IMPERIAL COLLEGE OF SCIENCE AND TECHNOLOGY

(University of London)

Department of Electrical Engineering

SLOT LOSS AND COUPLING STUDIES IN STACKED LINEAR ARRAY APPLICATIONS

By

Richard John Chignell, B.Sc., M.Sc., A.K.C.

A thesis submitted for the Degree

of Doctor of Philosophy of the University of London

March, 1975.

ABSTRACT

This study is concerned with some of the problems involved in realising a specific form of slotted waveguide monopulse array. The design considered differed from the usual monopulse configuration as a second set of waveguides was introduced into the aperture as the monopulse antenna difference channel. This allowed optimum illumination to be used for both channels. The problems associated with phase scanning in meeting the grating lobe criterion, dictated the use of a reduced height waveguide. The polarisation specified was parallel to the axis of the waveguide and as the resonant slots had to be fitted entirely within the narrow waveguide wall a non-standard geometry was essential. Earlier work has indicated that severe loss problems are associated with some slots of this type. Initially this thesis reviews the slot shapes available for array use and investigates their resonant properties. A slot loss model emerged the general behaviour of which was similar to that measured experimentally. The model indicated that a particular novel slot geometry had little loss associated with it and a wide range of slot couplings was available. Subsequently the problems encountered in designing large two dimensional phase scanned arrays using slots with this shape have been investigated. The principal problem was the inclusion of mutual impedance into a design particularly as cross polarisation suppression baffles were fitted which produced major changes in its behaviour. Several baffle shapes were investigated. They supported a guided wave so that the most important components of mutual impedance exist between slots in the same column but different waveguides. This was not helpful in phase scanning but at least ensured that an array could be designed, column by column,

and include the effects of mutual coupling.

The whole thesis is based on experimental approach and contains many practical results including those from the several arrays manufactured.

ACKNOWLEDGEMENTS

I would like to thank everyone who, in any way, helped me to complete this thesis.

I thank Mr. Roberts, my supervisor, for his advice during many discussions throughout the period of the work.

I thank the Admiralty for permission to present this thesis and for financial support under Contract No. N/CP47498/70/DC25(2)7L 220. Thanks are also due for use of the antenna test facilities of the Admiralty Surface Weapons Establishment, Hambrook, and for the helpful assistance of the Establishment's staff.

For workshop facilities, I thank the staff of the Electrical Engineering Department Workshop, Imperial College under the supervision of Mr. C. Jones. I am particularly grateful to Mr. R. Moore for meticulously cutting the many waveguide slots.

I am indebted to my colleagues at Imperial College who, through informal discussion, provided an environment in which ideas could flourish. Especially, I thank Mr. N. Williams for assistance with antenna site measurements.

I am grateful to my parents for my previous education and thank my mother for assistance with the preparation of figures.

I thank my wife Alexandra, for her patient and understanding encouragement in this work.

Finally, I thank Miss Elizabeth Farmer for the efficient manner in which she typed this thesis.

A LIST OF CONTENTS

A LIST OF FIGURES

A LIST OF PLATES

A LIST OF TABLES

CHAPTER 1

INTRODUCTION AND BACKGROUND

1.1. Introduction

Single slotted waveguide arrays were originally developed during the Second World War but have subsequently found wide application in marine radar. They can be seen fitted to pleasure craft of moderate size at any marina. They are ideal in this application producing a pencil beam in one plane, to locate radar targets, and a broad beam in the orthogonal plane which can accommodate the vessel rolling in a rough sea. They produce a horizontally polarised beam, without back radiation or spillover. This polarisation is generally considered optimum for marine use in the presence of sea clutter. The structure is also light and may readily be rotated.

Slotted waveguides have also been stacked (for instance Killick, Colley, Delaney and Eddles (1969)) to form two dimensional arrays which can be phase scanned. This enables a pencil beam to be formed in two planes but moved rapidly in one plane without the inertia problems associated with mechanical motion. For some radar applications, where the additional cost can be justified, more accurate angular information about a target can be more rapidly obtained by using a monopulse system. These systems use an additional channel in reception so that two different angular responses are obtained. By comparing the responses of the two channels to a single pulse the targets position can be obtained. In many monopulse systems a single antenna is fed through a hybrid and the two outputs obtained at different ports, but in others a second separate antenna system is introduced.

The object of this work was to develop a two channel array of interlaced slotted waveguides to give a monopulse response. The arrays were to be stacked so that the beam could be phase scanned in the vertical plane. The required range of phase scanning was $\pm 22\frac{1}{2}^{\circ}$ (1 beam width) but if a larger range could be obtained so much the better. Scanning in the horizontal plane was to be provided by mechanically rotating the whole array, but a small amount of scanning was required by changing the operating frequency. Vertically polarised arrays of this type have been made in the past using slots cut in ridged waveguide (Hu and Lunden 1961). A.S.W.E. required a horizontally polarised array and it is believed that no array of this type had previously been developed.

The scanning requirement of the array will be shown to require a compact radiating element and the phase distribution along each waveguide demands that the slots are resonant. One of the major problems in this work has been the development of a compact resonant slot radiating only the desired polarisation. A.S.W.E. did some preliminary work on a compact H-shaped slot before awarding a contract to Imperial College. Measurements on this type of slot showed that a substantial part (37.4%) of the power extracted from the waveguide was not appearing in the radiated power. A massive loss was associated with this slot. Some of the work presented in this thesis is directed at explaining this loss and ensuring that it does not occur in the slot configuration selected for use in arrays.

Many different types of slot were considered as the basic element of the array. The analysis and results from these slots are presented as an indication of their relative merits. One particular slot configuration was selected and subsequent work has been directed

towards its use in the type of phased array considered. This work included the design, manufacture and testing of two single slotted waveguide linear arrays. In these designs, mutual coupling was minimised by baffles which also improved their cross polarisation performance. However, for arrays consisting of more than one waveguide mutual coupling played a major role in modifying their individual performance. An analysis of mutual coupling is given. This is not complete but indicates the changes as different baffles are fitted or the array phase scanned. This work contributed to the design of an array of eight slotted waveguides which has been built and tested. The thesis includes the results of that array. However, before the work proceeds a more detailed consideration of some of the underlying concepts is presented.

1.2. Simple Phased Array Theory

An array antenna consists of several small antennas radiating in phase coherence. Many different individual antennas can be used as array elements but in this work slots are used. The original idea of using an array was to achieve better control of the antenna aperture illumination. In a multi channel array this is important as independent control of the individual aperture illuminations may be achieved. However, an array is also used because by changing the relative phase of the elements, the radiation pattern can be made to scan a volume of space.

A periodic planar phased array consists of similar radiating elements arranged in a planar and doubly periodic grid. In what, for need of a better name, is termed "classical" array theory, the mutual coupling between the array elements is neglected. The radiation pattern

of a finite sized phased array is expressed as a product of the array factor and the radiation pattern of the array element. The array factor determines the beam shape and sidelobe level of the array radiation pattern and relates the array geometry and steering phases to the direction cosines of the beam pointing directions. The functional relationship between these quantities is represented graphically by the figure known as the grating lobe diagram.

Amitay, Galindo and Wu (1972) considered a planar array of $(2M + 1) \times (2N + 1)$ identical elements in an infinite conducting ground plane at $z = o$ as shown in figure 1.2.1.. The apertures were arranged in a regular rectangular grid and the location of each was specified by indices (m, n) which corresponded to a physical location:

$$\bar{p}_{mn} = mb\hat{x} + nd\hat{y} \qquad (1.2.1)$$

where $\hat{x}$ and $\hat{y}$ were unit vectors and b and d the element separations in the directions x and y respectively. They showed that the electric field in the direction $\bar{r}$ was given by:

$$\bar{\mathcal{E}}(\bar{r}) = \bar{f}(T_x, T_y)S_a(T_x, T_y) \qquad (1.2.2)$$

$$|r| \to \infty$$

where $S_a(T_x, T_y)$ was a scalar quantity called the array factor and given by:

$$S_a(T_x, T_y) = \sum_{m=-M}^{M} \sum_{n=-N}^{N} V_{mn} \exp\left[j2\pi\left(m \frac{b}{\lambda} T_x + n \frac{d}{\lambda} T_y\right)\right] \qquad (1.2.3)$$

Similarly $\bar{f}(T_x, T_y)$ was a vector quantity called the element factor and given by:

FIGURE 1.2.1. A planar array of radiating elements.

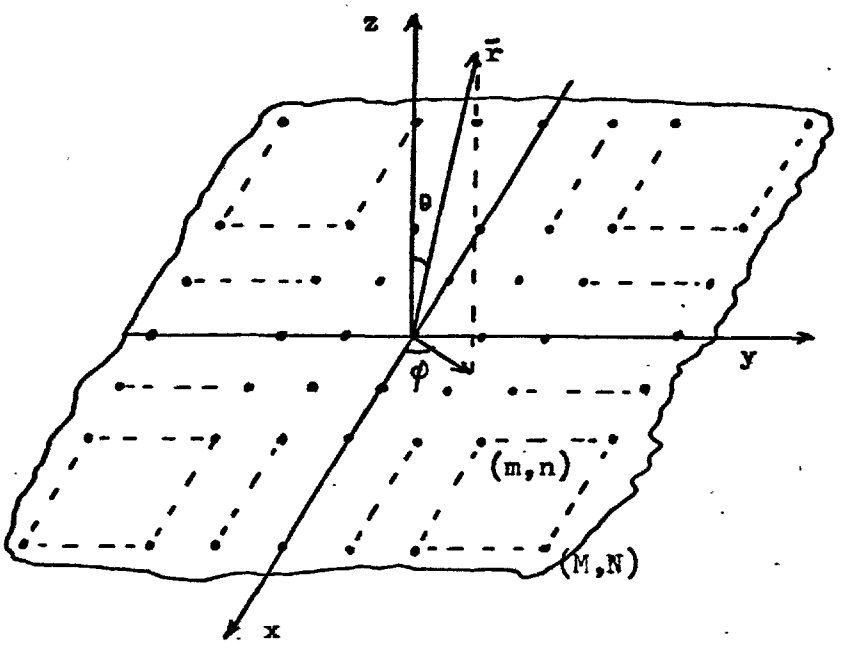

FIGURE 1.2.2. A grating lobe diagram for a rectangular grid array.

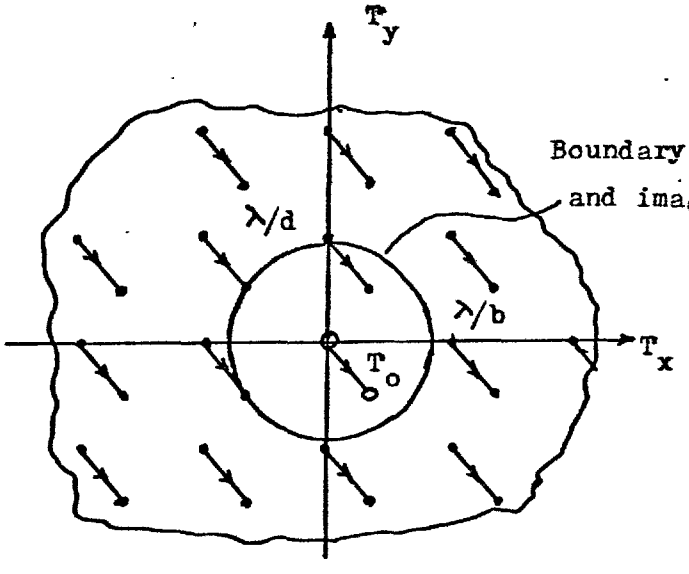

o Main beam.

• Grating lobe.

$$\bar{f}(T_x, T_y) = \frac{je^{-jkr}}{2\pi r}\left[k(1 - T_x^2 - T_y^2)^{\frac{1}{2}} - \hat{z}\,k\,(T_x x + T_y y)\right]$$

$$\wedge \iint_{A_o} \bar{E}_{oo}(x^o, y^o) e^{jk(T_x x^o + T_y y^o)}\, dx^o dy^o \qquad (1.2.4)$$

where:

V_{mn}	is the voltage on the (m,n)th. radiator,
λ	is the free space wavelength,
T_x and T_y	the direction cosines of $\bar{r}$,
k	the wavenumber,
and $\bar{E}_{oo}(x^o, y^o)$	is the field distribution of the element at the origin.

The array factor may be considered as the radiation pattern of an array of isotropic sources while the element factor introduces all the features of an individual element such as its radiation pattern and polarisation. Equation (1.2.2) is a statement of the principle of pattern multiplication, the far field radiation pattern being the product of the array factor and element pattern. Arrays usually use simple radiating elements for which the individual radiation patterns are broad. The beamwidth directivity and sidelobe structure are then determined mainly by the array factor. Radiation pattern synthesis thus involves a suitable choice of the V_{mn}'s in equation (1.2.3). V_{mn} is called the illumination function.

The equation (1.2.3) indicates that $S_a(T_x, T_y)$ is periodic both in T_x and T_y so that a knowledge of $S_a(T_x, T_y)$ in a rectangular region:

$$-\frac{\lambda}{2b} \leq T_x \leq \frac{\lambda}{2b} \; ; \qquad -\frac{\lambda}{2d} \leq T_y \leq \frac{\lambda}{2d}$$

is sufficient to completely characterise the array factor. A planar array radiates into a hemispherical region defined by $\frac{\pi}{2} > \theta > 0$ and $2\pi > \phi > 0$. Within the T_x, T_y plane this corresponds to the region $T_x^2 + T_y^2 < 1$ confined by a circle of unit radius. The region within the circle is termed real space or the visible region and the region outside the circle imaginary space or the invisible region.

If the voltages V_{mn} of an array have been properly synthesised to produce the prescribed radiation pattern then the array is phase scanned when its illumination is modified by adding a linear phase taper of the form:

$$V'_{mn} = V_{mn} e^{j(m\psi_x + n\psi_y)} \qquad (1.2.5)$$

ψ_x and ψ_y are the incremental phase shifts between adjacent elements in the x and y directions respectively. The corresponding array factor is:

$$S'_a(T_x, T_y) = \sum_{m=-M}^{M} \sum_{n=-N}^{N} V_{mn} \exp\left\{ j\left[\frac{2\pi mb}{\lambda}\left(T_x + \frac{\psi_x}{2\pi b/\lambda}\right) + \frac{2\pi nd}{\lambda}\left(T_y + \frac{\psi_y}{2\pi d/\lambda}\right)\right]\right\} \qquad (1.2.6)$$

The new array factor is the original one translated or scanned by T_{xo} and T_{yo} in the T_x and T_y directions where

$$T_{xo} = -\frac{\psi_x}{2\pi b/\lambda} \quad , \qquad T_{yo} = -\frac{\psi_y}{2\pi d/\lambda} \qquad (1.2.7)$$

In most applications an array is required to produce a directive radiation pattern with one large amplitude lobe or main beam; there are smaller lobes present due to the finite size of the array. If the

main beam is at broadside (i.e., $T_x = 0$, $T_y = 0$) then upon the application of a linear phase taper the main beam will be scanned to a new position. If the phase taper is correctly controlled the main beam may be made to scan the whole of the space. This is the principle of operation of a phased array.

The periodicity of the array factor in the $T_x - T_y$ plane means that the main beam and associated side lobes are repeated every λ/b and λ/d in the T_x and T_y directions respectively. Any repetition of the main beam is called a grating lobe. An infinite grid of grating lobes spaced at λ/b and λ/d intervals may be constructed. This is known as the grating lobe diagram and is shown in Figure 1.2.2..

The small circle at the origin corresponds to the broadside position of the main beam while the other circles indicate the grating lobes. The circle of unit radius showing the edge of real space is also shown. The figure indicates that if only one main beam is required the grating lobes must all be outside the unit circle. For a beam at broadside λ/d and λ/b must be greater than unity or the array elements must be closer than a wavelength apart.

If the array is to be phase scanned and a grating lobe is not to appear in real space then an even closer element spacing is required. When the main beam of the array is scanned to a new position T_o (where $T_o = \sin\theta_o$) the whole grating lobe structure is also translated by T_o as shown in Figure 1.2.2.. Grating lobes that were previously in imaginary space may now appear in real space and form a multiple beam. In most antennas this is avoided either by limiting the array scanning range or by decreasing the element spacing. In the principal directions, T_x and T_y, Blass and Rabinowitz (1957) have shown that the relationship between these quantities is:

$$\frac{b}{\lambda} \cdot \frac{d}{\lambda} < \frac{1}{1 + |\sin\theta_{max}|} \qquad (1.2.8)$$

where θ_{max} is the maximum scan angle for which a grating lobe peak does not appear in real space. For a single beam to be scanned to $\pm 90^{\circ}$ in the principal planes, the array elements must be closer than half a wavelength apart. If the scanning is limited to $\pm 30^{\circ}$ a spacing of up to two thirds of a wavelength is allowed.

If the beam is scanned in only one plane, as for an array of slotted waveguides, then different element spacings can be used in the two planes. For the plane in which there is no scanning a spacing of up to a wavelength is allowed.

When two arrays of slotted waveguides are interlaced the constraint applies separately to each array. There is only a third of a wavelength of space available to accommodate each waveguide if $\pm 30^{\circ}$ of scanning is required. In the particular antenna investigated in this thesis, the limit on the available space for each waveguide is of major importance and to satisfy it a completely new slot geometry has been evolved.

1.3. Slotted Waveguide Arrays

Phased arrays which can scan their main beam in two planes are extremely expensive because individual phase control is required for every element. In some applications the sophistication of phase scanning in two planes is unnecessary and unjustifiably expensive. The main advantage of electronically, rather than mechanically, steering an antenna beam is the fast scanning speed available without inertia. Electronic scanning rapidly moves an antenna beam, the required phase shifts being obtained by switching diode or ferrite phase control elements.

A radar aerial with a narrow beam may be required to search a volume for possible targets. The beam must be made to scan in two directions so that a three dimensional search is made: the third dimension being range. One systematic method of searching is to rapidly scan in one plane while at the same time slowly scanning in an orthogonal plane. The scanning speeds are adjusted so that after a complete search in one dimension the beam has scanned one beamwidth in the other direction. It may then be advantageous to make use of rapid phase scanning in one plane while using a comparatively slow mechanical rotation in the other. From a mechanical point of view the speed of rotation may still be high.

Reducing the phase scanning requirement to one plane, also reduces the number of phase control elements needed. Instead of each array element needing a phase shifter, each row or column of elements requires one, depending on the plane to be scanned. For a large square array of (N x N) elements this saves $(N^2 - N)$ phase shifters, which can represent a huge saving, because each phase control element can cost more than its antenna element.

This saving can only be realised if a suitable transmission network can be devised for each row or column of the array. At microwave frequencies, as large peak powers, typically for some radars in the megawatt range, are used, the obvious transmission system is waveguide. It is a totally screened transmission system and its characteristics are well known and well behaved.

The simplest method by which power may be radiated from a waveguide is through an aperture cut in one of its walls. For such an aperture to be a useful array element it must conform to certain requirements. One of these is that the phase characteristics of the aperture must be

independent of its amplitude coupling. If for instance, all the elements of the slotted waveguide array introduced a phase shift into the passing wave which was proportional to the coupling, a progressive phase shift would be produced similar to the array aperture distribution The radiated phase front would not be linear and a poor antenna performance would result. The apertures must thus be resonant, so that no reactance is introduced into the waveguide and a linear phase front is obtained independently of the aperture distribution. The most well known resonant aperture is the half wavelength long narrow slot. Its properties change with its position and orientation within the waveguide wall.

The proposed antenna was required to search a volume above the sea, typically defined by the horizon and an angle of elevation of 45°, from the surface vessel. A continuous search is needed in azimuth which is eminently suitable for mechanical scanning simply by rotating the whole antenna. Similarly, the rapid discontinuous nodding motion required of the beam in elevation is readily obtained using phase scanning without the inertia problems caused by rapidly reversing a large antenna. The waveguides must thus run horizontally and be stacked vertically above each other.

1.4. Angular Resolution and Monopulse

When a radar investigates a target many parameters may be measured but usually the most important is its relative position. The target's range is determined by the pulse circuitry attached to the antenna and the angular position by the scanning radiated beam. The radar transmits a continuous train of pulses which is reflected by the target. The time delay until the pulses return to the radar is a measure of the range. As the antenna beam is scanned past the target the amplitude of the

received pulses rises and falls in a similar fashion to the two way antenna radiation pattern as shown in Figure 1.4.1.. The amplitude of a single reflected pulse is a function not just of the target's angular coordinates but also of its scattering cross-section and range. For a single channel system, the angular position of the target can not be established from one reflected pulse but has to be obtained by comparing the amplitude of pulses arriving from slightly different angles. In this way the effects of range and scattering cross-section are removed. For simple radars this is done by storing the reflected pulses on a cathode ray tube. The operator then decides the brightest point on the display to give the target's position.

In a radar that is required to continuously search a volume for possible high speed targets, the use of a pulse train rather than individual pulses wastes time and reduces the possible scanning speed. This is obviously undesirable as the time between successive searches is increased. Other effects such as the suppression of sea clutter indicate that high scanning speeds are desirable.

It was realised early in the development of radar that a system that determined a target's angular coordinates from one reflected pulse would be advantageous and many different types of "monopulse" or one pulse systems have been devised. They all introduce an additional channel in reception with a different angular response. By comparing the outputs of the two channels the target's position can be determined. Rhodes (1950) attempted to unify all the monopulse systems into three categories which are:

(1) Amplitude comparison

(2) Phase comparison

(3) Sum and difference type.

FIGURE 1.4.1. A pulse train reflected by a target.

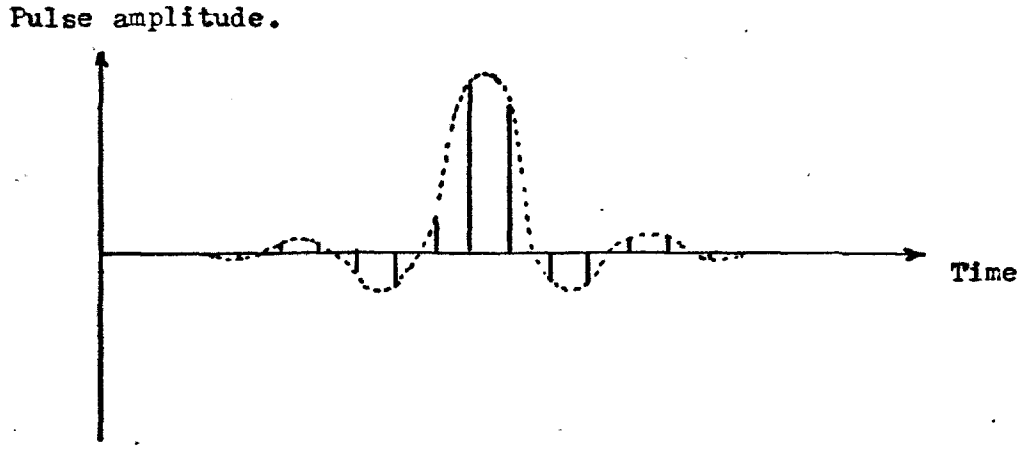

FIGURE 1.4.2. The block diagram of a two plane monopulse antenna.

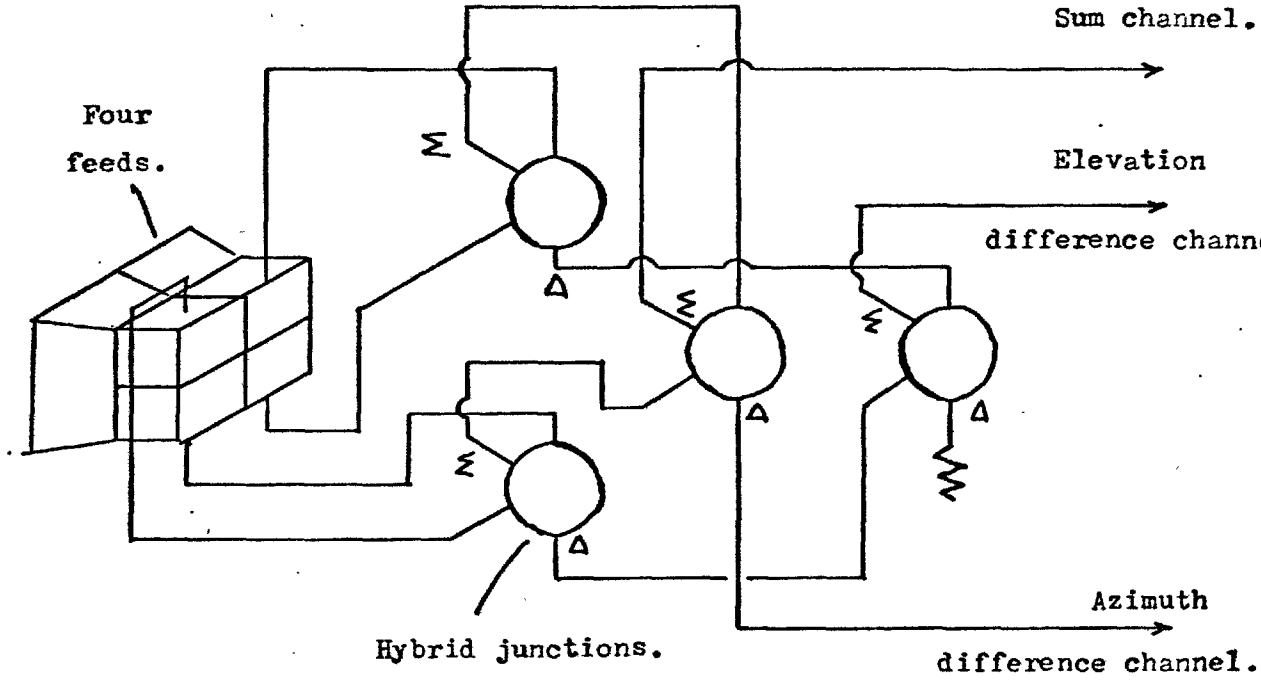

Amplitude comparison systems use a cluster of four antennas squinted at slightly different angles to each other. One antenna is used for transmission and the other three for reception. Due to the squint between the aerials a slightly different amplitude signal is received in each and upon comparison the angular position of the target may be obtained.

Phase comparison systems again use a cluster of four aerials, although in this case they are identical and all look out at the same angle. The angular position is determined from the difference in phase length from the target to each antenna. Both the comparison systems loose accuracy because the signals are frequently compared at the outputs of the two receivers which then have to be stable and of the same gain or phase characteristics.

The sum and difference type of monopulse is the most frequently used configuration in modern radars. A cluster of four antennas is used, frequently a cluster of four horns feeding a reflector. The antennas are interconnected by magic ties, rat races or short slot couplers as shown in Figure 1.4.2.. The radiation patterns obtained at the outputs of the network are one sum pattern with a single large lobe on axis and two difference patterns with lobes either side of a deep null as shown in Figure 1.4.3.. The signal in the difference channel is divided by that in the sum channel and the resulting signal is independent of the amplitude of the received signals or of the target's range and radar cross-section. Its amplitude is proportional only to the target's angular error from the antenna's boresight. The output voltage is an angular error signal ideally suited to control a tracking system. The single large sum channel lobe ensures that the target is well illuminated and maintains

FIGURE 1.4.3. A Monopulse Radiation Pattern.

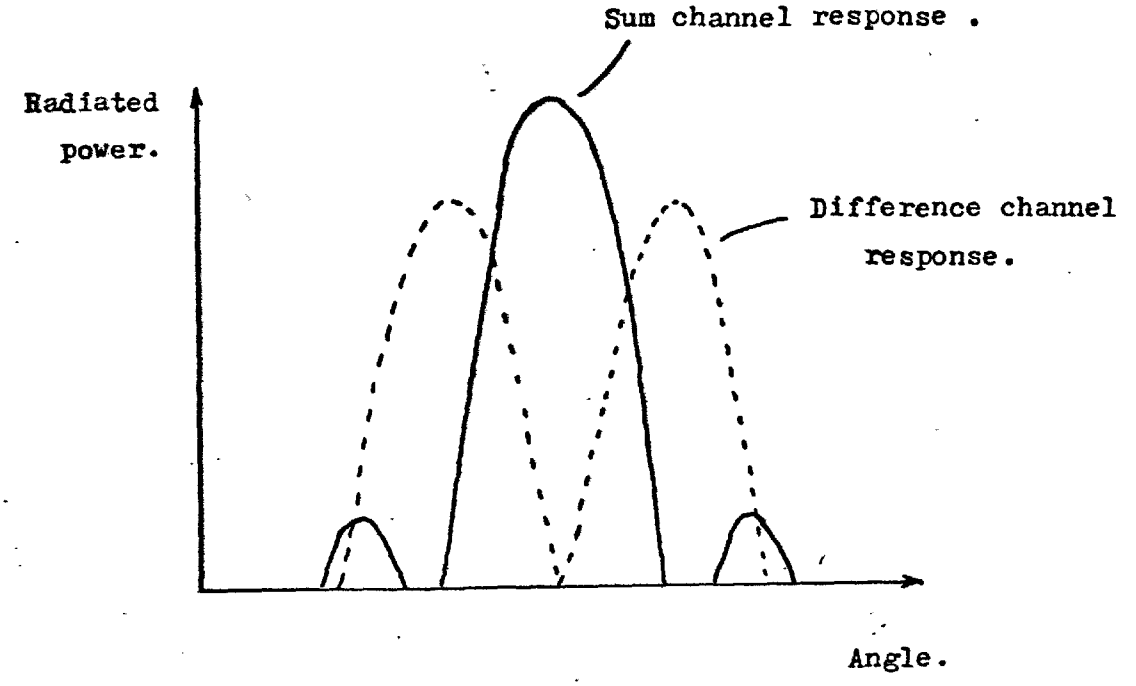

FIGURE 1.4.4. The envisaged waveguide system.

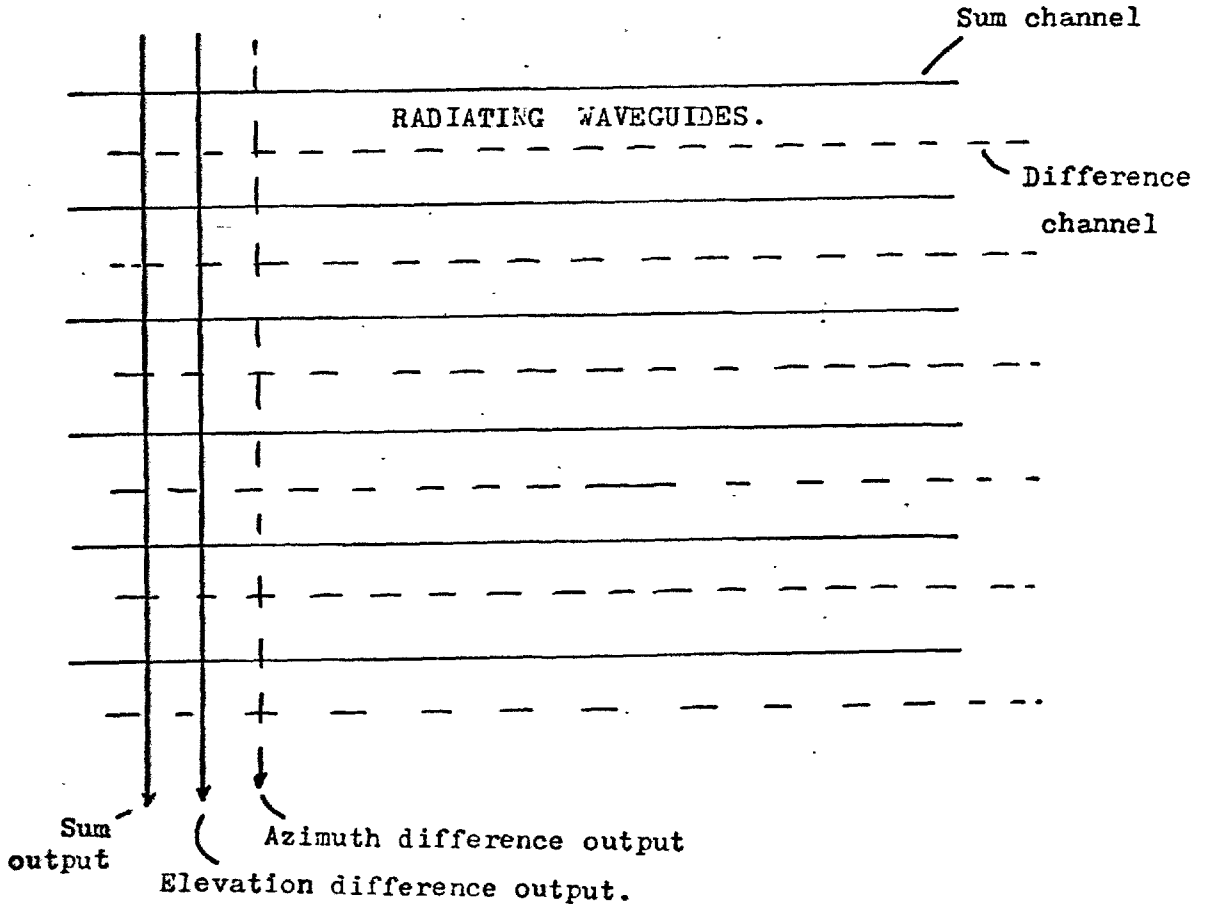

the radar's range. The deep null of the difference channel provides precise angular information. At microwave frequencies it relies for its position not on active components but on the stability of passive waveguide components. The fluctuation in gain of the receivers does however affect the magnitudes of the error voltages but not the null position.

A monopulse slotted waveguide array could be designed in a similar manner to the reflector antennas, using the same feed network with each quadrant of the array as a separate aerial. This solution was chosen by Lewis, Lee and McCarthy (1970). The main disadvantage of such a system is that the same aperture distribution with appropriate phasing must be used for both channels. This is usually a compromise and not the ideal distribution for either channel. Hannan (1961) showed that the periodicities in the aperture illuminations for the two channels should have been in the ratio of two to one. If only one distribution can be specified then some compromise is required in which one or more of sum channel gain, difference channel slope and sidelobe performance suffer. Usually the compromise favours the sum channel because it is used both in transmission and reception.

The system envisaged in this work introduced a second set of slotted waveguides with an additional feed network as shown in Figure 1.4.4.. The illumination functions for the two channels are now totally separated and can be independently optimised. The penalty paid for this freedom is an additional set of slotted waveguides within the same aperture. The grating lobe criterion applies separately to each channel so that the space for each waveguide has to be restricted to a third of the wavelength if scanning to $\pm 30^{\circ}$ from broadside is required. The slots are twice as closely spaced as they

would otherwise have been and the problems of mutual coupling are increased.

The mutual coupling problem is further complicated by the different modes in which the antenna is used. In transmission only the sum channels slots are directly excited, but the slots in the difference channel waveguides can not be neglected and must be treated as parasitic elements. In reception all the slots are illuminated by a plane wavefront and it can be shown by reciprocity that this is similar to using both channels in transmission. The relative voltages on the slots of the two channels are different in each case.

1.5. The Choice of Polarisation

The polarisation used by a radar system is influenced by many factors both environmental and mechanical. For instance over a calm sea horizontal polarisation may offer advantages in the suppression of sea clutter. If the sea becomes rough this improvement can be lost. Clutter caused by rain can be reduced using circular polarisation but the effective scattering cross-section of the target is also reduced.

The modern naval ship is equipped with several radars which should be complementary to each other. The choice of polarisation for one system should be related to the choices for the other systems and the changing operational and climatic conditions likely to be encountered.

For the system of waveguides shown in Figure 1.4.4., Hu and Lunden (1961) showed that vertical polarisation could be obtained using straight longitudinal slots cut in ridged waveguide as indicated in Figure 1.5.1..

A.S.W.E. required the capability of using horizontal polarisation.

FIGURE 1.5.1. Slots in ridged waveguide.

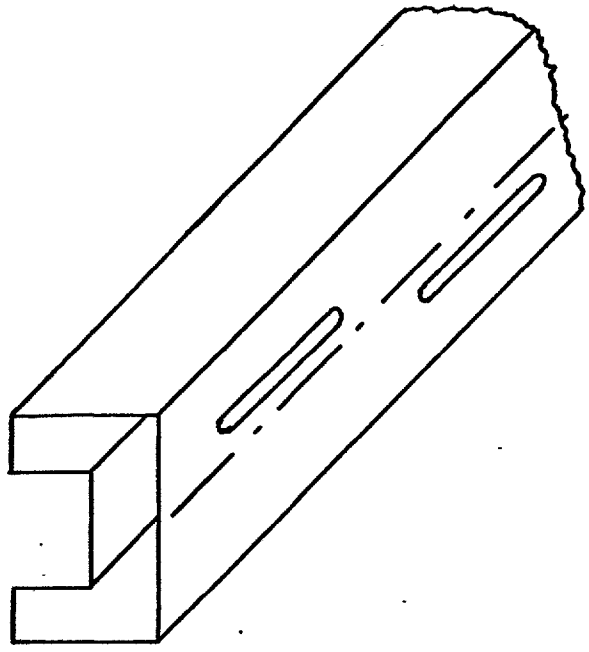

FIGURE 1.5.2. Shunt inclined slots.

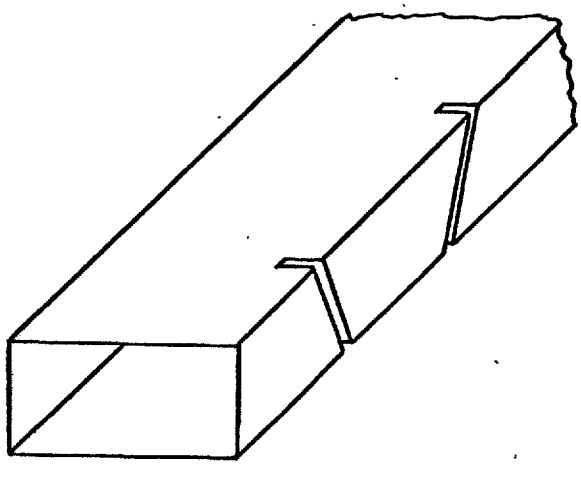

Shunt edge slots are normally used to obtain horizontal polarisation from a horizontal waveguide as indicated in Figure 1.5.2.. As the waveguide depth is usually less than half a wavelength, the slot length, the slot must be folded around onto the broad faces of the waveguide. In the envisaged application the complete slot and waveguide must occupy only a third of a wavelength. A waveguide much less than this depth must then be used so that the slot can be cut into the broad faces. Only a small portion of the slot is left in the narrow wall and capable of producing radiation. The parts of the slot on the broad face do not contribute to radiation at broadside but substantially increase mutual coupling between adjacent waveguides.

A different slot geometry was required preferably with all the slot contained in the narrow waveguide wall. Waveguides a third of a wavelength high could then be used and stacked touching each other. A.S.W.E. produced an H-shaped slot geometry as shown in Figure 1.5.3. which was designed by analogy to a double ridged waveguide. One slot profile was to be used and different couplings obtained by rotation in a similar manner to the shunt edge slot. A single waveguide array of slots of this type was made and it was found not to behave as expected. Careful measurements indicated that 37.4% of the power coupled out of the waveguide by these slots was not appearing as radiated power but was being dissipated in the slot. The surface finish of the slot was initially thought to be the source of the loss. Some slots were then made by spark erosion, the process which can produce a very high standard of surface finish by comparison to milling. For these slots the geometry was changed slightly as indicated in Figure 1.5.4.. This enabled the electrode used to be simply made

FIGURE 1.5.3. An H-shaped slot.

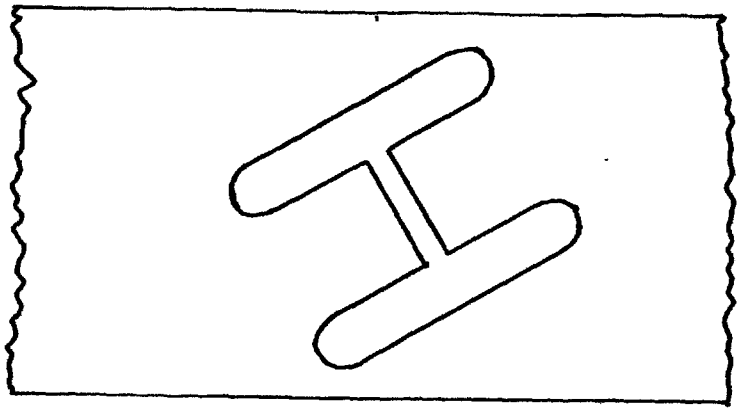

FIGURE 1.5.4. A modified H-shaped slot.

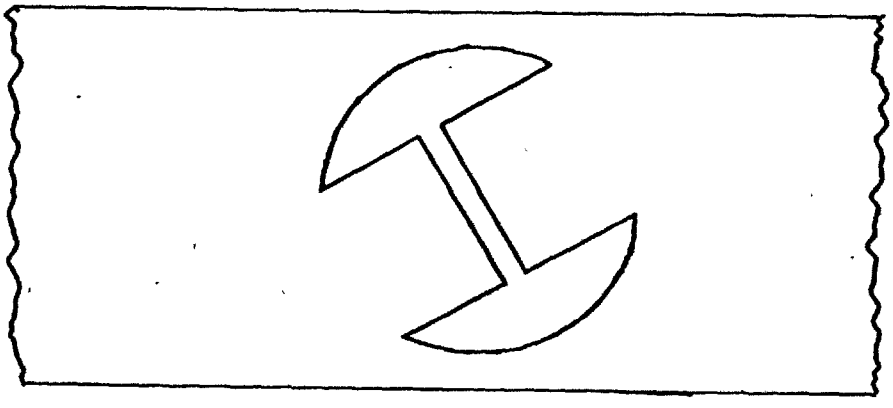

by milling two slots in a round bar. Measurements indicated that 52% of the power coupled out of the waveguide was being lost. The surface finish had improved, the slot geometry changed slightly and the loss had increased.

At this point a research contract was awarded to Imperial College to investigate these problems. This thesis is based on work performed by the author while employed on that contract.

CHAPTER 2

2.1. Historical Background

The waveguide array system envisaged required the development of a new radiating slot geometry and an examination of previous work was advantageous. The pioneering work in this field was done by a group working under W. H. Watson during the Second World War. He realised the inherent advantages of a slotted waveguide system with controllable aperture distribution and no spillover or back radiation, at a time when the parabolic dish antenna was almost universally used at microwave frequencies. The group were able to analyse several different slot geometries and built several arrays. Most of the group's work is summarised in Watson's book (Watson, 1947).

Stevenson (1948), a member of the group, presented a method of analysis for the equivalent circuit of a slot in waveguide. His method is elegant and gives the reactive component. The method is based upon the derivation of the vector potential within a waveguide of generalised cross section, using Green's functions, in terms of a specified electric field, due to the slot, at the waveguide wall. Stevenson's method though completely defining the slot parameters, subject to certain assumptions, is not easy to use in an engineering sense.

For engineering purposes a simpler but equivalent derivation has been given by Silver (1949) and Fradin (1961). They apply the reciprocity theorem to the fields in an unslotted waveguide and the field in the waveguide due to a slot. The result they obtain is similar to that of Stevenson's for the real part of the equivalent circuit of the slot. The advantage of their method is that the coupling of any section of a complicated slot can be readily obtained. In the development of

a new slot geometry this is advantageous as changes in geometry can easily be related to changes in coupling. The disadvantage of the method is that the reactive component of impedance is not obtained so the slot is only characterised at resonance.

Oliner (1957) also produced a method of analysis for waveguide slots. His work enabled some of the assumptions of the previous work, such as an infinitely thin waveguide wall, to be removed.

Slots in many different configurations have been used but none of them are suitable for the envisaged application. Initially the method of analysis of Silver and Fradin will be presented.

2.2. The Derivation of the Field Relationships for a Slotted Waveguide

The methods presented by Silver and Fradin both essentially start from a statement of the reciprocity theorem for a source free region. This has been derived from Maxwells equations by many authors (such as King and Harrison (1969), Section 8.2) and states that if two fields $\bar{E}_1$, $\bar{H}_1$ and $\bar{E}_2$, $\bar{H}_2$ exist in a source free volume V bounded by a surface S then:

$$\int_S \left\{ \hat{n} \cdot (\bar{E}_1 \wedge \bar{H}_2) + \hat{n} \cdot (\bar{H}_1 \wedge \bar{E}_2) \right\} dS = 0 \qquad (2.2.1)$$

where $\hat{n}$ is an outward directed normal unit vector to the surface S.

Equation (2.2.1) was applied to a section of waveguide bounded by planes S_L and S_R and containing the slot of interest as shown in Figure 2.2.1.. The waveguide was imagined extending to infinity in both directions. The field $\bar{E}_1$, $\bar{H}_1$ was taken as the known field due to the slot and $\bar{E}_2$, $\bar{H}_2$ as the known field in the waveguide. It was assumed that the waveguide wall was of negligible thickness and perfectly conducting. The waveguide walls would not support a tangential

FIGURE 2.2.1. A slotted section of waveguide.

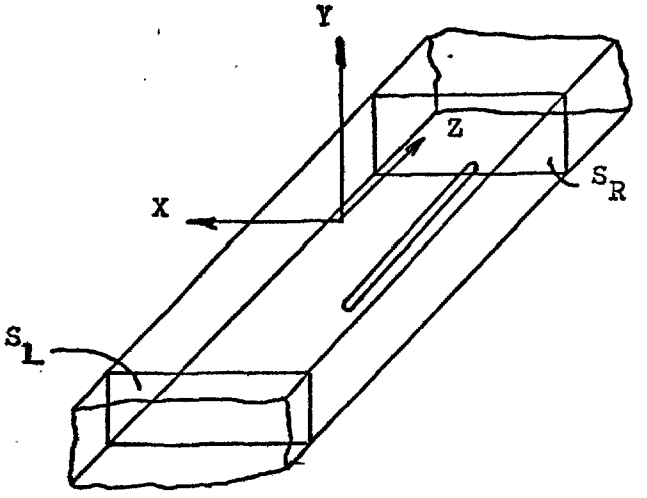

FIGURE 2.3.1. A rectangular waveguide containing a longitudinal slot in the narrow wall.

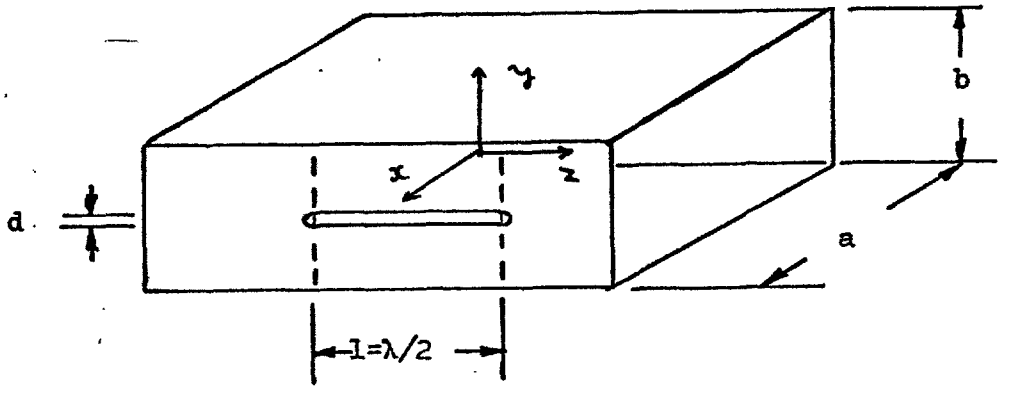

component of electric field, so that the area of integration in equation (2.2.1) was reduced to the planes S_L and S_R and the area of the slot, so that:

$$\int_{S_L \& S_R} \left\{ \hat{n} \cdot (\bar{E}_1 \wedge \bar{H}_2) + \hat{n} \cdot (\bar{H}_1 \wedge \bar{E}_2) \right\} dS$$

$$= - \int_{SLOT} \left\{ \hat{n} \cdot (\bar{E}_1 \wedge \bar{H}_2) + \hat{n} \cdot (\bar{H}_1 \wedge \bar{E}_2) \right\} dS \quad (2.2.2)$$

The electric field across the slot followed the path of maximum field gradient and lay in the plane of the slot with the magnetic field through the slot. Equation (2.2.2) could then be further simplified so that:

$$\int_{S_L \& S_R} \left\{ \hat{n} \cdot (\bar{E}_1 \wedge \bar{H}_2) + \hat{n} \cdot (\bar{H}_1 \wedge \bar{E}_2) \right\} dS = - \int_{SLOT} \hat{n} \cdot (\bar{E}_1 \wedge \bar{H}_2) dS \quad (2.2.3)$$

2.3. Application to Rectangular Waveguide

The most commonly used waveguide was of rectangular cross section and of dimensions such that only the lowest order TE_{01} mode would propogate. When waveguide of this type was used, the components of the fields could be specified. Referring to Figure 2.3.1., when the field $\bar{E}_2$, $\bar{H}_2$ was specified as a wave propagating in the positive z direction then its components were:

$$
\begin{aligned}
E_{2y} &= \cos\left(\frac{\pi x}{a}\right)e^{-j\gamma z} \\
H_{2x} &= -\frac{\gamma}{w\mu_o}\cos\left(\frac{\pi x}{a}\right)e^{-j\gamma z} \\
H_{2z} &= \frac{\pi}{a}\frac{1}{jw\mu}\sin\left(\frac{\pi x}{a}\right)e^{-j\gamma z} \\
E_{2x} &= E_{2z} = H_{2y} = 0
\end{aligned}
\qquad (2.3.1)
$$

where $\gamma = \frac{2\pi}{\lambda_g}$, λ_g being the wavelength within the waveguide. For propagation in the negative z direction the components became:

$$
\begin{aligned}
E_{2y} &= \cos\left(\frac{\pi x}{a}\right)e^{j\gamma z} \\
H_{2x} &= +\frac{\gamma}{w\mu_o}\cos\left(\frac{\pi x}{a}\right)e^{j\gamma z} \\
H_{2z} &= \frac{\pi}{a}\frac{1}{jw\mu}\sin\left(\frac{\pi x}{a}\right)e^{j\gamma z} \\
E_{2x} &= E_{2z} = H_{2y} = 0
\end{aligned}
\qquad (2.3.2)
$$

For a slotted waveguide used in reception, the field in the immediate vicinity of the slot depended upon the slot geometry. Within the waveguide however at sufficiently large distances from the slot the field must exist as travelling waves. The planes S_L and S_R were sufficiently removed from the slot for evanescent modes to have decayed so that the field at S_L must have been:

$$E_{1y} = A \cos(\frac{\pi x}{a}) e^{j\gamma z}$$

$$E_{1x} = \frac{A\gamma}{w\mu} \cos(\frac{\pi x}{a}) e^{j\gamma z}$$

$$H_{1z} = \frac{A\pi}{jw\mu a} \sin(\frac{\pi x}{a}) e^{j\gamma z} \qquad (2.3.3)$$

$$E_{1x} = E_{1z} = H_{1y} = 0$$

and at S_R:

$$E_{1y} = B \cos(\frac{\pi x}{a}) e^{-j\gamma z}$$

$$H_{1x} = -\frac{B\gamma}{w\mu} \cos(\frac{\pi x}{a}) e^{-j\gamma z}$$

$$H_{1z} = \frac{B\pi}{jw\mu a} \sin(\frac{\pi x}{a}) e^{-j\gamma z} \qquad (2.3.4)$$

$$E_{1x} = E_{1z} = H_{1y} = 0$$

The field in the slot has been related to that in the waveguide by the unknown quantities A and B . A was determined when the field $\bar{E}_2$, $\bar{H}_2$ was taken as that of a wave propagating in the positive z direction. Equations (2.3.1), (2.3.3) and (2.3.4) were substituted in equation (2.2.11) the left hand integrand of which was simplified by:

$$\hat{n} \cdot (\bar{E}_1 \wedge \bar{H}_2) + \hat{n} \cdot (\bar{H}_1 \wedge \bar{E}_2) = \pm (E_{2y} H_{1x} - E_{1y} H_{2x}) \qquad (2.3.5)$$

At S_R the integrand became zero so that:

$$\int_{S_L} \frac{2A\gamma}{w\mu} \cos^2\left(\frac{\pi x}{a}\right) dS = - \int_{slot} \hat{n} \cdot (\bar{E}_1 \wedge \bar{H}_2) \; dS \qquad (2.3.6)$$

from which:

$$A = - \frac{w\mu}{\gamma S_C} \int_{slot} \hat{n} \cdot (\bar{E}_1 \wedge \bar{H}_2) \; dS \qquad (2.3.7)$$

where S_C was the cross-sectional area of the waveguide.

Similarly when $\bar{E}_2$, $\bar{H}_2$ was taken as a wave propagating in the negative z-direction it could be shown that:

$$B = \frac{w\mu}{\gamma S_C} \int_{slot} \hat{n} \cdot (\bar{E}_1 \wedge \bar{H}_2) \; dS \qquad (2.3.8)$$

The magnitudes of A and B were the same as expected by symmetry. They could only be evaluated for particular slot geometries for which $\bar{E}_1$ could be specified within the slot.

For slots in the narrow wall of the waveguide which were of principal importance in this study, it is interesting to note the behaviour of the vector product in equations (2.3.7) and (2.3.8). At the narrow wall the only component of the waveguide field $\bar{H}_2$ is along the waveguide axis. A slot orientated along the length of the waveguide has its electric field $\bar{E}_1$ perpendicular to $\bar{H}_2$, forms a large vector product and is heavily coupled. Similarly a slot in the narrow face perpendicular to the waveguide axis results in $\bar{E}_1$ and $\bar{H}_2$ being parallel and no coupling. Thus for the narrow waveguide wall it is only slot sections extending along the length of the waveguide that are coupled.

The slots that had previously been investigated by this method were straight "half wavelength" long slots entirely within one face of the

waveguide. The analysis of these slots is again presented to illustrate the method and so that it could be investigated experimentally with what were thought to be regularly behaved slots before being applied to more novel geometries. These slots could be thought of as a transmission line short circuited at both ends so that when they were half a wavelength long they behaved like a resonant cavity with a sinusoidal field distribution along their length. The waveguide slots investigated were:

(a) the longitudinal slot in the narrow wall,

(b) the inclined slot in the narrow wall,

(c) the longitudinal slot in the broad wall.

(a) The longitudinal slot in the narrow wall.

The geometry of this slot is shown in Fig. 2.3.1. The electric vector $\bar{E}_1$ in the slot was given by:

$$\bar{E}_1 = E_{1y} = \frac{V}{d}\cos kz \qquad \left(\begin{matrix}V \text{ is the voltage} \\ \text{across the centre} \\ \text{of the slot}\end{matrix}\right) \quad (2.3.9)$$

where $k = 2\pi/\lambda$, λ being the wavelength. At the narrow face:

$$H_{2z} = \frac{\pi}{a}\frac{1}{jw\mu}e^{-j\gamma z} \quad (2.3.10)$$

so that from (2.3.7)

$$A = \frac{\pi V}{j\gamma a S_c d}\int_{-\frac{d}{2}}^{+\frac{d}{2}} dy \int_{-\frac{\lambda}{4}}^{+\frac{\lambda}{4}} \cos kz e^{-j\gamma z}\, dz$$

$$= \frac{\pi V}{j\gamma a S_c}\int_{-\frac{\lambda}{4}}^{+\frac{\lambda}{4}} \cos kz e^{-j\gamma z} dz = \frac{2V}{j\pi b}\cdot\frac{\lambda_g}{\lambda}\cdot\cos\left(\frac{\pi}{2}\cdot\frac{\lambda}{\lambda_g}\right)$$

(2.3.11)

and

$$B = A \tag{2.3.12}$$

(b) The inclined slot in the narrow wall.

This slot is illustrated in Figure 2.3.2 and was simply the longitudinal slot rotated by an angle θ. It was convenient to use an additional set of coordinate (x, y', z') as illustrated to analyse this slot. The electric field in the slot was:

$$\bar{E}_1 = E_{1y'} = \frac{V}{d} \cos kz' \tag{2.3.13}$$

and

$$H_{2z'} = H_{2z} \cos \theta \tag{2.3.14}$$

so that from (2.3.7)

$$A = \frac{\pi V \cos\theta}{j\gamma a S_c} \int_{-\frac{\lambda}{4}}^{+\frac{\lambda}{4}} \cos kz' e^{-j\gamma z' \cos\theta} \, dz'$$

$$= \frac{2V\pi\cos\theta\cos(\frac{\pi}{2}\frac{\gamma}{k}\cos\theta)}{ja\gamma S_c k\left\{1 - (\frac{\gamma}{k}\cos\theta)^2\right\}} \tag{2.3.15}$$

and $B = A.$ (2.3.16)

(c) The longitudinal slot in the broad face.

Figure 2.3.3. shows the geometry of this slot. The electric field within the slot lay in the x - z plane and was given by:

$$\bar{E}_1 = E_{1x} = \frac{V}{d} \cos kz \tag{2.3.17}$$

Its z component of the magnetic field was then

FIGURE 2.3.2. A straight inclined slot in the narrow wall of the waveguide.

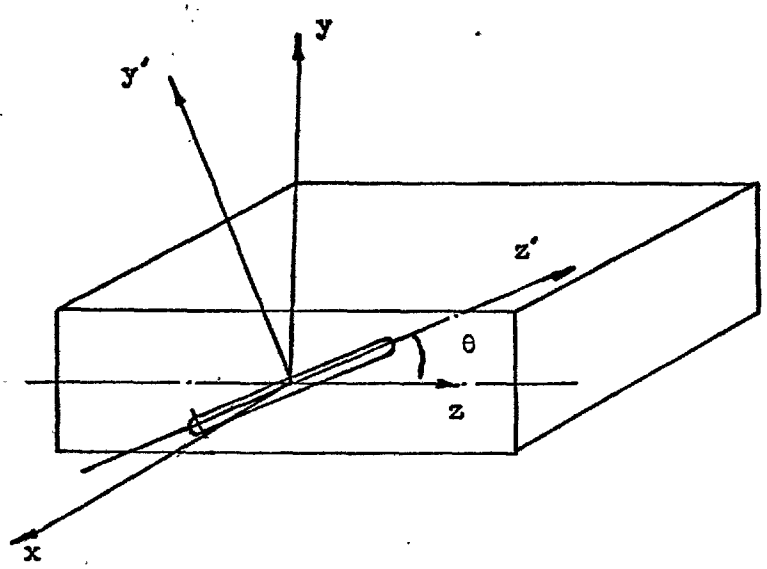

FIGURE 2.3.3. A straight longitudinal slot in the broad face of a waveguide.

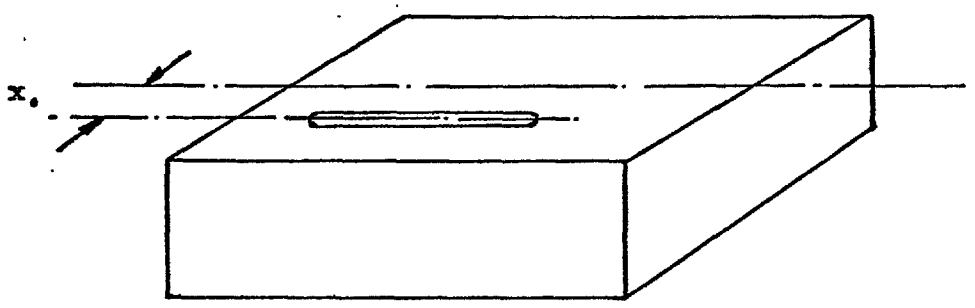

$$\bar{H}_2 = H_{2z} = \frac{\pi}{a} \cdot \frac{1}{jw\mu} \sin(\frac{\pi x}{a}) e^{-j\gamma x} \qquad (2.3.18)$$

and varied across the width of the slot which made the integral obtained by substitution in (2.3.7):

$$A = \frac{\pi V}{j\gamma S_c da} \int_{slot} \sin(\frac{\pi x}{a}) \cos kz e^{-j\gamma z} dS \qquad (2.3.19)$$

difficult to evaluate unless the slot width could be taken as small when:

$$\int_{x_1-\frac{d}{2}}^{x_1+\frac{d}{2}} \sin(\frac{\pi x}{a}) dx \simeq d \sin(\frac{\pi x_1}{a}) \qquad (2.3.20)$$

The integral then evaluated to give:

$$A = -\frac{2V}{j\pi b} \cdot \frac{\lambda_g}{\lambda} \cos(\frac{\pi}{2} \frac{\lambda}{\lambda_g}) \sin(\frac{\pi x_1}{a}) \qquad (2.3.21)$$

and

$$B = A \qquad (2.3.22)$$

For all the examples given it happened that B = A but for other cases such as a transverse slot in a broad wall it could be shown that B = - A. The significance of this difference will be shown later.

The relationship that had been established for the specified slots linked the voltage across a slot in reception with the amplitude of the waves launched into waveguide. The equivalent circuit could then be derived by launching a wave into the waveguide which induced a voltage across the slot producing secondary waves in the waveguide and radiation to space. Conservation of energy was then applied to this

situation and an equivalent circuit relationship emerged. Before this could be done an expression for the power radiated by the slot had to be determined.

2.4. Babinet's Principle and the Radiation Resistance of a Straight Dipole

Babinets principle was originally devised to determine the optical properties of complementary screens. It could also be applied to microwave problems but a fuller description was needed than the original optical statement. This was a standard piece of work and appeared in several books (see King and Harrison (1969), or Booker (1946)).

When a group of perfect electric conductors S_1, S_2,.... were considered, the boundary conditions were:

$$\begin{aligned} \hat{n} \cdot \bar{E} &= -\eta/\epsilon & \hat{n} \wedge \bar{H} &= -\bar{k} \\ \hat{n} \wedge \bar{E} &= 0 & \hat{n} \cdot \bar{H} &= 0 \end{aligned} \qquad (2.4.1)$$

on S_1, S_2,..... similarly a group of perfect magnetic conductors S_1^*,S_2^*,..... could be imagined for which:

$$\begin{aligned} \hat{n} \cdot \bar{H} &= -\eta^*/\mu & \hat{n} \wedge \bar{E} &= \bar{k}^* \\ \hat{n} \wedge \bar{H} &= 0 & \hat{n} \cdot \bar{E} &= 0 \end{aligned} \qquad (2.4.2)$$

where η and $\bar{k}$ were surface densities of electric charge and current and η^* and $\bar{k}^*$ were fictitious densities of magnetic charge and current.

It appeared that if fictitious magnetic currents were considered the electric and magnetic fields could be interchanged according to the plan:

$$\bar{E}_2 \equiv -\zeta \bar{H}_1 \qquad \text{and} \qquad \bar{H}_2 \equiv \zeta^{-1}\bar{E}_1 \tag{2.4.3}$$

if the electric and magnetic sources were interchanged as:

$$\begin{aligned} \bar{k}_2 &\equiv \zeta^{-1}\bar{k}_1^* & \eta_2 &\equiv -\zeta^{-1}\eta_1^* \\ \bar{k}_2^* &\equiv \zeta\bar{k}_1 & \eta_2^* &\equiv \zeta\eta_1 \end{aligned} \tag{2.4.4}$$

where ζ was the impedance of free space.

Magnetic currents were a fictitious expedient, however, the field configurations they would produce could be established by electric currents on the complementary structure. A filamentary dipole of perfectly conducting material was considered as shown in Figure 2.4.1., with the associated circularly symmetric magnetic field. As the magnetic field was circularly symmetric, the dipole could be surrounded by a perfectly magnetic conducting screen without changing the field. On interchanging electric and magnetic conductors, the resulting structure was a large electric conducting screen with a small filamentary magnetic conducting dipole or physically a slot cut in a large metallic ground plane. The concept of duality was established for complementary structures and particularly slots and dipoles. It could also be shown (see Rumsey (1966)) that if z and z' were the radiation impedances of a structure and its complement then:

$$zz' = \frac{\zeta^2}{4} \tag{2.4.5}$$

For a slot, it followed that if a voltage V was established at its centre and z_{slot} its radiation impedance then the power radiated was

$$P = \frac{V^2}{z_{slot}} \tag{2.4.6}$$

FIGURE 2.4.1. The duality between a slot and a dipole.

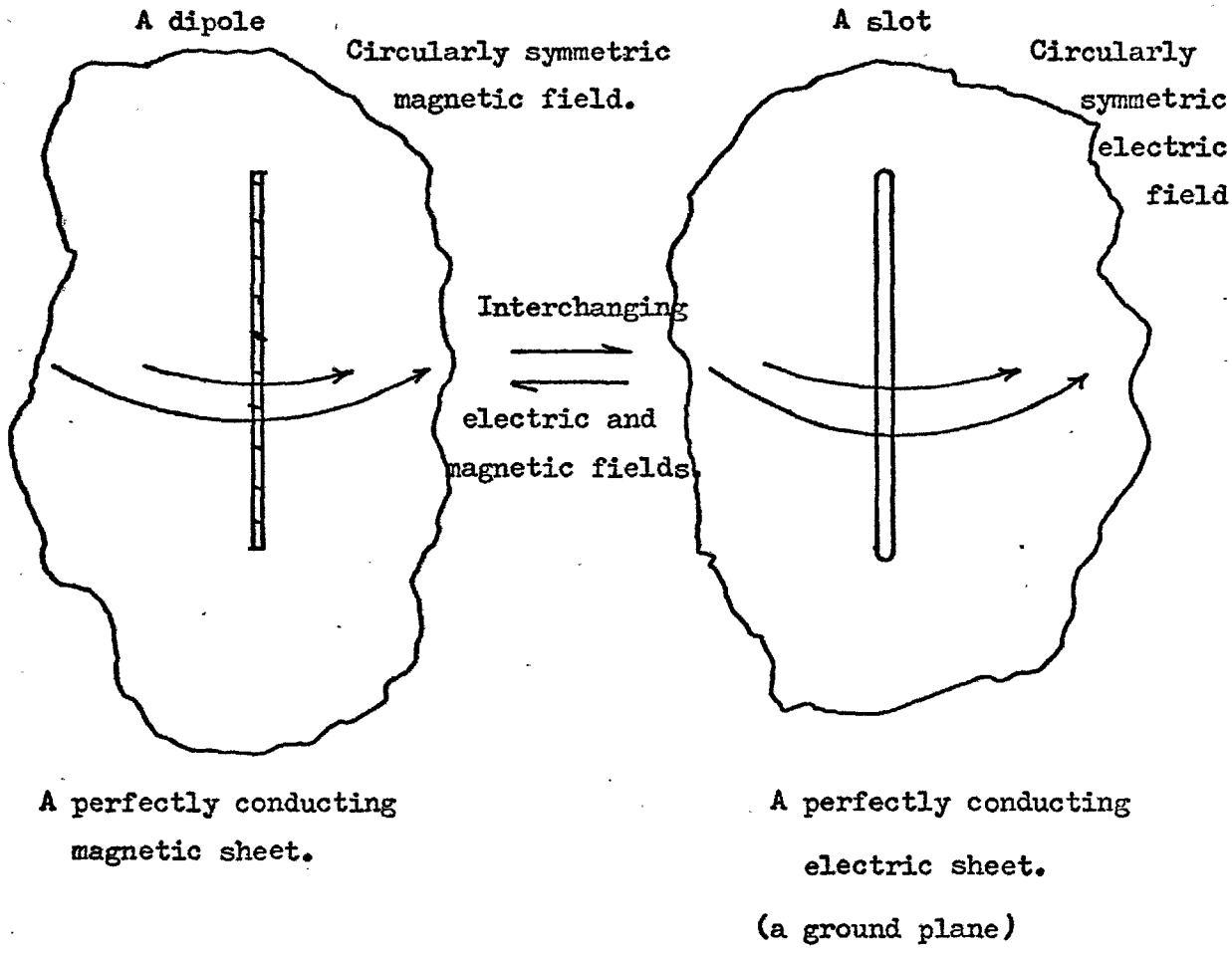

FIGURE 2.4.2. The coordinates used to determine the radiation resistance of a straight dipole.

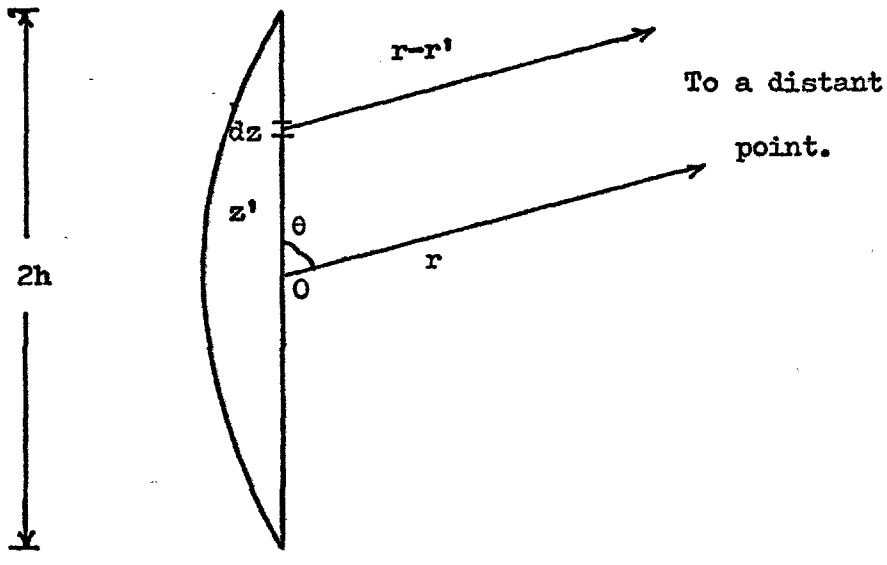

and from (2.4.5)

$$P = \frac{4V^2}{\zeta^2} R_{rad} \qquad (2.4.7)$$

where R_{rad} was the radiation resistance of the complementary dipole. This assumed that the slot was a two sided radiator but most slots and all waveguide fed slots were single sided radiators for which:

$$P = \frac{2V^2}{\zeta^2} R_{rad}$$

or

$$= \frac{V^2}{2(60\pi)^2} R_{rad} \qquad (2.4.8)$$

This last expression has been used to obtain the equivalent circuit of slots as it was much simpler to obtain the radiation resistance of a complementary dipole rather than that of a real slot by considering current flowing in the surrounding conducting sheet.

The radiation resistance of a straight dipole was then derived. This was a standard analysis (see King and Harrison (1969)) but is presented because dipoles of different shapes were later examined, and the derivation of their properties used the one basic method. The radiation resistance was found by analysing the total time averaged power radiated by a dipole which was given by:

$$\bar{P} = \mathrm{Re} \int_S \hat{n} \cdot \bar{S}(\bar{r}) dS$$

$$= \mathrm{Re} \int_0^{2\pi} d\varphi \int_0^{\pi} \bar{S}_r(\bar{r}) r^2 \sin\theta d\theta \qquad (2.4.9)$$

where $\bar{S}_r(\bar{r})$ was the complex Poynting vector defined by:

$$\bar{S}_r(r) = \tfrac{1}{2}\,\mu^{-1}\,.\,\bar{E}(\bar{r}) \wedge \bar{B}^*(\bar{r}) \qquad (2.4.10)$$

where $\bar{E}(\bar{r})$ and $\bar{B}(\bar{r})$ were the electric and magnetic fields. The integration was performed over a sphere in the far field or radiation zone, where:

$$\bar{E}^r(\bar{r}) = c\,\bar{B}^r(\bar{r}) \wedge \hat{r} \qquad (2.4.11)$$

so that

$$\bar{S}^r(\bar{r}) = \tfrac{1}{2}\,\mu^{-1} c\,\hat{r}\bar{B}^r\,.\,\bar{B}^{r*} \qquad (2.4.12)$$

but, by definition

$$\bar{B}^r = -\,jk\hat{r} \wedge \bar{A}^r(\bar{r}) \qquad (2.4.13)$$

where $\bar{A}^r(r)$ was the vector potential. The Poynting vector then became:

$$\bar{S}^r(\bar{r}) = \tfrac{1}{2}\,\mu^{-1} ck^2\,|\,\hat{r} \wedge \bar{A}^r(\bar{r})\,|^2\hat{r} \qquad (2.4.14)$$

but

$$\bar{A}^r(\bar{r}) = \frac{\mu}{4\pi}\,\frac{e^{-jkr}}{r}\int_V \bar{J}(\bar{r}')e^{jk_o(\bar{r}'\,.\,\hat{r})}\,dV' \qquad (2.4.15)$$

so

$$\bar{S}^r(\bar{r}) = \frac{k^2\zeta\hat{r}}{32\pi^2r^2}\,|\,\hat{r} \wedge \int_V \bar{J}(\bar{r}')e^{jk_o(\bar{r}'\,.\,\hat{r})}\,dV'\,|^2 \qquad (2.4.16)$$

where $\bar{J}(\bar{r}')$ was the current in the dipole. For a straight dipole of total height 2h illustrated in Figure 2.4.2., this was given by:

$$I_z(z') = I_z(o)\,\frac{\sin k(h - |z|)}{\sin hk} \qquad (2.4.17)$$

and the current integral was:

$$\frac{\hat{z}\, I_z(o)}{\sin hk}\left\{\int_o^h \sin k(h - z')e^{jkz'\cos\theta}dz' + \int_{-h}^{o} \sin k(h + z')e^{jkz'\cos\theta}dz'\right\} \tag{2.4.18}$$

This integral became:

$$\frac{2\hat{z} I_z(o)}{k \sin\theta} F_o(\theta, hk) \tag{2.4.19}$$

where:

$$F_o(\theta, hk) = \frac{\cos(hk\cos\theta) - \cos hk}{\sin hk \sin\theta} \tag{2.4.20}$$

From (2.4.16)

$$\bar{S}^r(\bar{r}) \equiv \frac{\hat{r}\,\zeta\,|I_z(o)|^2}{8\pi^2 r^2} F_o^2(\theta, hk) \tag{2.4.21}$$

and the time averaged power radiated was:

$$\bar{P} = \frac{\zeta\,|I_z(o)|^2}{4\pi}\int_o^{\pi} F_o^2(\theta, hk)\sin\theta d\theta \tag{2.4.22}$$

This was also defined to be

$$\bar{P} = \tfrac{1}{2}\,|I_z(o)|^2 R_{rad} \tag{2.4.23}$$

from which an evaluation of the integral (see King 1956)

$$R_{rad} = \frac{\zeta}{4\pi\sin^2 hk}\left\{-\cos 2hk\, Cin\, 4hk + 2(1 + \cos 2hk)Cin\, 2hk\right.$$

$$\left. + \sin 2hk(Si\,.\,4hk - 2Si\,.\,2hk)\right\} \tag{2.4.24}$$

where the following tabulated integrals were used:

$$\text{Si } x = \int_0^x \frac{\sin u}{u}\, du$$

$$\text{Cin } x = \int_0^x \frac{1 - \cos u}{u}\, du \qquad (2.4.25)$$

$$= C + \ell n\, x - C_i\, x$$

where

$$\text{Ci } x = \int_\infty^x \frac{\cos u}{u}\, du$$

and C was Eulers constant (C = 0.5772).

Equation (2.4.24) indicated the complexity of the integral for a simple dipole. If more complicated shapes were used it was likely that the integrals would be even more lengthy and evidently suitable for numerical analysis. From equation (2.4.24) by substituting $h = \lambda/4$, the well known result that for a half-wave dipole the radiation resistance was 73.1 ohms could have been obtained.

2.5. Derivation of the Equivalent Circuit Parameters

The power flowing in a rectangular waveguide carrying only the dominant mode has been shown (see Montgomery, Dicke and Purcell, 1948) to be given by:

$$\frac{E_o^2}{120\pi} \cdot \frac{Y}{k} \cdot \frac{S_c}{2} \qquad (2.5.1)$$

where E_o was the electric field at the centre of the waveguide. If a wave of amplitude E_o was incident upon a slotted waveguide section from the negative z direction, a voltage V would have been induced in the slot which would have launched secondary waves in the waveguide and produced radiation to space. Using the results of the last

sections the equation of energy balance would have been:

$$\frac{E_o^2}{120\pi} \cdot \frac{\gamma}{k} \cdot \frac{S_c}{2} = \frac{A^2}{120\pi} \cdot \frac{\gamma}{k} \cdot \frac{S_c}{2} + \frac{(E_o + B)^2}{120\pi} \cdot \frac{\gamma}{k} \cdot \frac{S_c}{2} + \frac{V^2 R_{rad}}{2(60\pi)^2} \tag{2.5.2}$$

so that:

$$\frac{V^2}{A^2} \cdot \frac{k}{\gamma} \cdot \frac{R_{rad}}{30\pi} \cdot \frac{1}{S_c} = -\left(1 + \frac{B^2}{A^2} + \frac{2BE_o}{A}\right) \tag{2.5.3}$$

The results obtained in section (2.3) indicated that either A = B or A = - B and A/E_o could be specified as the voltage reflection coefficient Γ so that:

$$\frac{V^2}{A^2} \cdot \frac{k}{\gamma} \cdot \frac{R_{rad}}{30\pi} \cdot \frac{1}{S_c} = -2\left(1 \pm \frac{1}{\Gamma}\right) \tag{2.5.4}$$

However, a normalised shunt conductance g introduced into an otherwise matched waveguide has a reflection coefficient given by:

$$\Gamma = -\frac{g}{2 + g} \tag{2.5.5}$$

or

$$g = -\frac{2}{1 + \frac{1}{\Gamma}} \tag{2.5.6}$$

Comparing (2.5.4) with (2.5.6) indicated that when A = B the slot could be represented by a normalised shunt conductance given by:

$$g = \frac{120\pi}{R_{rad}} \cdot S_c \cdot \frac{\gamma}{k} \cdot \frac{A^2}{V^2} \tag{2.5.7}$$

Similarly a normalised series resistance r introduced into an otherwise matched waveguide had a reflection coefficient given by:

$$\Gamma = \frac{r}{r + 2} \tag{2.5.8}$$

or:

$$r = \frac{2}{1 - \frac{1}{\Gamma}} \tag{2.5.9}$$

Comparison of equations (2.5.4) with (2.5.9) led to the conclusion that when A = - B the slot could be represented by a series resistance r given by:

$$r = \frac{120\pi}{R_{rad}} \cdot S_c \cdot \frac{\gamma}{k} \cdot \frac{A^2}{V^2} \tag{2.5.10}$$

For the three slots considered in Section (2.3) the ratio A/V had been determined and it had been shown that A = B. The equivalent shunt conductance of these slots could be established.

a) The longitudinal slot in the narrow wall of the waveguide.

When equation (2.3.11) was substituted in equation (2.5.7) the result was:

$$g = \frac{480}{R_{rad} \cdot \pi} \cdot \frac{a}{b} \cdot \frac{\lambda_g}{\lambda} \cos^2\left(\frac{\pi}{2} \cdot \frac{\lambda}{\lambda_g}\right) \tag{2.5.11}$$

b) The inclined slot in the narrow wall of the waveguide.

Substitution using equation (2.3.15) yielded the result:

$$g = \frac{30\lambda^3\lambda_g}{R_{rad}\pi a^3 b} \left\{ \frac{\cos\theta \cos\left(\frac{\pi}{2} \cdot \frac{\lambda}{\lambda_g} \cos\theta\right)}{1 - \left(\frac{\lambda}{\lambda_g} \cos\theta\right)^2} \right\}^2 \tag{2.5.12}$$

c) The longitudinal slot in the broad wall of the waveguide.

In this case equation (2.3.21) was used and resulted in the expression:

$$g = \frac{480}{R_{rad}\pi} \cdot \frac{a\lambda_g}{b\lambda} \cdot \cos^2\left(\frac{\pi}{2} \cdot \frac{\lambda}{\lambda_g}\right)\sin^2\left(\frac{\pi x_1}{a}\right) \qquad (2.5.13)$$

2.6. Experimental Investigation of Straight Slots in Rectangular Waveguide

It was proposed that the results so far presented in this chapter and which appeared in the literature should be thoroughly investigated experimentally, before possible application to novel slot geometries. This work could in principle have been performed at any frequency band, but practically this would not have been sensible. The lower the frequency used the larger the waveguide would have had to be, but for higher frequencies manufacturing tolerances became important. A compromise was required and the band from 4 to 8 GHz designated in England as C band was thought to be suitable. Within this band 5.70 GHz was selected as a possible centre frequency. A special size, thin walled, waveguide in 70/30 brass (I.D.: 1.270" x 0.590"; O.D.: 1.350" x 0.670") was available and when stacked equation (1.2.8) indicated that an array could be scanned to $\pm$ 33° at this frequency, before the peak of the grating lobe appeared in real space.

Most of the experimental work in this thesis was performed in the special waveguide. The work on individual slots was expected to involve the narrow wall of the waveguide and to save manufacturing effort a waveguide jig was made. The narrow wall of a section of special waveguide was removed by milling after the remaining faces had been reinforced. A plate was then located on straight parallel steel pins in place of the waveguide wall and was held in good contact by a series of screws. A drilling and a milling jig were made so that

the plates could be produced in large numbers with a minimum of workshop effort. The slots investigated were milled in the plates which when fitted to the waveguide jig and also provided the ground plane around the slot.

One series of four plates was made with straight longitudinal slots of different widths milled in them. A different series of four plates was made with inclined slots of the same dimensions cut in them but at different angles. For the purposes of investigating straight slots a series of longitudinal slots of different widths were milled in the broad face of sections of the special waveguide and fitted with an area of ground plane made from brass sheet.

All these slots were individually investigated using a Hewlett Packard swept frequency generator, Weinschel Engineering radio frequency ratiometer and data normaliser and a Waveguide 12 (R48; WR187) bench. Swept measurements of the attenuation past the slots were made to an accuracy of $\pm$ 0.03 dB and obtained as X - Y plots with normalised calibration lines.

Impedance measurements were also made on some slots using a slotted line, to establish that the frequency of maximum conductance and attenuation past the slot was close to the true resonance of zero slot reactance. For the straight slots the dispersion between these frequencies was small and to a good approximation the resonant frequency could be taken as that of peak attenuation past the slot.

The derivation of the equivalent circuit parameters assumed the length of the slot to be well defined by square ends. The literature (Knorr and Saerz (1973)) indicated that even for square ended slots this was not so as the slot magnetic field penetrated beyond the physical slot end which did not form a complete short circuit. Watson (1947)

obtained results for square ended resonant slots and found that their physical length was less than half a wavelength. Square ended slots would have been difficult to manufacture and the slots investigated experimentally were produced with round ends by milling. The effects associated with the round ends were unknown at the start of this study and this was initially investigated.

A recent paper, Yee (1974), has presented results for round ended longitudinal slots in the broad face and also indicates that for a particular slot dimension the resonant frequency varies slightly with displacement from the centre line of the waveguide.

The physical dimensions of the straight slots investigated are shown in Tables 2.6.1. and 2.6.2. in terms of the measured resonant wavelength. In all cases it appeared that the overall slot length was greater than half a wavelength but this sensibly described the length of the slot between centres of the end arcs. For round ended slots it appeared that the end effects were removed by considering the length between centres.

As the resonant dimensions and frequencies of the slots had been established theoretical values of conductance could be obtained for all the slots measured. The theoretical and experimental values for longitudinal slots in the narrow wall are compared in Table 2.6.3. Excellent agreement was obtained, for three cases the error was less than 0.2%, smaller than the range of experimental error, and for the fourth case approximately 2%. These results confirmed the method of slot analysis both in terms of coupling to the waveguide and the radiation from the slot. The finite slot width was included in the coupling to the waveguide but a line source was used to calculate the radiation resistance.

TABLE 2.6.1. The resonant electrical length of straight longitudinal slots in the narrow waveguide wall, radiating into half space.

Slot width. INCHES.	Electrical slot length ; Resonant wavelengths.	
	Overall	Between centres
0.020	0.513	0.504
0.031	0.522	0.507
0.047	0.525	0.501
0.062	0.534	0.502

TABLE 2.6.2. The resonant electrical length of straight longitudinal slots in the broad waveguide wall, radiating into half space.

Slot width. INCHES.	Electrical slot length ; Resonant wavelengths.	
	Overall	Between centres
0.020	0.503	0.493
0.031	0.507	0.492
0.047	0.513	0.491
0.062	0.520	0.491

TABLE 2.6.3. Experimental and theoretical results for the conductance of straight longitudinal slots in the narrow wall of the special size waveguide.

Slot width. INCHES.	Resonant frequency. GHZ.	Peak conductance values.	
		Experimental	Theoretical
0.020	5.844	2.623	2.560
0.031	5.950	2.330	2.325
0.047	5.990	2.193	2.213
0.062	6.094	2.084	2.087

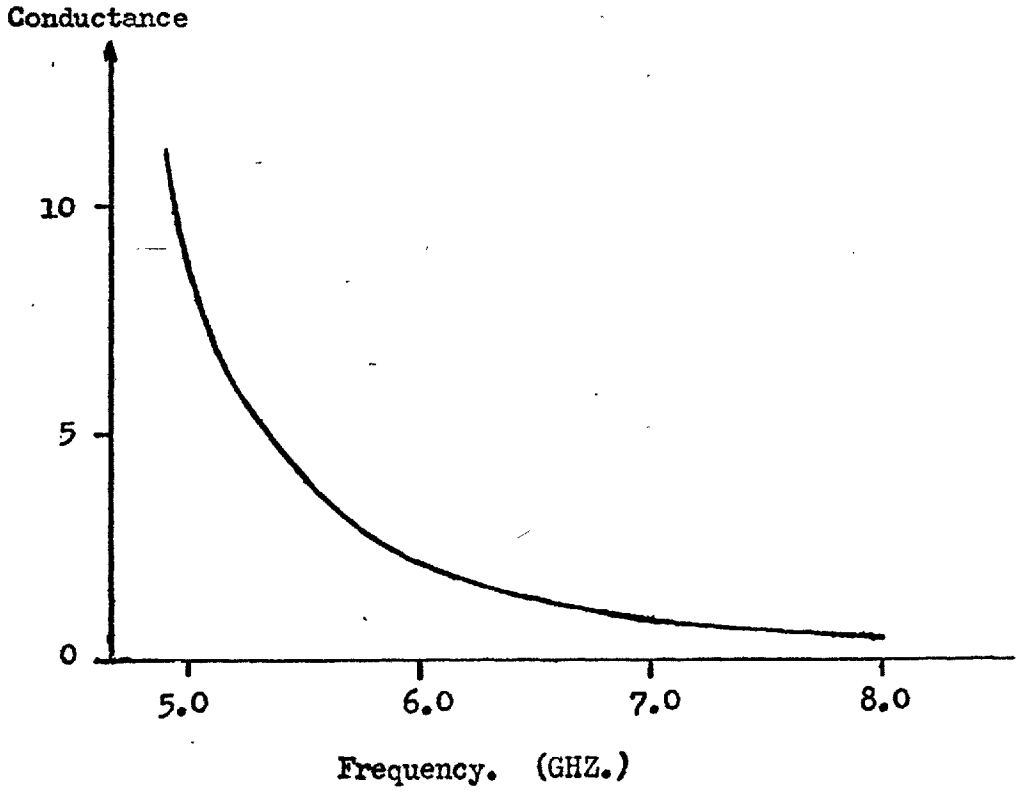

FIGURE 2.6.1. The frequency variation of the resonant conductance of a straight longitudinal slot in the narrow wall of the special size waveguide.

The radiating aperture of a slot can always be defined without any thickness unlike the case of a real dipole which always has finite dimensions. The non-filamentary nature of a practical dipole always changes its radiation impedance. The slot however must be less sensitive to its finite width as it is effectively of zero thickness.

The frequency variation of the resonant conductance of a straight longitudinal slot is shown in Figure 2.6.1. The variation is due to the longitudinal component of the waveguide magnetic field as the guide approaches cut-off.

Other theoretical and experimental results for inclined slots in the narrow wall and longitudinal slots in the broad wall of the waveguide are compared in Tables 2.6.4. and 2.6.5.. Good agreement was obtained but in all cases the experimental values were slightly larger than the theoretical values. The tables also indicate the resonant frequencies of the slots which varied because the slots of different widths were of similar overall lengths.

Figures 2.6.2. and 2.6.3. indicate both the theoretical and experimental radiation patterns obtained for a longitudinal slot in the narrow wall of the waveguide. Some agreement was obtained but the theoretical patterns were naively taken as the "far field patterns" of a slot in an "infinite" ground plane. Experimentally a finite ground plane was used and the departures were due to diffraction at its edges. The power at the ground plane edges was sufficiently low so that the discontinuity did not affect the power radiated by the slot and hence its conductance but was seen in the overall radiation pattern.

It appeared that the procedure for predicting slot conductance was useful and that the reference planes to be used in determining the

TABLE 2.6.4. Experimental and theoretical results for the conductance of straight inclined slots in the narrow wall of the special size waveguide.

Slot Inclination (Degrees)	Resonant frequency. GHZ.	Peak conductance values.	
		Experimental	Theoretical
5	5.854	2.635	2.452
10	5.855	2.566	2.403
15	5.844	2.523	2.354
20	5.795	2.431	2.371

TABLE 2.6.5. Experimental and theoretical results for the conductance of straight longitudinal slots in the broad wall of the special size waveguide. (x=a/4)

Slot width. INCHES.	Resonant frequency. GHZ.	Peak conductance values.	
		Experimental	Theoretical
0.020	5.667	1.544	1.522
0.031	5.600	1.598	1.651
0.047	5.600	1.699	1.651
0.062	5.496	1.995	1.878

FIGURE 2.6.2. The radiation pattern of a straight longitudinal slot in the narrow wall of the waveguide. The pattern is plotted in the plane of the waveguide's broad face with the transmitter vertically polarised.

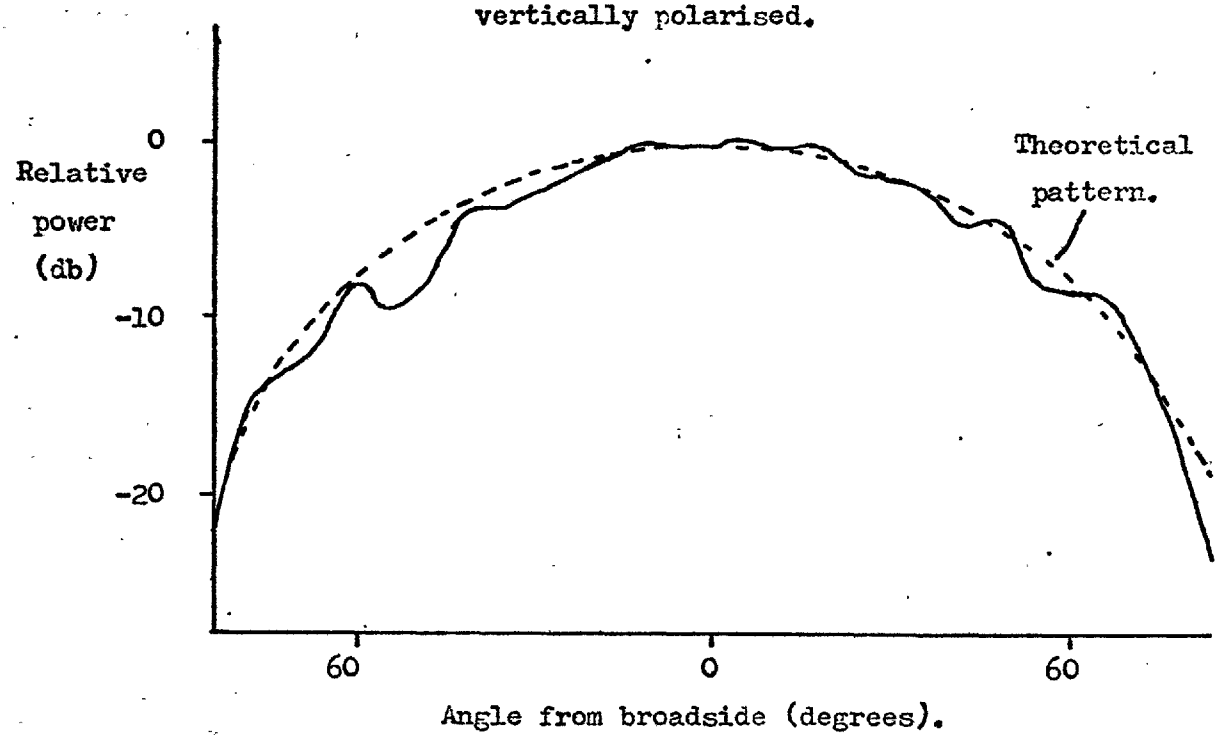

FIGURE 2.6.3. The radiation pattern of a straight longitudinal slot in the narrow wall of the waveguide. The pattern is plotted with the waveguide axis vertical and the transmitter horizontally polarised.

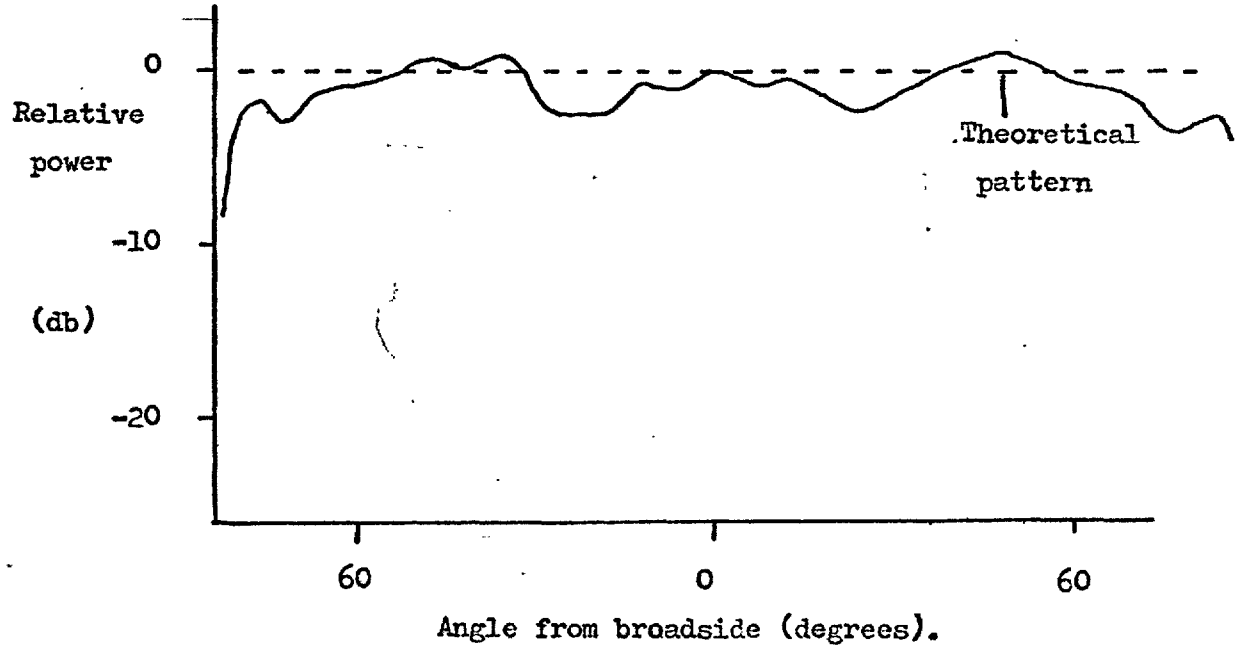

electrical length of rounded end slots were correct. These considerations were then used to investigate more novel slot geometries.

CHAPTER 3

NOVEL SLOT GEOMETRIES

3.1. The ⅂-Shaped Slot

The conventional short edge slot shown in Figure 1.5.2. was too long to fit the narrow face of the waveguide and had to be folded on to the broad face. In the application envisaged this was not possible and the obvious alternative was to fold the end arms round on to the narrow face as indicated in Figure 3.1.1.. The end arms now intercepted wall current and coupled power to the slot. The centre section could then be re-orientated as shown. The ⅂-shaped slot thus formed was analysed in a similar manner to the straight slots. A sinusoidal voltage distribution was fitted along the total length of the slot. The resonant slot was regarded as a transmission line short circuited at both ends with minor discontinuities at the corners so that the field was principally specified by the short circuits. This assumption was later verified by experiment. The ⅂-shaped slot was analysed in three sections, corresponding to the three slot limbs. After a sinusoidal voltage has been fitted along the entire length of the slot, the coupling coefficients were obtained by integration over the slot surface. In a real situation it is allowable to split the integral into components so that the coupling to each section is separately analysed and a physical understanding of the role of each obtained.

For the centre section of the slot:

$$\bar{E}_1 = E_{1z} = \frac{V}{d}\cos ky \qquad (3.1.1)$$

and

$$\bar{H}_2 = H_{2z} = \frac{\pi}{jw\mu a} e^{-j\gamma z} \qquad (3.1.2)$$

FIGURE 3.1.1. The geometry of a ⅂-shaped slot.

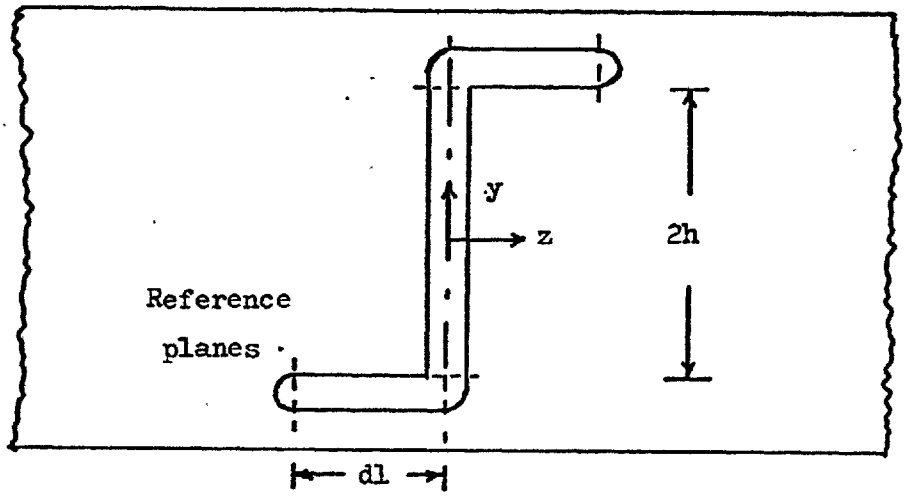

FIGURE 3.2.1. The geometry of a ⅂-shaped dipole.

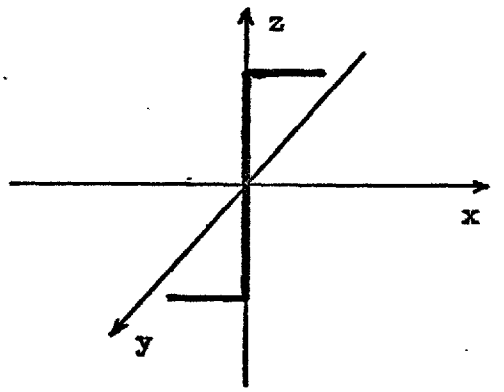

FIGURE 3.2.2. The ⅂-shaped dipole's radiation resistance.

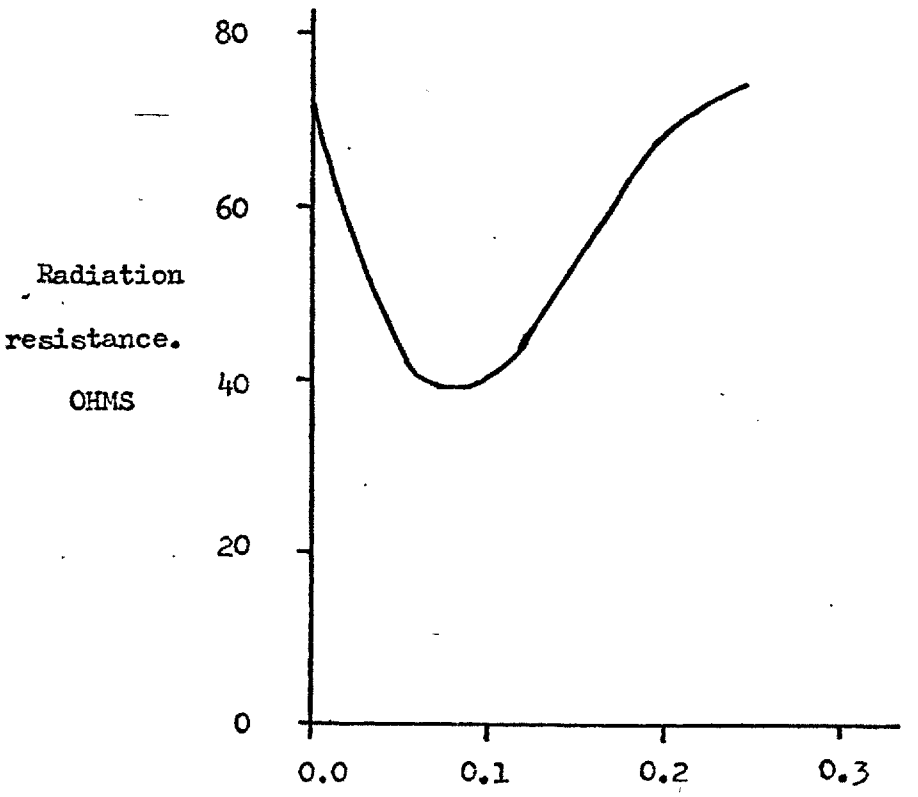

so that the vector product

$$\bar{E}_1 \wedge \bar{H}_2 = 0 \qquad (3.1.3)$$

and the centre section of the slot did not couple to the waveguide. For one end arm however

$$\bar{E}_1 = E_{1y} = \frac{V}{d}\cos k(z + h) \qquad (3.1.4)$$

where h was the electrical half height of the slot. From equation (2.3.7) the contribution to A from this end arm was:

$$A_1 = -\frac{\pi V}{j\gamma S_C}\int_0^{\lambda/4-h} \cos k(z + h)e^{-j\gamma z}dz \qquad (3.1.5)$$

Similarly for the other end arm:

$$\bar{E}_1 = E_{1y} = \frac{V}{d}\cos k(z - h) \qquad (3.1.6)$$

and

$$A_2 = -\frac{\pi V}{j\gamma S_C}\int_{-(\lambda/4-h)}^{0} \cos k(z - h)e^{-j\gamma z}dz \qquad (3.1.7)$$

so that the value of A was:

$$A = -\frac{\pi V}{j\gamma S_C}\left[\int_0^{\lambda/4-h} \cos k(z + h)e^{-j\gamma z}dz + \int_{-(\lambda/4-h)}^{0} \cos k(z - h)e^{-j\gamma z}dz\right] \qquad (3.1.8)$$

The integrals were evaluated by making the substitutions

$$u = z + h$$

and (3.1.9)

$$u = z - h$$

respectively so that the result was:

$$A = -\frac{2\pi V k}{j\gamma S_c(k^2 - \gamma^2)} \left\{ \cos\gamma(\lambda/4 - h) - \cos k(\lambda/4 - h) \right\} \qquad (3.1.10)$$

It could also be shown that:

$$B = A \qquad (3.1.11)$$

so that from (2.5.7), the equivalent circuit was a shunt conductance of value:

$$g = \frac{480a\lambda_g}{R_{rad}\pi b\lambda} \left\{ \cos\gamma(\lambda/4 - h) - \cos k(\lambda/4 - h) \right\}^2 \qquad (3.1.12)$$

where R_{rad} was now the radiation resistance of a ⅂-shaped dipole.

3.2. The Radiation Resistance of the ⅂-Shaped Dipole

The radiation resistance of the ⅂-shaped dipole was obtained in a similar manner to that of the straight dipole. An input current at the dipole centre was specified and a sinusoidal current distribution assumed along its length. The currents on the different sections were considered separately and then summed. Referring to Figure 3.2.1., the current integral contained contributions which were x and z directed. The dipole was assumed to be resonant so that a sinusoidal current distribution was fitted to it, the z contribution of which was:

$$I_z(z, t) = \mathrm{Re} I_z(0)\cos kz e^{jwt} \tag{3.2.1}$$

This produced a contribution to the current integral of:

$$J_z = I_z(0) \int_{-h}^{+h} \cos kz e^{jz\cos\theta} dz \tag{3.2.2}$$

$$= \frac{2I_z(0)F_1(\theta, hk)}{k\sin^2\theta} \tag{3.2.3}$$

where

$$F_1(\theta, hk) = \sin hk\cos(hk\cos\theta) - \cos\theta\cosh k\sin(hk\cos\theta) \tag{3.2.4}$$

The current in an end section was given by:

$$I_z(x, t) = \mathrm{Re} I_z(0)\cos k(x + h)e^{jwt} \tag{3.2.5}$$

and its contribution to the current integral was:

$$\int_0^{\lambda/4-h} I_z(0)\cos k(x + h)\exp[jk(x\cos\phi\sin\theta + h\cos\theta)]dx \tag{3.2.6}$$

Several substitutions were then made to simplify the form of the integral, these were:

$$u = x + h \tag{3.2.7}$$

$$V = hk(\cos\theta - \cos\phi\sin\theta)$$

and

$$\alpha = \cos\phi\sin\theta \tag{3.2.8}$$

so that the current integral was reduced to

$$I_z(0)\exp(jv) \int_h^{\lambda/4} \cos ku \cdot \exp(j\alpha ku)\,du \qquad (3.2.9)$$

and evaluated to give

$$\frac{I_z(0)}{k(1-\alpha^2)} \left\{ \exp[j(v + \tfrac{\alpha\pi}{2})] - [\sinh k + j\alpha\cosh k] \cdot \exp[j(v + \alpha hk)] \right\} \qquad (3.2.10)$$

Similarly for the other end section, the current integral was given by:

$$\int_{-(\lambda/4-h)}^{0} I_z(0)\cos k(x-h)\exp[jk(x\cos\phi\sin\theta - h\cos\theta)]\,dx \qquad (3.2.11)$$

In this case the substitution:

$$u = x - h \qquad (3.2.12)$$

was made and the result was:

$$\frac{I_z(0)}{k(1-\alpha^2)} \left\{ \exp[-j(v + \tfrac{\alpha\pi}{2})] - [\sinh k - j\alpha\cosh k] \cdot \exp[-j(v + \alpha hk)] \right\} \qquad (3.2.13)$$

The two x directed components (3.2.10) and (3.2.13) were then combined to give the total x directed component of the current integral:

$$J_x = \frac{2I_z(0)}{k(1-\alpha^2)} \left\{ \cos\beta - \sinh k\cos\gamma - \alpha\cosh k\sin\gamma \right\} \qquad (3.2.14)$$

where

$$\beta = v + \frac{\alpha\pi}{2} \qquad (3.2.15)$$

and

$$\gamma = v + \alpha hk$$
$$= hk\cos\theta \qquad (3.2.16)$$

The Poynting vector was defined when the straight dipole was considered by equation (2.4.16):

$$\bar{S}_r(r) = \frac{k^2\zeta_o \bar{r}}{32\pi^2 r^2} \left| \bar{r} \wedge \int_V \bar{J}(\bar{r}')e^{jk_o(\bar{r}' \cdot r)} dV' \right|^2$$

For the ⅂-shaped dipole the current integral was not circularly symmetric and the cross product introduced a more complicated term than the $\sin\theta$ of the straight dipole. The angle η between the total integrated current vector and $\bar{r}$ had to be found and was shown to be given by:

$$\eta = 2\sin^{-1}\left\{\frac{1}{\sqrt{2}}(1 - \sin\chi\sin\theta\cos\phi - \cos\chi\cos\theta)^{\frac{1}{2}}\right\} \qquad (3.2.17)$$

where χ was the angle between the total integrated current vector and the z axis. In order to find the total power radiated by the dipole, the Poynting vector had to be integrated over the surface of a sphere centred at the dipole. The time averaged power radiated $\bar{P}$ was given by:

$$\bar{P} = \int_0^{2\pi}\int_0^{\pi} \frac{k^2\zeta_o}{32\pi^2} \sin^2\eta(J_x^2 + J_z^2)\sin\theta d\theta d\phi \qquad (3.2.18)$$

but by definition:

$$\bar{P} = \tfrac{1}{2}\left|I_z(o)\right|^2 R_{rad} \qquad (2.4.23)$$

where R_{rad} was the radiation resistance which was hence given as:

$$R_{rad} = \frac{\zeta_o}{4\pi^2} \int_0^{2\pi} \int_0^{\pi} \sin^2\eta(i_x^2 + i_z^2)\sin\theta d\theta d\phi \qquad (3.2.19)$$

with

$$i_x = \frac{kJ_x}{2I_z(o)} \qquad (3.2.20)$$

and

$$i_z = \frac{kJ_z}{2I_z(o)} \qquad (3.2.21)$$

(3.2.19) was simplified, so that

$$R_{rad} = \frac{30}{\pi} \int_0^{2\pi} \int_0^{\pi} \sin^2\eta(i_x^2 + i_z^2)\sin\theta d\theta d\phi \qquad (3.2.22)$$

The double integration required for the evaluation of the ⅂-shaped dipole had to be performed without the simplification of circular symmetry and was hence programmed for numerical integration - by computer, using Simpson's rule. The programme was run several times with different numbers of integration intervals so that the convergence was checked and a sufficient number of integration points used. The results obtained are shown graphically in Figure 3.2.2..

The total length of the dipole was maintained resonant so that the case of zero half height corresponded to an x-directed half-wave dipole. When the half-height was quarter of a wavelength a z-directed half-wave dipole resulted. For both these geometries a radiation resistance of 73.1 ohms was obtained as expected. All intermediate values of half-height, corresponded to a ⅂-shaped dipole for which lower values of radiation resistance were obtained.

As numerical values for the radiation resistance of the bent dipole had been obtained, so could theoretical values of the conductance

of a ⅂-shaped slot. These were then investigated experimentally.

3.3. Experimental Investigation of the ⅂-Shaped Slot

The derivation of the radiation resistance of the ⅂-shaped dipole assumed filamentary current elements. For such a structure the lengths of the different sections were well defined. A physical slot had to be of finite width with rounded corners and there were several ways in which its lengths could be defined. The investigation of the straight slots had shown that if circular ends were treated as square ends at the position of the circle centres then the correct electrical length resulted. This influenced the choice of reference planes at the slot ends as shown in Figure 3.1.1. The figure also shows the reference planes which were suggested to divide the right angle bends of the slot. These planes though arbitrary had some logical foundation. The centre arm of the slot was responsible for most radiation and it was sensible to terminate this arm where the major impedance change occurred. Some allowance then had to be made for the corner region and this was included into the end arms by defining their length to the centre of the main arm as shown. These reference planes did not change when later a second arm was added at each end of the slot to make it I-shaped. The electrical length of the slot was first investigated experimentally.

A ⅂-shaped slot was milled in one of the plates of the special size waveguide jig using a one sixteenth inch diameter tool. The attenuation past the slot, radiating over a ground plane was measured over the band from 5.25 to 6.25 GHz. The frequency of peak attenuation past the slot was found to be 5.788 GHz. At this frequency the length of the slot defined using the reference planes shown in Fig. 3.1.1. was 0.496 wavelengths. The choice of reference planes appeared to be

justified.

In deriving the slot conductance, the slot field was assumed to be sinusoidal. This assumption was then tested. In the direction normal to the ground plane the component of electric field produced by the centre arm was proportional to:

$$\int_0^h \cos ky\,dy \qquad (3.3.1)$$

and by the end arms to

$$\int_h^{\lambda/4} \cos kz \cdot dz \qquad (3.3.2)$$

The two principal polarisations were in the ratio of:

$$\sinh k \;:\; (1 - \sinh k) \qquad (3.3.3)$$

This ratio was determined experimentally by fitting a section of circular waveguide to the slot. This did not change the slot resonant frequency, and it should not have substantially changed the field within the slot. The circular waveguide was terminated in a circular to rectangular transition which also incorporated an attenuating vane. This had originally been designed by Flann Microwave Instruments Ltd. as part of a precision rotary attenuator. In this manner the two orthogonal components of the electric field within the circular waveguide were terminated in matched loads but could be separately measured.

At the frequency of peak attenuation past the slot, the ratio of the polarisations was measured to be 3.57 dB, using the Weinschel Engineering radio frequency ratiometer described more fully

later. This value was compared to the theoretical value of 3.69 dB obtained using the specified reference planes. Reasonable agreement has been obtained indicating that the original assumption of a sinusoidal field distribution along the slot was substantially correct. The value of conductance derived using this distribution was then expected to be of similar accuracy. This was in fact so, as the theoretical value was 0.98 and the experimental value 0.85 determined from the measurement of peak attenuation past the slot.

The properties of the ⅂-shaped slot seemed well behaved. This view was reinforced by some early measurements of slot loss at X-band, which showed the slot to be substantially loss-free. These measurements are not reported here as they were repeated and more fully investigated at C-band. The C-band results appear in the next chapter. The results from the ⅂-shaped slot indicated that it could be used as an array element but at resonance only one value of conductance was available. Some method was required to vary the resonant conductance of the ⅂-shaped slot and retain its low loss behaviour. The first geometries investigated were ↿ and Z-shaped slots formed by rotating either the end arms or the central limb of the ⅂-shaped slot.

3.4. The ↿ and Z Shaped Slots

When the end arms of the ⅂-shaped slot were rotated the ↿-shaped slot was formed. The end arms of this slot intercepted less wall current and its coupling to the waveguide was likely to be reduced. Similarly, the centre arm could have been reorientated to form the Z-shaped slot in which the centre arm was excited in opposition to the end arms.

Distorting the straight slot to produce the ⅂-shaped slot did not

substantially change the sinusoidal distribution along its length. Further distortion to produce either the ↿ or Z shaped slot was unlikely to produce a major change in this distribution.

Both slots were divided into three sections in a manner similar to the ⅂-shaped slot, as indicated in Figure 3.4.1. and Figure 3.4.2.. The centre section of the ↿ shaped slot behaved in a similar manner to that of the ⅂-shaped slot, in that the slot electric field and waveguide magnetic field were parallel and not coupled. The coupling of the ↿-shaped slot to the waveguide was by the end arms and was analysed using a modified coordinate system x, y', z' as was used for the straight inclined slot in the narrow wall of the waveguide.

For one end section:

$$\bar{E}_1 = E_{1y'} = \frac{V}{d} \cos k \left\{ z' + h(1 + \sin \psi) \right\} \qquad (3.4.1)$$

and in the modified coordinates

$$H_{2z'} = \frac{\pi \cos \psi}{jw\mu a} \exp(- j\gamma z' \cos \psi) \qquad (3.4.2)$$

and as before from equation (2.3.7)

$$A = \frac{w\mu}{\gamma S_c} \int_{slot} \hat{n} \cdot (\bar{E}_1 \wedge \bar{H}_2) \, dS$$

so that for one end arm:

$$A_1 = \frac{\pi V \cos \psi}{ja\gamma S_c} \int_{-h\sin\psi}^{-h\sin\psi + (\lambda/4 - h)} \cos k \left\{ z' + h(1 + \sin \psi) \right\} e^{-j\gamma z' \cos\psi} \, dz'$$

(3.4.3)

FIGURE 3.4.1. The geometry of the λ-shaped slot.

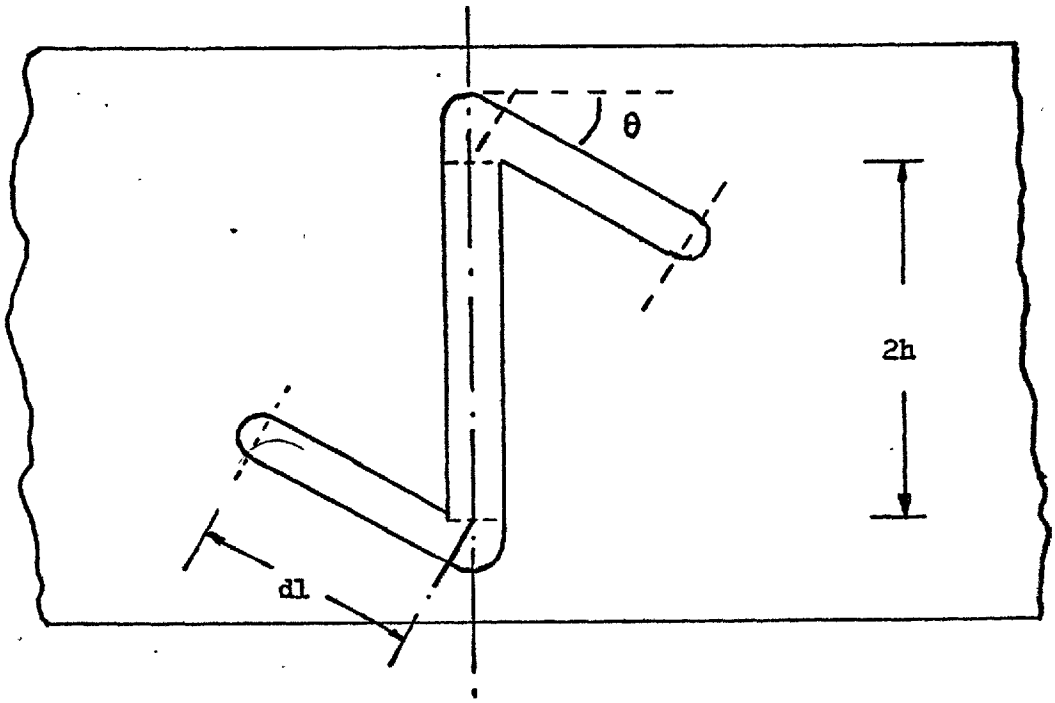

FIGURE 3.4.2. The geometry of the Z-shaped slot.

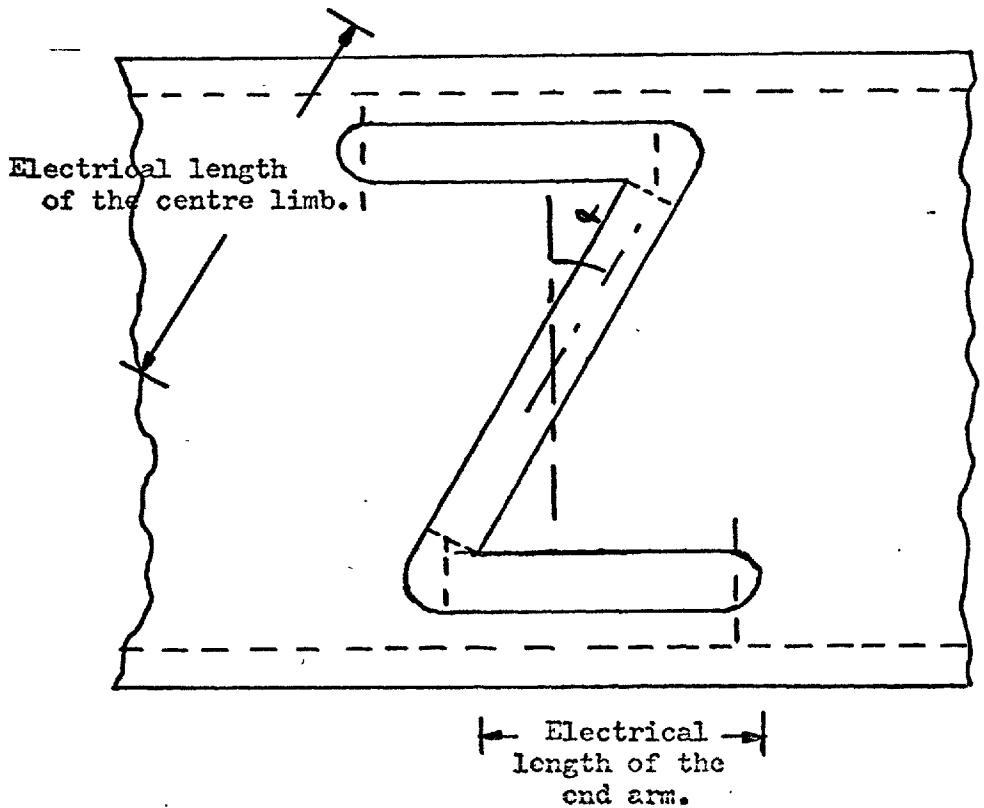

The simplifying substitution:

$$u = z' + h(1 + \sin\psi) \tag{3.4.4}$$

was made so that the integral became:

$$A_1 = \frac{\pi V \cos\psi}{ja\gamma S_c} \exp[j\gamma h(1 + \sin\psi)] \int_h^{\lambda/4} \cos ku \exp(-j\gamma u \cos\psi)\,du \tag{3.4.5}$$

which evaluated to give:

$$A_1 = \frac{\pi V \cos\psi}{ja\gamma S_c(k^2 - \gamma^2\cos^2\psi)} \left\{ k \exp[j\gamma\cos\psi \left\{h(1 + \sin\psi) - \lambda/4\right\}] \right.$$

$$\left. - (k \sin hk - j\gamma \cos\psi \cos hk) \cdot \exp(j\gamma h \cos\psi \sin\psi) \right\} \tag{3.4.6}$$

Similarly for the other end section:

$$\bar{E}_1 = E_{1y'} = \frac{V}{d} \cos k \left\{ z' - h(1 + \sin\psi) \right\} \tag{3.4.7}$$

and a similar integral was formed which was simplified by the substitution:

$$u = z' - h(1 + \sin\psi) \tag{3.4.8}$$

and evaluated to give:

$$A_2 = \frac{\pi V \cos\psi}{ja\gamma S_c(k^2 - \gamma^2\cos^2\psi)} \left\{ k \exp[-j\gamma\cos\psi \left\{h(1 + \sin\psi) - \lambda/4\right\}] \right.$$

$$\left. - (k \sin hk + j\gamma \cos\psi \cos hk) \cdot \exp(-j\gamma h \cos\psi \sin\psi) \right\} \tag{3.4.9}$$

Summing (3.4.6) and (3.4.9) gave the total value of A from which:

$$\frac{A}{V} = \frac{2\pi \cos\psi}{ja\gamma S_c(k^2 - \gamma^2\cos^2\psi)} \left\{k\cos\nu - k\sin hk\cos\xi - \gamma\cos\psi\cos hk\sin\xi\right\} \tag{3.4.10}$$

where

$$\nu = \gamma\cos\psi[h(1 + \sin\psi) - \lambda/4] \tag{3.4.11}$$

and

$$\xi = \gamma h\cos\psi\sin\psi \tag{3.4.12}$$

When ψ was set to zero the expression became that derived for the L-shaped slot (3.1.10).

It could also be shown that:

$$B = A \tag{3.4.13}$$

so that the equivalent circuit of the slot was a shunt conductance specified from (2.5.7) as:

$$g = \frac{120\pi\lambda\lambda_g\cos^2\psi\epsilon^2}{R_{rad}a^3b(k^2 - \gamma^2\cos^2\theta)^2} \tag{3.4.14}$$

where

$$\epsilon = k\cos\gamma - k\sin hk\cos\xi - \gamma\cos\theta\cos hk\sin\xi \tag{3.4.15}$$

and R_{rad} was in this case the radiation resistance of the equivalent L-shaped dipole.

The Z-shaped slot was analysed in a similar manner but the coupling to the waveguide by the centre limb had to be included. For this limb the modified coordinate system x, y', z' was used so that:

$$\bar{E}_1 = E_{1y'} = \frac{V}{d} \cos kz' \tag{3.4.16}$$

and the contribution to A was

$$A_C = \frac{\pi V}{ja\gamma S_C} \int_{+h}^{-h} \cos kz' \, e^{-j\gamma z'} \cos\beta \, dz' \tag{3.4.17}$$

which reduced to:

$$A_C = \frac{2\pi V \cos\beta}{ja\gamma S_C(k^2 - \gamma^2\cos^2\beta)} \left\{ \gamma \cos\beta \cos hk \sin(h\gamma\cos\beta) - k \sin hk \cos(h\gamma\cos\beta) \right\} \tag{3.4.18}$$

The original x, y, z coordinates were used to evaluate the contribution from the end arms. For one arm:

$$\bar{E}_1 = E_{1y} = \frac{V}{d} \cos k[z + h(1 + \sin\beta)] \tag{3.4.19}$$

so that:

$$A_1 = \frac{\pi V}{ja\gamma S_C} \int_{-h\sin\beta}^{\lambda/4 - h(1+\sin\beta)} \cos k[z + h(1 + \sin\beta)] e^{-j\gamma z} \, dz \tag{3.4.20}$$

The integration was facilitated by the substitution:

$$u = z + h(1 + \sin\beta) \tag{3.4.21}$$

and gave:

$$A_1 = \frac{\pi V}{ja\gamma S_c(k^2 - \gamma^2)} \left\{ k \exp[- j\gamma \{ \lambda/4 - h(1 + \sin\beta] \} \right]$$

$$+ (j\gamma \cos hk - k \sin hk)\exp(j\gamma h \sin\beta) \Big\} \qquad (3.4.22)$$

A similar result was obtained for the bottom section so that when all the contributions were summed the result was:

$$\frac{A}{V} = \frac{2\pi}{ja\gamma S_c} \left\{ M.P + N.R \right\} \qquad (3.4.23)$$

where

$$M = \frac{\sin\beta}{k^2 - \gamma^2 \sin^2\beta} \qquad (3.4.24)$$

$$N = \frac{1}{k^2 - \gamma^2} \qquad (3.2.25)$$

$$P = \gamma \sin\beta \cos hk \sin(h\gamma \sin\beta) - k \sin hk \cos(h\gamma \sin\beta) \qquad (3.4.26)$$

$$R = k \cos \left\{ \gamma[\lambda/4 - h(1 + \sin\beta)] \right\} - k \sin hk \cos(h\gamma \sin\beta)$$

$$- \gamma \cos hk \sin(h\gamma \sin\beta) \qquad (3.4.27)$$

As with other similar slots A and B could be shown to be of the same sign so that the equivalent circuit of the Z-slot was a conductance of value:

$$g = \frac{120\pi\lambda\lambda_g}{R_{rad} a^3 \beta} \left\{ M.P + N.R \right\}^2$$

R_{rad} was again the radiation resistance of a ⅂-shaped dipole.

3.5. The ⅂-shaped Dipoles Radiation Resistance

The radiation resistance of the ⅂-shaped dipole was found by evaluating the total radiated power, after fitting a sinusoidal current distribution along its length, in a manner similar to that used for other geometries. The contribution from the centre section was identical to that for the ⅂-shaped dipole, but different terms emerged for the end sections. The current in one end section was given by:

$$I_z(o)\ \cos k[x' + h(1 + \sin\beta)] \qquad (3.5.1)$$

where the geometry was defined by figure 3.5.1., and produced a component of the current integral:

$$x' \int_{-h\sin\beta}^{-h\sin\beta + (\lambda/4 - h)} I_z(o)\ \cos k[x' + h(1 + \sin\beta)] \cdot \exp\ \Big\{ jk[h\cos\theta + \cos\phi\sin(\theta - \beta)(x' + h\sin\beta)] \Big\} dx' \qquad (3.5.2)$$

This complicated expression was simplified using the substitutions:

$$u = x' + h(1 + \sin\beta) \qquad (3.5.3)$$

$$w = hk[\cos\theta - \cos\phi\sin(\theta - \beta)] \qquad (3.5.4)$$

and

$$e = \cos\phi\sin(\theta - \beta) \qquad (3.5.5)$$

FIGURE 3.5.1. The geometry of the ⅂-shaped dipole.

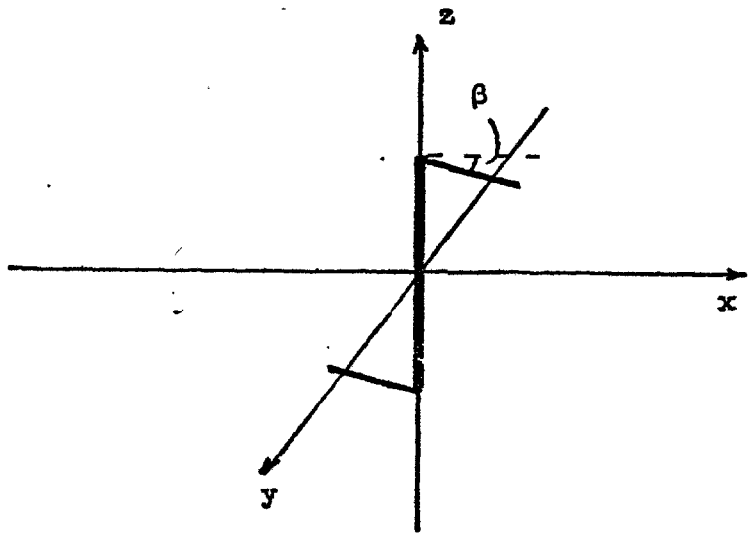

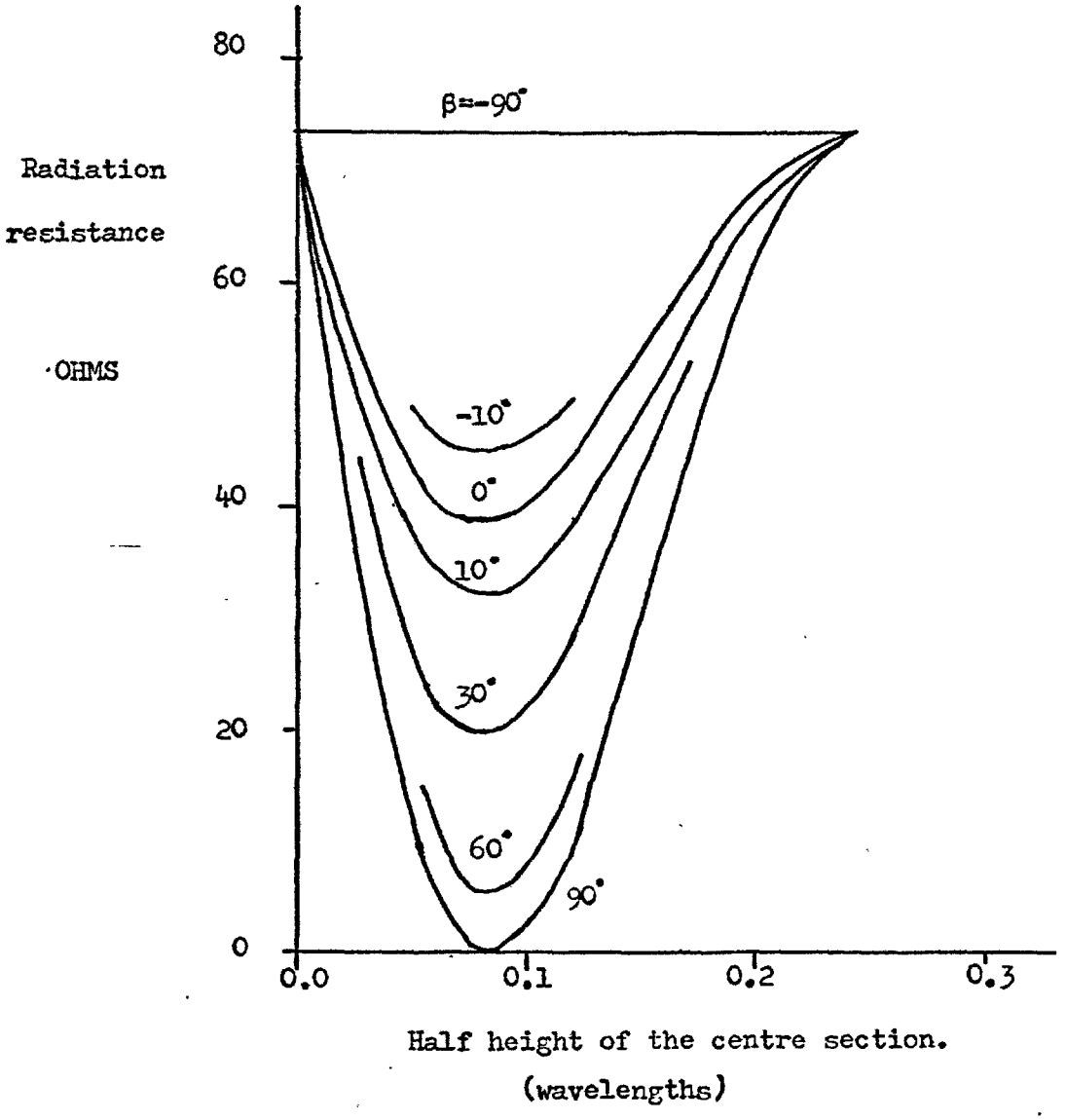

FIGURE 3.5.2. The computed results for the radiation resistance of the ⅂-shaped dipole.

so that it became:

$$x' I_z(o)\exp(jw) \int_h^{\lambda/4} \cos ku \exp(jk\epsilon u)\,du) \qquad (3.5.6)$$

This expression was similar to equation (3.2.9) with v and w replaced respectively by α and ϵ, and was evaluated in a like manner to give:

$$\frac{x' I\ (o)}{k(1 - \epsilon^2)} \left\{\exp j(w + \frac{\epsilon\pi}{2}) - \exp[j(w + \epsilon hk)](j\epsilon \cos hk + \sin hk)\right\} \qquad (3.5.7)$$

A comparable expression was obtained for the other end section so that the total x' directed contribution to the current integral was:

$$J_{x'} = \frac{2I_2(o)}{k(1 - \epsilon^2)} \left\{\cos(w + \frac{\epsilon\pi}{2}) - \sin hk \cos(w + hk\epsilon) + \epsilon \cos hk \cdot \sin(w + hk\epsilon)\right\} \qquad (3.5.8)$$

The components of the current integral vector were then expressed in orthogonal coordinates such that:

$$J_x = J_{x'} \cos\beta \qquad (3.5.9)$$

and

$$J_z = J_z - J_{x'} \sin\beta \qquad (3.5.10)$$

The radiation resistance was then obtained as

$$\text{Rad} = \frac{30}{\pi} \int_0^{2\pi} \int_0^{\pi} \sin^2\eta (i_x^2 + i_z^2) \sin\theta\, d\phi\, d\theta \qquad (3.5.11)$$

where

$$i_x = \frac{k J_x}{2 I_2(o)} \qquad (3.5.12)$$

and

$$i_z = \frac{k J_z}{2 I_2(o)} \qquad (3.5.13)$$

Equation (3.5.11) was similar to equation (3.2.19) and so was enumerated using the same numerical integration routine. The results for the radiation resistance of a ⅂-shaped dipole are shown in Figure 3.5.2.. The case when $\beta = -90^{o}$ corresponded to a straight half wave dipole and a value of 73.1 ohms was obtained. The radiated power decreased as the dipole was distorted and for a particular half height of the centre section with the end arms folded right back the radiation resistance was negligible. For a fixed dipole half height the radiation resistance was lowered the more bent it became. For the complementary slot this implied that the coupling to space was increased as the end arms were folded back. However the end arms were folded back to decrease the waveguide to slot coupling and hopefully reduce the waveguide to space coupling reducing the slot conductance. Folding the end arms back in fact increases the slot to space coupling but reduces the slot to waveguide coupling. As similar sinusoidal functions were used in the analysis of both component couplings it is unlikely that a major variation in slot conductance could be obtained.

3.6. Experimental Investigation of ⅂ and Z Shaped Slots

The experimental programme for these slots followed similar lines to that for the ⅂-shaped slot. Initially the choice of reference planes was investigated. They are shown in Figures 3.4.1. and 3.4.2., and were selected to be consistent with those of the ⅂-shaped slot.

The frequency of peak attenuation past series of slots of both types cut in plates of the special C band waveguide jig were determined. For the $\mathcal{L}$-shaped slots this presented certain difficulties as the resonant frequency was higher than the frequency at which more than one mode could exist in the waveguide 12. The measurements on this series of slots were made using coaxial components. The electrical lengths of the $\mathcal{L}$ and Z shaped slots at resonance are shown in Tables 3.6.1 and 3.6.2., using the defined reference planes. The lengths of the slots described in this manner appeared to be sensibly constant, justifying the choice of reference planes.

The polarisation angles of the slots were then investigated using the circular waveguide section already described. For the $\mathcal{L}$-shaped slots the measurements were unreliable, as the waveguide 12 measurement bench became overmoded, but are presented for completeness. Tables 3.6.3. and 3.6.4. show the experimental and theoretical values of the polarisation ratio obtained. Acceptable agreement was obtained for all the slots. The theoretical values supported by the measured data showed that the vertical polarisation was minimised using the Z-shaped slot rather than the $\mathcal{L}$-shaped slot. This was reasonable because for the Z-shaped slot, as the centre arm was rotated, it produced a rapidly increasing component of cross polarisation in opposition to that of the end arms. For the $\mathcal{L}$-shaped slot the cross polarisation fell comparatively slowly as the end arms were rotated.

The sinusoidal distribution fitted to the slots appeared to be correct, and as the derivation of slot conductance was based on this it was then expected to be similarly correct. This was in fact so and experimental results are compared to theoretical values in

TABLE 3.6.1. The electrical length of the ⅂-shaped slot.

β	Electrical slot length. (wavelengths)
10	0.473
20	0.482
30	0.489

TABLE 3.6.2. The electrical length of the Z-shaped slot.

β (degrees)	Electrical slot length (wavelengths)
-10	0.493
0	0.496
10	0.493
20	0.495
30	0.494

TABLE 3.6.3. The polarisation properties of ⅂-shaped slots coupling to circular waveguide.

α°	Ratio of main to cross polarisation db	
	Theoretical	Measured
0	5.55	5.62
10	5.15	4.59
20	4.90	3.98
30	4.95	5.31

TABLE 3.6.4. The polarisation properties of Z-shaped slots coupling to circular waveguide.

α°	Ratio of main to cross polarisation db	
	Theoretical	Measured
-10	1.27	1.51
0	3.69	3.57
10	6.44	5.52
20	9.26	8.80
30	12.50	9.34

TABLE 3.6.5. The conductance results for ⅂-shaped slots.

Angle θ (degrees)	Conductance	
	Theoretical	Measured
10	0.42	0.44
20	0.35	0.37
30	0.35	0.35

TABLE 3.6.6. The conductance results for Z-shaped slots.

Angle θ (degrees)	Conductance	
	Theoretical	Measured
-10	1.33	1.29
0	0.85	0.85
10	0.48	0.53
20	0.28	0.34
30	0.15	0.19

FIGURE 3.6.1. The geometry of a folded slot.

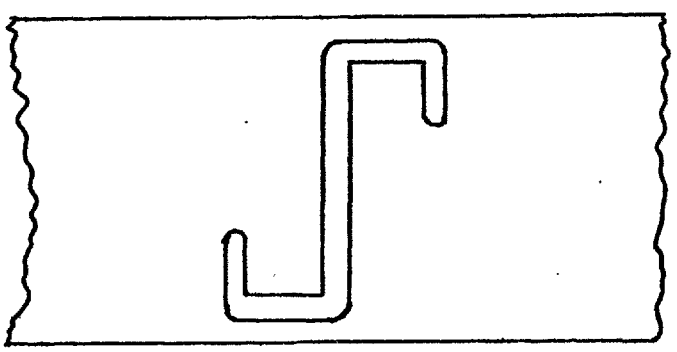

Tables 3.6.5. and 3.6.6..

The variation of the slot conductance was smaller than might have been originally expected. The coupling to the waveguide was decreased, but the radiation resistance varied in a similar but inverse manner. The functions used to calculate the coupling to the waveguide and the dipole radiation resistance were the same. The differences between the final results arose due to the different manners in which the functions were integrated and could be thought of as second order.

It appeared that to obtain a slot geometry with a wide range of conductances it was essential that either the coupling to the waveguide or the radiation conductance remained constant while the other varied widely. The ↿ and Z-shaped slots could not meet this requirement, neither could other possible slot geometries such as the folded slot shown in Figure 3.6.1.. The changes in the slot geometry required to produce changes in the coupling to the waveguide also changed the radiation resistance of the equivalent dipole. Consideration was then given to loaded ⅂-shaped slots in which the width or impedance of the slot was changed along its length. This changed the length of the end arms but the geometry of the slot stayed substantially constant as far as radiation was concerned.

3.7. The Loaded ⅂-shaped Slot

The geometry of this type of slot is shown in Figure 3.7.1. The slot width was different for the centre and end sections. The change in width was associated with a change in the characteristic impedance of the slot line short circuited at each end to form the slot. It was thought that to maintain the slot at resonance the lengths of the end

FIGURE 3.7.1. The geometry of the impedance loaded ⅂-slot.

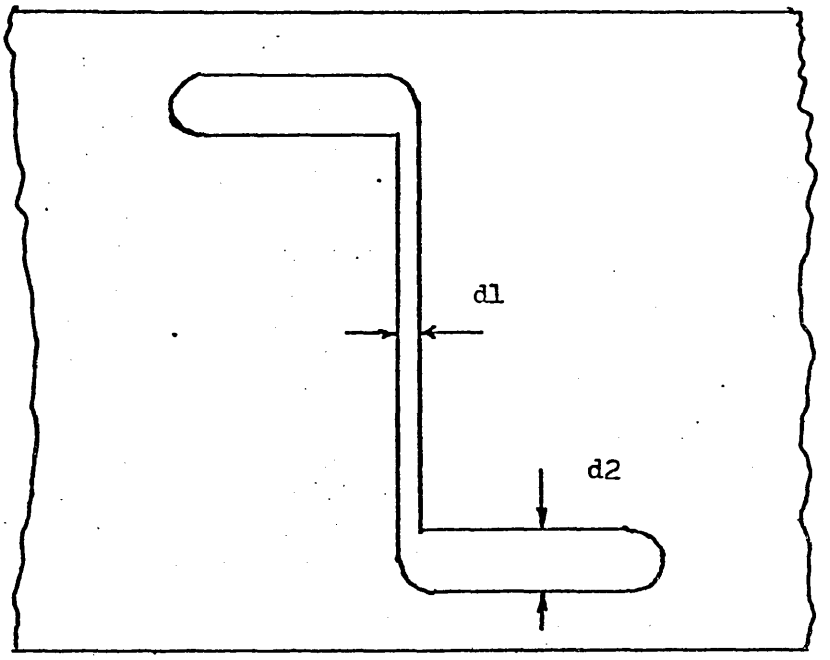

FIGURE 3.7.2. The equivalent circuit of the impedance loaded ⅂-slot.

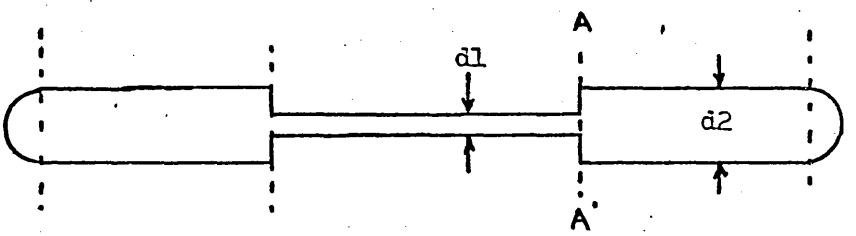

TABLE 3.7.1. The principal properties of loaded ⅂-slots coupling to waveguide 12.

d1 / d2	Frequency of peak coupling GHZ.	Peak coupled power db
0.50	5.696	4.34
0.75	5.806	3.52
1.00	5.854	3.52
1.33	5.902	3.53
2.00	5.956	3.69
3.12	5.904	3.71

arms would have to be changed and the amount of wall current intercepted would be different. Most of the radiation was from the centre limb and its distribution was unchanged while that from the end arms was maintained at the same angle. It was thus hoped that the coupling of the slot to the waveguide would change but that the radiation resistance of the equivalent dipole would be sensibly constant producing a variation in the slot conductance.

The investigation of the voltage distribution along the uniform ⅂-shaped slot indicated that the discontinuities produced at the corners were unimportant. The distribution along the loaded ⅂-slot was considered as if the corners were not present, so that the slot was straightened out as shown in Figure 3.7.2.. At the plane AA' the impedance looking towards the short was:

$$Z_b \tan \beta \ell_b \qquad (3.7.1)$$

but if the slot had been uniform it would have been:

$$Z_a \tan \beta(\lambda/4 - \ell_a) \qquad (3.7.2)$$

As the slots were both resonant the effective impedances were equal or:

$$Z_b \tan \beta \ell_b = Z_a \tan \beta(\lambda/4 - \ell_a)$$

so that:

$$\frac{Z_a}{Z_b} = \frac{\tan \beta \ell_b}{\tan \beta(\lambda/4 - \ell_a)} \qquad (3.7.3)$$

From the dimensions of a resonant loaded ⅂-slot it was possible to obtain

TABLE 3.7.2. The impedance results for ⅂-shaped slots.

Slot No.	d_1/d_2	$\sqrt{d_1/d_2}$	Z_o/Z_o'
1	0.32	0.57	0.53
2	0.50	0.71	0.66
3	0.75	0.86	0.82
4	1.00	1.00	0.99
5	1.33	1.15	1.22
6	2.00	1.41	1.48
7	3.12	1.76	1.98

the ratios of the impedances of the different sections of slot lines forming the slot.

A set of six plates for the special size waveguide jig were slotted with loaded ⅂-shaped slots. The ratio of the slot widths varied from 0.50 to 3.12. A thorough experimental investigation of these slots was mounted in a similar manner to that of previous slots. The important results are shown in Table 3.7.1.. They indicated that although the impedance loading substantially modified the lengths of the end arms, the slot conductance remained almost unchanged. The original object of impedance loading had been defeated but from the geometries an interesting relationship concerning the slot line impedances emerged. Table 3.7.2. lists the ratios of the slot line impedances and the square root of their relative widths from which it emerged that:

$$Z_{\text{slot line}} \propto \sqrt{\text{slot width}} \qquad (3.7.4)$$

It was a well known result that the impedance of a transmission line was given by:

$$Z_o = \sqrt{\frac{R + jwL}{G + jwC}} \qquad (3.7.5)$$

which in the high frequency limit became:

$$Z_o = \sqrt{\frac{L}{C}} \qquad (3.7.6)$$

so that for the slot line considered:

$$\frac{L}{C} \propto \text{Slot width} \qquad (3.7.7)$$

3.8. The I-Shaped Slot

The variations of the Z-shaped slot thus far investigated did not produce the desired range of conductances. In all cases the variation in the coupling to the waveguide did not vary sufficiently and was counteracted by a change in the radiation resistance of the equivalent dipole. This stimulated thought about terminating the centre arm of the slot not in one end arm, but by two arms in opposite directions. These end arms would excite the centre section in opposition and the ratio of their lengths could control the slot coupling. It was also postulated that the radiation resistances of dipoles top loaded with either one or two branch would be similar, so that a range of slot conductances would result.

The geometry of the slot is shown in Figure 3.8.1. and it was analysed in five sections as indicated. The reference planes at the branch arm junctions were picked so that the branch arms were symmetrically placed relative to the centre arm which was terminated at its impedance discontinuities. A sinusoidal voltage distribution was again fitted along the slot. For the centre section:

$$\bar{E}_1 = E_{1z} = \frac{V}{d} \cos ky \qquad (3.8.1)$$

and did not contribute to the coupling to the waveguide. At each junction, the two branch arms were in series and they had normalised input impedances given by:

$$\tan kd_1 \qquad \text{and} \qquad \tan kd_2 \qquad (3.8.2)$$

so that the normalised input impedance to the two branch arms was:

$$\tan kd_1 + \tan kd_2 \qquad (3.8.3)$$

FIGURE 3.8.1. The geometry of an I-shaped slot.

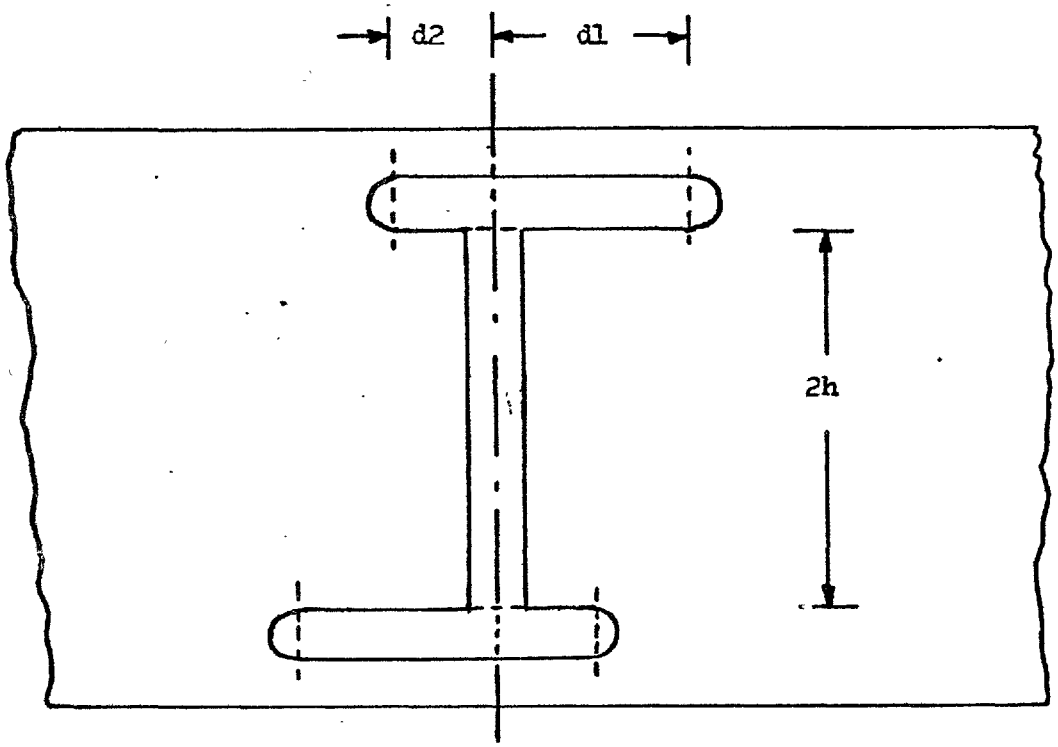

FIGURE 3.8.2. The radiation resistance of various dipoles.

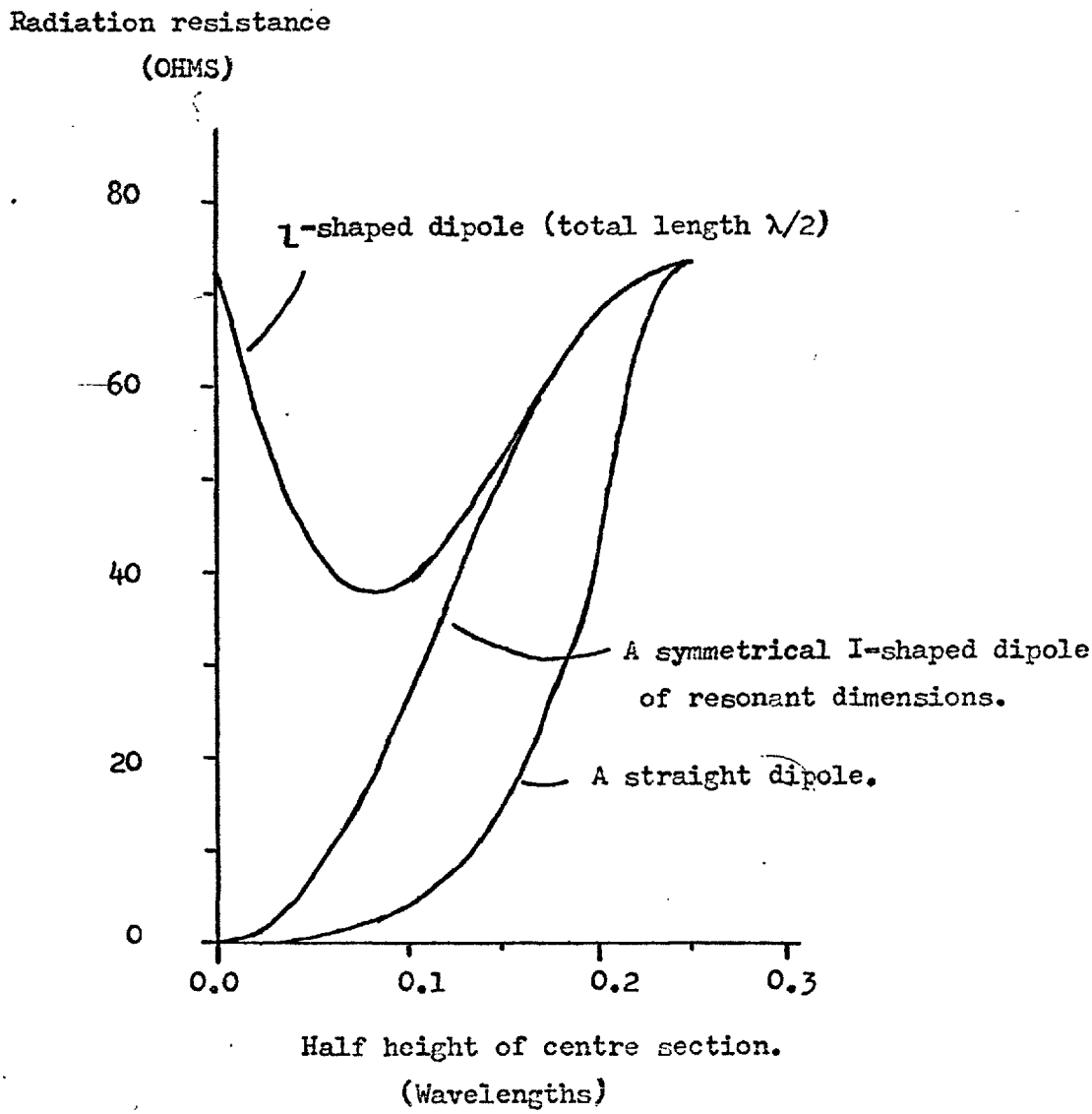

For an unbranched slot the normalised impedance at this point would have been:

$$\tan k(\lambda/4 - h) \tag{3.8.4}$$

from which it followed that:

$$\tan kd_1 + \tan kd_2 = \tan k(\lambda/4 - h) \tag{3.8.5}$$

and the resonant dimensions of the I slot have been defined.

The normalised input voltages to the branch arms were then:

$$\frac{\tan kd_1 \cos kh}{(\tan kd_1 + \tan kd_2)} \tag{3.8.6}$$

and:

$$\frac{\tan kd_2 \cos kh}{(\tan kd_1 + \tan kd_2)} \tag{3.8.7}$$

The voltages along the branch arms decayed sinusoidally to zero at their ends which corresponded to a variation of the form:

$$\cos k(\lambda/4 - d_1 + z) \tag{3.8.8}$$

The variation of voltage along the branch arm and the normalised input voltage were known so that they could be combined through an additional normalisation of the form $\cos k(\lambda/4 - d_1)$ to give the fields along the various branch arms as:

Arm 1:

$$E_{1y'} = \frac{V}{d} \frac{\tan kd_1 \cos kh \cos k(z + \lambda/4 - d_1)}{(\tan kd_1 + \tan kd_2)\cos k(\lambda/4 - d_1)} \tag{3.8.9}$$

Arm 2:

$$E_{1y2} = \frac{V}{d} \cdot \frac{\tan kd_2 \cos kh \cos k(z + \lambda/4 - d_2)}{(\tan kd_1 + \tan kd_2)\cos k(\lambda/4 - d_2)} \qquad (3.8.10)$$

Arm 3:

$$E_{1y3} = \frac{V}{d} \cdot \frac{\tan kd_1 \cos kh \cos k(\lambda/4 - d_1 - z)}{(\tan kd_1 + \tan kd_2)\cos k(\lambda/4 - d_1)} \qquad (3.8.11)$$

Arm 4:

$$E_{1y4} = \frac{V}{d} \cdot \frac{\tan kd_2 \cos kh \cos k(\lambda/4 - d_2 - z)}{(\tan kd_1 + \tan kd_2)\cos k(\lambda/4 - d_2)} \qquad (3.8.12)$$

These expressions were simplified using equation (3.8.5) and the properties of trignometric functions.

The centre section of the slot as with the ℸ-shaped slot did not contribute to the coupling integral, but there were still four components to be evaluated. For all these parts:

$$\bar{H}_2 = H_{2z} = \frac{\pi}{jw\mu a} e^{-j\gamma z} \qquad (3.8.13)$$

and the contribution to A from branch arm 1 was:

$$A_1 = -\frac{\pi V}{ja^2 b\gamma} \frac{\sin kh}{\cos kd_1} \int_0^{d_1} \cos k(\lambda/4 - d_1 + z) e^{-j\gamma z} dz \qquad (3.8.14)$$

which reduced to:

$$A_1 = -\frac{\pi V}{ja^2 b\gamma} \frac{\sin kh}{\cos kd_1} \frac{1}{(k^2 - \gamma^2)} \left\{ ke^{-j\gamma d_1} + j\gamma \cos k(\lambda/4 - d_1) - k \sin k(\lambda/4 - d_1) \right\} \qquad (3.8.15)$$

The integrals for the other three branch arms were evaluated in a like manner. The contributions from the long and short arms were initially summed separately so that:

$$A_1 + A_3 = - \frac{2\pi Vk}{ja^2 b\gamma} \frac{\sin kh}{(k^2 - \gamma^2)} \left\{ \frac{\cos \gamma d_1}{\cos kd_1} - 1 \right\} \qquad (3.8.16)$$

and

$$A_2 + A_4 = - \frac{2\pi Vk}{ja^2 b\gamma} \frac{\sin kh}{(k^2 - \gamma^2)} \left\{ \frac{\cos \gamma d_2}{\cos kd_2} - 1 \right\} \qquad (3.8.17)$$

It then followed that:

$$\frac{A}{V} = - \frac{2\pi k \sin kh}{ja^2 b\gamma(k^2 - \gamma^2)} \left\{ \frac{\cos \gamma d_1}{\cos kd_1} - \frac{\cos \gamma d_2}{\cos kd_2} \right\} \qquad (3.8.18)$$

It could also be shown that:

$$A = B \qquad (3.8.19)$$

so that from equation (2.5.7), the equivalent circuit was a shunt conductance of normalised value:

$$g = \frac{480\, a\lambda_g \sin^2 kh}{R_{rad} \pi b \lambda} \left\{ \frac{\cos \gamma d_1}{\cos kd_1} - \frac{\cos \gamma d_2}{\cos kd_2} \right\}^2 \qquad (3.8.20)$$

where R_{rad} was the radiation resistance of an I-shaped dipole.

If d_2 was set equal to zero in equation (3.8.20) the equation (3.1.12) was recovered corresponding to the result for the ⅂-shaped slot. Similarly when the length of the two branch arms were equal i.e., $d_1 = d_2$, then the conductance was zero, which showed that a complete

range of slot conductances would be produced by the I-slot providing its radiation conductance stayed reasonably constant.

The derivation of the radiation resistance of the I-shaped dipole was similar to that of the Z-shaped dipole except that there were four contributions to the x directed current J_x, which could be shown to be given by:

$$J_x = \frac{2AI_z(o)}{k(1-\alpha^2)} \left\{ \cos(u - \alpha kd_1) - \cos(u - \alpha kd_2) - \cos u(\cos kd_1 - \cos kd_2) + \alpha \sin u(\sin kd_1 + \sin kd_2) \right\} \quad (3.8.21)$$

where

$$A = \frac{\cos kh}{\sin kd_1 + \sin kd_2} \quad (3.8.22)$$

$$u = hk\cos\theta \quad (3.8.23)$$

and

$$\alpha = \cos\phi \sin\theta \quad (3.8.24)$$

For a symmetrical I-dipole $d_1 = d_2$ so that (3.8.21) was simplified to:

$$J_x = \frac{2I_z(o)\ \alpha \sin u \cos kh}{k(1-\alpha^2)} \quad (3.8.25)$$

If the centre section of the dipole tended to zero height, u went to zero with J_x; J_z was also zero so that the radiation resistance of a symmetrical I-dipole of zero height was also zero.

Equation (3.8.21) was incorporated into the numerical integration routine previously used to evaluate radiation resistance, subject to

the constraint of equation (3.8.5) to maintain resonant dimensions. The results obtained for the symmetrical I-dipole are shown in Figure 3.8.2., with the results for the ⅂-dipole and for completeness the straight dipole considered in Section 2.4.. The radiation resistances of the symmetrical I and straight dipoles of negligible height were, as expected, zero. This contrasted with the ⅂ shaped dipole of negligible height which became an x directed half wave dipole with a radiation resistance of 73.1 ohms. For half heights greater than zero the radiation resistance of the symmetrically top loaded dipole rose rapidly compared to that of the plain straight dipole. Similarly the radiation resistance of the ⅂-shaped dipole fell as it became more like a short top loaded antenna. For geometries with half heights in excess of a tenth of a wavelength, the effects of top loading with one, and then two, branch arms became similar and for half heights greater than 0.15λ the differences were negligible. This was important as it meant that provided the slot half height was sufficiently large the slot radiation conductance was unlikely to change with the coupling to the waveguide. It was then expected that the I-shaped slot would give a large range of values of conductance and its properties were then examined experimentally.

A series of twelve plates which fitted the special waveguide jig was used and I-shaped slots with the ends of various ratios were cut. These included a ⅂-shaped slot. The frequency of peak attenuation past each slot was found as it radiated above a ground plane, so that the original choice of reference planes could be examined. The equivalent electrical lengths of the slots were found at these frequencies from its physical dimensions. The results shown

in Table 3.8.1. indicated that the reference planes were appropriate as the slot length was well behaved.

The polarisation properties of the slots were then measured using the circular waveguide section as described earlier in this chapter. Theoretical values for the ratio of the main to the cross polarisation were also derived by integrating the voltage along each arm of the slot. Theoretical and experimental values were compared, as shown in Table 3.8.2.. It was found that a small amount of dispersion occurred between the frequencies of peak coupling to the major polarisations. This caused the polarisation angle of the slot to rotate around the resonant condition. It was not known at this point how the dispersion should be treated and the measured ratios of polarisation shown were in fact the ratios of the peak values. Reasonable agreement between theory and experiment was obtained for the first few slots but became progressively poorer for lower coupled slots. As the coupling was decreased by increasing the lengths of the shorter branch arms, the dispersion between the peak couplings to the two polarisations became larger. The vertical component corresponding to the branch arms descended to a coupling value of approximately - 26 dB and remained at that level. The horizontally polarised component progressively decreased as the branch arms were made more nearly equal until it reached the level of the cross polarisation at which point the whole slot resonance became ill defined. It was thought that a residual reactance could be associated with one polarisation which upset the slot resonance for small couplings. Highly coupled slots however, were generally well behaved with regard to their polarisation properties.

Experimental and theoretical values of the slot conductances

TABLE 3.8.1. The effective electrical length of I-shaped slots radiating in a ground plane.

Slot Coupling. (db)	Slot length. (wavelengths)
-5.8	0.5026
-8.9	0.5037
-10.9	0.5035
-12.4	0.5042
-14.1	0.5046
-14.8	0.5042
-16.5	0.5043
-17.6	0.5042

TABLE 3.8.2. The polarisation properties of I-shaped slots coupling to circular waveguide.

Length of the shorter branch arm. Inches.	Ratio of main to cross polarisation db	
	Theoretical	Measured.
0.000	3.69	3.57
0.100	6.73	7.00
0.150	11.27	11.70
0.160	12.97	12.39
0.170	14.8	13.4
0.175	15.9	13.2
0.180	16.6	13.5
0.185	19.3	14.1
0.190	21.5	13.0
0.195	24.2	9.3
0.200	29.6	1.6
0.205	46.7	-3.0

were obtained for the slots radiating over a ground plane. These are shown in Figure 3.8.3.. Good agreement was obtained for the highly coupled slots and reasonable agreement for the more lowly coupled slots, despite the poor cross-polarisation performance.

The I-shaped slot appeared to be a possible array element as its conductance could be readily controlled. Its cross polarisation performance was not as good as expected and at very low couplings the slot resonance was poorly defined. It appeared that some sort of cross-polarisation suppression grid would be required, possibly the slot would have to radiate into a parallel plate region and this was initially simulated by a waveguide 12 branch arm. The new slot parameters were as shown in Table 3.8.3.. The frequency of peak coup ling had been increased by 140 MHz and the cross polarisation suppressed. The slot resonance was now well preserved for couplings as low as - 35 dB. The I-shaped slot with some sort of cross polarisation suppression grid seemed to be an ideal array element as its coupling could be well controlled by changes in the relative lengths of its end arms.

For highly coupled I-slots radiating over a ground plane accurate theoretical values of conductance had been obtained. As a further check on these results it was decided to design three slots which would ordinarily have been highly coupled but to try to uncouple the slots by reorientating the centre limbs in opposition to the branch arms as shown in Figure 3.8.4.. When these slots were measured there was no discernible attenuation past the slots at the design frequency of, 5.70 GHz but two small peaks of attenuation 0.05 dB high were found 100 MHz either side of this frequency. The slots were successfully uncoupled further supporting the generally predictable behaviour of the

FIGURE 3.8.3. The variation of conductance of resonant I-shaped slots.

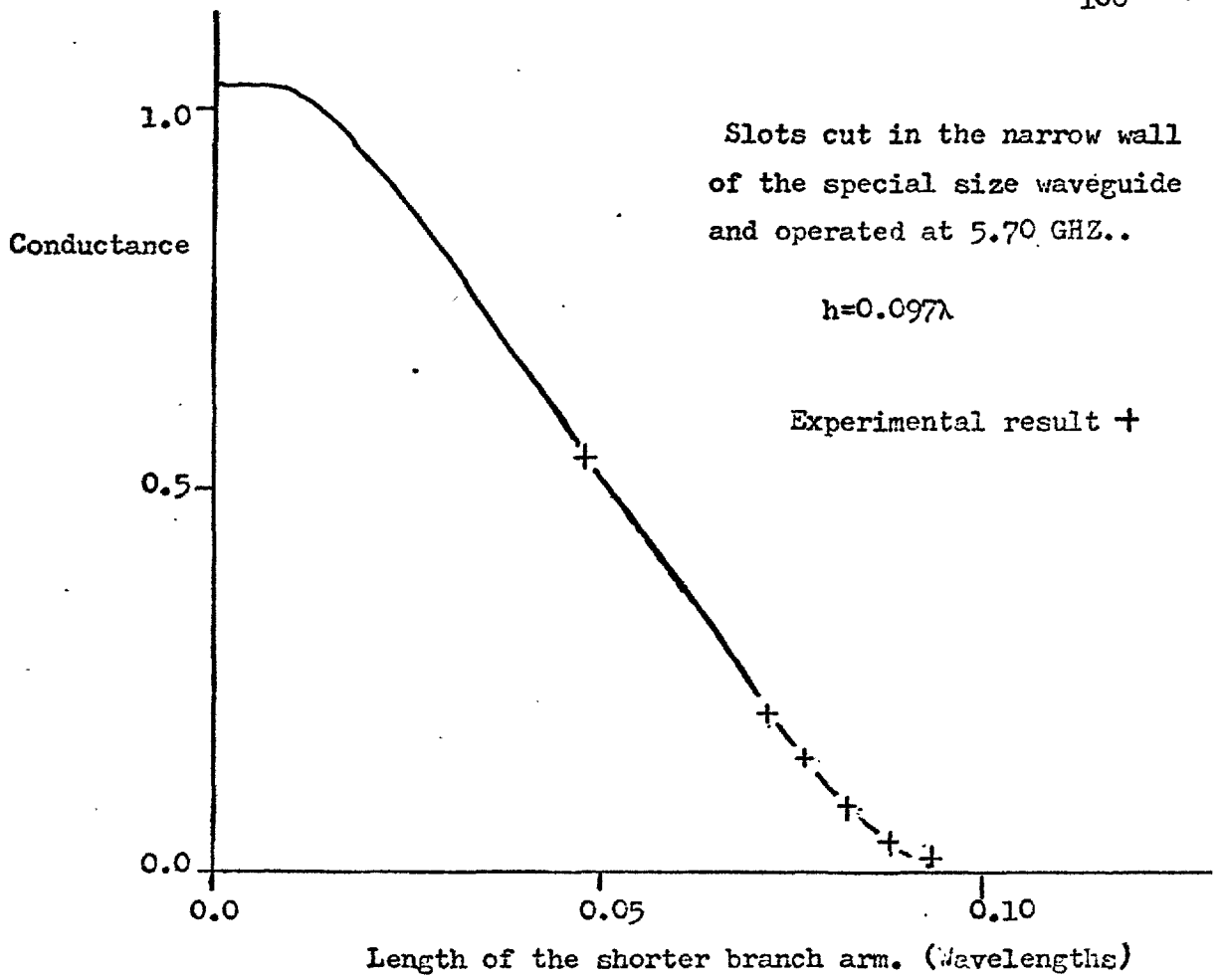

FIGURE 3.8.4. An uncoupled I-shaped slot.

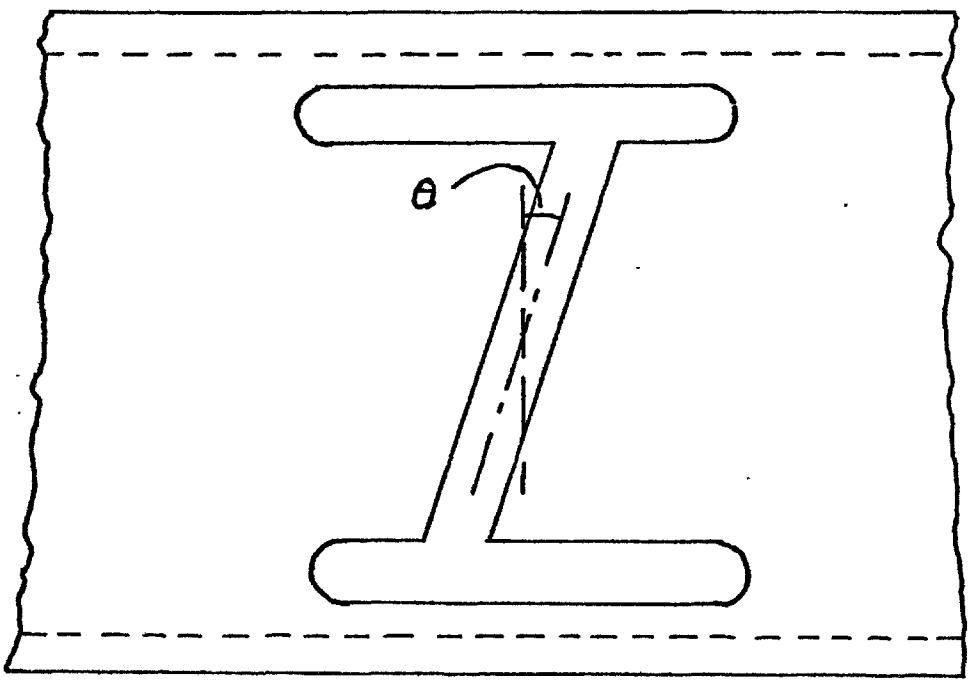

TABLE 3.8.3. The properties of I-shaped slots coupling to waveguide 12.

The length of the shorter branch arm. INCHES.	Frequency of peak coupled power. GHZ.	Peak coupled power db
0.000	5.902	3.99
0.100	5.860	4.78
0.150	5.868	8.01
0.160	5.856	9.46
0.170	5.868	11.0
0.175	5.888	12.8
0.180	5.866	13.4
0.185	5.852	14.2
0.190	5.868	17.5
0.195	5.872	19.7
0.200	5.874	26.7
0.205	5.860	35.1

I-shaped slots.

3.9. The Loaded I-Shaped Slot and the H-Shaped Slot

The last section indicated that the I-shaped slot appeared to be a useful array element. However, this slot, like the Z-shaped slot, could have been centre loaded by impedance changes to reduce its overall size. There would then have been few differences between centre loaded I-shaped slots and H-shaped slots of low coupling. The experimental results from both these types of slots are reported in this section. The loaded I-shaped slots were milled in plates which fitted the special C band waveguide jig and measurements were made with slots radiating and coupling to both rectangular and circular waveguide. The important results for this type of slot are summarised in Table 3.9.1.. It appeared that the slots were regularly behaved but it was noted that centre loading reduced their bandwidth.

The H-shaped slots (Figure 3.9.1.) measured were milled in an X band jig similar to the C band one, except standard waveguide 16 was used. The measurements were made on an X band bench which is further described in the following chapter and they are precised in Table 3.9.2.. The ratio of the slot line impedances was again found to be proportional to the square root of the slot width. The slots still appeared to be well behaved, although A.S.W.E. had reported the H-shaped slot to be lossy. The loss did not appear to upset the slot behaviour and thus had to be carefully investigated. The differences between the I-shaped slots and H shaped slots for low couplings were small and the H shaped slot had considerable loss associated with it. Before the I-shaped slot could be used as an array element its loss had to be shown to be small. If acceptable as an array element the

TABLE 3.9.1. The principal properties of centre loaded I-shaped slots.

(a) Coupling to waveguide 12.

Ratio of the widths of centre and end limbs.	Frequency of peak coupling. GHZ.	Peak coupled db
0.32	5.650	8.14
0.50	5.843	6.73
0.75	5.920	6.16

(b) Coupling to circular waveguide.

Ratio of the widths of centre and end limbs.	Frequency of peak coupling GHZ.	Peak coupled power main pol. db	Peak coupled power cross pol. db
0.32	5.594	6.64	17.52
0.50	5.724	5.92	16.41
0.75	5.832	5.50	12.96

(c) The polarisation properties coupling to circular waveguide.

Ratio of the widths of centre and end limbs.	Ratio of main to cross polarisation db	
	Theoretical	Measured
0.32	12.03	10.88
0.50	10.27	10.49
0.75	8.68	7.46

FIGURE 3.9.1. The equivalent circuit of an H-shaped slot.

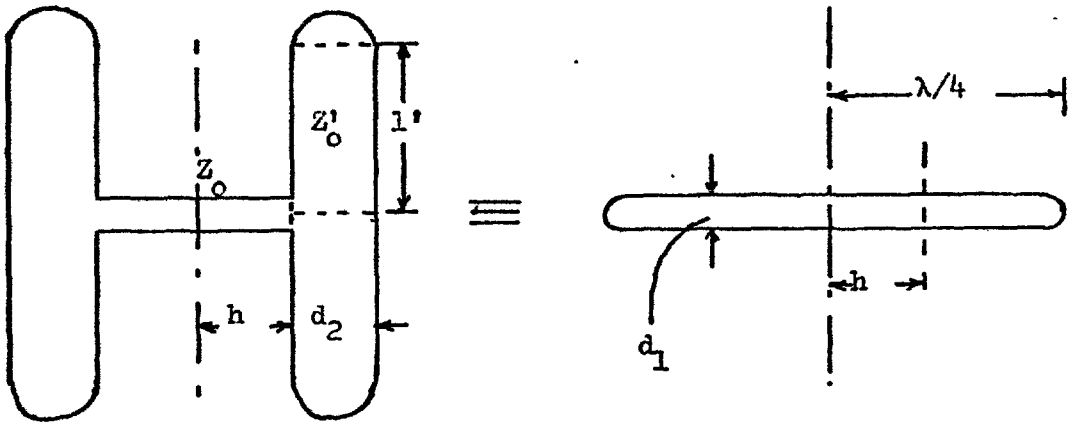

TABLE 3.9.2. The slot impedance results for X-band H-shaped slots.

Slot No.	Frequency of peak coupling to circular waveguide GHZ.	d_1 / d_2	$\sqrt{d_1 / d_2}$	Z_o / Z_o'
1	8.575	0.32	0.57	0.59
2	9.075	0.42	0.65	0.65
3	9.575	0.50	0.71	0.72
4	10.150	0.63	0.79	0.80
5	10.650	0.75	0.87	0.88

effects of the small differences between the I and H-shaped slots on loss had to be investigated. The next chapter is devoted to this study.

3.10. The Thick Dumb-Bell Slot

All the slot geometries which had so far been investigated, were cut in comparatively thin wall waveguide. The wall thickness of the waveguide had been ignored in deriving the slot conductance. The possibility of using a thick waveguide wall was investigated. If the wall was continued out to form a flange on the waveguide then a slot larger than the waveguide height could be used and coupled to the waveguide only over part of its length. It was postulated that if this type of slot proved useful then, all the slots could be realigned to remove the cross-polarised component and the waveguide cut by contour milling.

A single slot of this type was investigated at X band using a waveguide 16 jig. One wall of the waveguide was removed after reinforcing the other three. A thick plate in which a dumb-bell slot had been cut was then attached to the jig and its properties measured. A dumb-bell slot was used to reduce the over all slot length.

The slot was thought of as terminated at its junction with free space by a tuned circuit resonant at a frequency determined by the overall slot length. The slot-waveguide junction was considered to be another tuned circuit resonant at a higher frequency as determined by the length of the slot coupled to the waveguide. These tuned circuits were joined by a length of transmission line corresponding to the slot thickness and this could be regarded as a transformer. The final slot resonant frequency was expected to be intermediate between

FIGURE 3.10.1. The dependence of the resonant frequency of a dumb-bell slot on its thickness.

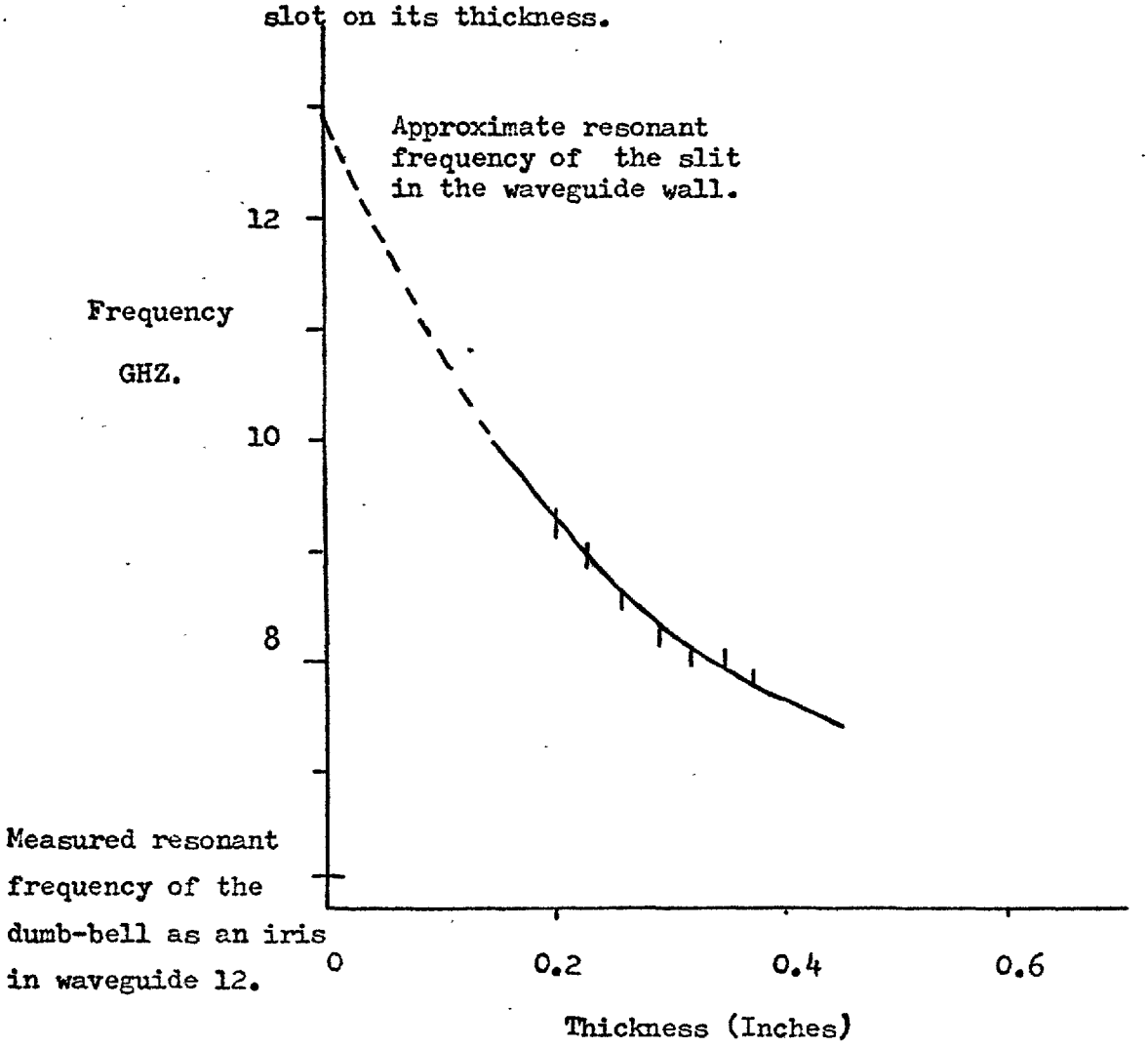

FIGURE 3.10.2. The conductance of dumb-bell slots of different thicknesses coupling to circular waveguide.

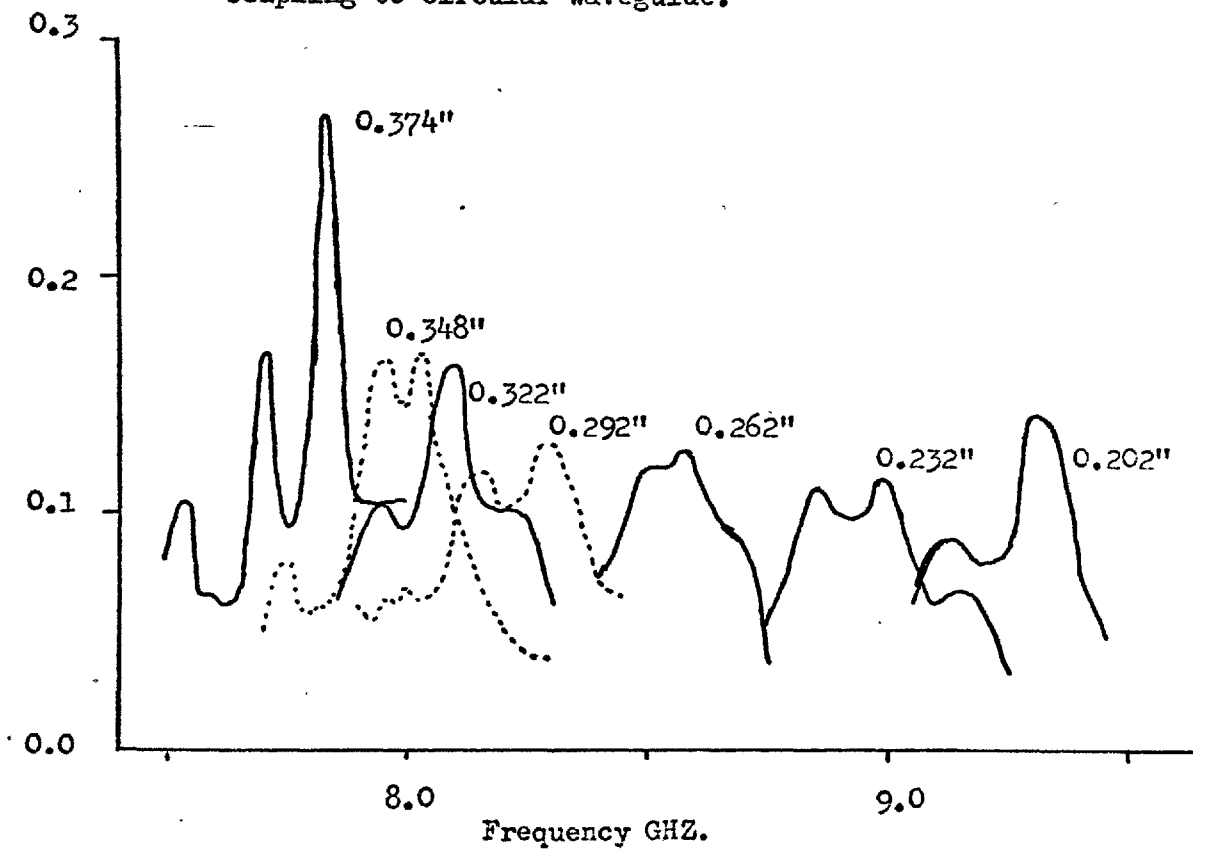

those of the tuned circuits and dependent upon the slot thickness.

The properties of the X-band slot were thoroughly investigated including loss coupling to a circular waveguide. The slot thickness was then reduced and the measurements repeated. This procedure was performed several times and the results for the slot resonant frequency are shown in Figure 3.10.1 and 3.10.2.. They indicated that the slot could be tuned over a wide frequency range by altering its thickness. The figure also shows the approximate resonant frequencies of the tuned circuits terminating the slot.

The measurements of slot loss produced values of between 19 and 37 percent of the coupled power, which were unacceptably high for array use. The loss was thought to be associated with large currents at the waveguide 16 to slot interface. The magnetic field in the slot was likely to be concentrated in the circular ends, but originates inside the waveguide. The magnetic field must have been squeezed into the dumb-bell ends within a short transition region. This was likely to be associated with high current densities which would have given rise to loss.

3.11. Slots in Triangular Waveguide

The method developed in Section (2.2) to analyse the conductance of slots had been applied only to rectangular waveguide. This limitation was not necessary as it could be applied to any waveguide cross-section capable of supporting only one propogating mode. Even this requirement was not strictly necessary but then terms corresponding to all the modes have to be considered as well as mode to mode coupling. Practically rectangular waveguide was the most readily available and few of the alternative cross sections offer advantages. However, in the

particular application envisaged it was thought that triangular waveguide could offer some advantages. Instead of having one side wall in which to cut slots, two pseudo-broad walls were exposed. It was hoped that slots could be cut in these faces which would not excite a cross-polarised component in the same way as transverse series slot cut in the broad wall.

A section of triangular waveguide was made by removing three walls from a length of waveguide 16 in such a way that when two plates were fitted, the required cross section resulted complete with transitions to rectangular waveguide.

Schelkunoff (1943) had previously analysed triangular waveguide of isosceles cross section and a symmetrical waveguide with one right angle. The waveguide formed from the waveguide 16 had a small apex angle and did not correspond to either of these geometries but was approximated by a segment of a circular waveguide carrying the TE_{o1} mode, as shown in Figure 3.11.1.. The TE_{o1} mode is circularly symmetric and so radial conductors could be erected without disturbing the field. The main error was likely to arise due to the flat rather than curved nature of the short side. The field within the waveguide was then given by:

$$H_z = J_o\left(S_{o1}\frac{r}{a}\right) \qquad E_z = 0$$

$$E_r = 0 \qquad H_r = -j\frac{\lambda_c}{\lambda_g} J'_o\left(S_{o1}\frac{r}{a}\right) \qquad (3.11.1)$$

$$E_\theta = j\frac{\lambda_c}{\lambda}\zeta J'_o\left(S_{o1}\frac{r}{a}\right) \qquad H_\theta = 0$$

where $S_{o1} = 3.832$, $\lambda_c = 0.820\ (2a)$ and a was the radius of the circular waveguide.

The cut-off of this waveguide was investigated experimentally using

FIGURE 3.11.1. The field in the triangular waveguide approximated by the TE_{01} mode in circular waveguide.

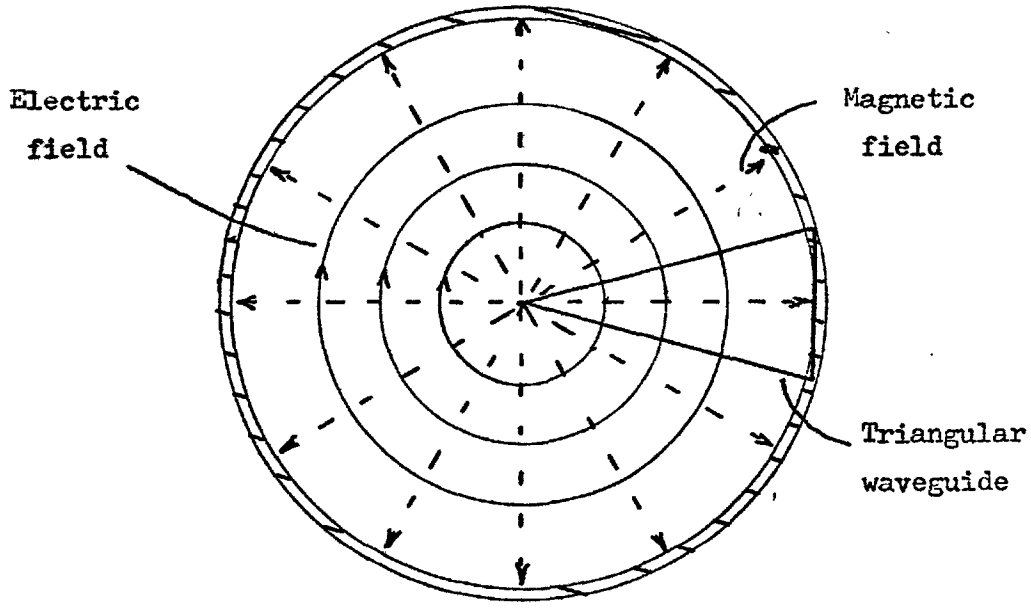

FIGURE 3.11.2. Slots cut in triangular waveguide.

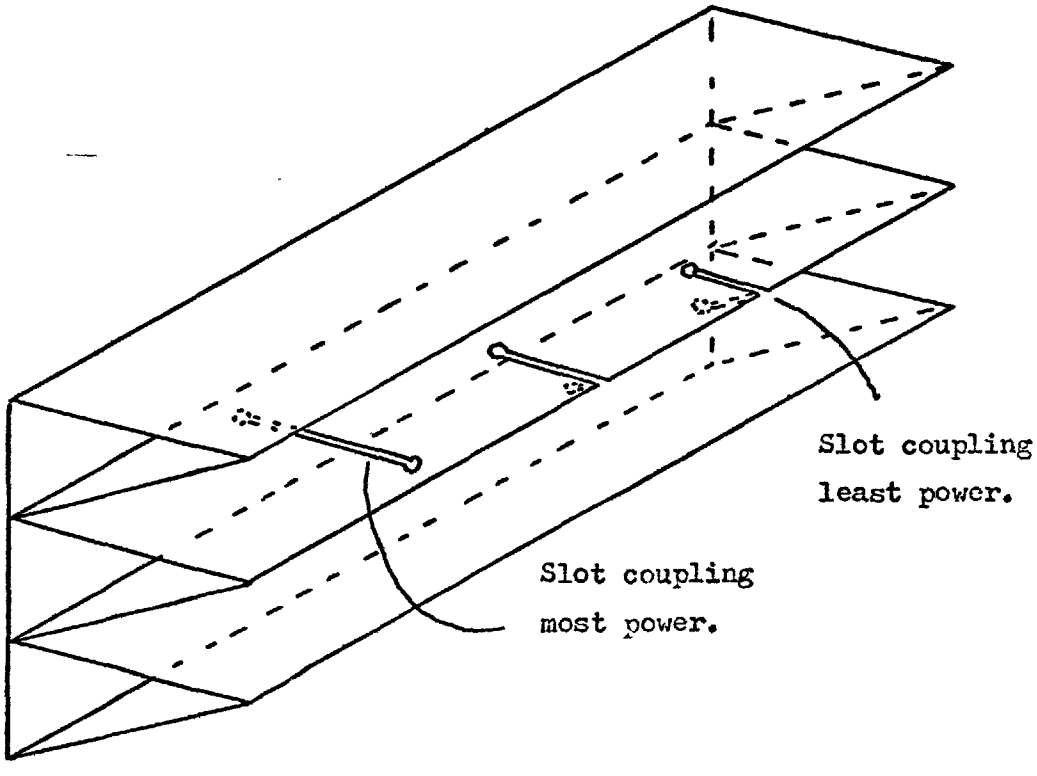

the section manufactured from waveguide 16 and found to be 8.35 GHz. The value of a was taken to be the shortest radius and if the waveguide had remained at its design dimensions this should have been 0.878". It was suspected that the dimension was smaller than this value but in any case:

$$\lambda_c = 1.414"$$

so that:

$$\frac{\lambda_c}{2a} = 0.805$$

This value agreed to within 2% of the expected value using the circular waveguide approximation and was better than the tolerance on a. The description of the field seemed acceptable and the methods of Section 2.2 and 2.3 could be used to analyse the properties of the slots shown in Figure 3.11.2.. It was thought that the coupling to the slot could be controlled by the fraction of the slot excited by each face of the waveguide, so that a slot completely on one face would be strongly excited and one folded equally on to the two faces would be uncoupled. Only slots on one face have been analysed.

The derivation of the equivalent circuit of the slot proceeded in a similar manner to that for the rectangular waveguide. The fields of waves travelling in both directions in the guide were known, the equation for the integration over the surface enclosing a section of waveguide was however computed in cylindrical polar coordinates, so that for the waveguide cross section

$$\hat{n} \cdot (\bar{E}_1 \wedge \bar{H}_2) + \hat{n}(\bar{H}_1 \wedge \bar{E}_2) = \pm (E_{2\theta}H_{1r} - E_{1\theta}H_{2r}) \qquad (3.11.2)$$

so that:

$$\int_S \frac{2A\gamma}{w\mu} J_o'^2(S_{ol}\frac{r}{a})dS = -\int_{slot} \hat{n} \cdot (\bar{E}_1 \wedge \bar{H}_2)dS \qquad (3.11.3)$$

so that:

$$A = \frac{w\mu}{2\gamma I_{02}} \int_{slot} \hat{n} \cdot (\bar{E}_1 \wedge \bar{H}_2)dS \qquad (3.11.4)$$

where

$$I_{o2} = \int_o^{\theta}\int_o^a J_o'^2(S_{ol}\frac{r}{a})drd\theta \qquad (3.11.5)$$

$$= \frac{\theta}{2\pi} \times 0.6383$$

by numerical integration.

For the half wavelength large slot cut in the broad face the electric field $\bar{E}_1$ was given by:

$$\bar{E}_1 = E_{1z} = \frac{V}{d}\cos k(r - d_1) \qquad (3.11.6)$$

and

$$\hat{n} \cdot \bar{E}_1 \wedge \bar{H}_2 = -E_{1z}H_{2r} + E_{1r}H_{2z} \qquad (3.11.7)$$

but the magnetic field at the wall was:

$$H_{2r} = \frac{\gamma}{w\mu} J_o'(S_{ol}\frac{r}{a})e^{-j\gamma z} \qquad (3.11.8)$$

so that:

$$A = \frac{V}{2I_{o2}d} \int_{\text{slot}} \cos k(r - d_1) \cdot J_o'(S_{ol}\frac{r}{a}) e^{-j\gamma z} dS$$

$$= \frac{V}{2I_{o2}d} \int_{d_1 - \lambda/4}^{d_1 + \lambda/4} J_o'(S_{ol}\frac{r}{a}) \cos k(r - d_1) dr \int_{-d/2}^{+d/2} e^{-j\gamma z} dz \qquad (3.11.9)$$

The z integral became:

$$\frac{2 \sin \gamma d/2}{\gamma} \qquad (3.11.10)$$

which on including another d became

$$\frac{\sin \gamma d/2}{\gamma d/2}$$

which for small d was approximately unity, so that:

$$A = \frac{V}{2I_{o2}} \int_{d_1 - \lambda/4}^{d_1 + \lambda/4} J_o'(S_{ol}\frac{r}{a}) \cos k(r - d_1) dr \qquad (3.11.11)$$

This integral could be evaluated numerically for any particular slot geometry.

It could also be shown that:

$$A = -B \qquad (3.11.12)$$

so that the equivalent circuit was a series resistance. Its value was determined after the power flow in the waveguide had been determined. It could be shown that for H type modes the power flow was given by:

$$P = \frac{1}{2}\,\frac{1}{\mathrm{Re}(Z_H)} \int |E_t|^2 dS \qquad (3.11.13)$$

where

$$Z_H = \frac{E_{\theta\,max}}{H_{r\,max}}$$

$$= \frac{jw\mu}{\gamma} \qquad (3.11.14)$$

so

$$P = \frac{\gamma}{2w\mu} \int |E_t|^2 dS$$

$$= \frac{\gamma\theta E_o^2}{4\pi w\mu} \int_o^a J_o'^2(S_{o1}\,\frac{r}{a})dr$$

$$= \frac{\gamma E_o^2}{2w\mu}\, I_{o2} \qquad (3.11.15)$$

The equation of energy balance when the waveguide was excited became:

$$E_o^2\,\frac{\gamma I_{o2}}{2w\mu} = A^2\,\frac{\gamma I_{o2}}{2w\mu} + (E_o + B)^2\,\frac{\gamma I_{o2}}{2w\mu} + \frac{V^2}{4(60\pi)^2}\, R_{rad} \qquad (3.11.16)$$

where R_{rad} was again the radiation resistance of a half wave dipole, 73.1 ohms. It had already been shown that the slot equivalent circuit was a series resistance so that its value was given by

$$r_o = \frac{4k_1}{R_{rad}} \cdot \frac{A^2}{V^2}$$

$$= \frac{k_1}{R_{rad}}\,\frac{I_{o1}^2}{I_{o2}^2} \qquad (3.11.17)$$

where

$$I_{o1} = \int_{d_1 - \lambda/4}^{d_1 + \lambda/4} J'_o(S_{o1}\frac{r}{a})\cos k(r - d_1)dr \qquad (3.11.18)$$

$$I_{o2} = \frac{\theta}{2\pi} \int_{o}^{a} J'^2_o(S_{o1}\frac{r}{a})dr \qquad (3.11.19)$$

and

$$k_1 = \frac{2(60\pi^2)\gamma I_{o2}}{w\mu} \qquad (3.11.20)$$

These expressions were evaluated numerically for a "half wavelength" long slot in the section of triangulated waveguide 16. Ground plane was fitted around the slot and the attenuation past it was measured compared to when the slot was taped over with adhesive aluminium tape. A peak value of series resistance of 1.09 was obtained experimentally compared to a theoretical value of 1.14. Good agreement was obtained showing that the field round the slot behaved in a predictable manner.

Although the isolated slot in triangular waveguide was well behaved considerable changes occurred in the slots properties when other dummy waveguides were introduced and work was not continued. Three principal reasons were given, firstly triangular waveguide was difficult to obtain or fabricate. Secondly it was thought that the problems of mutual coupling between slots would be greatly increased, when the waveguide were stacked. Slots in different waveguides would face each other and be highly coupled. Finally the triangular waveguide was lossy. The two "broad faces" were introduced parallel to lines of magnetic field. These faces introduced a large

attenuation into the otherwise low loss TE_{01} mode in circular waveguide. An expression for the waveguide attenuation was derived as:

$$\alpha = \frac{1}{\delta\sigma} \quad \frac{n}{a}\left(\frac{\lambda}{\lambda_c}\right)^2\left[1 - \left(\frac{\lambda}{\lambda_c}\right)^2\right]^{-\frac{1}{2}} + \frac{1}{\eta k \gamma I_{o2}}\left[\frac{4\pi^2}{\lambda_c^2} I_{a1} + \gamma^2 I_{o2}\right] \tag{3.11.21}$$

where

$\delta \equiv$ skin depth of the walls

$\sigma \equiv$ conductivity of the walls

and

$$I_{a1} = \int_o^a J_o^2\left(S_{o1}\frac{r}{a}\right)dr \tag{3.11.22}$$

Experimentally for the section of waveguide available a typical attenuation within its operating band was measured to be 0.5 dB/ft.

CHAPTER 4

SLOT LOSSES

4.1. Experimental Investigation

The slots in the special rectangular waveguide investigated in the last chapter appeared to be well behaved. A.S.W.E. had reported large losses associated with the H-shaped slot, but no reports of loss in the standard straight slot were known. It was to be expected that some loss could be associated with all slots, but there was considerable scope to investigate why the loss in some slots was negligible and in others unacceptably large.

It was very difficult to measure slot loss directly. The radio frequency energy dissipated must have appeared as heat, but most laboratory sources produce so little power that this could not be detected. A typical slot might couple a tenth of the power indident upon it and of this perhaps a third could be dissipated as heat. Only 3% of the incident power appeared as heat in the highly conducting waveguide wall. A sensibly detectable temperature rise would have required a massive radio frequency power source.

Slot loss had to be determined indirectly. This was done by measuring all the power sources and sinks of a slot and any power unaccounted for was assigned as loss. For a radiating slot this would have required the measurement of the attenuation past the slot, its reflection coefficient and the power radiated into the half space above the ground plane. This last measurement would have involved measuring the radiation pattern and gain at a sufficient number of points so that it could be integrated. There are many sources of error in such a measurement and it was felt that the power coupled by a slot

and hence the loss could only be accurately measured in a closed waveguide system. Measurements have been made of slot loss coupling to both rectangular and circular waveguide mainly at C band, although exploratory measurements were made at X band. The measurement of slot loss coupling to rectangular waveguide essentially involved three measurements; for coupling to circular waveguide one more measurement was required as it contained two orthogonal components.

The error in the value of the loss obtained had to be larger than the biggest error in measuring one of the slot power sinks. For slots with small couplings the least accurate measurement was that of the attenuation introduced into the passing waveguide. This measurement required a precision instrument capable of resolving small changes in attenuation. The equipment used was a Weinschel Engineering R. F. Ratiometer Model No. 1810. This instrument compared two radio frequency signals to an audio frequency precision attenuator at the modulation frequency of 1 kHz (Fig. 4.1.1). The result was displayed on a long linear scale and could also be processed by a data normaliser or plotted directly against frequency on an X-Y plotter. The makers claimed the accuracy of the instrument to be $\pm$ 0.02 dB. This was increased by mismatch and by the non-square law of the barretters used ($\pm$ 0.01 dB in 30 dB dynamic range). Measurements could be made to an accuracy of $\pm$ 0.03 dB if mismatch error was minimized. A schematic layout of the C band equipment used is shown in Fig. 4.1.3.. For some early slot measurements the simpler X band system shown in Figure 4.1.2 was used.

The C band measurement system was checked by measuring a waveguide 12 precision rotary attenuator made and calibrated by Flann Microwave Industries Limited. Figure 4.1.4. shows the swept frequency results

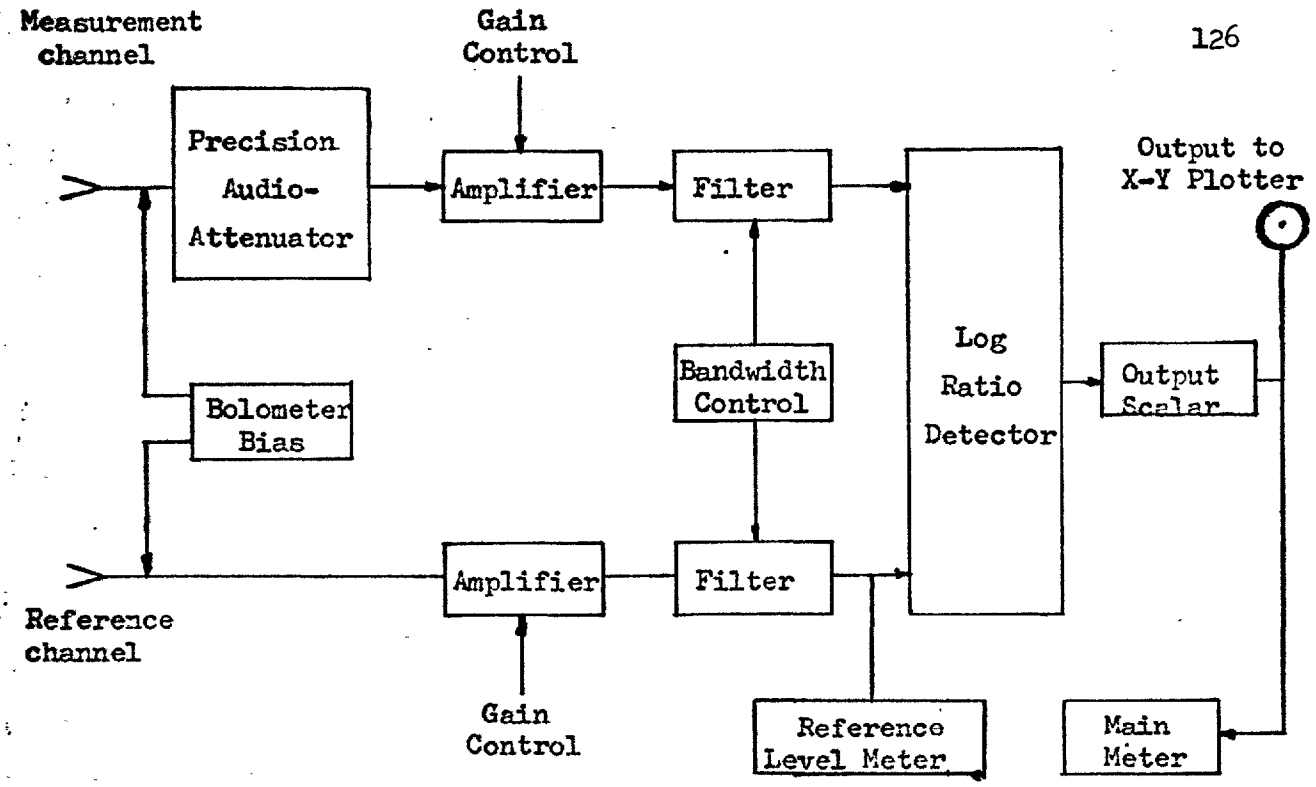

FIGURE 4.1.1. Block diagram of Weinschel Engineering Model 1810 R.F. Ratiometer.

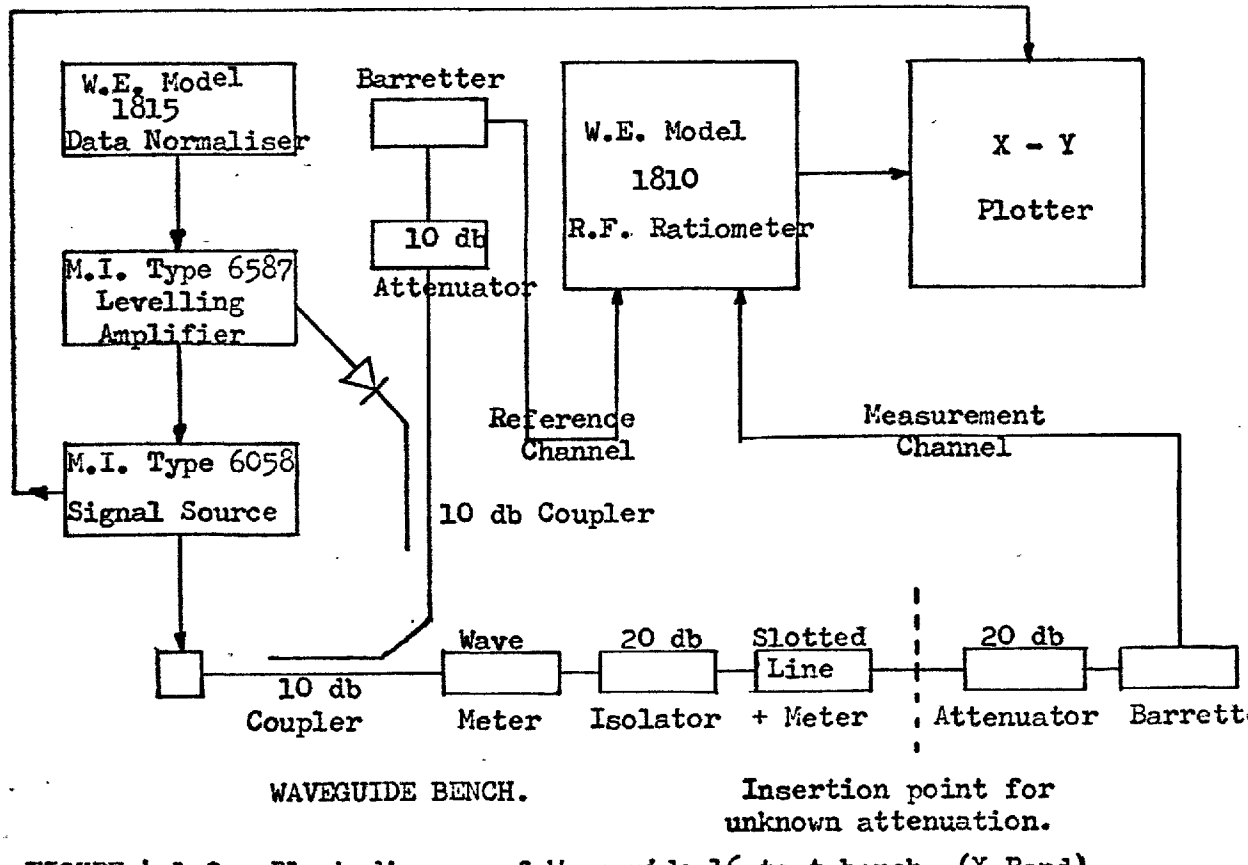

FIGURE 4.1.2. Block diagram of Waveguide 16 test bench. (X Band)

FIGURE 4.1.3. Block diagram of Waveguide 12 swept frequency test bench.
(C Band)

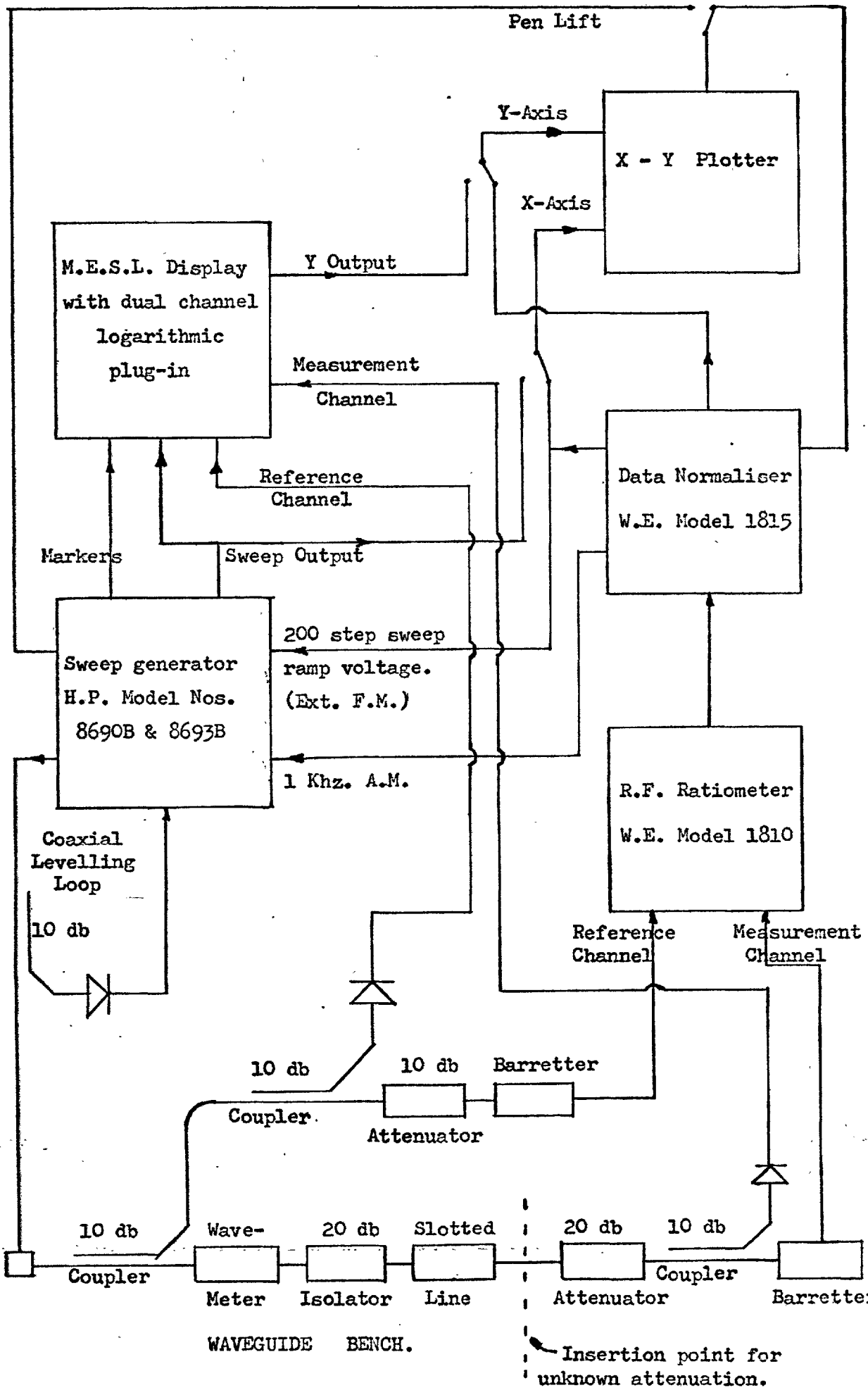

obtained over the band from 4.0 GHz to 5.85 GHz, the frequency range of the waveguide attenuator. It shows that the biggest discrepancy for small values of attenuation was approximately 0.03 dB and occurred around two frequencies. For other frequencies better agreement was obtained between the two attenuators, both of which were assumed to be correct.

The C band system could have been used to plot swept frequency results from which slot loss could be derived. In fact some uncertainty was introduced in comparing results and it was found better to obtain loss values from single frequency measurements. The frequency was initially determined by swept measurements. The slot V.S.W.R. was determined by using a slotted line which was also used to check the initial match.

Measurements were made on slots of various geometries but interest was chiefly attached to I-shaped slots as in all other respects they seemed ideal array elements. The I-shaped slot was in several respects similar to that of A.S.W.E.'s H-shaped slot and small differences could be important. Early X band measurements had shown that a ⅂ shaped slot was comparatively loss free and that an H-shaped slot was lossy. These measurements had also indicated that surface finish was comparatively unimportant as the ⅂-shaped slot was badly made.

At C-band, measurements were made on uniform width I-shaped slots of different centre heights coupling both to waveguide 12 and circular waveguide. I-shaped slots were used because H-shaped slots would not fit waveguide 12 unless centre loaded. The effect of centre loading could then be investigated separately.

When the waveguide 12 was fitted to the I-shaped slots, their resonant frequency was raised by approximately 150 MHz. This was

FIGURE 4.1.4. The calibration of the Flann waveguide 12 precision rotary attenuator against the Weinschel R.F. ratiometer.

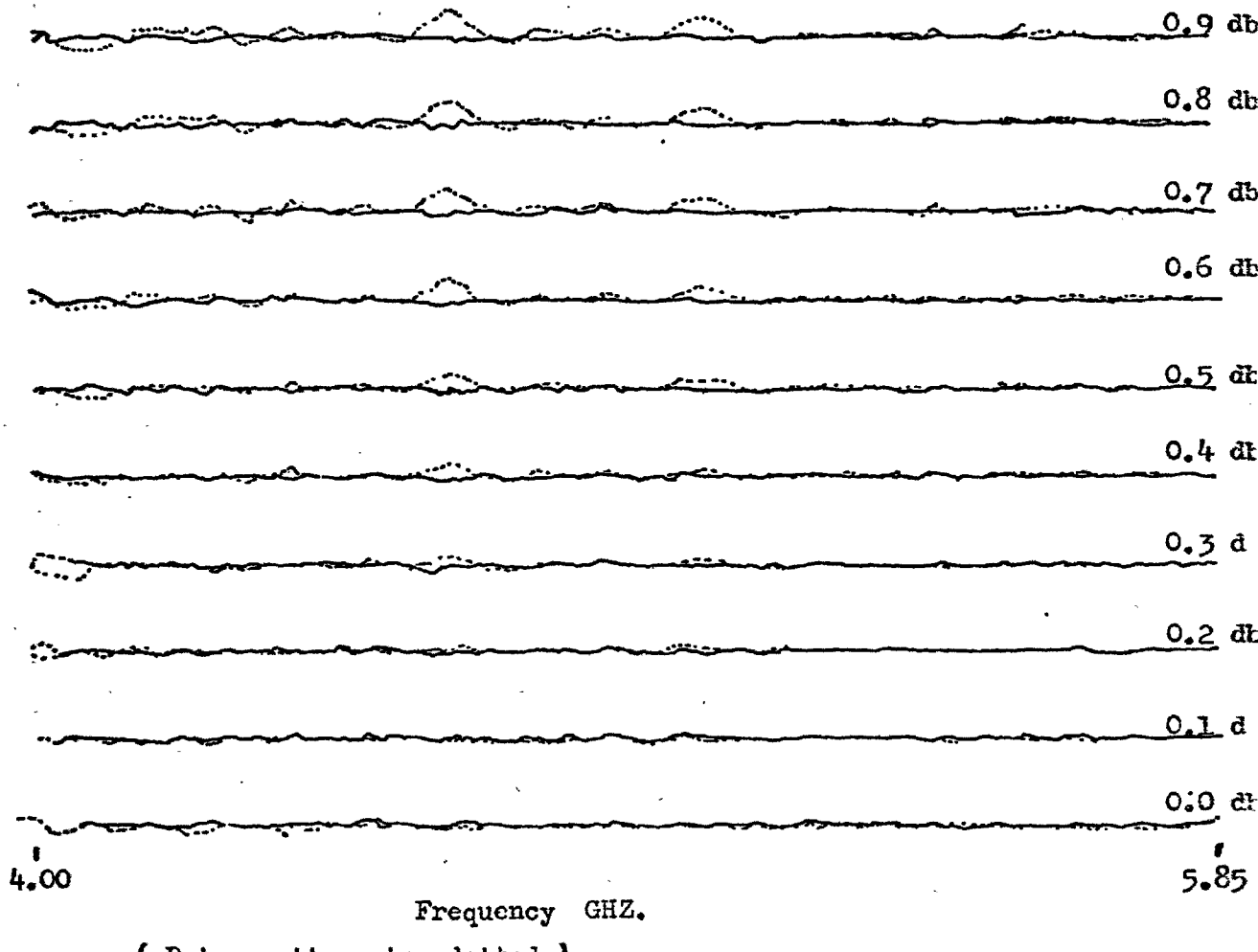

(Rotary attenuator dotted)

FIGURE 4.1.5. The loss of reduced height I-shaped slots coupling to waveguide 12 through the narrow wall of the special size waveguide.

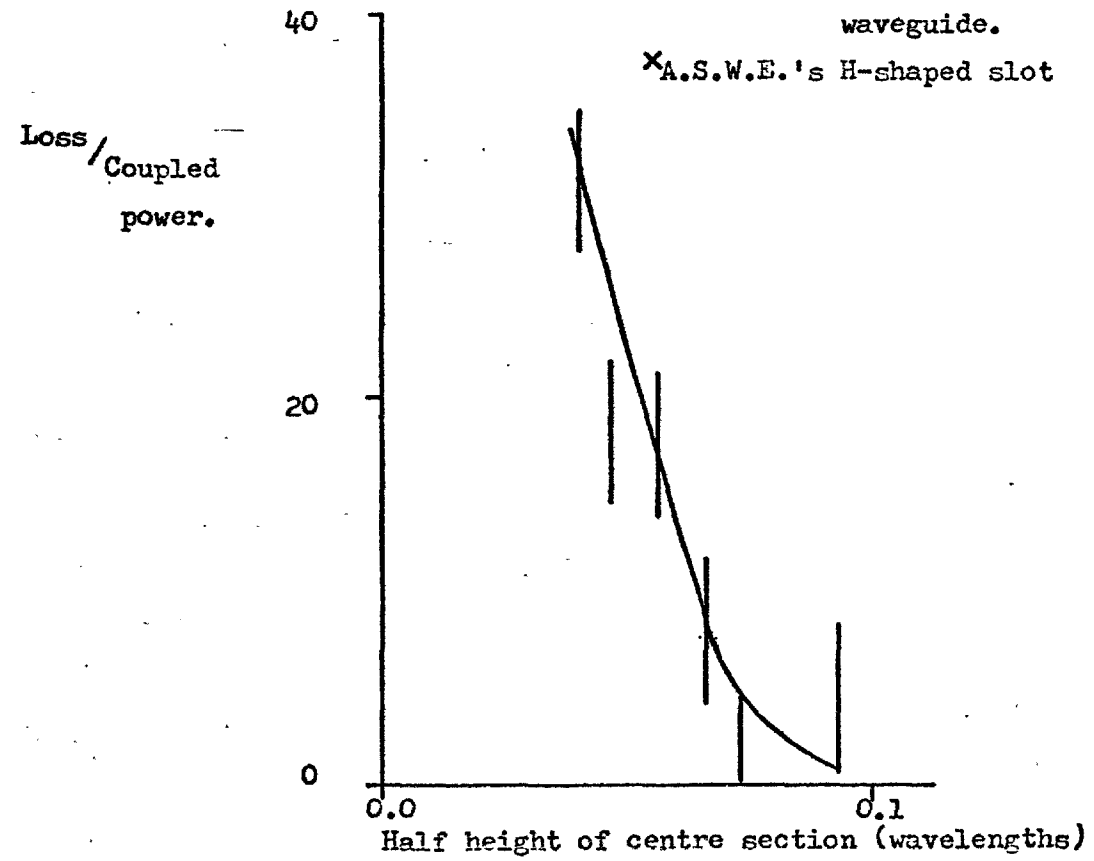

due to the cross polarisation being cut off. The cross polarisation produced a real component of the radiation impedance of the slot, which on being cut off changed to being imaginary. The waveguide 12 could also be regarded as producing an infinite number of reflections in its conducting walls so that the original slot radiation impedance changes to that in an infinite array.

Fitting the circular waveguide to the slot produced a large change in its conductance but no change in its resonant frequency. Some measurements were made at the frequency of peak attenuation past the slots.

The results obtained for I-shaped slots of various heights coupling to waveguide 12 are shown in Figure 4.1.5.. The results indicated that I-shaped slots occupying the full height of the special size waveguide were substantially loss free but as the height was reduced they became much more lossy. The full height I-shaped slot appeared to be a useful array element. The results of the last chapter indicated that in all other respects it was well behaved but it was similar to the H-shaped slot which was known to be lossy. One important difference as far as loss is concerned had been identified as the height of the centre section; in the H-shaped slot this was reduced to allow rotation. The other main difference between the two slot geometries was that the centre section of the H-shaped slot was impedance loaded. This was also necessary to allow for rotation but the I-shaped slot was of uniform width.

The effect of impedance loading on slot loss was initially investigated on a series of I-shaped slots of constant height but progressively centre loaded to reduce their overall size. The results shown in Table 4.1.1. demonstrate that the centre loaded I-shaped slot became progressively more lossy as the loading was increased. A

TABLE 4.1.1. The loss of centre loaded I-shaped slots coupling to waveguide 12.

d1 / d2 (see fig. 3.9.1)	Loss / Coupled power %
0.32	31.9±3.6
0.50	10.1±2.9
0.75	-0.6±2.0 (1.4)

TABLE 4.1.2. The loss of centre loaded ⅂-shaped slots coupling to waveguide 12.

d1 / d2 (see fig 3.9.1)	Loss / Coupled power. %
0.50	12.1±2.0
0.75	5.0±2.0
1.00	8.6±2.0
1.33	8.9±2.0
2.00	3.8±2.0
3.12	17.4±2.0

similar effect was found with centre loaded T-shaped slots as the results shown in Table 4.1.2. indicate.

All the loss measurements were repeated with the slots coupling to a section of circular waveguide. This was regarded as a two port device as it could support two orthogonal polarizations. Each was separately measured using a transition from circular to rectangular waveguide incorporating an attenuating vane, as described in Section 3.3.. Initially the transition was rotated and the polarisation within the circular waveguide investigated. At one position a deep null was measured indicating as expected that the wave in the circular waveguide was linearly polarised. Subsequently only the horizontal and vertical components have been measured. The loss values obtained with the various slots coupling to circular waveguide are given in Figure 4.1.6. and Table 4.1.3.. In general the results were similar to those coupling to a waveguide 12 branch arm but the variation of loss with the slot height and loading was less well defined. The effects on the conductance and frequency response of the slots in fitting the rectangular and circular waveguides were different but the slot loss characteristics were generally similar.

The measurements on the I-shaped slots of high coupling factor indicated that its loss was acceptably low. However, a completely symmetrical I-shaped slot would not radiate but it is likely that some loss can be associated with it. For lightly coupled slots it was possible that the loss as a function of coupled power could increase. Measurements of the loss of a series of I-shaped slots of different couplings were made. The results, shown in Table 4.1.4. apparently indicate that the loss increased for small couplings but the associated error also increased. A decisive result was not obtained.

FIGURE 4.1.6. The loss of reduced height I-shaped slots coupling to circular waveguide through the narrow wall of the special size waveguide.

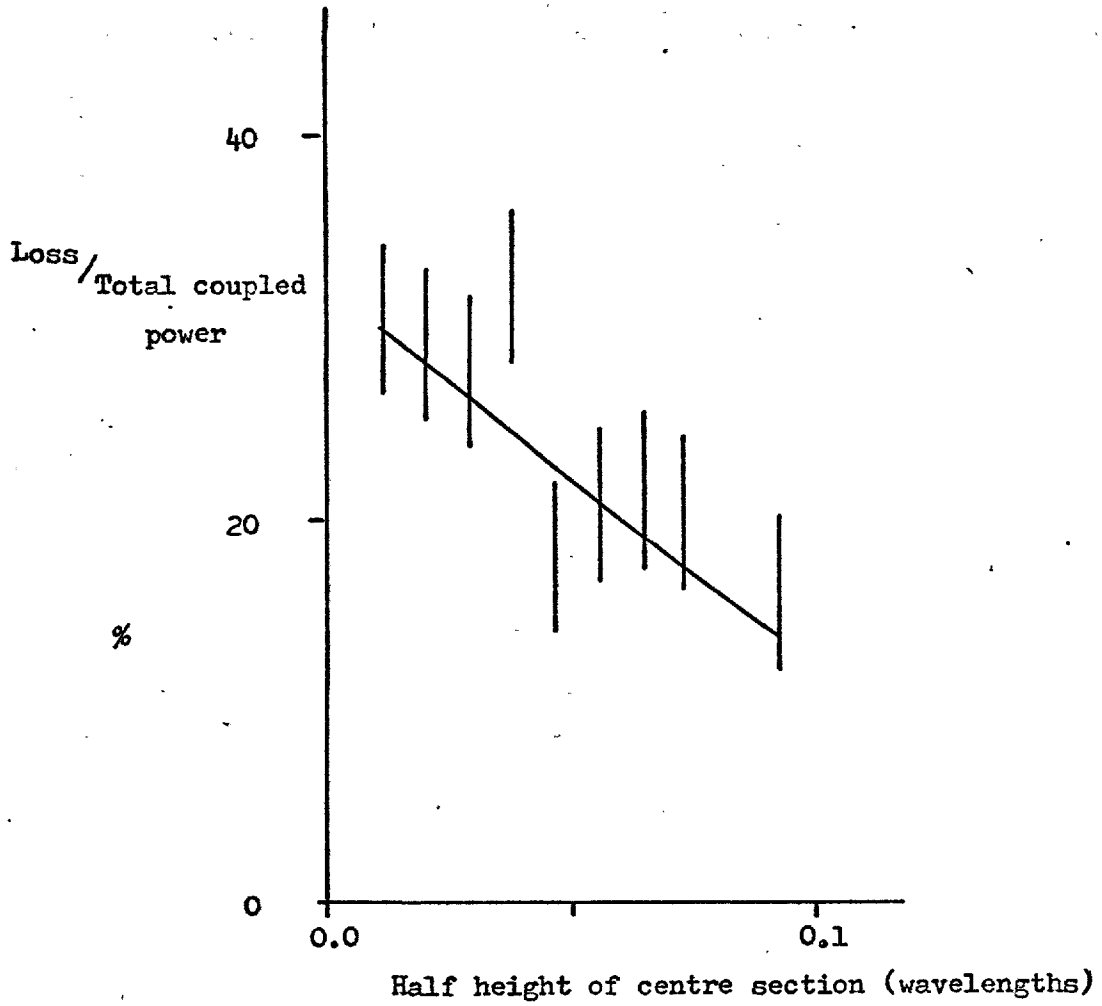

TABLE 4.1.3. The loss of loaded I-shaped slots coupling to circular waveguide.

The ratio of the widths of the centre and end limbs.	Loss / Power coupled to the main pol. %
0.32	26.4±3.6
0.50	12.2±3.6
0.75	12.4±2.1

TABLE 4.1.4. The loss associated with I-shaped slots of various couplings feeding a waveguide 12 branch arm.

The length of the shorter branch arm INCHES	Coupling to waveguide 12 -db	Loss/Coupled power %
0.000	3.99	10.1±1.2
0.100	4.78	4.5±1.5
0.150	8.01	0.9±3.2
0.160	9.46	-4.6±5.8 1.2
0.170	11.02	-4.5±7.0 2.5
0.175	12.77	1.2±12.0
0.180	13.3&	19.1±13.7

FIGURE 4.1.7. The loss of reduced height I-shaped slots coupling to circular waveguide through the end wall of waveguide 12, as measured by the modified V.S.W.R. method.

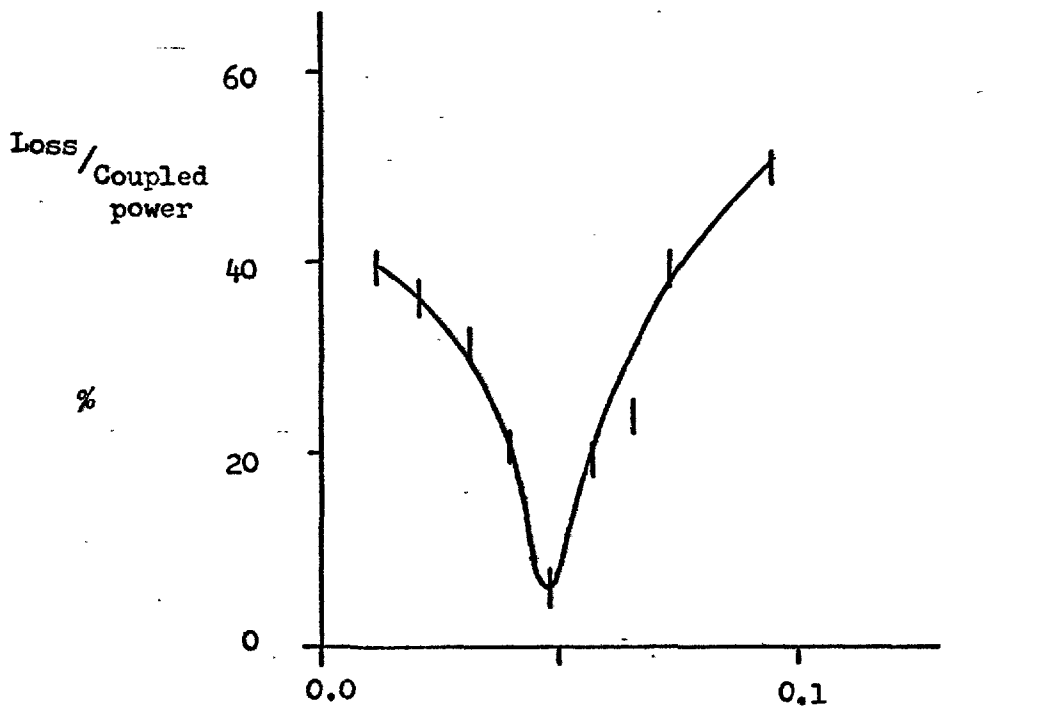

It was postulated that more accurate loss measurements could be obtained if the slot was introduced as a resonant iris in a waveguide. At resonance, there would be no reactance associated with the slot and the conductance should also be zero. If the V.S.W.R. of the slot followed by a matched load is measured the V.S.W.R. should be that of the load. Any change in the V.S.W.R. could then be associated with a residual conductance due to slot loss.

A resonant slot in the end wall of a waveguide though, fed in a different manner to a slot in the narrow wall is likely to have the same field configuration. The relative power sinks were however likely to be changed and the actual value of slot loss was expected to be different. The form of the loss variation was expected to be independent of which wall the slot was cut in.

The series of reduced height I-shaped slots were measured in this way coupling between waveguide 12 and circular waveguide. The minimum V.S.W.R. within the waveguide 12 was measured using a swept frequency generator and reflectometer coupler. The results obtained interpreted as described are shown in Figure 4.1.7.. The form of the loss variation appeared to be totally different to that measured for side-wall coupling. The results suggested that the slot was resonantly loss free for a half height of 0.05 wavelengths.

This result was further investigated as it was unexpected. The same slots were introduced as resonant irises in waveguide 12 and the attenuation past them as well as the V.S.W.R. were measured. In this way the loss was measured both by the minimum V.S.W.R. method and as power unaccounted for. The results shown in Figure 4.1.8., indicate that for this case good agreement was obtained between the two methods. The loss rose for this configuration, as the half height increased,

FIGURE 4.1.8. The loss of reduced height I-shaped slots used as irises in waveguide 12.

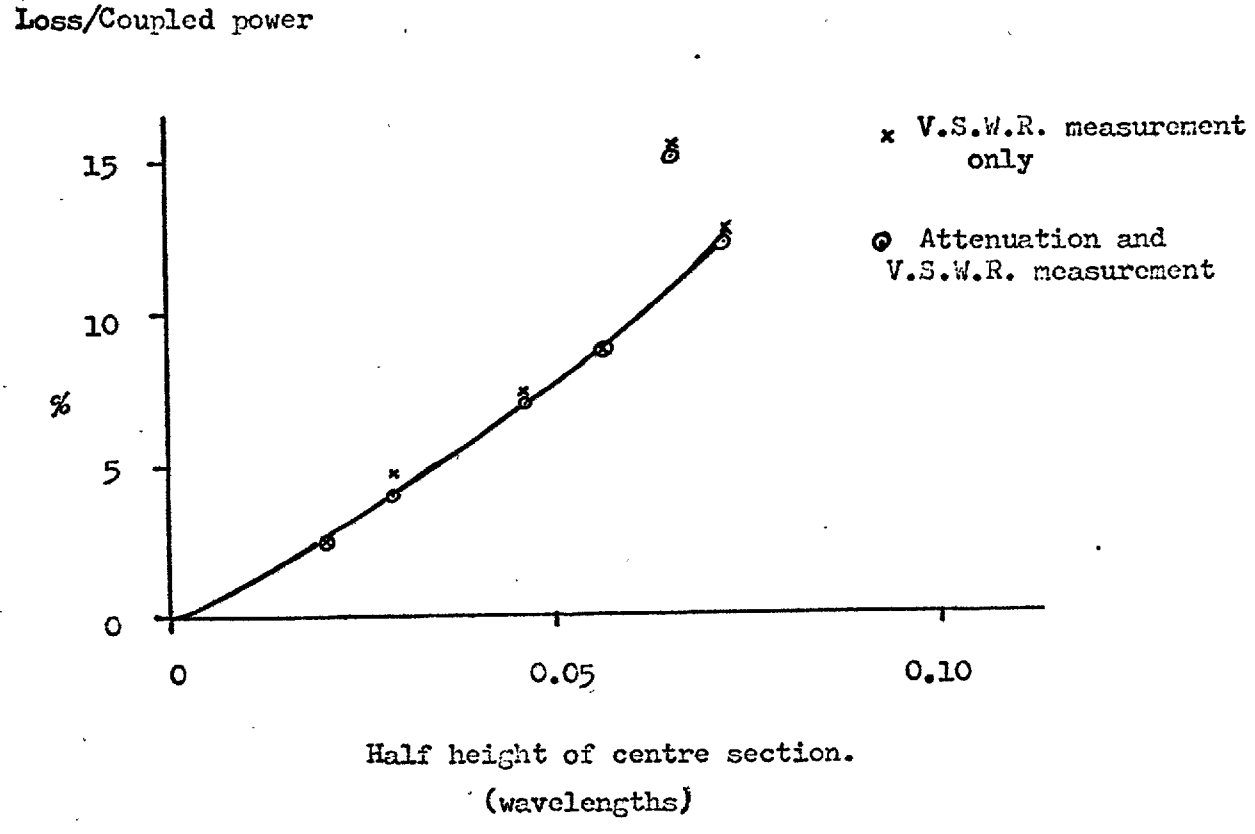

FIGURE 4.1.9. The loss of reduced height I-shaped slots used as polarisation rotation transformers between orthogonal sections of waveguide 12.

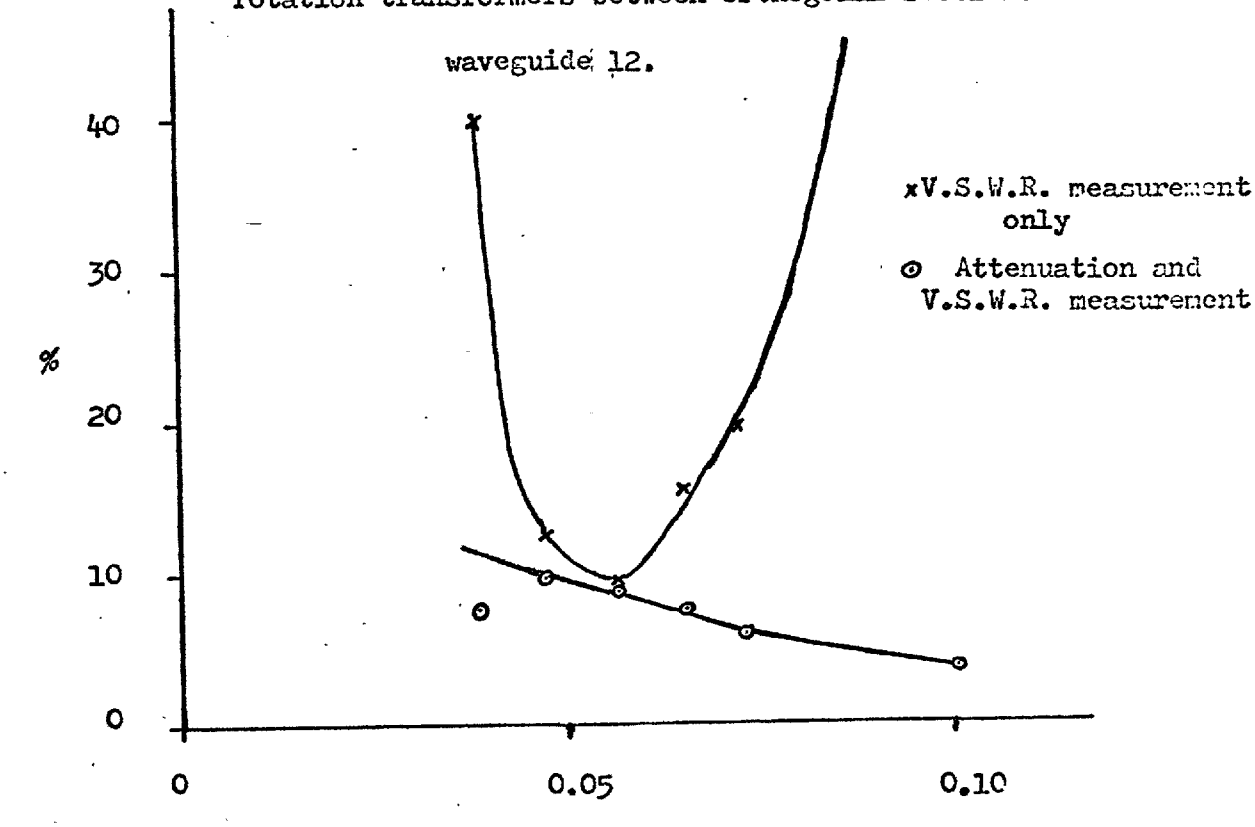

because all the coupling was via the end arms. The two methods of measuring iris loss were repeated using the reduced height I-shaped slots as a polarisation rotator between sections of waveguide 12 twisted at 90° relative to each other. In this case, (Figure 4.1.9) agreement between the two methods of loss measurement occured only for a half height of 0.05 wavelength. For all other heights the change of V.S.W.R. method gave a much higher loss than there was power unaccounted for. The change in V.S.W.R. was associated with a residual reactance which was zero for a half height of 0.05 wavelengths. This residual reactance was only associated with the polarisation excited by the centre section of the slot. It invalidated the modified V.S.W.R. method when this polarisation was excited. It was also responsible for the dispersion between the frequencies of peak coupling to the two orthogonal polarisations within circular waveguide and the break down of the slot resonance for low couplings.

The loss assigned as unaccounted power with the slots as polarisation rotation elements was consistent in its variation with measurements of coupling through the narrow waveguide wall. The values obtained were however different due to the change in geometry and relative power sinks.

I-shaped slot loss had been measured coupling to both rectangular and circular waveguide and the highly coupled full waveguide height slots found to be low loss. It was thought reasonable to assume that these slots would remain similarly free from loss when radiating into space. In addition the loss of the lightly coupled slots has been shown to be within reasonable bounds but any information regarding these slots would be useful. It was decided to check the relative gain of a series of I-shaped slots against some other antenna. This was done by forming an

interferometer from a slot and an open ended waveguide through a rat-race, as shown in Figure 4.1.10.. The interferometer so formed was slowly rotated and the radiation pattern recorded, paying particular attention to the null depths. The slot was then taped over with adhesive aluminium tape and the level of the open ended waveguide recorded. The interference fringes were less than 2° wide and they were recorded over an angle of 20° - 30° so that many nulls were sampled. From the null depth compared to the level of the radiation from the waveguide the difference in gain of the two antennas was determined.

Bench measurements were also made on the radiating slots and the power lost from the waveguide at the slot was compared to its relative gain. This is done in Table 4.1.5.. If the slot loss and radiation pattern shape remained sensibly constant with coupling then these quantities should have varied in a similar manner. The results obtained were numerically similar in this case, although that is coincidental. It appeared that the loss of the full waveguide height I-shaped slots radiating over a ground plane stayed substantially constant with coupling.

The loss of the full waveguide height I-shaped slot was small but measurements indicated that the loss increased rapidly if its height was reduced or if it was loaded by changes in impedance. The H-shaped slot originally investigated by A.S.W.E. was an impedance loaded reduced height slot and its high loss seemed sensible from experimental evidence.

4.2. Investigation of the Field of a V.H.F. Waveguide Slot

The results of the last section established the phenomena of slot loss experimentally and a model of slot loss was required. The

FIGURE 4.1.10. The system used to measure the relative gain of a series of slots.

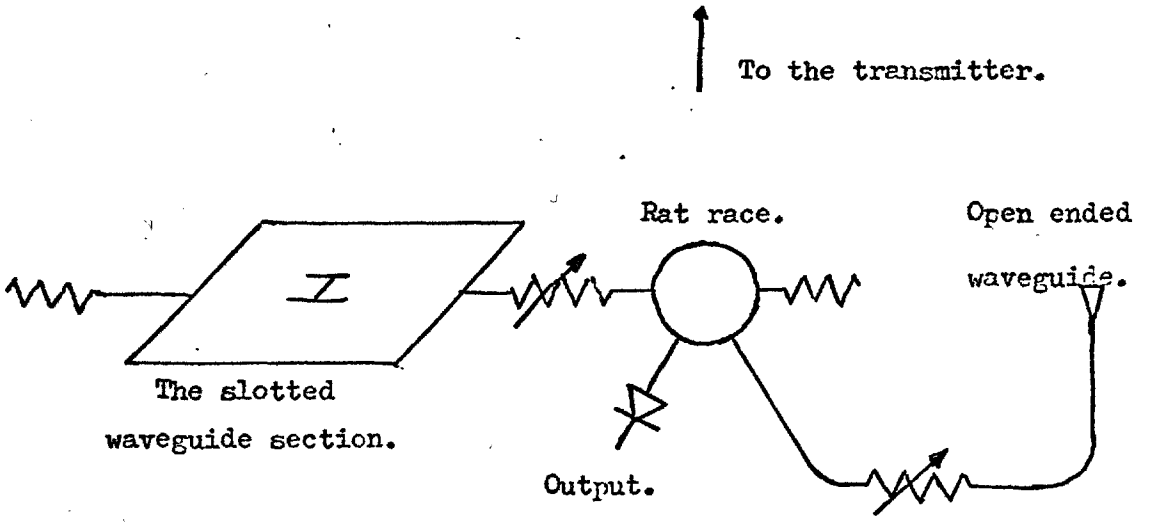

TABLE 4.1.5. The results from the measurement of the relative gain of a series of slots.

Slot No.	Power unaccounted for by bench measurements.		Relative gain of slot compared to waveguide. db.	Difference.
	%	-db		
1	31.16	5.06	-5.2	+0.1
2	17.60	7.54	-7.0	-0.5
3	11.44	9.42	-10.6	+1.2
4	7.95	11.00	-11.8	+0.8
5	5.86	12.32	-12.0	-0.3
6	4.45	13.52	-13.0	-0.5
7	3.73	14.28	-15.0	+0.3
8	1.02	19.92	-20.0	+0.1

assumption of a sinusoidal slot field was shown to be substantially correct in determining slot conductance, but before a loss model could be established with confidence it was desirable to obtain a more complete knowledge of the slot electromagnetic field. The simplest experimental approach was to probe the field around the slot. A C-band slot was too small to be accurately probed, and a much larger slot was required. A section of V.H.F. waveguide was made from aluminium sheets bent to form a nine foot length of waveguide approximately to the dimensions of waveguide 00 (WR2300). The waveguide was terminated at one end with a load made from a hollow wooden pyramid filled with carbon loaded foam rubber. Power was introduced at the other end by an offset electric probe in front of an adjustable short circuit. The probe was made of copper sheet and approximately four inches in diameter by five inches long. Its position across the waveguide could be altered by means of the compressed paper rods used for its mechanical support. The position of the short and probe were adjusted for the best input match while the V.S.W.R. was monitored over a large frequency range using a "Polyskop". It was set to be no worse than 1.5 over the frequency range from 300 to 400 MHz.

An H-shaped slot scaled from C-band in all dimensions including thickness and of overall size $7\frac{1}{2}$" x $7\frac{1}{2}$" was introduced into the narrow waveguide wall. Some ground plane was introduced around the slot. This was approximately a wavelength in extent in all directions from the slot. Its size had to be restricted due to limitations of space but as only the field in the immediate slot vicinity was to be sampled, it was sufficient.

The "Polyskop" indicated the frequency at which peak power was coupled by the slot as 336 MHz. All subsequent measurements of this slot

have been made at this frequency using a General Radio oscillator as a source.

The probe used for most of the measurements was a small circular magnetic field type. It was a shielded loop symmetrically loaded at the point furthest from the ground plane and feed cable. Any current picked up by the cable and injected into the loop flowed symmetrically into the two halves of the loop. At a point diametrically opposite the cable entry the two currents were equal and opposite and should not have affected the measurement. The electric field component normal to the surface investigated should have induced similarly symmetrical currents on the loop and again not affected the measurement of tangential magnetic field. It was also assumed that the tangential electric field near the surface was small.

The variation of the magnitude and polarisation of the magnetic field tangential to the ground plane have been measured. The results, normalised at each point for the variation of polarisation are shown in Figure 4.2.1.. The polarisation was linear in line with and perpendicular to the central limb of the H-shaped slot. These were the directions in which the electric field of a half-wave dipole was linearly polarised. Figure 4.2.1. also shows the lines along which King and Harrison (1969) have shown that the electric field of a half-wave dipole is circularly polarised. These contours also correspond to the regions in which the magnetic field of the H slot was circularly, or at least elliptically, polarised. The duality between the electric field of a dipole and the magnetic field of a slot was further established.

The magnetic field coupled through the slot has also been measured. Its general profile is shown in Figure 4.2.2.. There is a well defined null bisecting the central arm of the slot, while in the end sections

FIGURE 4.2.1. The measured polarisation of the magnetic field above a ground plane in the region of a waveguide fed H-shaped slot.

Frequency - 336 MHZ.

The dotted line represents points for which the electric field of a half-wave dipole is circularly polarised.

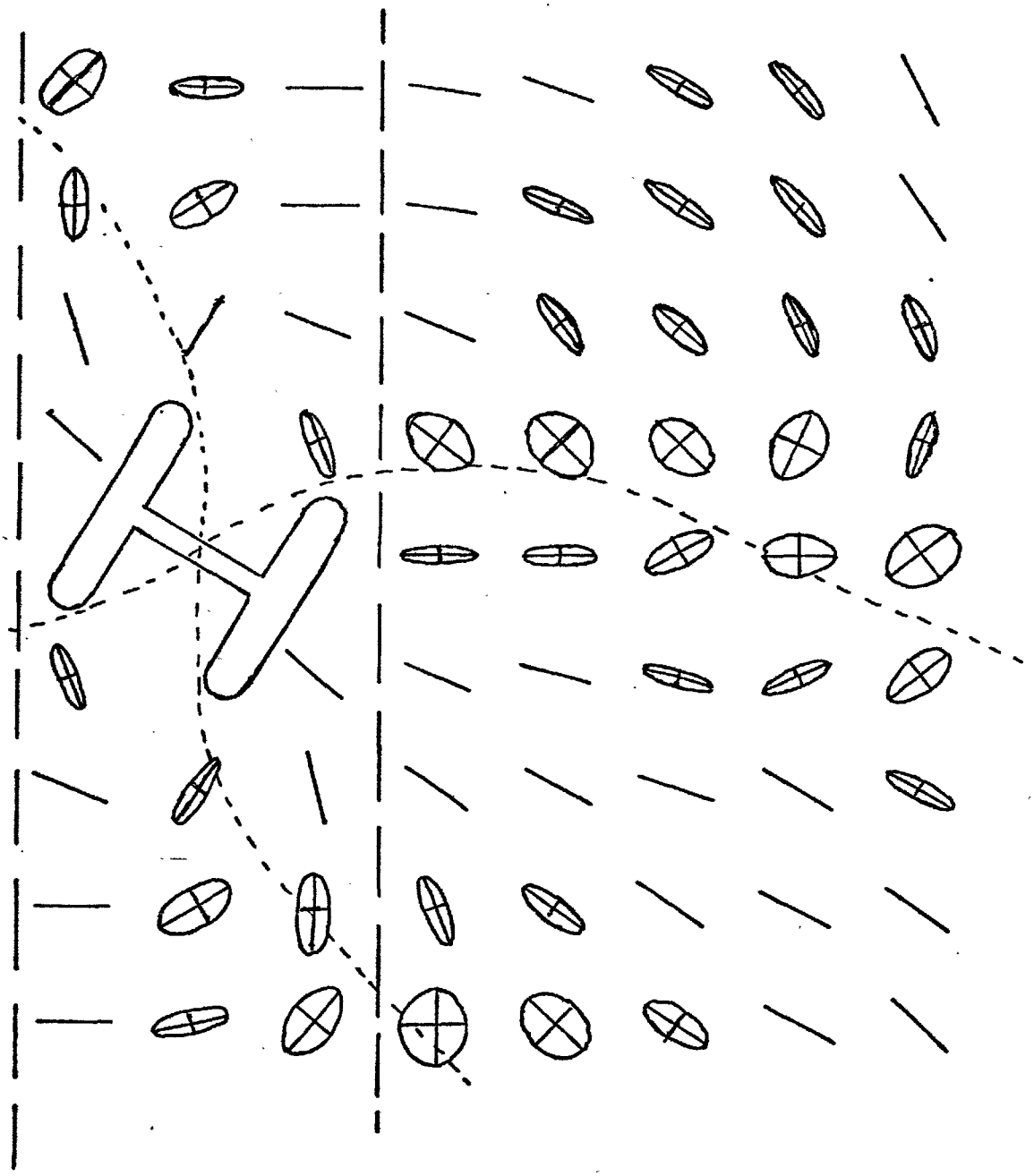

The principal polarisation is normalised at each point . The scale for the orthogonal polarisation is 1 db/mm.

All the points lie on a 4 inch square grid.

FIGURE 4.2.2. The profile of the normal component of magnetic field of a waveguide fed H-shaped slot.

Vertical scale ; 3db / 4mm.

Frequency ; 336 MHZ.

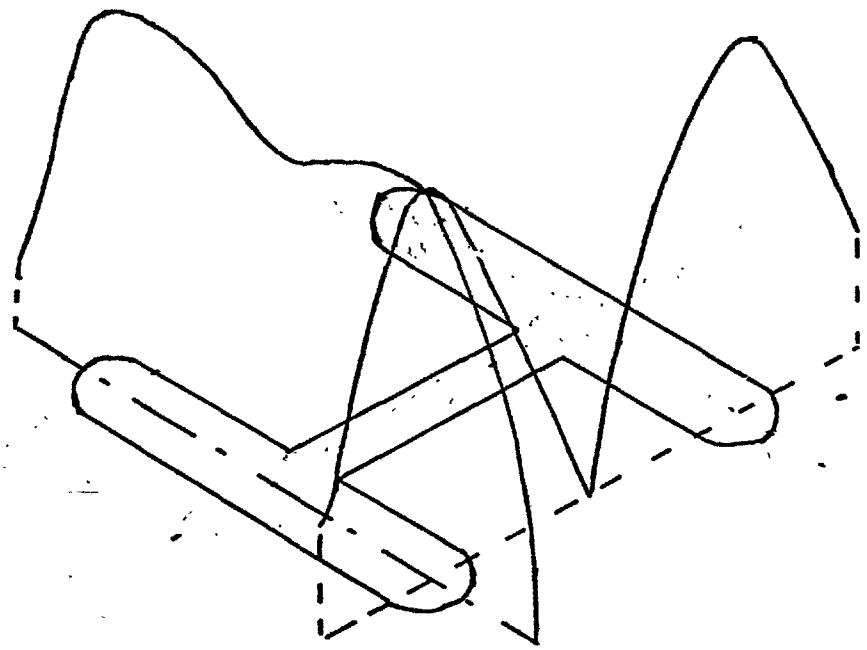

the field was concentrated near the extremities, as shown by Figure 4.2.3.. The phase variation of the magnetic field through the slot was measured. This was done using a Hewlett Packard network analyser, and the results are plotted in Figure 4.2.4..

The magnetic field coupled through each end section was at a single phase but on moving along the central section there was a phase shift of approximately 180°. It appeared to be coupled out by one end section and back in again by the other end section so that it was concentrated in two rings threading the four extremities of the slot.

The concentration of magnetic field at the corners of the slot must have been maintained by conduction currents flowing into the slot between the end arms. As copper losses are proportional to the square of the current density it was likely that these currents gave rise to the loss associated with this type of slot. A.S.W.E.'s evidence that modifying the slot corners to facilitate spark erosion increased loss, supported this view. Referring to Figure 4.2.5. the rings of magnetic field shown must have been maintained by conduction currents flowing across the plane AA'. These became displacement currents to cross the slot and emerged from the plane BB' as conduction currents. The current crossing the slot was concentrated within the metallic regions confined by the end arms of the slot and an investigation of its distribution was useful.

The conduction current within the surface of a metal can not be easily measured. Usually the "tangential" magnetic field is measured but this can vary extremely rapidly away from the surface. The best that can be done is to measure the magnetic field at various heights and attempt to extrapolate to the surface. The shielded loop magnetic field probe can only give a measure of the average field over its area. It

FIGURE 4.2.3. The magnitude of the magnetic field through the end section of an H-shaped slot.

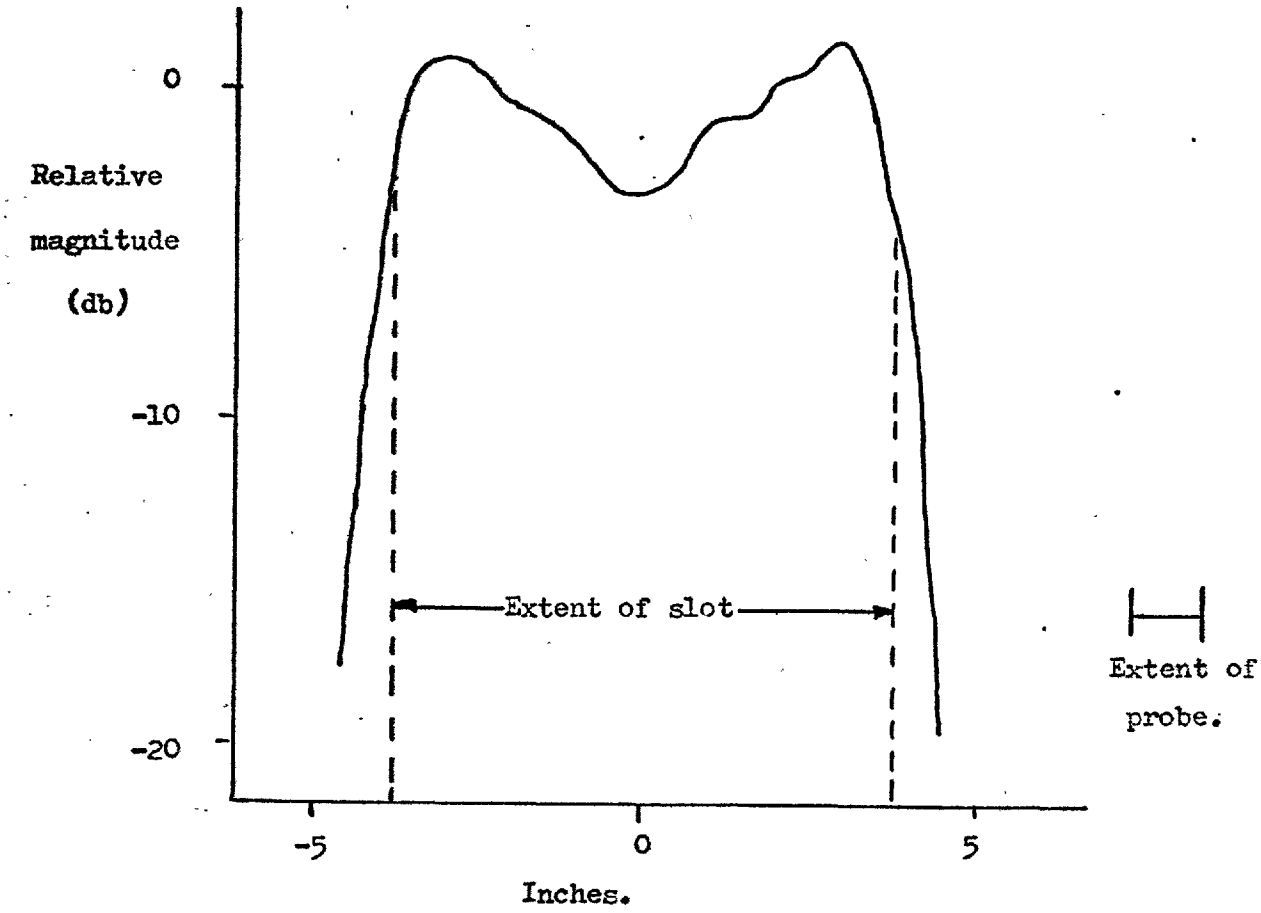

FIGURE 4.2.4. The relative phase of the magnetic field through a waveguide fed H-shaped slot (a) Along the centre limb.
(b) Along the end setion.

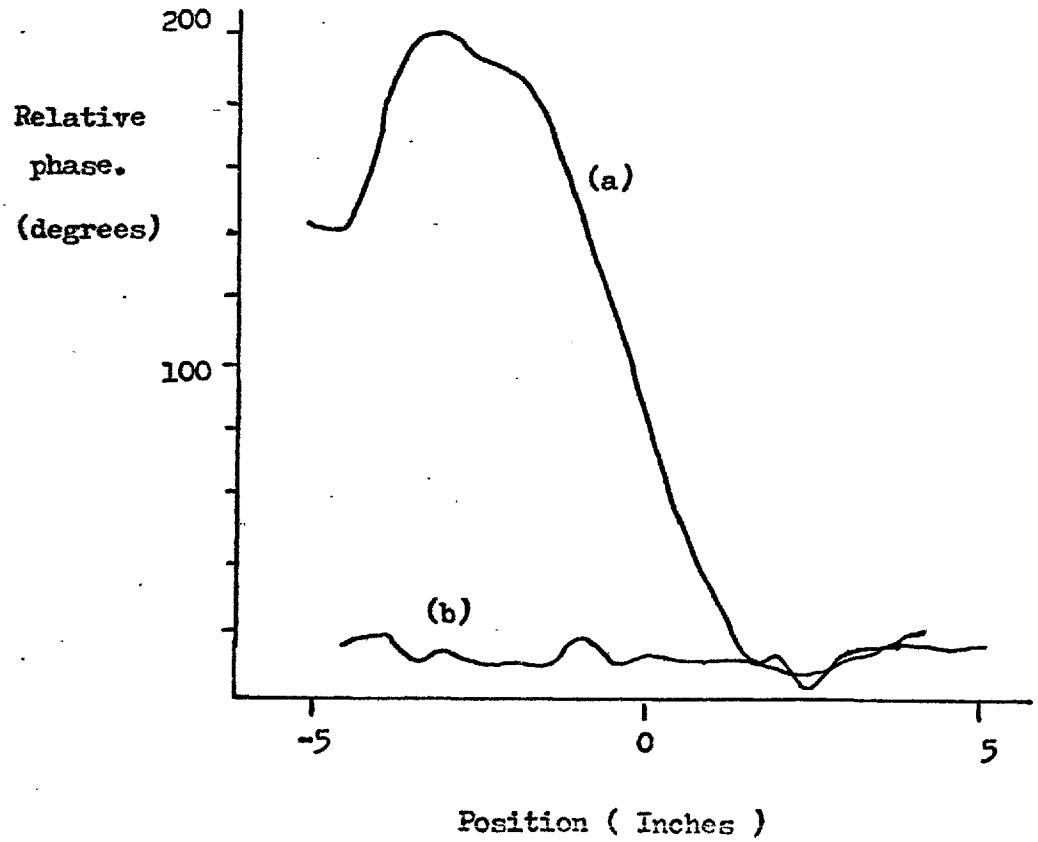

FIGURE 4.2.5. The geometry of the H-shaped slot's currents.

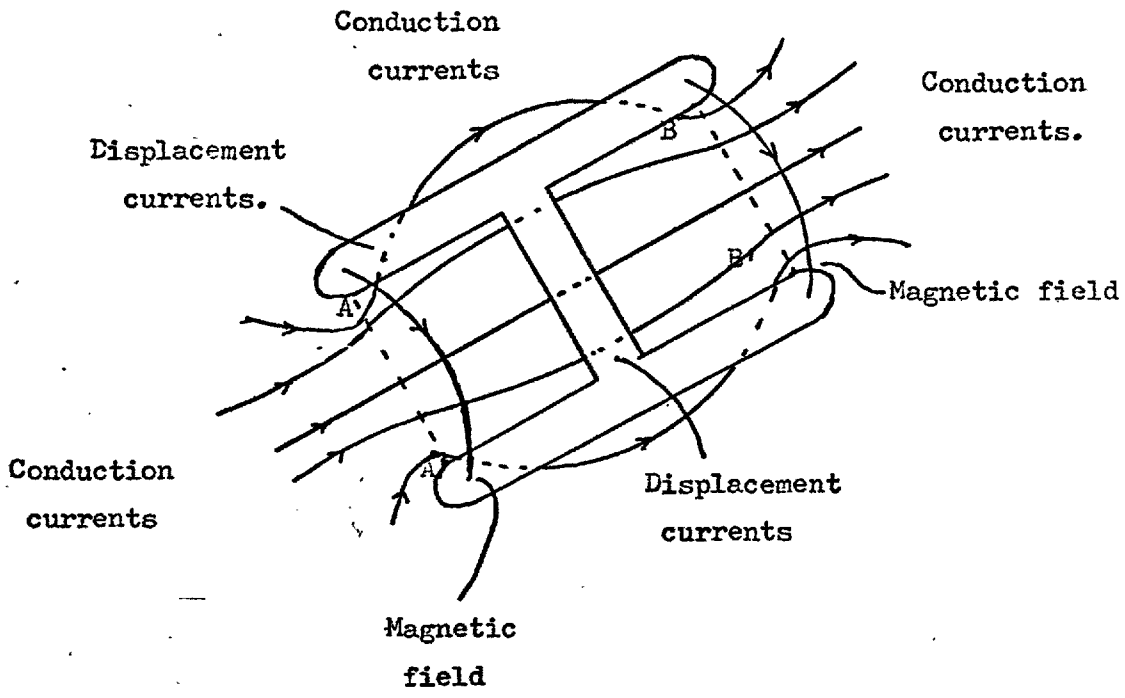

cannot give the magnetic field at a point but only over an area in which rapid variations can occur. The simplest way to improve the measurement was to decrease the area of the loop but this unfortunately reduced the power received and the measurement sensitivity. In this case the field varied rapidly away from the surface but comparatively slowly along the end arms so that a compromise could be achieved using an asymmetric but balanced loop. It was extended along the slot in the direction in which the field varied slowly but reduced in height. The probe used was a rectangular shielded loop araldited to a perspex former of approximate dimensions 1½" x ⅜".

The tangential magnetic field above the metal surface between the end arms of the H-slot was measured using this probe both between the slot extremities and adjacent to the centre limb. The probe was initially placed on the ground plane but the measurements were repeated with its raised $^3/_{16}$" and then $^3/_8$". The results are shown in Figures 4.2.6. and 4.2.7. and they indicate that the field varied rapidly above the surface. With the probe resting on the surface its centre was at a height of $^3/_{16}$" above the ground plane so that measurements should be averaged to this height. On raising the probe $^3/_{16}$" the height at which measurements were made was effectively doubled. The measured field half way between the end arms also doubled indicating that the tangential magnetic field at the surface was negligible. The conduction current must also have become negligible so that it must have been carried predominantly by the metal close to the slot edges. A high current region existed close to the edges of the slot end arms and this was probably responsible for the loss of the H-slot.

FIGURE 4.2.6. The tangential magnetic field across the centre tag of an H-shaped slot measured near the slot ends.

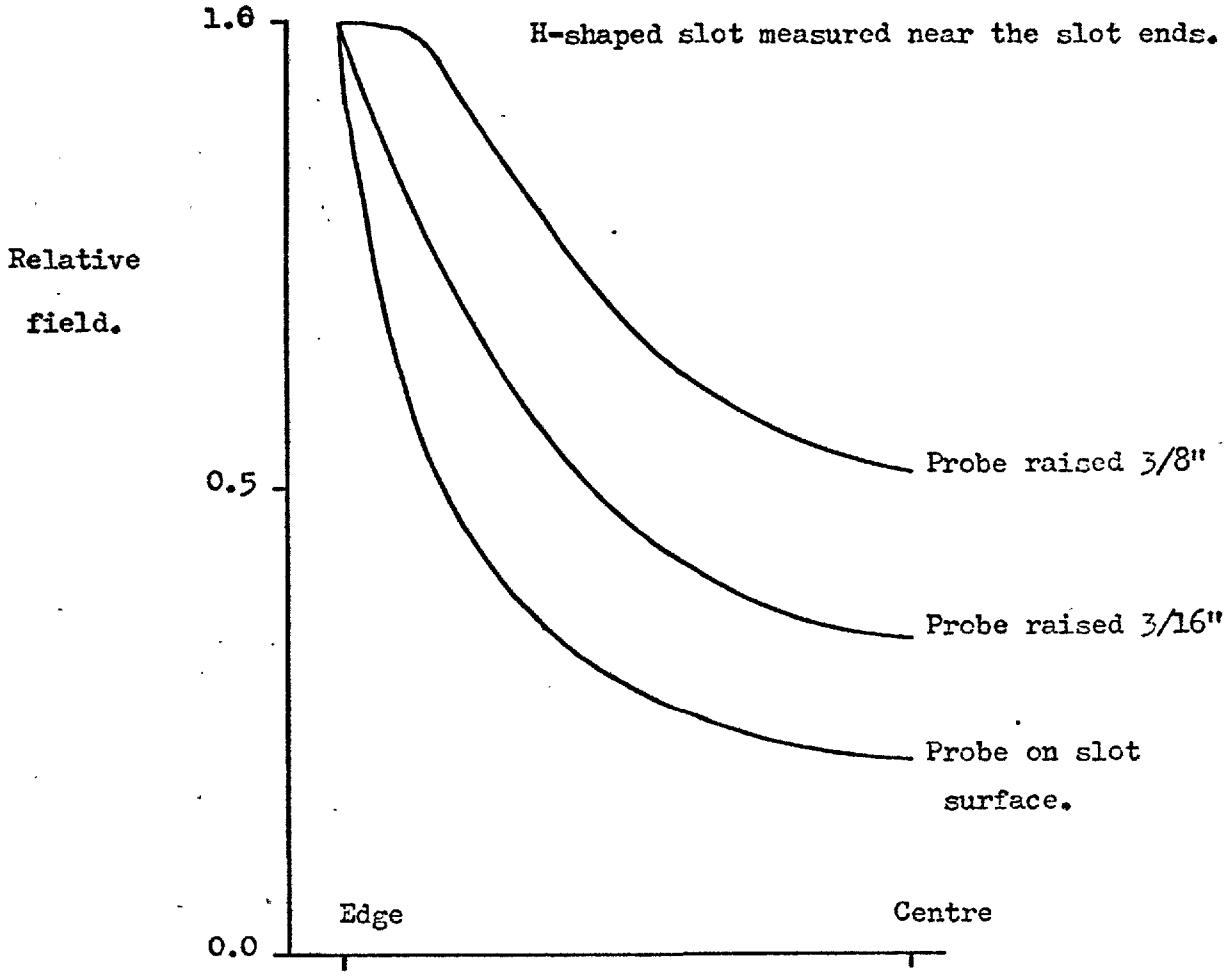

FIGURE 4.2.7. The tangential magnetic field across the centre tag of an H-shaped slot measured near the centre section.

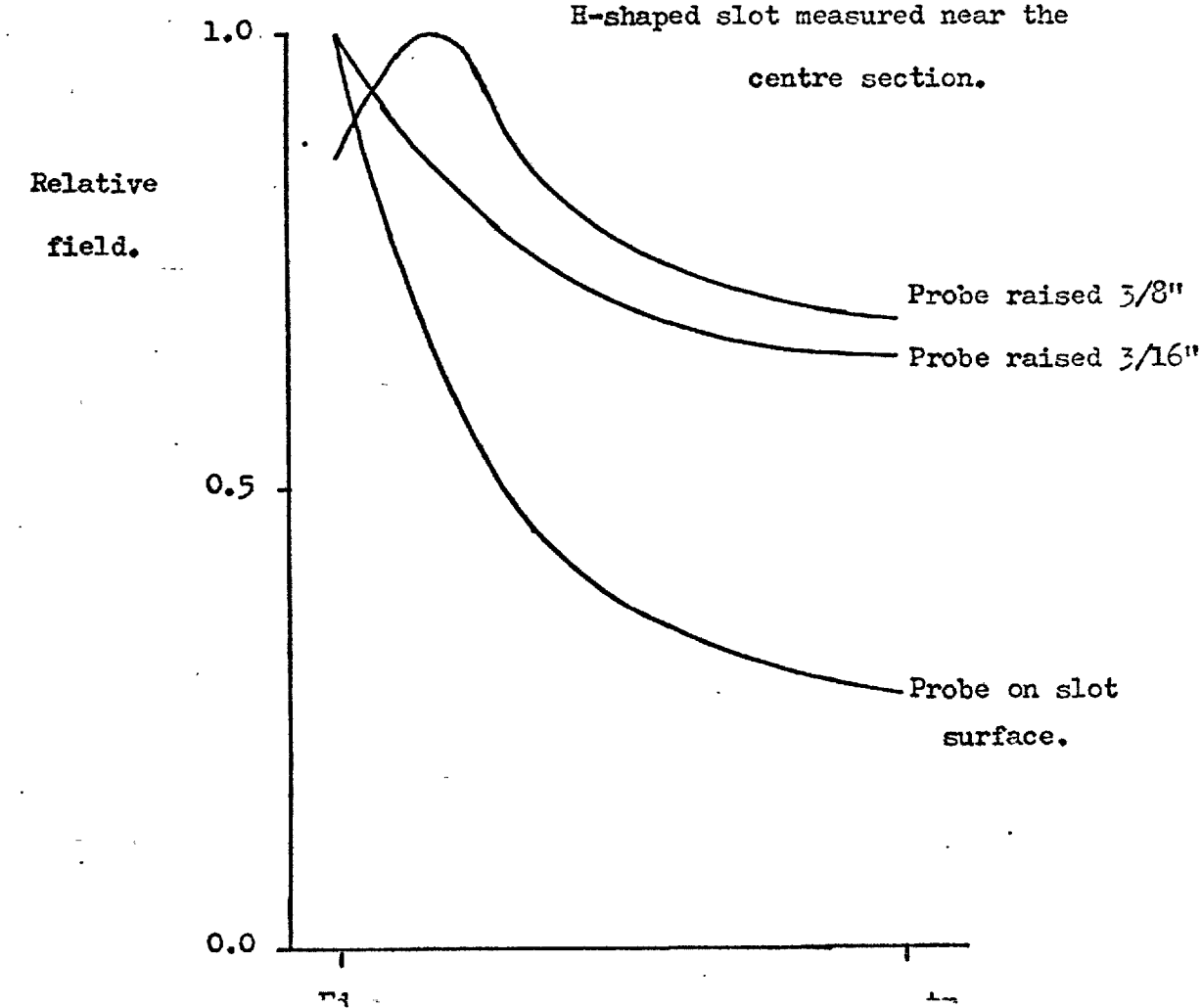

4.3. The H Slot Loss Model

The field measurements on the V.H.F. slot indicated that a conduction current flowed in between the end arms of the H slot, and crossed the slot as a displacement current. The difficulties involved in estimating the surface current density had also been demonstrated. However, the success of Chapter 3 in predicting slot conductance depended upon establishing the voltage across the slot centre. This was known reasonably accurately and could be used to give the displacement current across the slot centre via the relationships:

$$\text{Displacement current} = \frac{\partial D}{\partial t} \qquad (4.3.1a)$$

$$= \epsilon \frac{\partial E}{\partial t} \qquad (4.3.1b)$$

and

$$E = \frac{V}{d} \qquad (4.3.2)$$

where

D = Electric flux density

and ϵ = Permittivity

The differentiation with respect to time introduced an w into the expression, from the assumed time variation of the field so that the displacement current at the slot centre was given by:

$$\epsilon w \frac{V}{d} \qquad (4.3.3)$$

The variation of current along the slot was sinusoidal as demonstrated in deriving the conductance. The current distribution out of the plane of the slot was not known, but a variation given by f(x) was assumed so that it could be integrated to give an effective slot thickness.

The total current flowing across the centre section of the slot was

$$\int_{-\infty}^{+\infty} f(x)dx \int_{-h}^{+h} \epsilon_w \frac{V}{d} \cos ky.dy \qquad (4.3.4)$$

which reduced to:

$$\frac{2\epsilon_w V t_{eff} \sinh kh}{kd} \qquad (4.3.5)$$

where t_{eff} was the effective slot thickness such that:

$$t_{eff} \times f_{max} = \int_{-\infty}^{+\infty} f(x)dx$$

If the field with $f_{max} = 1$ was uniform and entirely confined to the region within the slot, the effective slot thickness would have been its physical thickness but the variation out of the plane of the slot had to be investigated.

The current crossing the plane AA' in Figure 4.2.5. and then the slot end arms was similarly:

$$2t_{eff} \int_{0}^{d_1} \frac{V}{d} \epsilon_w \frac{\cosh kh}{2} \frac{\cos k(\lambda/4 - d_1 + z)dz}{\cos k(\lambda/4 - d_1)} \qquad (4.3.6)$$

$$= \frac{V\epsilon_w t_{eff} \cosh kh}{kd \cos k(\lambda/4 - d_1)} [1 - \sin k(\lambda/4 - d_1)] \qquad (4.3.7)$$

The total conduction current flowing across AA' and the slot was then:

$$\frac{V\epsilon_w t_{eff} Y}{kd} \qquad (4.3.8)$$

where:

$$Y = [2\sin kh + \frac{\cos kh}{\cos k(\lambda/4 - d_1)} - \cos kh \tan k(\lambda/4 - d_1)] \quad (4.3.9)$$

Most of this current crossed the centre limb of the slot and was carried from AA' mostly by the metal close to the end arms of the slot. For a full loss derivation the complete distribution of the field would have been required but this was not readily available and the two extreme cases of the current being carried uniformly by the metal between the slot end arms and entirely by the slot edges were considered. This enabled bounds to be placed on the loss values. It was also assumed that the currents dispersed so rapidly away from the slot that the only significant loss occurred between the slot end arms.

If the current was carried uniformly by the skin depth of metal between AA' and BB' then the cross sectional area involved was:

$$2(2h + t) \cdot \delta \quad (4.3.10)$$

where δ is the skin depth. The resistance of the metal was then:

$$\frac{2d_1}{2(2h + t)\delta\sigma} \quad (4.3.11)$$

σ being the conductivity. The loss associated with the current in the metal was,

$$\frac{V^2 e^2 w^2 t_{eff}^2 d_1 Y^2}{k^2 d^2 (2h + t)\delta\sigma} \quad (4.3.12)$$

but the power radiated by the slot was known to be:

$$\frac{V^2 R_{rad}}{2(60\pi)^2}$$

so that the loss/coupled power could be derived after simplification as:

$$\frac{t_{eff}^2 d_1 \gamma^2}{2R_{rad} d^2 (2h + t)\delta\sigma} \qquad (4.3.13)$$

This result assumed that the current was carried uniformly between the end arms of the slot. The other extreme case assumed the current was carried entirely by the slot edges and resulted in the expression for loss/coupled power of:

$$\frac{t_{eff}^2 d_1 \gamma^2}{2R_{rad} d^2 t\delta\sigma} \qquad (4.3.14)$$

Upper and lower limits to the loss of the uniform H slot have been set. It appeared that as the slot height was reduced the loss would increase because the radiation resistance of the equivalent dipole decreased. Numerical values could be obtained if a value of the effective slot thickness was first obtained. This involved the fringing field and could not be easily investigated by direct means. However, if the exponential time variation assumed throughout was removed then a stationary field resulted. This could be investigated by static techniques such as modelling using a resistive sheet. For two dimensional problems space may be represented by a resistive film introduced between appropriately shaped conductors. When voltages are applied to the conductors a current flows between them in a manner similar to the original high frequency problem. The field within a region can be determined from voltage measurements between two adjacent points.

The fringing slot field was investigated by a similar technique

which used a network of many discrete good quality and nominally identical resistors. If a sufficient number are used they model space in a similar manner to finite difference methods (Silvester (1968)). Using discrete resistors the positions at which voltages are measured become well defined and contact problems are removed.

A quadrant of the slot cross-section was modelled in this manner using a network of 35 x 35 resistors. Most C band slots investigated were cut using a 0.062" diameter tool in the special size waveguide with a wall thickness of 0.040". The slot cross-sections modelled were equivalent to slots 0.020" and 0.060" wide in the special size waveguide. Eight resistors corresponded to the wall thickness. The profiles obtained for the electric field through the centre of the slot are shown in Figure 4.3.1. For the narrower slot the field within its thickness was approximately uniform and the fringing field fell off rapidly. When the slot was widened, the field varies more within its thickness but the fringing field dropped slowly and could be well approximated by an inverse relationship as shown. The fringing field of the narrower slot was not so well approximated by this type of relationship. The inverse behaviour was expected consistent with power spreading out into space. Unfortunately this type of distribution could not be integrated to infinity and give a finite result. The distribution could either be truncated or approximated so that a finite integration result is obtained. It was decided to truncate the distribution one third of a wavelength from the slot. This was an arbitrary figure but at this distance from a complicated slot it became difficult to decide to which branch the field was bound. The distribution was then integrated and the effective thickness found. For the 0.060" wide slot it was found to be five times its physical

FIGURE 4.3.1. A cross-section of the slot field as modelled on the resistive network.

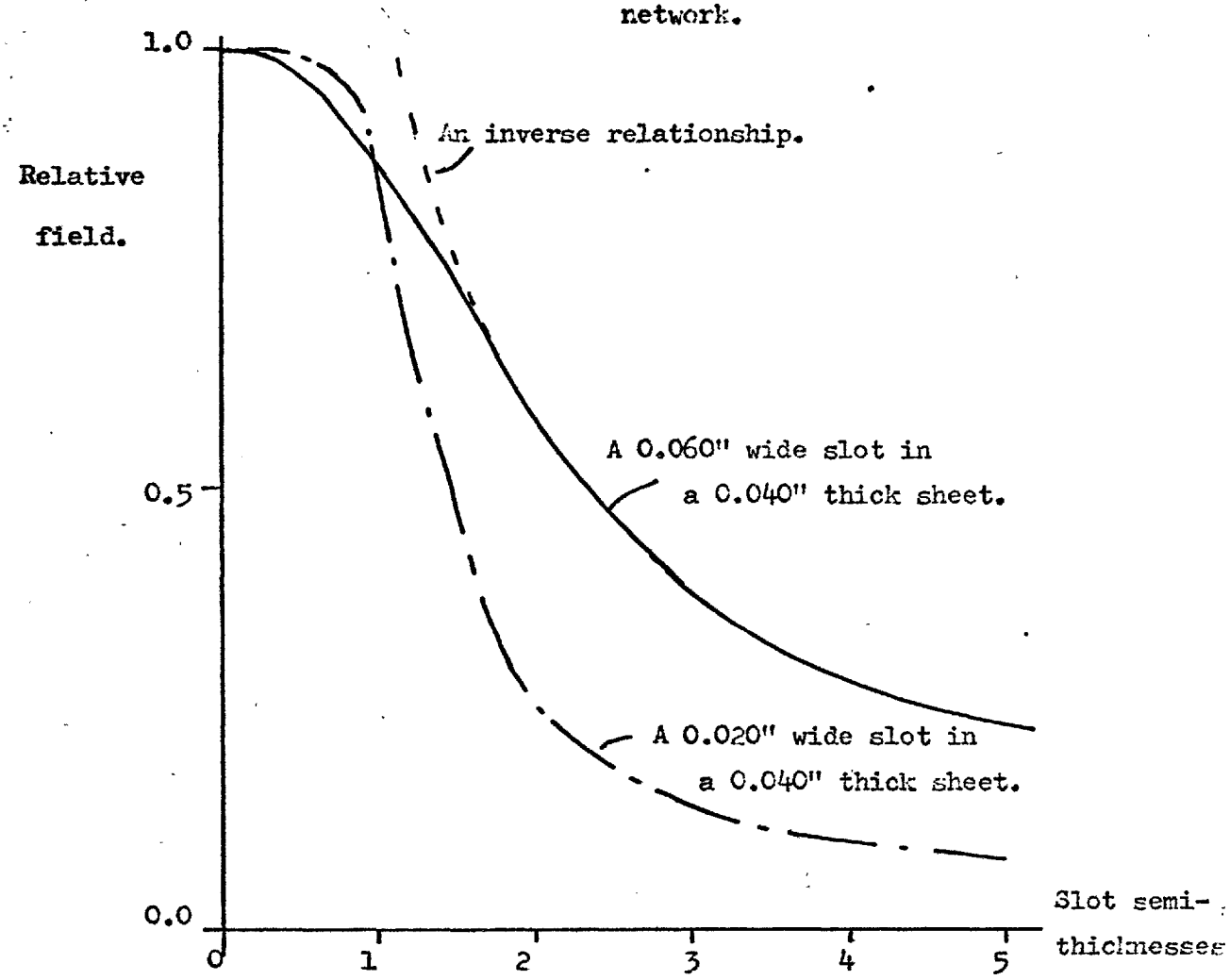

FIGURE 4.3.2. The results of the slot loss model.

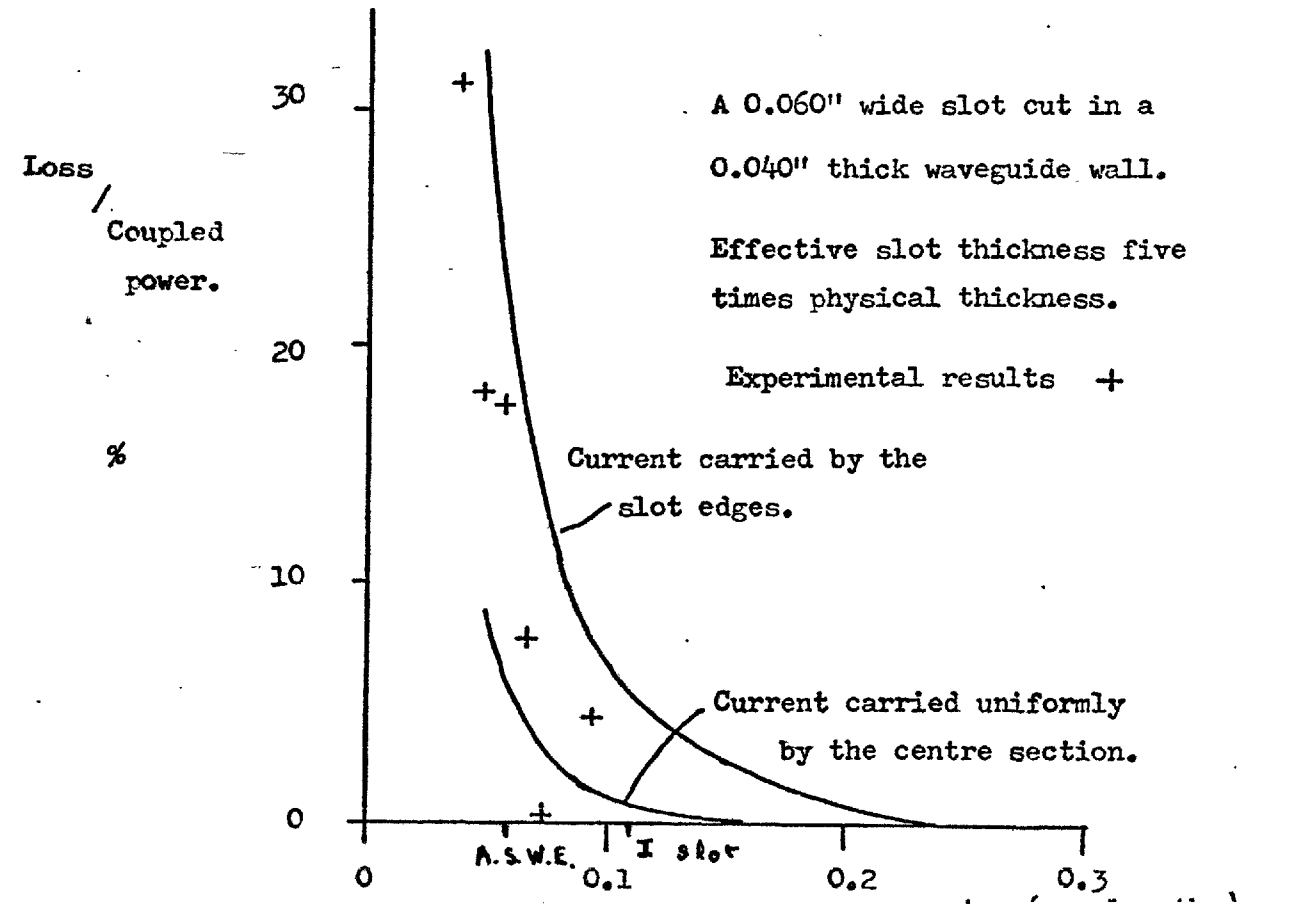

thickness and two and a half times for the 0.020" wide slot. This result was reasonable, as the effective slot thickness was a measure of the total current crossing the slot, or with constant electric field across the slot a measure of its characteristic impedance. This has been shown experimentally to be proportional to the square root of the slot width. The slots considered had widths in the ratio of three to one and should have had impedances in the ratio of the square root of three to one. In fact the truncation appeared to be appropriate and it gave impedances in the ratio of two to one. The effective slot thickness was used in calculating the upper and lower bounds to the slot loss shown in Figure 4.3.2.. The Figure also shows experimental results for I-shaped slots. When the lengths of the end arms were similar there was little difference between the I and H shaped slots. The curves showed that the loss rose rapidly if the slot height was reduced. The experimental results lie between the two extreme cases presented showing that the general description of loss was substantially correct, with the current being predominantly carried by the slot edges. The dimensions of the full waveguide height I-shaped slot is indicated and the corresponding loss was approximately five percent of the coupled power. This was thought to be acceptable. The height of A.S.W.E.'s H slot is shown. The corresponding loss for uniform 0.060" wide slots was about fifteen percent of coupled power. However, the H slot's centre section was centre loaded to allow rotation. Reducing the slot width to 0.020" reduced the effective thickness to a half of its previous value and would have increased the loss by a factor of two and a quarter. The model predicts a loss of 34% of coupled power for A.S.W.E.'s H-shaped slots, compared to their measured value of 37.4%.

The loss associated with the I and H shaped slots has been successfully modelled, despite the lack of knowledge concerning slot impedance and current distributions. In these respects the model is certainly capable of improvement. However, the loss has been shown to be critically dependent on the slot height and width. The I and H slot geometries differ in these two important aspects. The high loss of the H-shaped slot has been accounted for and the loss of the full height I-shaped slot has been shown to be much lower at an acceptable value of about 5% of coupled power. The full height I-shaped slot appears to be a most useful array element.

CHAPTER 5

THE DESIGN AND PERFORMANCE OF LINEAR WAVEGUIDE ARRAYS USING THE I-SHAPED SLOT

5.1. Introduction

The last two chapters indicated that the I-shaped slot seemed ideally suited for use in large two-dimensional waveguide arrays. However, the design of such an array was expected to include many components of mutual coupling between all pairs of slots. An intermediate design was that of a single slotted waveguide array, in which mutual coupling needed only to be considered in a single direction; it was thought that it could be minimised. The problem was thus reduced to producing a specified radiation pattern from a linear aperture distribution and required accurate control of the individual slot conductances.

Initially an eight slot array was built and tested but all the problems associated with a long array such as the accumulation of errors were not present. Later a thirty slot linear array was made.

5.2. The Radiation Pattern-Aperture Distribution Relationship

It is well known in antenna theory that the far field radiation pattern of the antenna and the aperture field distribution are Fourier transform pairs. In reflector antennas the far field patterns are basically the diffraction patterns of the feed modified by the reflector. Control of the far field depends upon the design of the feed and the range of shapes of the far field patterns are limited. For a linear array individual control of the coupling at each slot enables any distribution to be specified, and more care was needed to designate the pattern of

an individual array. The compromise that had to be made was as usual between the antenna gain and sidelobe level but the shape of the sidelobe envelope was also a variable. A uniform amplitude and phase aperture distribution gave the maximum forward antenna gain but produced large sidelobes. The sidelobes limited the angular discrimination of the antenna and the range of the radar system as a high threshold level had to be set to avoid false echoes. Any other amplitude distribution reduced the antenna gain and radar range, although if certain distributions are used the sidelobe level can be reduced. These distributions generally involved limiting the power at the aperture edges so that little diffraction occurs. Two classes of functions were generally used for the aperture amplitude distributions one involved sinusoids and the other polynomials. The usual orthogonal polynomials used were the subclass of Chebyshev polynomials, Dolph (1946) showed how they could be used to give a uniform sidelobe level. However, polynomials whose order was at least equal to half the number of array elements were required and as few Chebyshev polynomial table give coefficients greater than twelve (Abramowitz and Stegren 1964) for most users designs are limited to twenty four elements. For larger linear arrays Van der Mass (1954) noted that the discrete functions could be well described by a continuous function, and this work was persued by Taylor (1955). He obtained a class of functions which gave for continuous distributions equal amplitude sidelobes.

For radars designed to operate in a hostile electromagnetic environment uniform amplitude sidelobes might not be the best compromise and more discrimination against wide angle jamming could be obtained using a decaying sidelobe structure. Sinusoidal aperture voltage distributions of the form cosine^n are then usually used. The higher

the value of n the more power is concentrated at the centre of the amplitude distribution with a consequential reduction in both the antenna gain and sidelobe level. The properties of this type of distribution are well known, and were tabulated by Barton and Ward (1969). For most practical systems a value around two is selected for n being a good compromise between sidelobe level and gain. For linear slotted arrays the distribution is often placed on a small pedestal because slots can not be made with the small couplings required near the feed end. For a $\cos^2$ distribution it happens that a $\frac{1}{7}$ pedestal reduces the first and largest sidelobe at the expense of others so that a $\frac{1}{7} + \frac{6}{7} \cos^2$ voltage aperture distribution is suitable for linear slotted array use.

5.3. The Eight Slot Array

Some of the problems associated with slotted arrays were initially investigated using an eight element waveguide array of I-shaped slots. A $\frac{1}{7} + \frac{6}{7} \cos^2$ voltage distribution was used for this array simply because it required a large range of conductances.

It was proposed that the array should be operated with a cross-polarisation suppression grid. If this simulated the waveguide 12 branch arm used to measure slot loss the resulting slot and baffles were likely to be low loss. In addition, for low coupling slots, the resonance would be maintained. The cross polarization grid consisted of bars placed either side of the slot so that it coupled into a parallel plate region. The separation of the plates was established as the narrow dimension of waveguide 12 or 0.872 inches. It was considered that if the parallel plate region extended at least three inches either side of the slot this would be sufficient. The only

other dimension to be established was the depth of the parallel plate region. Accordingly a series of bars were made so that baffles of different heights could be made up using different combinations, and investigated experimentally.

It was found by rotating a small horn in front of the slot that baffles less than half an inch high did not sufficiently cut-off the cross polarisation. A series of measurements of phase shift past the slot (Table 5.3.1.) indicated that increasing the baffle height beyond half an inch decreased the effective bandwidth of the slot. The total phase shift associated with any slot remained constant but it occurred in a smaller bandwidth. From measurements on individual slots it appeared that the optimum baffle height was half an inch. The derivation of this dimension ignored the other function of the baffles that of reducing coupling between slots. However, at 5.7 GHz half an inch was approximately a quarter of a wavelength so ditches of this depth were introduced between alternate slots of a single waveguide array.

It was found experimentally that fitting baffles half an inch high to a series of I-slots altered their frequency of operation on average by + 158 MHz. (3%) The other modification to the basic I-shaped slot required for incorporation in an array, was the fitting of a 0.010" thick layer of P.T.F.E. to the outside of the waveguide as weather protection. This was expected to make the slot appear larger and the resonant frequency of a batch of slots was decreased on average by 307 MHz.. (6%) Bailey (1970) investigated dielectric covered straight slots and this result was consistent with his finding. The combined effects of the baffles and P.T.F.E. produced an average frequency shift of - 113 MHz (2%) and only small changes in the slot conductances.

The eight slot waveguide array was then designed. A waveguide

TABLE 5.3.1. The gradient of the phase shift past a slot with frequency for various baffle heights.

Baffle height. INCHES	Phase gradient. °/MHZ.
0.00	0.057
0.25	0.048
0.50	0.060
0.67	0.089
1.00	0.118

FIGURE 5.3.1. An array of N radiating slots.

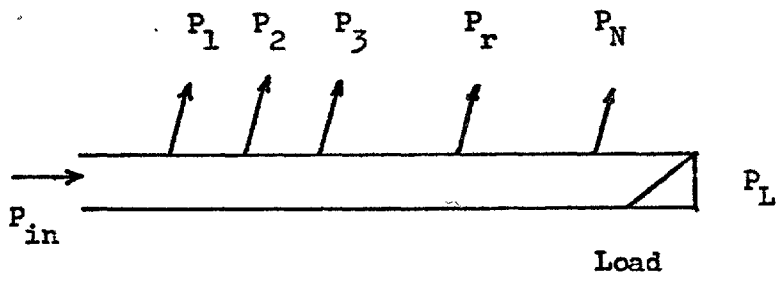

TABLE 5.3.2. The required power division with 8 slots to approximate a $(1/7+6/7\cos^2)$ distribution and waste -6 db in the load.

Slot No.	Required coupling. -db	Power past slot. %
1	22.86	99.48
2	16.27	97.13
3	9.35	85.84
4	5.67	62.56
5	4.29	39.28
6	5.41	27.99
7	10.76	25.64
8	16.94	25.12

with N radiating slots was considered as shown in Figure 5.3.1.. For a matched waveguide the input power P_{in} was equal to the sum of the load power P_L and the radiated powers P_r so that:

$$P_{in} = P_L + \sum_{r=1}^{N} P_r \qquad (5.3.1)$$

assuming no reflected power. P_r was a specified function of position f(r) so that the power radiated at slot r should be:

$$P_r = \alpha \times f(r) \qquad (5.3.2)$$

where α was a normalising constant to be determined.

$$\sum_{r=1}^{N} P_r = \sum_{r=1}^{N} \alpha \times f(r) = P_{in} - P_L \qquad (5.3.3)$$

so

$$\alpha = \frac{P_{in} - P_L}{\sum_{r=1}^{N} f(r)} \qquad (5.3.4)$$

$$\alpha = \frac{(1 - \eta)P_{in}}{\sum_{r=1}^{N} f(r)} \qquad (5.3.5)$$

where

$$\eta = \frac{P_L}{P_{in}} \qquad (5.3.6)$$

for unity input power the power radiated at each slot should have been:

$$P_r = \frac{(1 - \eta)}{\sum_{r=1}^{N} f(r)} f(r) \qquad (5.3.7)$$

At slot r the power radiated was equal to:

$$\frac{g_r}{1 + g_r} \quad x \quad \text{Power incident on the rth. slot} \qquad (5.3.8)$$

The previous assumption of a matched array implied that $g_r \ll 1$ so that the rth. slot the power radiated was:

$$g_r \quad x \quad \text{Power incident on rth. slot}$$

$$= g_r \; x \; \prod_{n=0}^{r-1} (1 - g_n) \qquad (5.3.9)$$

with $g_o = 0$, so that:

$$g_r = \frac{(1 - \eta) f(r)}{\sum_{r=1}^{N} f(r) \prod_{n=0}^{r-1} (1 - g_n)} \qquad (5.3.10)$$

In this form the required conductances were programmed for computer evaluation. Initially the values of f(r) were determined by definition, and subsequently normalised and summed. The conductances were then obtained sequentially. This was done for a range of values of load powers and it was found that to reduce the coupling of the fifth slot below - 4 dB, the highest coupling available from I-shaped slots, the power in the load had to be at least a quarter of the input power (- 6 dB). The required power division was then as shown in Table 5.3.2.. The only remaining design variable was the slot spacing. Slots are normally placed close to half a wavelength apart so that when alternate slots of opposite hand are used a uniform phase front results. If the slots are spaced half a guide wavelength apart the conductances of all the slots can be transformed to the first slot by the half

wavelength 1:1 transformers. The input V.S.W.R. is then far from unity and related to the design power in the load, as indicated in Figure 5.3.2.. The figure also shows that a small departure from a half a guide wavelength spacing rapidly reduces the input V.S.W.R.. The slots when transformed to the first slot are more uniformly spaced around the Smith Chart. Changing the slot spacing from half a guide wavelength moved the radiating beam away from broadside. For spacings less than half a guide wavelength the beam moved towards the feed. For spacings greater than half a guide wavelength the beam moved towards the load as shown in Figure 5.3.3.. For spacings less than half a wavelength the change in the beam position or squint varied more rapidly with frequency. This was considered to be a desirable feature of an experimental array in which the variation of squint with frequency was to be investigated. Accordingly the slot spacing was set to be less than half a guide wavelength. Figure 5.3.2. indicated that for a slot spacing of 1.42" at 5.7 GHz a good match was obtained. The match was preserved at lower frequencies to be better than 1.2 and at higher frequencies up to 5.9 GHz. The squint of the beam at 5.7 GHz was predicted using Figure 5.3.3. as 8.3° towards the feed.

The individual slots of the array were then specified from extrapolated results of attenuation past individual slots. The array was then made together with nine half inch high removable baffles. Measurements of the attenuation past individual slots when that slot alone radiated were made with, and without, baffles and with, and without, P.T.F.E.. The attenuation past the slots with all the slots radiating was also measured. The results are shown in Table 5.3.3.. The Table shows the peak attenuation past each individual slot when it alone radiated both with and without baffles. It should be noted that there

FIGURE 5.3.2. The input V.S.W.R. of an 8 slot array with (1/7+6/7 cos) voltage illumination function and -6 db of input power in the load.

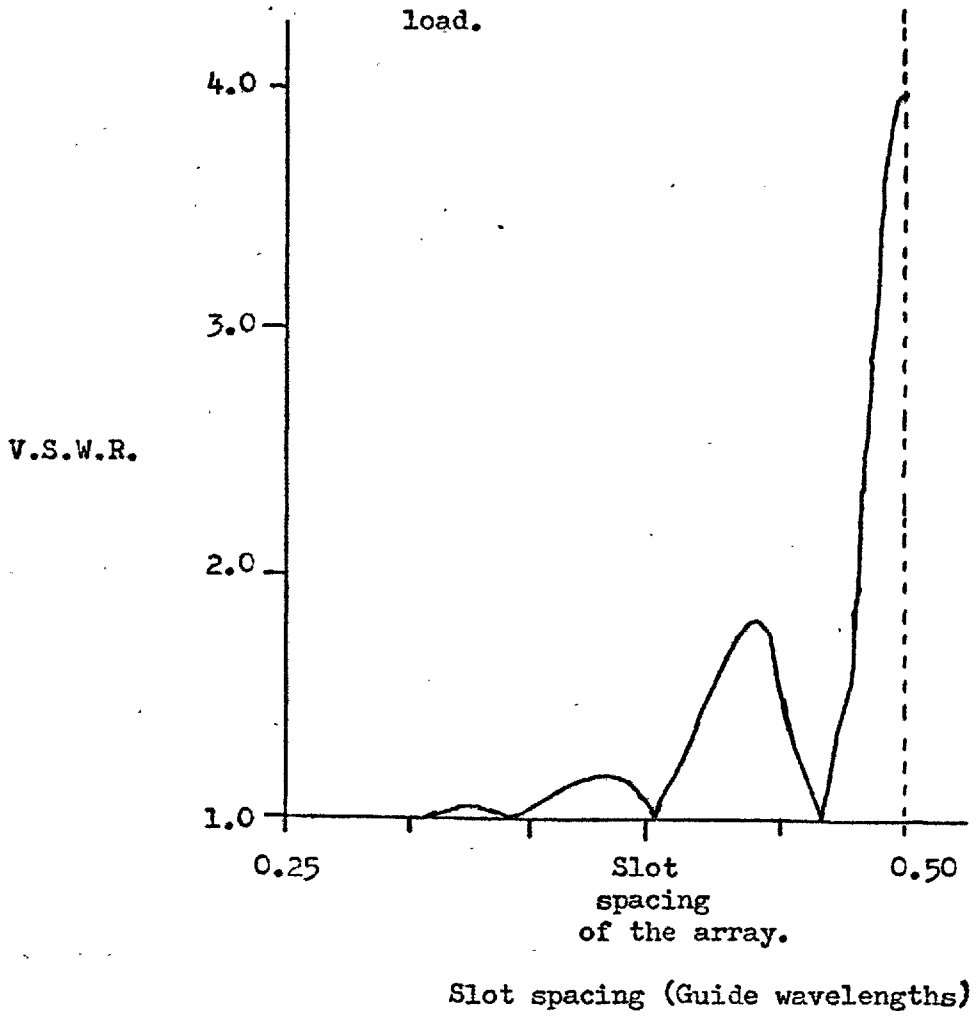

FIGURE 5.3.3. The variation of squint with slot spacing for arrays cut in the special size waveguide and operated at a frequency of 5.70 GH

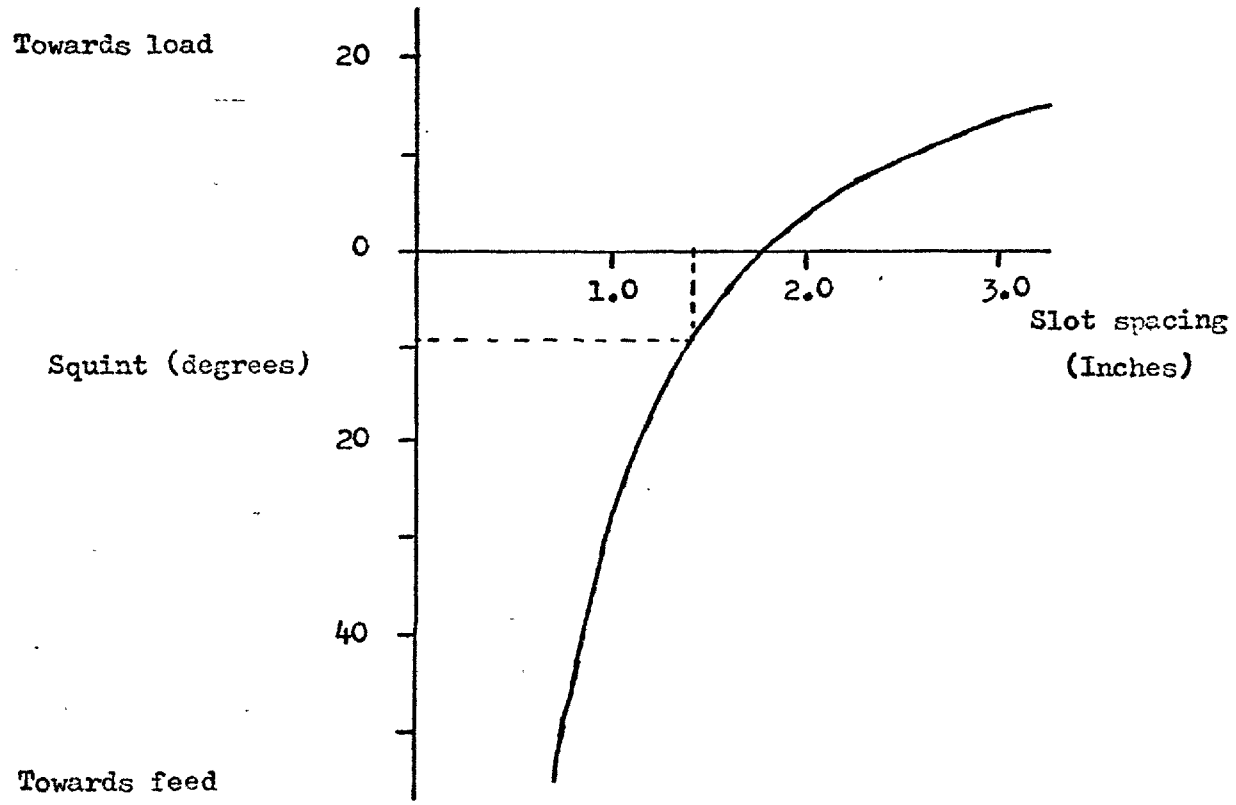

TABLE 5.3.3. The individual peak attenuations past each slot of the eight slot array.

Slot No.	Attenuation past individual slots alone db	
	Ground plane	Baffles
1	0.05	0.05
2	0.10	0.09
3	0.41	0.53
4	1.33	1.29
5	2.34	2.41
6	1.35	1.33
7	0.39	0.34
8	0.07	0.09
Total =	6.04	6.13

The peak attenuation past all 8 slots radiating in a ground plane =11.0 db

The peak attenuation past all 8 slots radiating with baffles = 5.28 db

was a dispersion of 50 MHz, in the frequencies of peak coupling. The sum of the component peak couplings radiating without baffles above a ground plane was 6.04 dB but when all the slots radiated a peak attenuation of 11.00 dB was measured. Mutual coupling between the slots was responsible for this increase in conductance or, incremental conductance. The baffles were however designed to reduce mutual coupling along the array. The sum of the peak component attenuations with the baffles fitted was 6.13 dB and the peak attenuation past the slots with them all radiating was only 5.28 dB. The discrepancy between the two figures was reasonable and it was due to the dispersion between the peak attenuations. The baffles appeared to be successful at reducing mutual coupling.

This was further investigated using two sections of waveguide fitted with short circuits. Slots were cut in the narrow wall of each section at the open circuit position nearest the short and the waveguide sections arranged in line as shown in Figure 5.3.4.. Ground plane and baffles could be fitted and the slot spacing was adjustable to the values found in the eight slot array. A Hewlett Packard Model 8410A network analyser was used to measure the radiative coupling between the slots.

The coupling was investigated for both coupling between slots of the same hand (⌐¬) and slots of opposite hand (⌐⌐). The results indicated that coupling between slots of either band had the same magnitude but the change of hand produced a phase reversal as expected. Results of coupled power for two slots of opposite hand and to the dimensions of the sixth slot of the eight slot array are shown in Figure 5.3.5. The results of coupled power both with and without baffles are shown. The reduction of coupling for adjacent slots was only 4 dB when the intervening baffle was introduced. This was probably

FIGURE 5.3.4. The experimental arrangement used to measure mutual coupling along a linear array.

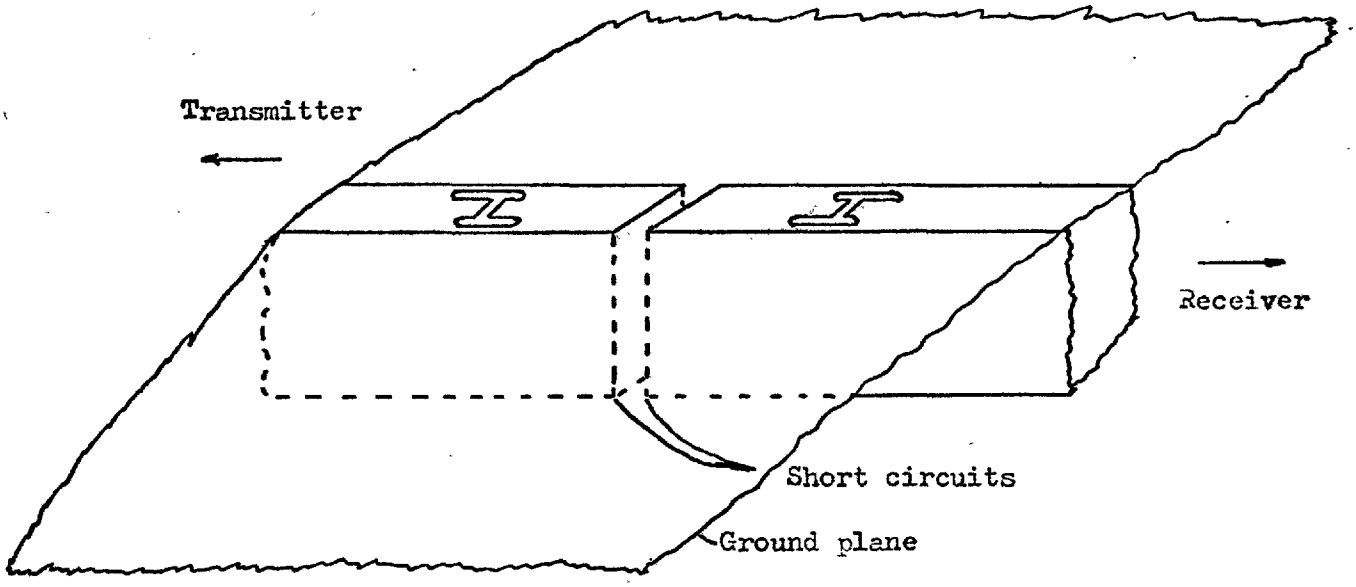

FIGURE 5.3.5. The measured coupling between similar open-circuited slots.

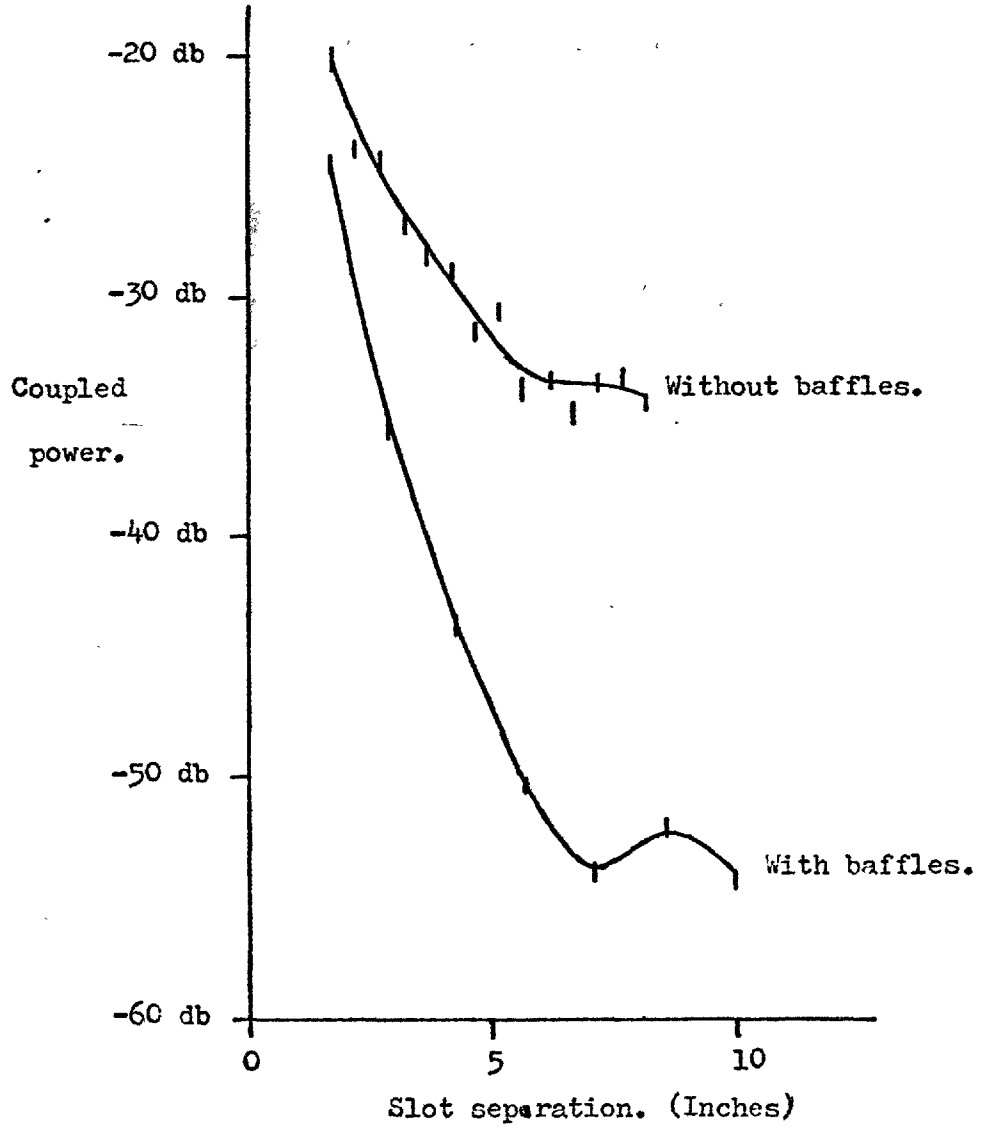

the difference in coupling between slots in a ground plane and open ended parallel plate waveguides at the same separation. The baffles produced a much greater reduction in the coupling between widely-spaced slots, and this was reasonable as two baffles fitted between coupled slots was equivalent to one choke groove separating them. Further separation introduced more choke grooves and further suppressed coupling.

The measurements past individual slots and past the whole array indicated that mutual coupling was a serious problem in linear arrays without baffles but that when fitted they greatly reduced its effect. The substantial reduction in coupling was between non-adjacent slots.

Far field radiation patterns of the eight slot array have been plotted however, it was more enlightening and convenient to measure near field patterns as errors associated with individual slots were revealed. A small rig was made to perform these measurements. It consisted of a half wave dipole fitted with a small reflector and mounted on a perspex trolley. The trolley slide, in front of the array, on P.T.F.E. mountings along a "Speediframe" track. A motor, gearbox and chain-drive were used to move the trolley. A helical potentiometer was geared to the main chain wheel's shaft and gave an output voltage proportional to the trolley's position. This was used to drive the x-axis of an x-y plotter. The output from the dipole was connected to the network analyser and thence to the y axis of the plotter. In this manner aperture phase and amplitude plots were obtained.

A typical plot is shown in Figure 5.3.6.. It indicated that a linear phase front was obtained over the length of the array. The phase gradient corresponded with the squint of the beam. The amplitude distribution was similar to that required but showed some error because the slot conductances were not sufficiently accurately specified. The

FIGURE 5.3.6. The aperture amplitude and phase distribution of the 8 slot array fitted with baffles and P.T.F.E. and operated at a frequency of 5.60 GHZ..

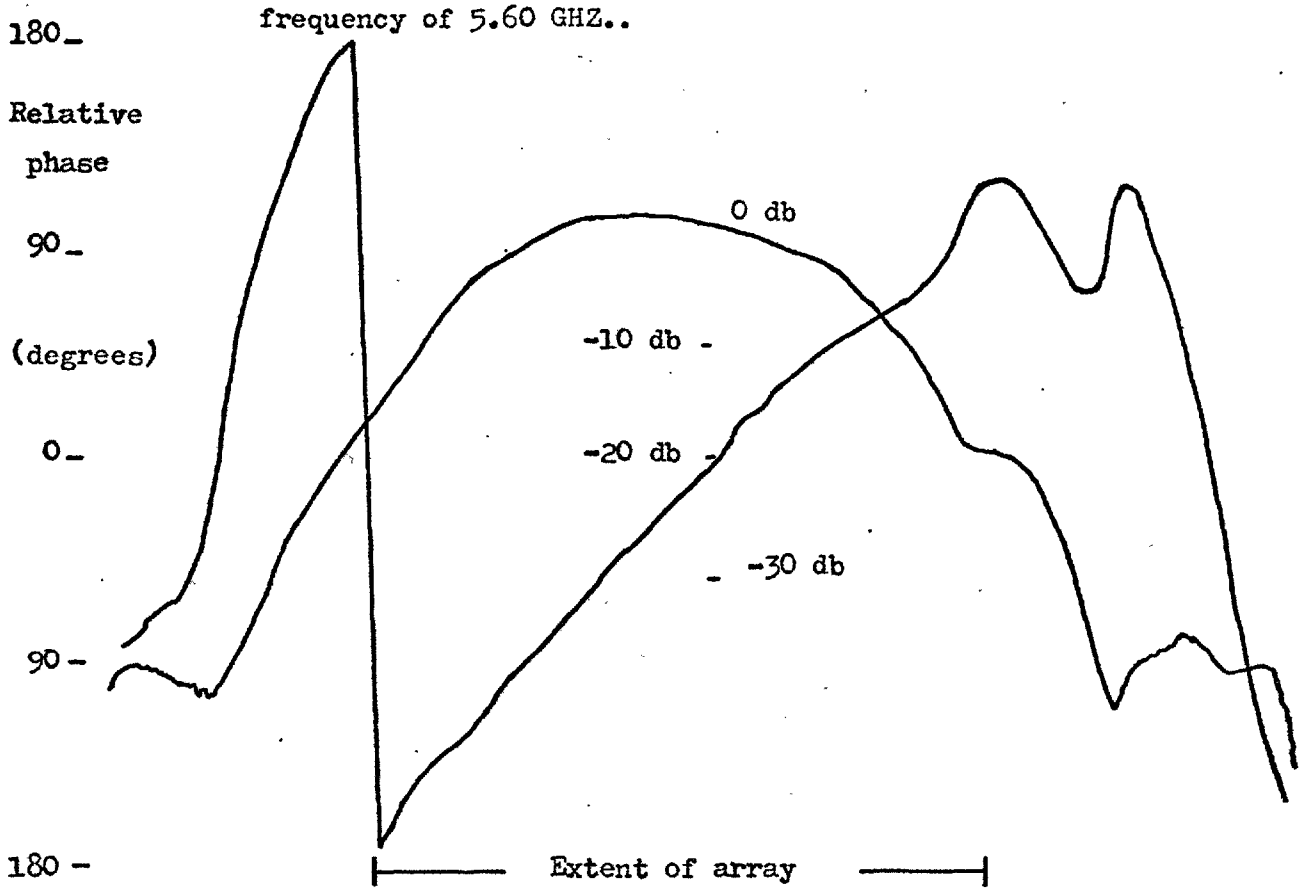

FIGURE 5.3.7. The far field radiation pattern of the 8 slot array with baffles and P.T.F.E. at 5.60 GHZ.

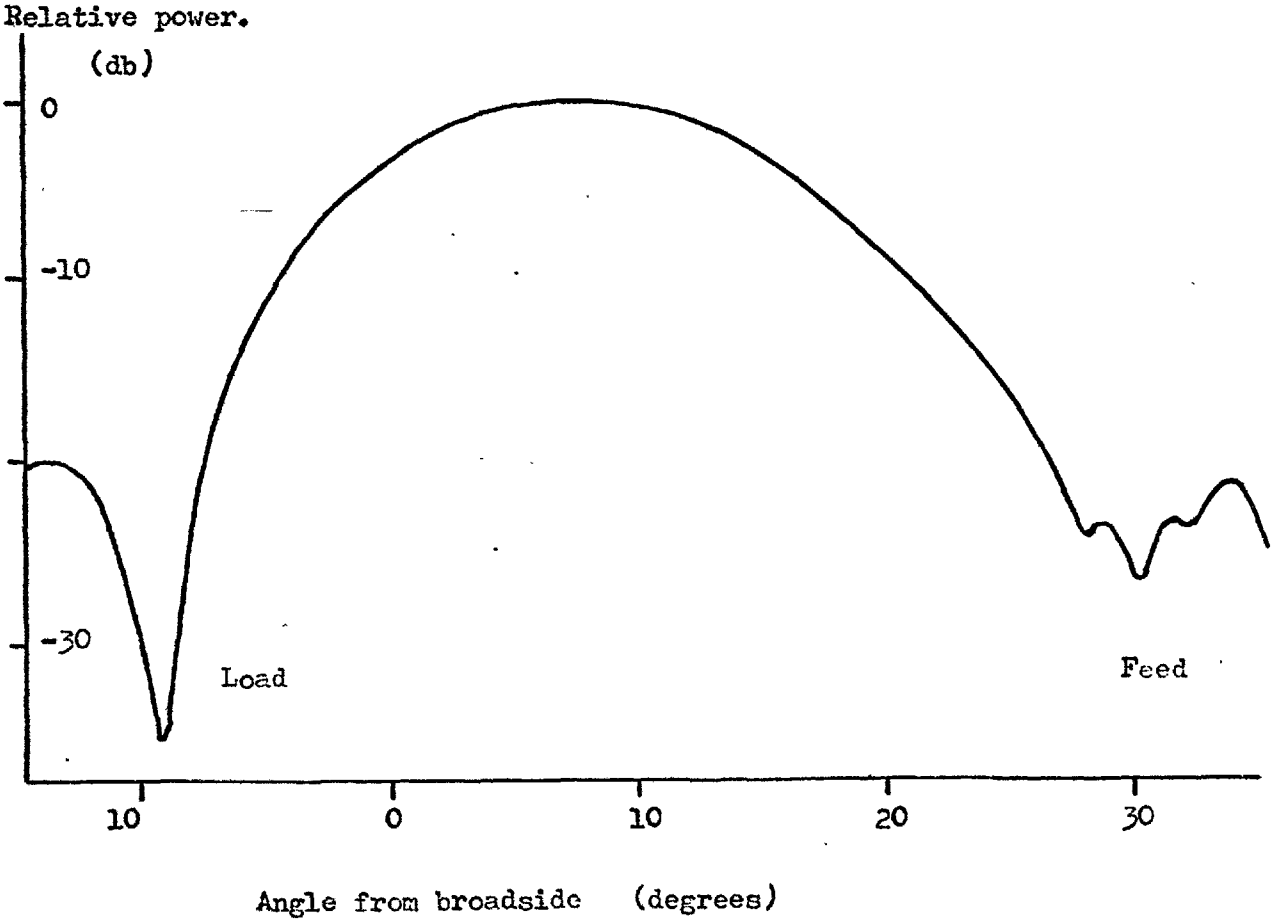

amplitude error was reflected in the corresponding far field pattern, which is shown in Figure 5.3.7.. This pattern was plotted using A.S.W.E.'s facilities.

Aperture distributions were obtained over a band of frequencies for the array both with and without baffles and P.T.F.E.. From these plots the variation of squint with frequency was obtained. The results for the array fitted with just a ground plane are shown in Figure 5.3.8. and for the array fitted with baffles and P.T.F.E. in Figure 5.3.9.. These curves should have been smooth for arrays of slots with no reactance associated with them. The phase behaviour of individual slots was similar independently of whether they were fitted with baffles or P.T.F.E.. For coupling over a ground plane there must have been a substantial reactive component associated with mutual coupling which greatly affected the frequency scanning performance of the array.

5.4. The Thirty Slot Array

The results obtained for the eight slot array were considered to be good but some of the problems associated with long arrays were not so pronounced with shorter arrays. A short array does not require the same range of couplings nor do manufacturing errors accumulate so badly in a shorter length. Accordingly it was decided to manufacture one larger array. After discussion it was found that a waveguide four feet long was the longest that could readily be coped with, and this was sufficient to accommodate an array of thirty slots. The aperture voltage distribution selected for the array was $(\frac{1}{7} + \frac{6}{7}\cos^2)$ as previously described. It theoretically should have produced sidelobes at least 36 dB below the level of the main beam. The required power division at each slot was evaluated for differing amounts of power

FIGURE 5.3.8. The variation of squint with frequency for the 8 slot array fitted with a ground plane.

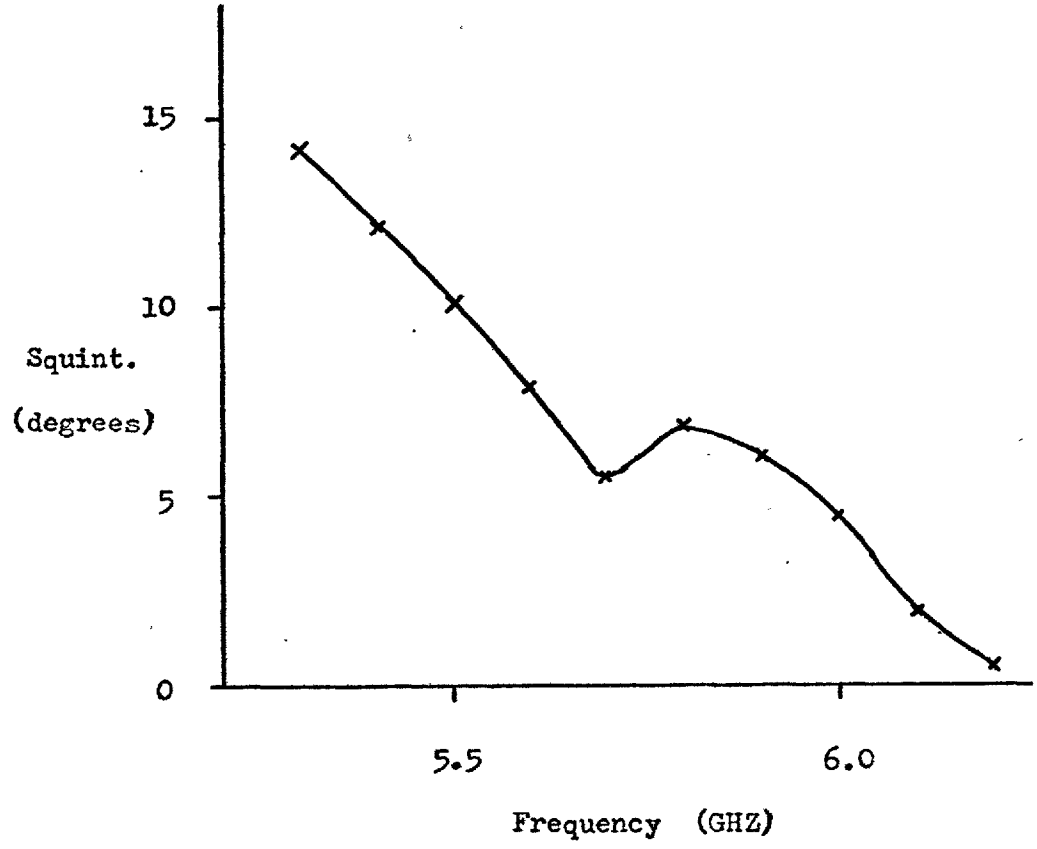

FIGURE 5.3.9. The variation of squint with frequency for the 8 slot array fitted with baffles and P.T.F.E..

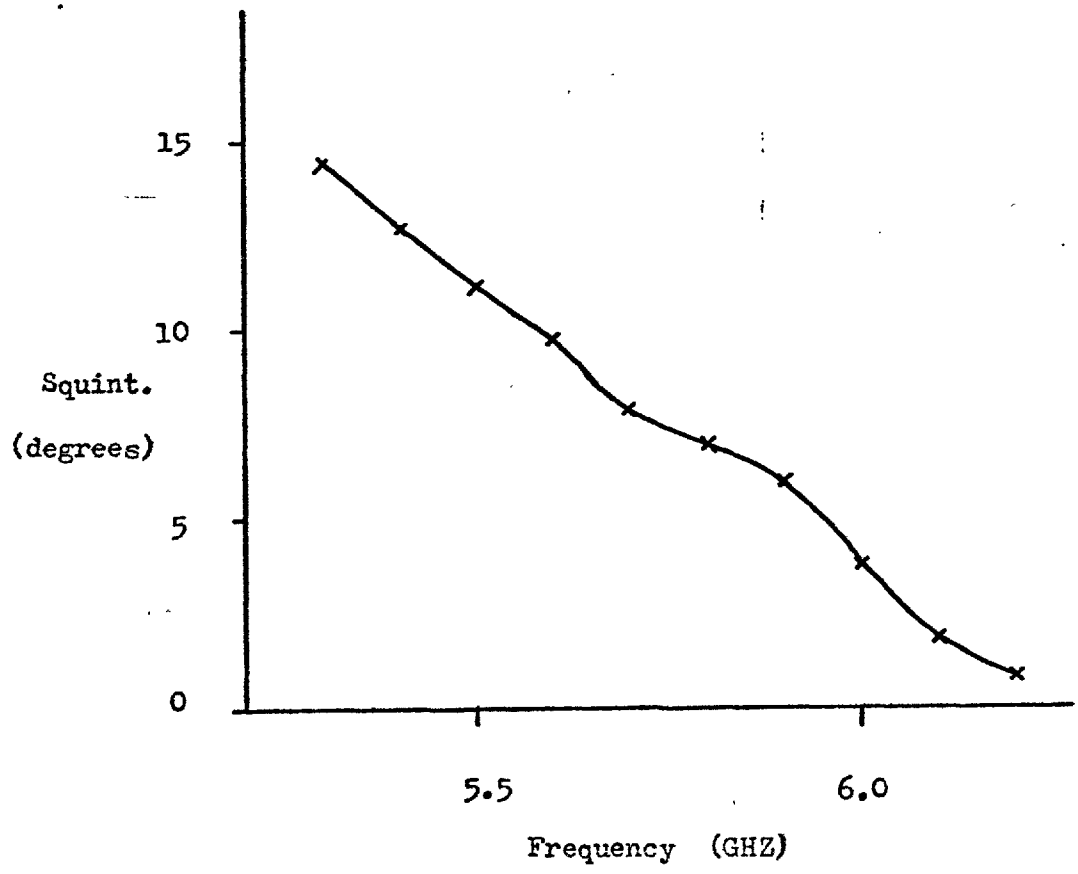

deposited in the load. From the computed results shown in Figure 5.4.1. the amount of power to be wasted in the load was minimised consistent with the range of coupling required. The range of coupling available from I shaped slots was approximately - 4 dB to - 30 dB. A choice of - 20 dB of input power wasted in the load required a coupling range of from - 5 dB to - 27 dB and this value was selected.

The required values of coupling were converted to shunt conductances assuming a perfect match beyond each slot. The shunt conductances were then placed across a transmission line and the input V.S.W.R. computed for various slot separations. The result is shown in Figure 5.4.2.. For a slot spacing of half a guide wavelength there was as expected a large resonant mismatch. At smaller spacings the V.S.W.R. was closer to unity and at spacings less than 0.45 of a guide wavelength it was never greater than 1.02. From Figure 5.4.2., a slot spacing of 1.500" ($\equiv 0.42\ \lambda_g$) was selected. For this spacing a good input match was maintained over a reasonable bandwidth (7%) around the design frequency of 5.70 GHz. The beam squint was of the order of 6° towards the feed.

The assumption of a perfect match beyond each slot was then tested. Starting with the load impedance, the impedance beyond each slot in turn was calculated by transforming back along the appropriate length of transmission line. The required conductance at each slot was thus calculated allowing for the actual impedance beyond it. In terms of coupling coefficient this correction was maximum and approximately - 0.5 dB around slots numbered 16 and 26 from the feed end. This was reasonable as maximum couplings were beyond slot 16 and there were only a few slots and little power beyond slot 26.

The baffles of the eight slot array were of cross-sectional dimensions 0.548" x 0.500", with slot spacings of 1.420". For the thirty slot array the slot spacing was increased to 1.500" for simplification

FIGURE 5.4.1. The variation in required coupling with position for slots of the thirty element array.

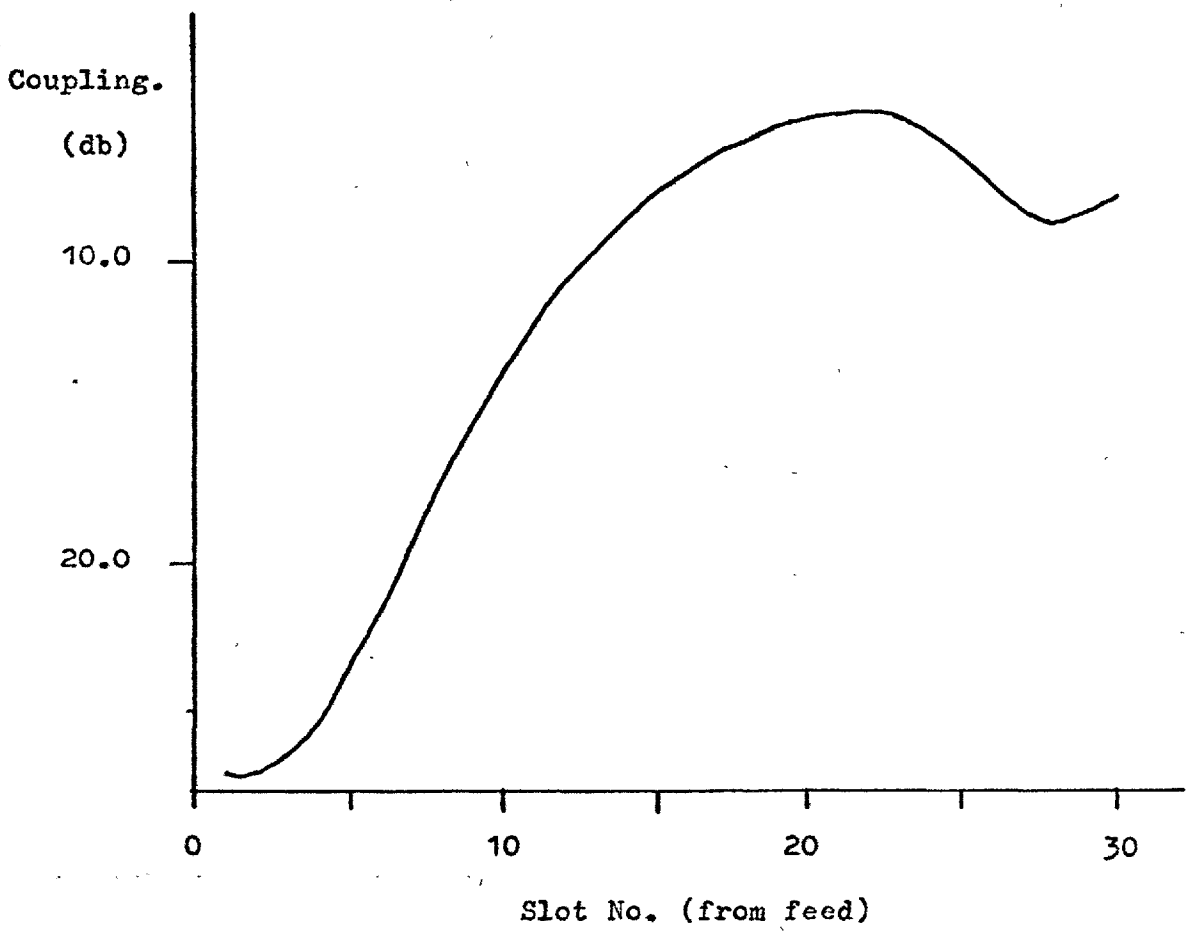

FIGURE 5.4.2. The input V.S.W.R. of a 30 slot array with $(1/7+6/7\cos^2)$ voltage illumination function and -20 db of input power in the load.

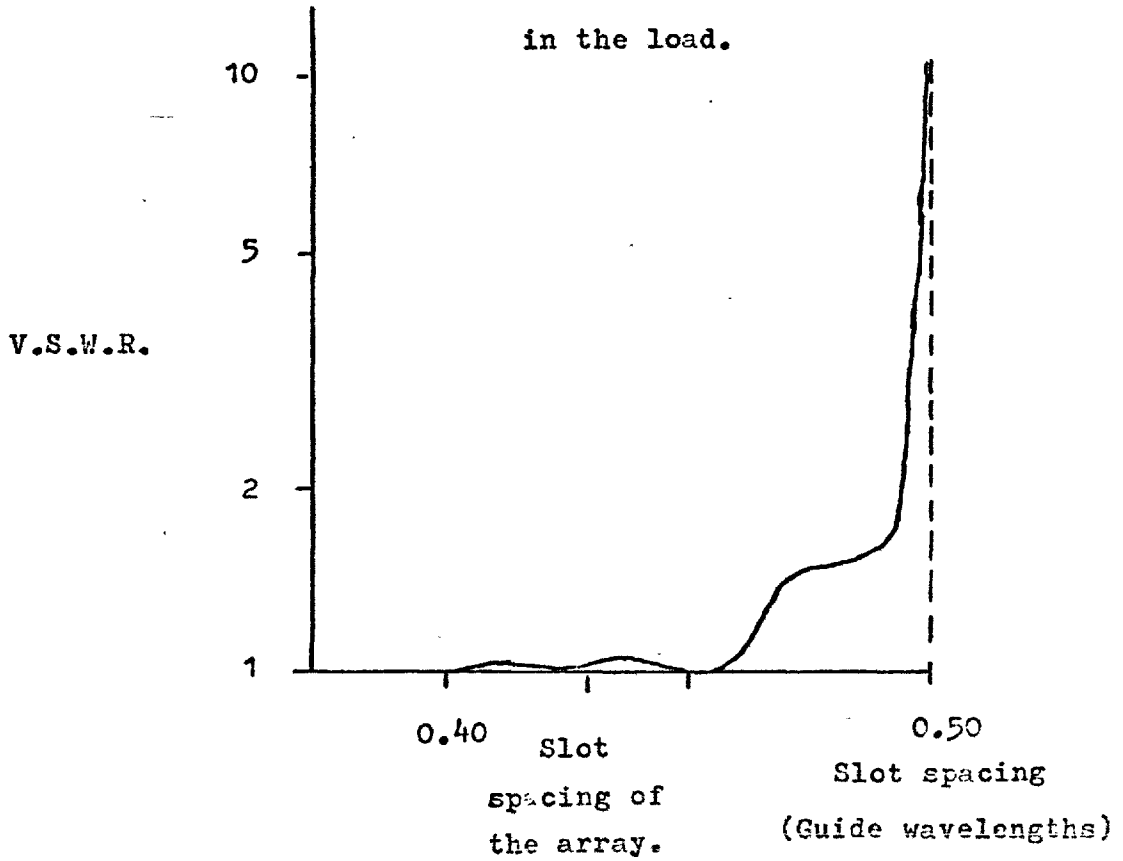

in manufacture as no mismatch problem arose. If the window between the baffles was to remain the same dimensions the baffles would have been of dimensions 0.628" x 0.500". However, considerable weight and cost reductions occurred if a standard size tube could be used. Thus $\frac{5}{8}$" x $\frac{5}{8}$" x 18 S.W.G. square brass tube was specified for the baffles. The window was nominally changed by 0.003" and they were $\frac{1}{8}$" higher. To check the effect of this on electrical performance, six slots were measured fitted with a pair of the redesigned baffles both with and without P.T.F.E.. Small changes of both sign were detected in the value of peak slot conductance but their frequency characteristics appeared unchanged. The conclusion was made that redesigning the baffles had an insignificant effect.

A curve of slot coupling against the length of the shorter branch arm was then constructed from experimental evidence. Difficulties were encountered in characterising lowly coupled slots because of the small amount of attenuation they introduced into the waveguide. However, using a set of moderately coupled slots it was found from measurements that the difference in coupling between an I-shaped slot fitted with baffles and P.T.F.E. and the same slot fitted with P.T.F.E. and coupling to waveguide 12 was 0.7 dB. This relationship was applied to lightly coupled slots because the coupling to a waveguide 12 branch arm could be accurately measured. The dimensions of the thirty slots of the array were then specified using the computer corrected values of required coupling and the experimental slot coupling curve.

The array was then manufactured complete with thirty one tubular baffles which were soldered to its front face. The array could be tested both with and without P.T.F.E.. The first tests performed on the array were swept frequency measurements of the attenuation past individual slots. The slots not being measured were covered with

adhesive aluminium tape. These tests showed that the frequency response of the slots both with and without P.T.F.E. was as expected but that the P.T.F.E. produced a larger increase in the slot conductance than had previously been measured. It was thought that this was due to a complete set of baffles being present. Some of the earlier measurements were made with only two baffles fitted to a single slot. As the array had been designed for use with P.T.F.E., this meant that at resonance with P.T.F.E. all the slots were over coupled. From the attenuation measurements past individual slots with P.T.F.E. at 5.70 GHz the power coupled by each slot was calculated to give an outline of the aperture distribution. This is shown in Figure 5.4.4..

Near field measurements of the array were then performed using the rig used to measure the eight slot array. These measurements were later repeated using a phase-amplitude plotter at A.S.W.E.. Good agreement was obtained between the two sets of results.

The amplitude distribution of the thirty slot array with P.T.F.E. at a frequency of 5.70 GHz is shown in Figure 5.4.3.. This was compared to the distribution shown in Figure 5.4.4. obtained from thirty separate measurements. Both distributions showed the same main features which indicated that mutual coupling was not important in this array. As all the slots were over-coupled, the slots near the feed coupled out too much power and insufficient power reached the slots near the load. Maximum power was thus coupled out before the centre of the array which appeared to be shorter than designed. The main beam of the array was then expected to be wider than the design. The measured radiation pattern shown in Figure 5.4.5. confirmed this. With P.T.F.E. fitted however, the array was expected to operate over a wider bandwidth than the intended design because the correct amplitude aperture

distribution occured at two frequencies either side of the design frequency rather than just at one frequency. This was so and reasonable far field patterns were obtained at frequencies as low as 5.40 GHz, as shown in Figure 5.4.6..

Without P.T.F.E. even at resonance (5.84 GHz) the slots were all under coupled. Too much power reached the slots near the load and was coupled out to distort the aperture distribution as shown in Figure 5.4.7.. The total error in the amplitude distributions at resonance was similar whether P.T.F.E. was present or absent. The near field phase distribution of the array at 5.85 GHz without P.T.F.E. is shown in Figure 5.4.8.. There was a ripple in the distribution because the array consisted of discrete slots. When the ripple was ignored the phase front could be approximated by three straight lines as shown. The reason for the breaks in the phase front was not clear but was thought to be associated with the lightly coupled slots being slightly detuned relative to the heavily coupled slots. The breaks were present in many traces but were most abrupt near the resonant frequency of the slots. They were obviously detrimental to the far field pattern.

It was realised that in principle far field patterns could have been computed from the near field distribution. However as the near field patterns were measured immediately in front of the array, it was problematical as to whether the distributions should be treated as belonging to a discrete array of points sources or a continuous aperture. In addition extremely accurate near field data was required to predict the sidelobe structure at least -30 dB below the main beam. The value of this exercise, if good agreement had been obtained, would have been in confirming the measured near field distributions. It was felt however, that the distributions were sufficiently well established

FIGURE 5.4.3. The aperture amplitude distribution of the 30 slot array fitted with P.T.F.E. at a frequency of 5.70 GHZ..

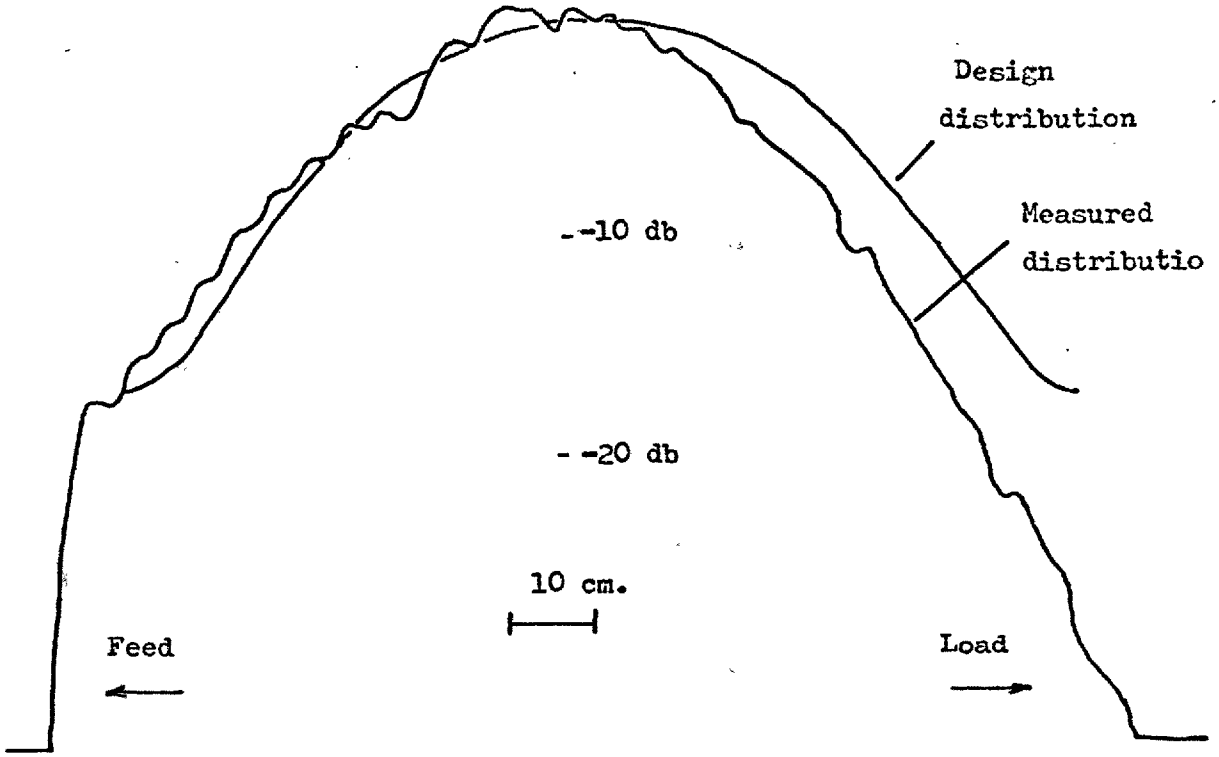

FIGURE 5.4.4. The aperture distribution of the 30 slot array with P.T.F.E. computed at 5.70 GHZ. from attenuation measurements on individual slos.

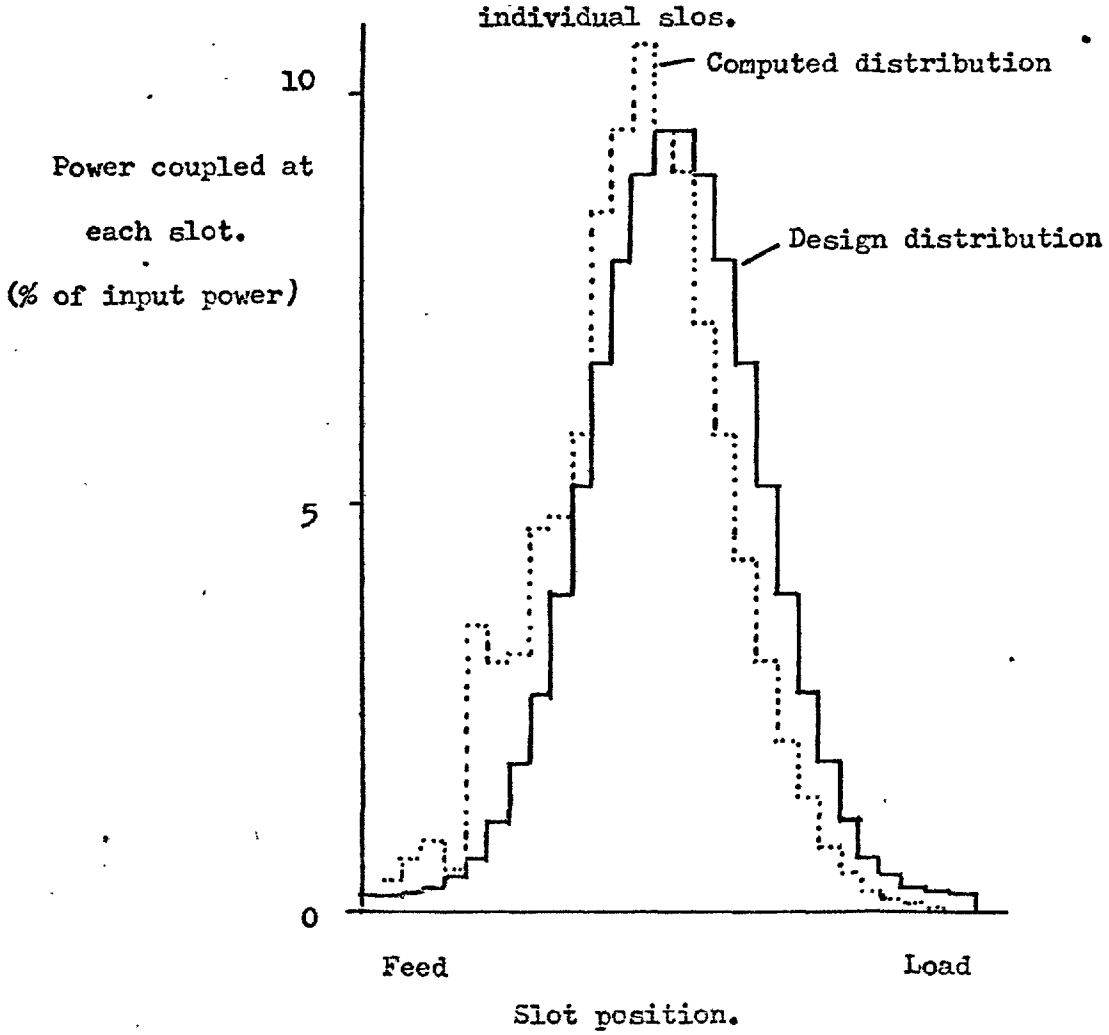

FIGURE 5.4.5. The far field radiation pattern of the 30 slot array fitted with P.T.F.E. and operated at 5.70 GHZ..

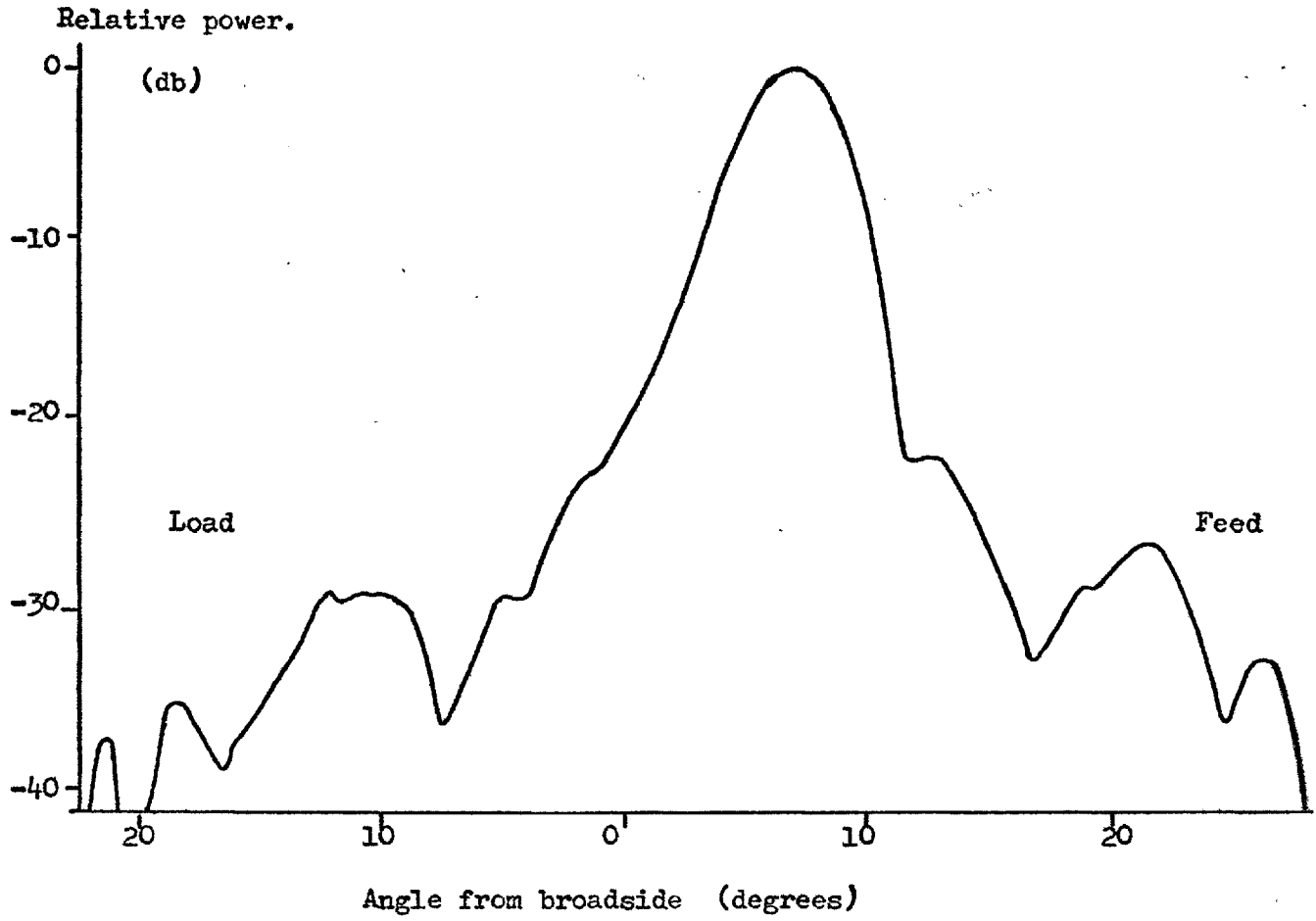

FIGURE 5.4.6. The far field radiation pattern of the 30 slot array fitted with P.T.F.E. and operated at 5.40 GHZ..

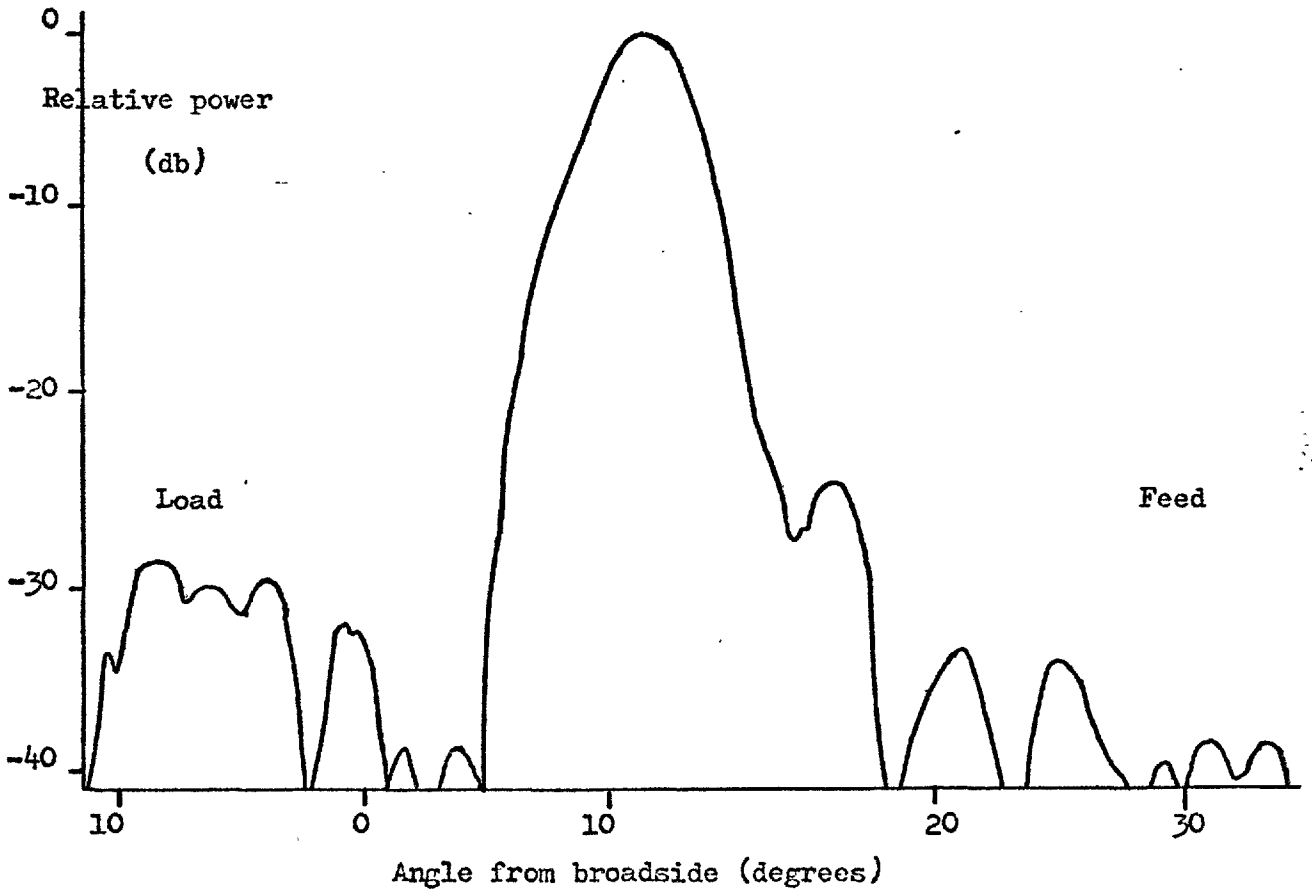

to indicate the errors in the specification of the array.

The far field patterns of the array without P.T.F.E. remained essentially unchanged over a band of at least 200 MHz. Although the amplitude aperture distribution was further distorted away from resonance the phase front became more linear. A typical pattern is shown in Figure 5.4.6..

A cross polarisation radiation pattern was plotted at 5.85 GHz without P.T.F.E.. This showed two peaks approximately 40^{o} either side of the main beam. The level of the peaks was only 20 dB below that of the main beam. The position of the cross polarised beams was as expected. Alternate slots were of opposite hand so that approximately at broadside all the main polarisation components were in phase, but a phase reversal occured between the cross polarised components of adjacent slots. This phase reversal was compensated by moving away from broadside until at approximately 40^{o} away from the main beam all the cross-polarised components were in phase. The precise positions of the cross polarised beams were determined by the ratio of the guide to free space wavelength and the slot spacing. The level of the cross polarisation was higher than expected but previous measurements of cross polarisation had been made only with single slots. With single slots the measurement relies on an accurate mechanical movement of a horn to separate the two polarisations, but with an array they were separated by the different phase relationships. The level of the cross polarisation was not as good as desired but it was thought that this could be improved by changing the window seen by the slot. This has not been investigated.

In general the performance of the thirty slot array was satisfactory for the first attempt to design a long array of I-shaped slots. Some error was present in the aperture amplitude distribution due to the

FIGURE 5.4.7. The aperture amplitude distribution of the 30 slot array without P.T.F.E. at a frequency of 5.85 GHZ..

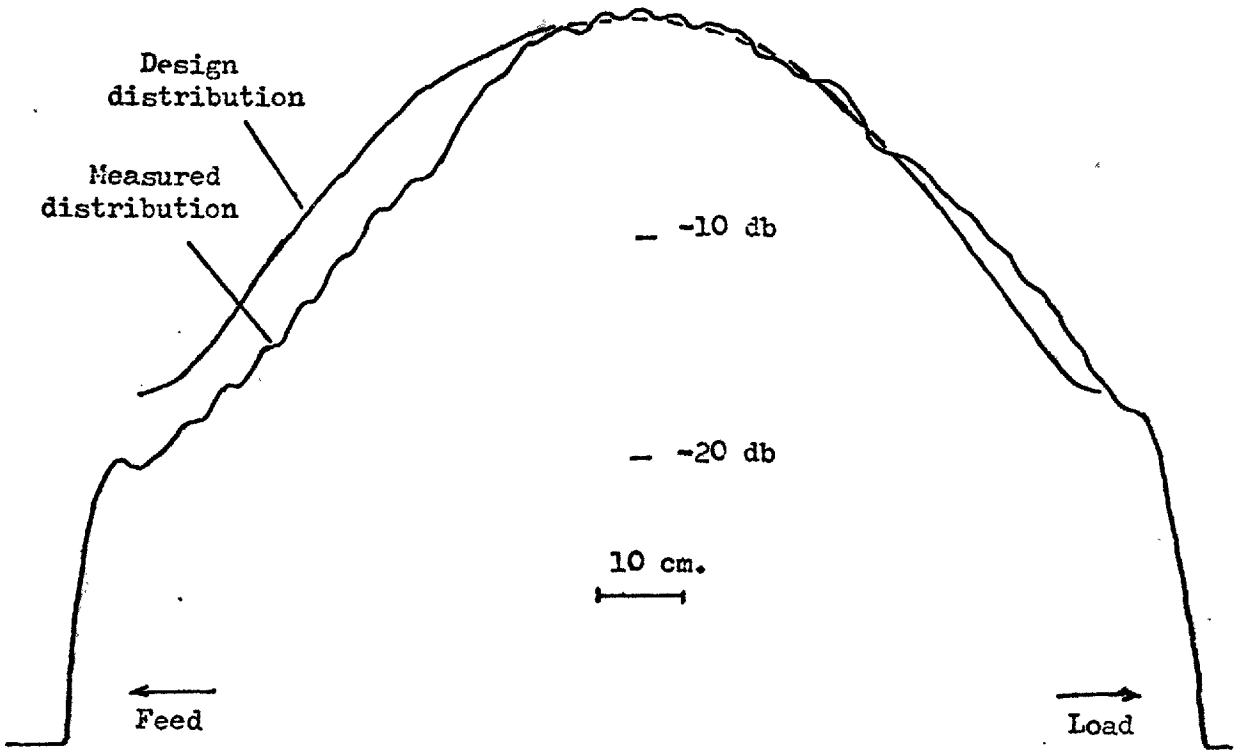

FIGURE 5.4.8. The aperture phase distribution of the 30 slot array without P.T.F.E. at a frequency of 5.85 GHZ..

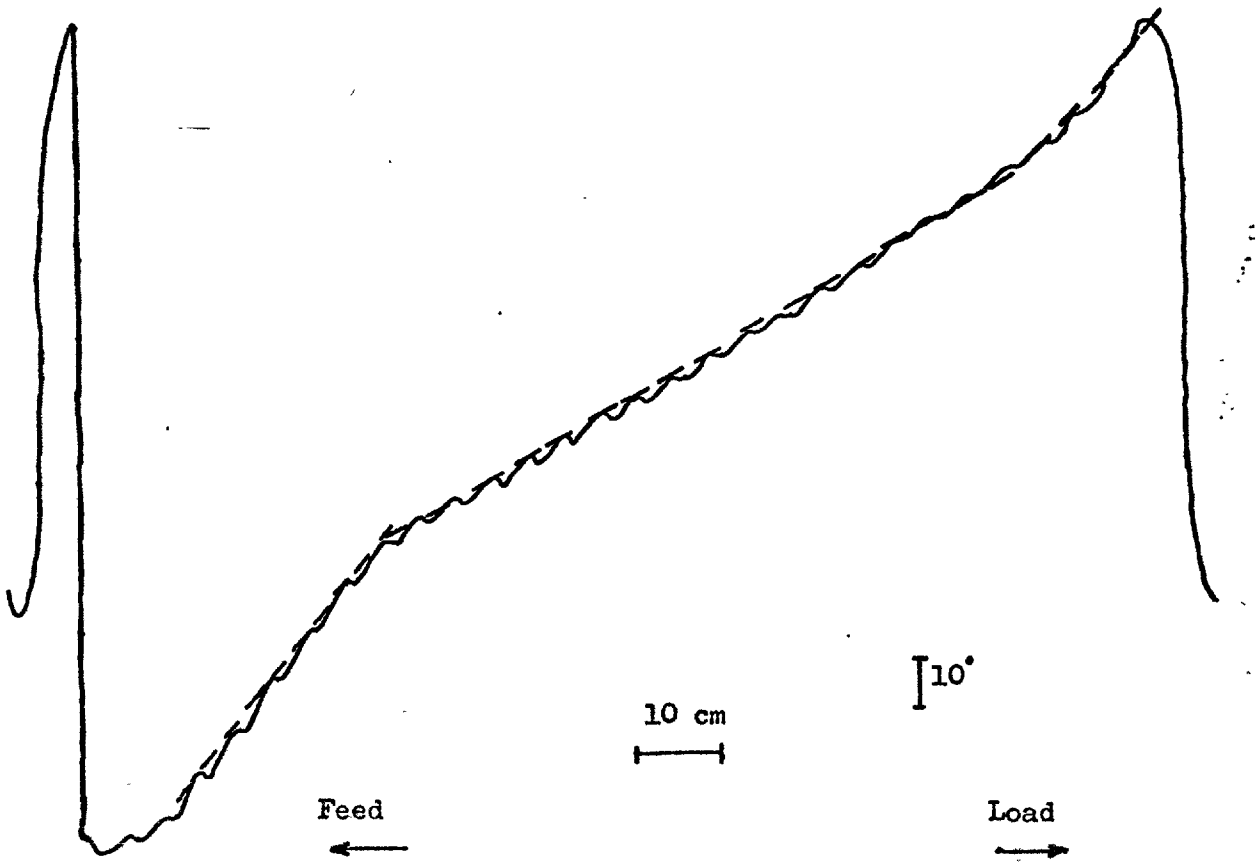

original slots being measured with only two baffles. Small breaks in the otherwise linear phase front were present and these helped to degrade the performance of the array. This was thought to be due to a small dispersion between the resonant frequency of the lightly and heavily coupled slots.

The results of measurements of individual slots of the thirty slot array, represented a major increase in the amount of information available about I-shaped slots fitted with baffles and P.T.F.E.. In Chapter 3 expressions for the conductance of an I-shaped slot radiating over a ground plane were derived. The fitting of the baffles and P.T.F.E. did not affect the coupling of the slot to the waveguide it only changed the radiation impedance of the slot. The only unknown in equation (3.8.20) for the conductance of an I-shaped slot with baffles and P.T.F.E. was the radiation resistance of the equivalent dipole. However, the conductances of the thirty slot array had been measured so that from these measurements values of R_{rad} could be obtained. The values are plotted in Figure 5.4.9. against slot conductance. A remarkable uniformity was obtained and an average value of R_{rad} of 22.8 ohms was obtained for I-shaped slots fitted with $\frac{5}{8}$" square baffles and a 0.010" thick layer of P.T.F.E..

Similarly, the effects of P.T.F.E. were considered on the frequency of peak conductance of the slots. The expression used in Chapter 3, equation (3.8.5) was modified to include a factor a so that the frequency shifts caused by the baffles and P.T.F.E. could be allowed for in later designs:

$$\tan kd_1 + \tan kd_2 = \alpha \tan k(\lambda/4 - h)$$

Values of α were then derived from experimental results and are plotted

FIGURE 5.4.9. The equivalent dipole radiation resistance of the slots of the thirty element linear array.

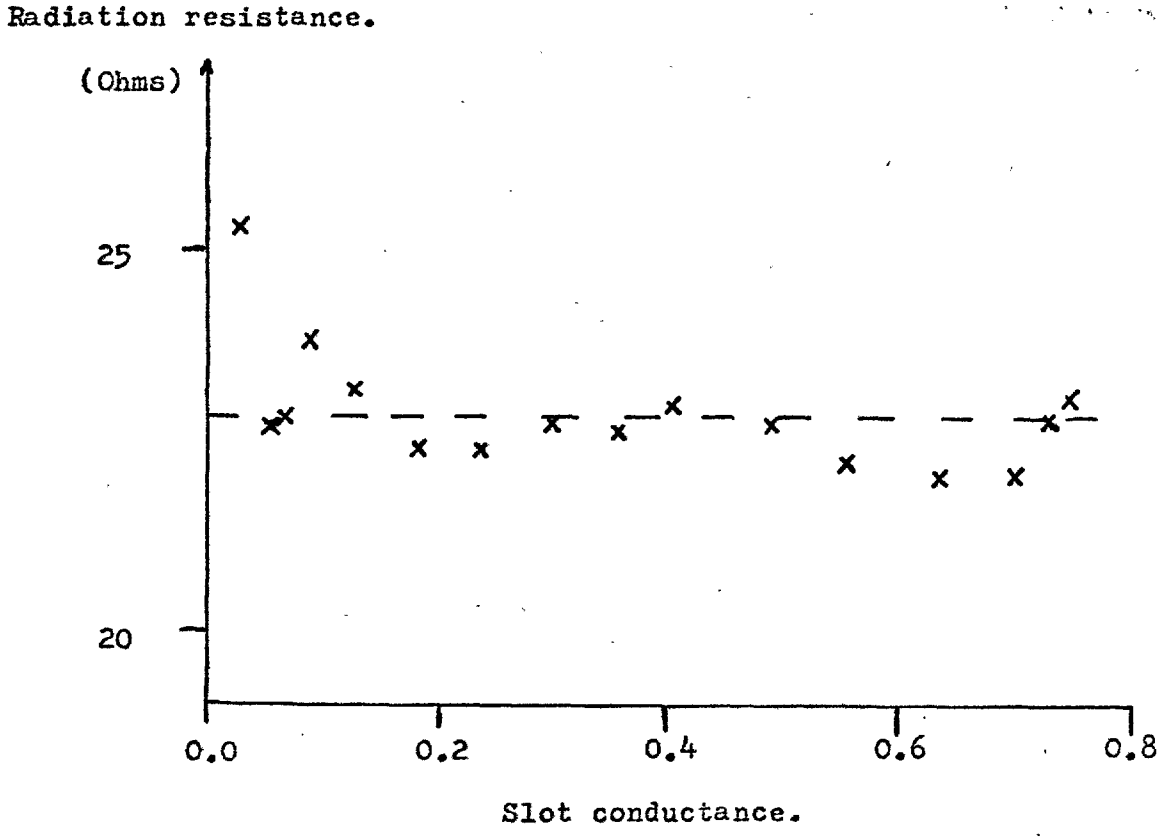

FIGURE 5.4.10. The dependence of the slot resonant frequency on dimensions.

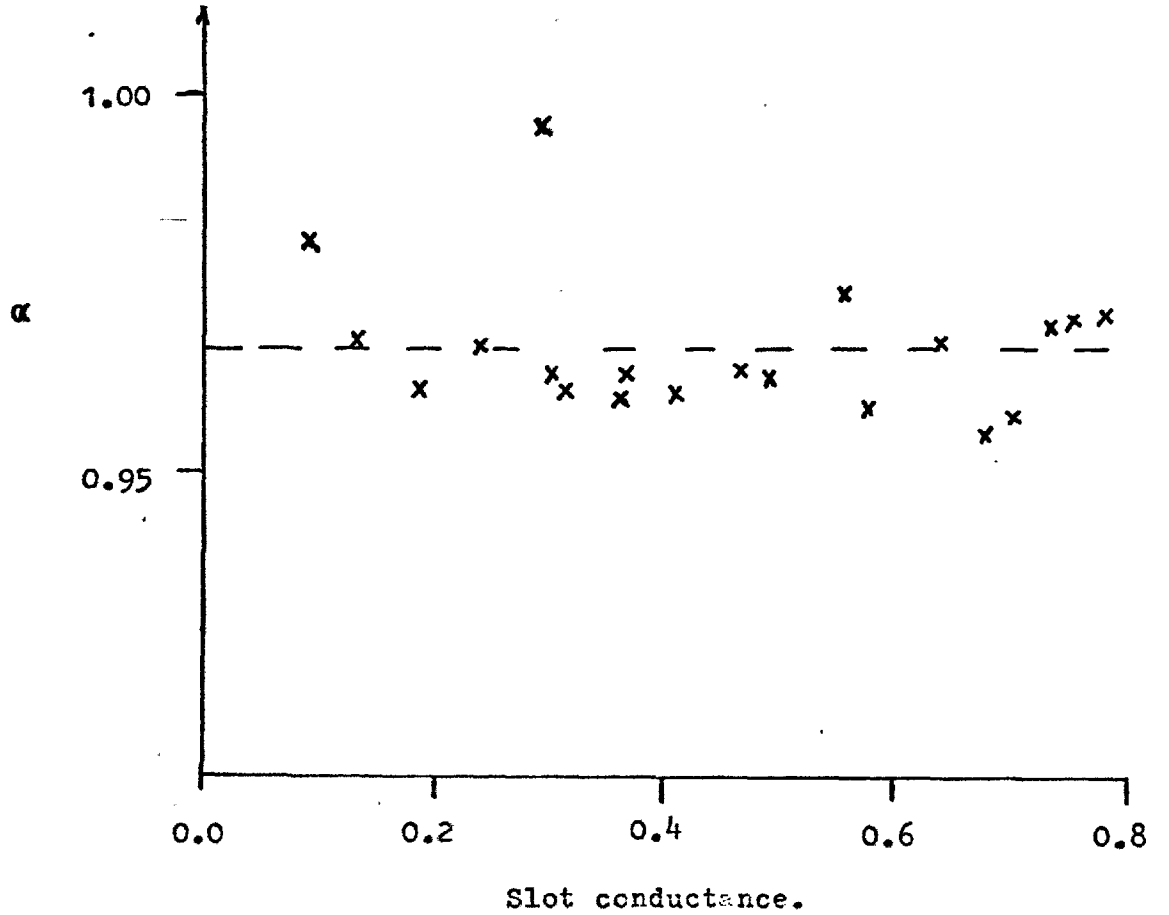

against slot conductance in Figure 5.4.10. A constant value for α emerged and gave an average value of 0.966.

Some errors were present in the thirty slot array due to insufficient experimental evidence being used to specify the slot conductances. However, the evidence provided by the thirty slot array should have ensured that the errors would not be present in later designs.

CHAPTER 6

MUTUAL COUPLING BETWEEN SLOTS

6.1. Introduction

It was shown in the last chapter that mutual coupling between slots in a single waveguide could be minimised by the use of baffles, which changed the direction of coupling. For a two dimensional array the problems associated with mutual impedance were much more complicated and deserved more careful study.

The mutual coupling between passive antennas arose due to their reciprocal nature. An aerial acted both in transmission and reception, so that when two of them were transmitting in proximity both received energy transmitted by the other modifying their individual performances. This effect was obviously most severe when the elements were close together and one subtended a large solid angle at the other. For large two dimensional arrays of closely spaced elements mutual coupling must have played a major role in the overall antenna performance.

There were numerous variations in the way that mutual impedance could have been investigated, almost as many as there were types of radiating elements. The two main approaches were to regard an individual element not as a member of a finite array but as a member of an infinite periodic array. Floquet's theorem could then be applied to the structure and the problem confined to within a unit cell in a similar manner to that used in crystallography. The element pattern of a unit cell within an infinite array environment could in principle be derived if the field within the array element could be specified. The array factor of an infinite array became the delta function which sampled the element pattern to give the power radiated by the array at a particular angle. The remaining incident power must have been reflected and so the

reflection coefficient of the array as a function of beam angle could be determined. This was a powerful technique when the individual radiator was simple, such as an open ended waveguide supporting only one mode. It was still a powerful method if dielectric plugs or similar modifications were made providing the fields could be fully specified and has been well reported (Amitay, Galindo and Wu, 1972). The method determined the angle at which the array blindspots or angles at which no radiation took place. For finite array designs using simple radiators this approach has indicated the angles at which large reflections could be expected. The main objections to this method were that simple elements had to be used, with each element individually fed and that arrays are never infinite. Some finite arrays could be well approximated by the infinite array technique but the difficulty was deciding how good the approximation was. The infinite array approximation also assumed a uniform amplitude distribution as within the plane of the array the axes could be translated by amounts corresponding to whole unit cells without changing the solution.

The second general approach was to analyse the mutual impedance between two elements as one of them was moved about the other. More elements could be introduced and a matrix established to describe the resulting array. The matrix could be solved to determine the main properties of the array. Other considerations such as the aperture distribution could be included into the solution as the model became more sophisticated. The main problem with this approach was that although the mutual impedance between two elements could be solved quite accurately to give a 2 x 2 matrix representation, when further elements were added to give a 3 x 3 and then 4 x 4 representation, the original errors were

magnified so that the final result could become unacceptably inaccurate.

For the type of array envisaged however, it was expected that the second approach would be more useful especially as the elements of even quite a large matrix could be obtained experimentally. The problems associated with using a travelling wave feed and shaped aperture distributions, different for the two channels, could then also be included.

The coupling between two individual I-slots could be analysed in several ways. One approach which has been investigated by a colleague (N. Williams, 1975) was to use the so-called "induced E.M.F. method" on equivalent dipoles. This method was proposed by Carter (1932) and essentially involved calculating the E.M.F. induced in a segment of one dipole by current flowing in the other. The induced E.M.F.'s were then summed to give the mutual impedance. The implicit assumption of this method was that the second antenna did not disturb the field of the first. The second antenna appeared "invisible" to the first. If this assumption was made explicitly a whole class of antennas could be specified for which certain general conclusions emerged which were useful when examined with experimental data.

6.2. Canonically Minimum Scattering Antennas (C.M.S.)

Montgomery and Dicke (1948) first referred to a minimum scattering antenna which they defined "as an antenna for which the scattering is a minimum for each eigensolution" and they derived the symmetry properties associated with such an antenna. The subject then, was not pursued until relatively recently, when Wasylkiwskyj and Kahn (1970) derived the properties of a class of canonically minimum scattering antennas. A brief account of their derivation will be given as the results they obtained could be directly applied to the array analysis problem, and enabled the amount of experimental work necessary to be kept within

reasonable bounds.

The method differed from other treatments which proceeded from a particular antenna structure with its electromagnetic properties as implicit. This method defined a class of idealised antennas the electromagnetic properties of which were rigorously expressed explicitly in terms of their radiation pattern. Such idealised antennas were termed minimum scattering, which was defined so that they became "invisible" when their ports were terminated in a particular set of reactive loads. If these loads were pure open circuits the antennas were described as canonically minimum scattering (C.M.S.) and the invisibility property could be used directly to calculate the elements of the open circuit impedance matrix of an array.

For slots in a ground plane clarification of the invisibility condition was required. The definition of invisibility for an antenna in a conducting sheet was modified so that the sheet scattered in the same way as if the slot had not been cut. It was easy to see that this condition could be met for a slot if a short circuit was placed at the same plane. Normal transmission line techniques showed that a short at the plane of the slot could for one mode at least, be equivalent to a pure open circuit a quarter of a wavelength away. The antenna input ports could be defined at this plane so that a thin waveguide fed slot supporting only one mode could be regarded as C.M.S.. In fact as for the radiation resistance in Chapters 2 and 3 equivalent dipoles were considered but by duality this was acceptable.

The radiation and scattering properties of a finite lossless but otherwise arbitrary antennas have been shown by Montgomery and Dicke (1948) to be related by the scattering matrix equation:

$$\bar{b} = \bar{\bar{S}}\,\bar{a} \qquad (6.2.1a)$$

or more fully:

$$\left|\begin{array}{c} b_\alpha \\ \\ b_\beta \end{array}\right| = \left|\begin{array}{c|c} S_{\alpha\alpha} & S_{\alpha\beta} \\ \hline S_{\beta\alpha} & S_{\beta\beta} \end{array}\right| \left|\begin{array}{c} a_\alpha \\ \\ a_\beta \end{array}\right| \qquad (6.2.1b)$$

where $\bar{S}^+ \bar{S} = 1$, $\bar{S}^+$ being the complex conjugate transpose of $\bar{S}$. For convenience $\bar{S}$ was normalised to a set of one ohm resistors. The a_α and b_α were column matrices each containing respectively incident and reflected waves at the N locally accessible ports. Similarly a_β and b_β were infinite column matrices corresponding to incident and reflected wave amplitudes of the spherical modes in free space outside a sphere or for a slot in an infinite ground plane a hemisphere enclosing the antenna. An input a_α at the antenna ports produced a radiated wave $b_\beta = S_{\beta\alpha}a_\alpha$ into space and a wave reflected back into the antenna ports $b_\alpha = S_{\alpha\alpha}a_\alpha$. The N-dimensional sub-matrix $S_{\alpha\alpha}$ described the mutual and self-coupling among the accessible ports while $S_{\alpha\beta}$, $S_{\beta\alpha}$ and $S_{\beta\beta}$ described respectively the receiving, transmitting and scattering properties of the antenna. The quantities $S_{\alpha\beta}$ and $S_{\beta\alpha}$ were termed respectively the modal receiving and transmitting patterns to distinguish them from the conventional far-field radiation pattern which was expressed explicitly in angular coordinates. For a reciprocal lossless antenna it could be shown that $S_{\alpha\beta}$ was the same as the complex conjugate transpose of $S_{\beta\alpha}$.

C.M.S. antennas were defined to be "invisible" when their local ports were correctly terminated in pure open circuits. This meant that the field scattered by the antenna must have been identical with the incident field i.e., the field produced by b_β must have been the same as that originally produced by a_β in the absence of the antenna. This

condition with the constraint of losslessness gave the scattering matrix of a C.M.S. antenna as

$$S = \left[\begin{array}{c|c} 0 & S_{\beta\alpha}^{+} \\ \hline S_{\beta\alpha} & I_{\beta\beta} - S_{\beta\alpha}S_{\beta\alpha}^{+} \end{array}\right] \qquad (6.2.2)$$

where $I_{\beta\beta}$ was a unitary matrix. It was also shown by Montgomery and Dicke (1948) that the modal radiation pattern of a reciprocal antenna had to be real and that purely real modal radiation patterns had to have point symmetry about the origin. In addition when the excitations at the local ports of reciprocal C.M.S. antennas were purely real the radiation fields defined with respect to the axes shown in Figure (6.2.1) must have the symmetry property:

$$F_{\theta}^{*}(\pi - \theta, \varphi + \pi) = - F_{\theta}(\theta, \varphi) \qquad (6.2.3)$$

and

$$F_{\varphi}^{*}(\pi - \theta, \varphi \pm \pi) = F_{\varphi}(\theta, \varphi) \qquad (6.2.4)$$

Armed with the properties of individual C.M.S. antennas Wasylkiwskyj and Kahn developed the theory of mutual coupling between two such antennas, radiating into a three dimensional region using the coordinates shown in Figure 6.2.1.. As the antennas were C.M.S. their individual scattering matrices were:

$$S_1 = \left[\begin{array}{c|c} 0 & S_1^{+} \\ \hline S_1 & I_{\beta\beta} - S_1 S_1^{+} \end{array}\right] \qquad (6.2.5)$$

and

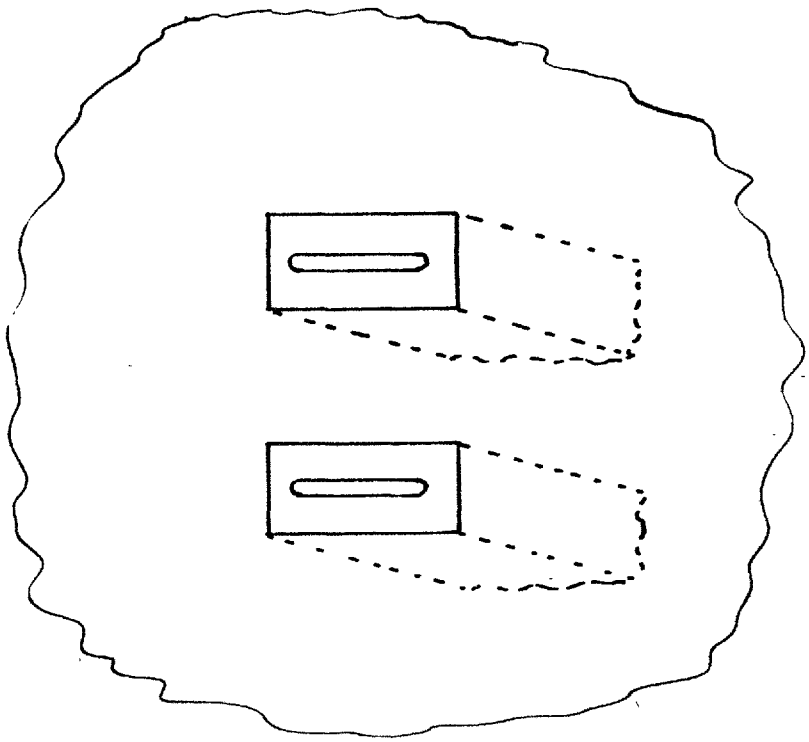

A sketch of parallel straight slots inthe end walls of the waveguide.

FIGURE 6.2.1. The coordinates used to analyse two C.M.S. antennas radiating into a three-dimensional region.

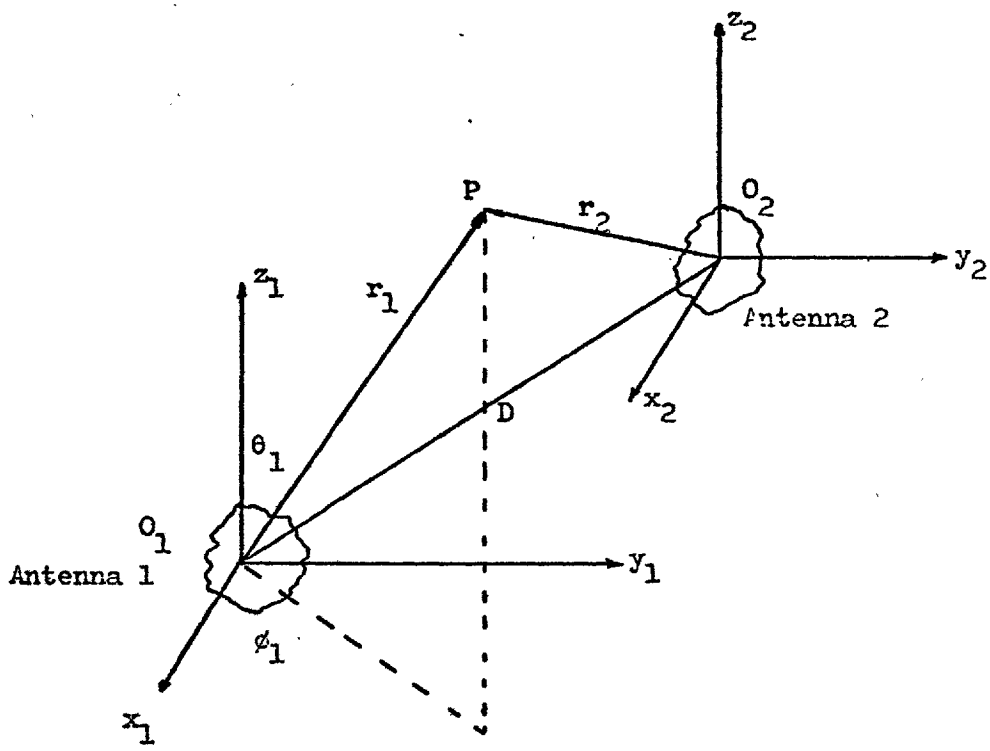

FIGURE 6.2.2. The coupled power between parallel straight slots in the end walls of waveguides.

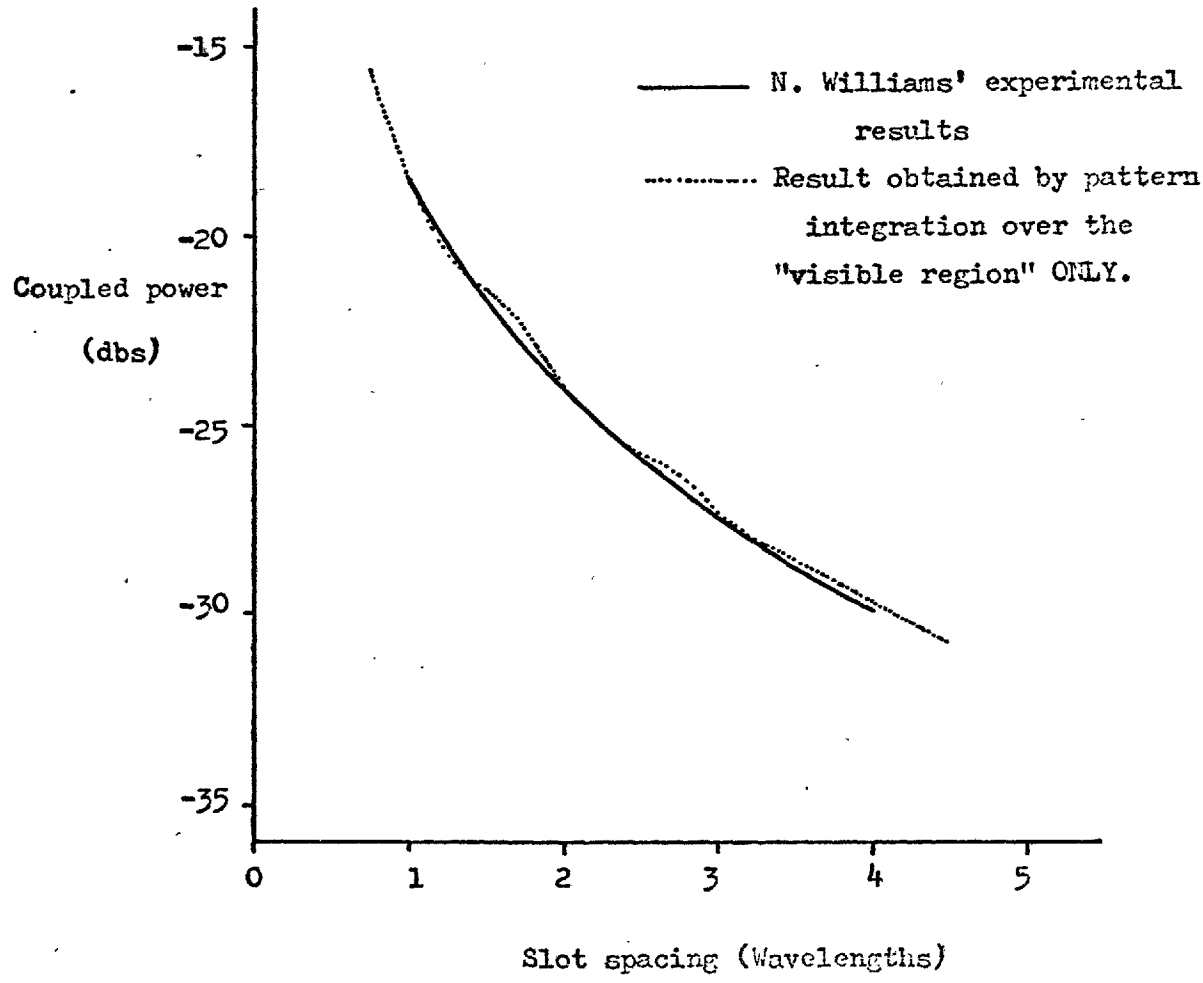

$$S_2 = \left[\begin{array}{c|c} 0 & \tilde{S}_2 \\ \hline S_2^* & I_{\beta\beta} - S_2^*\tilde{S}_2 \end{array}\right] \qquad (6.2.6)$$

where the scattering matrices were referred respectively to origins O_1 and O_2, and S_1 and S_2^* were the modal transmitting patterns which were given by:

$$\tilde{S}_1 = \left[\ldots\ldots S_{1nm}^{\prime(e)} \; S_{1nm}^{\prime(o)} \; S_{1nm}^{\prime\prime(e)} \; S_{1nm}^{\prime\prime(o)} \ldots\ldots\right] \qquad (6.2.7)$$

and

$$S_2^+ = \left[\ldots\ldots S_{2nm}^{\prime(e)} \; S_{2nm}^{\prime(o)} \; S_{2nm}^{\prime\prime(e)} \; S_{2nm}^{\prime\prime(o)} \ldots\ldots\right] \qquad (6.2.8)$$

(m = local ports, n = spherical ports)

Antenna 1 was excited at its local port with a unit amplitude wave and antenna 2 was open circuited and indistinguishable from free space. Refering to Figure 6.2.1., the transverse electric field at P due to antenna 1 expanded in terms of Hankel functions was then:

$$r_1\bar{E}_t(\bar{r}_1) = \zeta^{\frac{1}{2}} \sum_{n=1}^{\infty} \sum_{m=o}^{n} \sum_{e,o} \left\{ S_{1nm}^{\prime(e,o)} H_n^{(2)}(kr_1) e_{nm}^{\prime(e,o)}(\theta_1,\varphi_1) \right.$$

$$\left. + S_{1nm}^{\prime\prime(e,o)} H_n^{(2)}(kr_1) e_{nm}^{\prime\prime(e,o)}(\theta_1,\varphi_1) \right\} \qquad (6.2.9)$$

By means of addition theorems for spherical vector mode functions developed by Stein and Cruzan (Stein 1961 and Cruzan 1961) the field at P could be expanded about the origin of antenna two in terms of its

coordinates r_2, θ_2, ϕ_2. As the field at O_2 had to remain finite the result was of the form:

$$r_2\bar{E}_t(\bar{r}_2) = \zeta^{\frac{1}{2}} \sum_{n=1}^{\infty} \sum_{m=o}^{n} \sum_{e,o} \left\{ a'^{(e,o)}_{1nm}\, 2\hat{J}_n(kr_2) e'^{(e,o)}_{nm}(\theta_2,\phi_2) + a''^{(e,o)}_{1nm}\, 2\hat{J}_n(kr_2) e''^{(e,o)}_{nm}(\theta_2,\phi_2) \right\} \qquad (6.2.10)$$

where $\hat{J}_n$ were spherical Bessel functions and the $a^{(e,o)}_{1nm}$ were the amplitudes of incoming and outgoing spherical modes with respect of O_2. If these were arranged to form a column matrix $a^{(1)}$ then:

$$\tilde{a}^{(1)} = [\, a_1^{(1)(e)} a_1^{(1)(o)} a_2^{(1)(e)} a_2^{(1)(o)} \ldots\ldots] \qquad (6.2.11)$$

This was the incident and scattered wave at antenna 2 with its local ports open circuited so that the scattering matrix equation became:

$$\begin{bmatrix} b_2 \\ a^{(1)} \end{bmatrix} = \left[\begin{array}{c|c} 0 & \tilde{S}_2 \\ \hline S_2^* & I_{\beta\beta} - S_2^*\tilde{S}_2 \end{array}\right] \begin{bmatrix} b_2 \\ a^{(1)} \end{bmatrix} \qquad (6.2.12)$$

The antennas were assumed to be tuned to free space so that the reflected waves b_1 at the input ports of antenna 1 was zero. The incident wave a_1 was unity so that the mutual impedance was given by

$$Z_{21} = \left.\frac{V_2}{I_1}\right|_{I_z=0} = \frac{2b_2}{a_1 + b_1} = 2b_2 \qquad (6.2.13)$$

Using the scattering matrix representation this was given by

$$\bar{Z}_{21} = 2\tilde{S}_2 a^{(1)}$$

$$= 2 \sum_{n=1}^{\infty} \sum_{m=o}^{n} \sum_{e,o} \left\{ a'^{(e,o)}_{1nm} S'^{(e,o)}_{2nm} + a''^{(e,o)}_{1nm} S''^{(e,o)}_{2nm} \right\}$$

(6.2.14)

Using the addition theorems of Stein expressions for $a^{(e,o)}_{1nm}$ in terms of the modal radiation pattern of antenna 1 could have been obtained to give an expression for mutual impedance in terms of spherical mode coefficients. Kahn and Wasylkiwskyj (1966) adopted this approach for elementary dipoles but its generalisation to arbitrary C.M.S. antennas was cumbersome. The simpler approach they adopted (Wasylkiwskyj and Kahn, 1970) was to express the fields of antenna 1 as a superposition of plane waves. The results were then compared to the corresponding spherical mode expansions so that $a^{(e,o)}_{1mn}$ could be identified as integrals involving the far field pattern of antenna 1. The details of the manipulation appeared in the paper but the results were of the form:

$$a'^{(e,o)}_{1nm} = \int_0^{2\pi} d\beta \int_\Gamma d\alpha (-j)^n \exp(-j \bar{K} \cdot \bar{D}) \sin\alpha F_{1t}(\alpha,\beta) e'^{(e,o)}_{nm}(\alpha,\beta)$$

(6.2.15)

where α and β were the angular coordinates, F_{1t} the transmitted normalised field pattern of antenna 1 and the path of integration Γ as shown in Figure 6.2.3.. Equations of the last type could then be substituted back in equation (6.2.14) to give, after some manipulation:

$$\bar{Z}_{21} = 2 \int_0^{2\pi} d\phi \int_\Gamma \sin\alpha \, d\alpha \exp(-j\bar{K}.\bar{D}).F_{1t}(\alpha,\phi).F^*_{2t}(\alpha^*,\phi)$$

(6.2.16)

FIGURE 6.2.3. The contour of integration in the complex α plane.

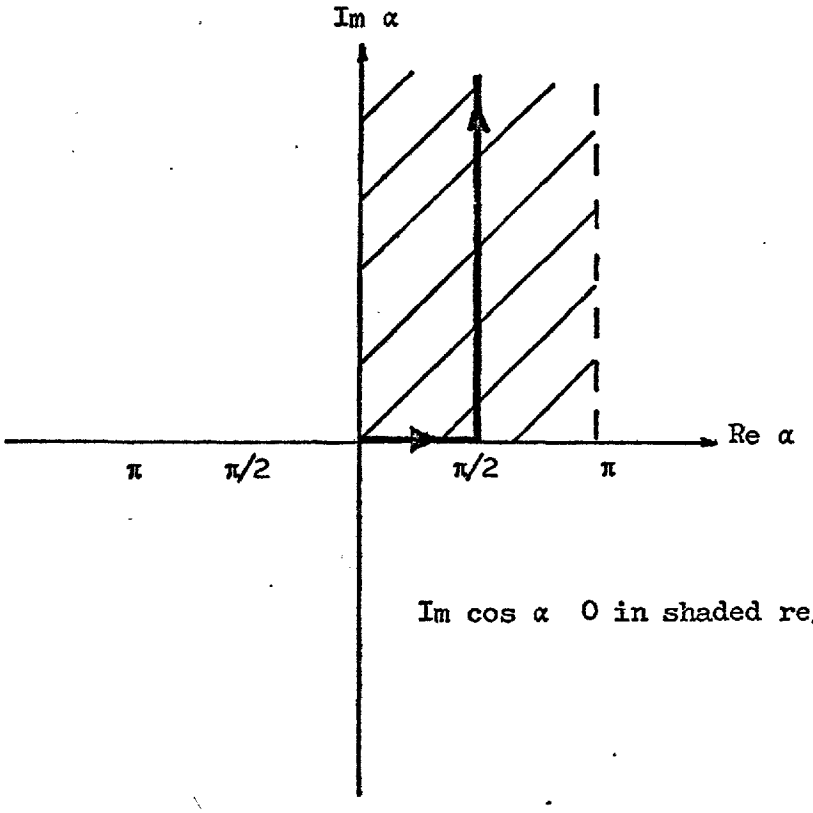

For identical reciprocal C.M.S. antennas the mutual impedance could be specified in terms of the power pattern P and if both antennas lay on the Z axis $\bar{D} = \hat{z}_o D$ and with $t = \cos\alpha$:

$$Z_{21} = 2 \int_0^{2\pi} d\phi \int_{-j\infty}^{1} \exp(-jkDt) P(t,\phi) dt \qquad (6.2.17)$$

Similarly for antennas in the xy plane $\bar{D} = \hat{x}_o D_x + \hat{y}_o D_y$ so that in terms of k variables:

$$\bar{Z}_{21} = \frac{2}{k} \int_{-\infty}^{\infty} \int_{-\infty}^{\infty} \frac{\exp[-j(k_x D_x + k_y D_y)]}{(k^2 - k_x^2 - k_y^2)^{\frac{1}{2}}} P(k_x, k_y) dk_x dk_y \qquad (6.2.18)$$

Equation (6.2.17) has been programmed for computer evaluation and the results indicated the limitations of the method. However, in the discussion of the proposed array numerical results were not the most useful result of the method. The I-slot was selected because it was capable of producing a large range of coupling values. The coupling to the waveguide could be varied but the coupling to space or radiation resistance was almost independent of the ratio of the lengths of the branch arms. This implied that the power pattern showed only small changes, with variations of the branch arm lengths, but this function was the only variable in equation (6.2.17) other than the slot separation. It appeared that Z_{21} could only change slowly as the branch arms lengths were altered while maintaining the slots at resonance.

Power patterns over real space were integrated in Chapters 2 and 3 to give values of radiation resistance. It was a trivial matter to include the exponential in the integrand and integrate over real space but the continuation of the integral into imaginary space would have been

exceedingly difficult. Numerically it has been shown that if the power function tends to zero where the contour entered the imaginary space then the contribution from the latter could be ignored, but otherwise an error resulted. This was demonstrated using parallel straight slots. The radiation pattern had a null at the angle corresponding to t = o so that when it was included in equation (6.2.17) and integrated over only the real range of t the results were as shown in Figure 6.2.2.. It also shows experimental results obtained by N. Williams for slots in the end wall of waveguide 16. Good agreement was obtained which showed that ignoring the contribution from the imaginary range was acceptable in this case.

The arrangement in which colinear slots were considered was very different, the radiation pattern was uniform with respect to α and was effectively unity for all the real range. Obviously a considerable component to the integration would have been produced if this function had been analytically continued into the imaginary plane, but how this could be done was extremely problematical. However, the integration was again performed over the visible region, and the results were compared to equivalent experimental results again by N. Williams in Figure 6.2.4.. At some separations the agreement obtained was acceptable but at other separations the computed results were greatly in error as if a large component was omitted, as indeed it had been. These results showed the problems associated with this method, but realising its limitations the more interesting case of I-shaped slots was considered. The two extreme cases of Γ-shaped slots and completely symmetrical I-shaped slots were investigated remembering that where α departed from the real axis the radiated power was not zero. The results obtained are shown in Figure 6.2.5. and indicated that the amplitude and variation of the

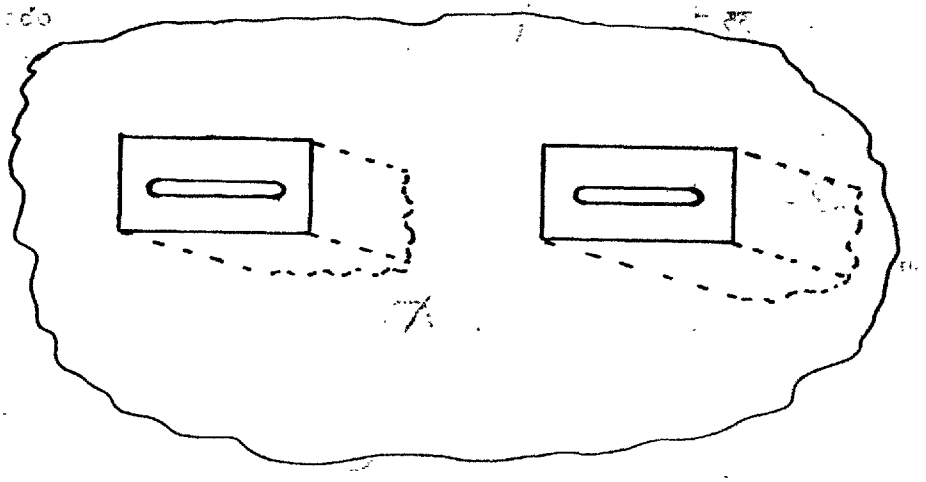

A sketch of colinear straight slots in the end walls of the waveguide.

FIGURE 6.2.4. The coupled power between colinear straight slots in the end walls of waveguides.

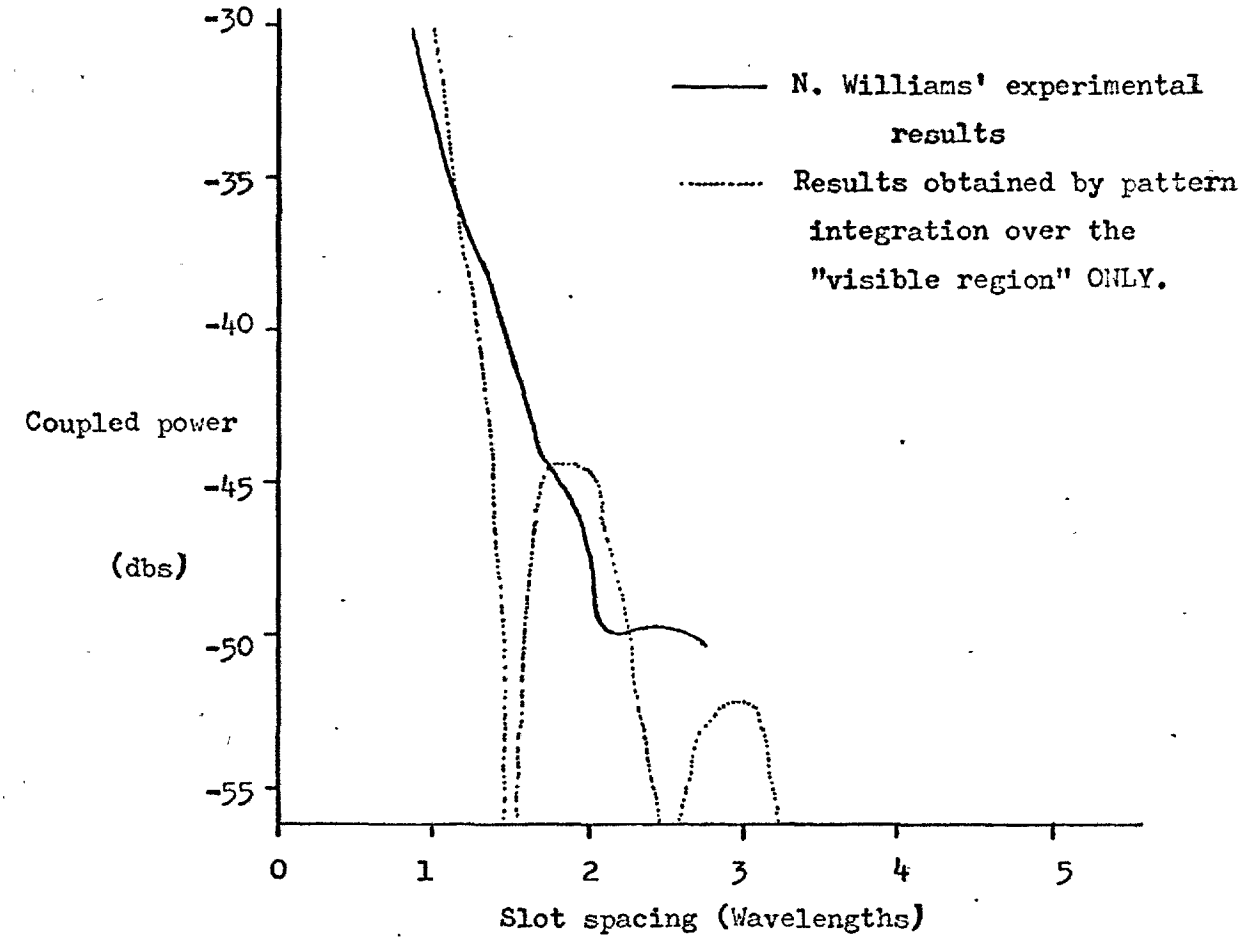

FIGURE 6.2.5. The coupled power between ⅂ and I-shaped slots in the end walls of waveguides.

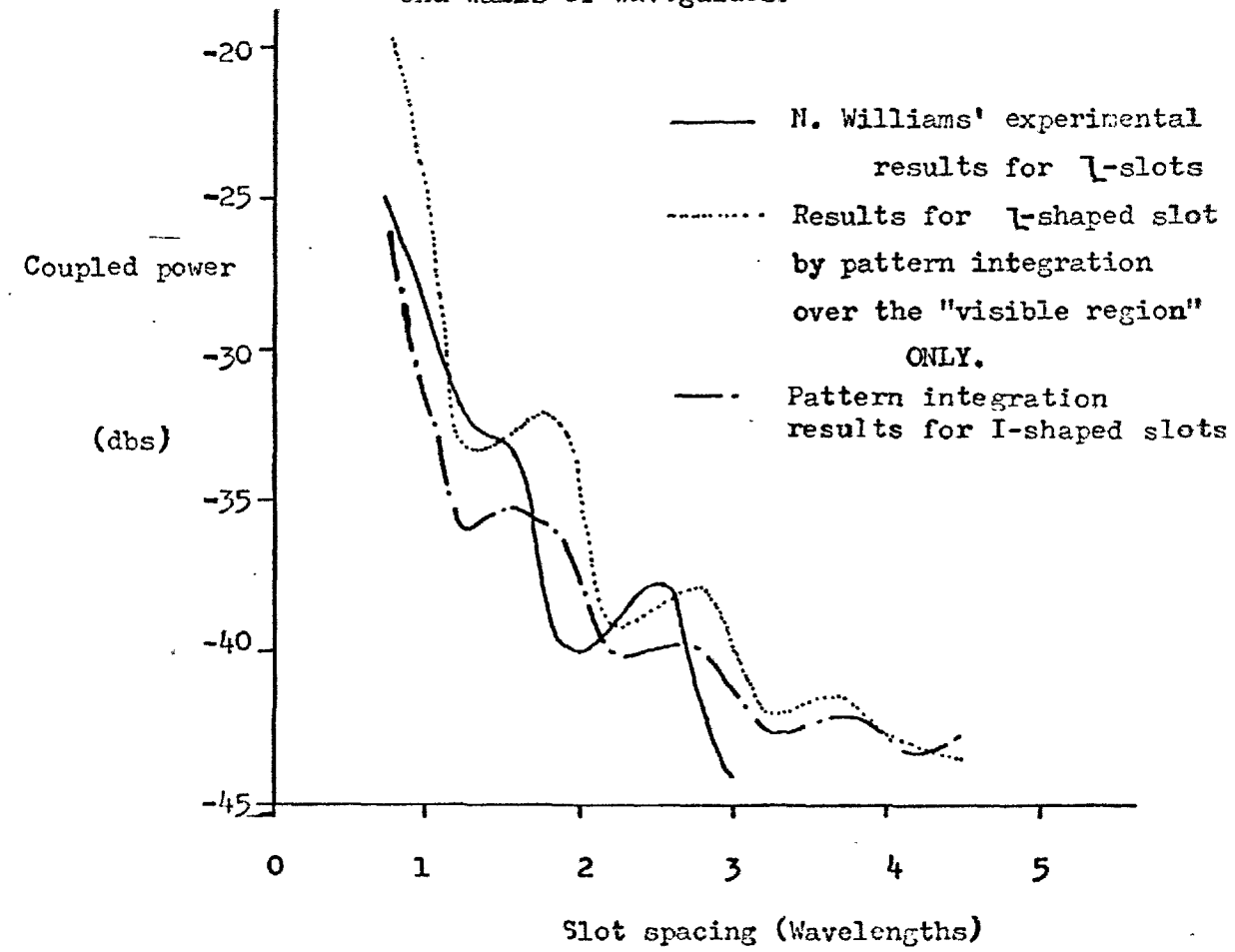

curves was substantially similar and the maximum difference was about 2 dB. The figure also shows experimental results obtained by Williams and it was interesting to note that the experimental and theoretical results both showed a ripple with a similar period and amplitude. The ripple in the theoretical curve was due to omitting the component due to the imaginary space and that in the experimental curve to a small amount of detuning between the principal polarisations, and will be discussed in the next section.

Wasylkiwskyj and Kahn's method had indicated that for slots in the end wall of a waveguide radiating above a ground plane, the maximum change in coupled power changing from ⅂-shaped slots to symmetrical I-slots was likely to be about 2 dB. For slots in the side wall the coupling between the slot and the waveguide had to be included but this result applied for slot to slot coupling.

When the baffles and P.T.F.E. were fitted to the slots they were no longer C.M.S. antennas as if the slots had not been cut the baffles would not have scattered like a ground plane. However, if a specialist re-definition of the term "invisible" was allowed so that when the antenna terminals were open circuited the slots scattered like a corrugated surface similar arguments could be applied. The results for the thirty slot array showed that with P.T.F.E. and $\frac{5}{8}$" square baffles fitted the radiation resistance of the equivalent dipoles for slots of all values of coupling was 22.8 ohms. This indicated that there was negligible change in the radiation pattern with slot coupling and by Wasylkiwskyj and Kahn's arguments negligible change in the radiation coupling between slots. This argument could have broken down for adjacent slots where coupling could have taken place by higher order evanescent modes but was checked experimentally by Williams and found to be

correct for adjacent slots.

The value of this approach has been that it showed that the radiation coupling of the slots was almost independent of their coupling to the waveguide. This was useful as it meant that the elements of the radiation coupling matrix had only to be measured for one slot coupling and could then be assumed for all other couplings.

6.3. An Experimental Investigation of Mutual Coupling

In order to study the effects of mutual coupling experimentally a network of twenty four nominally identical I-shaped slots was made. It consisted of eight waveguides with three slots cut in each, and was made this size as it was envisaged that the final array would contain eight waveguides and the elements of the 8 x 8 coupling matrix corresponding to a column of slots could be measured. Three slots were considered sufficient as when fitted with baffles the coupling along each waveguide had been shown to be small.

Initially the network was surrounded by ground plane and the frequency and value of peak attenuation past each slot was measured with the other slots covered by adhesive aluminium tape. The results which were plotted as histograms were shown in Figures 6.3.1. and 6.3.2.. The results showed that the mean frequency of peak attenuation past the twenty four slots was 5.842 GHz with a standard deviation of 30 MHz. Similarly the mean value of peak attenuation was 0.58 dB with a standard deviation of 0.07 dB which was equivalent to a conductance of 0.138 with a deviation of $\pm$ 0.017. These results illustrated the range of manufacturing errors associated with I-shaped slots.

Mutual coupling measurements were then made on the network. A slot at the corner of the network was used in transmission and the other

FIGURE 6.3.1. A histogram of the measured values of peak attenuation past individual slots of the 8×3 slot network.

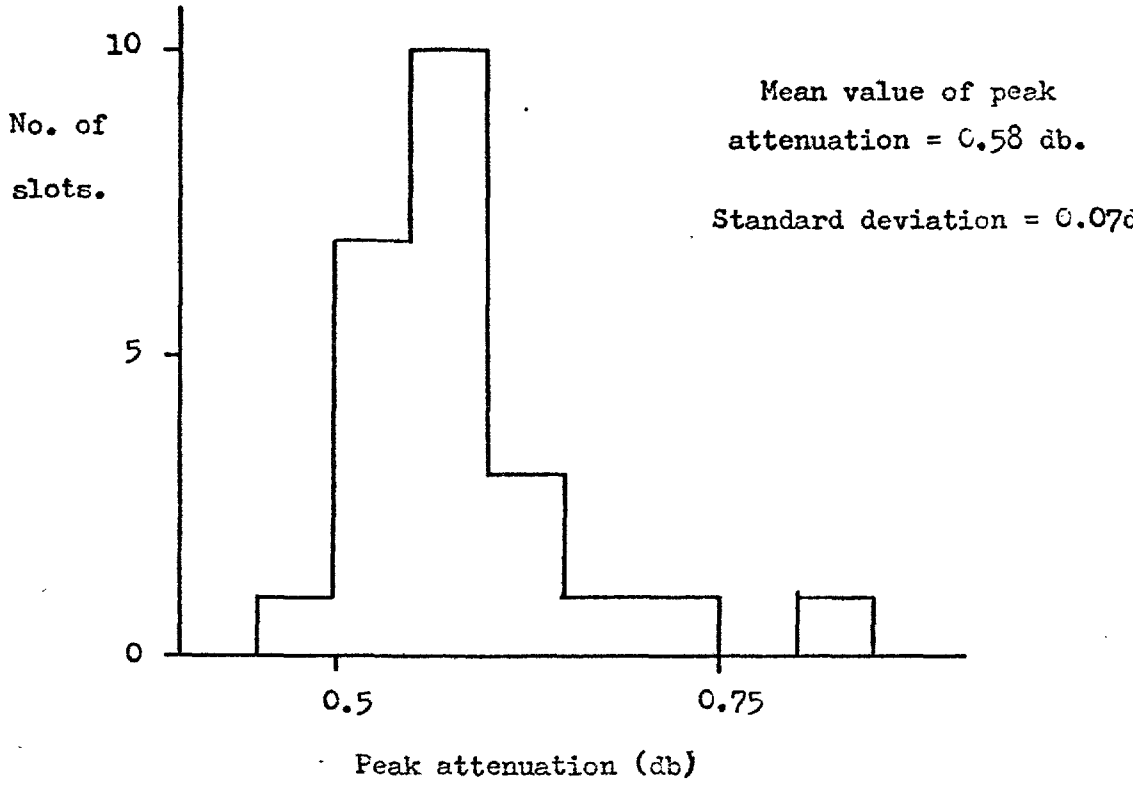

FIGURE 6.3.2. A histogram of the measured values of the frequency of the peak attenuation past individual slots of the 8×3 slot network.

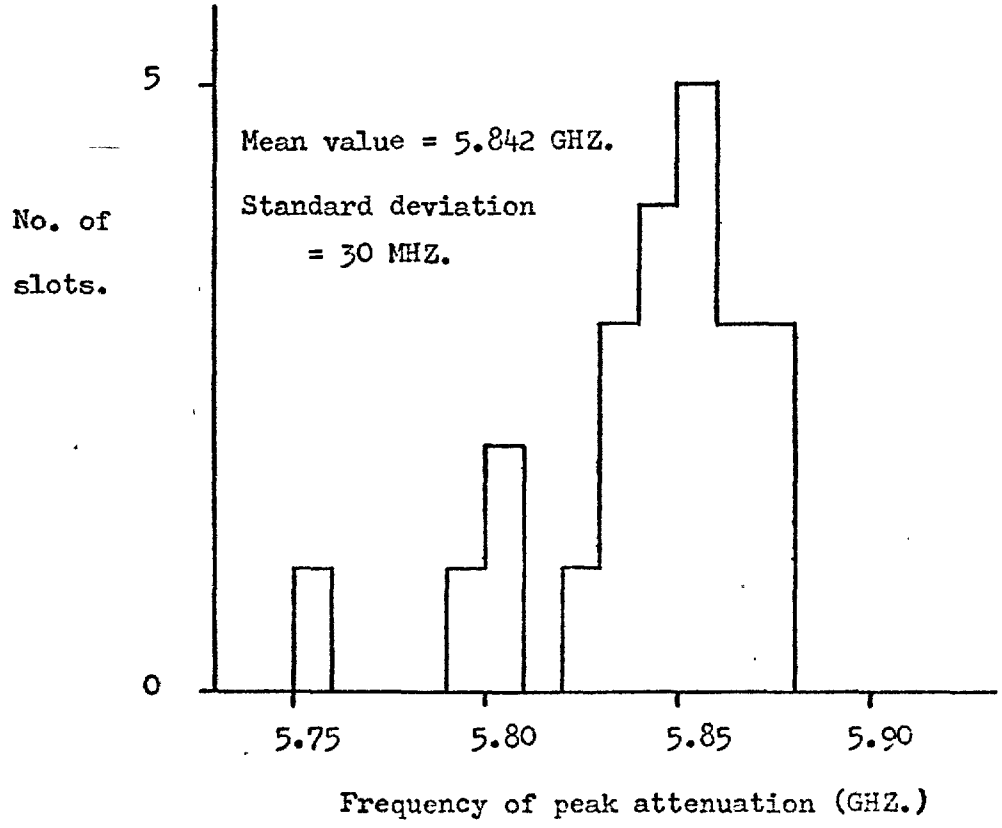

slots occupying approximately a quadrant around it used sequentially in reception. The slots that were not being used at any time were covered with adhesive aluminium tape. In order to compensate for the effects of dispersion between the slots, swept frequency measurements were made over a wide frequency band using a Hewlett-Packard swept frequency oscillator and network analyser with the Weinschel Engineering data normaliser. On careful examination of the results which were obtained as X-Y recordings, it was found that there was not just a single peak of coupled power but three principal peaks at widely separated, but well defined, frequencies. For some pairs of slots one peak dominated, for other combinations two peaks were enhanced and in others all three peaks were at approximately the same level as shown in Figure 6.3.3.(a). Other subsidiary maxima occurred but their frequency and level appeared to be unpredictable. The explanation of this behaviour lay with the residual reactance associated with the main polarisation of the I-shaped slot reported earlier. The lowest frequency peak was associated with cross polarisation to cross polarisation coupling which involved no residual reactance. The highest frequency peak was associated with main polarisation to main polarisation coupling which included two residual reactive components. Similarly the middle peak was accounted for by coupling between different polarisations which included only one residual reactance. These three circuits were resonant at different frequencies and gave rise to the three well defined coupling peaks.

The complicated frequency behaviour of mutual coupling above a ground plane made the results a little difficult to summarise but Figure 6.3.4 shows the peak coupled power between the waveguides containing the slots irrespective of frequency. The variation of the coupled power along the waveguides was slow compared to the rapid decay across the

FIGURE 6.3.3. (a) The coupled power between two waveguides of the 8x3 slot network above a ground plane without baffles or P.T.F.E..
(Slot 8A - Slot 4C)

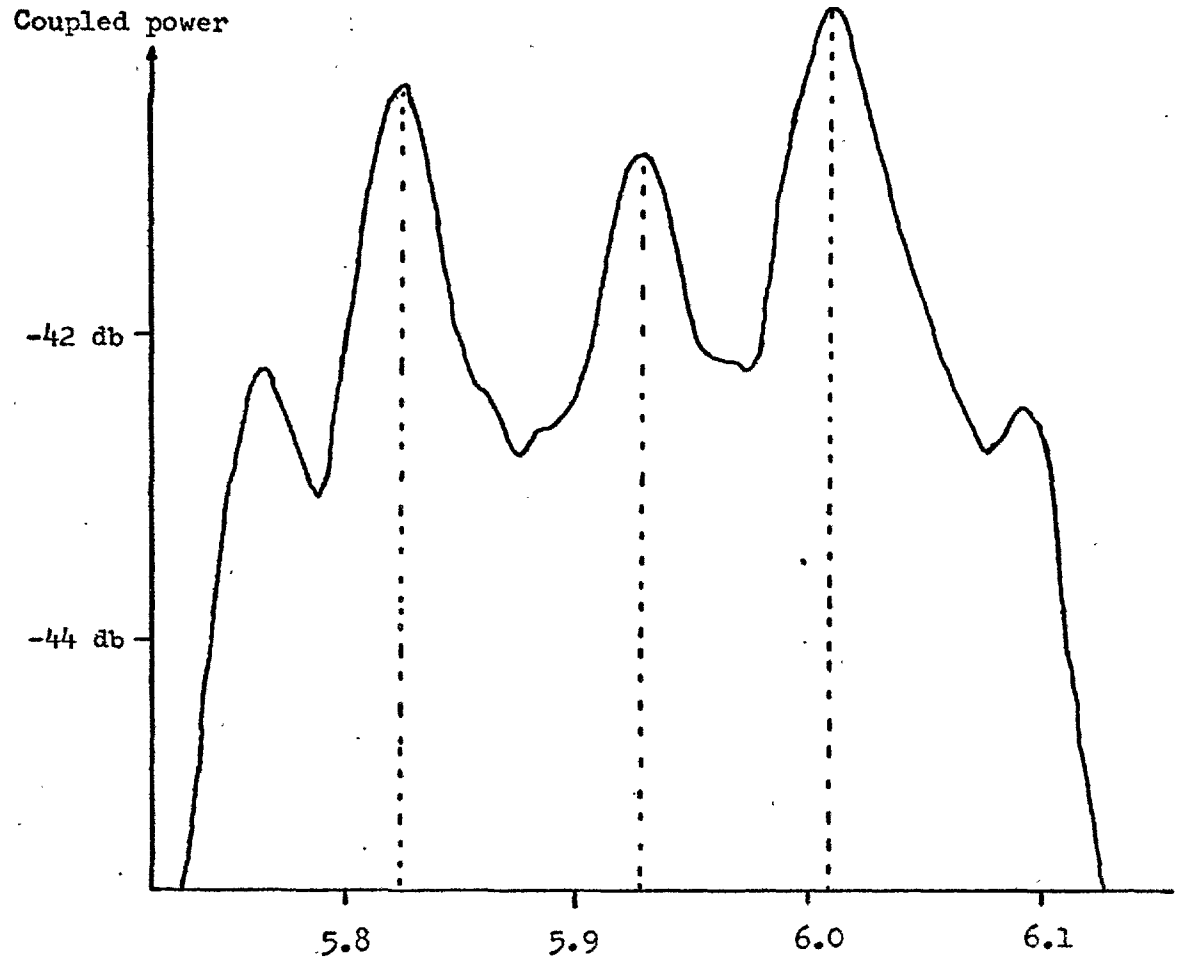

(b) The coupled power for the same slots with the network fitted with 5/8" square baffles

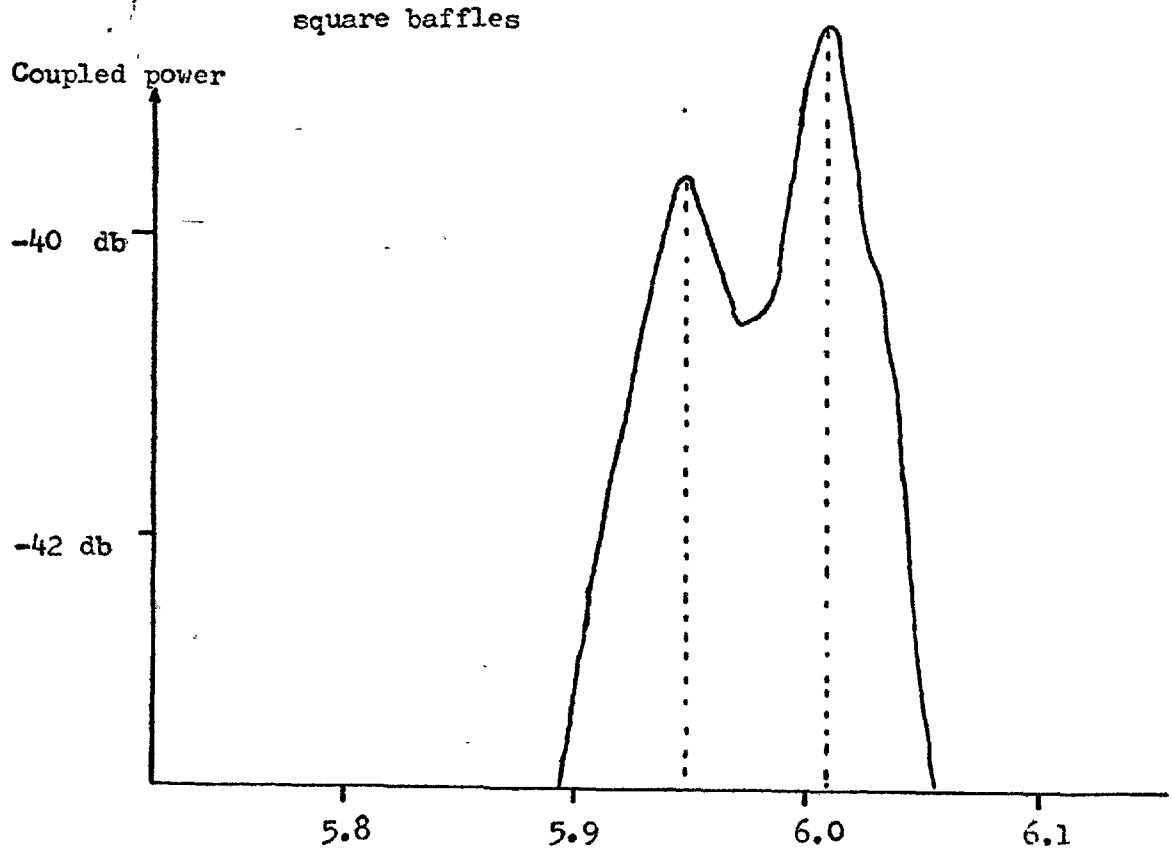

FIGURE 6.3.4. The peak coupled power between two slots of the 8x3 network when fitted with ground plane. One slot is fed and the others used sequentially in reception.

No P.T.F.E. used.

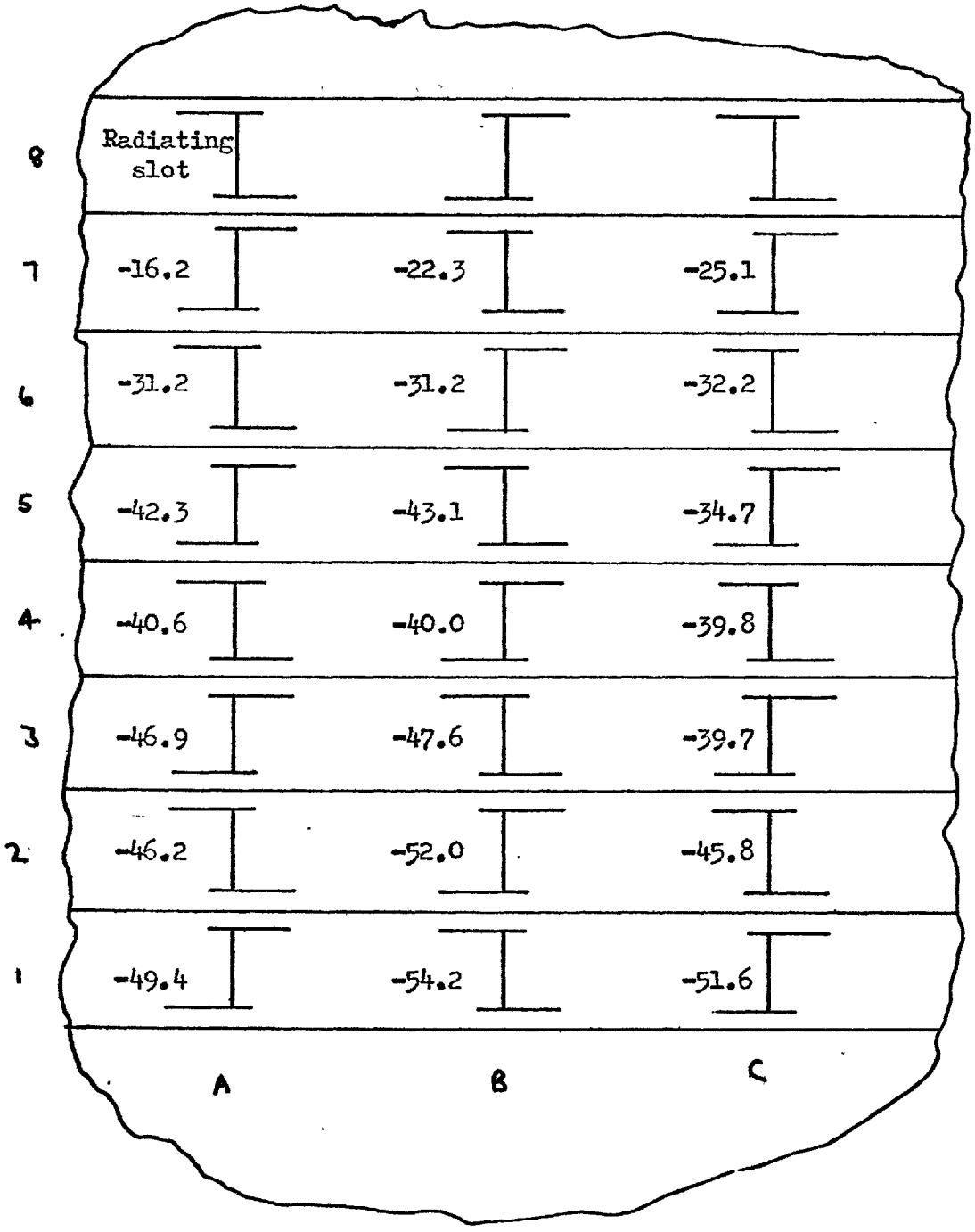

The measurements (db) were made in the coupled waveguide relative to the power in the incident waveguide.

waveguide. This indicated as expected that the centre sections of the slots were dominant in the coupling. The coupling between parallel straight slots was shown in the last section to decay more slowly than between co-linear straight slots.

The frequency dispersion between the components of mutual coupling was also responsible for the ripples in N. Williams experimental results for ⅂-shaped slots. He performed single frequency measurements and if all the components of mutual coupling had resonated at this frequency he would have obtained a smooth curve. However, in different areas around a slot the components of mutual impedance contributed varying amounts to the total so that if a dispersion was introduced between them, a ripple would have resulted in the measured coupled power.

Swept frequency coupled power measurements were also made when $\frac{5}{8}$" square baffles were fitted to the network. It was found that all the major peaks of coupled power occured at the same frequency as the highest frrquency peak when coupling over a ground plane. It appeared that the baffles selected the coupling between main polarisation elements and produced no substantial frequency change in this component other than raising its power level at the expense of the cross-polarisation. A typical swept frequency result is shown in Figure 6.3.3.(b) and this utilised the same pair of slots as used in Figure 6.3.3.(a). Subsidiary maxima occured for some pairs of slots but their behaviour did not follow any discernible pattern. The peak values of coupled power are summarised in Figure 6.3.5.

The phase of the mutual coupling was examined initially at the average frequency of peak attenuation past the individual slots used. A single column of eight slots was employed and the measurements were made both with only the two slots concerned present and with all eight

FIGURE 6.3.5. The peak coupled power between two slots of the 8x3 network when fitted with baffles made from sections of 5/8" square tube. One slot is fed and the others used sequentially in reception.

No P.T.F.E. used.

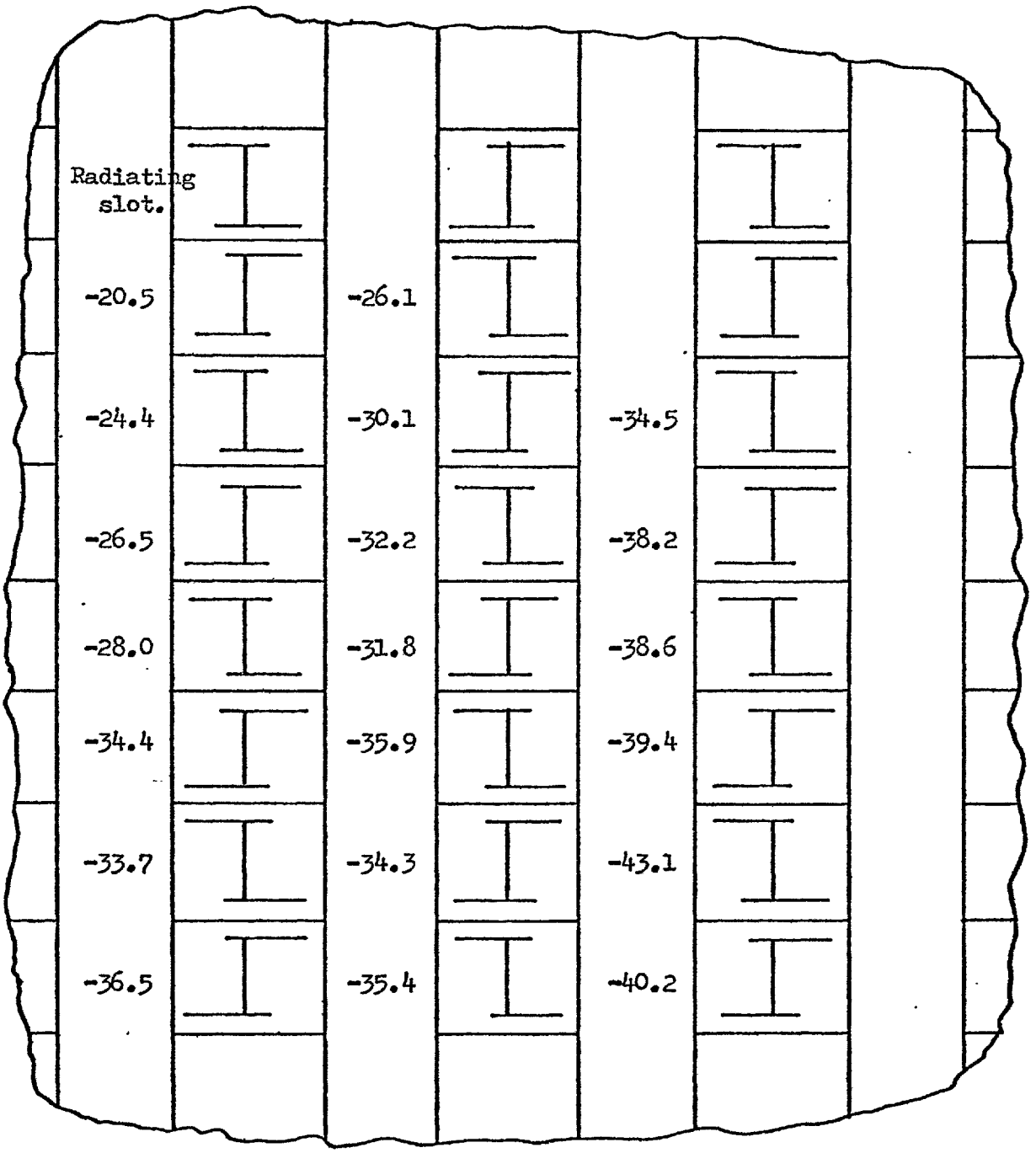

The measurements (db) were made in the coupled waveguide relative to the power in the incident waveguide.

slots present. All excited waveguides were fitted with matched loads made from iron loaded araldite. Initial measurements were made above a ground plane using a Hewlett-Packard network analyser. The waveguides forming the network were all of the same length and the instrument was initially set up with its measurement channel terminating the waveguide containing the radiating slot via a waveguide to coaxial transformer. This was then moved to the coupled waveguide and a load inserted into the fed waveguide. The measured change in the path length had no contribution from the waveguides but was due to the phase length through the slots and to mutual coupling. The phase paths measured in this way for a column of I-slots at resonance radiating over a ground are shown in Figure 6.3.6. after allowance had been made for the phase reversal due to the different hands of the slots and the 90° phase shift through the slots. The latter was associated with the j term in the expression for $^{A}/_{V}$ developed for slot conductances in Chapters 2 and 3. It ensured that secondary waves generated at an excited slot were of the correct phase to produce a net attenuation past the slot.

The results showed that with all eight slots present the phase length between slots was less than the free space separation of their centres. This implied that a fast-wave or leaky-wave was supported by the column of slots. Further evidence for this idea was provided by the results obtained when only two slots were present. For the smaller separation little difference was noted but for large separations the absence of the intermediate guiding structure resulted in a phase length greater than free-space being measured, corresponding to coupling above the ground plane rather than by a guiding structure.

The phase measurements were repeated with the $^{5}/_{8}$" square baffles

FIGURE 6.3.6. The measured phase variation between I-shaped slots radiating over a ground plane at 5.834 GHZ..

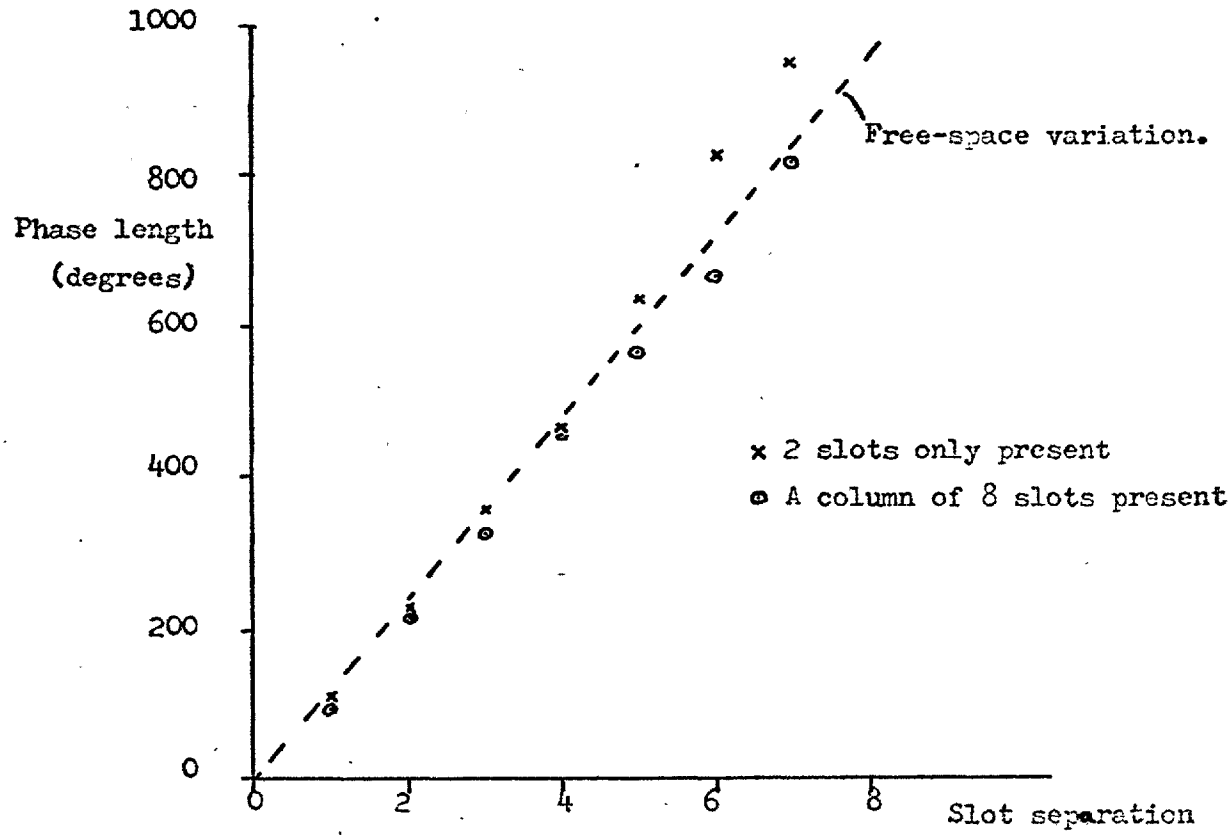

FIGURE 6.3.7. The measured phase variation among I-shaped slots radiating between 5/8" square baffles at 6.063 GHZ..

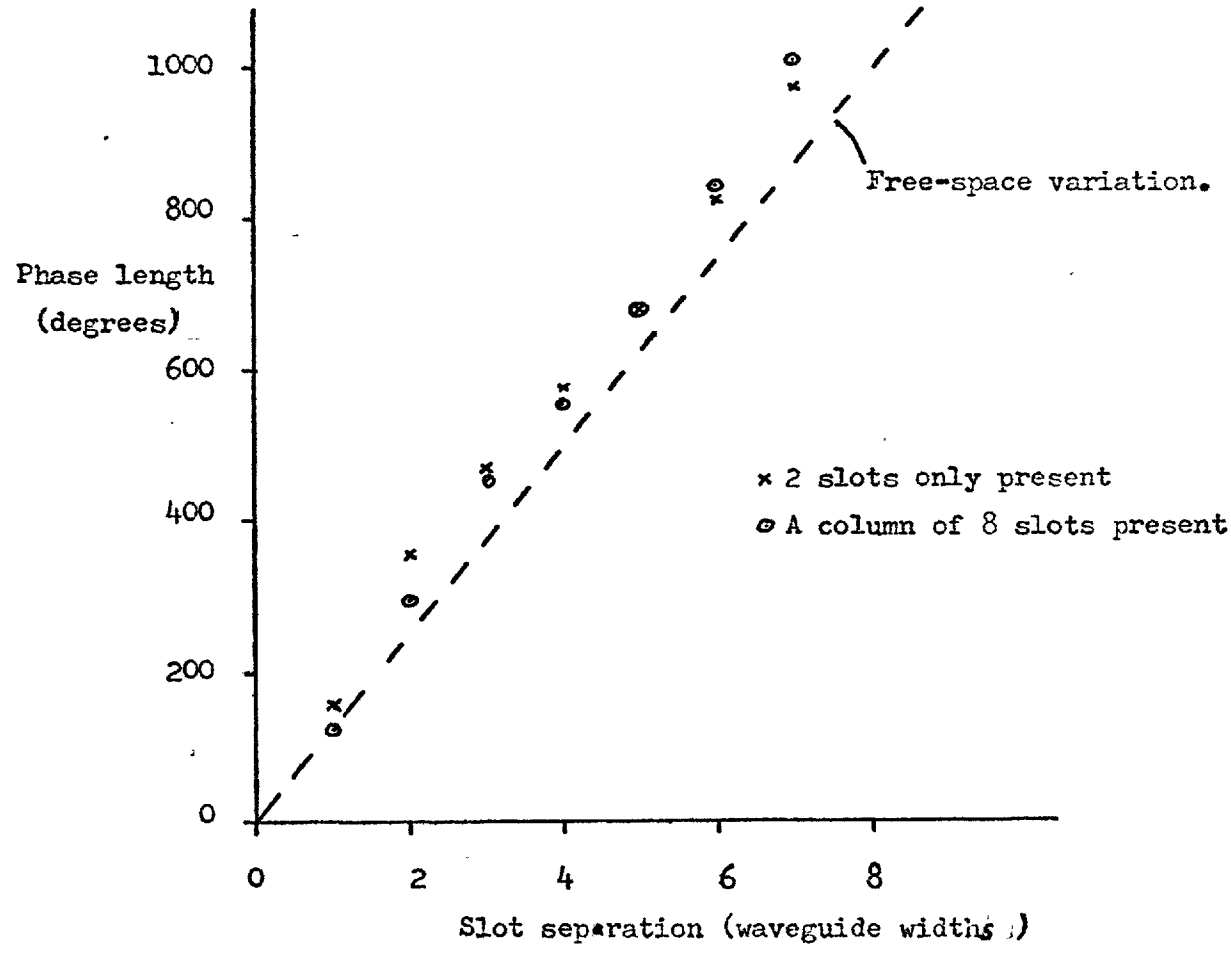

fitted to the network. The results obtained are shown in Figure 6.3.7., and indicated that the phase length of mutual coupling with the baffles was substantially larger than free space even for small slot separations. This type of behaviour could have resulted if a slow--wave was present on the structure but it was extremely difficult to see how such a mode could exist. It was more likely that the additional phase length resulted from the energy being transported away from the ground plane near the top of the baffles. The effect of intermediate slots was negligible which further suggested that there was little energy at the bottom of the baffles away from the fed slot.

The measurements were all repeated with the protective layer of P.T.F.E. fitted and the results are shown graphically in Figures 6.3.8. and 6.3.9.. The phase lengths over a ground plane were substantially increased relative to the free space variation and little change was observed with the $\frac{5}{8}$" square baffles fitted. This was further evidence that when coupling with baffles the field was not so closely bound to the ground plane, the region in which the P.T.F.E. was fitted.

6.4. Leaky-Waves and the Channel Waveguide

It was shown experimentally in the last section that a fast-wave could exist on the slots in a ground plane. The more useful structure for the envisaged application consisted of slots fitted with baffles and P.T.F.E. and some thought was given to what waves could propagate along this structure. The fields that could exist in the channel had to be established and then any additional modes caused by the presences of the P.T.F.E.. Finally on introducing the slots a small perturbation might be observed.

Goldstone and Oliner (1959) investigated a structure they termed

FIGURE 6.3.8. The measured phase variation between I-shaped slots radiating over aground plane fitted with P.T.F.E. at 5.538 GHZ

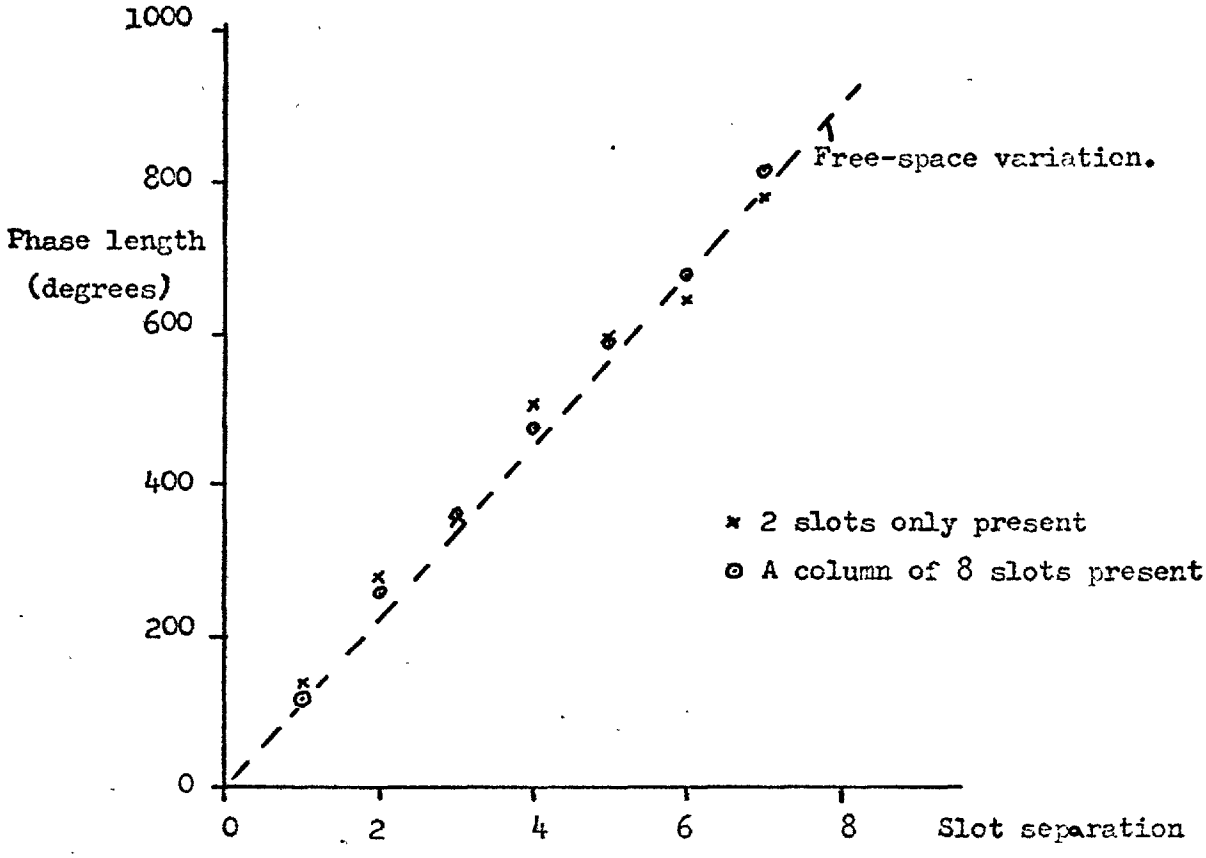

FIGURE 6.3.9. The measured phase variation among I- shaped slots fitted with P.T.F.E. and radiating between 5/8" square baffles at 5.705 GHZ..

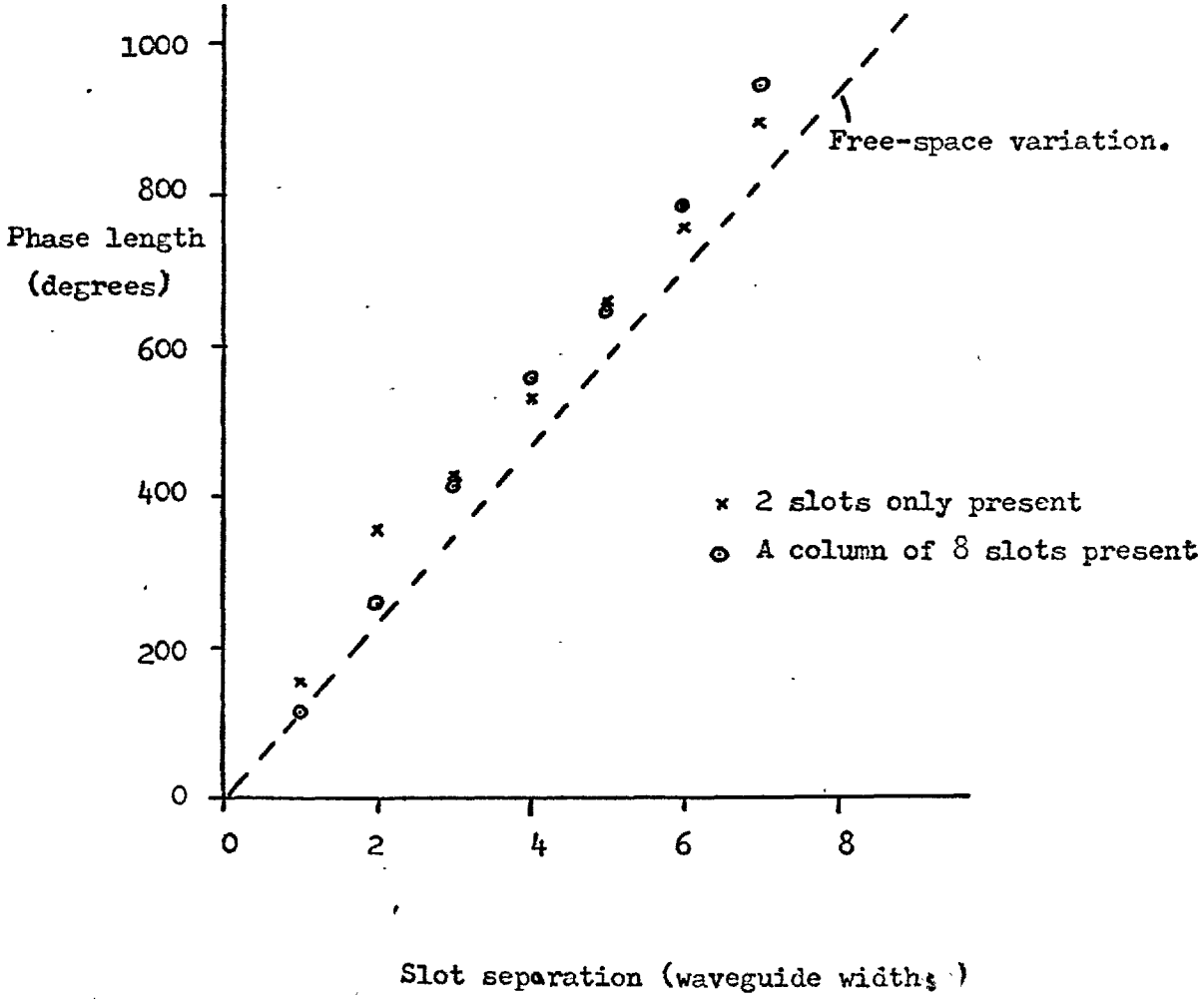

the channel waveguide as part of a study of leaky-wave antennas. The structure they were interested in was a rectangular waveguide with a long continuous slot in the narrow wall which radiated over a ground plane. In the extreme case the slit became the same height as the waveguide and the resulting structure was that of a channel cut in a ground plane. When the baffles were fitted to an array a whole series of channel waveguides resulted. The solutions Goldstone and Oliner obtained corresponded to leaky waves, and were characterised by a complex propogation constant in the direction of propogation. This implied the wave was attenuated as it travelled the attenuation being due to a continuous leakage of energy. In addition they had phase velocities faster than the speed of light, and were not characterised by modes, being associated with regions open to space.

Goldstone and Oliner's method essentially involved finding a perturbation solution of the transverse resonance equation of the structure of interest. The general form of the terminated transmission line which was used to represent a transverely viewed waveguide is shown in Figure 6.4.2.. The transverse wavenumbers k which corresponded to source-free fields in the waveguide were obtained from the solution of the resonance equation.

$$\overleftrightarrow{Y}(k) = \overleftarrow{Y}(k) + \overrightarrow{Y}(k) = 0 \qquad (6.4.1)$$

where $\overleftarrow{Y}$ and $\overrightarrow{Y}$ were the admittances looking to the left and right respectively from some arbitrary reference plane. This equation was difficult to solve for an exact solution but solutions by numerical methods were available. These did not give any insight into the physical behaviour of such systems and Goldstone and Oliner opted for a perturbation approach.

FIGURE 6.4.1. A section of channel waveguide.

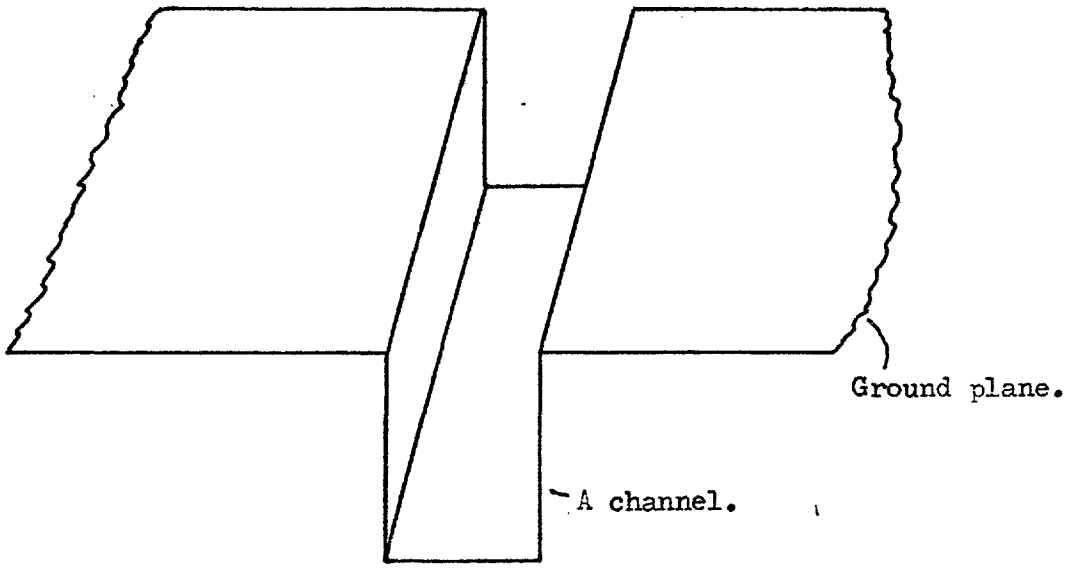

FIGURE 6.4.2. A terminated transmission line representing a waveguide cross-section.

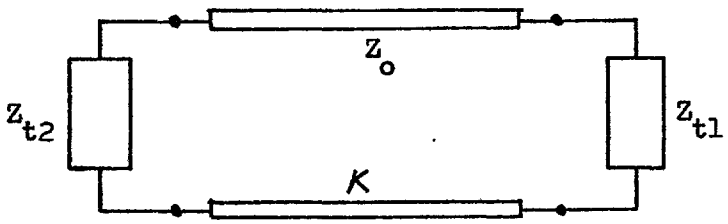

FIGURE 6.4.3. The transverse equivalent network of a uniform leaky rectangular waveguide, in particular the channel waveguide.

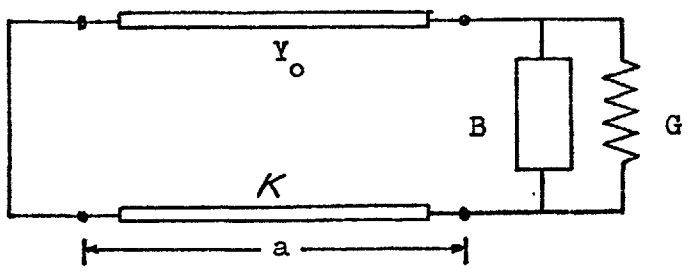

The leaky-wave solution could be regarded as a perturbation of a mode in a "closed" or non-radiating waveguide, so that the transverse wavenumber of the leaky wave could be written as:

$$\kappa = \kappa_o + \Delta\kappa \tag{6.4.2}$$

where κ_o was the wavenumber of the unperturbed mode and $\Delta\kappa$ was the perturbation to be determined. Expansion of the normalised form of (6.4.1) about the point $\kappa = \kappa_o$ to a first order in $\Delta\kappa$ yielded:

$$\Delta\kappa = - \frac{\overleftrightarrow{Y}'(\kappa_o)}{\left(\frac{d\overleftrightarrow{Y}'(\kappa)}{d\kappa}\right)_{\kappa=\kappa_o}} \tag{6.4.3}$$

where

$$\overleftrightarrow{Y}' = \frac{\overleftrightarrow{Y}}{Y_o} \tag{6.4.4}$$

The reference plane for the resonance equation was chosen to be at the mouth of the channel and the admittance at Y_{T_2} was taken to be that of a short circuit. The length of the transmission line was equal to the channel depth. The propagation wavenumber along the z direction for this type of leaky guide was:

$$K_z = \sqrt{K^2 - K_y^2 - \kappa^2} \tag{6.4.5}$$

where $K = 2\pi/\lambda$ and K_y was the propogation wavenumber in the y direction. When (6.4.1) was substituted in (6.4.5), the result obtained neglecting terms involving $(\Delta\kappa)^2$ was

$$K_z \approx \sqrt{K^2 - K_y^2 - \kappa_o^2 - 2\kappa_o \Delta\kappa} \tag{6.4.6}$$

$$\approx \frac{2\pi}{\lambda_{go}} \left(1 - \frac{\kappa_o \lambda_{go}^2}{4\pi^2} \Delta\kappa \right) \tag{6.4.7}$$

where

$$\lambda_{go} = \frac{2\pi}{\sqrt{K^2 - K_y^2 - \kappa_o^2}} \tag{6.4.8}$$

and was the guide wavelength of the unperturbed mode. The real and imaginary parts of the propogation constant along z were then:

$$\frac{\beta}{K} = \frac{\lambda}{\lambda_g} \approx \frac{\lambda}{\lambda_{go}} \left(1 - \frac{\kappa_o \lambda_{go}^2}{4\pi^2} \Delta\kappa_r \right) \tag{6.4.9}$$

$$\alpha\lambda \approx \frac{\lambda\lambda_{go}}{2\pi} \kappa_o \Delta\kappa_i \tag{6.4.10}$$

where

$$K_z = \beta - j\alpha \tag{6.4.11}$$

and

$$\Delta\kappa = \Delta\kappa_r + j\Delta\kappa_i \tag{6.4.12}$$

The perturbation $\Delta\kappa$ of a rectangular leaky waveguide was obtained from (6.4.3) as:

$$\Delta\kappa \approx - \frac{Y_{T'}(\kappa_o) - j \cot \kappa_o a}{\left(\frac{dY_{T'}}{dK}\right)_{=o} + j a \cos^2 \kappa_o a} \tag{6.4.13}$$

The discontinuity for the channel waveguide was not resonant so that the

derivative term could be neglected

$$\Delta K \approx \frac{j}{a} \frac{Y_{T'}(K_o) - j \cot K_o a}{\cos^2 K_o a} \qquad (6.4.14)$$

The problem has thus been reduced to finding the circuit parameters corresponding to the discontinuity at the interface with the half-space. Goldstone and Oliner (1957) calculated the conductance from the relationship

$$G = \frac{P}{|V^2|} \qquad (6.4.15)$$

where P was the real transverse power flow per unit cell and V the modal voltage of the propagating mode in the aperture plane. The transverse power flow per unit cell within the guide must have been equal to the outward radial power flow per unit cell in the half space so that the numerator of (6.4.15) could be calculated from the far field in the half space. The result was of the form:

$$G \approx \frac{bK^2}{2w\mu} \qquad (6.4.16)$$

or when normalised

$$G' = \frac{G}{Y_o} \approx \frac{Kb}{2} \qquad (6.4.17)$$

For the channel waveguide, the wavenumber could be better approximated by regarding the discontinuity at the half plane not as a perturbation of a "closed" waveguide, but as a perturbation of a magnetic wall. The corresponding unperturbed wavenumber was then $K_o = \pi/2a$. When $a \gg b$ corresponding to a very flat channel guide this result was satisfactory.

For the dimensions of the trough formed by the $\frac{5}{8}$" square baffles a different approach was necessary. Since the phase part of the desired propogation constant depended mainly on the energy storage property or susceptance of the discontinuity the method was formulated in terms of the resonance problem involving the susceptance only:

$$\cot K_o a = B'(K_o) \tag{6.4.18}$$

This equation for real K_o could be solved to any desired degree of accuracy by successive approximations and yielded

$$K_o \approx \frac{\pi}{2a} - \frac{1}{a} B'\left(\frac{\pi}{2a}\right) \tag{6.4.19}$$

The solution of (6.4.18) was substituted in (6.4.14) and resulted in:

$$\Delta K = \frac{j}{a} \frac{G'(K_o)}{\csc^2 K_o a} \tag{6.4.20}$$

The attenuation constant and guide wavelength of the H type leaky wave in the channel guide were obtained by Oliner and Goldstone as:

$$\frac{\beta}{k} = \frac{\lambda}{\lambda_g} \approx \sqrt{1 - \frac{\lambda^2 K_o^2}{4\pi^2}} \tag{6.4.21}$$

$$\alpha\lambda \approx \left(\frac{\lambda}{a}\right) \frac{\lambda_g K_o}{2\pi} \frac{G'(K_o)}{\csc^2 K_o a} \tag{6.4.22}$$

These results indicated that if the baffles were made taller the attenuation constant of the guide would be less and the guide wavelength would approach the free-space value. This behaviour was characteristic of leaky waves.

6.5. Analysis of Trough Guide Modes

The structure consisting of the baffles and dielectric was similar to the trough waveguide structure investigated by Cohn in (1960) and which also appeared in Benson (1969). Initially an H-guide formed by a slab of dielectric between two parallel plates, as shown in Figure 6.5.1., was considered by Cohn. It emerged that there were two classes of mode designated PE_{mn} and PM_{mn}, where the letters stood for parallel electric or parallel magnetic and indicated that the relevant field was parallel to the dielectric-air interface.

The analysis proceeded with the assumption being made that the permeability in all three regions was that of free space but for the permittivity:

$$\epsilon_1 = K_1 \epsilon_o \qquad (6.5.1)$$

and

$$\epsilon_2 = \epsilon_3 = K_2 \epsilon_o \qquad (6.5.2)$$

where ϵ_o was that of free space. The symmetry resulted in the modal solutions being either even or odd depending on whether E_y was an even or odd function of x.

The trough guide structure resulted when a conducting wall was erected in the y-z plane, as shown in Figure 6.5.2.. The conducting wall suppressed the even modes of the H-guide so that only the odd modes could propogate.

Cohn showed that the field components for the odd symmetry PM modes were after neglecting a time dependence of the form $e^{j(wt - \beta z)}$:

FIGURE 6.5.1. A cross section of an H guide.

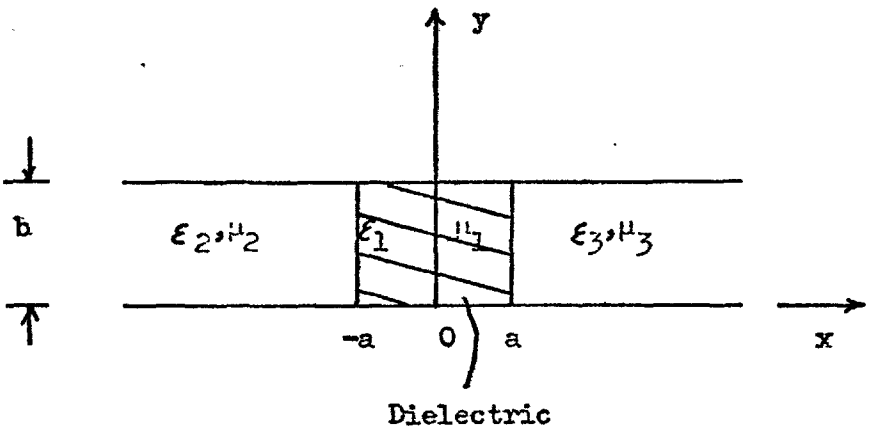

FIGURE 6.5.2. Across section of a trough guide.

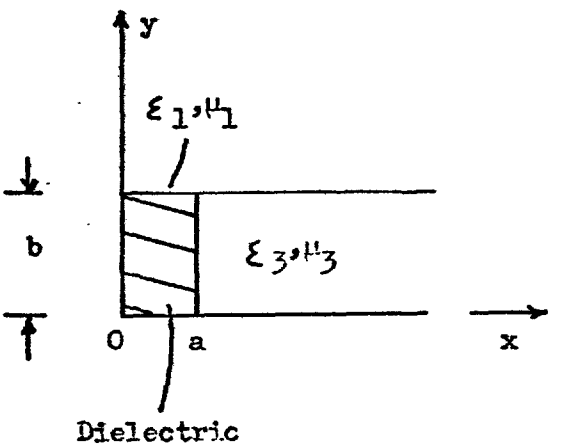

In Region 1:

$$
\left.
\begin{aligned}
E_{x1} &= j \frac{\beta^2 + (\frac{n\pi}{b})^2}{w\epsilon_1(\frac{\pi n}{b})} \cos k_d x \sin \frac{n\pi}{b} y \\
E_{y1} &= - j \frac{k_d}{w\epsilon_1} \sin k_d x \cos \frac{n\pi}{b} y \\
E_{z1} &= - \frac{k_d \beta}{w\epsilon_1(\frac{n\pi}{b})} \sin k_d x \sin \frac{n\pi}{b} y \\
H_{x1} &= 0 \\
H_{y1} &= \frac{j\beta}{(\frac{n\pi}{b})} \cos k_d x \sin \frac{n\pi}{b} y \\
H_{z1} &= \cos k_d x \cos \frac{n\pi}{b} y
\end{aligned}
\right\} \quad (6.5.3)
$$

and for Region 3:

$$
\left.
\begin{aligned}
E_{x3} &= j \frac{\beta^2 + (\frac{n\pi}{b})^2}{w\epsilon_2(\frac{n\pi}{b})} \cos k_d a \, e^{k_2(a-x)} \sin \frac{n\pi}{b} y \\
E_{y3} &= - j \frac{k_d}{w\epsilon_1} \sin k_d a \, e^{k_2(a-x)} \cos \frac{n\pi}{b} y \\
E_{z3} &= - \frac{k_d \beta}{w\epsilon_1(\frac{n\pi}{b})} \sin k_d a \, e^{k_2(a-x)} \sin \frac{n\pi}{b} y
\end{aligned}
\right\} \quad (6.5.4)
$$

$$\left.\begin{aligned} H_{x3} &= 0 \\ H_{y3} &= j \frac{\beta}{(\frac{n\pi}{b})} \cos k_d a \; e^{k_2(a-x)} \sin \frac{n\pi}{b} y \\ H_{z3} &= \cos k_d a \; e^{k_2(a-x)} \cos \frac{n\pi}{b} y \end{aligned}\right\} \quad (6.5.4)$$

Similar expressions were derived by Cohn for the other types of mode, all of which were in general hybrid with E_z and H_z non-zero.

The transverse wavenumbers in the inner region k_d and the outer region k_2 were connected by equating the tangential electric field E_y at the boundary. The quantity $k_d a$ had to be specified in a particular quadrant, i.e.,

$$(m - 1)\frac{\pi}{2} \leqslant (k_d a) \leqslant m\frac{\pi}{2} \quad (6.5.5)$$

For the odd symmetry PM modes:

$$k_2 = \frac{k_2}{k_1} k_2 \tan k_2 a \quad \text{with m odd} \quad (6.5.6)$$

while for the odd symmetry PE modes:

$$k_2 = - k_2 \cot k_2 a \quad \text{with m even} \quad (6.5.7)$$

Cohn also showed that for all modes of the H-guide:

$$k_d^2 + (\frac{n\pi}{b})^2 = w^2 \mu_o \epsilon_o K_1 - \beta^2 \quad (6.5.8)$$

$$k_2^2 - (\frac{n\pi}{b})^2 = \beta^2 - w^2 \mu_o \epsilon_o K_2 \quad (6.5.9)$$

When these equations were added:

$$k_d^2 + k^2 = w^2\mu_o\epsilon_o(K_1 - K_2) \qquad (6.5.10)$$

which when substituted in (6.5.6) or (6.5.7) could be solved for $k_d a$.

For odd symmetry PM modes:

$$\pi^2(\frac{2a}{\lambda_o})^2(K_1 - K_2) = (k_d a)^2\left[1 + (\frac{K_2}{K_1})^2 \tan^2 k_d a \right] \qquad (6.5.11)$$

and for odd symmetry PE modes

$$\pi^2(\frac{2a}{\lambda_o})^2(K_1 - K_2) = \left[\frac{kd_a}{\sin kd_a} \right] \qquad (6.5.12)$$

Equations (6.5.11) and (6.5.12) were used by Cohn to show that a necessary requirement for the mth. rank mode to propogate was that the inequality:

$$\frac{2a}{\lambda_o} > \frac{m - 1}{2\sqrt{\Delta K}} \qquad (6.5.13)$$

be satisfied where:

$$\Delta K = K_1 - K_2 \qquad (6.5.14)$$

For the trough guide formed by the baffles and P.T.F.E. fitted to the array a ~ 0.01", λ_o ~ 2" and ΔK ~ 1.4, so that m could be no bigger than one. The odd symmetry PE modes required by equation (6.5.7) that m be even. The case m equal zero was trivial and so odd symmetry PE modes could not be supported by the P.T.F.E. at the bottom of the baffles.

There was also a requirement on b except for the n = 0 order PE modes. From equation (6.5.8) it could be seen that b had to exceed a certain critical value b_c for the propogation constant β to be real. By setting $b = b_c$ and $\beta^2 = 0$ the value of b_c was found as:

$$\frac{b_c}{n\lambda} = \frac{\pi(\frac{2a}{\lambda})}{\left\{\pi^2(\frac{2a}{\lambda})^2 K_1 - (k_d a)^2\right\}^{\frac{1}{2}}} \qquad (6.5.15)$$

By using equations (6.5.11) and (6.5.12) the $\frac{2a}{\lambda}$ term could be eliminated to leave for odd symmetry PM modes:

$$\frac{b_c}{\lambda} = \frac{n}{2}\left\{\frac{K_1^2 + K_2^2 \tan^2 k_d a}{K_1 K_2^2 \tan^2 k_d a + K_1^2 K_2}\right\}^{\frac{1}{2}} \qquad (6.5.16)$$

and for odd symmetry PE modes:

$$\frac{b_c}{\lambda} = \frac{n}{2}\left\{K_1 \cos^2 k_d a + K_2 \sin^2 k_d a\right\}^{\frac{1}{2}} \qquad (6.5.17)$$

For the trough formed by the baffles and P.T.F.E. the thickness of the P.T.F.E. only allowed odd symmetry PM modes to propogate. Equation (6.5.16) however provided a further constraint on these modes. As $\frac{2a}{\lambda_o}$ was small $k_d a$ approached $(m - 1)\frac{\pi}{2}$ and $\frac{b_c}{\lambda}$ approached $\frac{n}{2}(K_2)^{-\frac{1}{2}}$. Region 2 was air so K_2 was unity and:

$$b_c \sim \frac{\lambda}{2} \qquad (6.5.18)$$

b_c was however maintained less than half a wavelength so that the cross

polarisation was suppressed. This condition and the small thickness of the dielectric ensured that no trough guide mode could be supported. It had already been shown however that a channel guide mode could be supported on the structure by the discontinuity at the top of the baffles where they formed an interface with the half space.

6.6. Possible Modifications to the Baffle Design

It was realised early in this study that the mutual impedance between elements would play a major role in the performance of an array. If sufficient information was available it ought to have been possible to correct errors caused by mutual coupling for one beam position. However, on phase scanning the beam, a different correction would be required, so that to maintain an acceptable sidelobe level over a reasonable scan volume, the mutual impedances and hence the required corrections had to be minimised. Some thought was given to re-designing the baffles to achieve this aim. It was also desirable that the baffles should further suppress the cross-polarisation, although this was expected to involve either reducing their separation of increasing their height. It was however realised that if the baffle heights was increased the attenuation of the leaky-wave would decrease and it would radiate over a bigger effective aperture, perhaps introducing nulls into the element radiation pattern. This was highly undesirable as if the beam of a phased array was steered to a null direction a severe mismatch would have occurred.

The fitting of the $\frac{5}{8}$" square baffles to a linear array had already been shown to reduce coupling between non-adjacent slots presumably due to the choke action of the intervening ditches. It was thought that a further improvement could have been obtained by introducing an additional

choke into the top face of the baffles. Accordingly some $\frac{5}{8}$" square baffles were made out of brass bar and $\frac{1}{16}$" wide grooves 0.5" deep were cut in their top face using a slitting saw. When fitted to the 8 x 3 slot network, operated without P.T.F.E. at the average frequency of peak slot conductance the grooves were fractionally deeper than a quarter of a wavelength. The peak coupled powers between pairs of slots occurred around the same frequency and the values obtained are shown in Figure 6.6.1. When compared with the results for plain baffles shown in Figure 6.3.5., a considerable reduction in the mutual coupling was revealed. These baffles had demonstrated the advantage of having a choke groove but for even a reasonable sized array would have been excessively heavy. If their particular cross section was highly desirable for large arrays, a special extrusion could have been made. However, for the purposes of this study a simpler solution was required and thought was given to forming a choke groove by fitting side plates to tubular baffles. Although Goldstone and Oliner's results could not be applied directly to this geometry it was expected that the leaky-wave would be enhanced so that the radiation pattern of a single slot fitted with these baffles would have to be investigated.

The structure formed by the baffles fitted with side plates was similar to that investigated by Dufort (1968). He investigated an infinite array of parallel plate waveguides which radiated into the half-space. Alternate waveguides were fed by matched generators and the intervening waveguides were terminated in short circuits at a certain depth from the aperture. As the array was of infinite extent he was able to apply Floquet's theorem in a similar manner to Amitay, Galiner and Wu (1972) and reduced the problem to consideration of a unit cell. This consisted of two waveguides, one fed and one parasitic

FIGURE 6.6.1. The peak coupled power between two slots of the 8x3 network when fitted with 5/8" square baffles with grooves 0.5" deep by 1/16" wide cut in the top face. One slot is fed and the others used sequentially in reception.

No P.T.F.E. used.

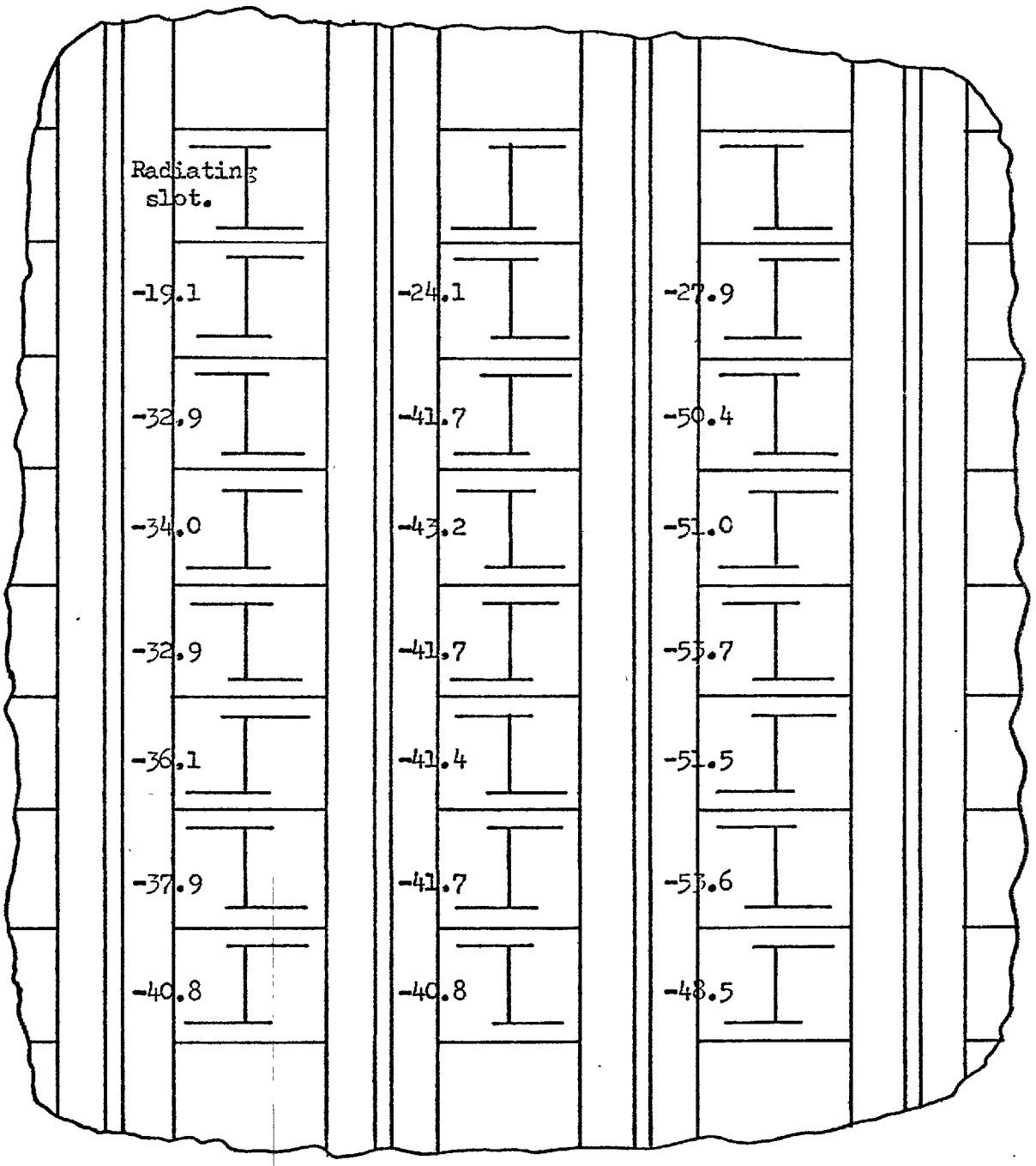

The measurements (db) were made in the coupled waveguide relative to the power in the incident waveguide.

and a region of free space, and could be considered as a three port device. The properties of such a lossless device (Montgomery, Dicke and Purcell (1948)) could be used to show that the power coupled between two ports depended upon the impedance of the third. For the baffles this was interpreted to mean that the reflection coefficient at the aperture fed by the slots depended upon the depth of the ditch, in their top face. Dufort (1968) attempted a complete analysis using a modification of the method of Whitehead (1951) which was similar to work done by Heins and Carlson (1947). For an array with alternate waveguides fed and parasitic he showed that for broadside operation the shorts should be 0.3 wavelengths inside the waveguide. For arrays scanned only in the E-plane the optimum value was smaller and for arrays scanned only in the H-plane larger. From a practical point of view it was likely to be critically important that the impedance seen at the aperture was capacitive rather than inductive. This result was also in broad general agreement with several recent papers (e.g. Hannan and Litt (1968)) in which various devices have been used to capacitively load the apertures of phased array antennas.

The result was also investigated experimentally using two sets of side plates which were fitted in turn to the sides of the $\frac{5}{8}$" square baffles, of the 8 x 3 slot network. One set of plates was 1.03" high and produced an inductive ditch between columns of slots while the other set was 1.18" high and produced a capacitive ditch. Neither set of plates, when fitted, resulted in major changes in the frequency response of the individual slots. The peak coupled powers between pairs of slots are however shown in Figures 6.6.2. and 6.6.3.. The capacitive baffles produced a major reduction in the power coupled between all pairs of slots except for adjacent slots compared to when fitted with $\frac{5}{8}$" square

FIGURE 6.6.2. The peak coupled power between two slots of the 8x3 network when fitted with baffles made from sections of 5/8" square tube with side plates 1.18" 21 S.W.G..(Capacitive) One slot is fed and the others used sequentially in reception.

No P.T.F.E. used.

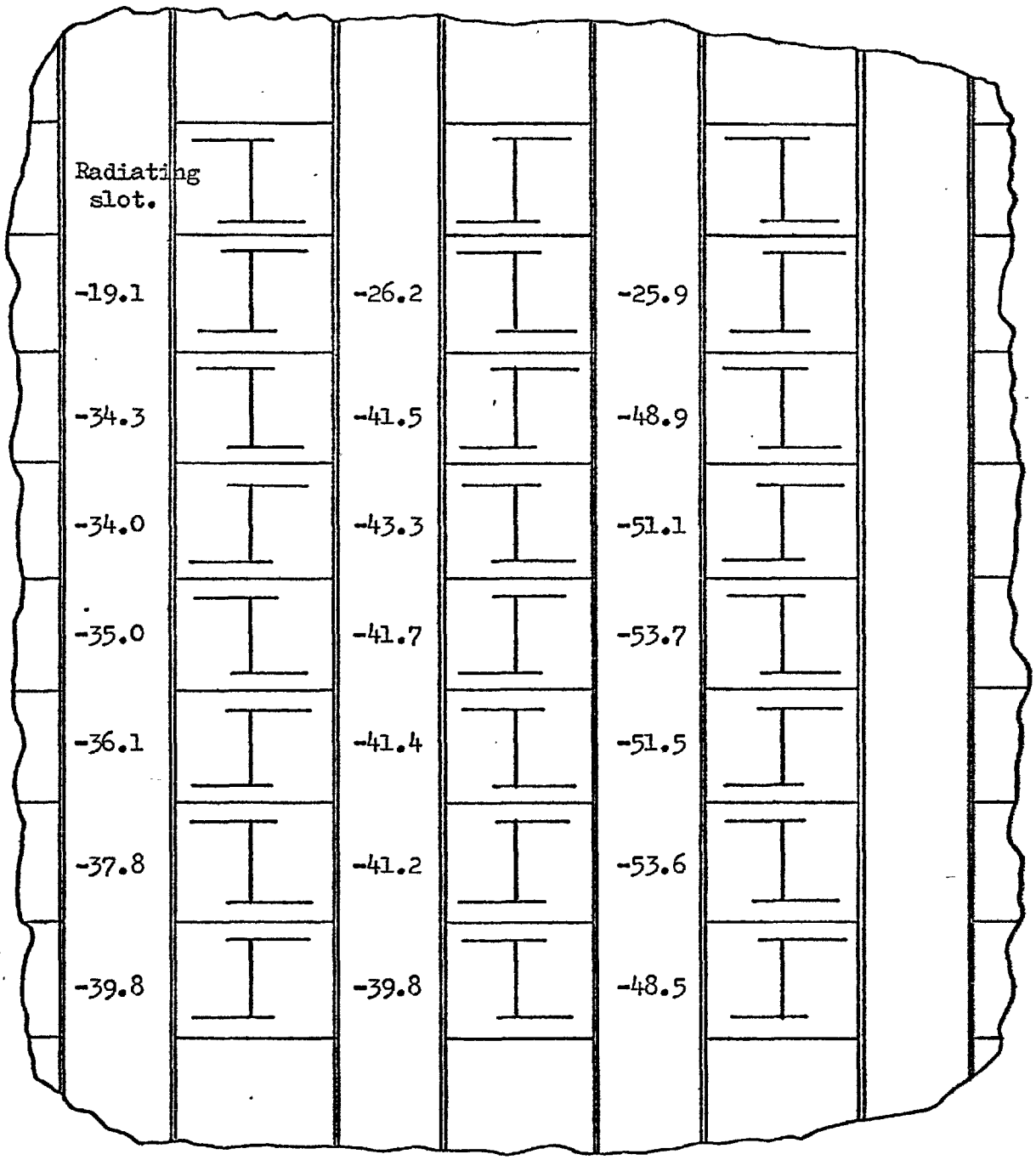

The measurements (db) were made in the coupled waveguide relative to the power in the incident waveguide.

FIGURE 6.6.3. The peak coupled power between two slots of the 8×3 network when fitted with baffles made from sections of 5/8" square tube with side plates 1.03" high 18 S.W.G. (Inductive). One slot is fed and the others used sequentially in reception.

No P.T.F.E. used.

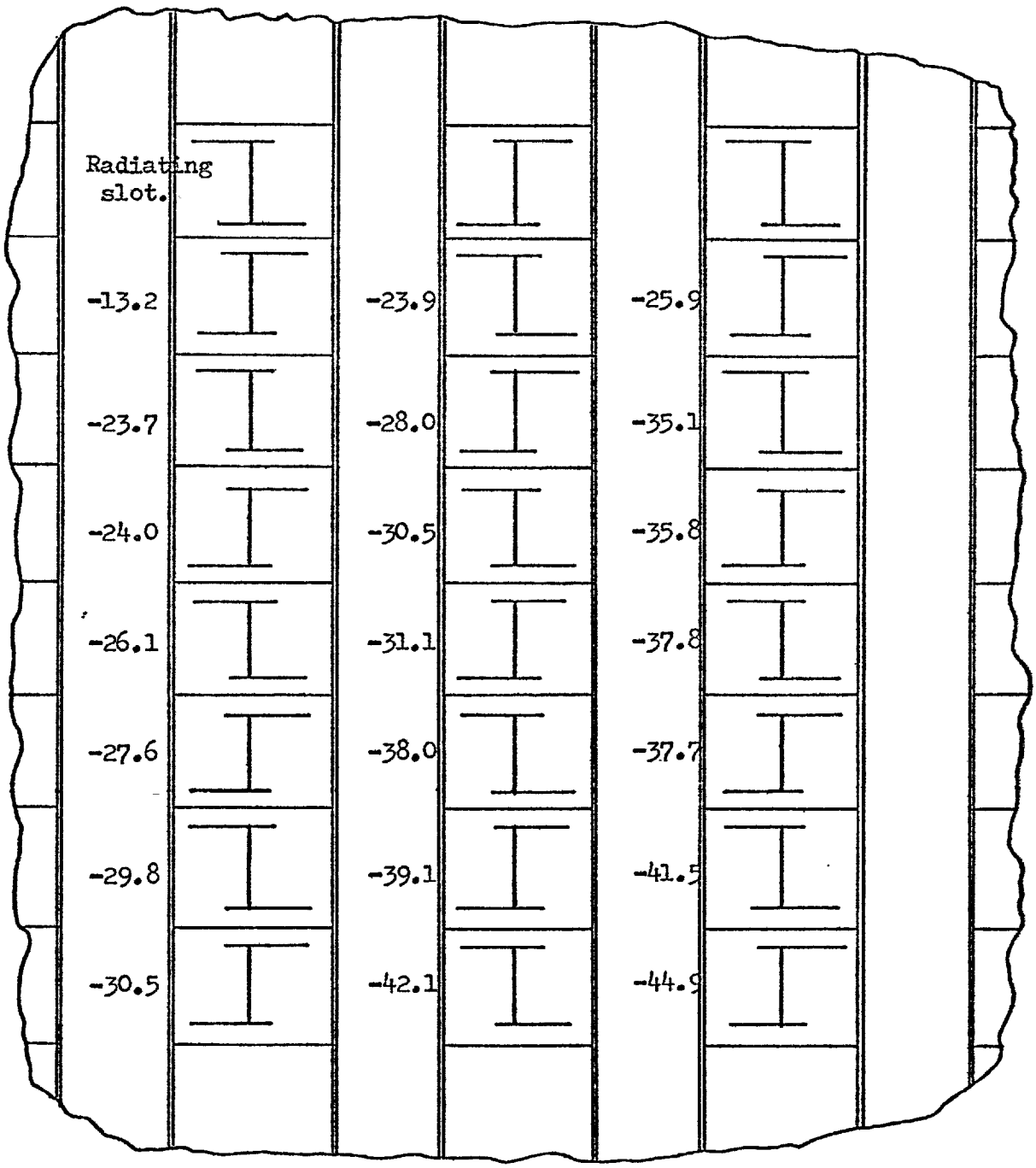

The measurements (db) were made in the coupled waveguide relative to the power in the incident waveguide.

baffles. However an increase in the slot conductances was noted, presumably due to the reduced mismatch at the top of the baffles. When the coupling was expressed in terms of coupled voltages across the slots an improvement was noticed even for adjacent slots in the same column. Similarly when the inductive baffles were used the power coup led between pairs of slots was increased, as shown in Figure 6.6.3..

The radiation properties of a slot fitted with baffles were then investigated. Initially both the near and far field radiation patterns of a slot radiating over a ground plane were measured. It was found that the slot had a broad radiation pattern with some ripple which was thought to be due to the large ground plane surrounding the slot being of finite dimensions, as shown in Figure 6.6.4.. The near field pattern of the slot was measured using the rig used in the last chapter to investigate the near field properties of the thirty slot linear array. The amplitude pattern is shown in Figure 6.6.5., and the effective aperture of the slot was confined to a fairly small area, which gave the broad far field radiation pattern. The phase distribution shown in Figure 6.6.6. corresponded to waves propogating away from the slot above the ground plane.

The same measurements were then repeated with the slot fitted with $\frac{5}{8}$" square baffles. In this case the near field patterns were of particular interest because the presence of leaky wave could be determined. Typical near field amplitude and phase measurements are shown in Figures 6.6.7. and 6.6.8.. From such measurements the attenuation gradient and phase velocity of the energy propogating between the baffles was found. The measured values are compared in Table 6.6.1. with theoretical results obtained using Goldstone and Oliner's formulae, ignoring the presence of the P.T.F.E.. Excellent agreement was obtained

FIGURE 6.6.4. The radiation pattern of a single I-shaped slot in a large ground plane. The pattern is plotted in the plane containing the central arm of the slot.

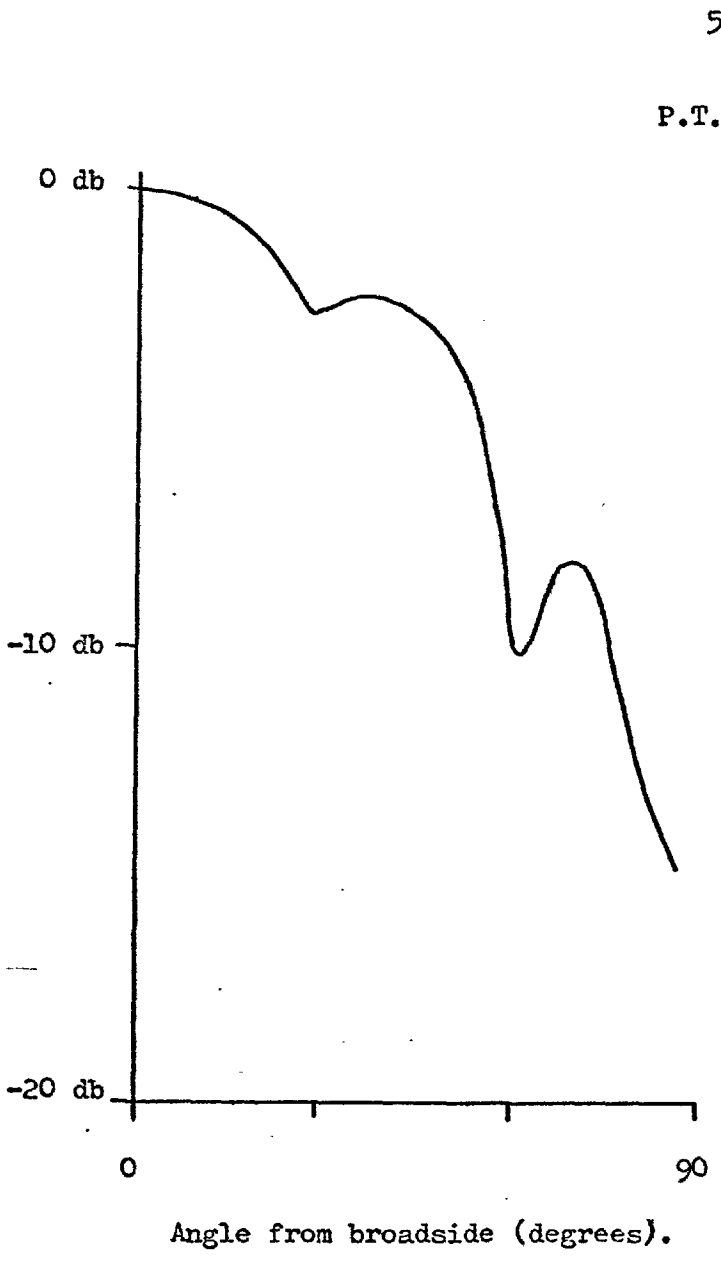

FIGURE 6.6.5. The aperture amplitude distribution of an I-shaped slot, radiating above a ground plane.

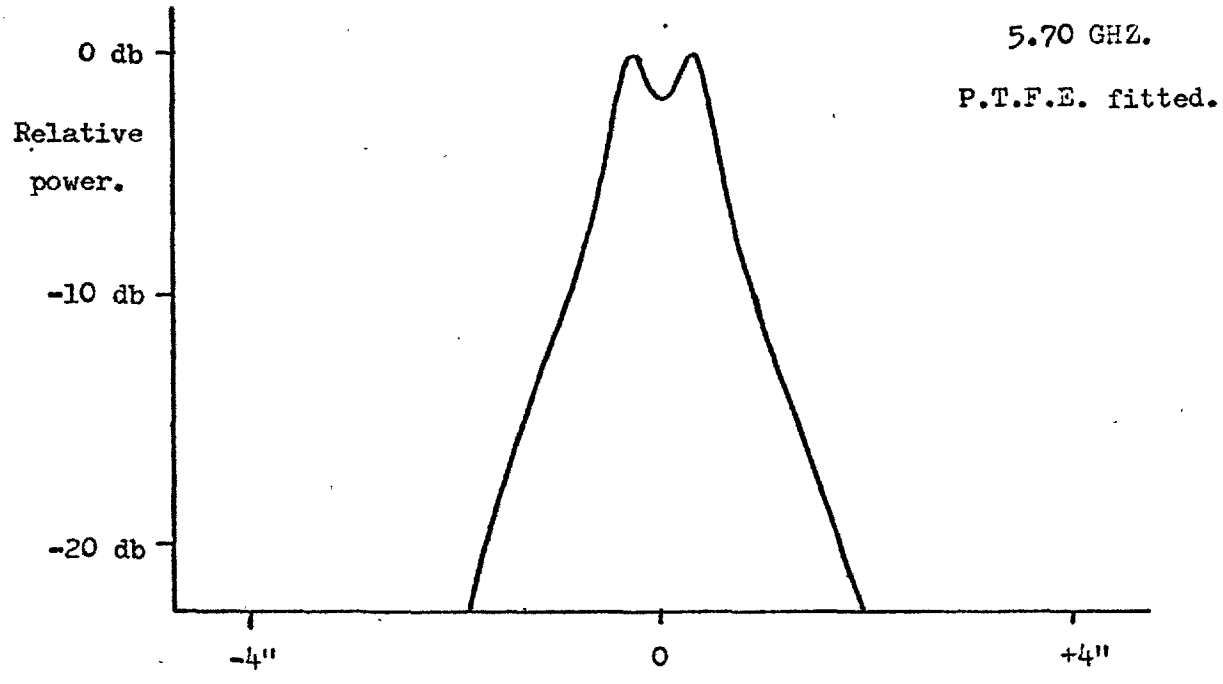

FIGURE 6.6.6. The aperture phase distribution of an I-shaped slot, radiating above a ground plane.

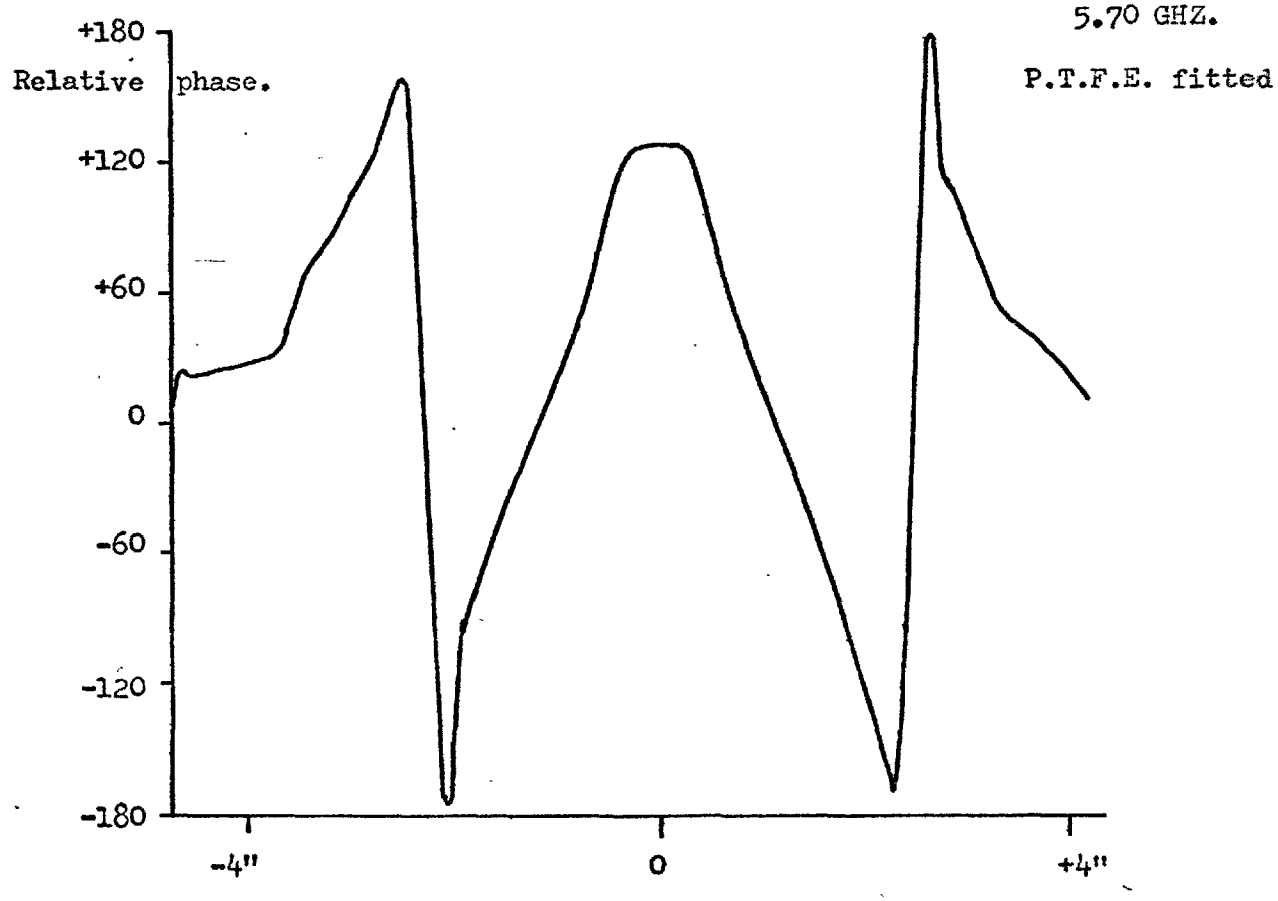

FIGURE 6.6.7. The aperture amplitude distribution measured between 5/8" square baffles .

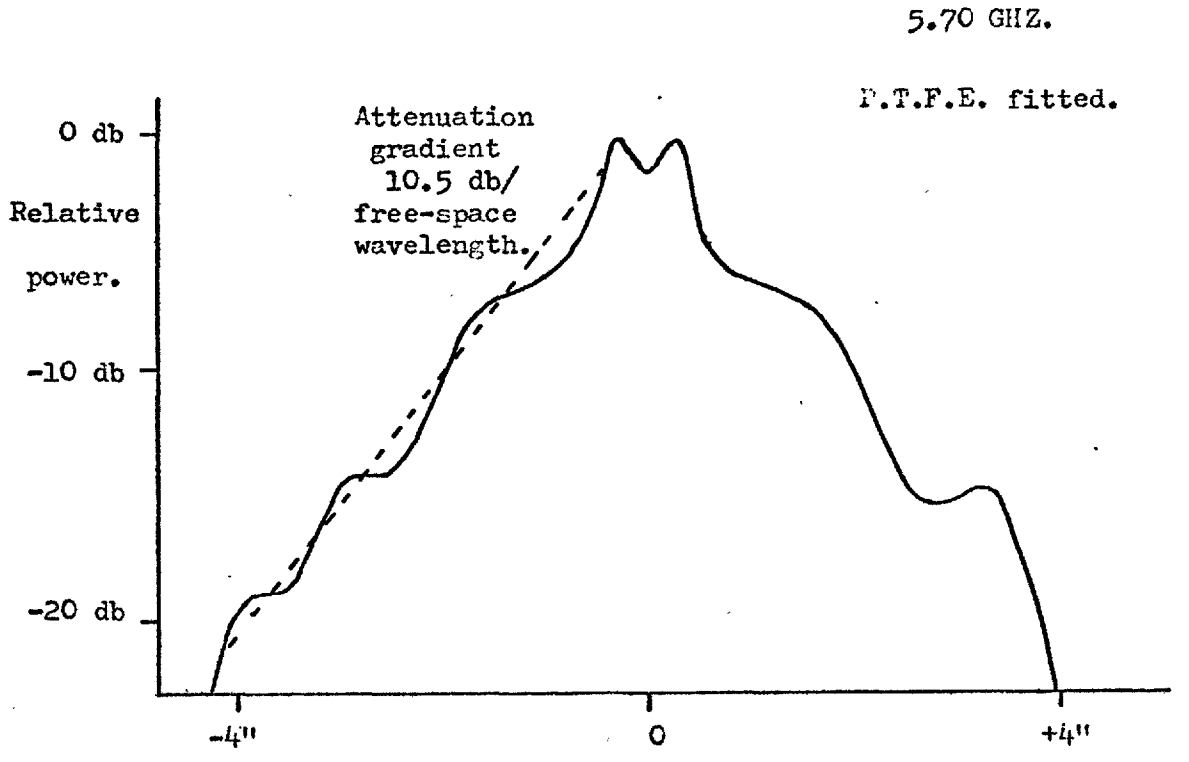

FIGURE 6.6.8. The aperture phase distribution measured between 5/8" square baffles.

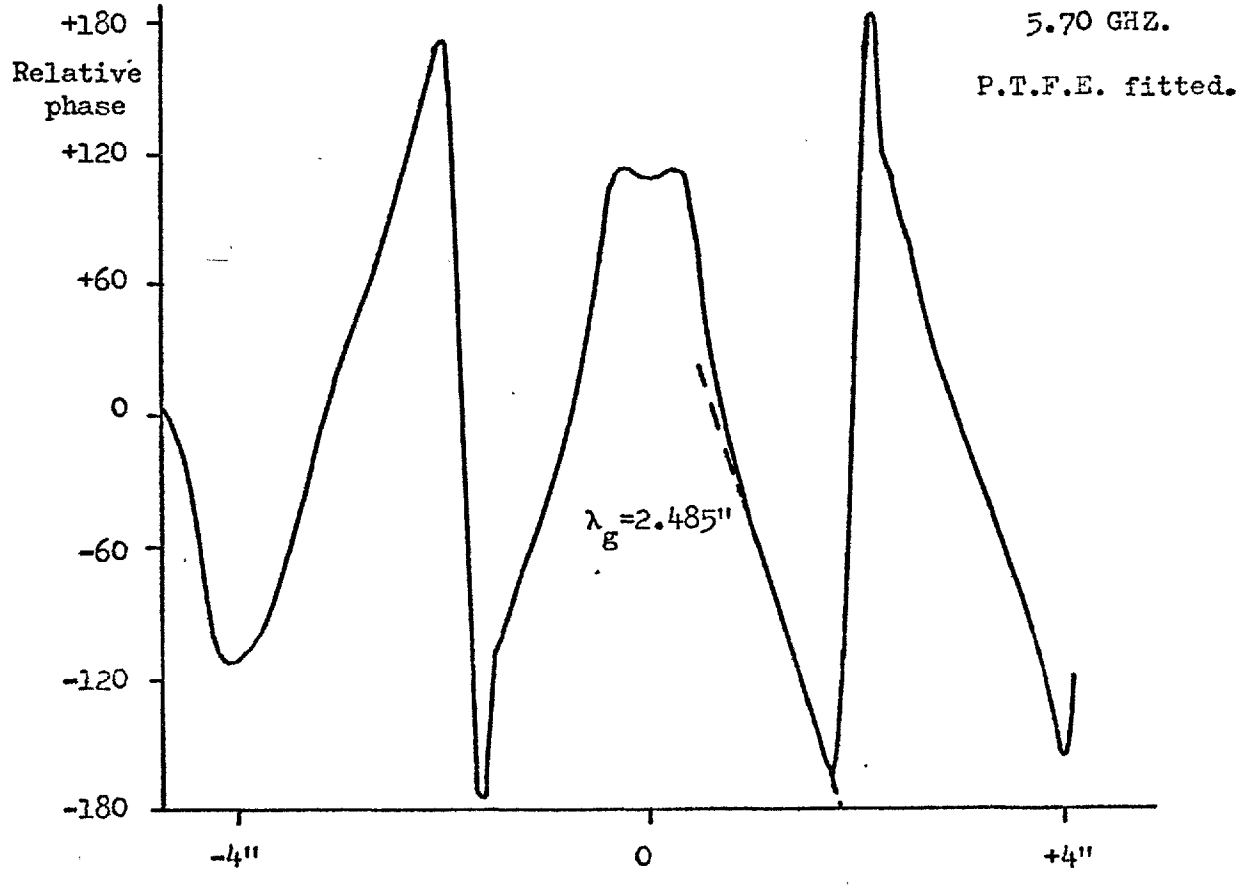

TABLE 6.6.1. A comparision of the theoretical and experimental results obtained for the channel waveguide formed by the 5/8" square baffles.

(a) Attenuation gradient.

Frequency GHZ.	Attenuation gradient db/λ	
	Experimental	Theoretical
5.60	10.6	10.9
5.70	10.5	10.5
5.80	9.2	10.0

(b) Guide wavelength.

Frequency	Guide wavelength (inches)	
	Experimental	Theoretical
5.70	2.484	2.485
5.80	2.432	2.423

identifying the leaky wave they described. Its presence between the baffles, modified the far field radiation pattern of the slot as shown in Figure 6.6.9.. The pattern showed a small dip of $1\frac{1}{2}$ dB away from broadside but recovered and then stayed at a high level before rapdily decaying. This pattern was acceptable for an array element because even though a dip occurred away from broadside, the power level was maintained at large scan angles with no major nulls, which could have been associated with large mismatches.

The inductive and capacitive baffles were then investigated. Although Goldstone and Oliner's results could not be applied directly to these structures due to the modified surface impedance on top of the baffles it was expected that the attenuation gradient of the leaky wave would be reduced. The measured near field amplitude distributions shown in Figures 6.6.10. and 6.6.11., supported this view. These broad distributions were expected to produce nulls in the far field patterns. The measured patterns are shown in Figures 6.6.12. and 6.6.13.. The inductive baffles produced a deep null 30° from broadside and a substantial sidelobe (- 5 dB for the main beam) at 50°. For the capacitive baffles however a null was obtained at around 40° from broadside with a small sidelobe at 50° giving a directive pattern in the elevation plane with the main beam at broadside. The 3 dB beamwidth was of the order of 23° and the capacitive baffle appeared to be a sensible choice for an array required to look out only at broadside with a narrowed elevation plane pattern. The major differences in the far field patterns of these two types of baffle were produced by subtle differences in the near field distributions.

It was also found that for the solid baffles with the $\frac{1}{16}$" wide half inch deep groove the leaky wave again propogated with reduced attenuation because the effective surface impedance on top of the baffle

FIGURE 6.6.9. The radiation pattern of a single I-shaped slot fitted with 5/8" square baffles .The pattern is in the plane containing the central arm of the slot.

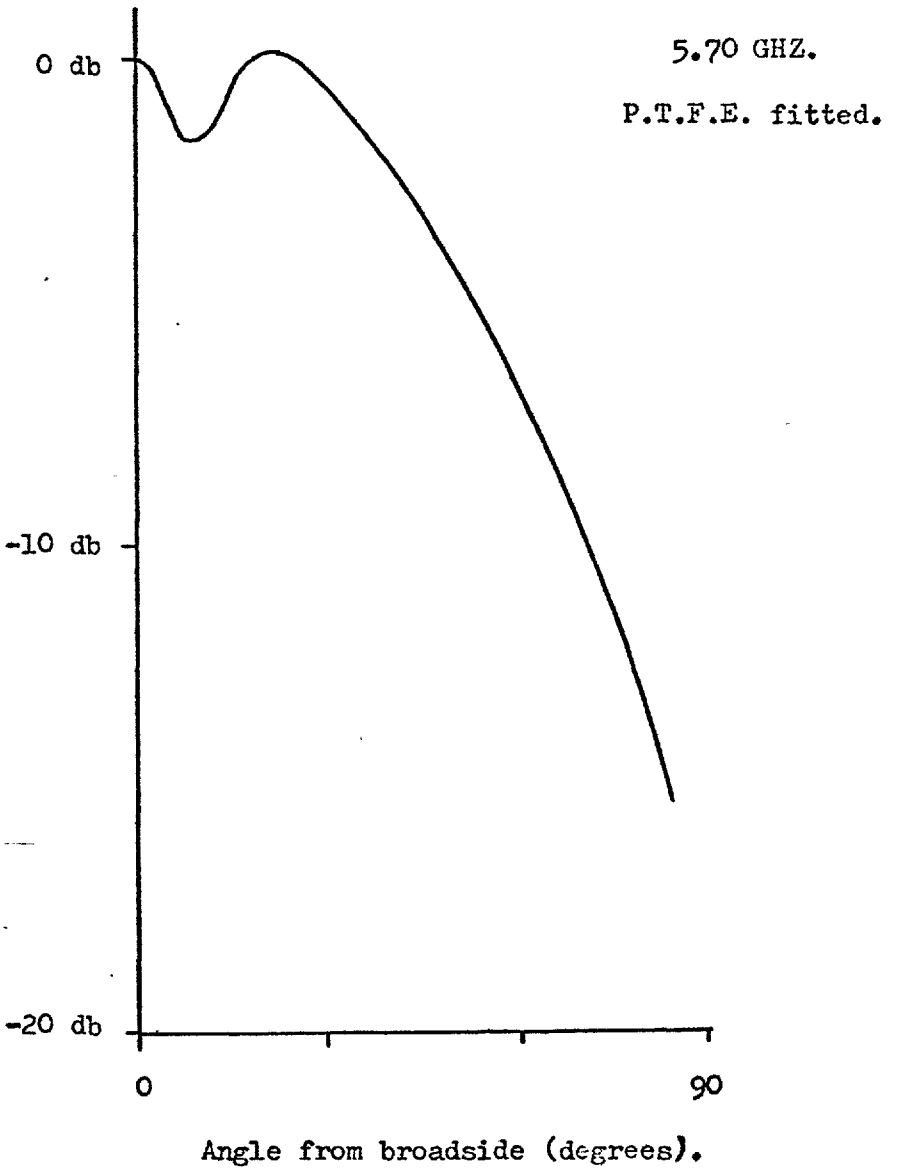

FIGURE 6.6.10. The aperture distribution measured between inductive baffles. (5/8" square tubes with 1.03" high side plates).

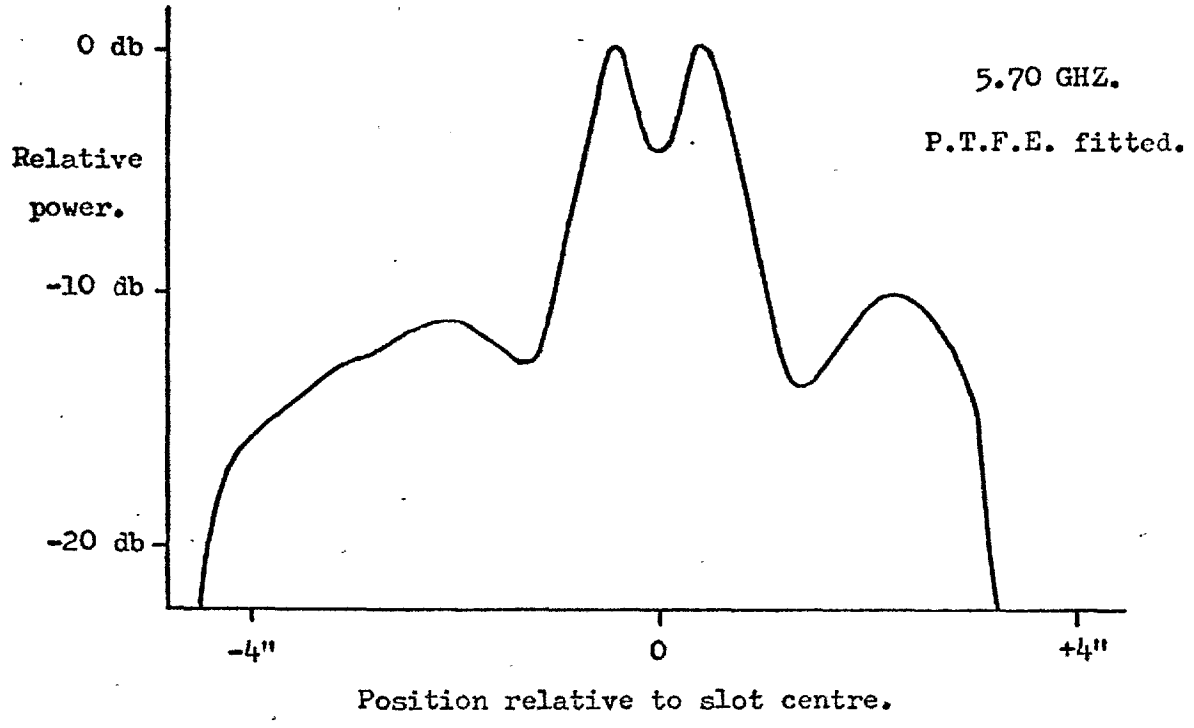

FIGURE 6.6.11. The aperture distribution measured between capacitive baffles. (5/8" square tubes with 1.18" high side plates).

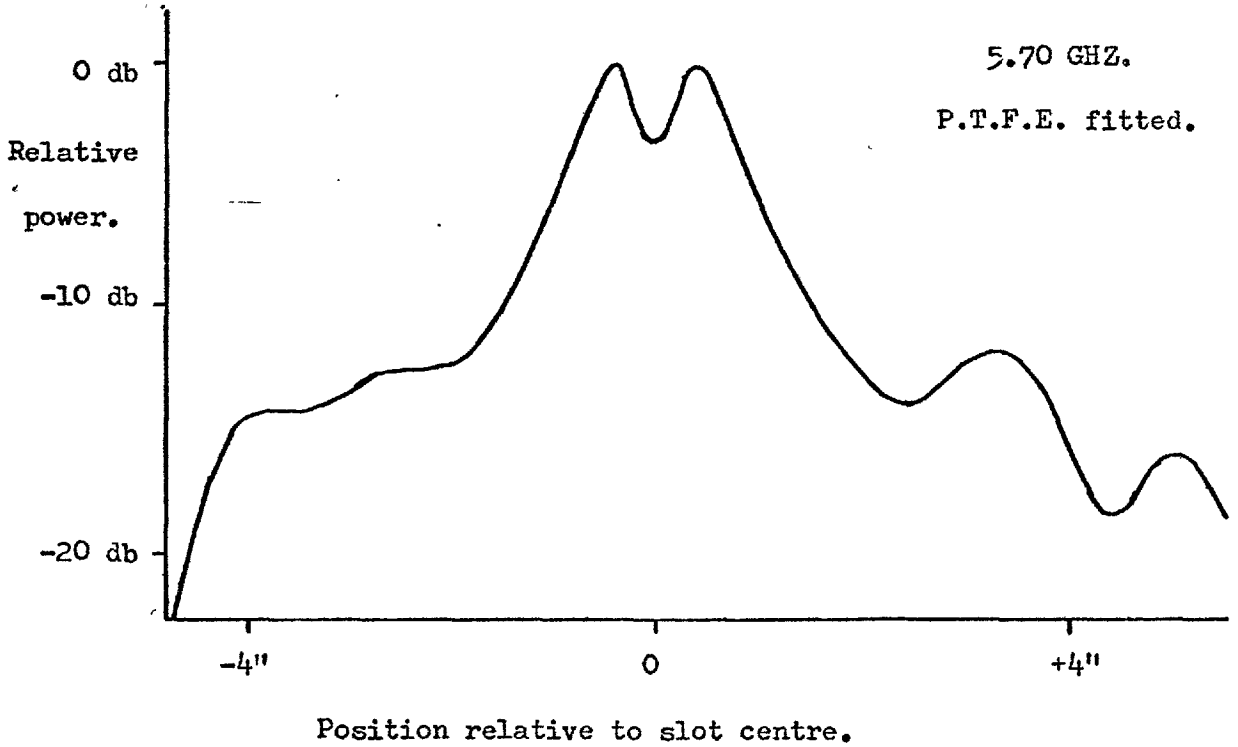

FIGURE 6.6.12. The radiation pattern of a single I-shaped slot fitted with inductive baffles. The pattern is plotted in the plane containing the central arm of the slot.

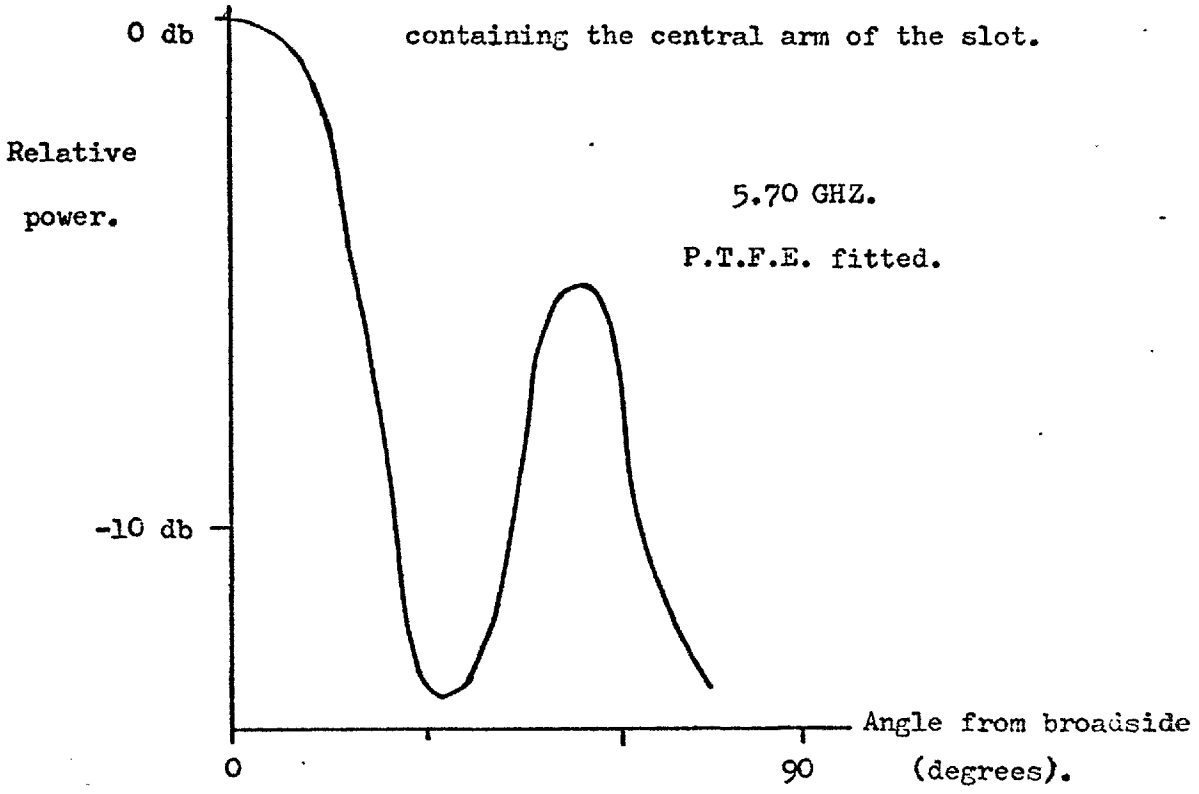

FIGURE 6.6.13. The radiation pattern of a single I-shaped slot fitted with capacitive baffles. The pattern is plotted in the plane containing the central arm of the slot.

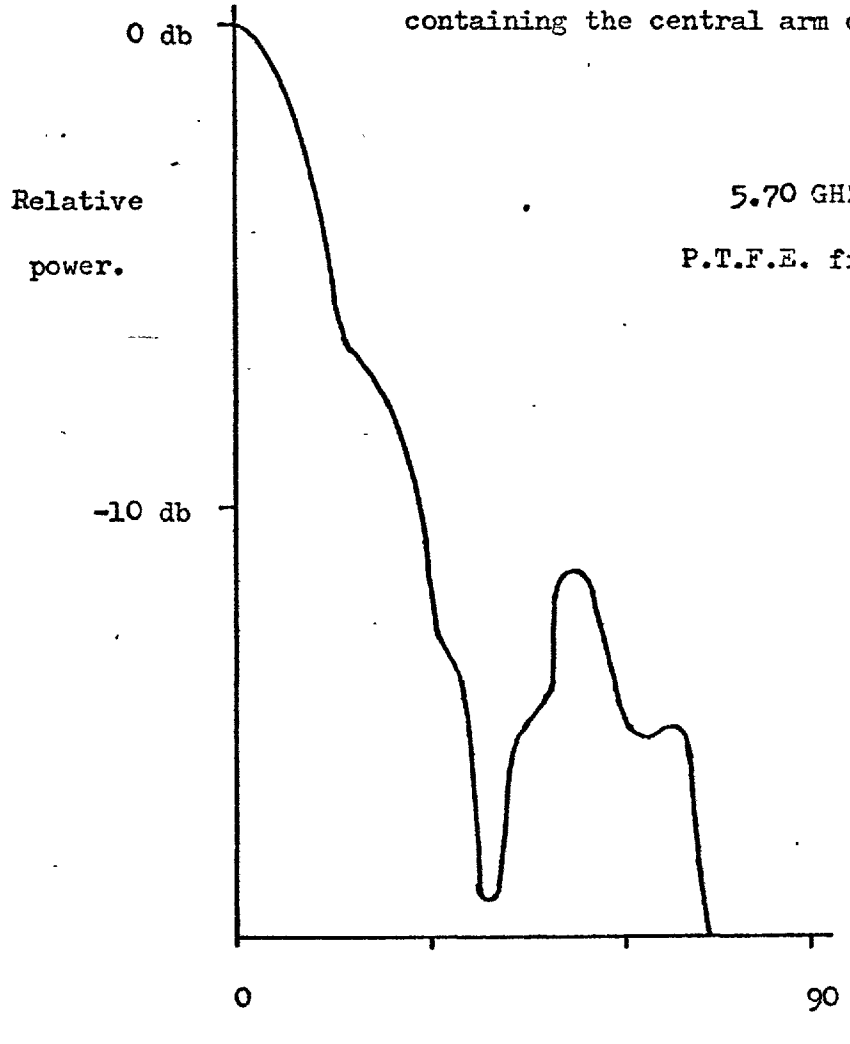

had changed. A broad near field distribution was measured as shown in Figure 6.6.14. and this produced a 6 dB null in the far field radiation pattern only 20° from broadside (Figure 6.6.15).

A different set of baffles was also investigated for which not only the ditch on top of the baffles but also the channels between them were capacitive. They consisted of sections of Waveguide 15 with tall side plates attached. When fitted to the network the measured coupled powers were as indicated in Figure 6.6.16. and an increase in the isolated slot conductance was noted. The coupled power for neighbouring slots in the same column was reduced although for more distant slots the coupled power increased. This was presumably due to an improved reflection coefficient at the top of the baffles producing less reflected power to near neighbours but an enhanced leaky wave coupling between more distant slots. The measured near field radiation pattern is shown in Figure 6.6.17. It was broad and could reasonably have been expected to produce a null in the far field radiation pattern. This was in fact found to be so, the measured pattern shown in Figure 6.6.18. indicated that a deep null (20 dB) was present at an angle less than 20° from broadside. The baffle length used for this case was unrepresentative of that necessary in an array and the null position could have changed.

The only baffles that have been investigated that could usefully be incorporated into an array were the $\frac{5}{8}$" square plain tubular baffles and the capacitive baffles formed by fitting side plates to $\frac{5}{8}$" square tubes. The former type was suitable for use in phase scanned arrays and the latter type in arrays only required to look out at broadside, with increased directivity in the elevation plane. The cross polarisation performance of the plain baffles suitable for phase scanned arrays was perhaps not as good as would have been liked. The only sensible way of improving it would have been to decrease the slot

FIGURE 6.6.14. The amplitude aperture distribution measured between the 5/8" square baffles with a 1/16" wide groove cut in the top face.

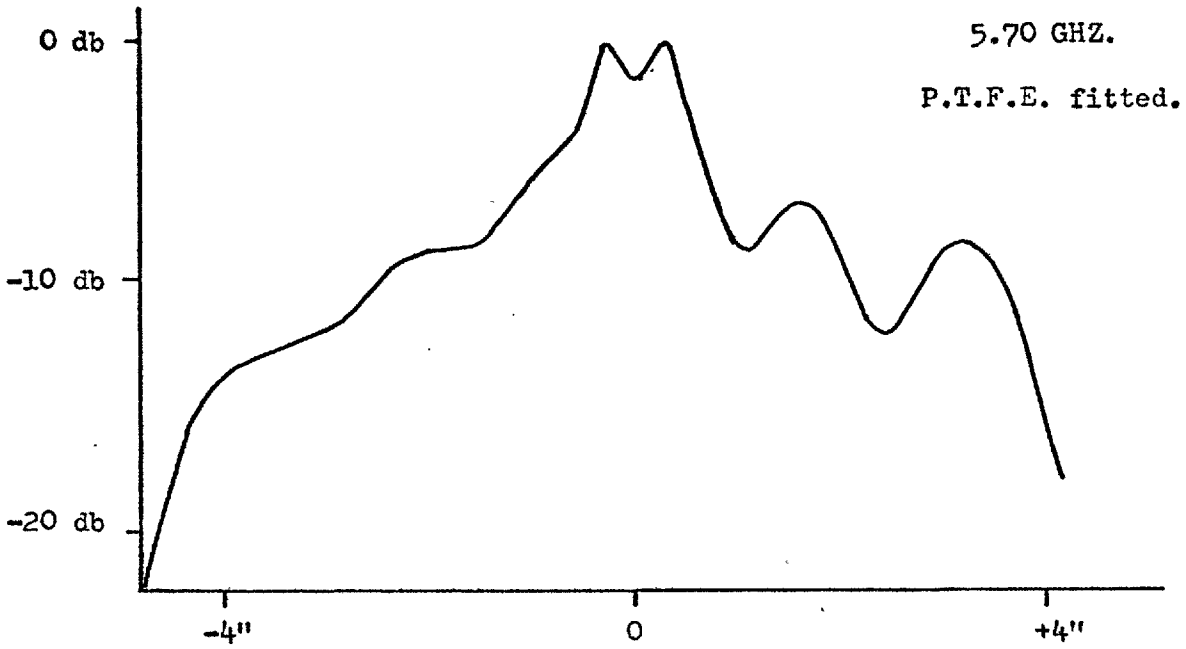

FIGURE 6.6.15. The radiation pattern of a single I- shaped slot fitted with 5/8" square baffles with a 1/16" wide groove cut in the top face. The pattern is in the plane containing the central arm of the slot.

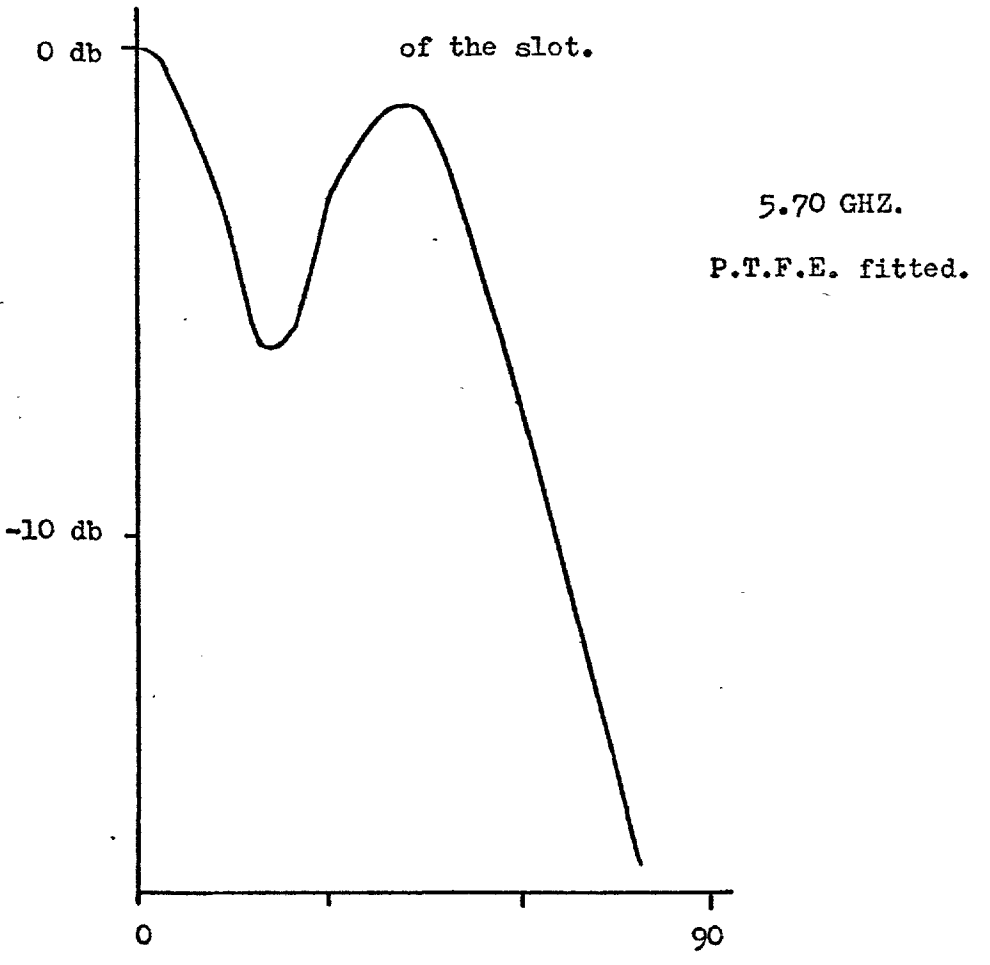

FIGURE 6.6.16. The peak coupled power between slots of the 8x3 network when fitted with baffles made from sections of waveguide 15 with side plates 1.80" high 21 S.W.G.. One slot is fed and the others used sequentially in reception.

P.T.F.E. fitted.

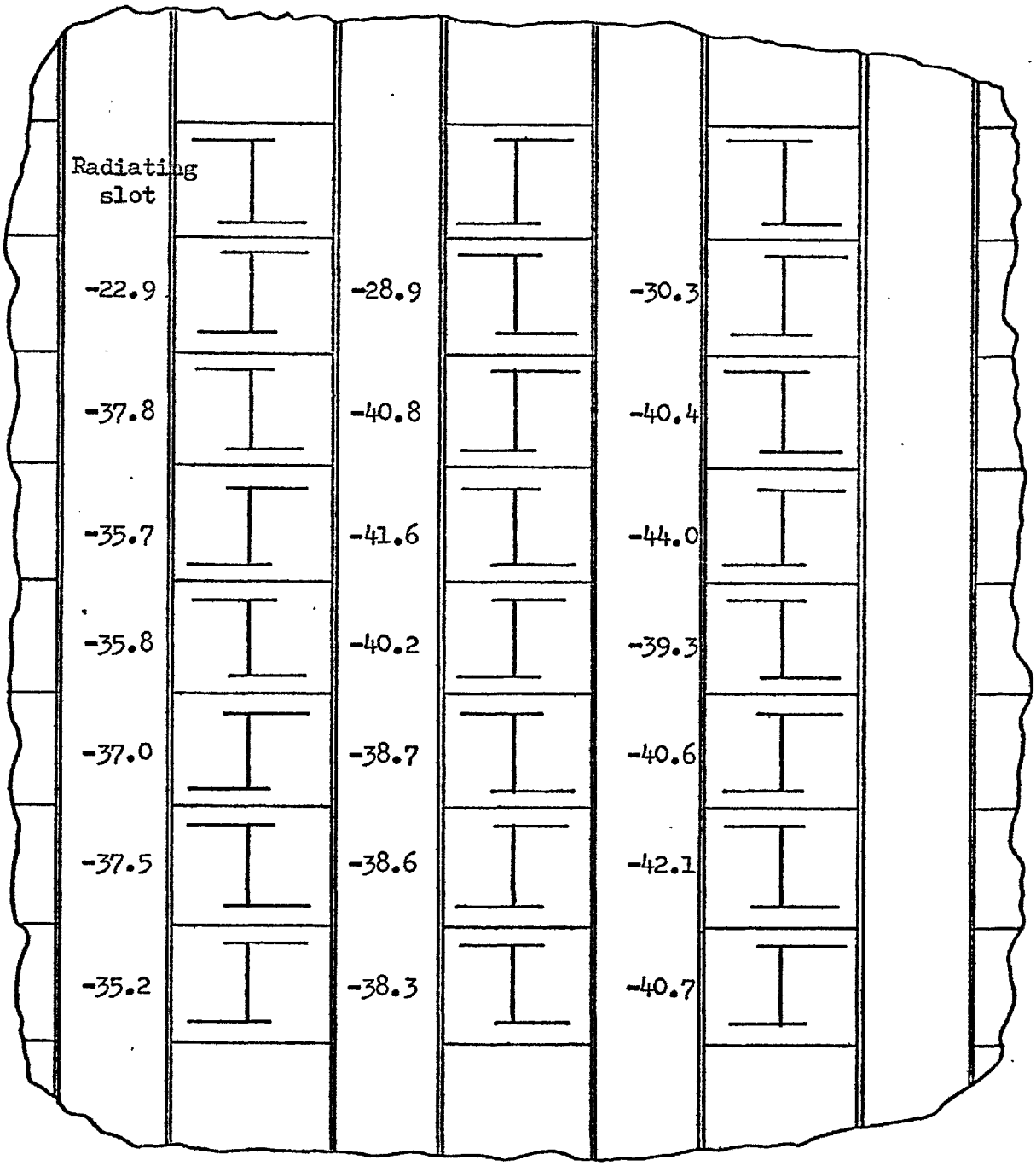

The measurements (db) were made in the coupled waveguide relative to the power in the incident waveguide.

FIGURE 6.6.17. The aperture distribution measured between baffles consisting of sections of waveguide 15 with side plates 1.80" high.

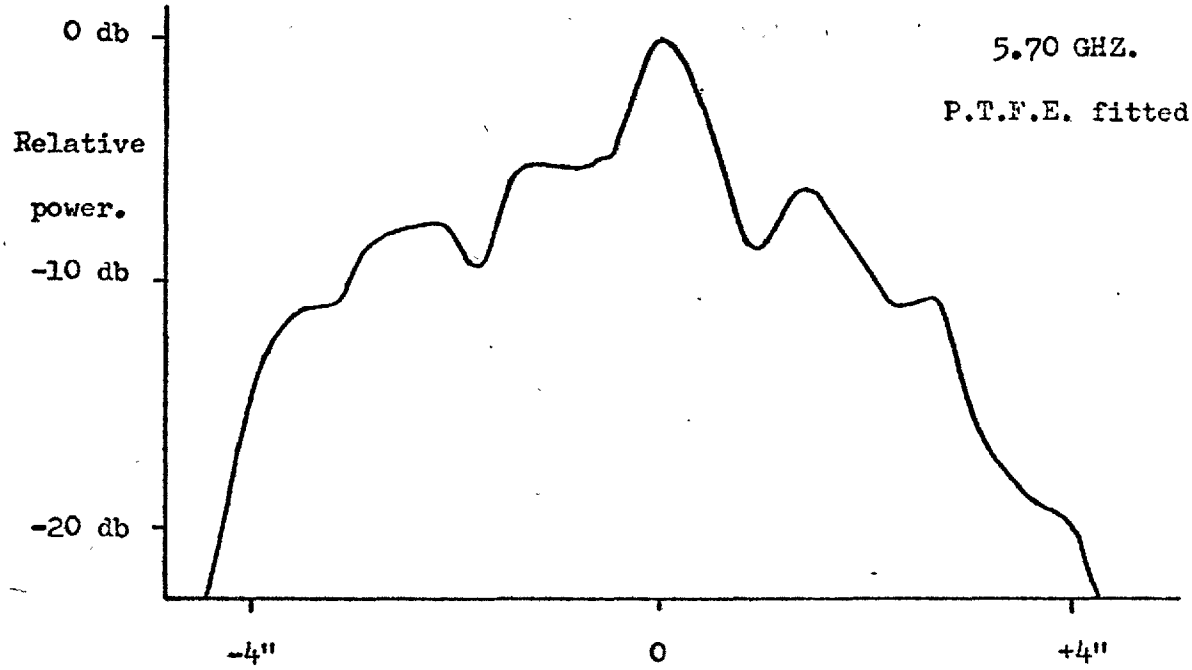

FIGURE 6.6.18. The radiation pattern of a single I-shaped slot fitted with baffles consisting of sections of waveguide 15 with side plates 1.80" high . The pattern is in the plane containin the central arm of the slot .

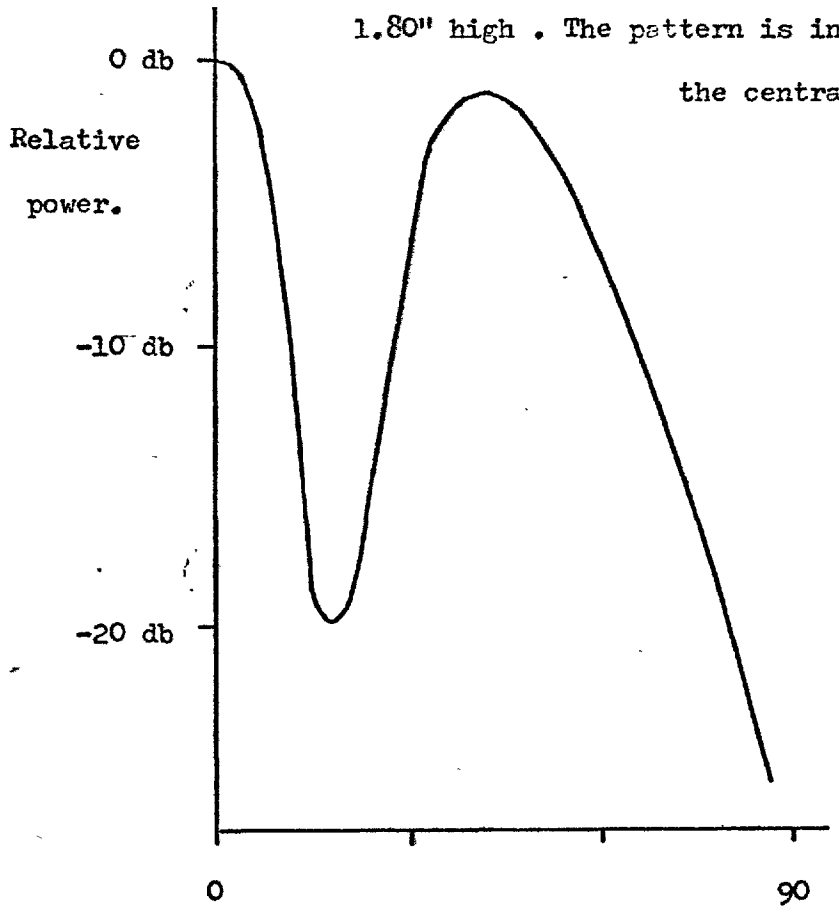

separation to bring the baffles closer together, alternate methods involved taller baffles for which the leaky wave attenuation would have decreased. It might have been possible to introduce more attenuation into the leaky wave by cutting periodic chokes across the baffles at regular intervals along their length. This possibility was not investigated as it was thought that the chokes might excite the cross polarisation and the additional machining would contribute a significant increase to the overall cost of an array. All the baffle cross sections investigated could have been made as a straight forward extrusion with the only machining required to cut the sections to length. It was fortunate that in fact the most suitable cross section for subsequent use in phase scanned arrays was the $\frac{5}{8}$" square tubular baffle and this was available as a stock size.

CHAPTER 7

MULTIPLE WAVEGUIDE ARRAYS

7.1. Incremental Admittance

The previous chapter indicated the occurence of mutual coupling within a group of slots and how modifications to the radiating apertures changed its behaviour. Such studies were most interesting but alone could not be used to predict the performance of a large array. Consideration had to be given to how the measured mutual couplings appeared within the waveguides. A modified equivalent circuit could then be constructed for each slot and the performance of the whole array deduced.

Initially only two slots were considered in separate waveguides as shown in Figure 7.1.1.. When a generator was attached to the first waveguide a voltage was induced across the first slot as indicated in the second and third chapters. The voltage on the first slot induced a voltage on the second slot by mutual coupling and this in turn induced subsidiary waves in the second waveguide. When this waveguide was also excited the secondary waves appeared to be a modification of the slot reflection coefficient. As the voltage reflection coefficient and terminating admittance are uniquely linked, a modified slot admittance could be used to represent the presence of mutual coupling. The position of the radiated beam of a phased scanned array depended upon the relative phase of the waveguide excitations. The apparent slot reflection coefficient or active admittance was hence sensitive to the beam position, and inter-element spacing. For the envisaged array slots in the same column and adjacent waveguides were approximately 120° apart in space. The results of the last chapter indicated that the

FIGURE 7.1.1. The voltages coupled between two slots in different waveguides.

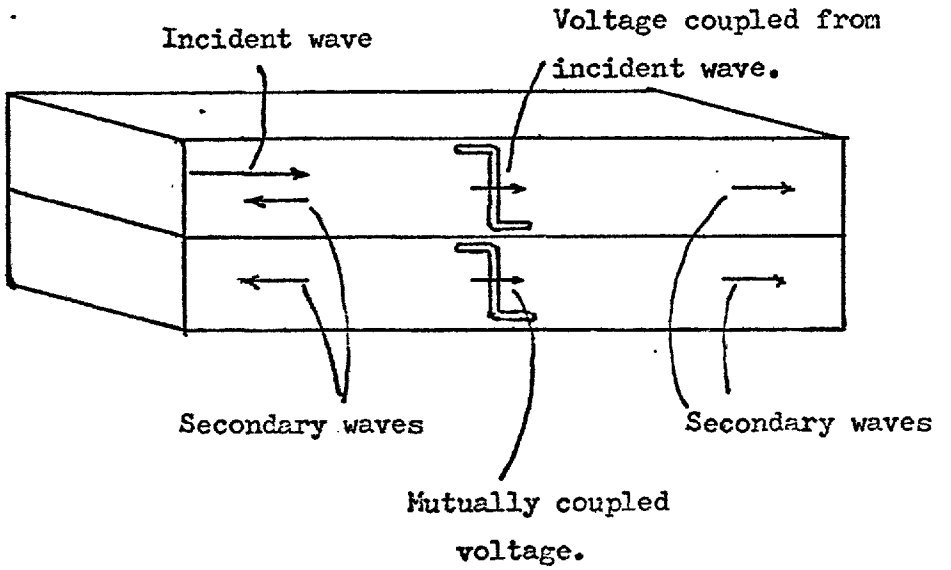

FIGURE 7.1.2. The two slot phase scanned array.

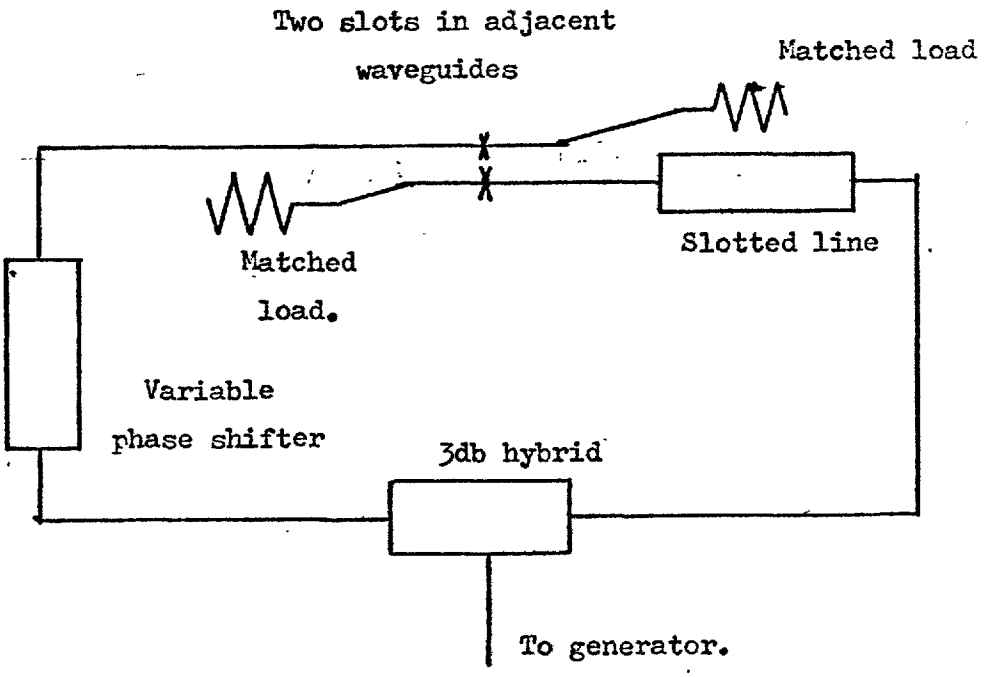

phase length of mutual coupling was approximately 120° - 130° so that for the array of two slots shown in Figure 7.1.1. with the beam at broadside the mutual impedance appeared as a modification to the slot conductance with a susceptance. This contrasted with the concept of "incremental conductance" (Watson (1947)) usually used in designing single waveguide arrays of shunt inclined slots. These slots are usually close to half a free-space wavelength apart and the phase length of mutual coupling is close to 180° so that the secondary waves excited by mutual coupling appear to be from a modified conductance only.

These ideas were tested experimentally using two slots of the 8 x 3 network. All the other slots were covered with adhesive aluminium tape. The two waveguides were fed via a 3 dB hybrid and phase shifters. A coaxial slotted line was included in one feed arm as shown in Figure 7.1.2.. Initially a reference phase was recorded by fitting a short beyond the slot in the waveguide containing the slotted line. Its position was adjusted to minimise the power radiated (decrease of 30 dB) and form an effective short circuit across the slot. The remaining power radiated was due to residual series resistance components. The null positions along the slotted line were noted. The short was replaced by a matched load and the two slot array phase scanned. The active admittance of one slot was plotted for each beam position and is shown in Figure 7.1.3.. The active admittance traced out a circle although the isolated slot admittance was not at its centre due to problems associated with the residual V.S.W.R. of the load. The power in the measurement waveguide was less than in the other waveguide because of difficulties with the power division and incorporating a slotted line. Figure 7.1.3. also indicated that larger phase shifts were required to move the beam near broadside than at wide

FIGURE 7.1.3. The measured active admittance of one slot of a two slot phase scanned array.

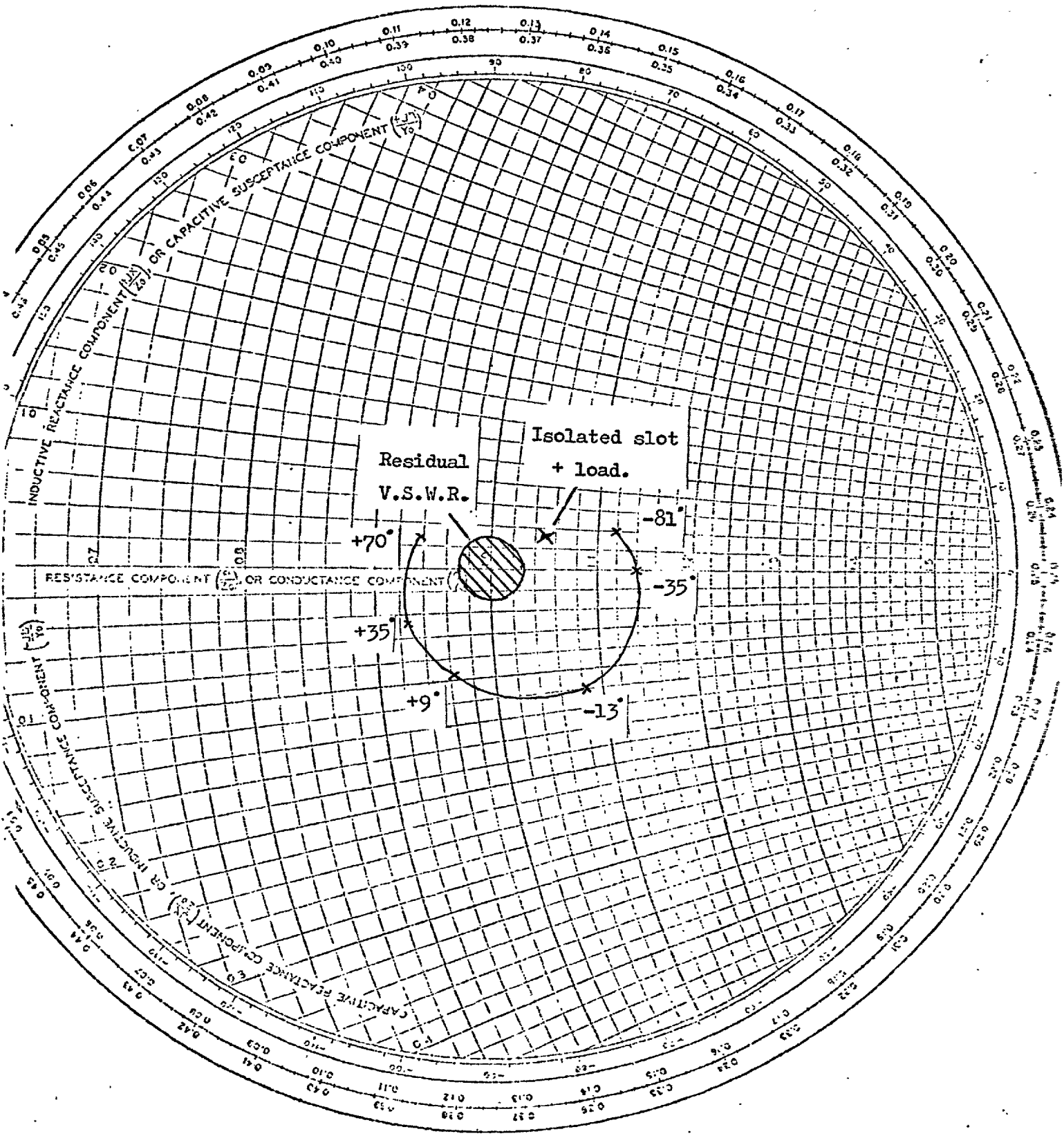

The figures indicate the beam position.

angles. So if an array could be designed to phase scan a beam successfully over a range of angles about broadside its performance was likely to be reasonable at wide angles, apart from grating lobes.

The concept of including mutual coupling as an incremental slot admittance appeared to be justified and was used in some design examples. As monopulse arrays were considered details of the designs will be given after the radiation patterns used have been justified.

7.2. Monopulse Antenna Difference Patterns

In Chapter 5 some consideration was given to the choice of aperture illumination function for a sum channel waveguide. For the array now considered separate waveguides were used for the difference channel so that an independent choice of difference channel illumination could be made. For the more conventional dish type radar antennas this choice is not available. The sum aperture distribution is obtained from four horns fed through a suitable network. The difference channel illumination function, obtained through a different port of the network, is intimately linked to that of the sum channel. Hannan (1961) showed, using appropriate sinusoidal functions how the optimum monopulse performance could be obtained. For dish type radar antennas, because the sum channel is used both in transmission and reception the optimum illumination favours the sum channel at the expense of the difference channel. Only in the type of antenna envisaged in this work in which the difference channel is separately established can real consideration be given to its optimum performance rather than an optimum compromise between the channels.

For the difference channel the important feature is not directly its gain but the pattern slope at boresight. The slope of the pattern

determines the angular resolution of the system when one channel is divided by the other. Kirkpatrick (1953) demonstrated that of all the possible odd uniform phase, constant power distribution functions the linear distribution shown in Figure 7.2.1., gives the pattern whose slope is maximum at boresight. Any other distribution results in a smaller slope.

Powers (1967) linked this distribution with the uniform amplitude distribution giving maximum gain for the sum channel. He took the well known relationship between a line source distribution f(w) and its far field radiation pattern F(μ) involving a Fourier transform pair given by:

$$F(\mu) = \int_{-1}^{1} f(w) e^{j\mu w} dw \qquad (7.2.1)$$

$$f(w) = \frac{1}{2\pi} \int_{-\infty}^{+\infty} F(\mu) e^{-j\mu w} dw \qquad (7.2.2)$$

$$F(\mu) \rightleftarrows f(w) \qquad (7.2.3)$$

He differentiated (7.2.1) and (7.2.2) with respect to μ and w, respectively and obtained two additional Fourier transform pairs.

$$\frac{dF(\mu)}{d\mu} \rightleftarrows jwf(w) \qquad (7.2.4)$$

$$mF(\mu) \rightleftarrows j \frac{df(w)}{dw} \qquad (7.2.5)$$

Now in (7.2.1), if f(w) is a constant the maximum gain sum channel pattern results and similarly in (7.2.4) the maximum slope difference channel illumination is obtained. Thus the maximum slope difference channel

FIGURE 7.2.1. The maximum slope difference channel illumination function.

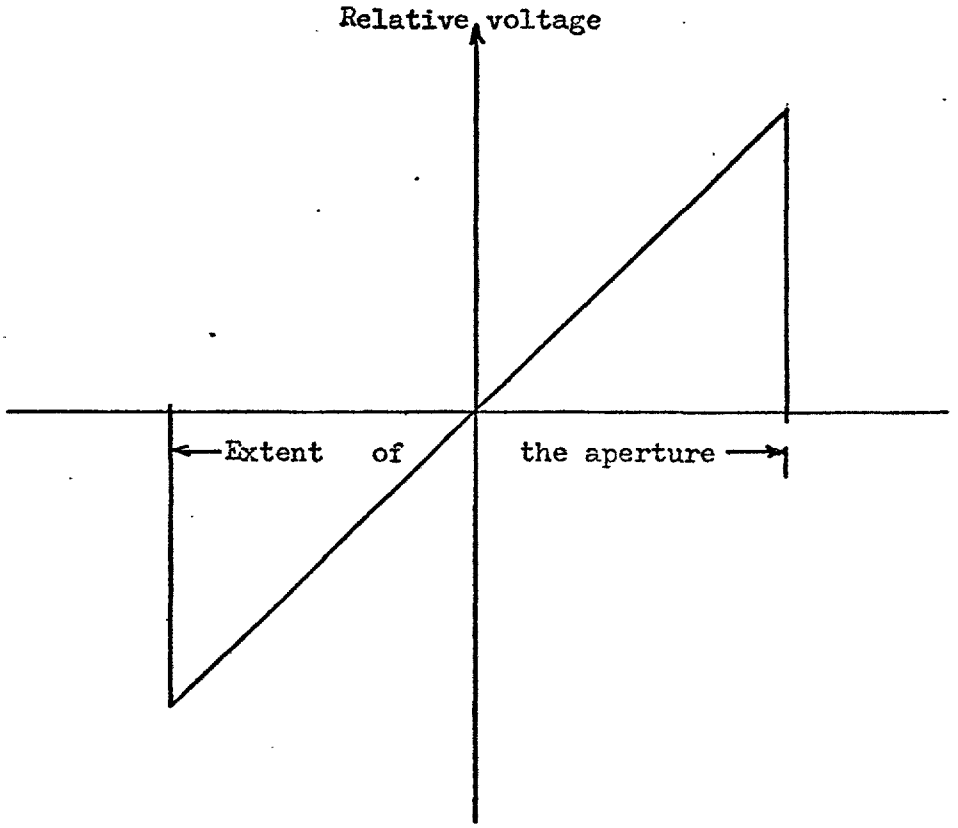

FIGURE 7.2.2. The normalised radiation patterns produced by parabolic and cubic illumination functions.

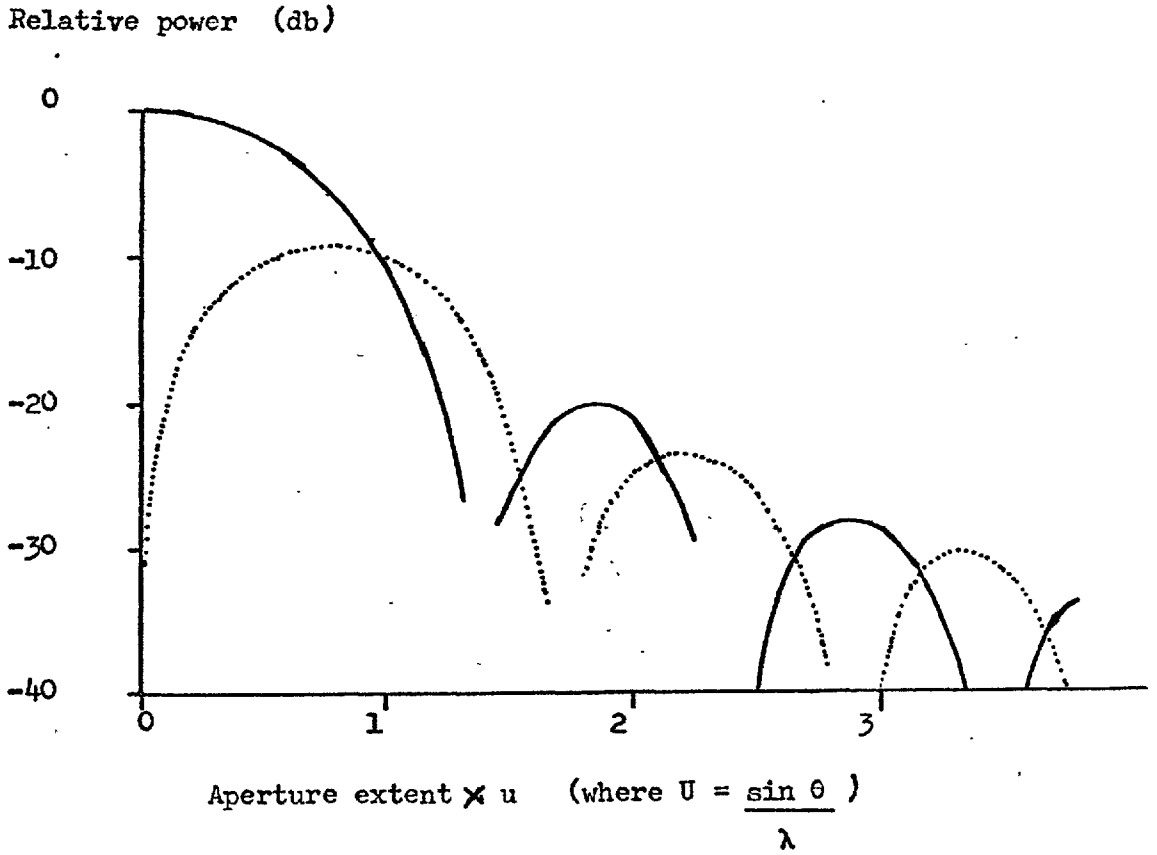

apart from a constant is the derivative of the maximum gain sum channel result. The difference channel illumination function is the aperture variable times that of the sum channel.

Price and Hyneman (1960) had previously obtained this type of result with more relevant illumination functions. They wanted to obtain polynomial descriptions of optimum difference patterns when they already had the required sum channel results. They showed for Chebyscheff polynomials that, a good approximation at least, to a uniform sidelobe difference pattern could be generated in this manner from an equal sidelobe sum pattern. They also applied the method to other functions such as a binomial distribution.

Powers (1967) worked in terms of Lambda functions which have been shown by Ramsay (1967) to be a class of functions which include all the usual antenna radiation patterns. On differentiation, he obtains functions which he calls the L functions. These are in fact Lambda-Struve functions. The Lambda functions and corresponding Lambda-Struve functions behave similarly to the cosine and sine functions. They have the same envelope but are $\frac{\pi}{2}$ apart in phase. Thus if any sum pattern illumination function is acceptable in the compromise between gain and sidelobe then if the distribution is multiplied by the aperture variable a similar compromise is made between difference channel slope and sidelobes. In addition it is the round trip sidelobe performance that is important for a monopulse antenna, when the sum channel is used in transmission and the difference channel in reception. The 90^{o} phase shift between the patterns ensures that a peak of one channel coincides with a null of the other so that no large round-trip sidelobes occur. Figure 7.2.2. shows the radiation pattern obtained from the parabolic and cubic distributions. The patterns both have the same envelope but it must be remembered that

both channels are not radiating the same power. For equal power radiated in this case the difference pattern should be raised 8.4 dB relative to the sum pattern.

In Chapter 5 a $\frac{1}{7} + \frac{6}{7} \cos^2(\frac{\pi}{2} x)$ distribution was specified for the sum channel array. It seemed appropriate to specify an $x \times (\frac{1}{7} + \frac{6}{7} \cos^2(\frac{\pi}{2} x))$ for the difference channel.

7.3. Mutual Coupling and Monopulse Arrays

The direct inclusion of the effects of mutual coupling in a large two dimensional Monopulse slotted waveguide array is extremely difficult. The sum channel of the array is initially used to illuminate the radar target but both channels are simultaneously used to determine the targets position. The critical performance of the array for tracking is thus when both channels are used, in reception. It is desirable to ensure that the required monopulse response is obtained in the presence of mutual coupling and at a range of beam positions. The response of the antenna in reception is thus of most interest but this case is the most unweildy to consider. In the last chapter it was shown that the mutual impedance between slots of the whole range of coupling above a ground plane was reasonably constant. The mutual impedance between slots was however a relationship between the current and voltages at their respective terminals. The network formed by the waveguides and slots presents an impedance to each slot which determines the current flowing in that element. This is critically dependent upon the angle of arrival of a plane wave from space so that the array factor radiation pattern is generated. To include the effects of mutual impedance into a computed received radiation pattern would thus involve for each angle of arrival determining the impedance

terminating each slot to give the current in each element. Values of mutual impedance could then be used to determine the additional voltages injected into each element and the powers received by individual slot could then be summed along each waveguide. This process if used to determine the radiation patterns over a reasonable angular range would involve a massive computer programme. There would be no guarantee that small errors in the values of mutual impedance used would not severely limit the accuracy of the patterns obtained. In addition it is hard to see how corrections could be made to the slots to eliminate any adverse effects of mutual coupling.

Instead of considering the array in reception, the problem may be simplified by envoking the principle of reciprocity and investigating the array in transmission. The principle of reciprocity has been used to determine the slot conductances. When applied to a one port antenna it can be used to show that if a source is placed at that port and a field radiation pattern $F(\theta, \phi)$ obtained, then if this source is replaced by one which is moved about in space at θ and ϕ the voltage at the antenna port is proportional to $F(\theta, \phi)$. In other words the same radiation pattern is obtained both in transmission and reception. This relationship applies equally to a two port antenna such as a monopulse array but care is required to ensure that the correct relative powers are used at the two ports when the transmission case is used to replace the array in reception.

The advantage of considering arrays in transmission is that the network formed by the slotted waveguide impresses a particular voltage across each slot. As the slots all have the same radiation impedance, if the waveguide loading can be neglected, the current in each is proportional to its impressed voltage, so that the mutual impedance

effects can be regarded as a voltage to voltage coupling. The voltage injected into one slot from another slot can be regarded as proportional to the voltage on the excited slot. This is a great simplification as the individual impedances terminating each slot can be neglected. Ignoring the impedance loading of the waveguide is certainly justified for lightly coupled slots and is probably reasonable for all but the most tightly coupled slots.

The reduction of mutual impedance to a voltage to voltage coupling also has other simplifying effects particularly when baffles are fitted. It has been shown that in their presence the most important components of mutual coupling are associated with coupling within a column of slots all in separate waveguides. If for simplicity only a sum and difference pair of waveguides are considered then with only the sum waveguide transmitting the voltages on the difference channel slots will have the same distribution as the sum channel. The difference channel will then radiate as a parasitic sum array with a different phase and amplitude, as determined by the voltage to voltage coupling coefficient. The effect of the presence of the difference channel is thus to reduce the effective gain of the sum channel without major changes in the shape of its radiation pattern. Similarly when the difference channel alone radiates the presence of the sum channel reduces its effective gain. When both channels transmit the proximity of the two arrays reduces the gain of both. If the aperture distribution of each waveguide was examined it would show large errors from that intended. It should be remembered however that the distributions would be a suitable mixture of those from both channels and might appear a lot worse than the actual array performance.

If the impedance loading of the slots can be ignored then the

effect of mutual coupling is simply to reduce the antenna gain at the expense of the elevation pattern sidelobes. Unfortunately in all cases of practical interest low azimuth sidelobes are required and these are sensitive to small aperture errors such as those introduced by the impedance loading effects.

Other properties of mutual coupling within a monopulse array of this type have been derived by Killick, Salt and Porter (1969). They showed that because the amplitude distributions used for a monopulse array are symmetric and antisymmetric the input ports are decoupled.

For a single channel antenna at one frequency and beam position it should be possible to recover the desired aperture distribution and radiation pattern by modifying the slot conductances and detuning to introduce the correct susceptances. The modification required would just remove the incremental admittance introduced by mutual coupling. For a two channel antenna the situation is more complicated. When both channels simultaneously transmit changing the slots to give the correct aperture distribution would not give the correct radiation patterns, because each slot voltage would include components from both channels. The correction to the sum channel would be antisymmetric and the correction to the difference channel symmetric. The input ports would not be decoupled. Although in principle the correct radiation patterns would be obtained, the outputs of the sum pattern would appear at both ports. As no way exists of separating components the patterns at the two input ports would not be those required. With a two channel antenna the only correction that can be made is when each channel alone is excited. Sum channel slots can be corrected when the sum channel is excited but no correction can be made for excited difference channel slots, and similarly vice versa.

7.4. The Measurements Required for the Design of an Eight Waveguide Array

It has been indicated that in a sum and difference pair of waveguides, when both are excited each behaves as a parasitic array on the other. It is important to allow for the impedance change in a driven slot due to the presence of the second element. A slot to be operated in an array environment must be designed to allow for its surroundings and note taken of frequency shifts or conductance changes that occur. However, once the slot has been specified surrounded by other parasitic elements, its apparent impedance will change when the other slots are excited and with the inter-waveguide phase shifts required to scan the beam. Before an eight waveguide array could be designed the effects of mutual coupling had to be more fully explored. The terms of the mutual coupling matrix had to be determined and the effects of adjacent parasitic slots on individual slot performance established.

The 8 x 3 slot network was available and an intensive experimental study of mutual coupling was mounted. The network was fitted with the prescribed $\frac{5}{8}$" square baffles. With these present the most important components of mutual coupling were between slots in the same column as indicated in the last chapter. When all eight slots of a column were present this effect was more pronounced because not only the baffles but also the slots acted as a guiding structure. Initial measurements Figure 7.4.1. showed that mutual coupling did not decay as fast as measurements with only two slots might indicate. It was decided that in order to simplify the analysis, coupling over the baffles could rationally be ignored. Two columns of slots from the 8 x 3 slot network were effectively removed by covering with adhesive aluminium tape. Measurements were then performed on eight slots, one per waveguide.

Initially the effects of parasitic slots were investigated. A phase

FIGURE 7.4.1. The peak coupled power between eight slots in the same column fitted with 5/8" square baffles and P.T.F.E..

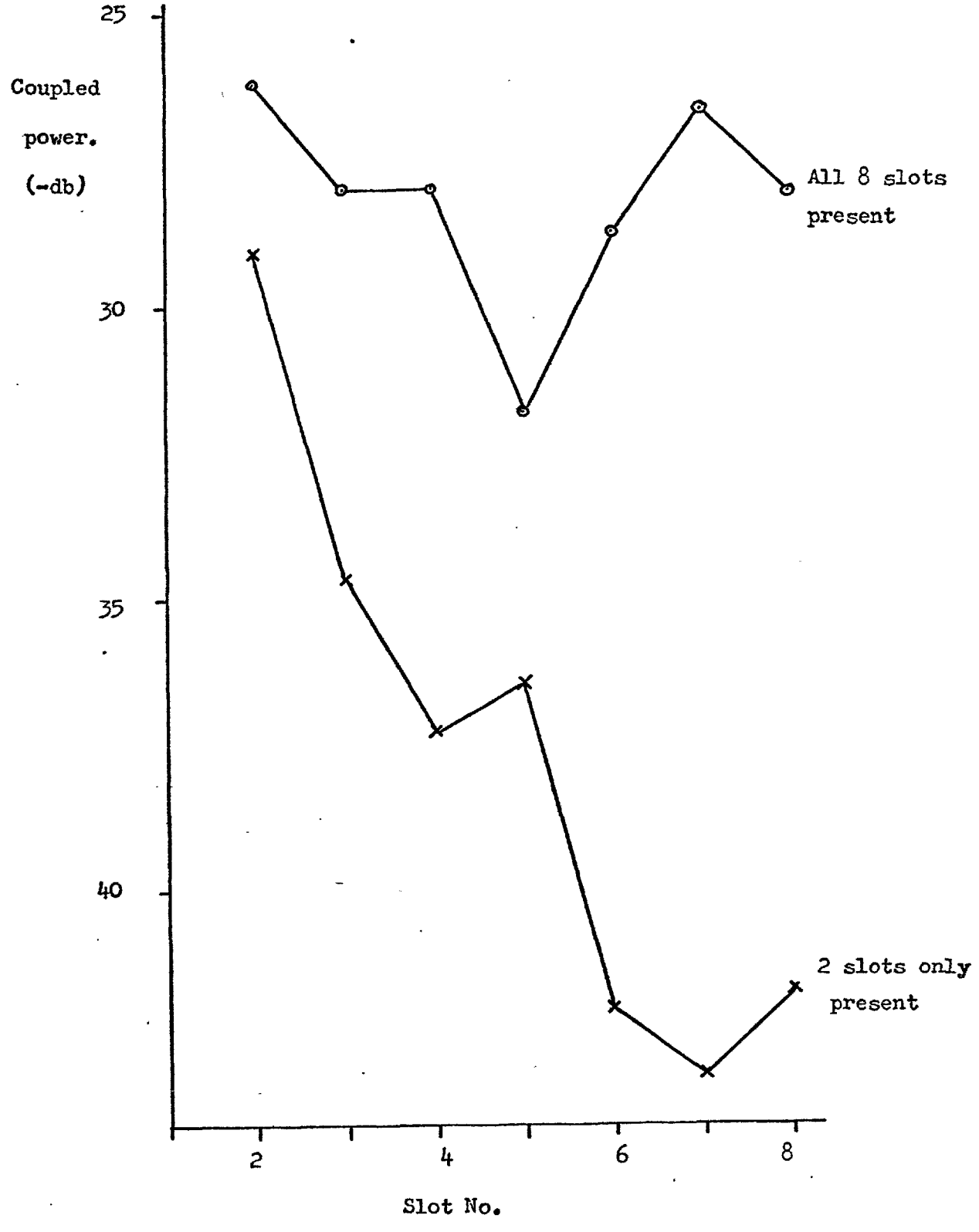

bridge was set up using Hewlett-Packard network analyser to perform swept measurements of phase shift past a slot. The analyser required a reference signal and in order to do swept frequency measurements the phase length to the instrument in both channels had to be approximately the same. Accordingly the bridge was used with similar lengths of special and standard waveguide, and cable in each channel. Phase shifters were also used so that the lengths could be adjusted. However, no two similar pieces of equipment are identical and because the reference channel was obtained through a waveguide coupler, the phase bridge could not be simultaneously balanced at all frequencies. The output from the Network Analyser was thus fed to the data normaliser, described in Chapter 4, so that the effects of in-balance could be removed. When set up in this manner it was found that swept transmission phase measurements could readily be made through a large waveguide system over a 1 GHz bandwidth. The output of the network analyser had a total variation of 90^{o} but this could be removed by the data normaliser. Phase measurements were obtained as X-Y recordings with the whole Y axis representing only 30^{o} of phase.

In this manner the phase shift past a slot could be measured by making the data normaliser recording with it taped over. Parasitic slots could then be introduced and the effects noted. Typical results are shown in Figure 7.4.2. for a central slot. The results for edge slots were similar and indicated that the resonant frequency was likely to be changed by the introduction of parasitic elements. However, the measurement could not show what the respective resonant frequencies were. A residual phase shift occured past a taped over slot. If the slot was taped over on the inside of the waveguide a different zero was obtained but there was then likely to be a phase

FIGURE 7.4.2. The measured phase shift past a central slot of the 8×3 network when fitted with 5/8" square baffles and P.T.F.E..

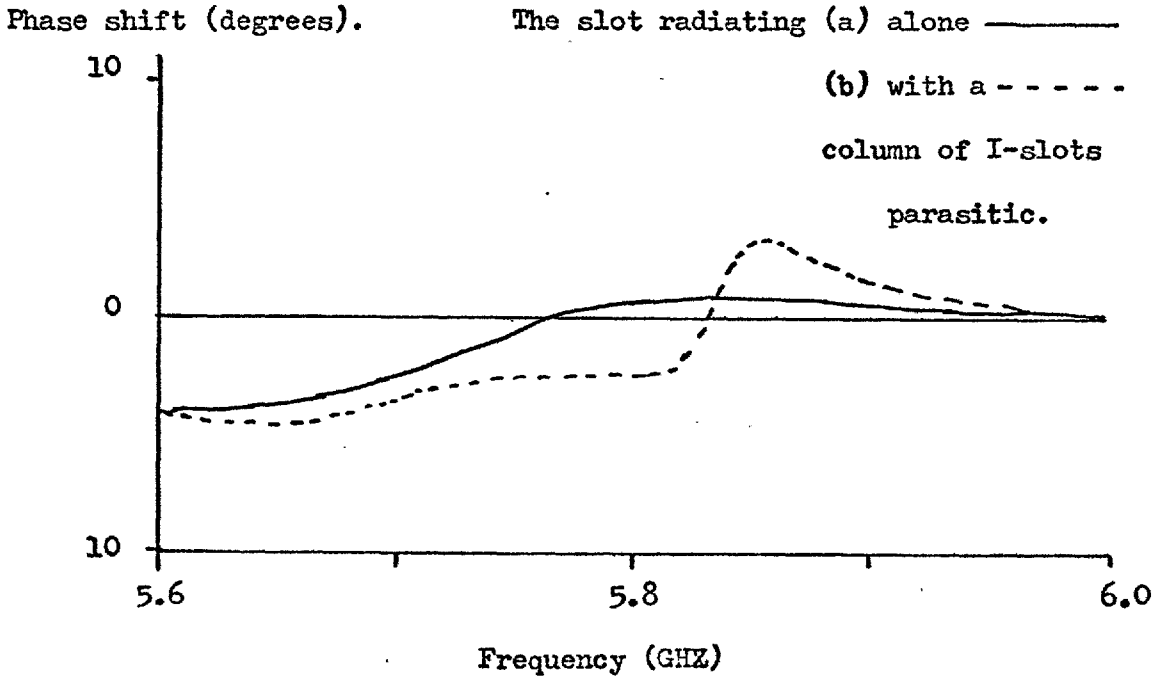

FIGURE 7.4.3. The phase length of the coupling between adjacent waveguide containing I-shaped slots of opposite hand.

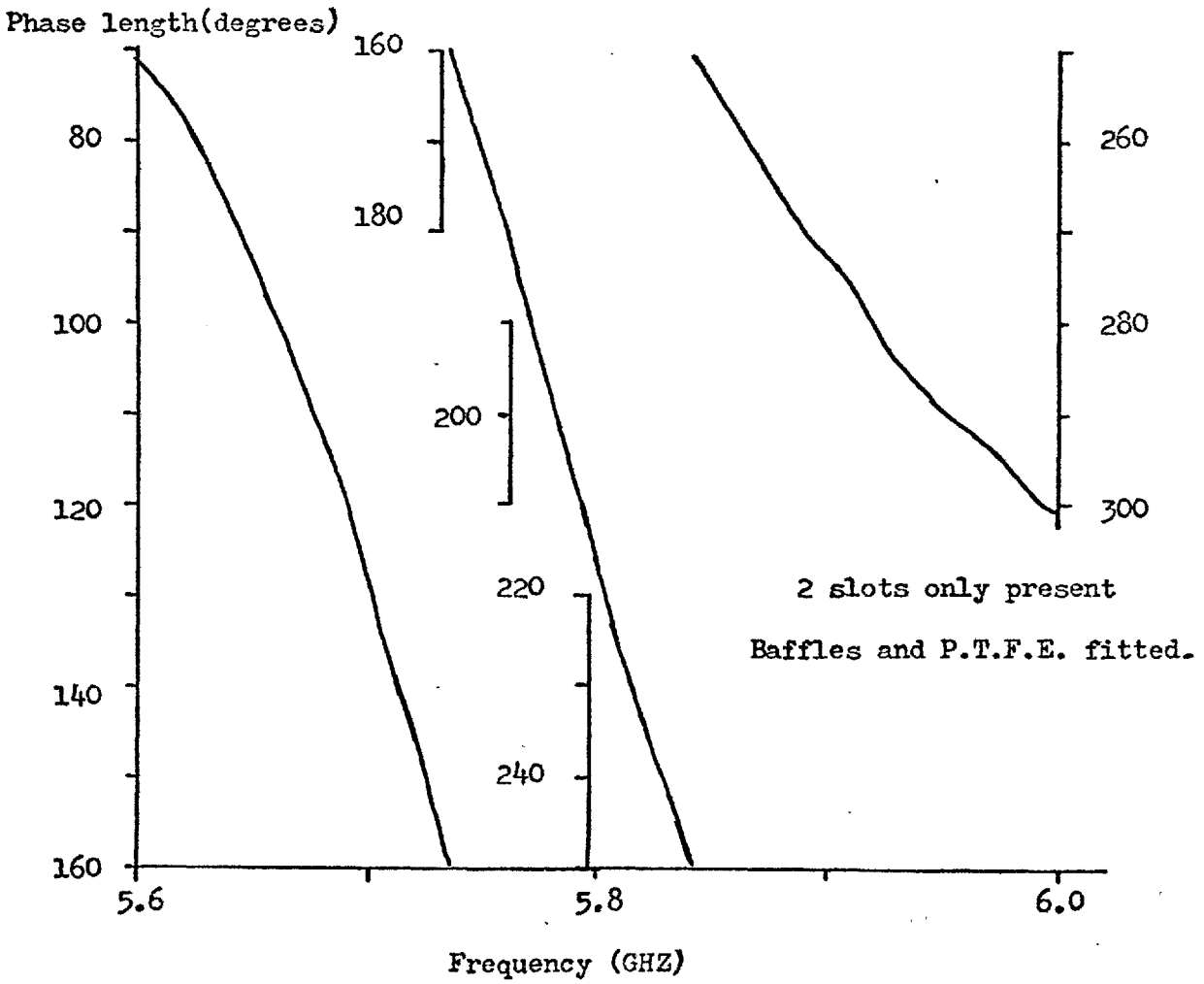

shift past the tape.

A different method of measuring the slot resonant frequency was required. Hansen (1966) has shown that the phase shift past a slot is:

$$\tan^{-1} \frac{b}{2}$$

whereas the phase shift through a slot is:

$$\frac{\pi}{2} + \tan^{-1} \frac{b}{g}$$

where g and b are respectively the slot conductance and susceptance. For a lightly coupled slot both b and g are small and the phase shift past the slot varies only slowly but that through the slot is a rapdily varying function. It was desirable to attempt to measure the rapdily varying function. The phase length of the mutual coupling out of one waveguide and back into another through identical slots was:

$$\pi + 2 \tan^{-1} \frac{b}{g} + \text{coupled phase length}$$

for slots of the same hands. Slots of opposite hand required an additional π term. This was indeed a rapidly varying function as the experimental result shown in Figure 7.4.3. indicates. This result was again obtained using the network analyser and data normaliser. The eight waveguides of the twenty four slot network were all nominally the same length so that coupled phase measurements could readily be obtained simply by transferring the detector from one waveguide to the next. Matched loads being inserted inside the appropriate waveguides. The slots of the network were all nominally identical so that the $2 \tan^{-1} \frac{b}{g}$ term was common to coupling between all pairs of slots. When

measurements of phase length were made between pairs of slots in one column of the 8 x 3 network with all redundant slots taped over the rapidly varying 2 $\tan^{-1}\frac{b}{g}$ term could be eliminated by subtracting pairs of results to leave an incremental phase length. This could be done for all combinations except coupling to an adjacent slot. As all the values obtained were similar an average value was assumed for this increment so that all the coupled lengths could be determined as shown in Figure 7.4.4.. The swept frequency coupled phase lengths were then used to determine the average resonant frequency of a pair of slots as the frequency at which the 2 $\tan^{-1}\frac{b}{g}$ term was zero. For measurements between pairs of slots with all the other slots absent the average resonant frequency was found to be 5.688 GHz with only a spread of 10 MHz. Once the slot resonant frequencies were established the rapid variation caused by the $\tan^{-1}\frac{b}{g}$ term could be considered. This gave a ratio between b and g and as the effect of b on attenuation measurements was small g was known and hence b could be determined. The phase shift past a slot was then computed as $\tan^{-1}\frac{b}{2}$ and is shown in Figure 7.4.5. The slope and magnitude of the variation is similar to that previously measured and shown in Figure 7.4.2..

This method of characterising slots by swept coupled phase measurements appeared to be valid. It was most useful as it gave the resonant frequency of the slots. There was a small spread in the results obtained which was smaller than the standard deviation in making all twenty four slots of the network. It must be remembered however that the spread in the results was reduced by always using the same slot in transmission. The method also gave the coupled phase lengths between slots. With only two slots present the results were most interesting as at large spacings the incremental phase length corresponded with a

FIGURE 7.4.4. The measured mutual coupling phase lengths taken from swept frequency measurements at 5.688 GHZ. of I-shaped slots radiating between 5/8" square baffles.

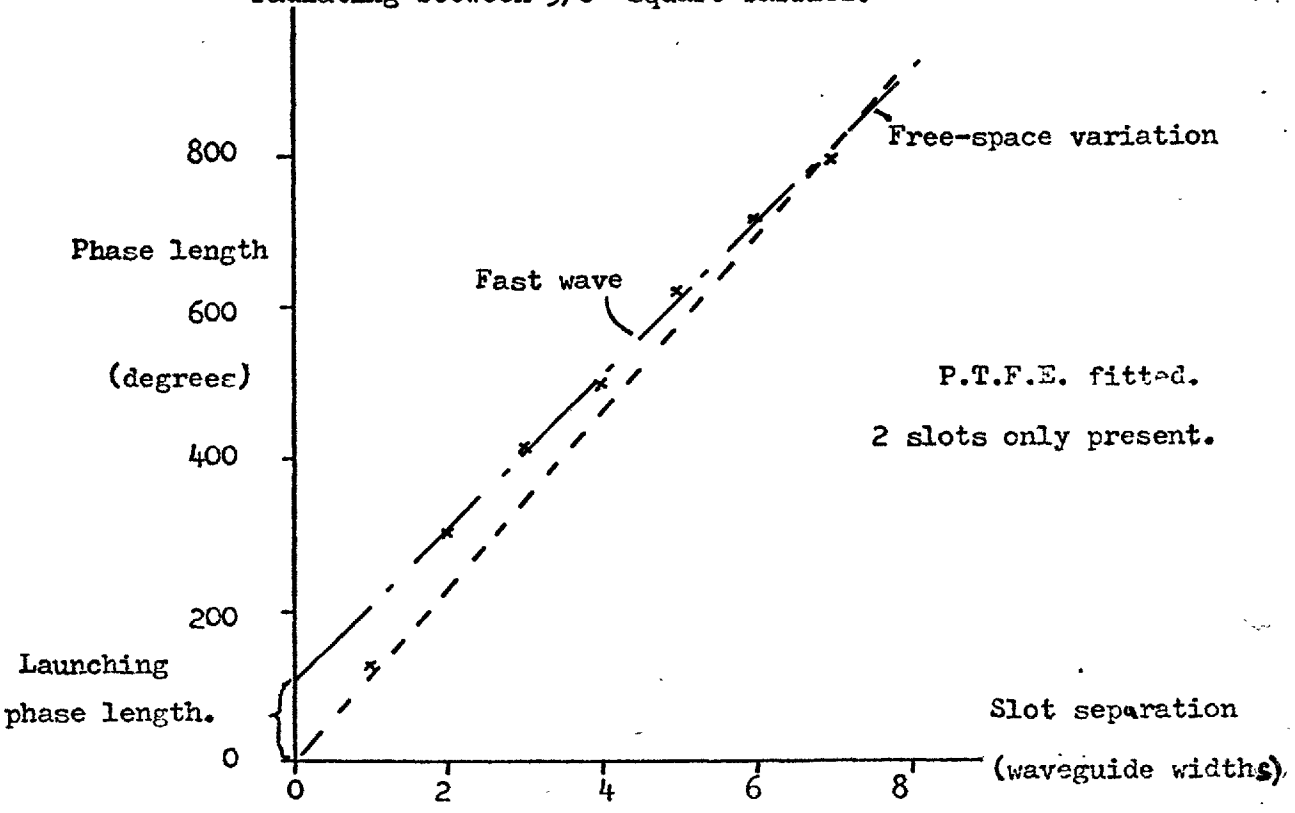

FIGURE 7.4.5. The computed phase shift past a single slot from measurements of coupled phase length.

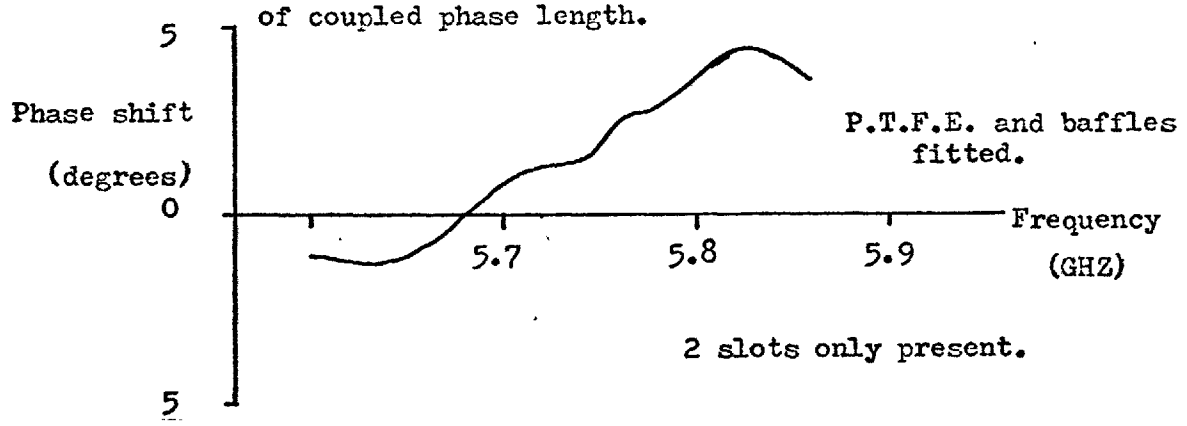

FIGURE 7.4.6. The computed equivalent circuit parameters from measurements of coupled phase length.

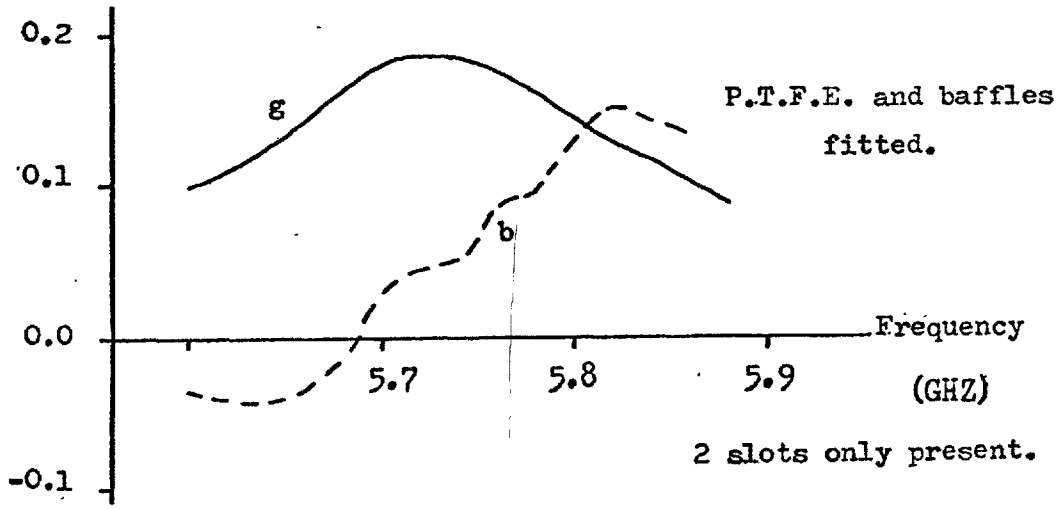

fast wave. This was the leaky wave identified in the last chapter. However, if the results are extrapolated to zero slot separation the launching phase length is obtained as approximately 100^{o}. The method enables the slots to be completely characterised and the slot susceptance measured. The results obtained also enabled the phase shift past the slot to be predicted and agreement was obtained with measured data.

The measurements were repeated with all eight slots present. The first feature noticed was that the phase length varied even more rapidly with frequency. The resonant frequencies were found to be on average 5.752 GHz and have a similar spread as with only two slots present. With all eight slots present the coupled phase lengths shown in Figure 7.4.7. did not clearly demonstrate the fast wave behaviour. This is thought to be due to the additional guiding action of the slots reducing the attenuation of the leaky wave and lowering its phase velocity. In addition when the phase shift past a slot was predicted as described previously a massive phase shift resulted. This is related to off resonance slots loading the coupled phase length and giving it, its fast variation. The measurements were repeated with non-edge slots as transmitters but the results indicated that 5.752 GHz was a good estimate of resonant frequency. When a central slot is used in transmission, two incremental phase lengths become unknown and the method is less reliable. However all the measurements of phase shift past individual slots with all the other seven slots parasitic agree with the resonant frequency indicated.

The effects of parasitic slots on the conductance of isolated slots was then investigated. Initially all the slots of the 8 x 3 network were taped over with adhesive aluminium tape and the measurement bench

FIGURE 7.4.7. The measured mutual coupling phase lengths taken from swept frequency measurements at 5.752 GHZ..

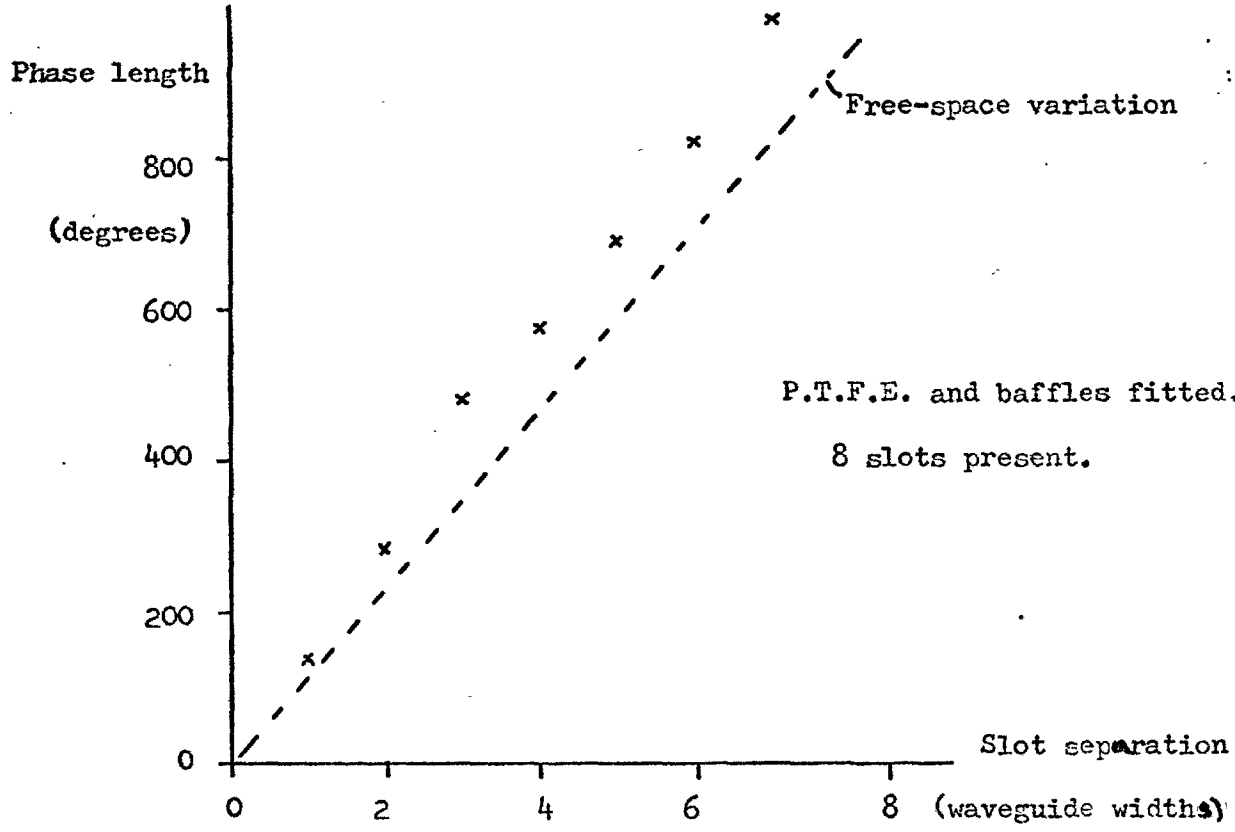

FIGURE 7.4.8. The computed phase shift past a single slot from measuremen of coupled phase lengths with 8 slots present.

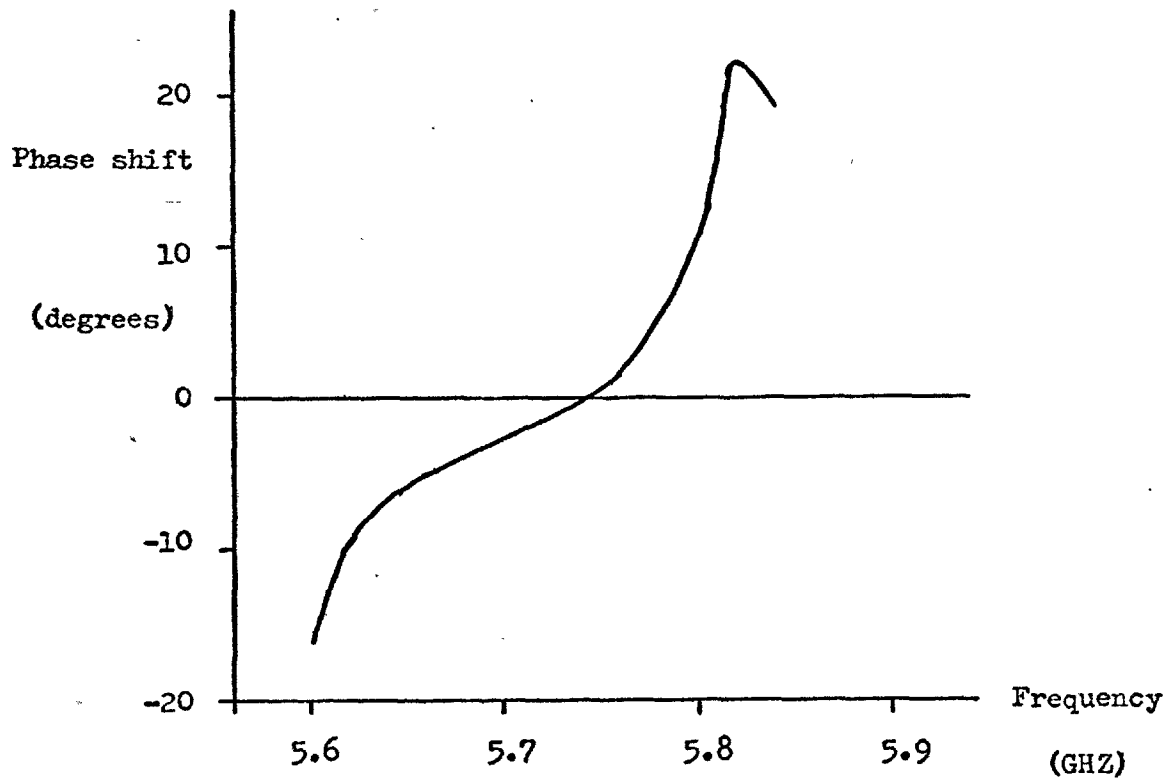

connected to one waveguide. The calibration of the ratiometer output was recorded on the data normaliser and the aluminium tape removed from the single slot used in the measurement waveguide. P.T.F.E. was then fitted and the attenuation past this slot measured. The other slots in the same column were then uncovered and fitted with P.T.F.E.. The measurement was repeated and the effect of parasitic slots revealed. Typical results for an edge and central slot are shown in Figure 7.4.9. and 7.4.10.. Introducing the parasitic slots had a major effect on the attenuation past the individual slots, particularly for central elements. As the reactive component of the slot only introduces a small contribution to the attenuation of the passing wave, the changes measured were principally associated with the slot conductance. The parasitic slots caused an increase in the peak conductance of the slot and for central elements produced a shift to higher frequencies. However, around 5.75 GHz which the previous measurements had shown to be the frequency at which the slots were phase resonant the slot conductances appeared unchanged by the parasitic elements. It was thus logical to design an experimental array to operate at 5.75 GHz as the slot information derived from the linear thirty element array could be used directly. A small correction being required to allow for the decrease in conductance in shifting the operating frequency from 5.70 GHz to 5.75 GHz.. Performing this shift was likely to account for all the effects of operating a slot with other parasitic elements. The shift in resonant frequency is included and no change in the conductance appeared to be required.

Before proceeding with the array design it was thought useful to feed all eight slots in a single column and ensure that they behaved regularly. To do this each waveguide was provided with a waveguide phase

FIGURE 7.4.9. The measured attenuation past an edge slot of the 8×3 network when fitted with 5/8" square baffles and P.T.F.E..

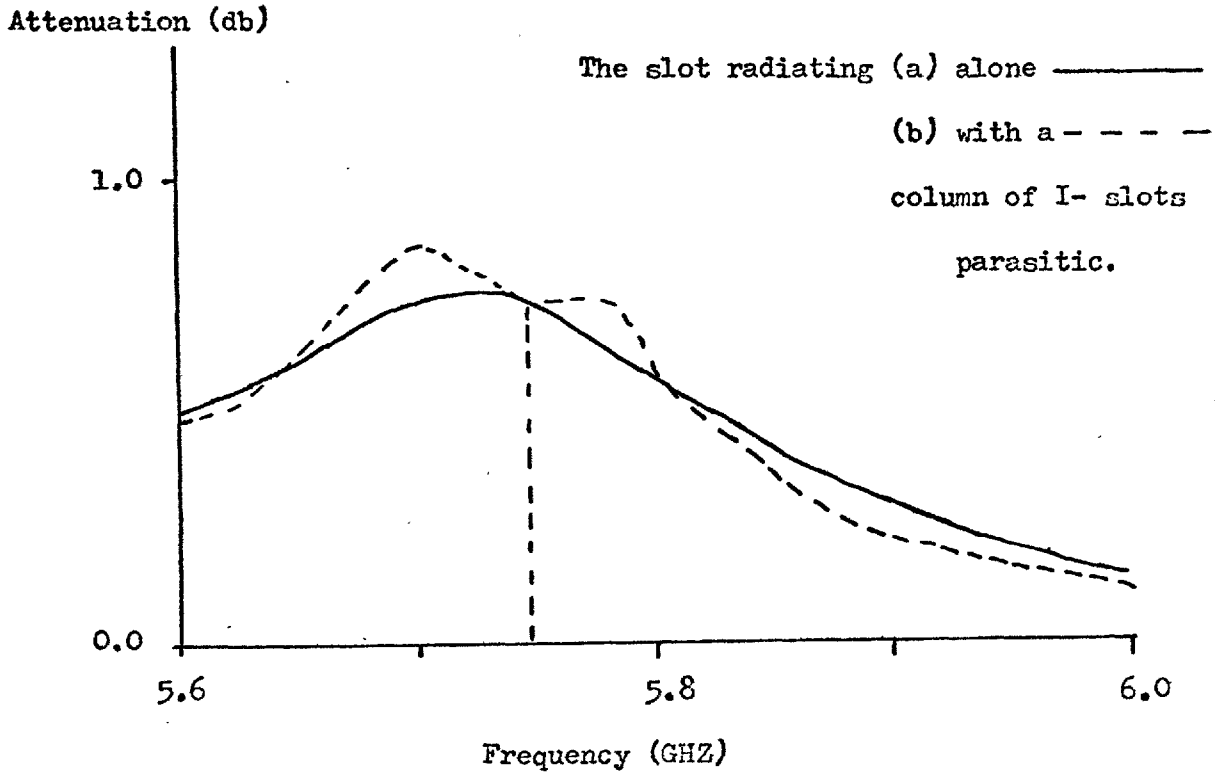

FIGURE 7.4.10. The measured attenuation past a centre slot of the 8x3 network when fitted with 5/8" square baffles and P.T.F.E..

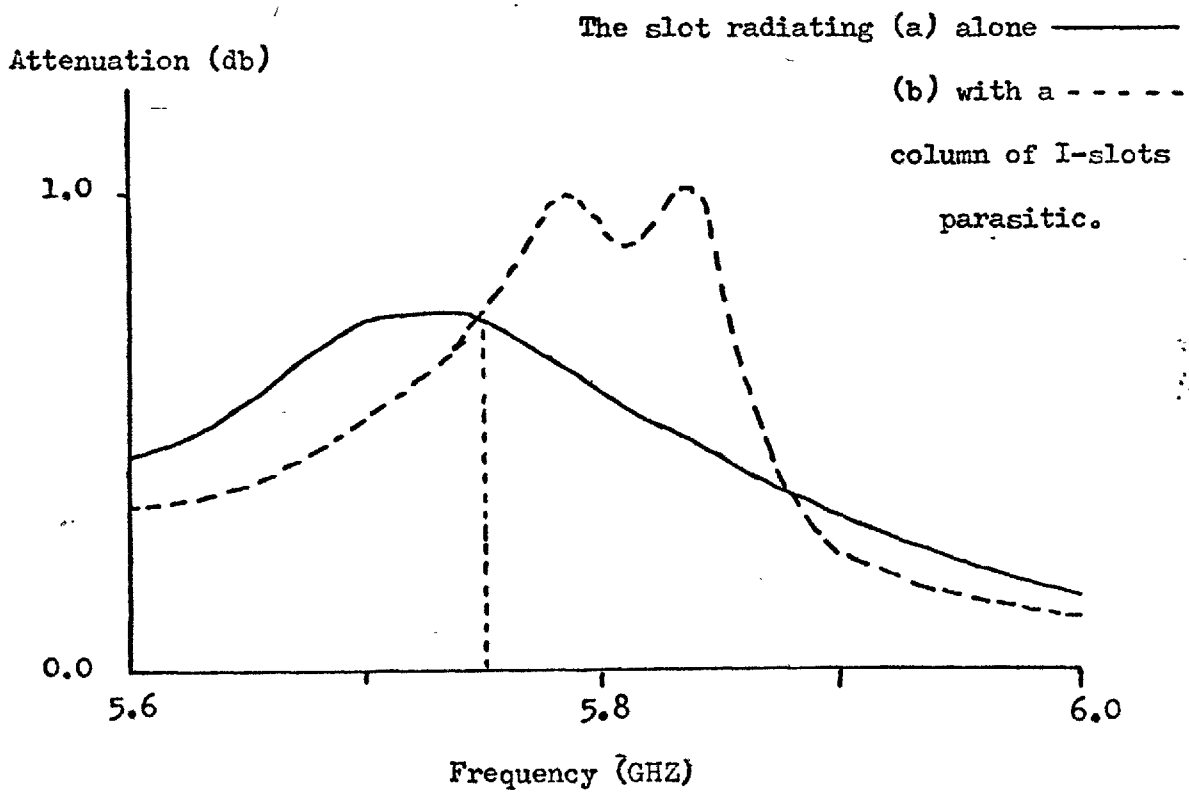

shifter in the special size waveguide. Four waveguides were fed from each end of the network. Bifurcated waveguide sections were used to combine the outputs of the four waveguides and the final combination was done using a 3 dB hybrid. The network was placed on an antenna test site and the phase shifters set to give a beam at broadside. The radiation pattern was plotted and the beam phase scanned. This procedure was repeated. In this manner the far field performance of the phase scanned beam was established. The important results were summarised in Figure 7.4.11.. The position of the beam varied as set by the phase shifters out to an angle of approximately 50^{o} from broadside. For larger scan angles although the phase shifters were correctly set the beam moved more slowly than expected. Similarly the gain of the eight slot array varied in a manner similar to an individual element pattern out to approximately 50^{o} from broadside. For larger beam angles the gain did not fall as expected but remained substantially constant. This unusual behaviour was due to the leaky wave being more strongly excited as the beam was scanned from broadside. The leaky wave could be expected to produce a beam approximately 60^{o} from broadside. This corresponds to the angle maintained by the beam when larger scan angles were set by the phase shifters. The gain was enhanced by the leaky wave. The active admittance of a centre slot of the eight slot phase scanned array was also measured by introducing a slotted line into one channel in a similar manner to that described in Section 7.1.. The results obtained are shown in Figure 7.4.12. The active admittance of the slot was in fact comparatively well behaved and confined to a reasonably small area of the Smith Chart. This contrasted with the result obtained with two slots in which a circle was obtained, and was regarded as encouraging. Little variation in admittance was measured and if this result applied in a full array then it was likely that a well behaved

FIGURE 7.4.11. A summary of the results obtained by phase scanning a column of eight I-shaped slots fitted with 5/8" square baffles.

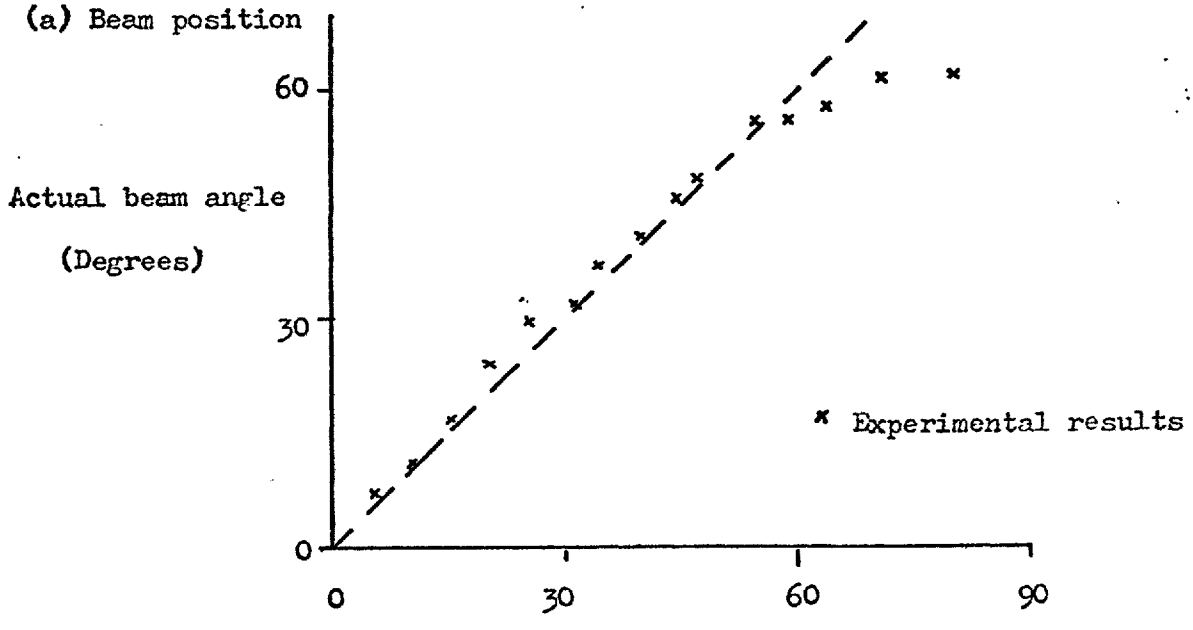

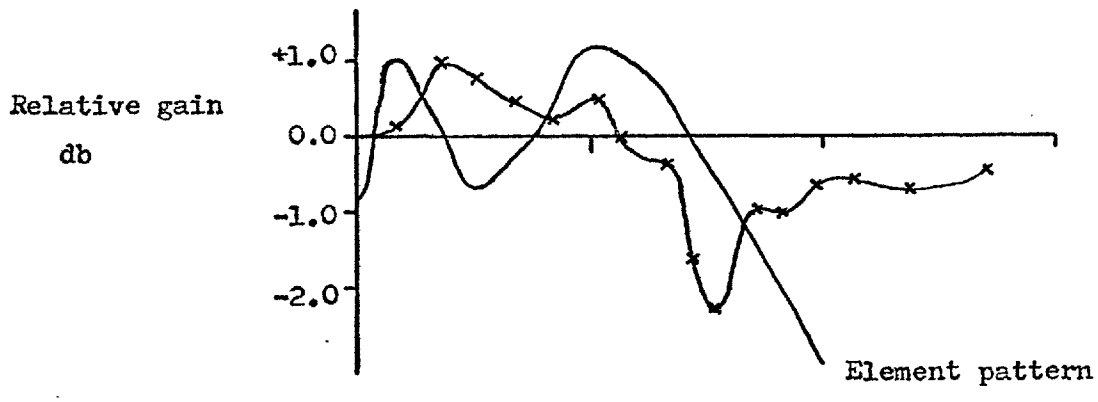

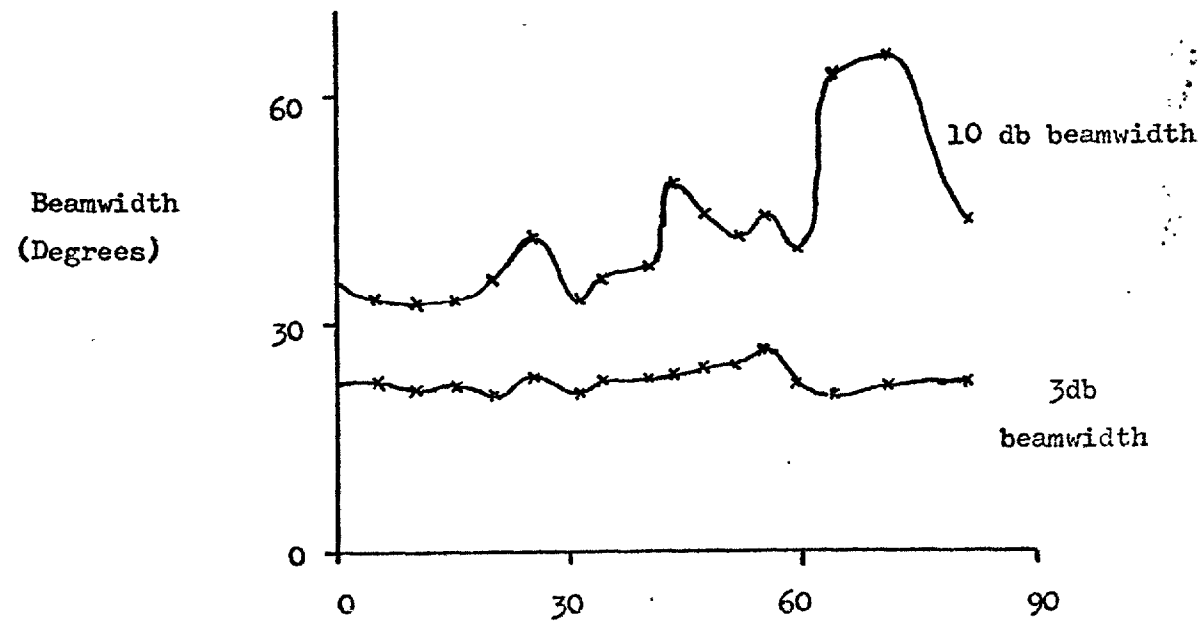

FIGURE 7.4.12. The measured active admittance of a central slot of the eight element phase scanned array.

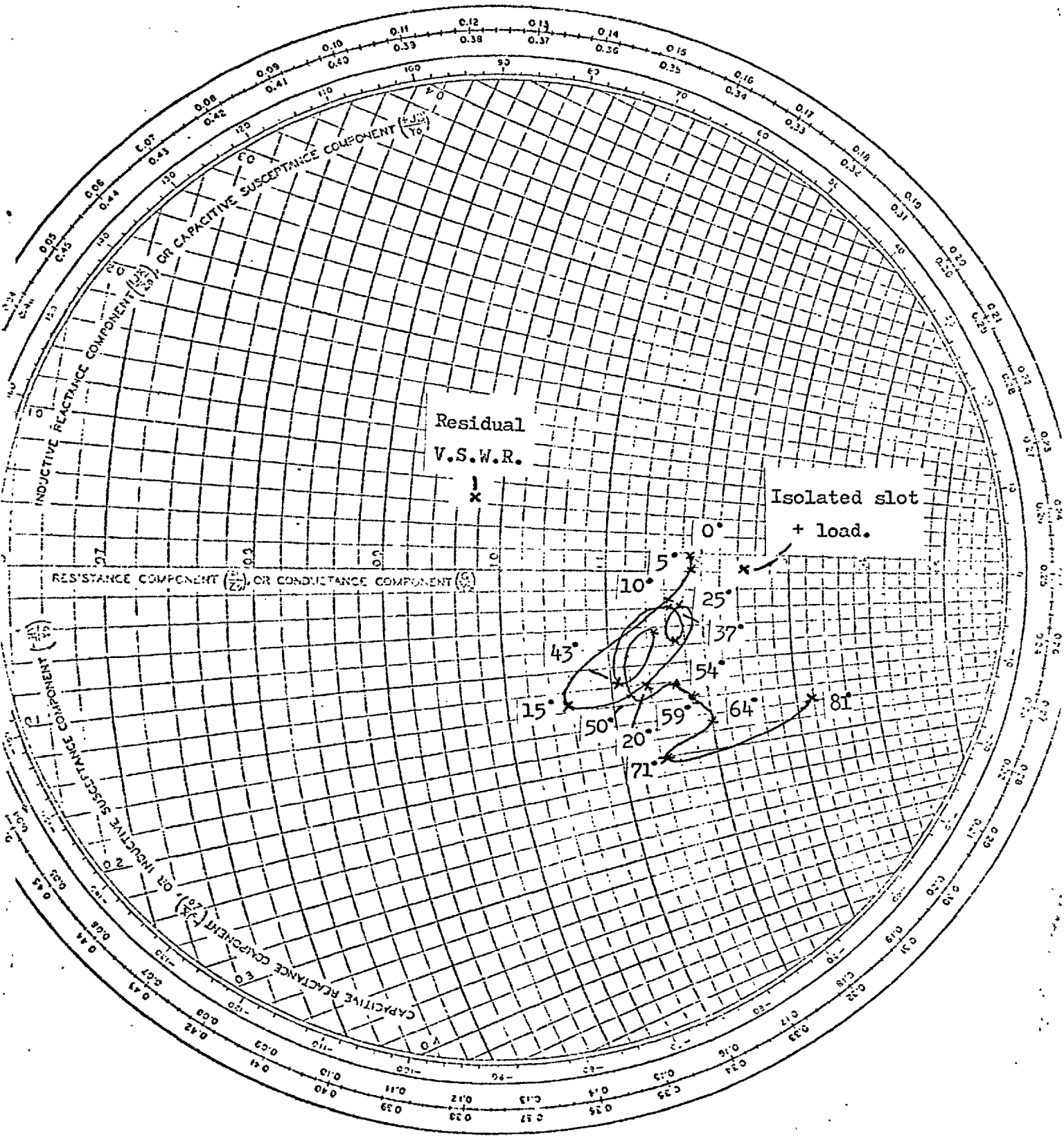

5.70 GHZ. 5/8" square baffles + P.T.F.E..

The figures indicate the beam position.

phase scanned performance would be obtained.

The elements of the coupling matrix were then measured for a column of eight slots in separate waveguides. Essentially the mutual impedance matrix linking the eight slots ought to have been used so that the voltage induced on one slot by a current in another was investigated. As the slots all had the same self radiation impedance a voltage to voltage description was used. This ignored the effect of the waveguide loading of the slot and was essentially a scattering matrix representation, with all the element impedances assumed to be the same. The coupling matrix was required at 5.75 GHz, the array design frequency, but measurements were made over a band of frequencies. All the phase components had essentially been measured to determine the resonant frequencies and attention focussed on the amplitude components.

When one waveguide was excited a voltage was induced across its slot. This in turn produced voltages across all the other slots by virtue of the mutual impedances. All the slots then excited secondary waves in their respective waveguides and since all the slots were the same the amplitudes of the secondary waves were in the same ratio as the voltages across the slots. The measurement thus essentially involved comparing the amplitude of the reflected signal in the excited waveguide with the secondary waves induced in the other waveguides. Practically all quantities were compared to the input level but the coupled voltage amplitudes were readily obtained. In this manner a coupling matrix could be established for the voltages induced on other slots when a particular slot was excited.

The matrix was required at 5.75 GHz but swept measurements indicated that there was considerable variation in the frequency of peak coupled power as shown in Figure 7.4.13.. There seemed to be a regular pattern about

FIGURE 7.4.13. The frequency of peak coupling between pairs of slots all eight slots of one column present.

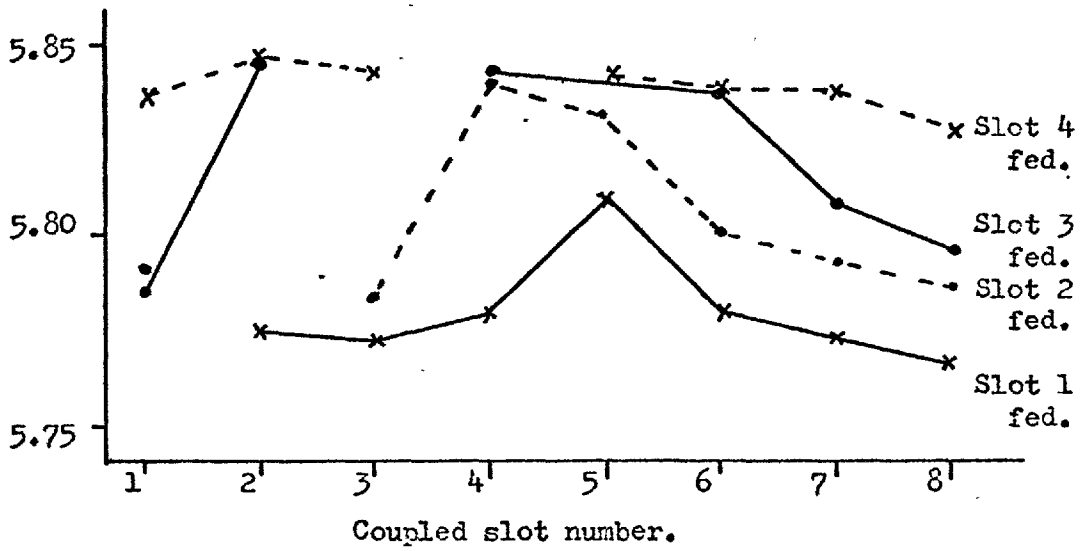

FIGURE 7.4.14. The measured values of coupled power.

(a) Slots 1 & 2 radiating.

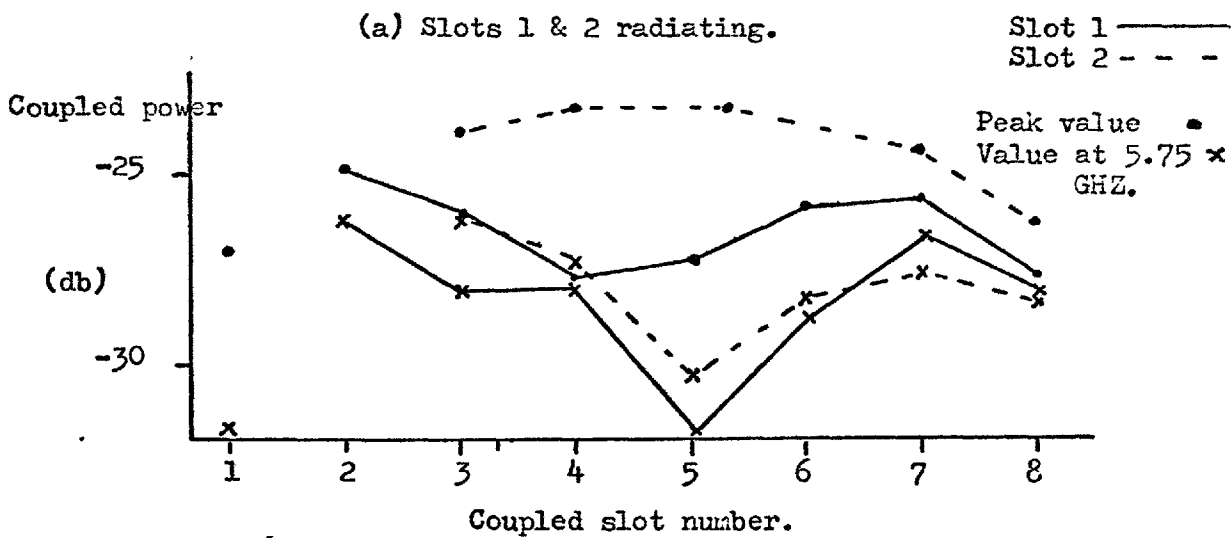

(b) Slots 3 &4 radiating.

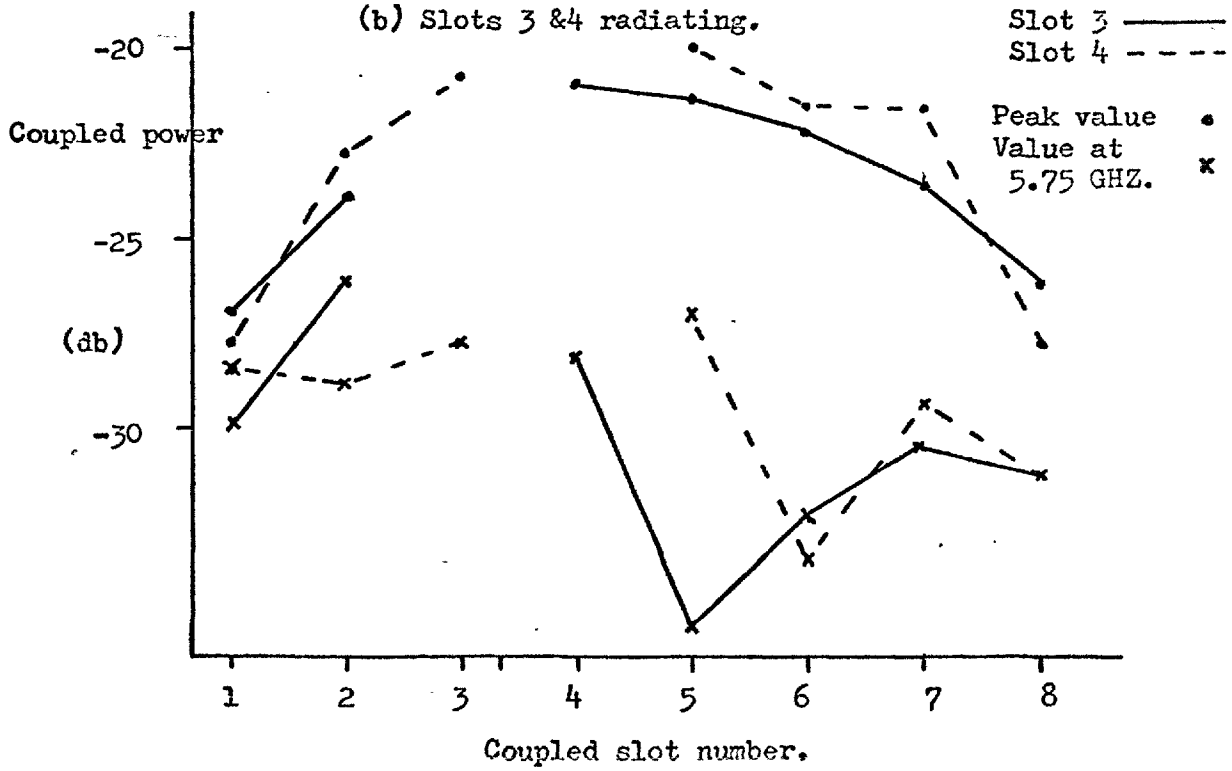

the behaviour with pairs of slots nearer the middle of the column having the highest frequency of peak coupled power. This was taken as an indication that with eight slots in a column none of them could be regarded as elements of an infinite array. The peak coupled powers between slots and the values at 5.75 GHz are shown in Figure 7.4.14. Apart from when an edge slot is excited, there seems to be some sort of resonant distribution within the column of slots, with coupling from slot 2 to slot 5 being larger than the coupling from slot 2 to slot 3. These measurements showed that although an eight waveguide array would provide a useful indication of the behaviour of a many waveguide array extrapolation would have to be made with extreme care. From these measurements the mutual coupling matrix was established. Despite the dispersion of the amplitude results all the phase measurements indicated that the slots were phase resonant around 5.75 GHz.

7.5. The Design of the Eight Waveguide Array

The coupling matrix was fed into the computer programme used to design the eight waveguide array. Each set of sum and difference waveguides were initially designed in isolation. They were then brought together and mutual coupling introduced. The sum waveguides were made 28 slots long with a $1_7 + 6_7 \cos^2(\frac{\pi}{2} x)$ aperture distribution similar to the single waveguide array considered earlier. The difference waveguides were of the same length and an $x \quad x \quad (1_7 + 6_7 \cos^2(\frac{\pi}{2} x))$ distribution was used. The two centre slots of the difference array did not radiate a significant amount of power and they were omitted so that the difference channel waveguide could be split. This allowed phase trimming between the two halves, to obtain a deep null. The computer programme used to design the array, initially worked out the slot conductances, required to establish the prescribed aperture distribution

with a given amount of power wasted in the terminating loads, in the absence of mutual coupling. The arrays were then considered in transmission and mutual coupling introduced with the experimentally determined values. A column of slots at a time was considered starting from the feed end. The correct relative powers were considered as incident on these slots establishing the required voltages. The coupling matrix was then used to determine the modified voltages on each slot. The total voltage on each slot was regarded as exciting secondary waves in the waveguide rather than just the voltage component coupled out of the waveguide by that slot. Effectively mutual coupling was treated as modifying each slots' voltage reflection coefficient and hence by definition the effective admittance at each slot.

The modified slot admittance was calculated in the presence of mutual coupling for each slot and beam position. The modification to the power getting past each slot was calculated to give the power incident on the next column. In this manner the phase and amplitude error on each slot was calculated at various beam positions and some of the effects of the waveguide loading included. However, a matched load was considered to exist beyond each slot. The slot spacing was such that in the absence of mutual coupling this was a fair assumption. When it was introduced the impedance beyond each slot became unknown so that an iterative procedure would have been required to include it. This was not considered to be necessary. The programme calculated the phase and amplitude on each slot which in effect gave the aperture distribution of the antenna. Predicting the far field distribution was a little more problematical. If only two waveguides are considered and all the slots so lightly compiled that the waveguide loading is negligible then the error on the sum array has the distribution of the

difference and similarly vice versa. In such a case the distribution on the sum array is as prescribed plus a correct difference distribution at a different phase. Then the difference channel pattern should include the power radiated as desired and the contribution from the sum channel. This last component will have the correct azimuth distribution and a desirable pattern in that plane. It is however likely to be at an incorrect phase and hence reduce the antenna gain increasing the elevation sidelobes. This is only a marginal decrease in performance compared to that which would be predicted if all the voltages on the sum channel slots only contributed to the sum channel far-field patterns and all the voltages on the difference channel slots only contributed to the difference channel far field patterns. In essence when considering the far field patterns the voltages on all the slots have to be considered together with the origin of each component, so that all the voltages originating at the sum channel feed are included into the sum channel pattern. The programme used to design the array was not capable of making this distinction so no theoretical far-field patterns are presented. Instead the programme only predicted near field performance, because errors could then be associated with individual slots. If systematic errors had emerged corrections could be made. In this connection the most important result that emerged was that if the power deposited in the sum channel loads had been specified as - 20 dB, as for the thirty slot linear array, the waveguide loading of the slots nearest the load would have resulted in large asymetric errors. For the sum channel the error was greatly reduced by specifying the power in the loads as only - 10 dB on the input. Equal power was radiated by the two channels so - 10 dB was also deposited in the difference channel loads. Some unbalanced error was then associated with the slots near the load end of the first half of the difference array but this was

thought to be tolerable. The amplitude and phase distributions calculated for the waveguides of the array for various beam positions are as shown in Figure 7.5.1. to 7.5.8..

The distributions obtained appear to show major errors associated with each channel but it must be remembered that the distributions show the total power radiated or effectively the voltage present at each slot and that this includes components originating from both types of distribution. The odd character of the difference distribution makes the sum channel distributions appear asymmetric. The even nature of the sum distribution enhances one half of the difference channel at the expense of the other. Although the individual waveguide distributions may initially appear to be bad they can generally be shown to be a simple mixture of the sum and difference distributions. More serious errors occur due to the waveguide loading of the slots. The heavily coupled slots distort the distribution particularly if very different powers exist in the two waveguides. These errors are minimised by increasing the power in the terminating waveguide reducing the loading of the slots.

In general the near field behaviour of the antenna is complicated and due to the different phase relationships required for phase scanning the distributions can, and do, take all manner of variations. Apart from the effects of waveguide loading it is not sensible to attempt to eliminate mutual coupling from the design. The sum waveguide slots must be allowed to be parasitic difference slots and vice versa. The origin of all contributions must be included if any corrections are to be made so that the sum channel is a correctly behaved parasitic difference radiator as well as a sum channel element. In any case for the required range of scan angle it appeared that the actual distributions embraced the design, so that it is most unlikely that any correction could be introduced.

FIGURE 7.5.1. The computed aperture distribution of No. 1 waveguide of the eight waveguide array.

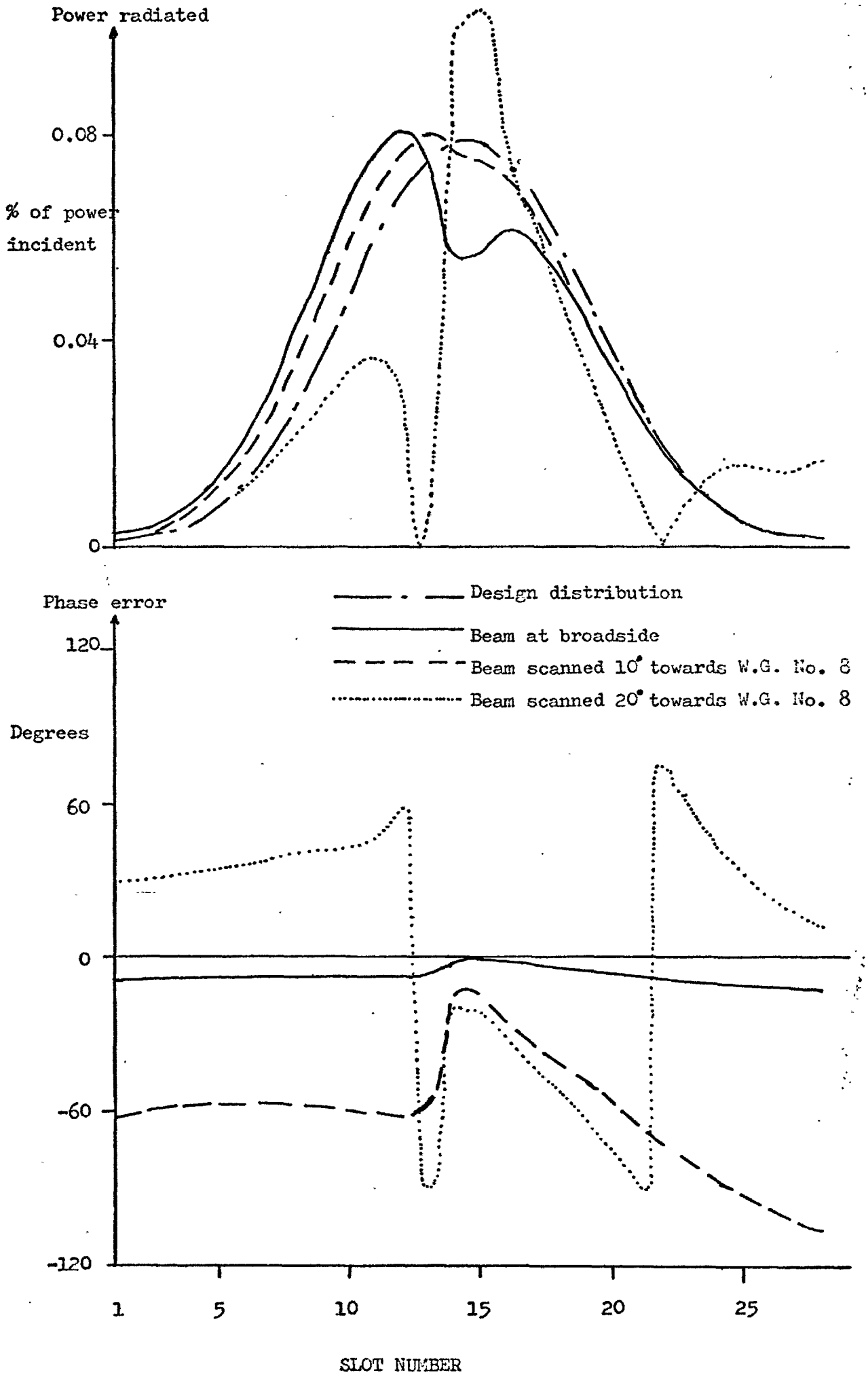

FIGURE 7.5.2. The computed aperture distribution of No. 2 waveguide of the eight waveguide array.

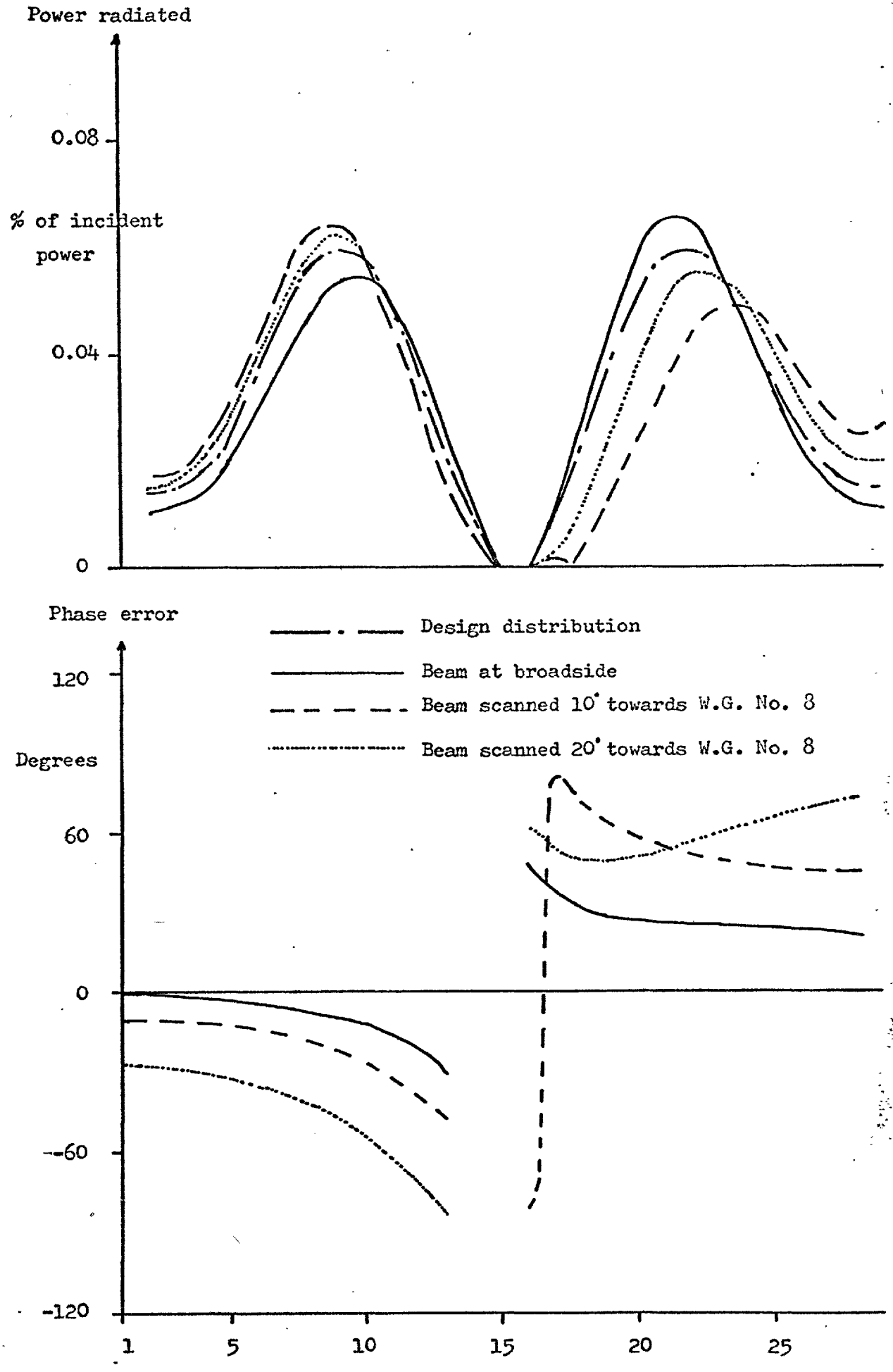

FIGURE 7.5.3. The computed aperture distribution of No. 3 waveguide of the eight waveguide array.

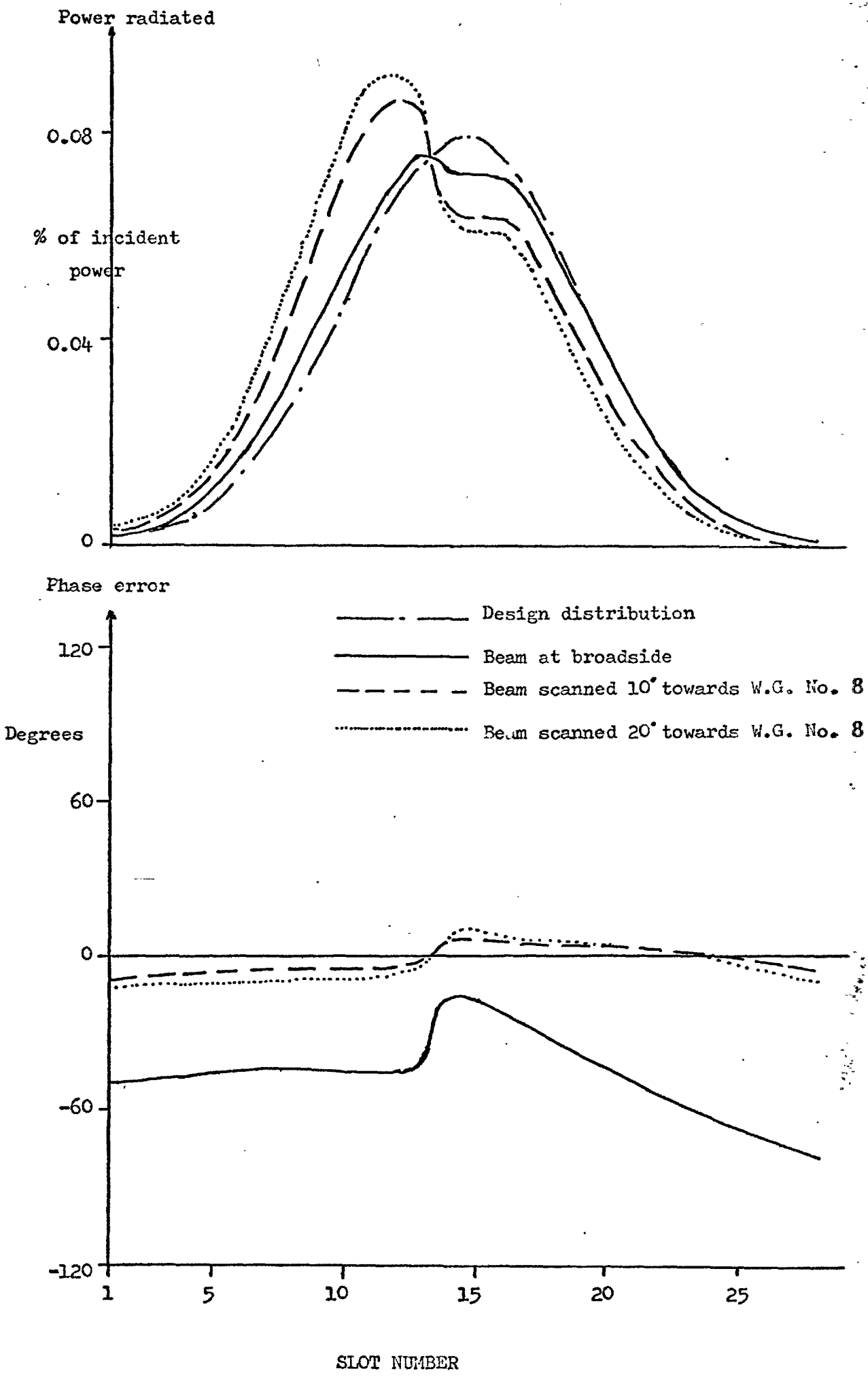

FIGURE 7.5.4. The computed aperture distribution of No. 4 waveguide of the eight waveguide array.

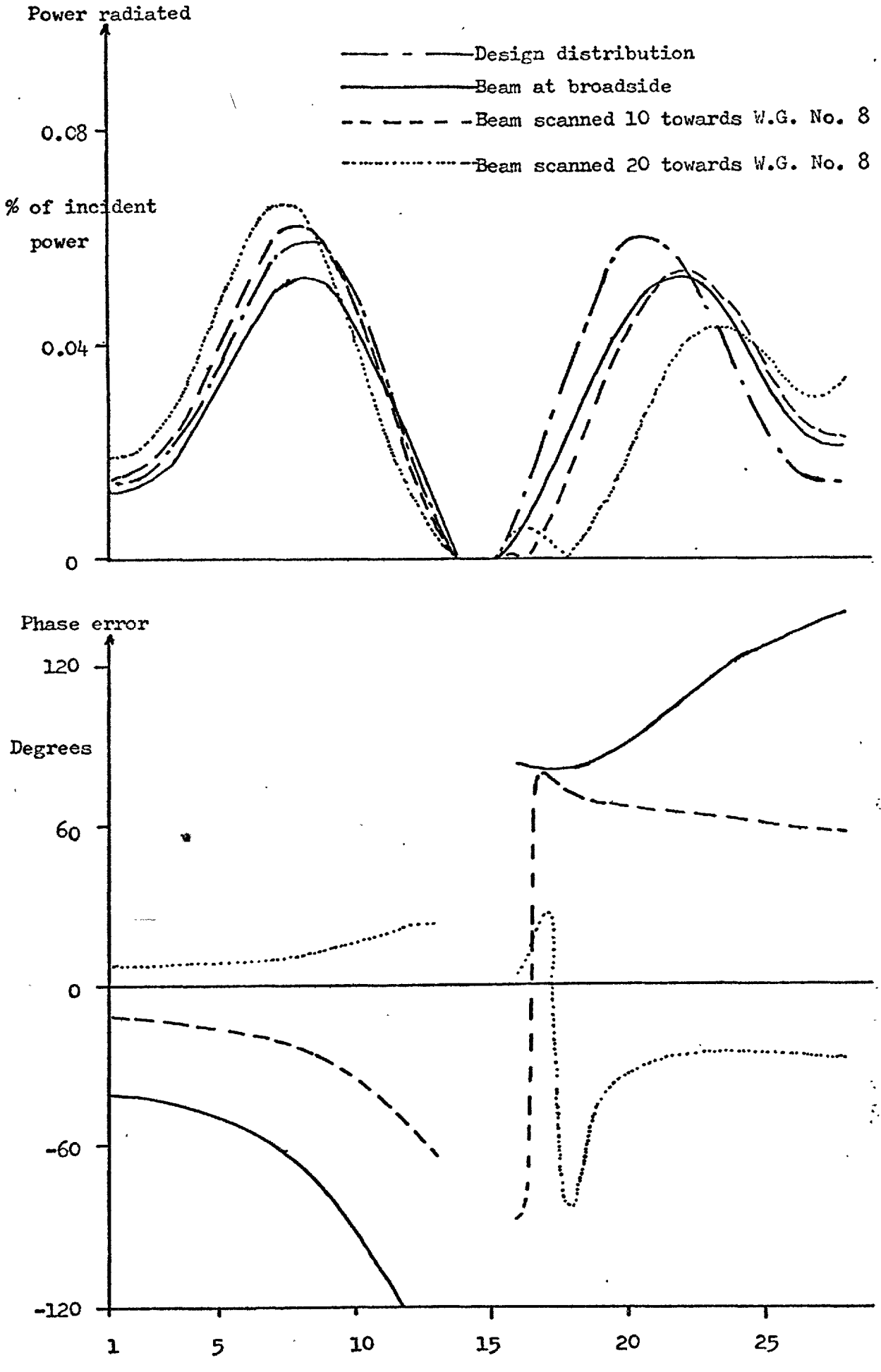

FIGURE 7.5.5. The computed aperture distribution of No. 5 waveguide of the eight waveguide array.

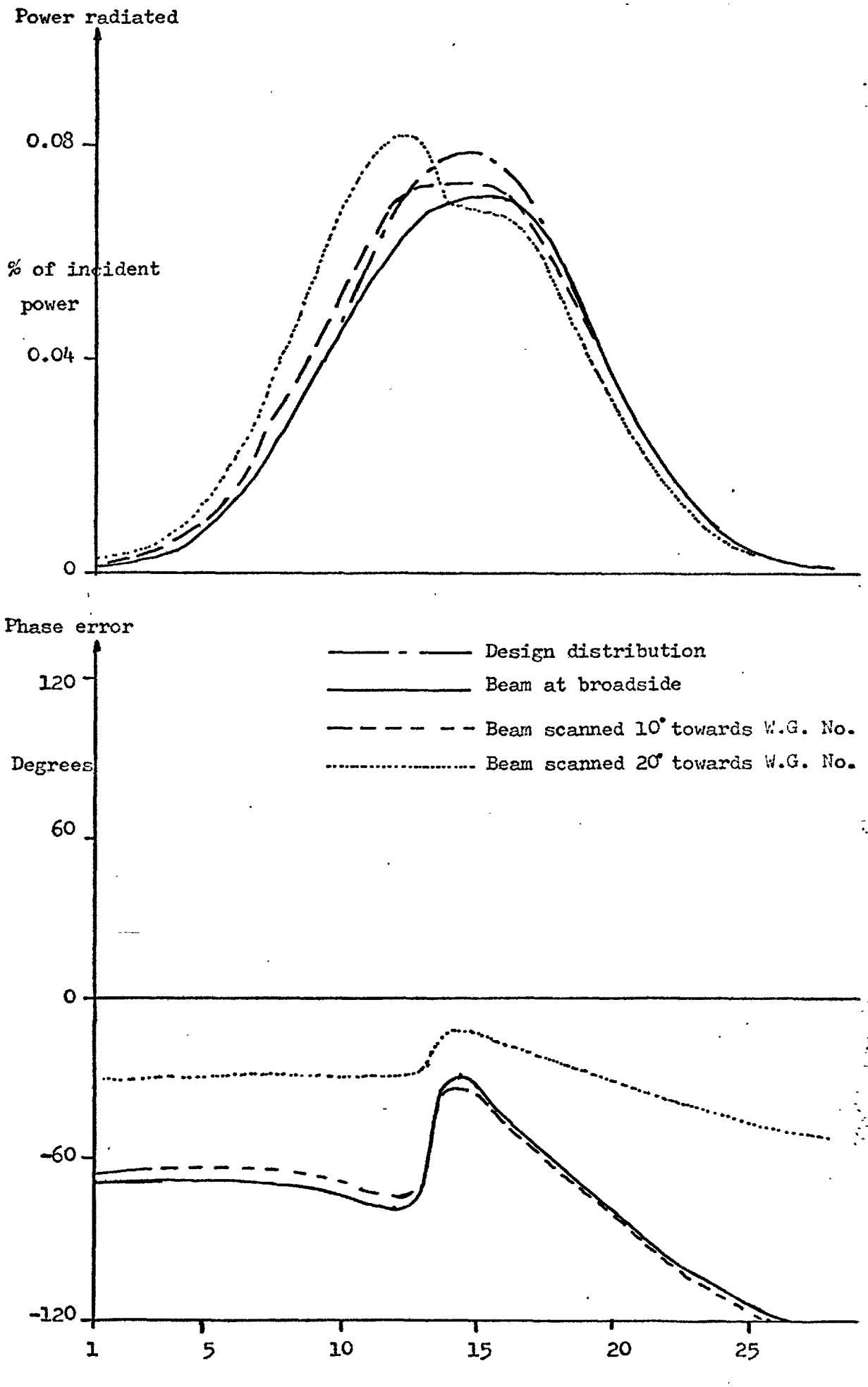

FIGURE 7.5.6. The computed aperture distribution of No. 6 waveguide of the eight waveguide array.

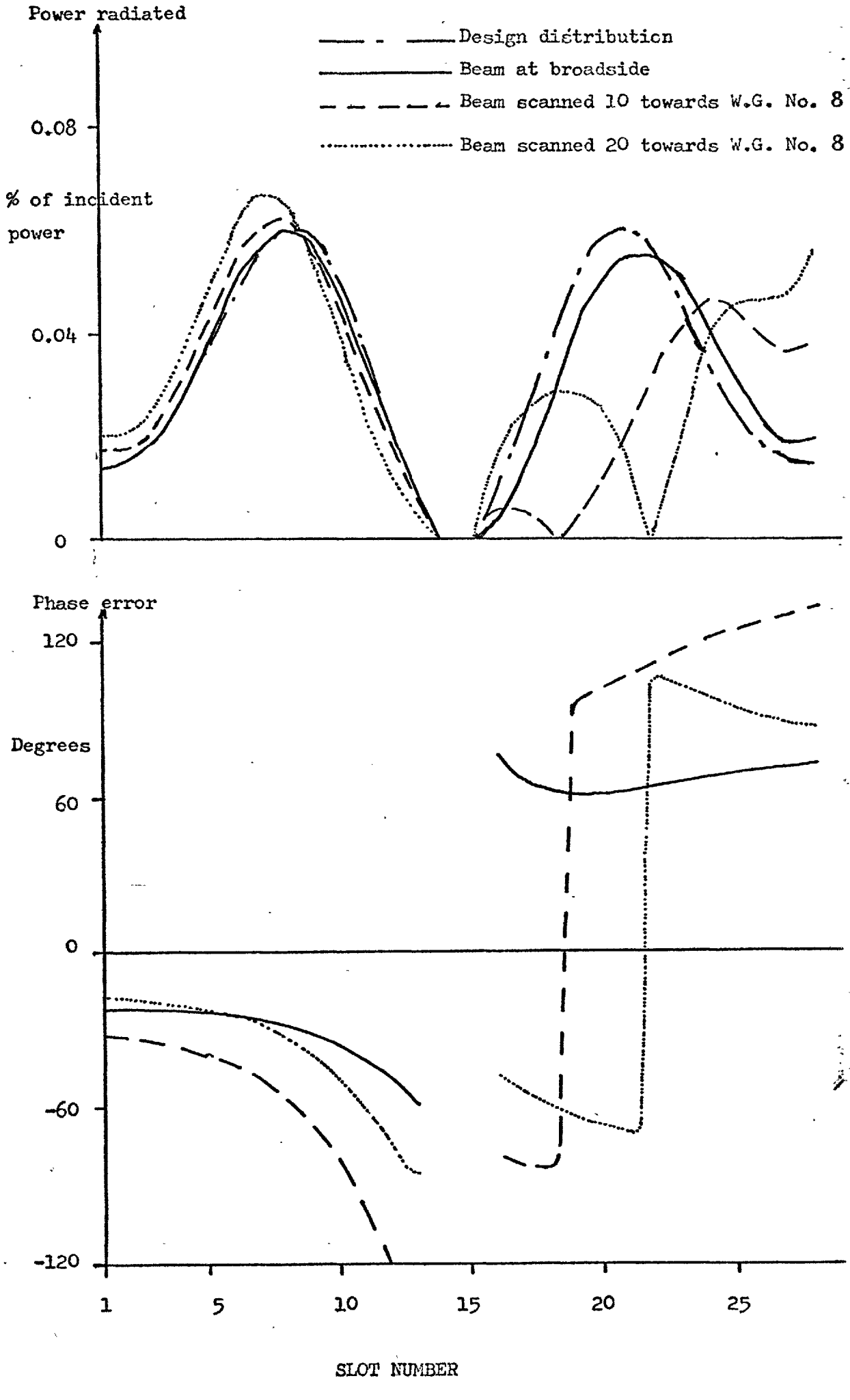

FIGURE 7.5.7. The computed aperture distribution of No. 7 waveguide of the eight waveguide array.

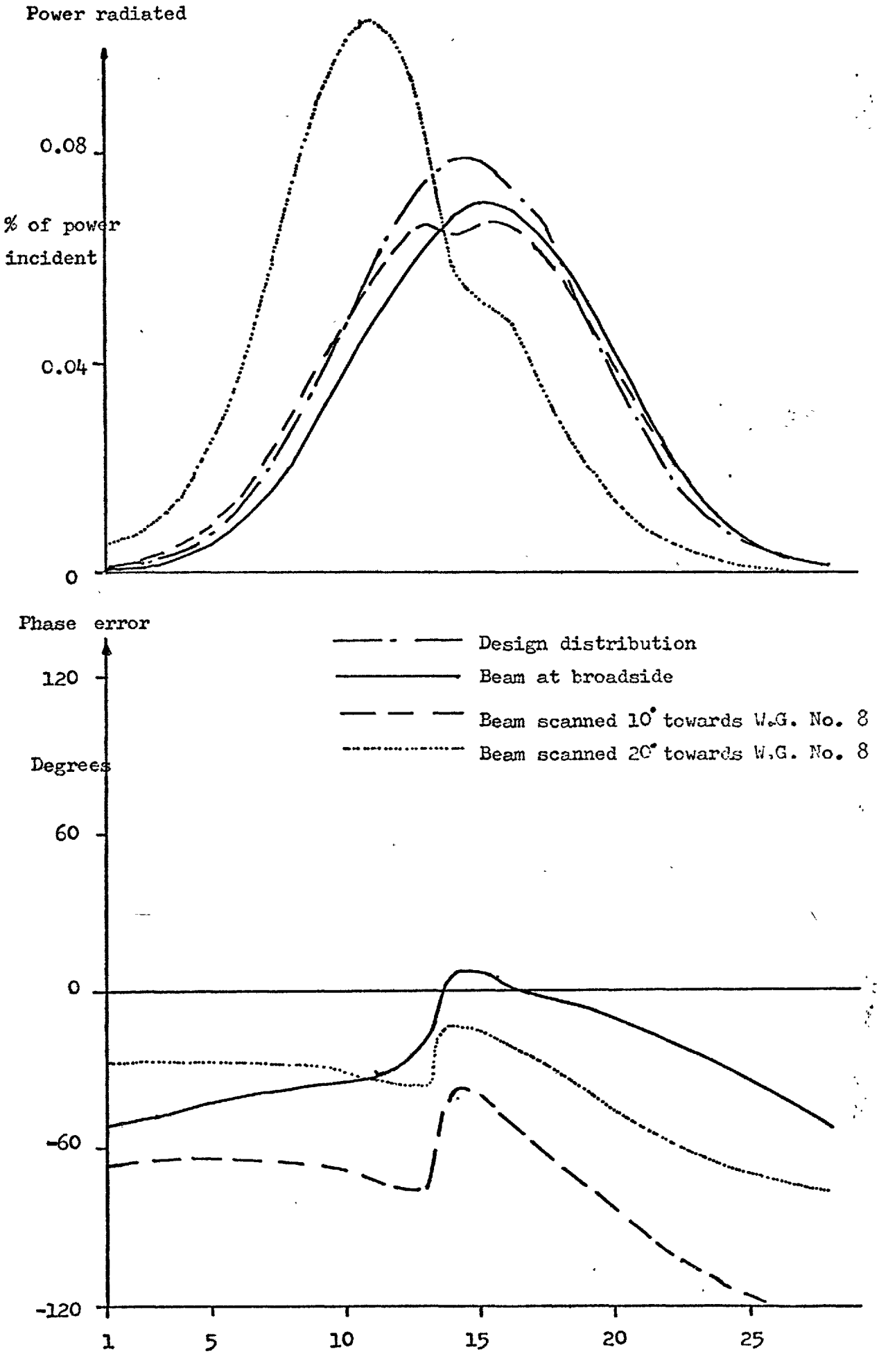

FIGURE 7.5.8. The computed aperture distribution of No. 8 waveguide of the eight waveguide array.

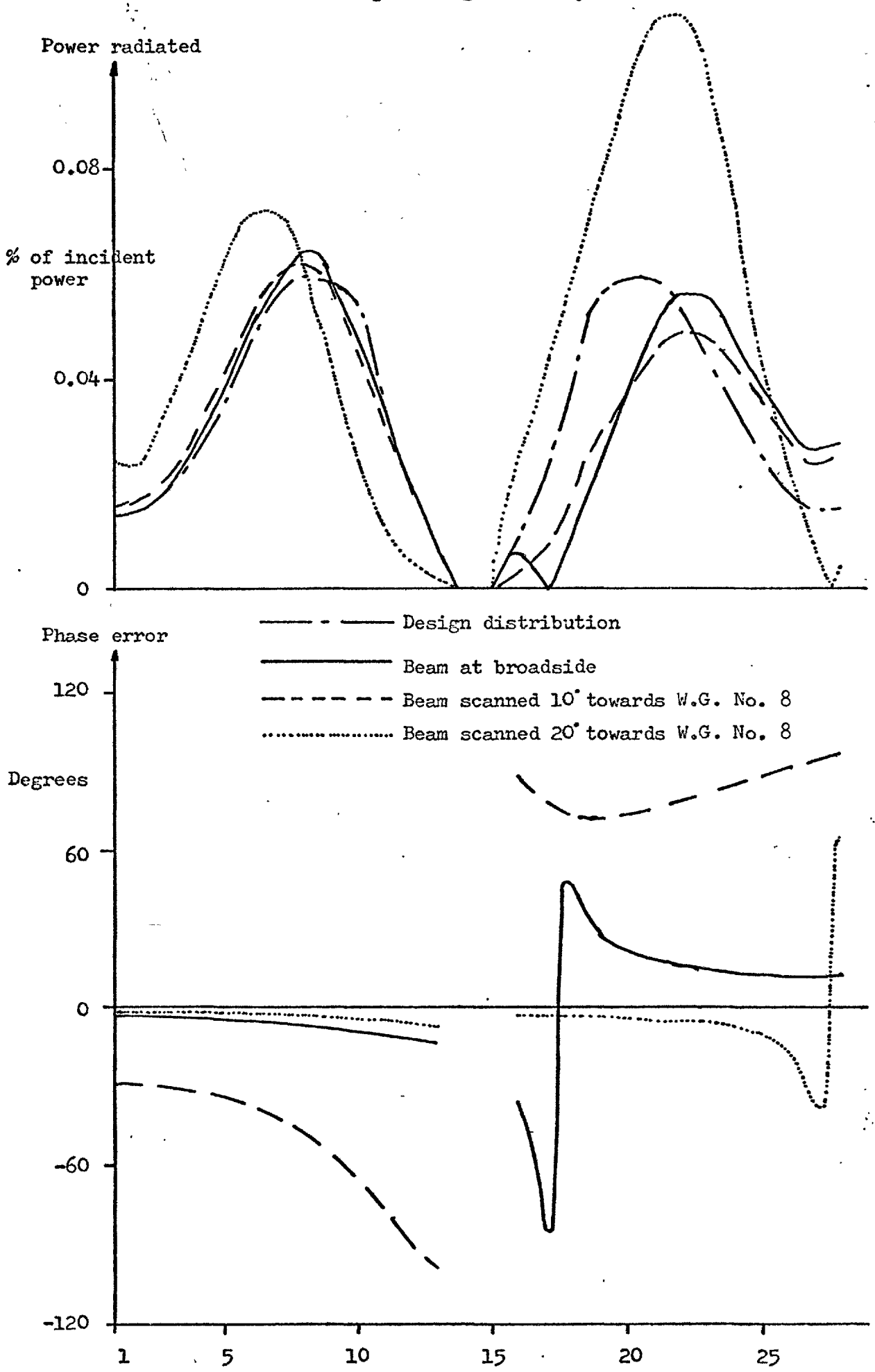

7.6. The Performance of the Eight Waveguide Array

A practical demonstration of the far field performance of this antenna was desired and the computer programme was then used to dimension the required slots. It did this in an iterative manner, initially assuming an average value for the length of the shorter branch arm of the slot. The other slot dimensions and its conductance were then evaluated and the latter compared to the desired value. The length of the shorter branch arm was then suitably incremented, the increment being halved when the conductance error changed sign. The interactions were continued until a suitable accuracy was achieved, five or six iterations generally being sufficient. The slots dimensions were then printed out in a form directly suitable for workshop use and the array manufactured (see Plate 1).

A considerable waveguide network was required to feed the array (see Figure 7.6.1), all in the special size waveguide used. Eight beam steering phase shifters were required together with the combining bifurcations. As the difference channel was split to allow phase trimming, four additional phase shifters were required together with magic tees and loads. To combine the difference channel waveguides and reduce the overall size of the network sixteen waveguide corners were required. Apart from the bifurcations all the components (see Plate 2) were designed and then built in Imperial College's workshops. The input V.S.W.R. of all the components over the required bandwidth was comparable or better than the specifications claimed by component manufacturers for full waveguide band equipment. The bifurcations had previously been made by outside manufacturer's to A.S.W.E. designs. The whole array and network was assembled in an aluminium alloy channel frame approximately six feet long by two and a half feet square (see Plates 3

FIGURE 7.6.1. The arrangement of the eight waveguide array and feed network.

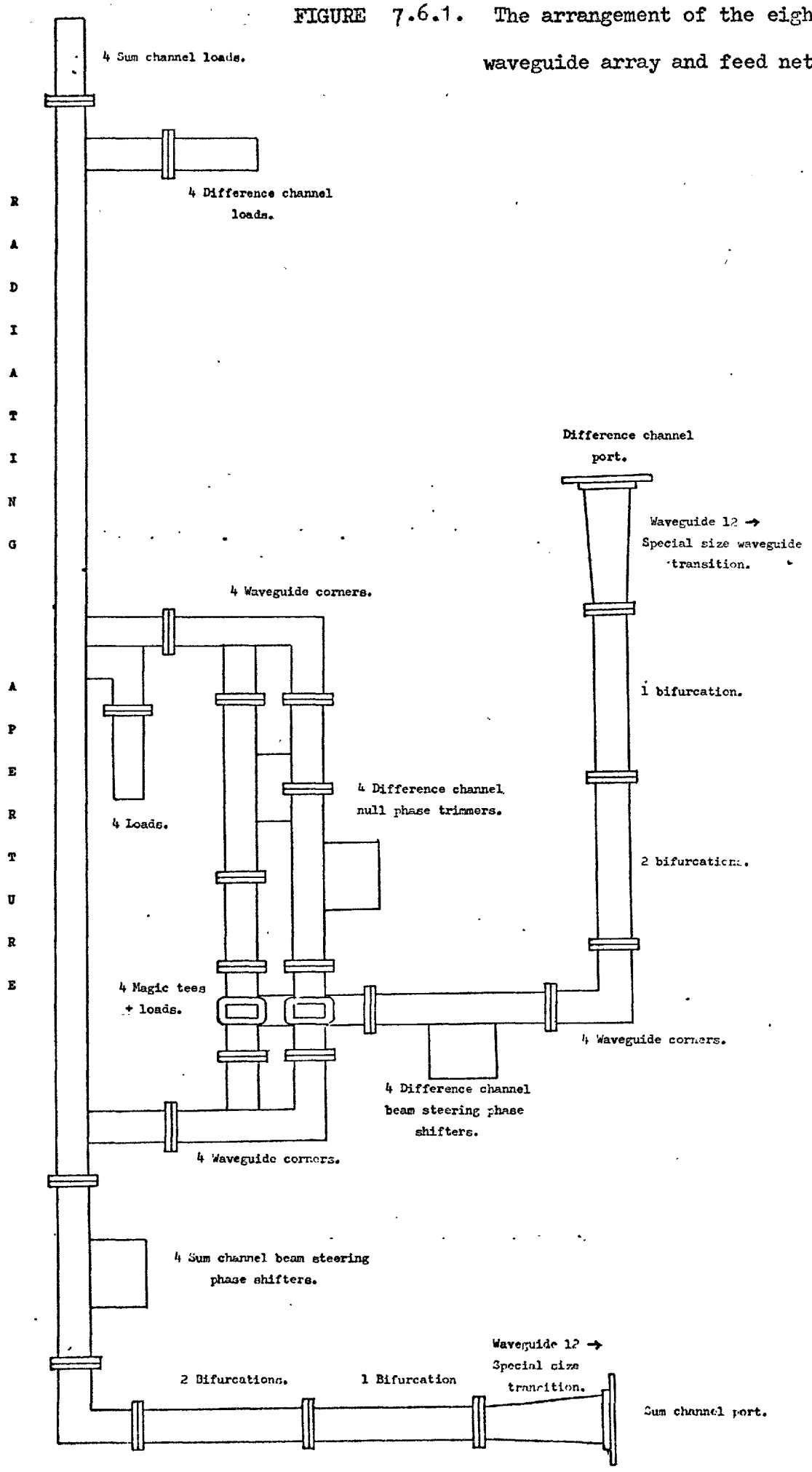

and 4). The performance of individual waveguides was checked during manufacture. The phase shifters had also been calibrated. In fact they all behaved similarly over the required frequencies so that once a broadside beam had been established it stayed at that position over the frequency range. The dispersion of the two halves of the difference array feed was dissimilar so that the null phase trimmers should have been adjusted at each change of frequency. They were set for the design frequency of 5.75 GHz and not adjusted for other frequencies. Large errors occured in the measured difference patterns at the edges of the measurement band.

Initially the array was placed on a C-band measurement site. The antenna was raised approximately thirty feet above the ground. The transmitting antenna, at a similar height was situated approximately 850' away from the array. Suitably sited fences were used to break up the ground reflection. The difference channel phase trimmers were then set one waveguide at a time with the bifurcations removed and the antenna pointing in the correct direction relative to the transmitter. The bifurcations were then replaced and the sum and difference azimuth radiation patterns plotted, with the beam at broadside, over a wide frequency range. These results are shown in Figure 7.6.2. to 7.6.7., although the lowest frequency difference channel results are omitted, because the phase trimming error was excessive.

The results show considerable variation over the band. Very good patterns with sidelobes generally lower than - 30 dB on the sum channel main beam being obtained at the lowest frequencies around 5.40 GHz. As the frequency was raised the sidelobe level deteriorated, with the worst performance being obtained at 5.80 GHz close to the frequency of peak coupled power between slots. In particular a large sidelobe existed on the load side of the main beam. This was thought to be due to

FIGURE 7.6.2. The sum channel radiation pattern at broadside and a frequency of (a) 5.40 GHZ.

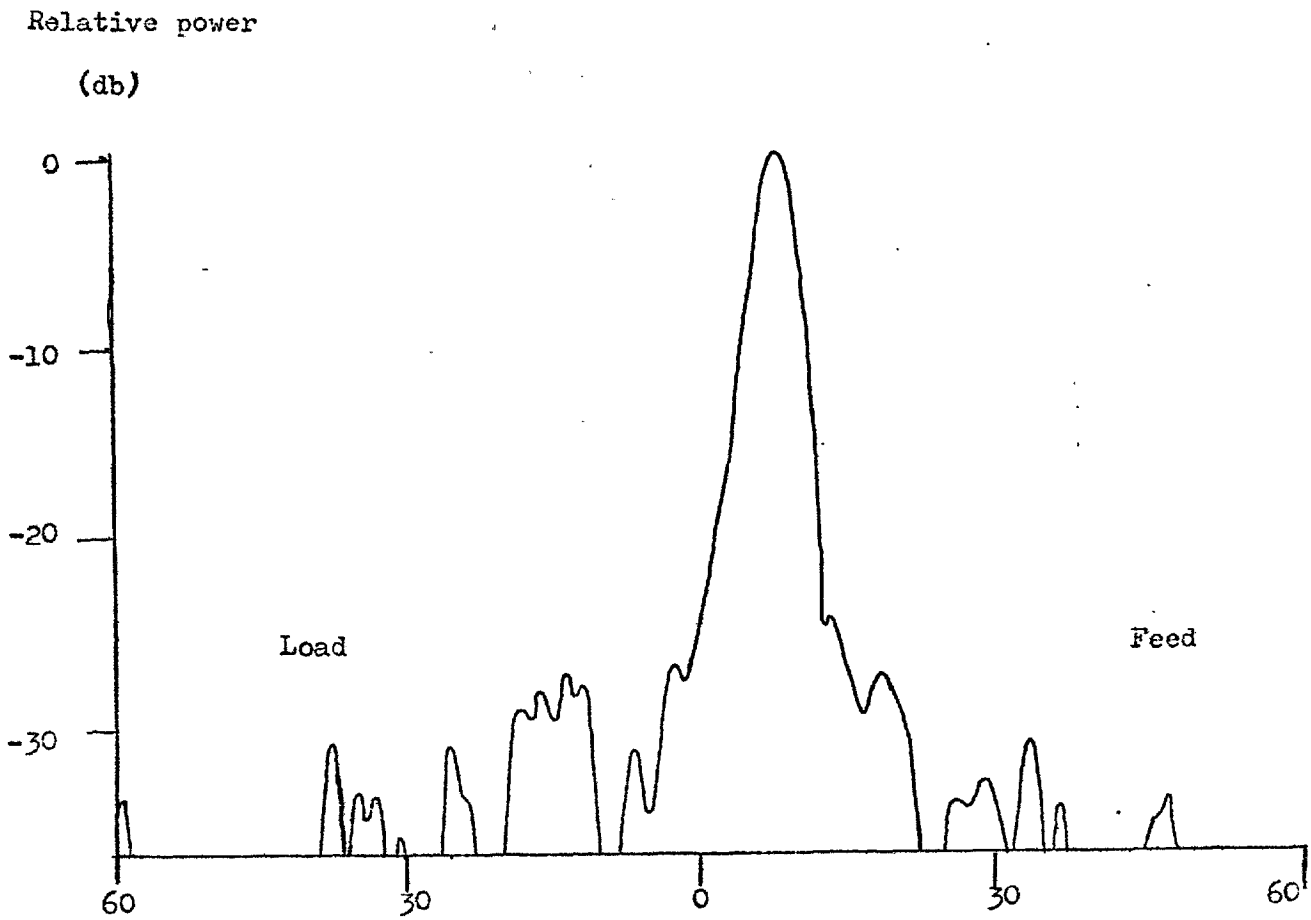

(b) 5.45 GHZ.

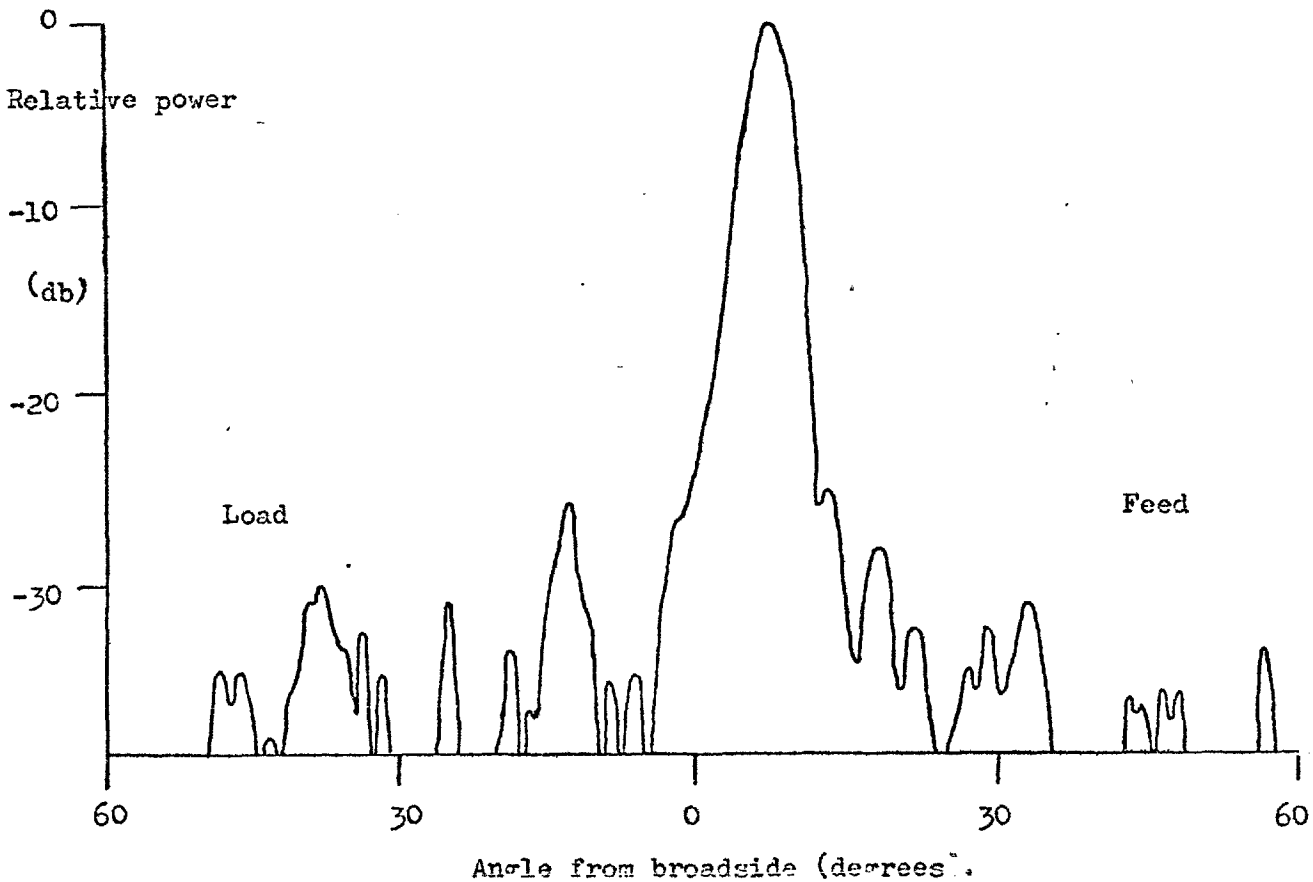

FIGURE 7.6.3. The sum channel radiation patterns at broadside and a frequency of (a) 5.50 GHZ.

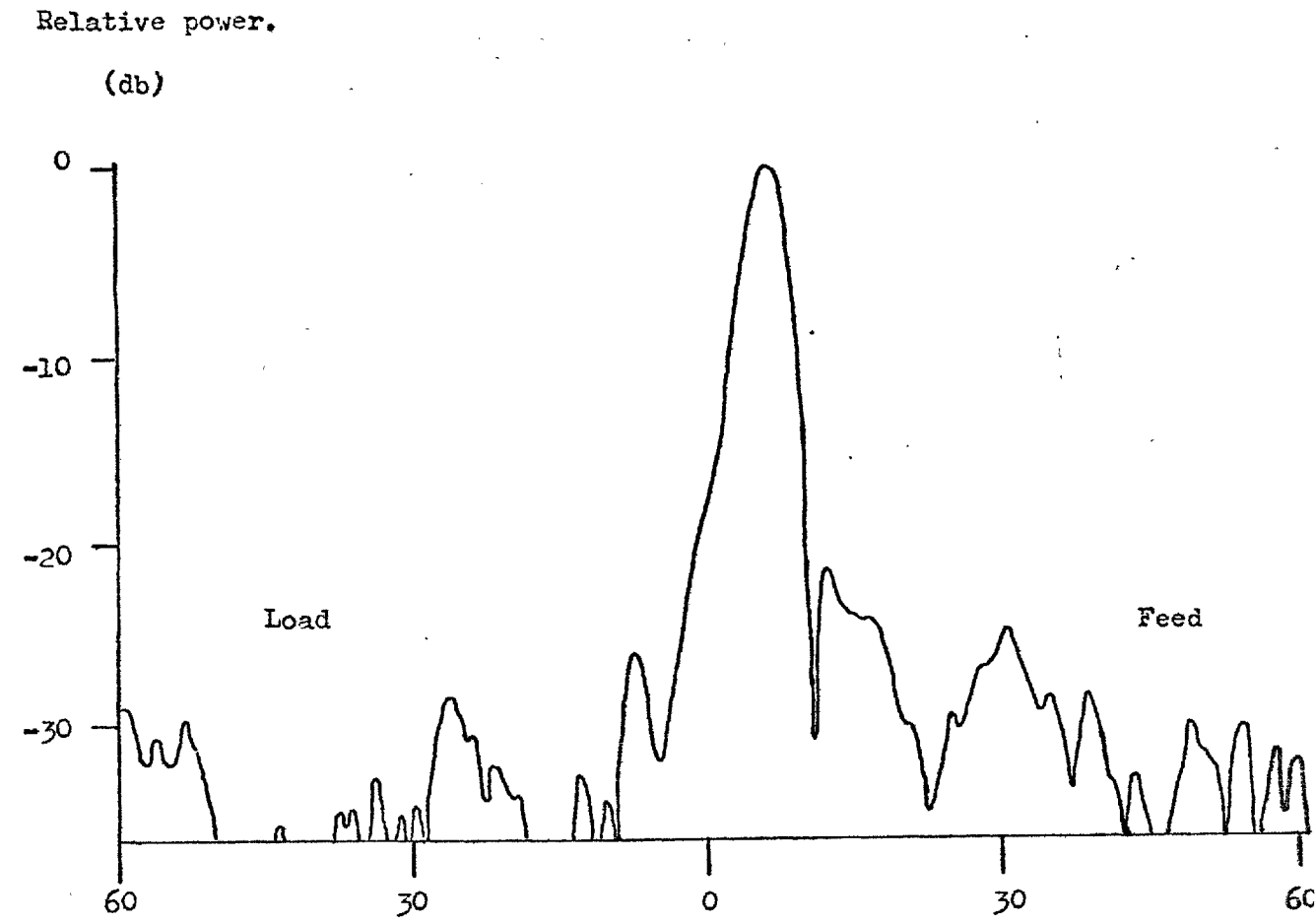

(b) 5.55 GHZ.

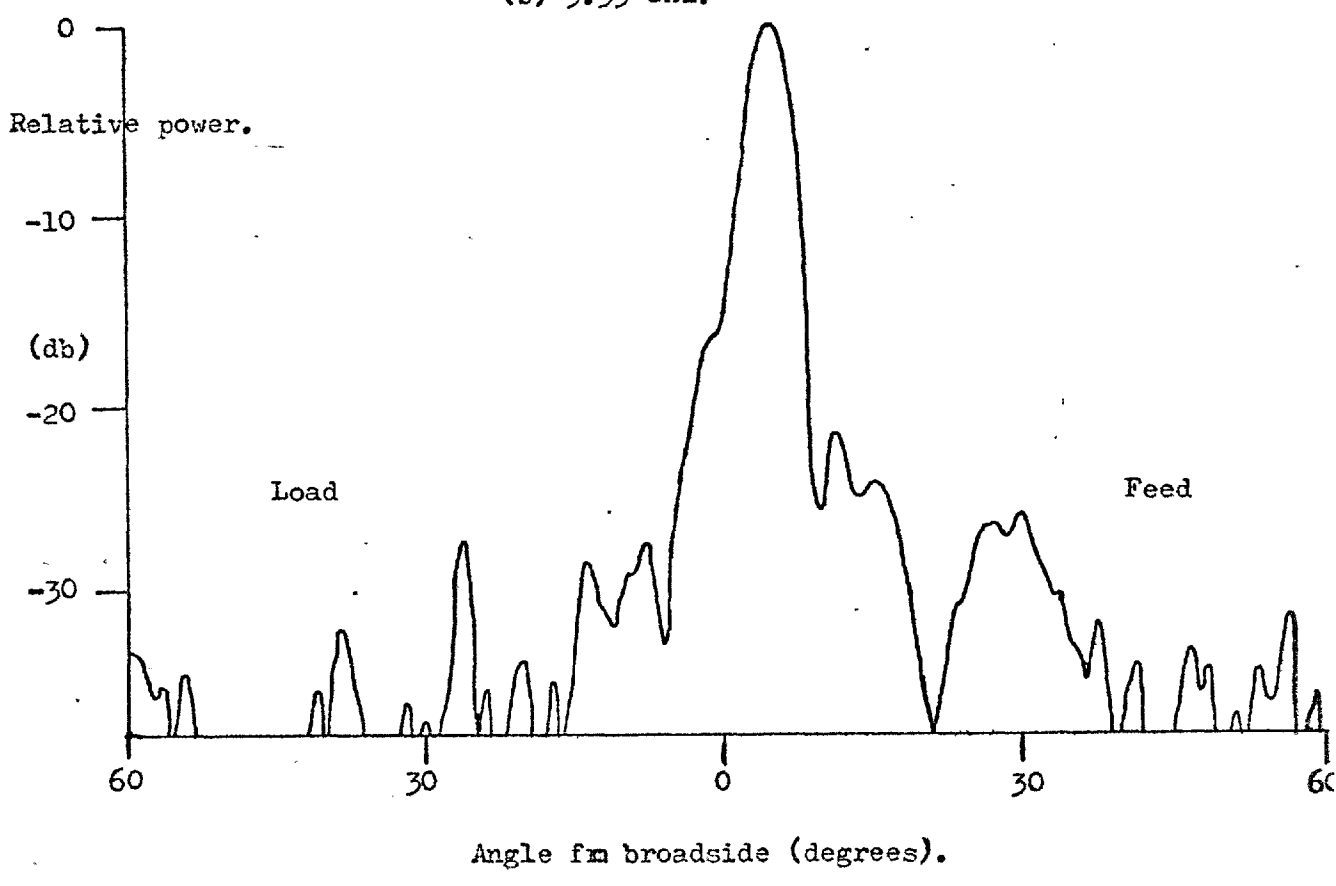

FIGURE 7.6.4. The radiation patterns of the array at broadside and a frequency of (a) 5.60 GHZ.

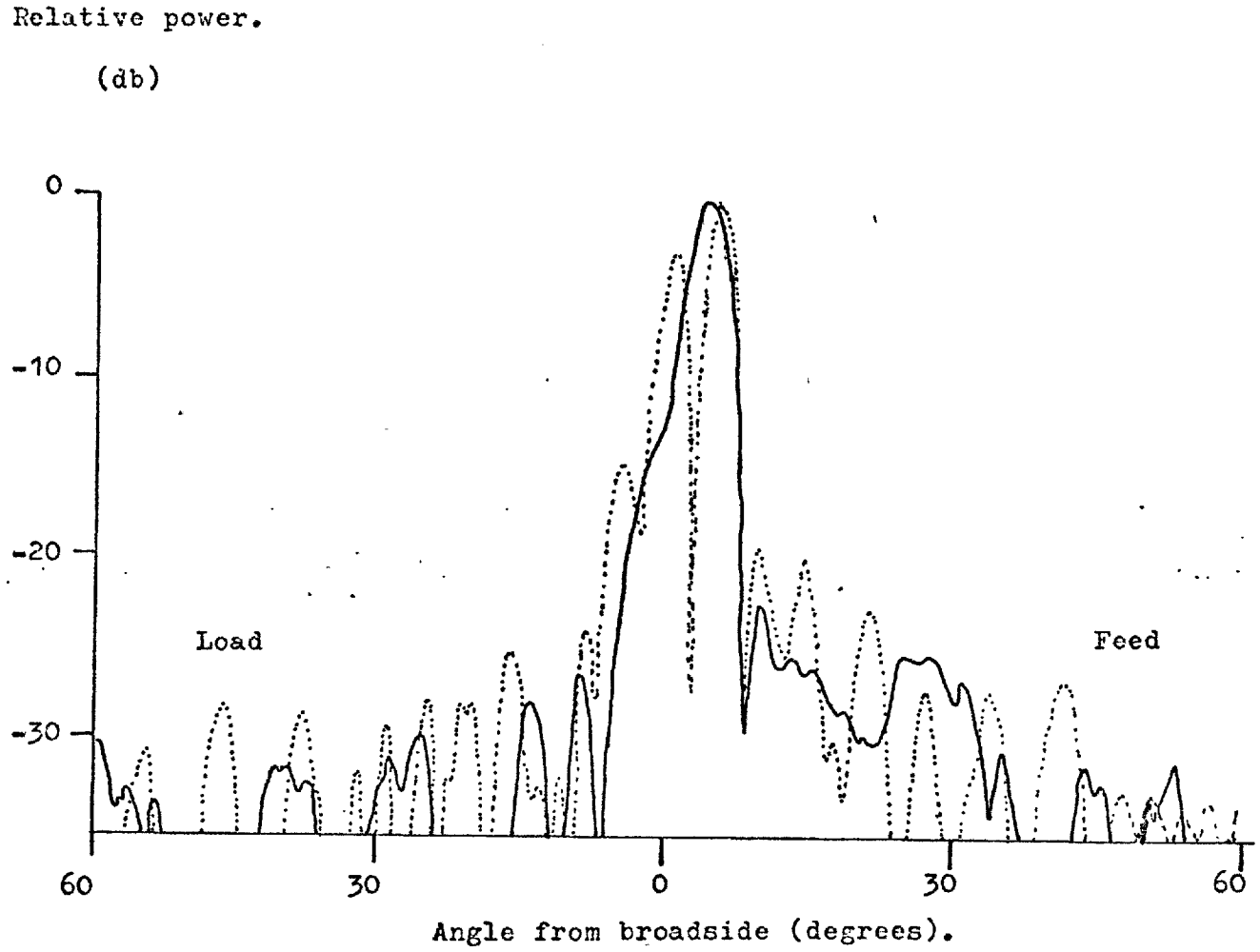

(b) 5.65 GHZ.

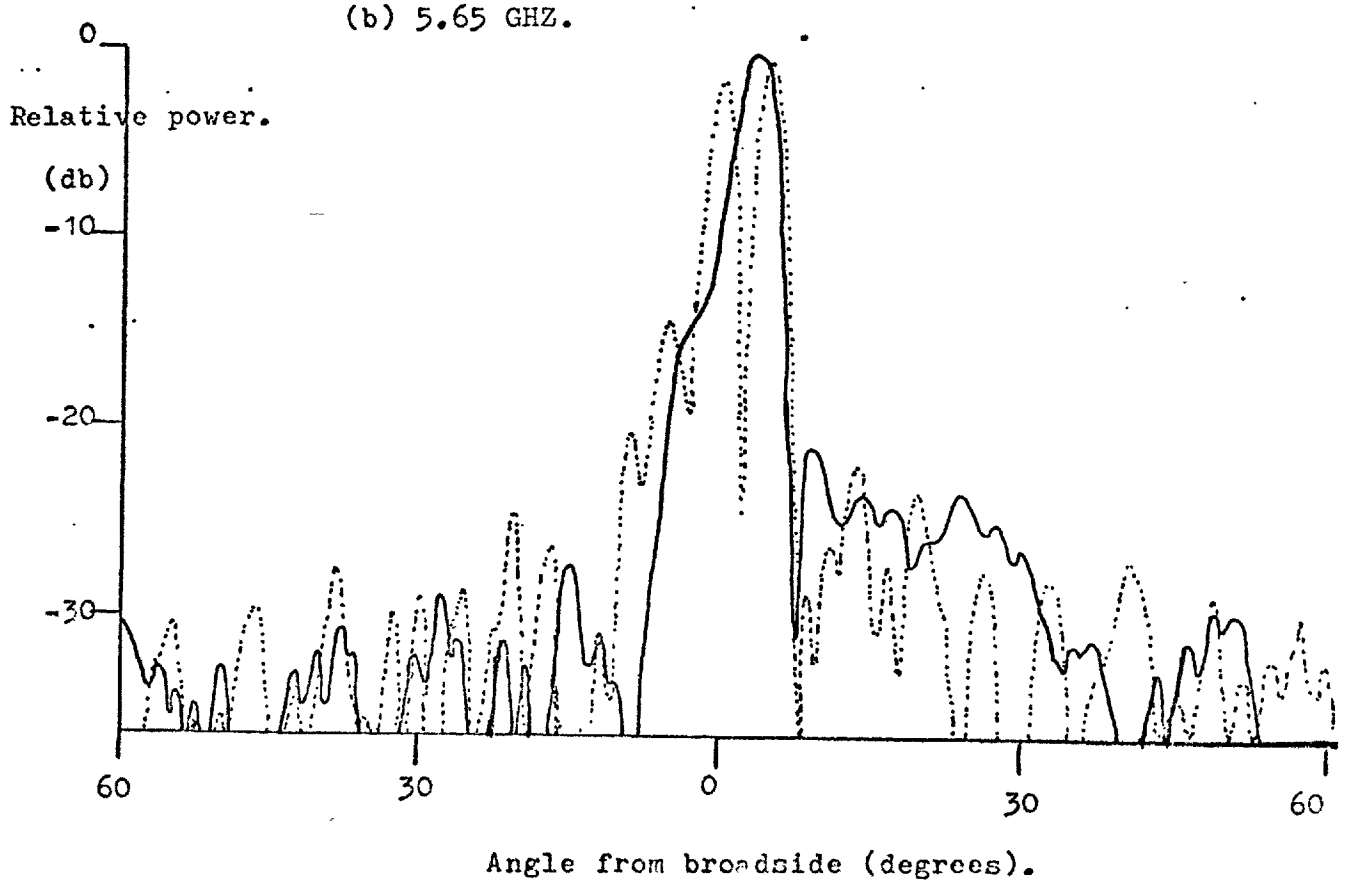

FIGURE 7.6.5. The radiation patterns of the array at broadside and a frequency of (a) 5.70 GHZ.

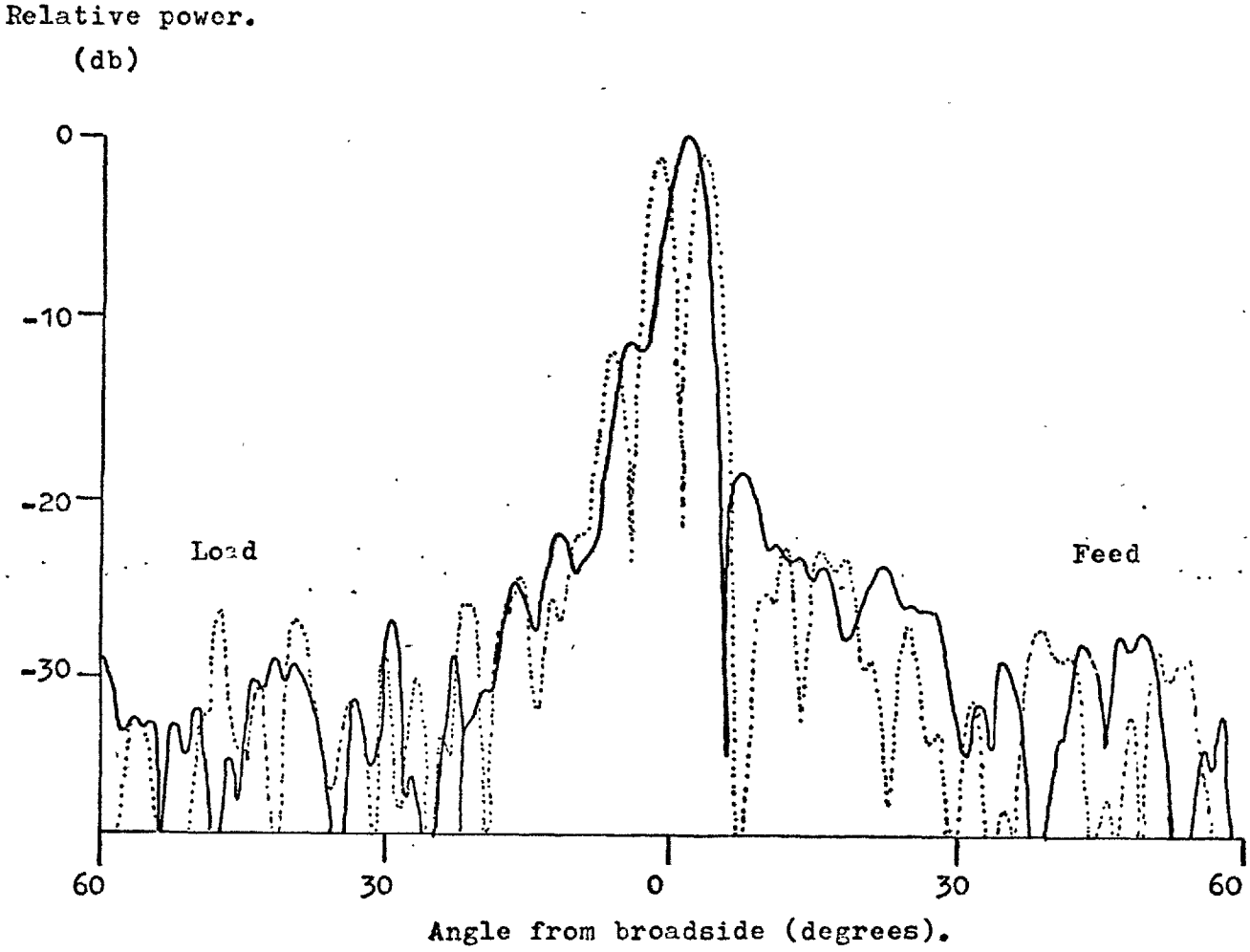

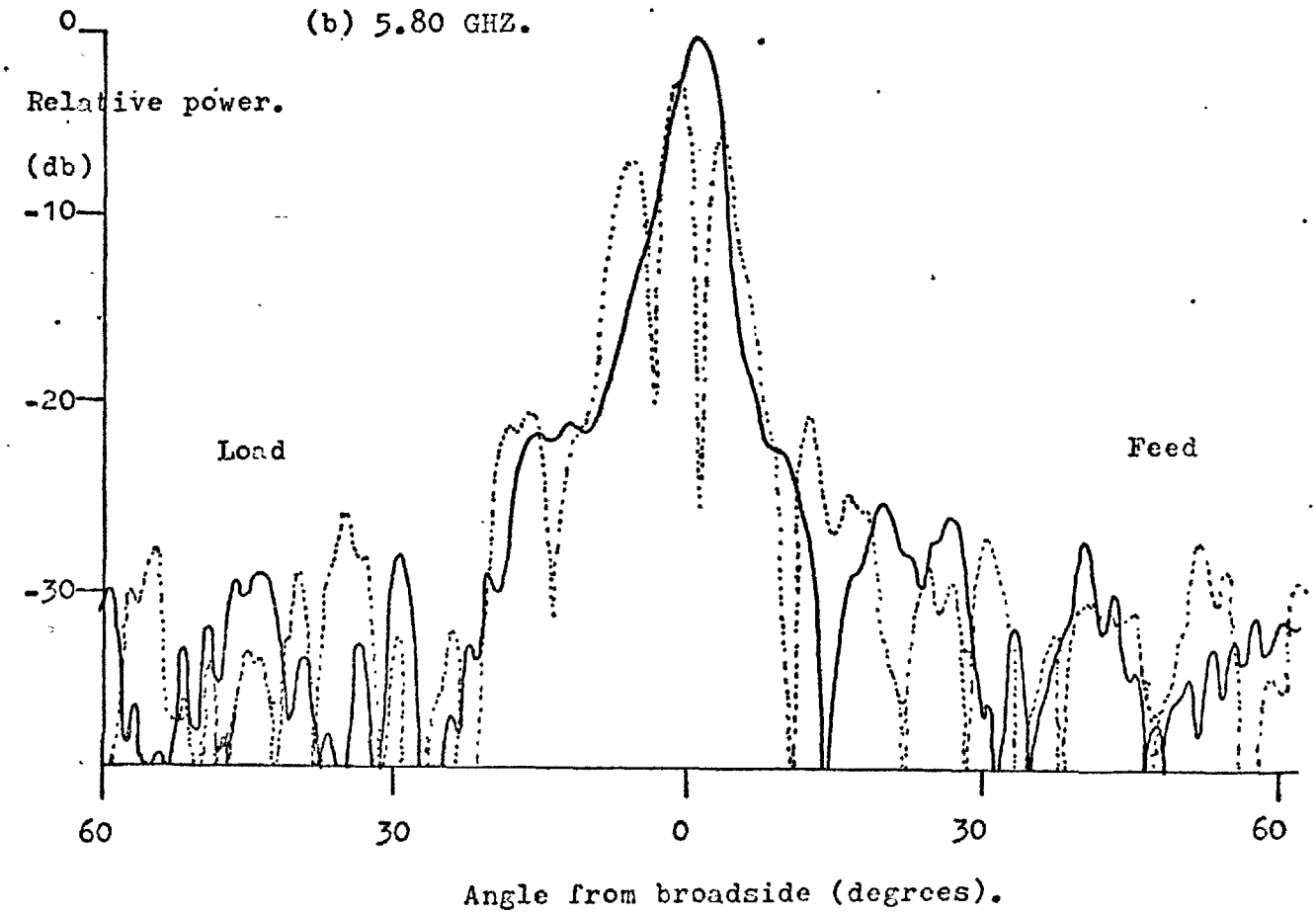

FIGURE 7.6.6. The radiation patterns of the array at broadside and a frequency of (a) 5.85 GHZ.

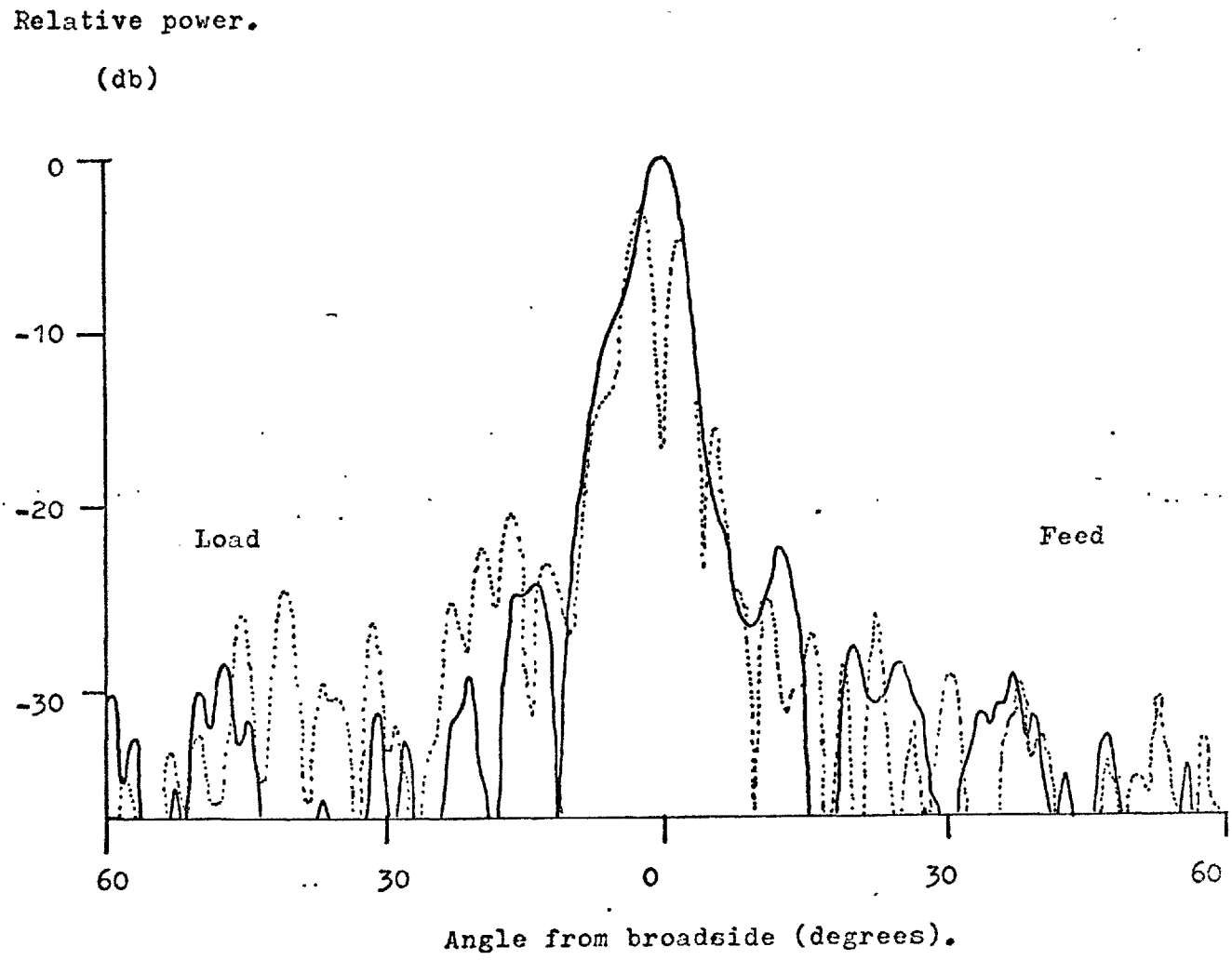

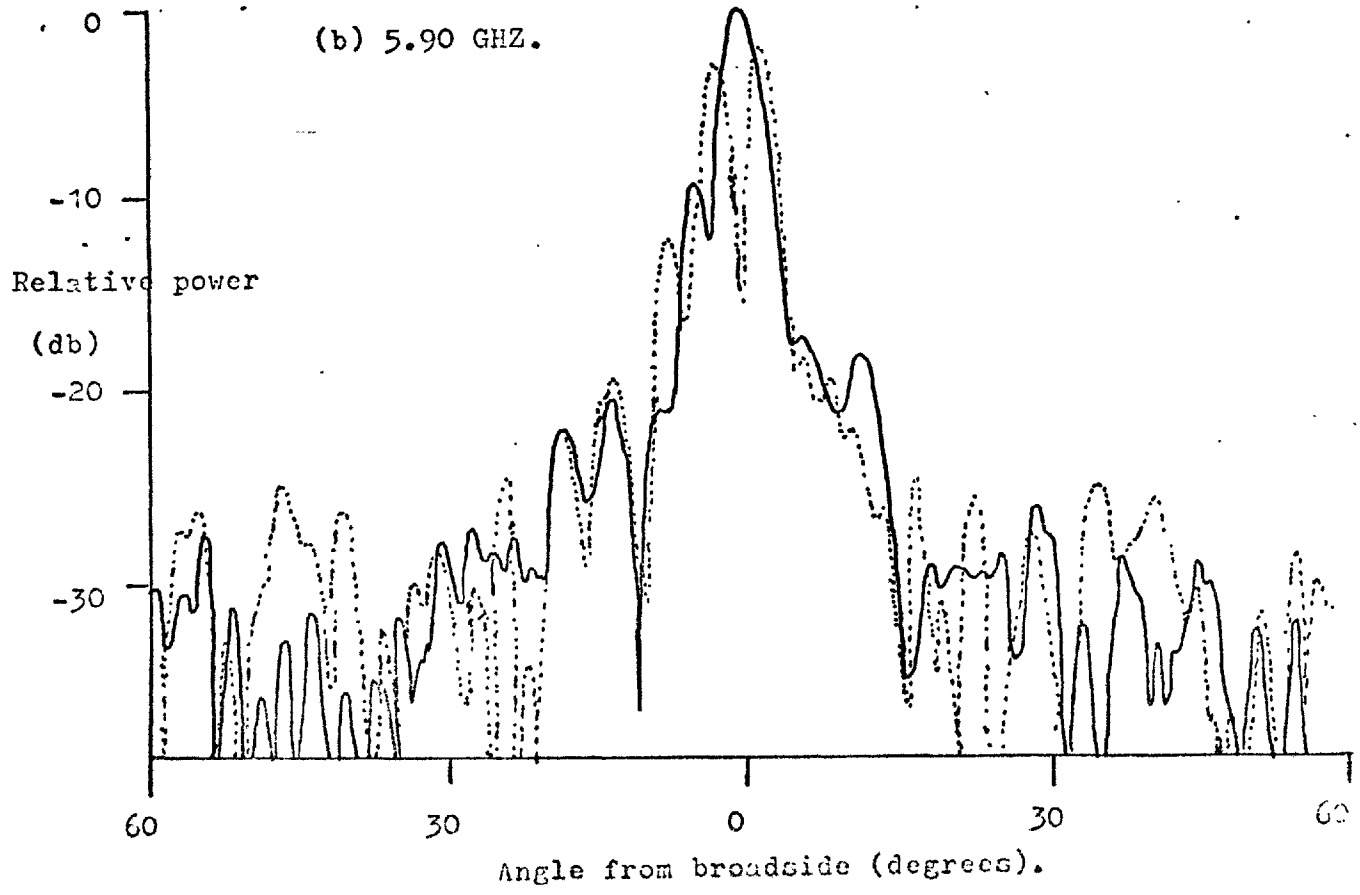

FIGURE 7.6.7. The radiation patterns of the array at broadside and a frequency of (a) 5.95 GHZ.

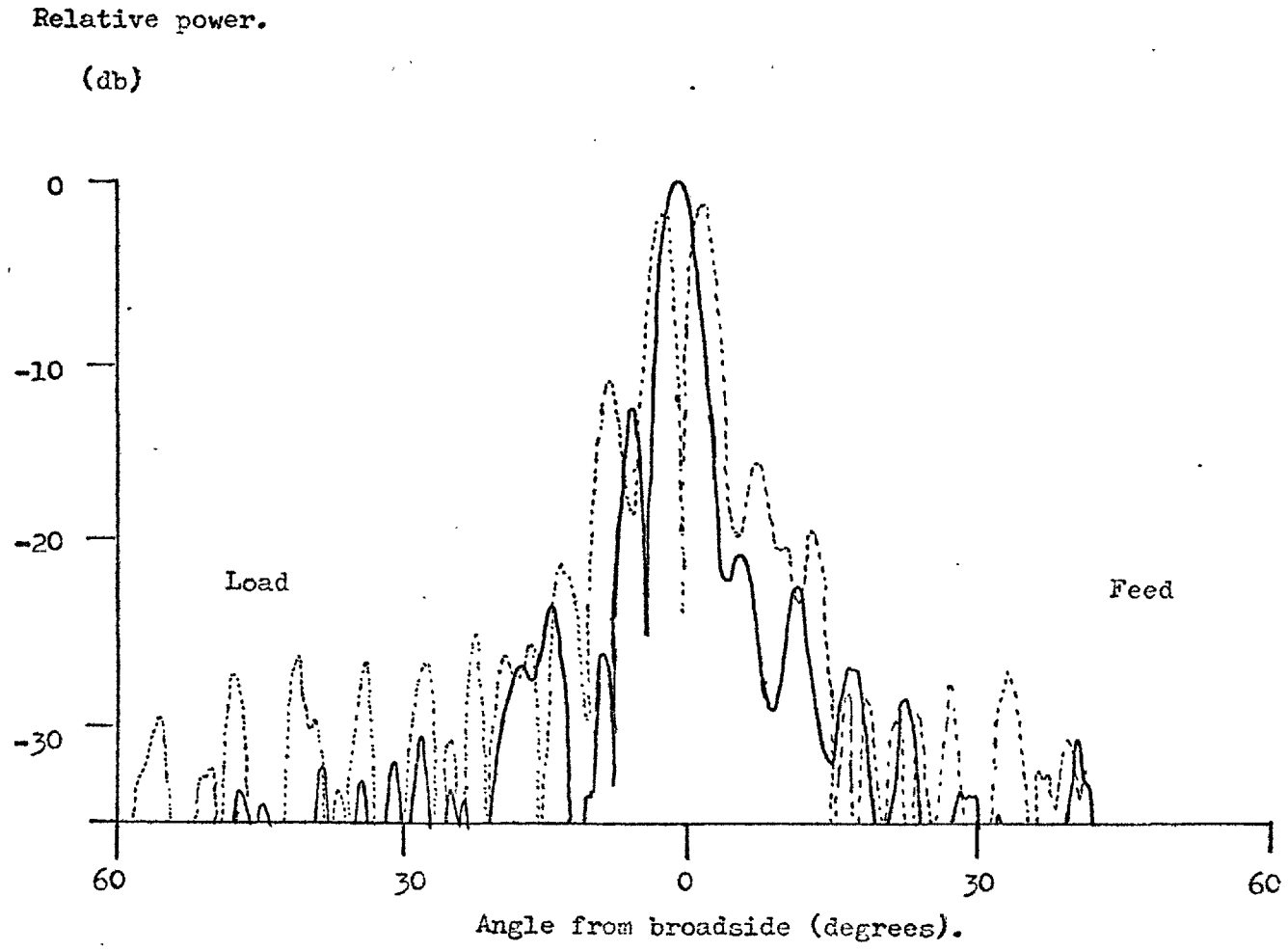

(b) 6.00 GHZ.

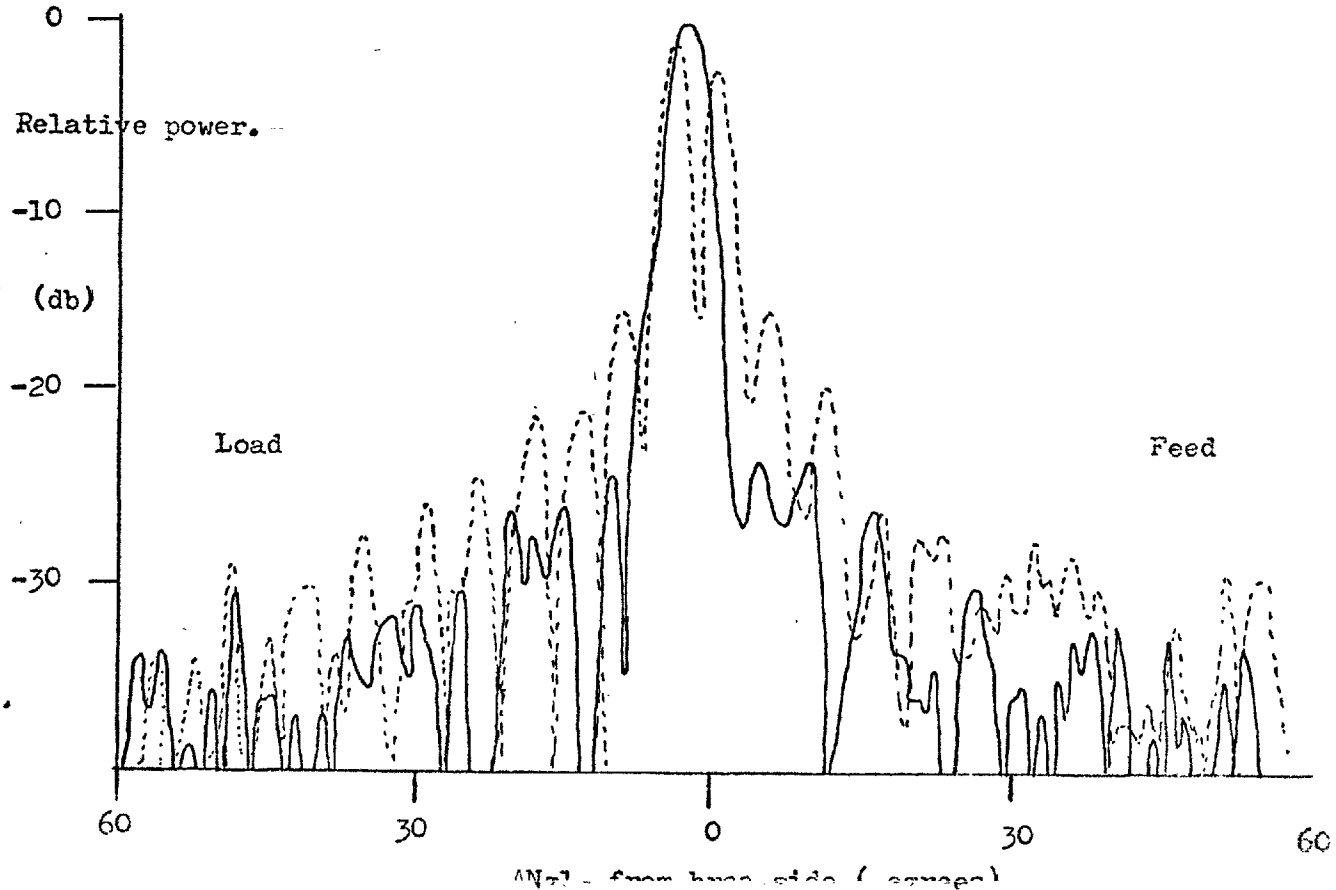

a wave travelling along the waveguide in the opposite direction to that intended. The waveguides were mismatched. Normally this would not have been a problem due to the slot spacing. The incremental susceptance introduced by mutual coupling must increase the effective slot spacing, so that they appear close to half a wavelength apart along the waveguide and cause a mismatch. Away from the frequency of peak mutually coupled power the radiation patterns were generally reasonable with acceptable patterns obtained at the top and bottom of the frequency range investigated.

The phase scanning performance of the array was then investigated. This was done at several frequencies but the results at 5.75 GHz the nominal design frequency are presented. Initially the elevation patterns were plotted. These are shown in Figure 7.6.8.. The beam phase scanned as expected remaining at the same peak level out to 20° from broadside. The $25\frac{1}{2}^{\circ}$ pattern showed a decrease in gain and this coincided with the predicted appearance of the grating lobe. The grating lobe could not be measured due to the limited range of the mounting used but the decrease in gain was taken as a sign of its existence. The elevation scan performance was then as expected and attenuation focussed on the azimuth patterns with the beam phase scanned. The results at 5.75 GHz are shown in Figures 7.6.9. to 7.6.12.. At this frequency the azimuth sidelobe level of the antenna appeared to improve as the beam was scanned. At broadside the first sum channel sidelobe was only 12 dB down but by the time a scan angle of 37° was reached this had improved to approximately 20 dB. The improvement generally applied to all the sidelobes. The antenna's phase scanning performance was as expected and at 5.75 GHz its sidelobe level improved with phase scanning.

The cross polarisation of the array with the beam at broadside

FIGURE 7.6.8. The elevation plane phase scanned radiation patterns at a frequency of 5.75 GHZ.

(a) 0° - 15° scan angles.

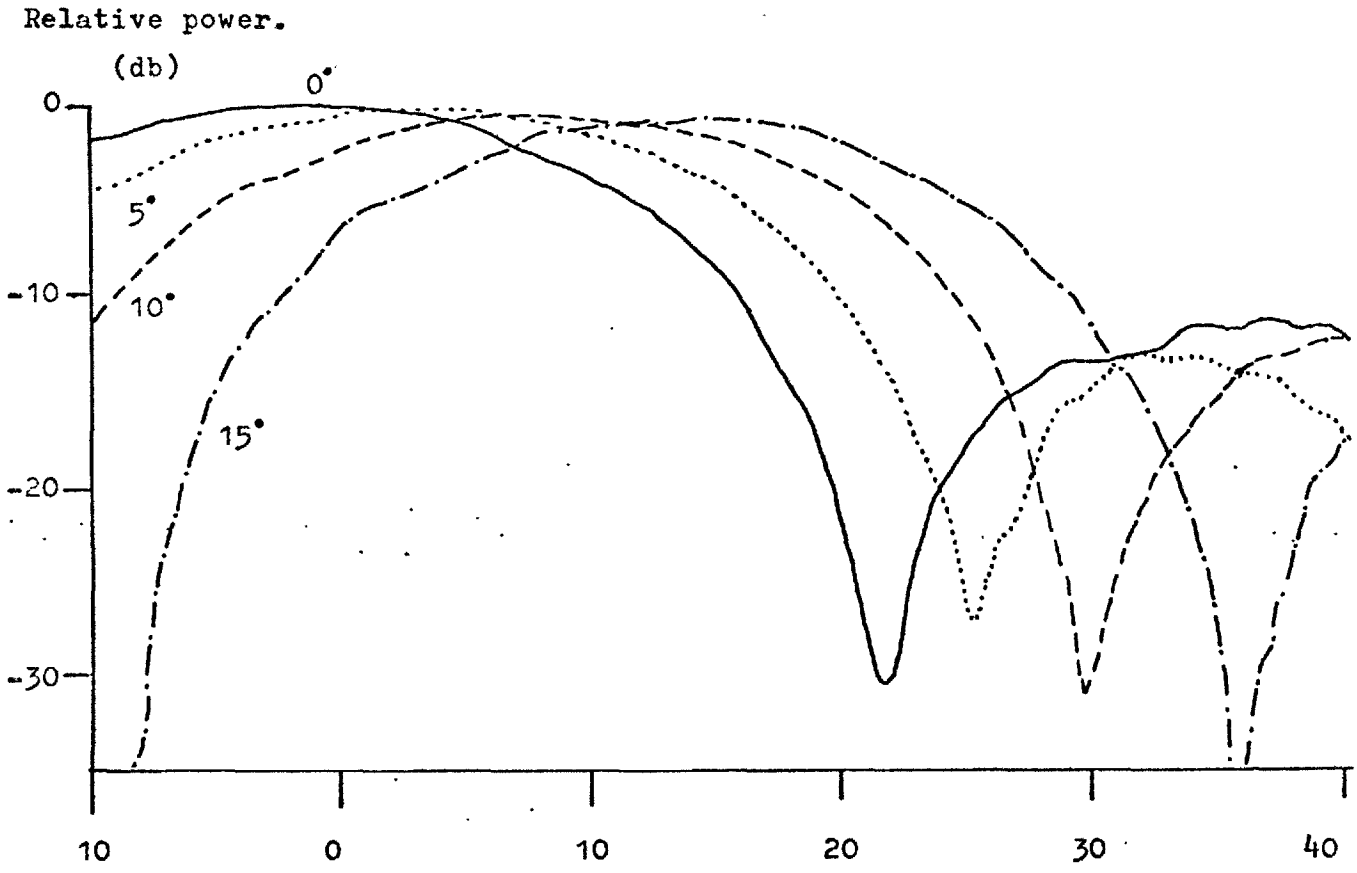

(b) 20° - 37° scan angles.

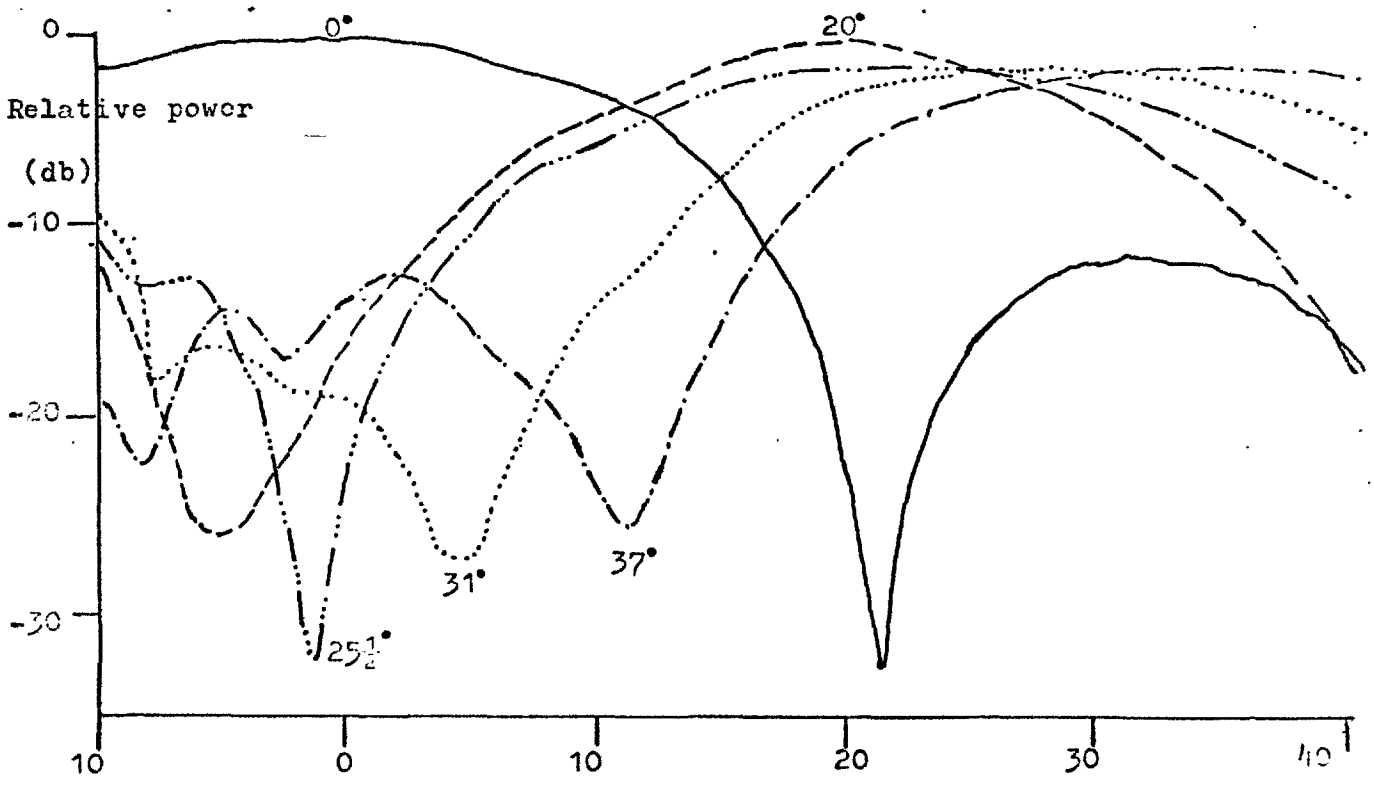

FIGURE 7.6.9. The radiation patterns of the array at a frequency of 5.75 GHZ and a scan angle of (a) 0 degrees

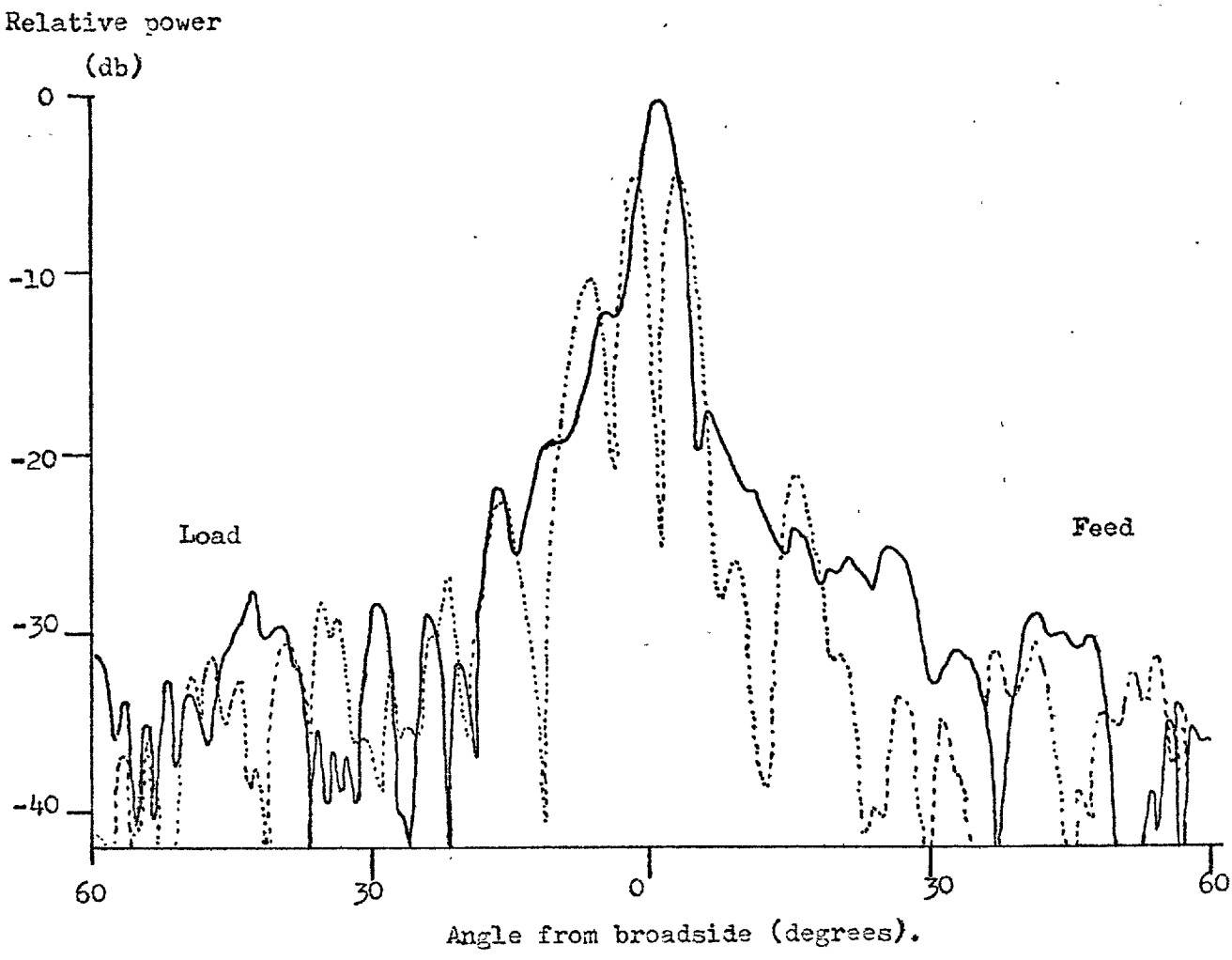

(b) 5 degrees.

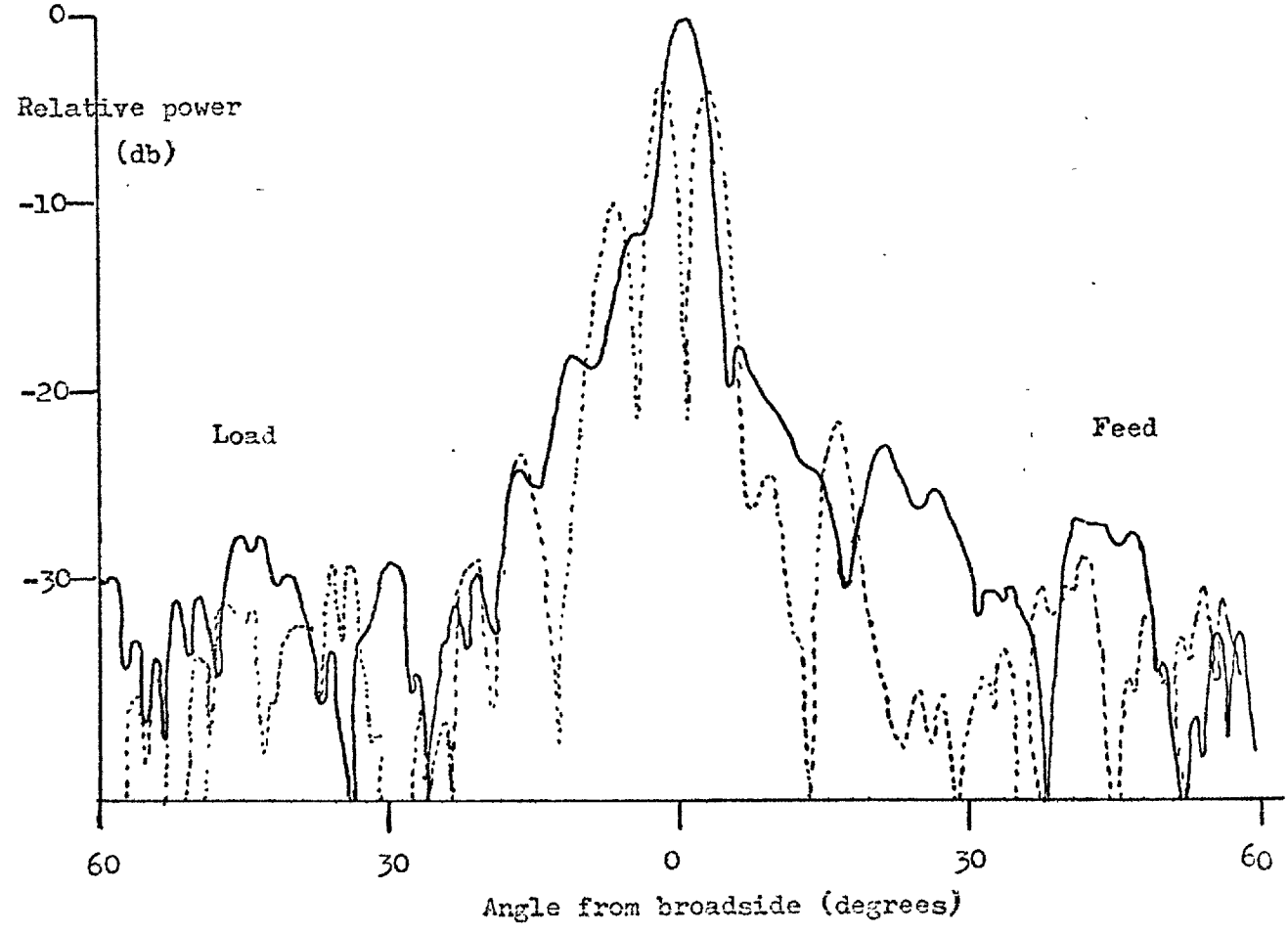

FIGURE 7.6.10. The radiation patterns of the array at a frequency of 5.75 GHZ and at a scan angle of (a) 10 degrees.

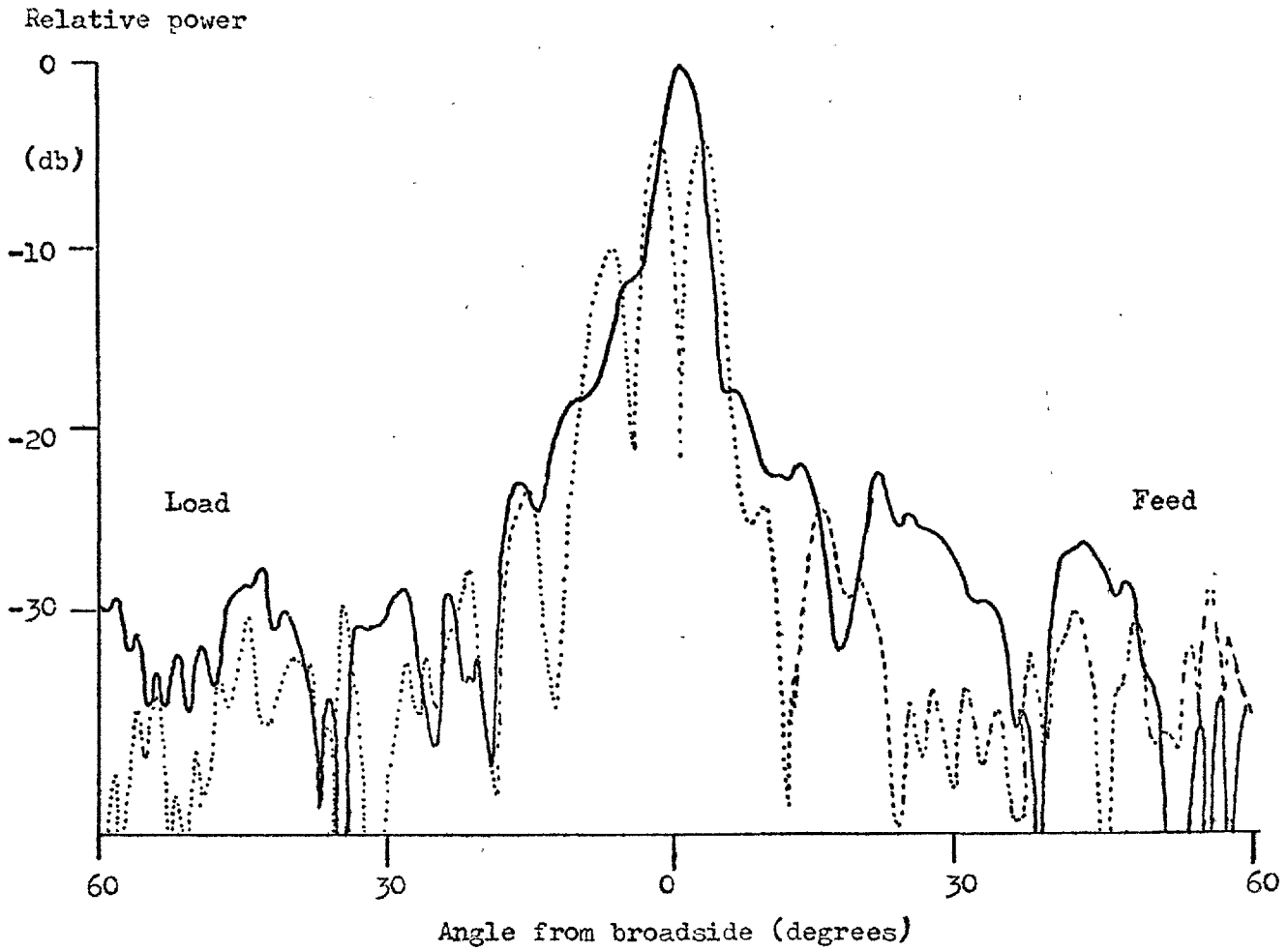

(b) 15 degrees

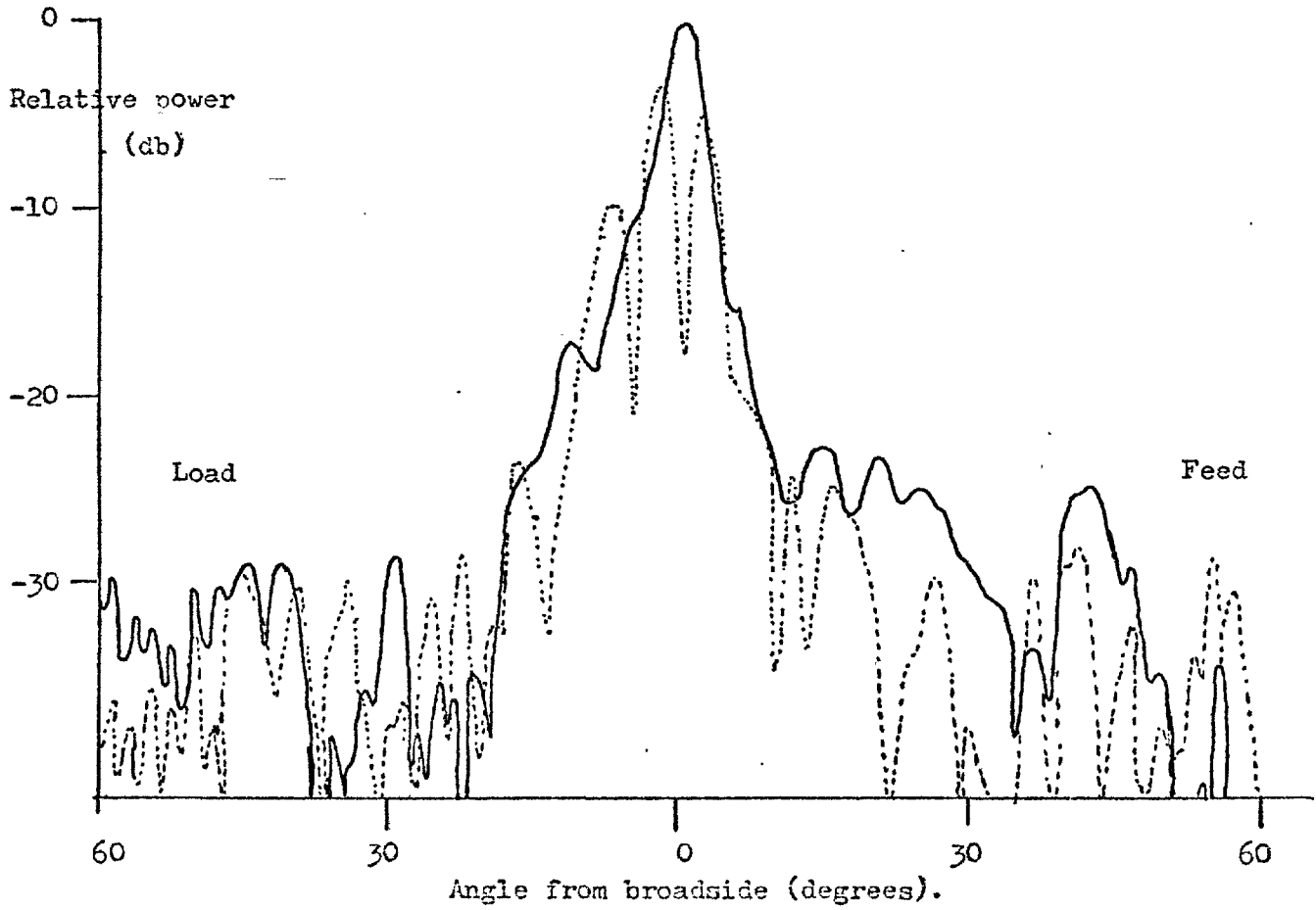

FIGURE 7.6.11. The radiation patterns of the array at a frequency of 5.75 GHz and a scan angle of (a) 20 degrees.

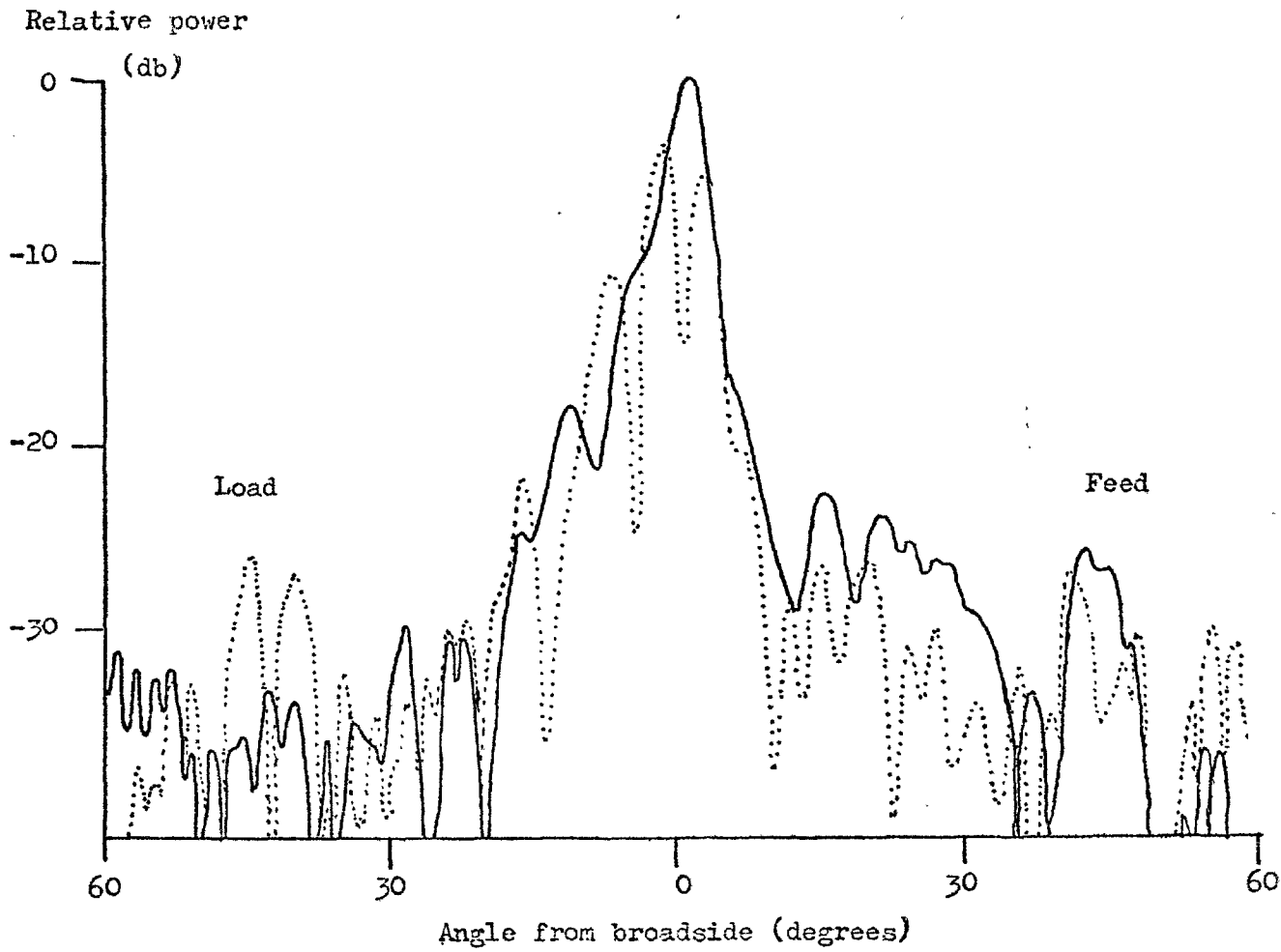

(b) 25.5 degrees

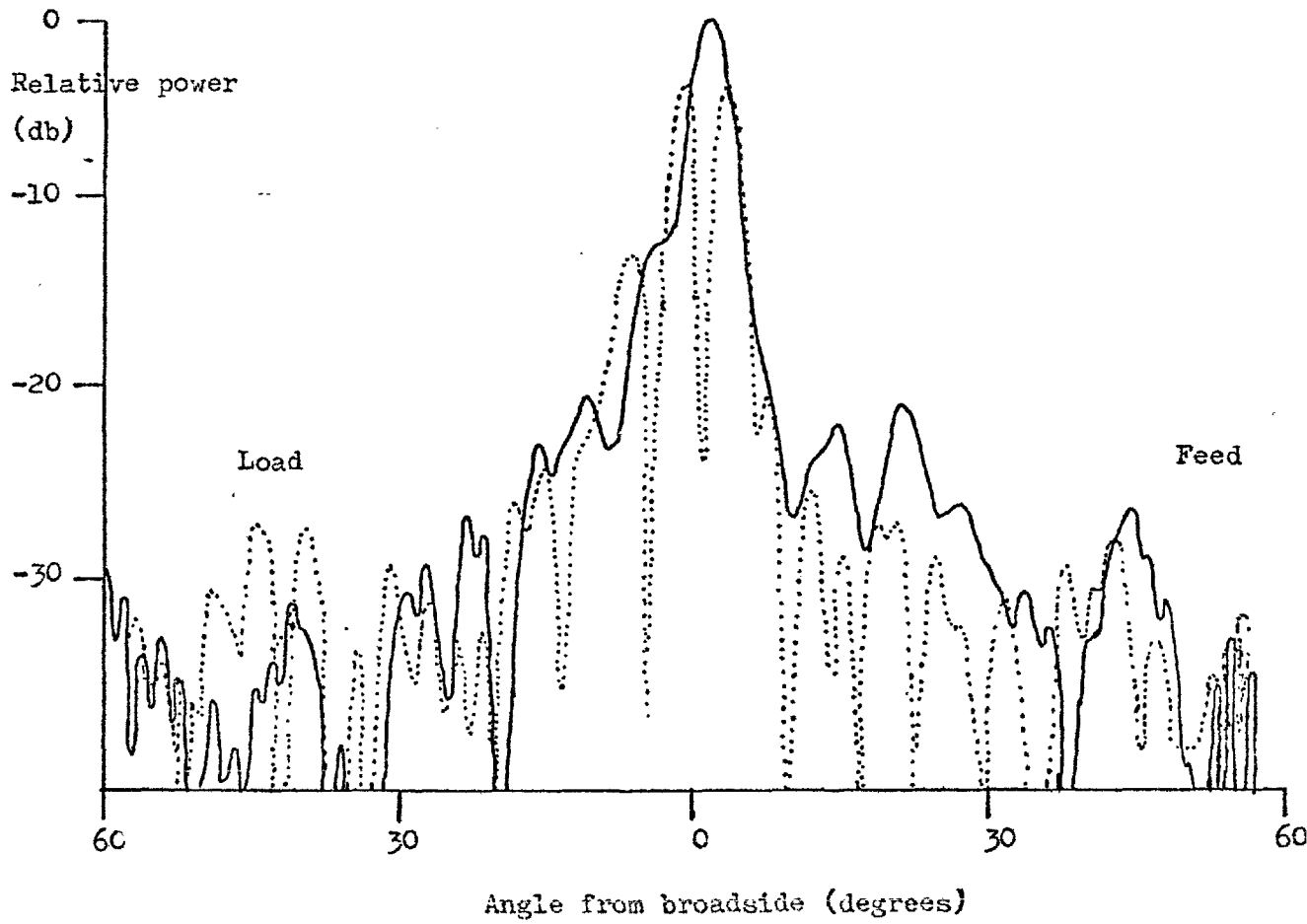

FIGURE 7.6.12. The radiation patterns of the array at a frequency of 5.75 GHZ. and a scan angle of

(a) 31 degrees.

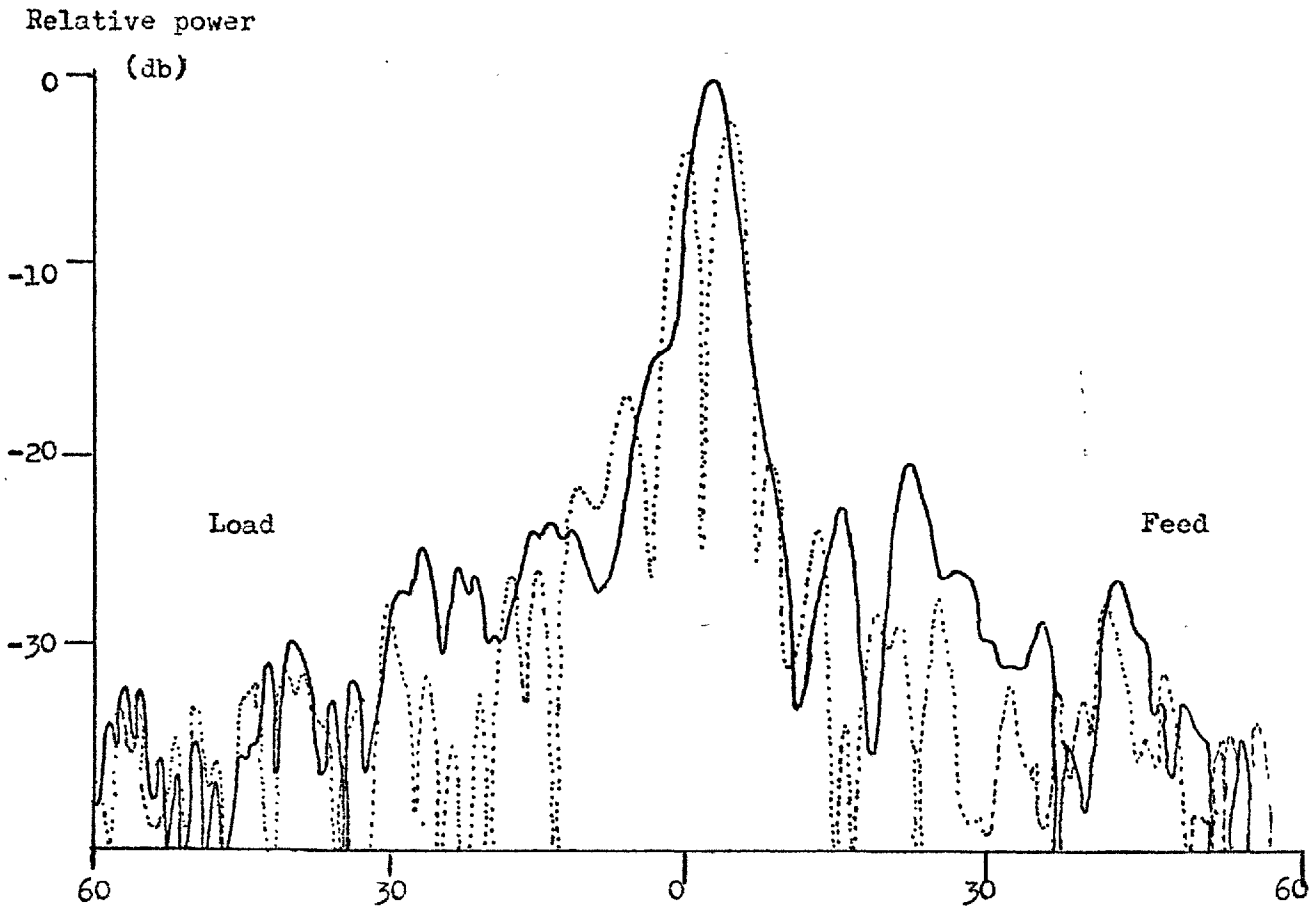

Angle from broadside (degrees).

(b) 37 degrees.

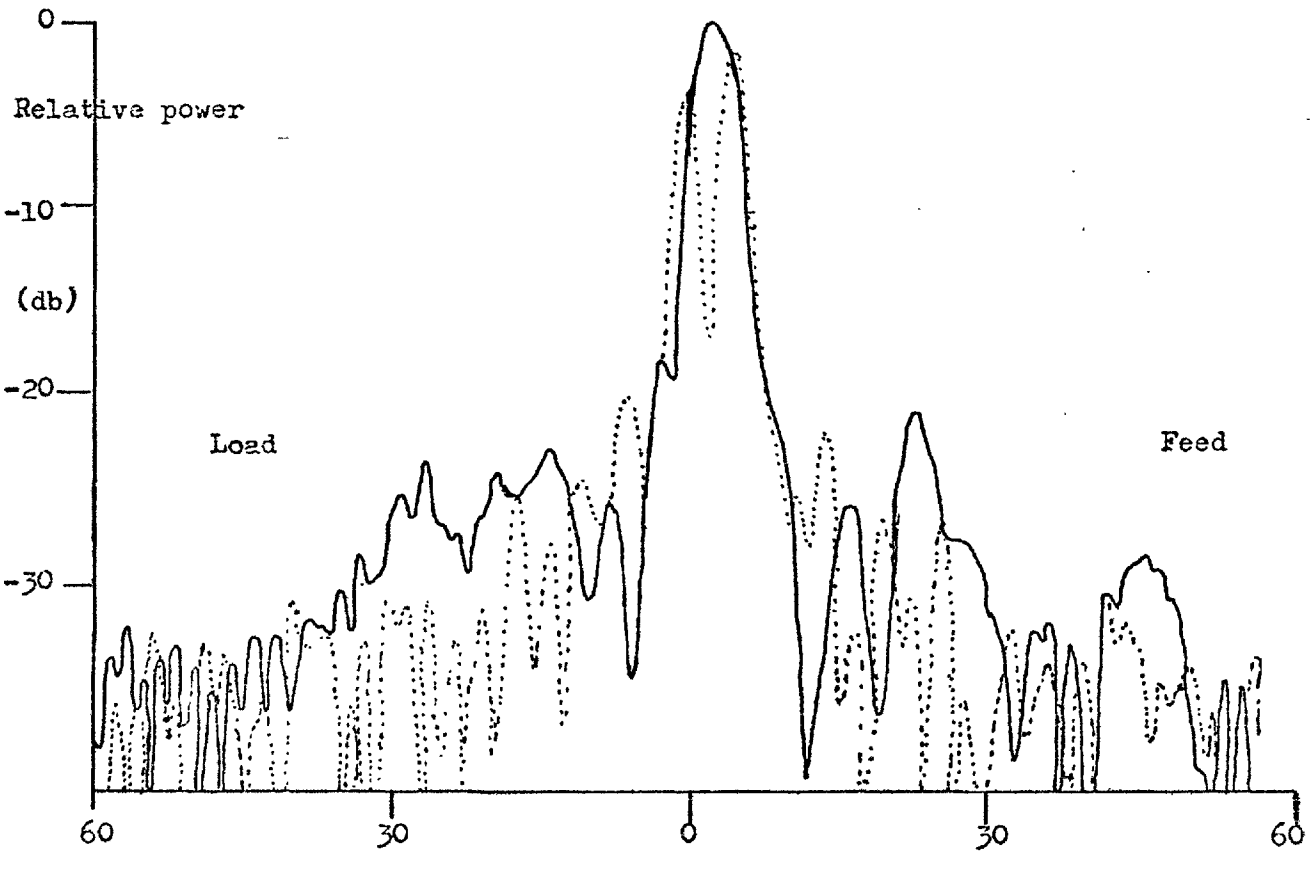

was also investigated. The results obtained are shown in Table 7.6.1.. The cross polarisation performance of the array was approximately 5 dB worse than for a single array. This must have been associated with the change in the environment of each slot by introducing close neighbours in the same column.

The gain of the array at broadside was measured. No standard gain horn was available but only a well made nominally 20 dB horn. Its dimensions were carefully noted and its gain worked out from tables (Jasik (1961)), making allowance for the phase error across its aperture. In fact its calculated gain was accurately 20 dB in the middle of the waveguide 12 frequency band. Measurements were made relative to this horn and the results obtained are shown in Figure 7.6.13.. A figure of gain for the array was also computed. If the overall dimensions of the array enclosing slots were used to work out an effective area, then at 5.80 GHz the uniform phase and amplitude aperture would have a gain of 28.3 dB. For the actual array a non uniform amplitude distribution was used and this would have reduced the gain by 3.8 dB to 24.5 dB. All the power fed into the sum channel port was not radiated but some of it was fed into the terminating loads. This reduced the gain by a further 0.5 dB to 24.0 dB. In fact the peak gain measured was 24.2 dB at a frequency of 5.825 GHz. It was appreciated that some experimental error could be associated with this result but never the less it appeared to be sensible.

Attention was then focussed on the performance of an individual array with all the others taped over with adhesive aluminium tape. For comparison the first results presented will be the gain of a single sum array, as shown in Figure 7.6.13. If 24.0 dB was a reasonable array gain figure then that of a single array should have been approximately 18.0 dB. This was in fact the peak gain measured, indicating that

TABLE 7.6.1. The cross polarisation performance of the eight waveguide array.

Frequency GHZ.	Level relative to main beam. (-db)	Angle between cross polarised beams (degrees)
5.70	16	87
5.75	17½	86
5.80	17	85
5.85	19	84½

FIGURE 7.6.13. The measured array gain.

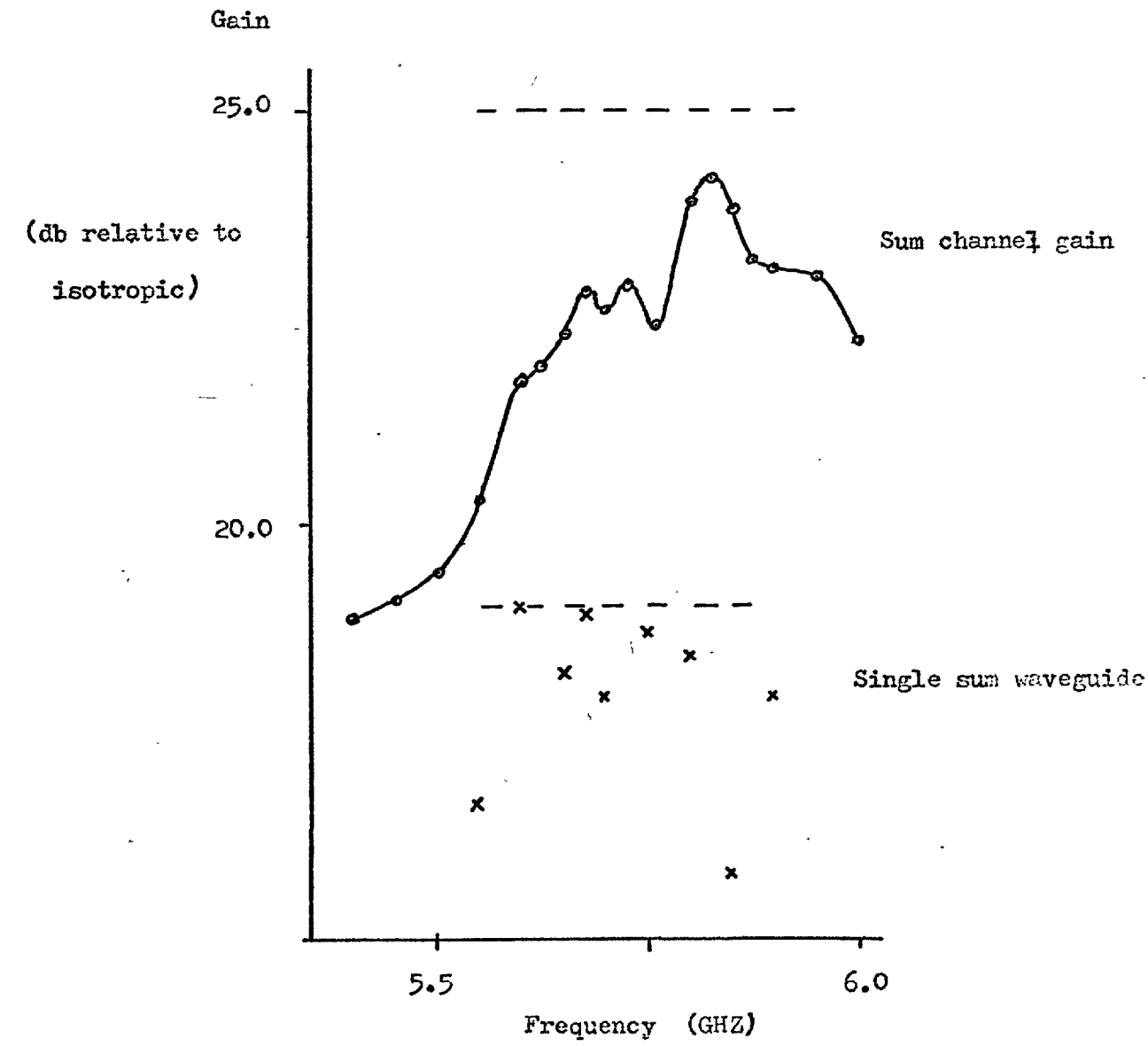

provided the approximate distribution required had been achieved, the array was well behaved. Little loss could be associated with any of the slots and the effect of mutual coupling in reducing the gain was not noticed.

The radiation patterns of the single sum waveguide and of a single difference waveguide are shown in Figures 7.6.14 to 7.6.17. In general good patterns were obtained with sidelobes at least 20 dB below the level of the main beam, showing that the approximate aperture distribution required must have been established.

The aperture distributions of the array were then measured using A.S.W.E.'s phase-amplitude plotter. The measured near field of a single sum array is shown in Figure 7.6.18.. A linear phase front was established. The design amplitude distribution is also shown. In general at 5.70 GHz the distribution is well approximated by the antenna although all the slots were slightly over-coupled. This was deliberately done to allow for the decrease in conductance in tuning to the phase resonant frequency within an array environment. The near field behaviour of the single waveguide was in general better than that measured previously for the thirty slot array. Its phase was more linear and the amplitude distribution was better established but its far-field sidelobe level was worse. This raised questions about the standard of the far field site used. This was probed and variations found in the incoming "plane" wave. In general the variations were small but their presence means that care has to be exercised in interpreting low level sidelobe results. Subsequently the near field measurements have been included in an A.S.W.E. programme to predict far field patterns. At 5.70 GHz the first sidelobes of the single sum waveguide pattern (Figure 7.6.14) improved to - 25 dB with all other sidelobes below - 30 dB. The single

FIGURE 7.6.14. The radiation pattern of a single sum waveguide

(a) 5.70 GHZ.

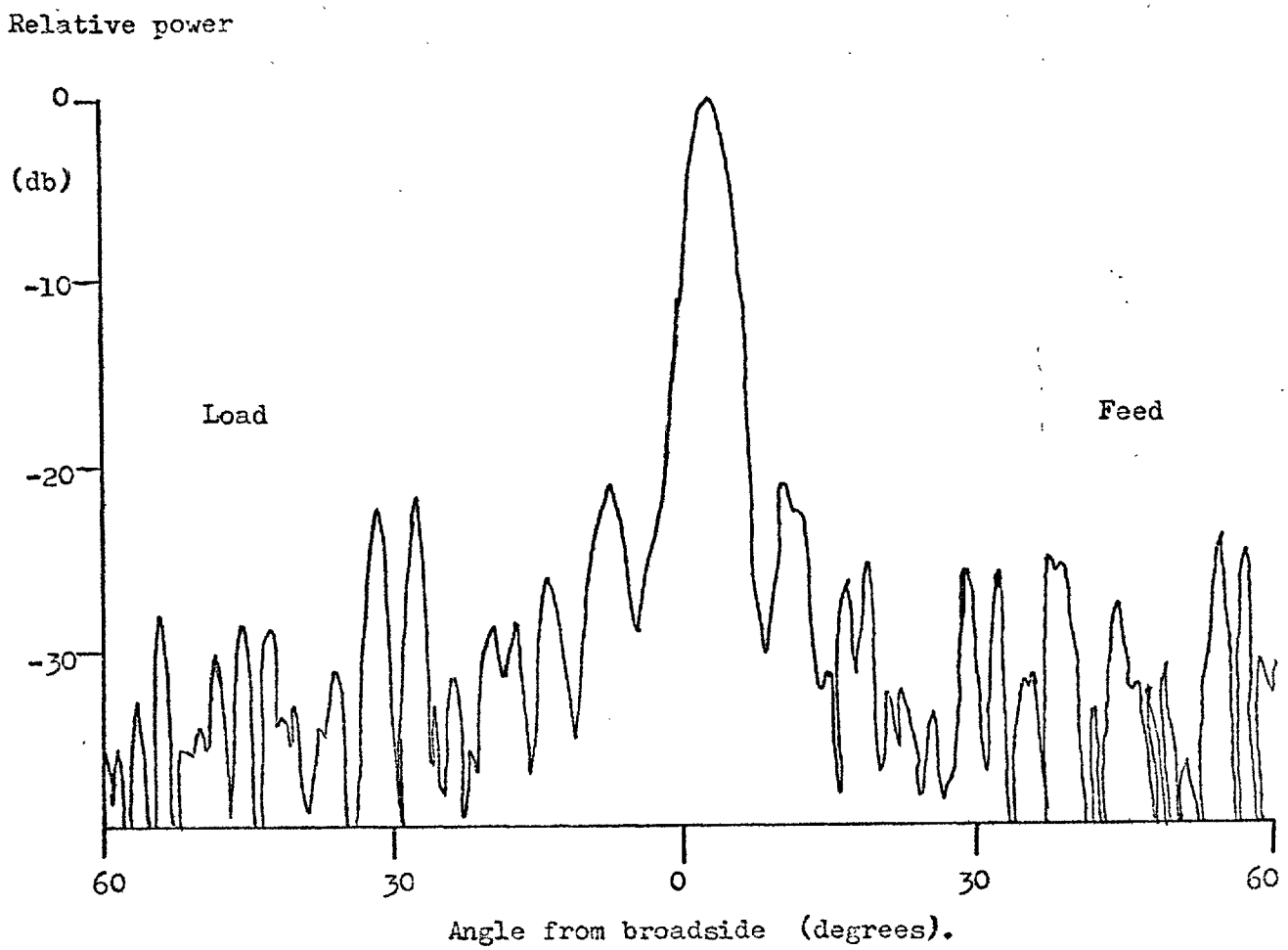

(b) 5.75 GHZ.

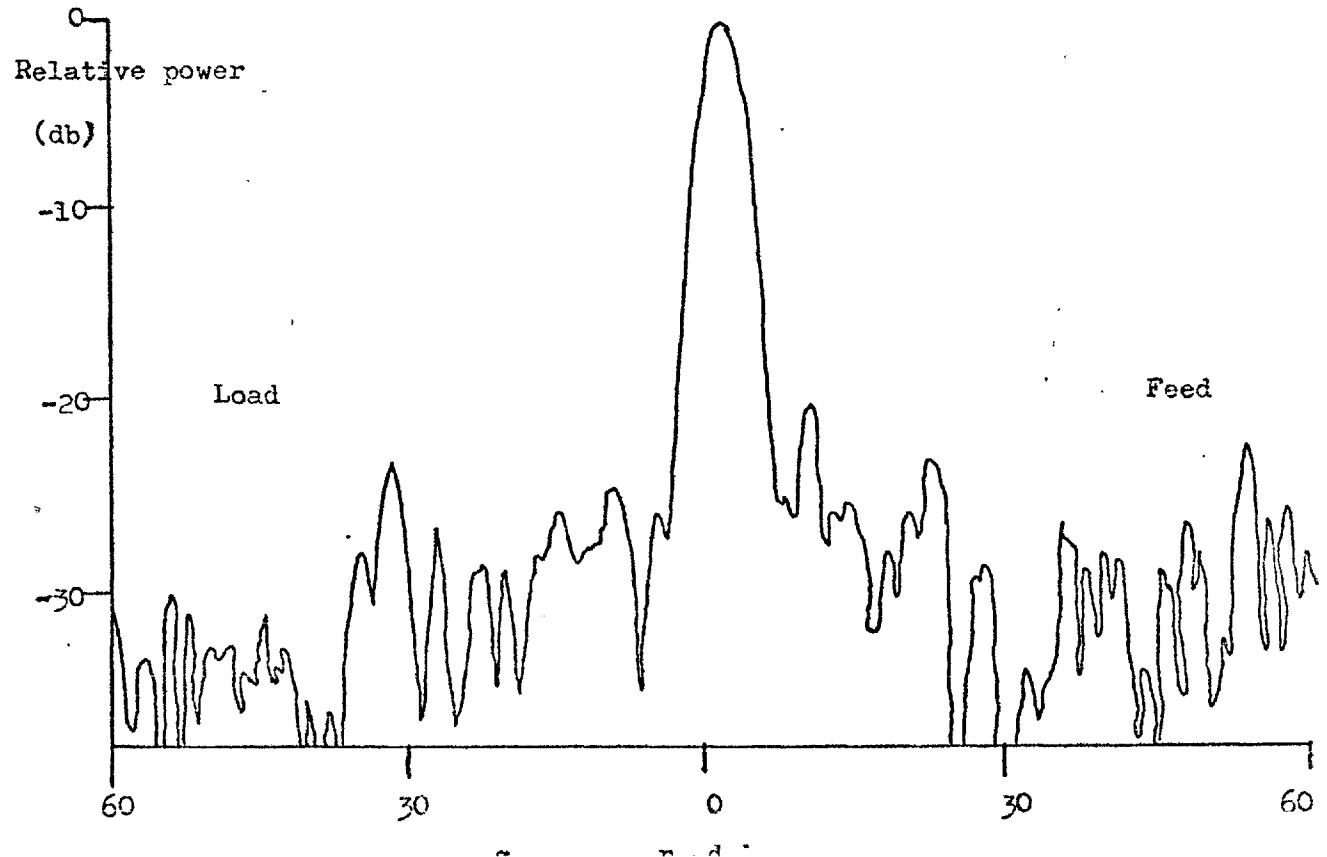

FIGURE 7.6.15. The radiation pattern of a single sum waveguide.

(a) 5.80 GHZ.

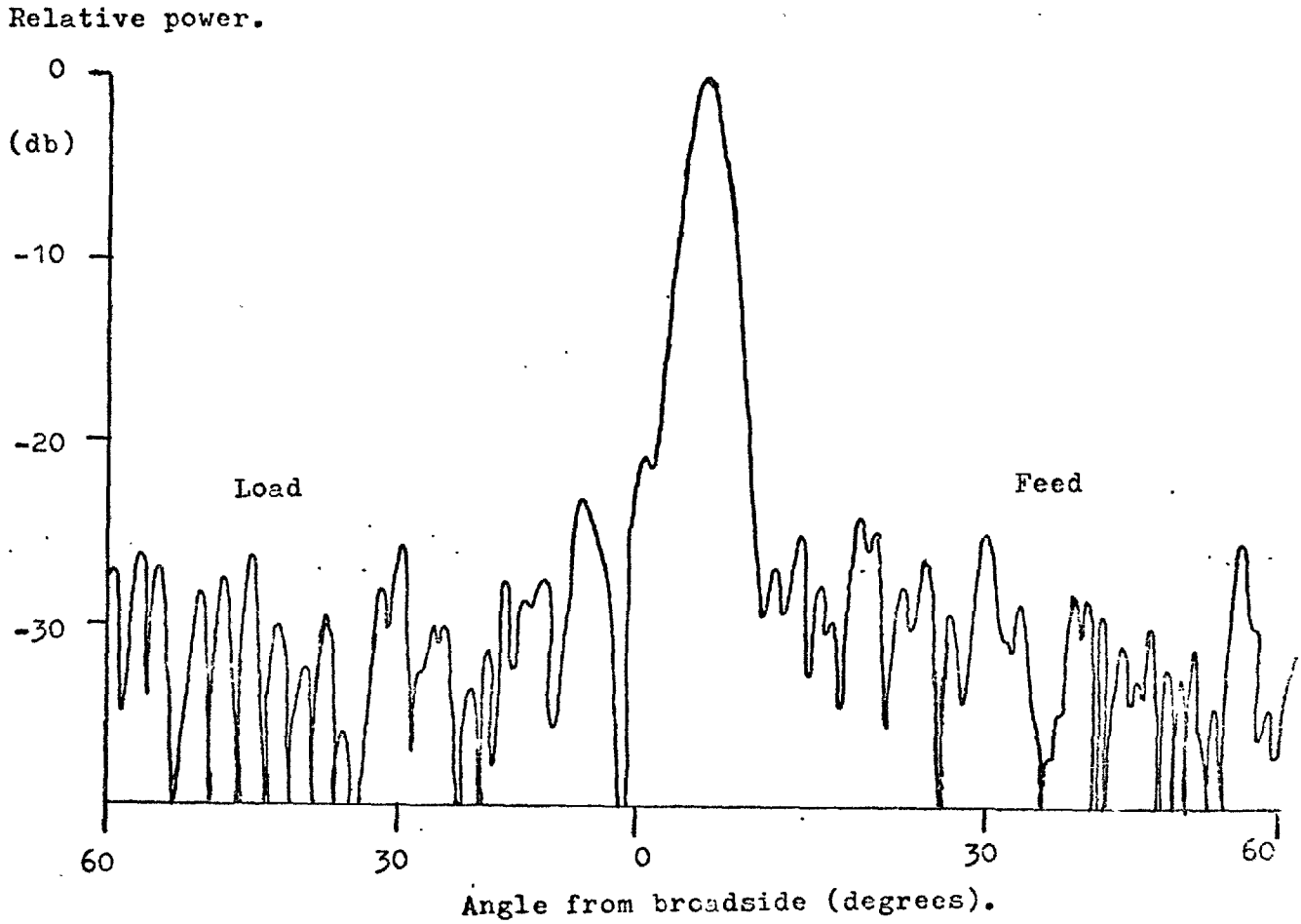

(b) 5.90 GHZ.

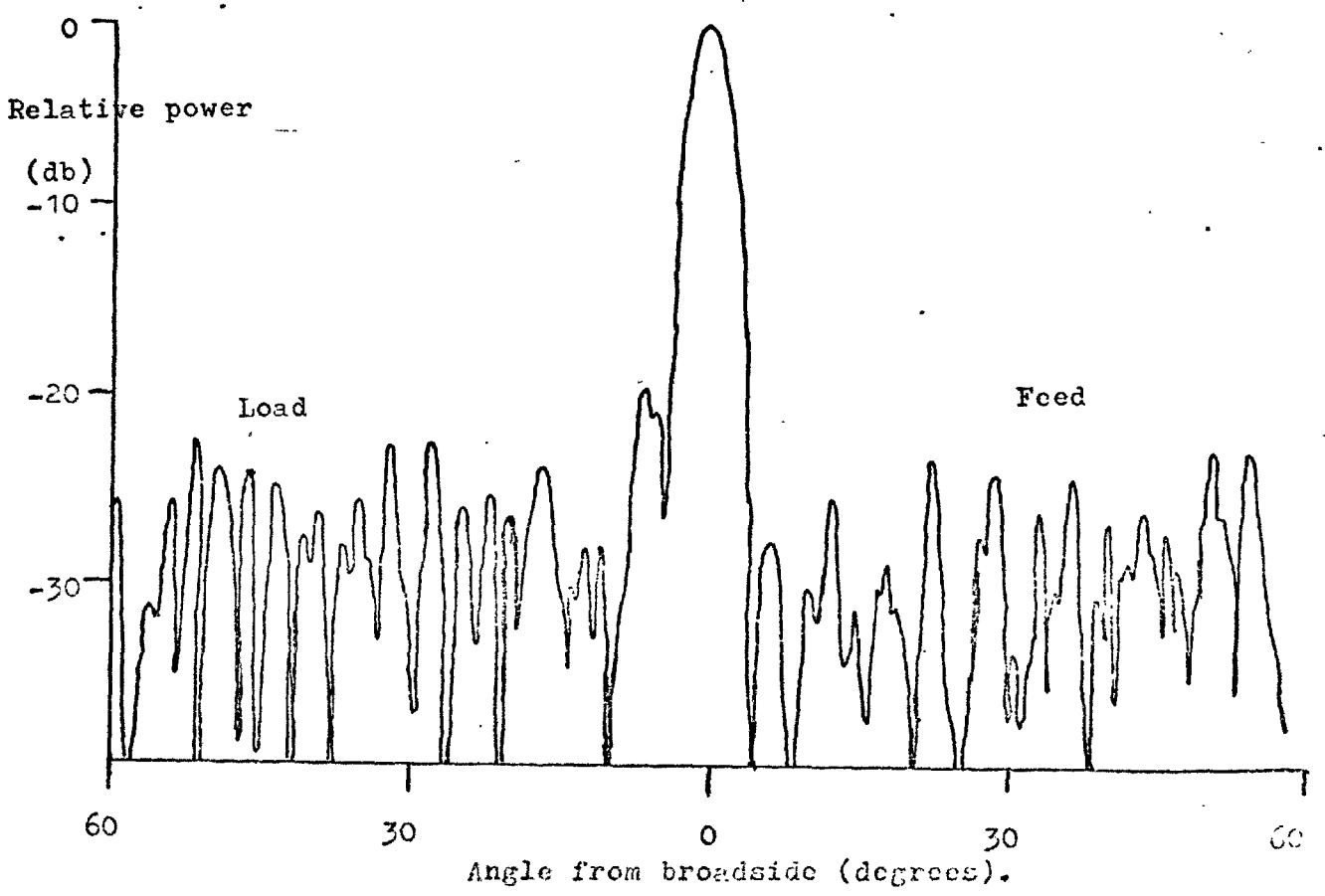

FIGURE 7.6.16. The radiation pattern of a single difference waveguide.

(a) 5.70 GHZ.

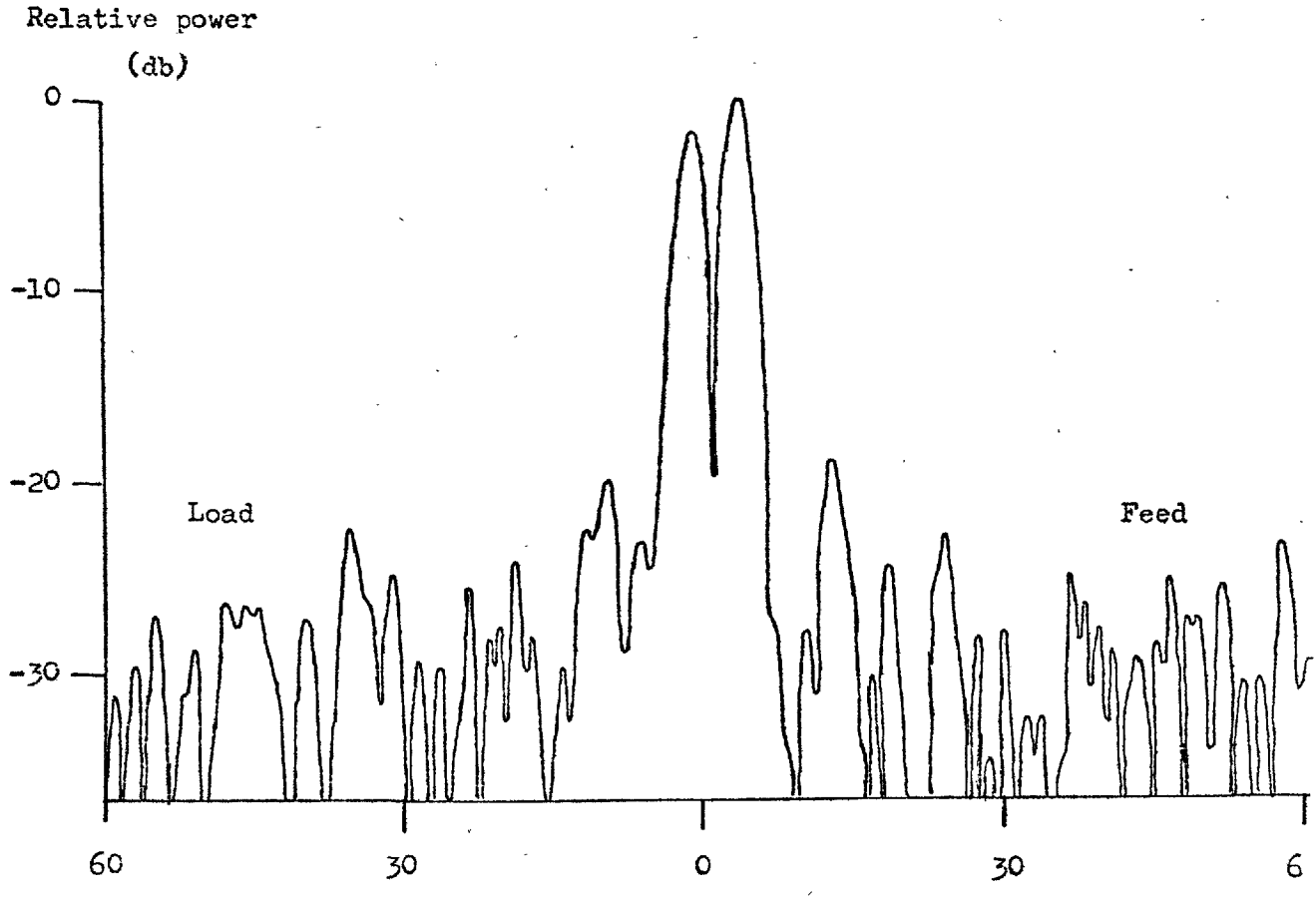

(b) 5.75 GHZ.

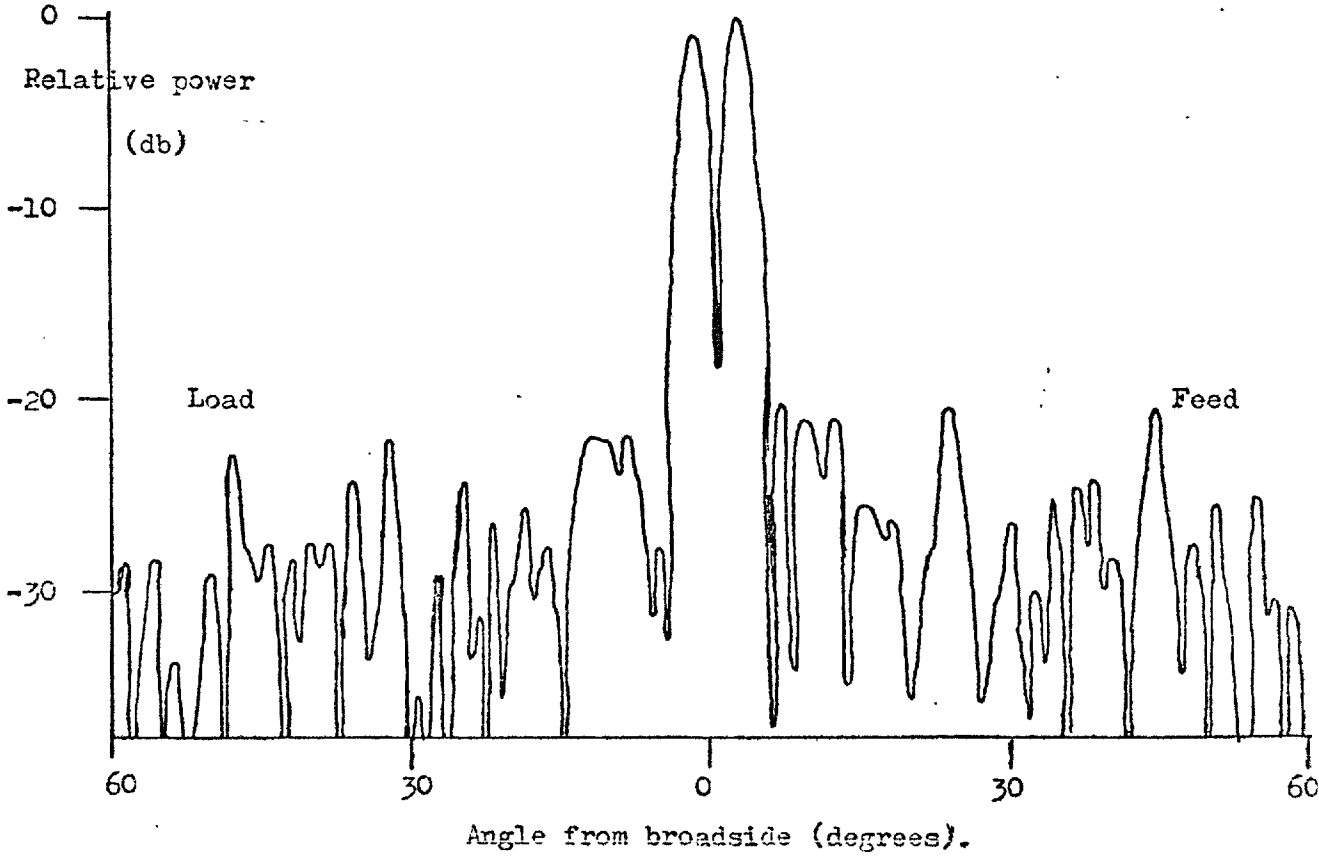

FIGURE 7.6.17. The radiation pattern of a single difference waveguide.

(a) 5.80 GHZ.

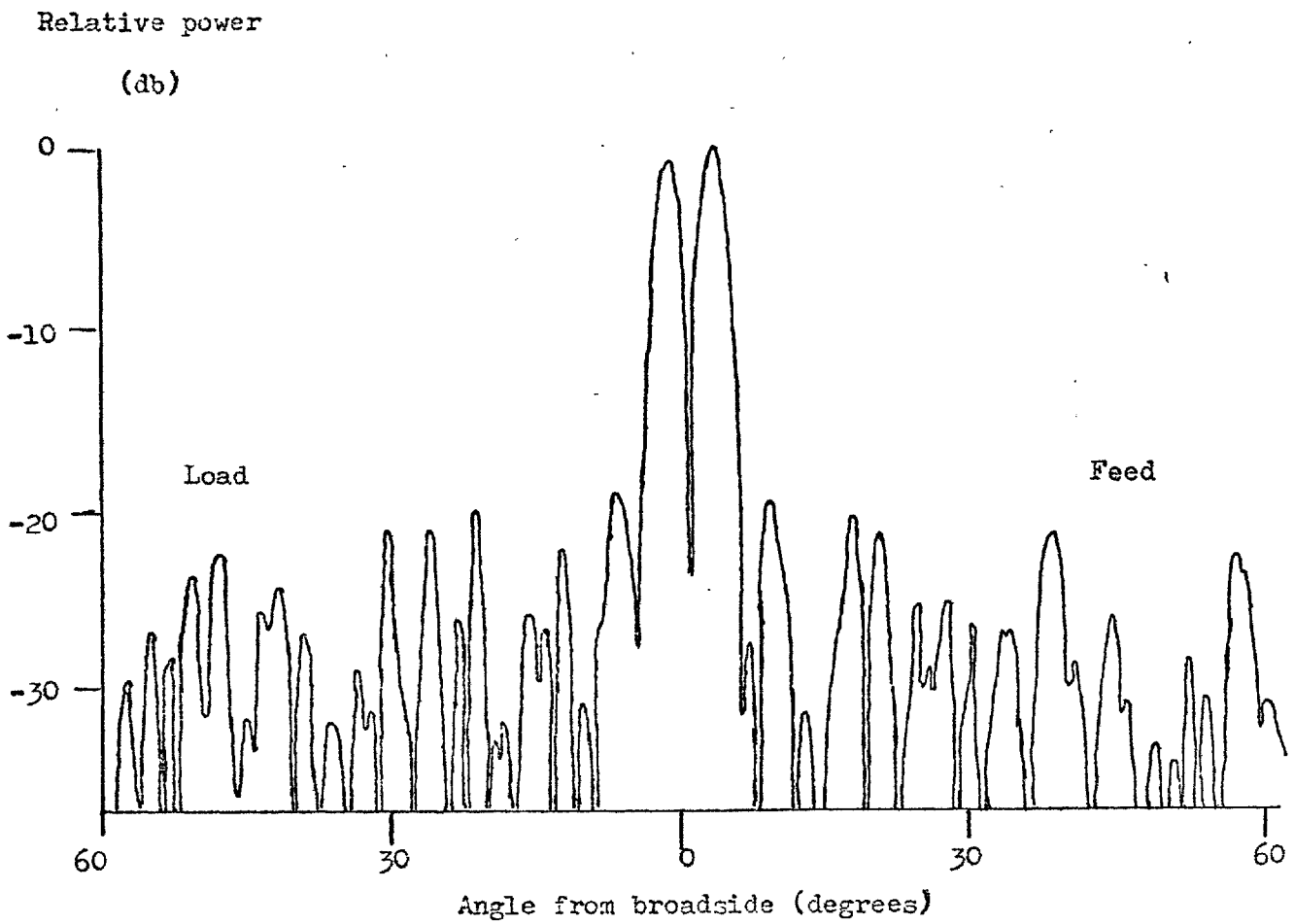

(b) 5.90 GHZ.

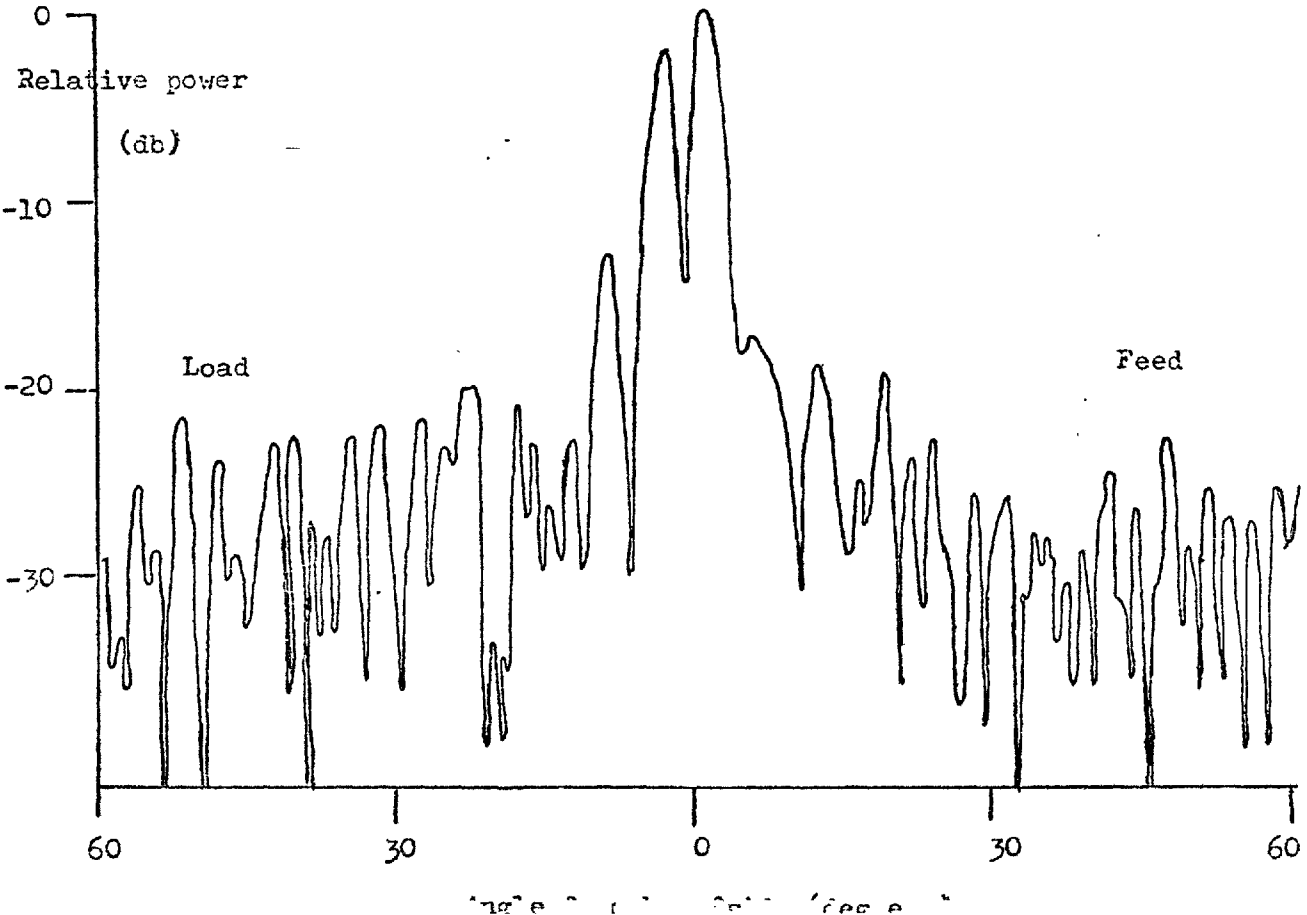

FIGURE 7.6.18. The aperture distribution of a single sum waveguide at 5.70 GHZ..

(a) Amplitude.

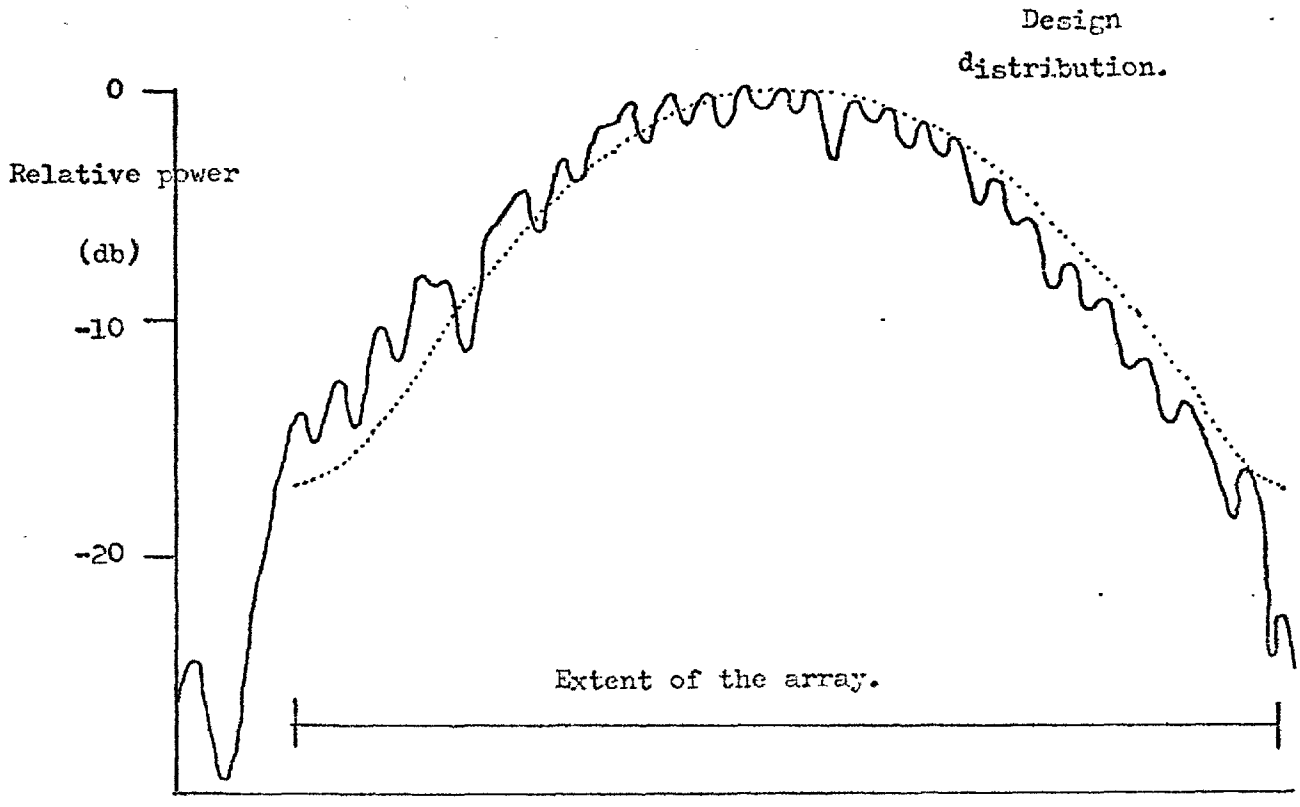

(b) Phase.

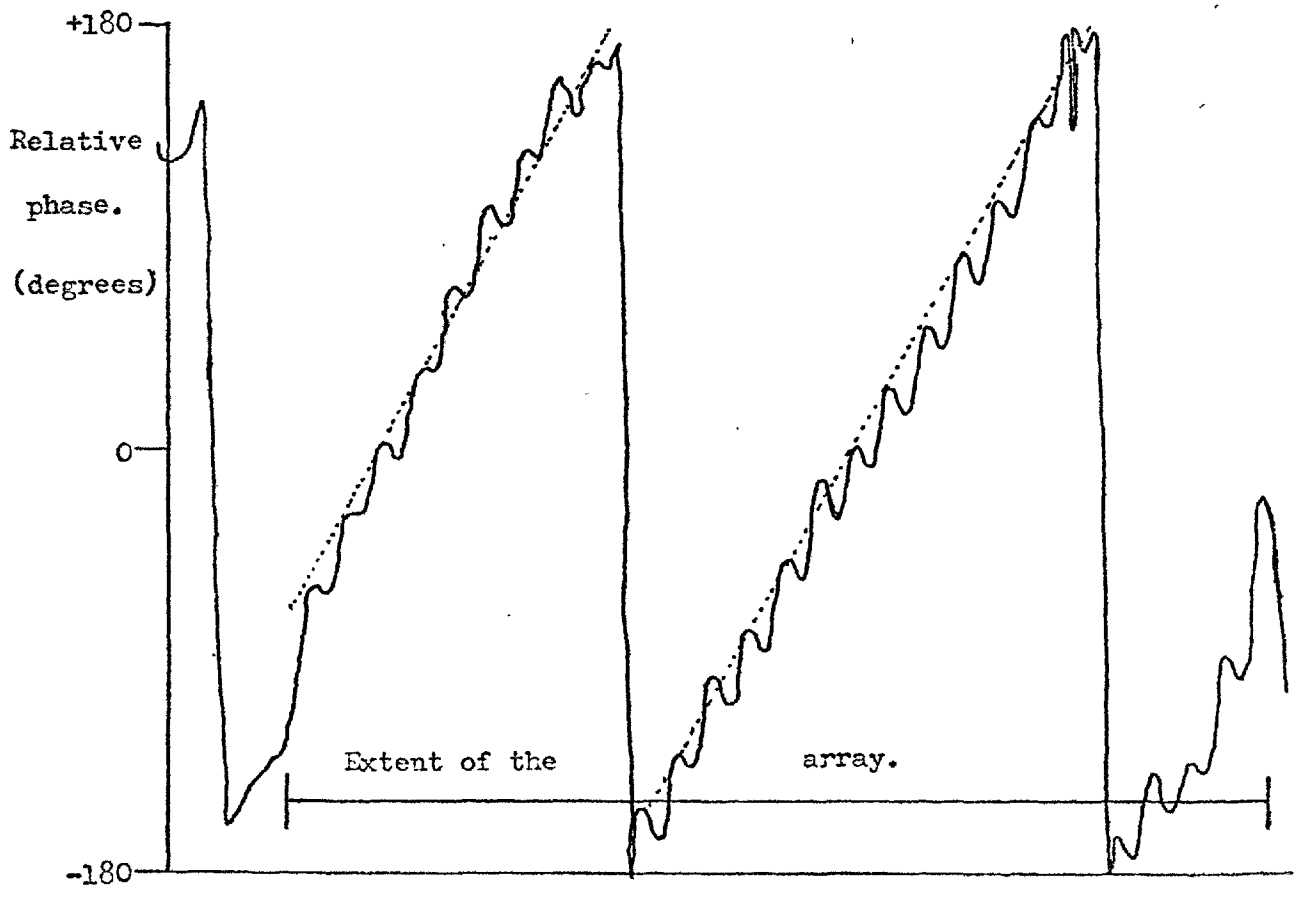

FIGURE 7.6.19. The aperture distribution of a single difference waveguide at 5.70 GHZ..

(a) Amplitude

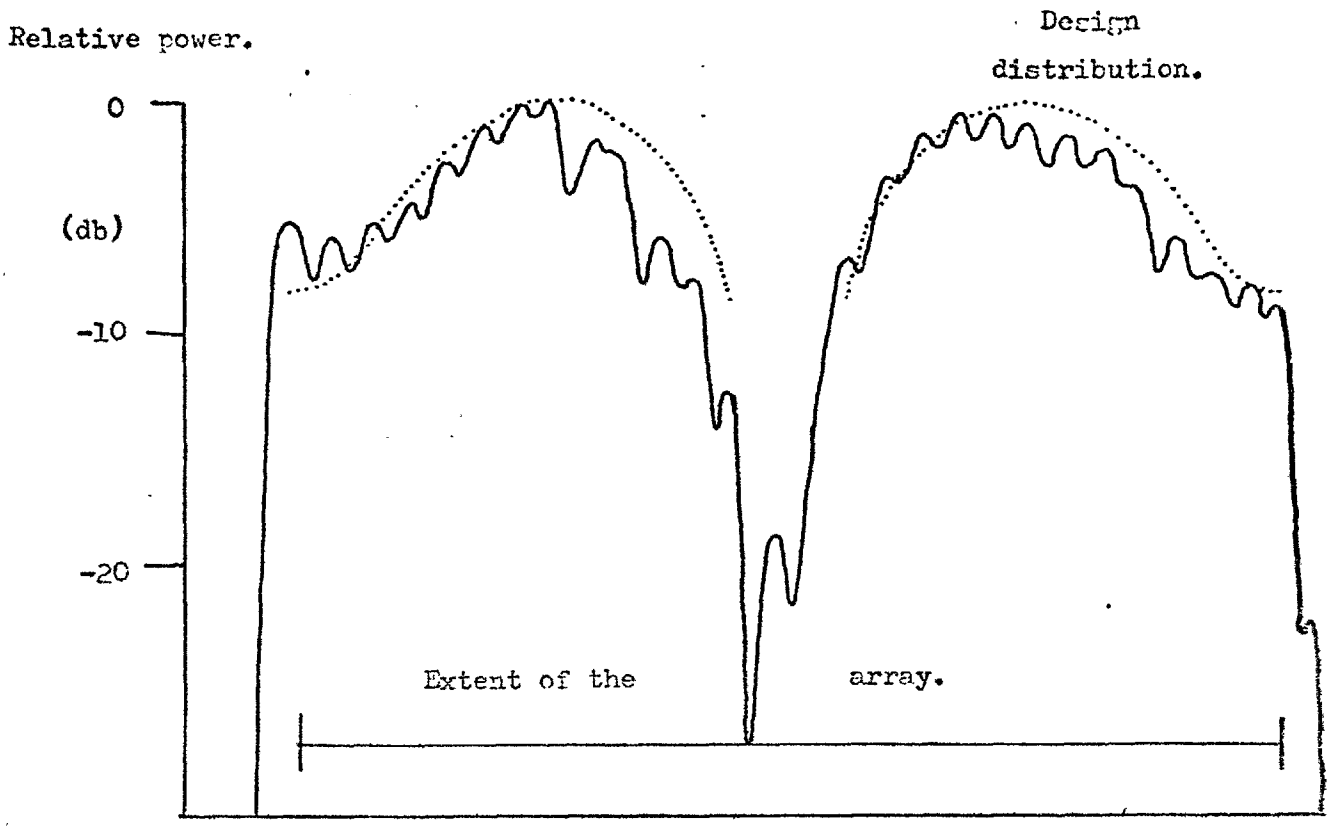

(b) Phase

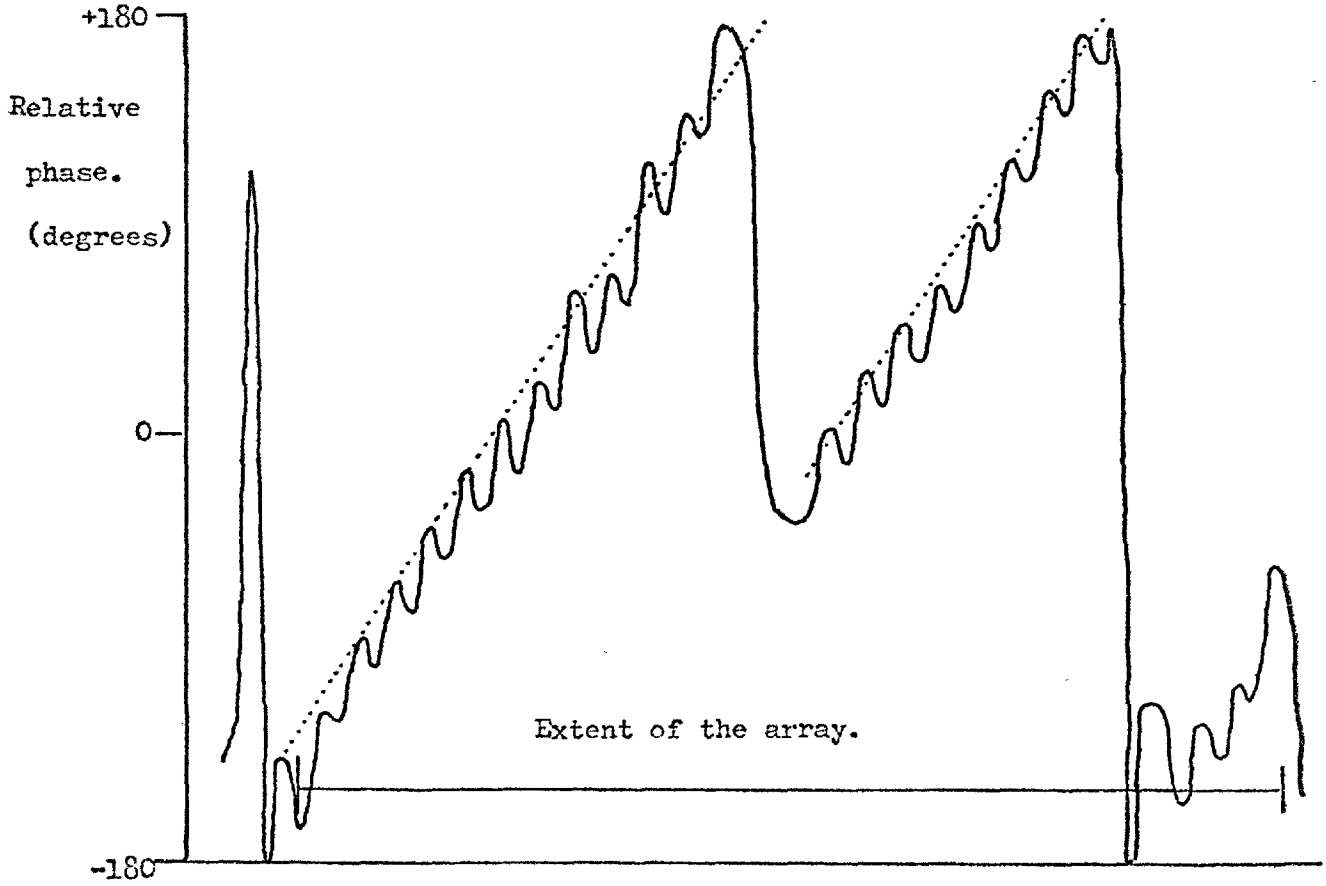

difference array distributions showed (see Figure 7.6.19) effects similar to those noted on the single sum waveguide.

When all the other waveguides were reintroduced and the measurements repeated initially with all the sum waveguides fed the results showed considerable changes. Figure 7.6.20. shows that the phase front is not as linear as it was and that the amplitude distribution is more ragged. The changes were principally due to mutual coupling and were worst around 5.85 GHz the frequency of peak coupled power. The distribution for this frequency is shown in Figure 7.6.21. with that at 5.60 GHz. The 5.60 GHz distribution is well behaved, consistent with all the slots being under-coupled. The 5.85 GHz plot has taken on the character of the difference channel with a deep hole near its centre. The two main regions of the distribution were at the correct phase consistent with the squint of the beam. There was however a small peak between the two major peaks and the phase of this was reversed. A similar type of behaviour was also noted with the difference channel. At 5.60 GHz and 5.70 GHz the patterns became more untidy but at 5.85 GHz the central hole in the distribution was completely filled in, as shown in Figures 7.6.22 and 7.6.23. The difference channel had taken on the character of the sum channel because of mutual coupling.

In general the behaviour of the array produced no major surprises. The gain of the single sum waveguide appeared to be very reasonable and mutual coupling seemed to only degrade the sidelobe performance of the array. The beam could be phase scanned as expected and no major change in gain occured until the grating lobe appeared. The difference channel null was perhaps not as deep as was desirable but in principle this can be made as deep as required by sufficiently accurate phase and amplitude trimming. The array sidelobes particularly around 5.80 GHz were higher than was wanted and this was due to mutual coupling. This was also

FIGURE 7.6.20. The aperture distribution of a sum waveguide with the difference parasitic at 5.70 GHZ..

(a) Amplitude.

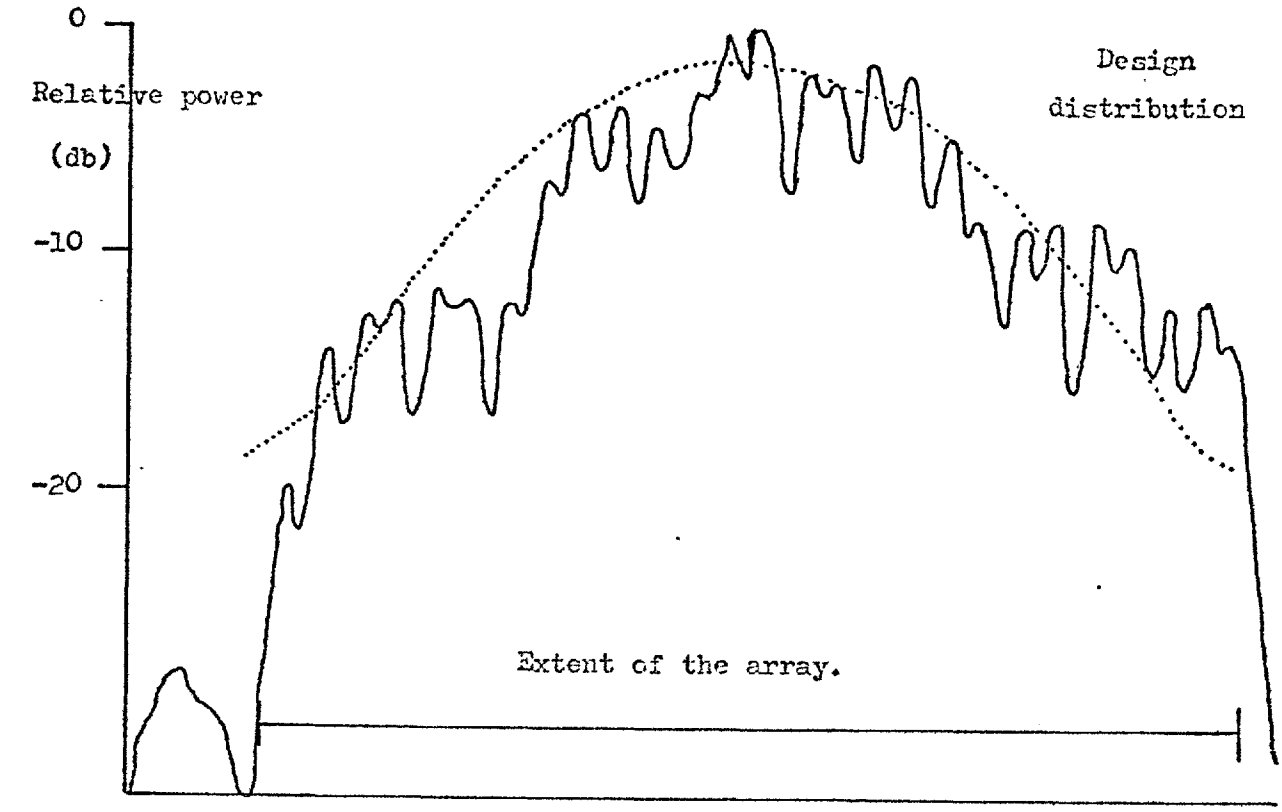

(b) Phase.

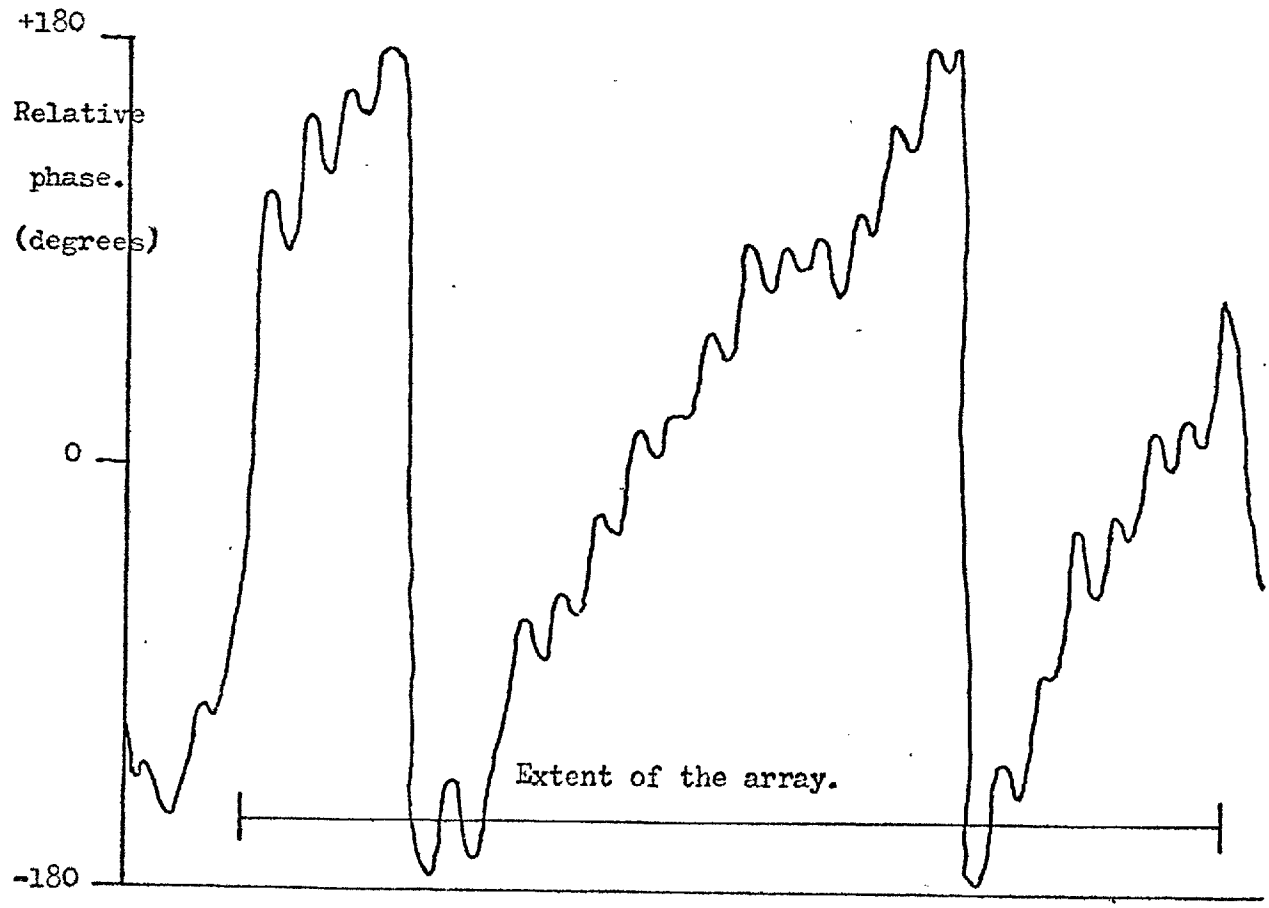

FIGURE 7.6.21. The amplitude distribution along a sum waveguide with the difference waveguides parasitic.

(a) 5.60 GHZ.

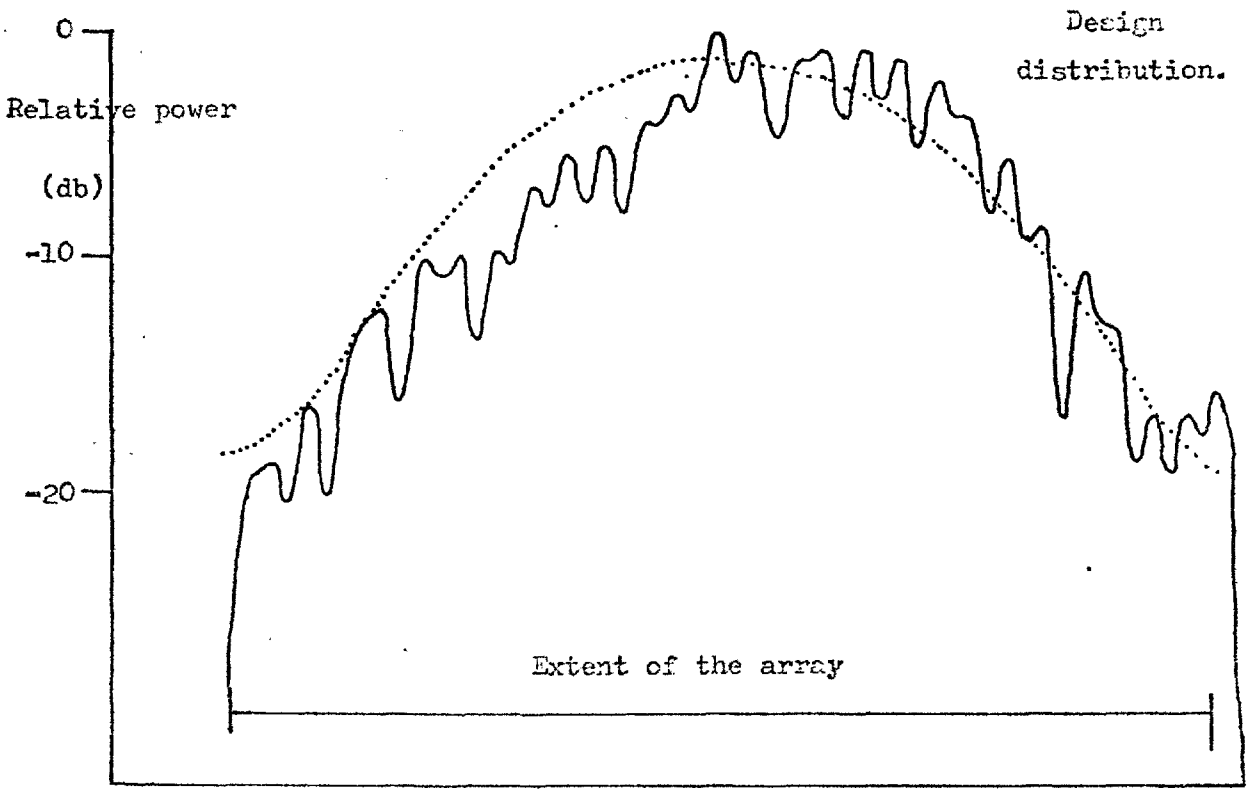

(b) 5.85 GHZ.

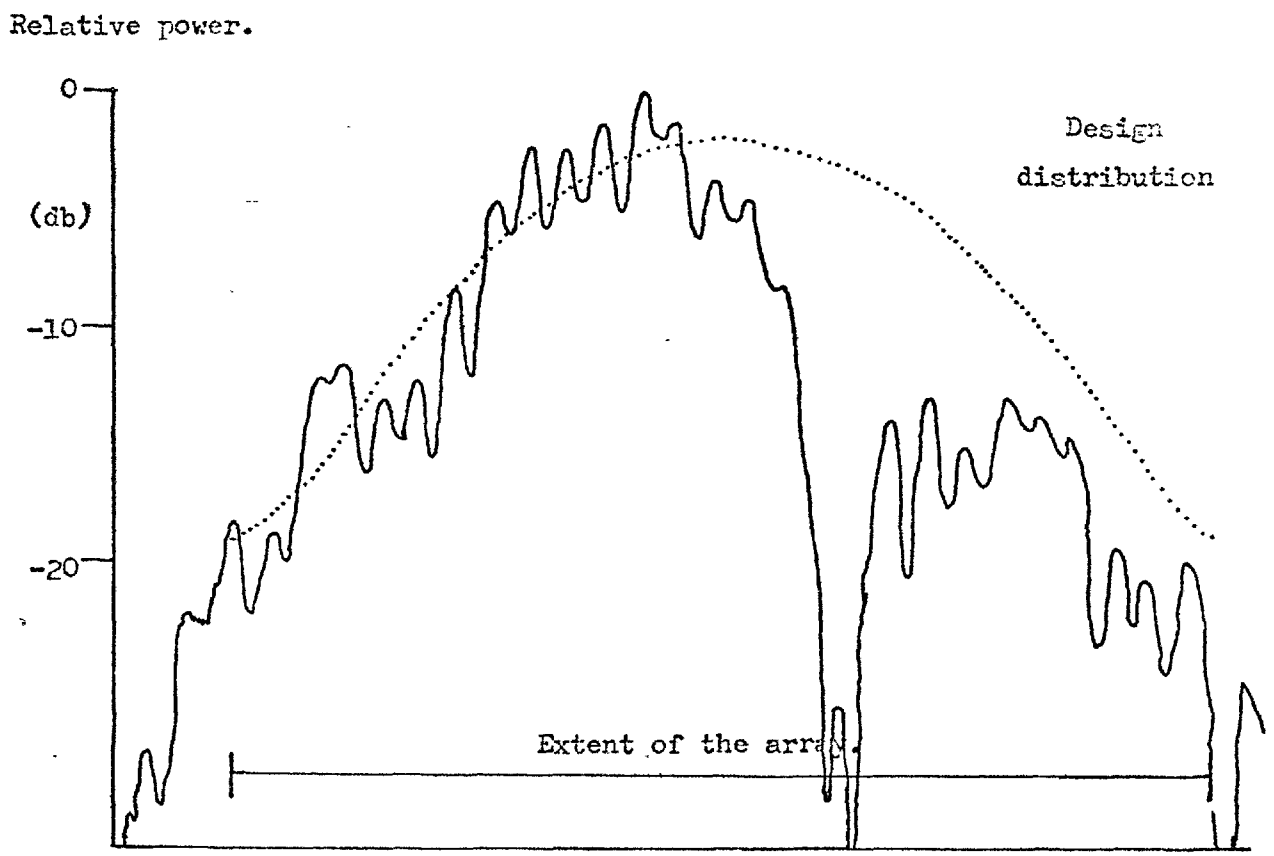

FIGURE 7.6.22. The aperture distribution of a difference waveguide with the sum array parasitic at 5.70 GHZ..

(a) Amplitude.

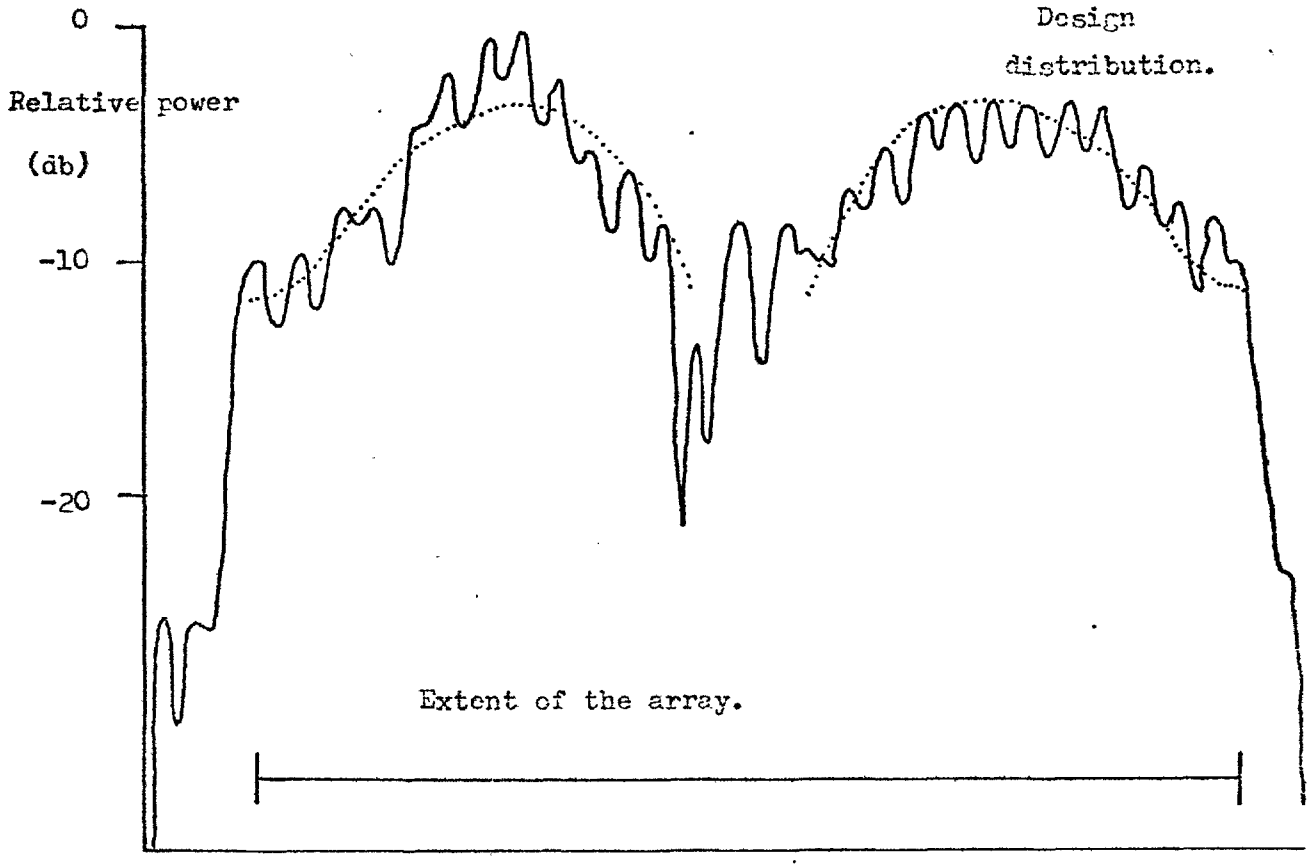

(b) Phase.

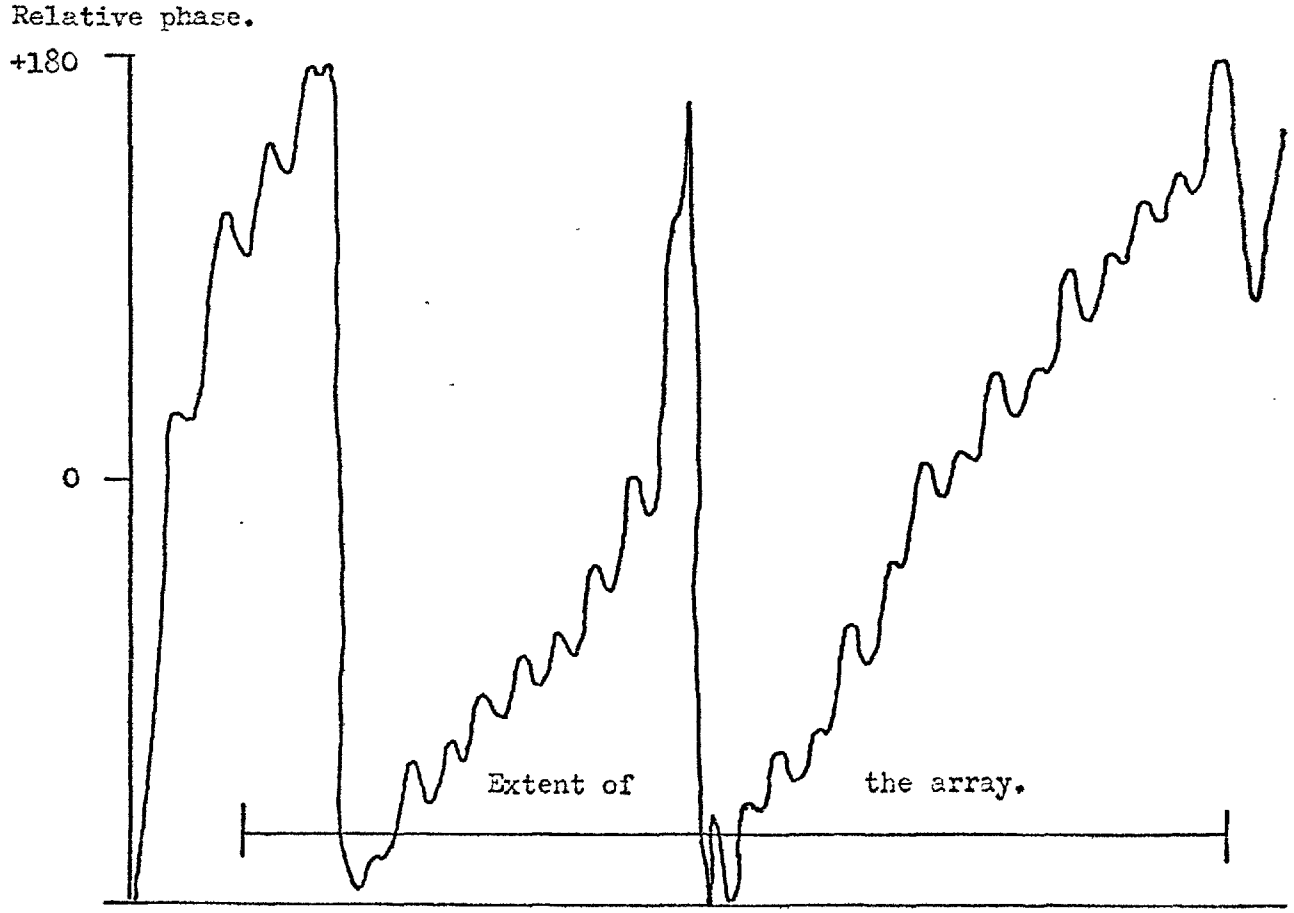

FIGURE 7.6.23. The amplitude distribution along a difference waveguide with the sum waveguides parasitic.

(a) 5.60 GHZ.

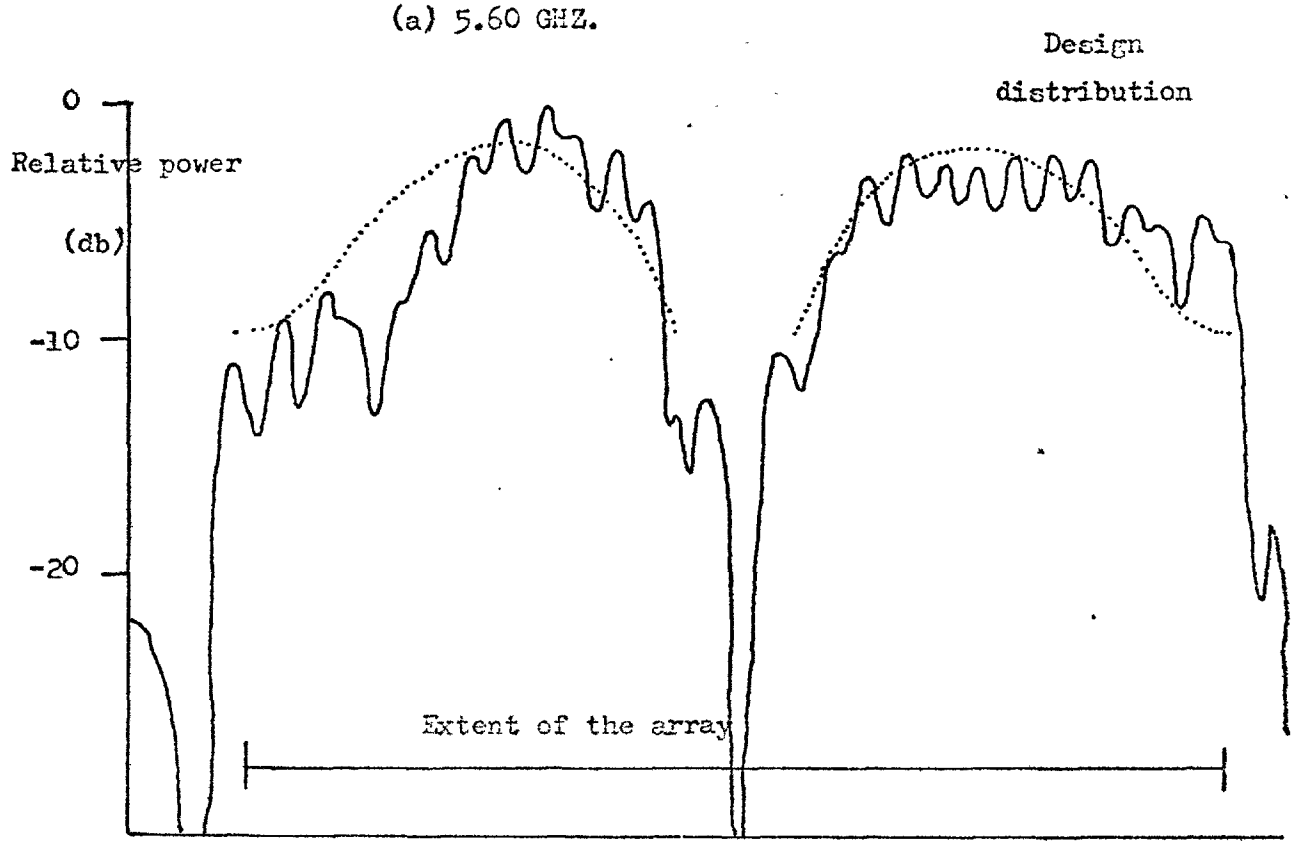

(b) 5.85 GHZ.

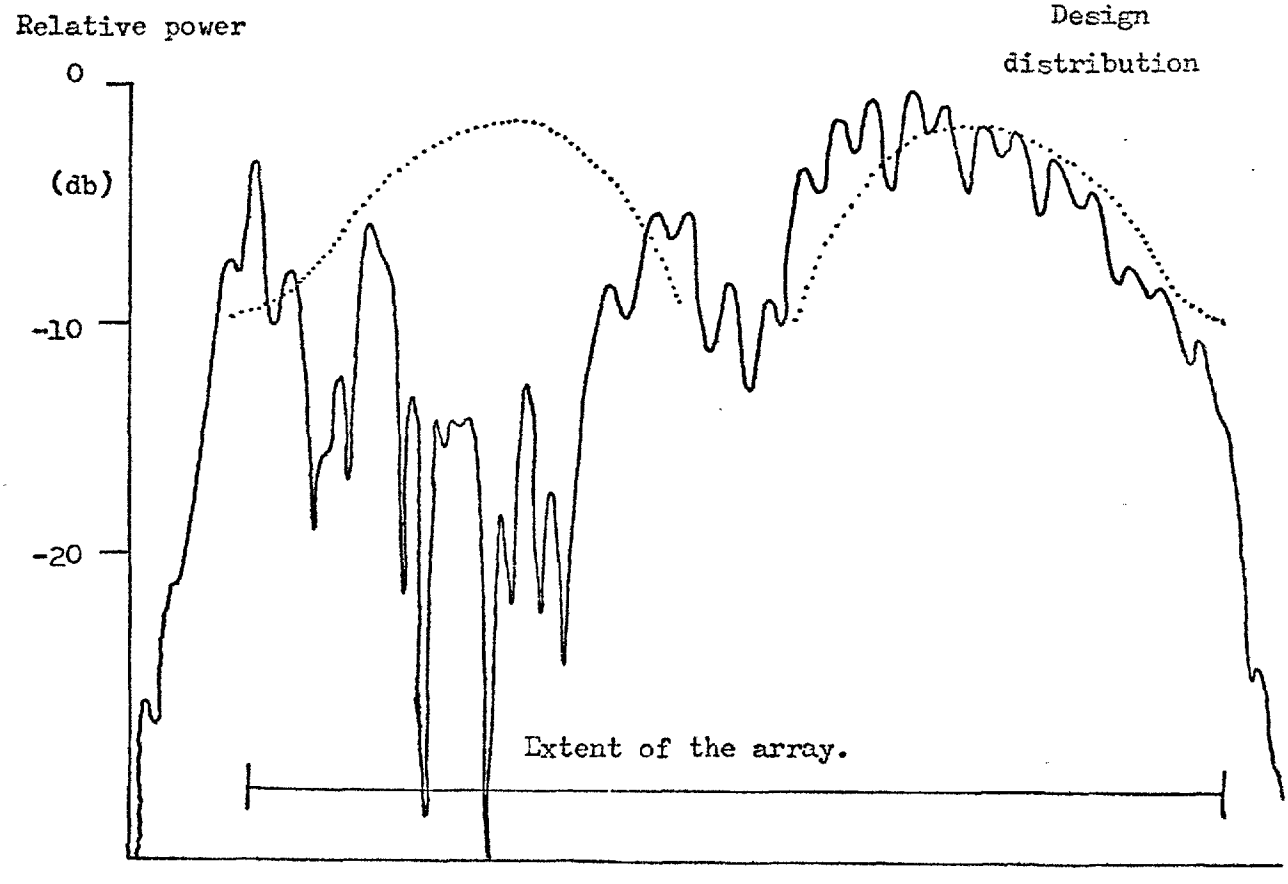

enhanced by the resulting mismatches within the main waveguides giving a large sidelobe at a particular angle. The performance of the single waveguides appeared to be good from near field measurements but larger sidelobes then expected were measured on the far field site. The cross polarisation of the array was approximately 5 dB bigger than expected from previous measurements on single slotted waveguides.

CHAPTER 8

A SUMMARY WITH CONCLUSIONS

This thesis has been concerned with finding an engineering solution to a specific practical antenna problem. The project grew from a need of A.S.W.E. for a horizontally polarised monopulse phase-scanned array in which the sum and difference channels were separately established. The grating lobe criterion dictated the use of a compact slot and initially the project was concerned with the search for a suitable geometry. This was complicated by the loss problems found by A.S.W.E..

The work presented was firmly based on an experimental approach as at the outset it was considered desirable if possible to build a prototype antenna. As each problem has been encountered an experimental investigation has been initiated because of the time required for manufacture. In the mean time theoretical studies have been undertaken so that experimental and theoretical results could be compared as early as possible. In most cases agreement was obtained so that the work could confidently and quickly be carried forward.

Straight, half wavelength long, slots have now been used for thirty years and their behaviour has been well documented, however they were initially considered. This was primarily done to establish the likely discrepancies between theoretical and experimental results and indicate the likely magnitude of end effects. This served to introduce the theory used and indicate the effects of rounded ends on slots as opposed to the square ends used in most papers. Good agreement between theory and experiment was obtained in predicting the conductance of these slots, in most cases better than the range of experimental error. It

was realised that the theory used was simpler than that of some of the more recent papers on slots, particularly the work of Oliner (1957) and work based on his results. However agreement between theory and experiment, at resonance was good. Although the off resonance performance of the slots could not be predicted this work was concerned with finding a new slot geometry and the simple theory was likely to be sufficient. Indeed any greater sophistication in the theory was likely to cloud the effects of changes in geometry.

The search for a suitable slot geometry proceeded in a fairly logical manner. The ⅂-shaped slot resulted naturally from the inability to fold the end arms of the shunt inclined slots on to the broad face. Early X-band measurements on this slot showed it to be relatively loss free and confirmed that the H-slot was lossy. The ⅂-shaped slot appeared to be a suitable array element but in a particular waveguide size it only had one value of resonant conductance so that complicated aperture distributions could not be specified. Some method was required to vary the resonant conductance. Initially ⅃- and Z-shaped slots were tried in an attempt to reduce the coupling of the slot to the waveguide. Unfortunately the radiation impedance of these slots varied in a similar manner to the coupling to the waveguide so that the required conductance variation was not obtained. However, the work on these slots showed that a suitable slot would have a variable coupling to the waveguide with constant radiation impedance. The I-shaped slot then emerged as a suitable geometry once it was remembered that top loading a dipole with an additional element was not likely to radically change its radiation resistance. The coupling to the waveguide could readily be controlled by altering the ratio of the lengths of the end arms as they excited the slot in opposition. The end arms could be regarded as series branch arms so that

the slot dimensions emerged. It was also experimentally demonstrated that the slots had a wide range of conductances. Lightly coupled slots in a ground plane were not so well behaved due to residual reactive components associated with the main polarisation. For very lightly coupled slots these components introduced such a frequency shift between the principal polarisations that the whole slot resonance was destroyed. However, well behaved lightly coupled slots could be obtained by fitting cross-polarisation suppression baffles.

At this stage the I-shaped slot seemed to be a useful array element but there appeared to be remarkable similarities in geometry between an uncoupled I-shaped slot and an uncoupled H-shaped slot. From A.S.W.E.'s results the H-shaped slot was known to be lossy. A substantial programme of loss measurement was undertaken to investigate loss in I-shaped slots of various dimensions. The results of this work showed that the loss of the I-shaped slot was critically dependent upon the height of the centre section. Small height reductions caused large increases in slot loss. The loss also changed with changes in slot width. Two important differences had been indentified between the geometries of the I and H slots on regard loss. The full waveguide height uniform width I-shaped slot was relatively loss free but the H shaped slot was of reduced height and impedance loaded so that it could be rotated. These differences appeared sufficient to account for its large loss.

A slot loss model was developed for the I or H shaped slot, after field measurements were made on a V.H.F. slot. The model provided a reasonably correct picture of the variation of loss with slot height. It was however, deficient in two major respects. The voltage across a slot at any point was accurately defined and known but the loss model

required the total current crossing the slot. This effectively meant that the slot line impedance was required. Unfortunately this can not be found directly because as the region of integration is further extended to infinity more capacitance is added. In the results presented the current density was modelled on a resistive network and arbitrarily truncated at a suitable value. The other major problem is the distribution of current between the end arms of the slot. Measurement indicated that the current was likely to be principally carried by the slot edges, but measurements can only be made above a surface not at a surface. The model could be further refined if a current gradient could be established. A knowledge of the slot line impedance would however make the theoretical slot loss figures derived more convincing. However, the model gives a variation of loss with dimensions that behaves in a manner similar to experimental results and is likely to be a correct description of the loss mechanism. The full waveguide height I-slot appeared to be loss free and the H-shaped slot lossy.

The full waveguide height I-shaped slot thus appeared to be a useful array element. It had a readily controlled conductance and in addition was most suitable for manufacture using numerically controlled machine tools, either a milling machine or jig borer. The slot only required cutting movements along or across the axis of the waveguide. This type of movement is available on all numerically controlled machines and means that there are considerable production advantages in this type of slot compared to the shunt inclined slot. Each shunt inclined slot requires an angle to be set on a rotary table. This movement is frequently not numerically controlled. This specific production advantage has been taken up by Plessey Radar Limited, Cowes. They, under Admiralty guidance, and in cooperation with Imperial College have adopted the I-shaped slot

developed in this study for their proposal to the F.A.A. for the C-band azimuth ground antenna of the Microwave Landing System (M.L.S.).

The work presented in this thesis was then concentrated on building large two dimensional monopulse arrays incorporating the I-shaped slot. This was done in two stages. Initially single waveguide arrays of I-shaped slots were developed and later these were stacked to produce a two dimensional array. The problems involved in making single slotted waveguide arrays were greatly reduced by fitting baffles to the slots. These effectively removed mutual coupling along the arrays and they could be designed effectively as a collection of isolated slots. The main design variables in the type of array are simply the number of slots, the aperture distribution, the power in the terminating load and the slot separation. In Chapter 5, the design of such arrays was presented and although errors were present on the thirty slot array made, the results enabled other arrays to be specified more accurately. The near-field distribution of the single sum waveguide of the eight waveguide array reflects this improvement. It is felt that single waveguide arrays of I-slots can now be accurately specified at C-band in the special size waveguide. Any aperture distribution or array length can in principle, be specified, subject to the range (- 4 dB → - 30 dB) of slot coupling available. Single waveguide arrays requiring a lower range of coupling can either be obtained by using a composite feed or by using a larger waveguide size with less magnetic field at the narrow wall. Extrapolation to other frequency bands should involve no major problems, although it is probably necessary to make a short array of say, sixteen slots to check end effects and radiation impedances.

Single waveguide arrays fitted with baffles appear to have no major design problems, but this is not so for two dimensional arrays. When the single arrays are stacked, mutual coupling becomes a major feature of their operation. The mutual impedance between slots effectively connects a network between all the slots in the space outside the aperture. As the waveguides connecting the slots also form networks the overall performance and even the voltage on an individual slot become difficult to predict. Fortunately for the case investigated the mutual impedance between slots over a ground plane varied by only 2 dB with coupling to the waveguide. When baffles were fitted even this variation was removed so that the mutual impedance between all slots at the same relative positions was the same. The other simplification made was that because baffles were fitted the mutual coupling across the waveguides was the only important component. The baffles supported a leaky wave that was partly responsible for this. Various alternative baffles were investigated but although some of these successfully matched the slot to space reducing short range mutual coupling, they reduced the attenuation of the leaky wave, increasing long range coupling and destroying the element pattern.

The simplification that the most important component of mutual impedance is within a column of slots enables some sort of rationalisation in treatment. The mutual coupling within one column of slots can be included and each column treated in turn. The other important feature to note is that consequential to fitting the baffles all the slot radiation impedances are identical. If the waveguide loading of the slots can be ignored, which is a reasonable approximation for lightly coupled slots then all the slots have the same impedance. The mutual impedance between slots is invariant with coupling

to the waveguide. It is a relationship between the current and voltages at the various terminals of the array elements. The constancy of the impedances within the array enables them not to be considered, and effectively removed, by using a voltage to voltage coupling description of mutual impedance. Being able to neglect the waveguide loading of the slots also has a more subtle effect on the overall performance of a multiple waveguide array. If one waveguide is excited with a prescribed aperture distribution the adjacent ones will also have that distribution, because of the constancy of the radiation and mutual impedances. Thus all the other arrays, to a first approximation, behave as parasitic elements with the correct azimuth aperture distribution. These elements are however at the wrong phase, so that the principal effects of mutual coupling on an array of stacked waveguides fitted with baffles, is to reduce the array gain and increase the elevation pattern sidelobes. Only on a second approximation when the effects of waveguide loading are included is the azimuth radiation pattern affected. For the eight waveguide array investigated the decrease in gain was not appreciable and the elevation side-lobe structure was not investigated. The azimuth patterns measured showed appreciable deterioration due to mutual coupling but comparatively little error is required to increase sidelobes from - 30 dB to - 20 dB. The patterns also showed a large sidelobe due to reflections within the waveguide.

Before other multiple waveguide monopulse arrays are built, there is thus a considerable amount of work to be done to predict azimuth radiation patterns. Arrays could be built with very lightly coupled slots so that the approximation improves but this would probably result in an inefficient antenna and although its azimuth sidelobes were likely to be better than the eight waveguide array built they could

still not be predicted. A complete mutual impedance description rather than a mutual coupling description of the effects of neighbouring slots is required. This would also require a complete network description of individual slots. It is felt that it should not be too difficult to characterize an array in this way with the slots at reasonance. The computer programme involved to calculate azimuth radiation patterns would be large. It would also have to be iterative so as to include the actual impedance beyond each slot including incremental impedances.

The other aspect of the array performance that needs more effort is its performance over a band of frequencies. This requires the reactive component of the slot impedances to be investigated. The more sophisticated methods of slot analysis could probably be used but more directly for engineering applications the results of experimental measurements could be included into a suitable computer programme. The likely performance obtained by frequency scanning the beam in azimuth could then be predicted.

This thesis has only considered two channel monopulse arrays. The problems encountered have been more difficult than with a single channel array or with an array required to produce only beams at broadside. For either of these applications the problems of mutual coupling are greatly reduced by increasing the slot spacing. For a single channel array the problems are further reduced because the same aperture distribution is used for all waveguides. In any column all the slots are identical and have the same coupling. Under these circumstances the scattering description of mutual impedance is likely to be more valid. With a single channel array the problems of mutual impedance are reduced because a greater inter-waveguide spacing is allowed. This not only

reduces the amplitude of the coupling between adjacent waveguides but if a half wavelength spacing is selected the coupling appears inside the waveguides as an "incremental conductance" with no reactive components. The frequency shifts associated with mutual impedance in the eight waveguide array are then removed.

A monopulse array can be made by splitting the waveguides of a single channel array and using devices like magic tees to produce the multiple beams. The problems associated with this type of monopulse array are much simpler than with the specific geometry investigated in this study, although the aperture amplitude distribution used must be the same for both channels. However, good sidelobe performances can be obtained from this type of geometry (Lewis, Lee and McCarthy (1970)) with inefficient use of the aperture. The configuration investigated in this study attempted to separately establish the different monopulse channels so that a good sidelobe performance may be obtained with reasonable aperture efficiency. The final array manufactured was partially successful in achieving this aim. However, the degradation in the sidelobe performance due to mutual coupling can not yet be determined, although a large computer programme is proposed to give this type of result.

For most systems the extra expense and complications caused by including a second set of waveguides in the aperture can not be justified by the marginal improvement in aperture efficiency. The use of two sets of waveguides must be dictated by particular system requirements such as gain, side-lobe level and available space.

To summarise, in order to meet the particular requirements of an array of closely spaced slotted waveguides a fresh look has been taken at the type of radiating slots used. Various possible novel alternative slots were investigated but most of them were rejected. One particular

slot geometry emerged as most useful for this application and has been closely studied. The I-shaped slot was found to have important production advantages as it is most suitable for numerically controlled machining. In time this manufacturing advantage may lead to its wide spread use. The emergence of the I-shaped slot may be the most important contribution of this work.

REFERENCES

ABRAMOWITZ, M. and STEGEN, I.A. (1964) "Handbook of Mathematical Functions with Formulas, Graphs and Mathematical Tables", National Bureau of Standards, U.S. Government Printing Office, Washington D.C..

AMITAY, N., GALINDO, V. and WU, C.P. (1972) "Theory and Analysis of Phased Array Antennas", Wiley-Interscience, J. Wiley, New York.

BAILEY, M.C. (1967) "Design of Dielectric-Covered Resonant Slots in a Rectangular Waveguide", I.E.E.E. Trans. on Antennas and Propogation, Vol. AP-15, No. 5, pp 594-8, Sept. 1967.

BARTON, D.K. and WARD, H.R. (1969) "Handbook of Radar Measurement", Prentice Hall Inc., New Jersey.

BENSON, F.A. (1969) "Millimetre and Submillimetre Waves", Iliffe Books, London.

BLASS, J. and RABINOWITZ, S.J. (1957) "Mutual Coupling in Two Dimensional Arrays", I.R.E. Wescon Convention Record, Vol. 1, Part 1, pp 134-150, 1957.

BOOKER, H.G. (1946) "Slot Aerials and Their Relation to Complementary Wire Aerials", Proc. I.E.E., Vol. 93, Part IIIA, No. 4, p. 620, 1946.

CARTER, P.S. (1932) "Circuit Relationships in Radiating Systems and Applications to Antenna Problems", Proc. I.R.E., Vol. 20, No. 6, pp 1004-41, June 1932.

COHN, M. (1960) "Propogation in Partially Dielectric Loaded Parallel Plane and Trough Waveguides", Technical Report No. AF-78, The John Hopkins University Radiation Lab., Baltimore, Md. (1960).

CRUZAN, O.R. (1962) "Translation Addition Theorems For Spherical Vector Wave Functions", Quart. Appl. Math., Vol. 20, No. 1, pp 33-40.

DOLPH, C.L. (1946) "A Current Distribution for Broadside Arrays Which

Optimises the Relationship Between Beam Width and Side-Lobe Level", Proc. I.R.E., Vol. 34 , No. 6, pp 335-48, June 1946.

DUFORT, E.C. (1968) "Design of Corrugated Plates for Phased Array Matching", I.E.E.E. Trans on Antennas and Propogation, Vol. AP-16, No. 1, pp 37-46, Jan. 1968.

FRADIN, A.Z. (1961) "Microwave Antennas", (Translation from the Russian by M. Nadler), Pergamon Press, Oxford 1961.

GOLDSTONE, L.O. and OLINER, A.A. (1959) "Leaky-Wave Antennas 1 : Rectangular Waveguide", I.R.E. Trans. on Antennas and Propogation, Vol. AP-7, No. 4, p. 307, Oct. 1959.

HANNAN, P.W. (1961) "Optimum Feeds for all Three Modes of a Monopulse Antenna 1 : Theory", I.R.E. Trans. on Antennas and Propogation, Vol. AP-9, No. 5, p. 444, Sept. 1961.

HANNAN, P.W. and LITT, S.P. (1968) "Capacative Ground Plane for a Phased Array Antenna", 1968, G-AP International Symposium Digest, pp 115-123, Sept. 1968.

HANSEN, R.C. (1966) "Microwave Scanning Antennas", Academic Press, New York.

HEINS, A.E. and CARLSON, J.F. (1947) "The Reflection of an Electromagnetic Plane Wave by an Infinite Set of Plates : I and II", Quarterly of Mathematics 4, pp 313-329 and 5, pp 82-88, 1947.

HU, A.Y. and LUNDEN, C.D. (1961) "Rectangular-Ridge Waveguide Slot Array", I.R.E. Trans. on Antennas and Propogation, Vol. AP-9, No. 1, pp 102-5, Jan. 1961.

JASIK, H. (1961) "Antenna Engineering Handbook", McGraw Hill, New York.

KAHN, W.K. and WASYLKIWSKYJ, W. (1966) "Coupling, Radiation and Scattering by Antennas", Proc. Symp. on Generalised Networks, Vol. 16, pp 83-114, Polytechnic Press, Brooklyn, N.Y., 1966.

KILLICK, E.A., COLLEY, G.J., DELANEY, W.D. and EDDLES, J.A. (1969) "A Ferrite Controlled Phase Scanned Microwave Antenna", Proc. 1969 European Microwave Conference.

KILLICK, E.A., SALT, H. and PORTER, N.E. (1969) "The Design of Waveguide Arrays Providing Sum and Difference Beams and Suitable For Scanning in One Plane", Proc. 1969 European Microwave Conference.

KING, R.W.P. (1956) "Theory of Linear Antennas", Harvard University Press, Cambridge, Mass.

KING, R.W.P. and HARRISON, C.W. (1969) "Antennas and Waves - A Modern Approach", The M.I.T. Press, Cambridge, Mass. and London.

KIRKPATRICK, G.M. (1953) "Aperture Illuminations for Radar Angle of Arrival Measurements", I.R.E. Trans. on Aeronautical and Navigational Electronics, Vol. AE-9, pp 20-27, Sept. 1953.

KNORR, J.B. and SAENZ, J. (1973) "End Effect in a Shorted Slot", I.E.E.E. Trans. on Microwave Theory and Technique, Vol. MTT-21, No. 9, p. 579, Sept. 1973.

LEWIS, D.J., LEE, J.R. and McCARTHY, D.K. (1970) "A Single Plane Electronically Scanned Antenna for Airbourne Radar Applications", Phased-Array Antenna Symposium, June 2-5, 1970, Polytechnic Institute of Brooklyn, Graduate Center, New York. Later published in "Phased Array Antennas", edited by OLINER, A.A. and KNITTEL, G.H., Artech House, Mass., 1972.

MONTGOMERY, C.G., DICKE, R.H. and PURCELL, E.M. (1948) "Principles of Microwave Circuits", M.I.T. Radiation Lab. Series Vol. 8, McGraw Hill, New York.

OLINER, A.A. (1957) "The Impedance Properties of Narrow Radiating Slots in the Broad Face of Rectangular Waveguide. Part 1 - Theory", I.R.E. Trans. on Antennas and Propogation, Vol. AP-5, No. 1, pp 4-20, Jan. 1957.

POWERS, E.J. (1967) "Utilisation of the Lambda Functions in the Analysis and Synthesis of Monopulse Antenna Difference Patterns", I.E.E.E. Trans. on Antennas and Propogation, Vol. AP-15, No. 6, p. 771, Nov. 1967.

PRICE, O.R. and HYNEMAN, R.F. (1960) "Distribution Functions for Monopulse Antenna Difference Patterns", I.R.E. Trans. on Antennas and Propogation, Vol. AP-8, No. 6, pp 567-76, Nov. 1960.

RAMSAY, J.F. (1967) "Antenna Design Supplement; Lambda Functions Describe Antenna / Diffraction Patterns", Microwaves, June, 1967.

RHODES, D.R. (1950) "Introduction to Monopulse", McGraw Hill, New York.

RUMSEY, V. (1966) "Frequency Independent Antennas", Academic Press, New York and London.

SCHELKUNOFF, S.A. (1943) "Electromagnetic Waves", D. Van Nostrand, Princeton, N.J.

SILVER, S. (1949) "Microwave Antenna Theory and Design", M.I.T. Radiation Lab. Series, Vol. 12, McGraw Hill, New York.

SILVESTER, P. (1968) "Modern Electromagnetic Fields", Prentice-Hall Inc., New Jersey.

STEIN, S. (1961) "Addition Theorems for Spherical Wave Functions", Quart. Appl. Math., Vol. 19, No. 1, pp 15-24.

STEVENSON, A.F. (1948) "Theory of Slots in Rectangular Waveguide", J. Appl. Phys., 19, pp 24-38, 1948.

TAYLOR, T.T. (1955) "Design of Line Source Antennas for Narrow Beam Width and Low Sidelobes", I.R.E. Trans. on Antennas and Propogation, Vol. AP-3, No. 1, pp 16-28, Jan. 1955.

VAN DER MASS, G.J. (1954) "A Simplified Calculation for Dolph-Chebyshev Arrays", J. Appl. Phys., 25, pp 121-4, 1954.

WASYLKIWSKJ, W. and KAHN, W.K. (1970) "Theory of Mutual Coupling a Among Minimum Scattering Antennas", I.E.E.E. Trans. on Antennas and Propogation, Vol. AP-18, No. 2, pp 204-16, March 1970.

WATSON, W.H. (1947) "The Physical Principles of Waveguide Transmission and Antenna Systems", Oxford University Press, London and New York, 1947.

WHITEHEAD, E.A.N. (1951) "Theory of Parallel Plate Media for Microwave Lenses", Proc. I.E.E., Vol. 98, Part 3, p. 133, March 1951.

WILLIAMS, N. (1975) "Mutual Coupling Studies in Waveguide Slot Arrays", Ph.D. Thesis, University of London.

YEE, H.Y. (1974) "Impedance of a Narrow Longitudinal Shunt Slot in a Slotted Waveguide Array", I.E.E.E. Trans. on Antennas and Propogation, Vol. AP-22, No. 4, p. 589 , July 1974.

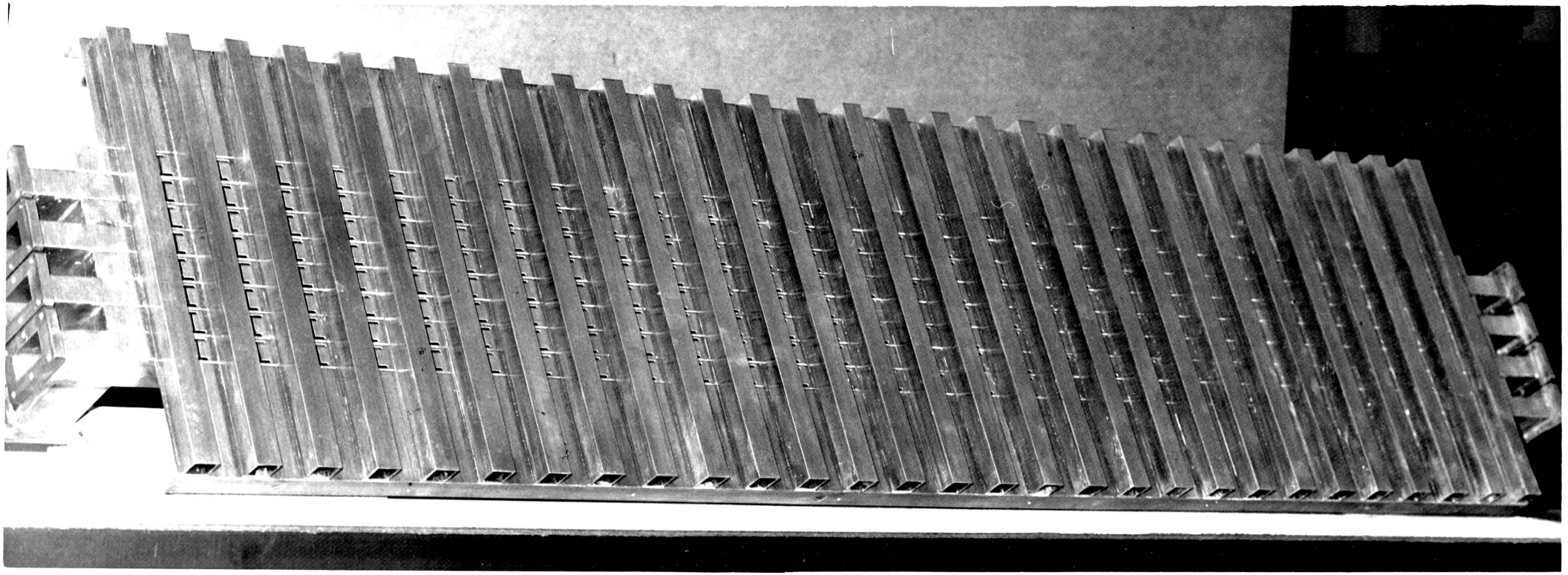

Plate I THE EIGHT WAVEGUIDE SLOTTED ARRAY

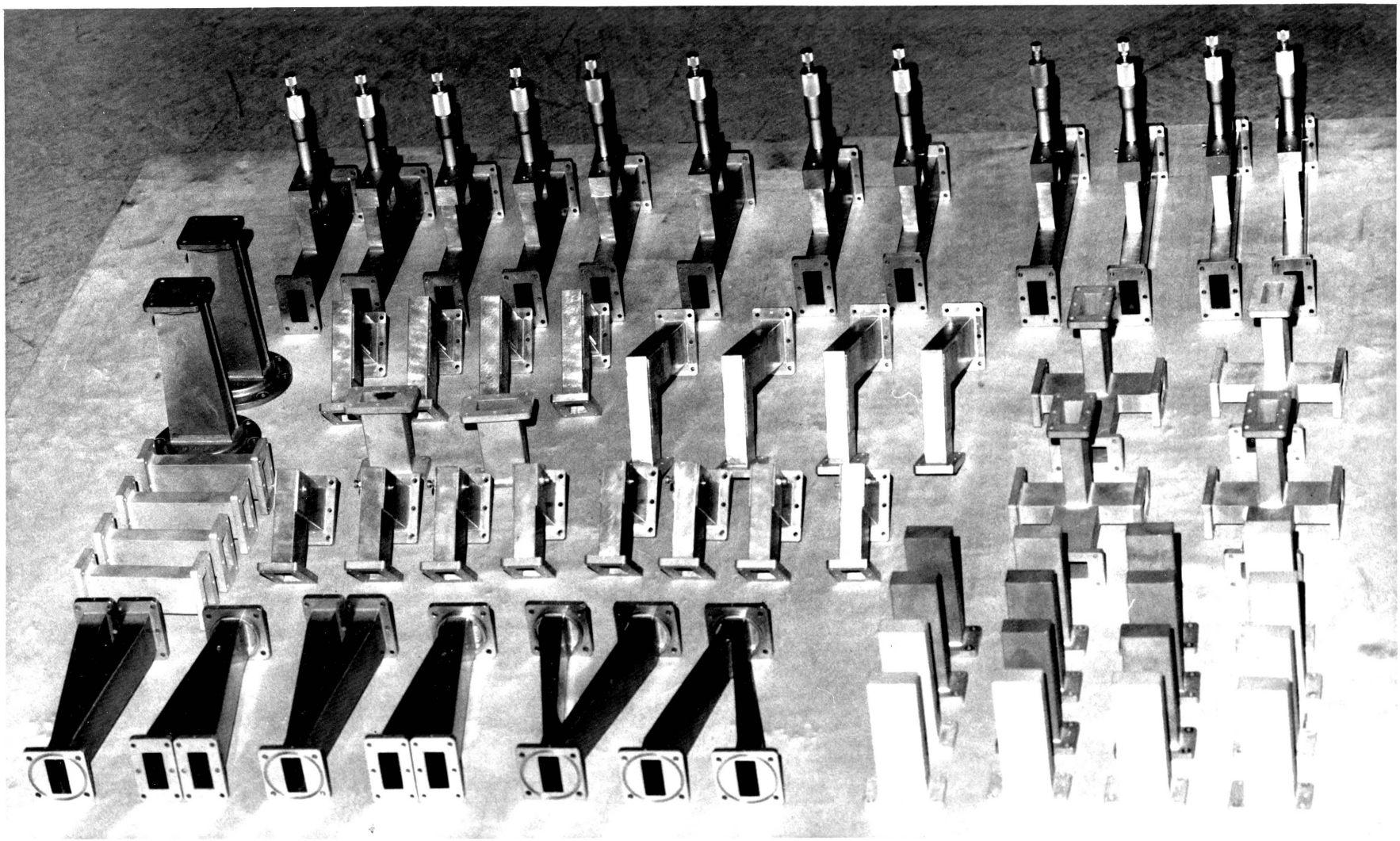

Plate 2 THE COMPONENTS OF THE FEED NETWORK

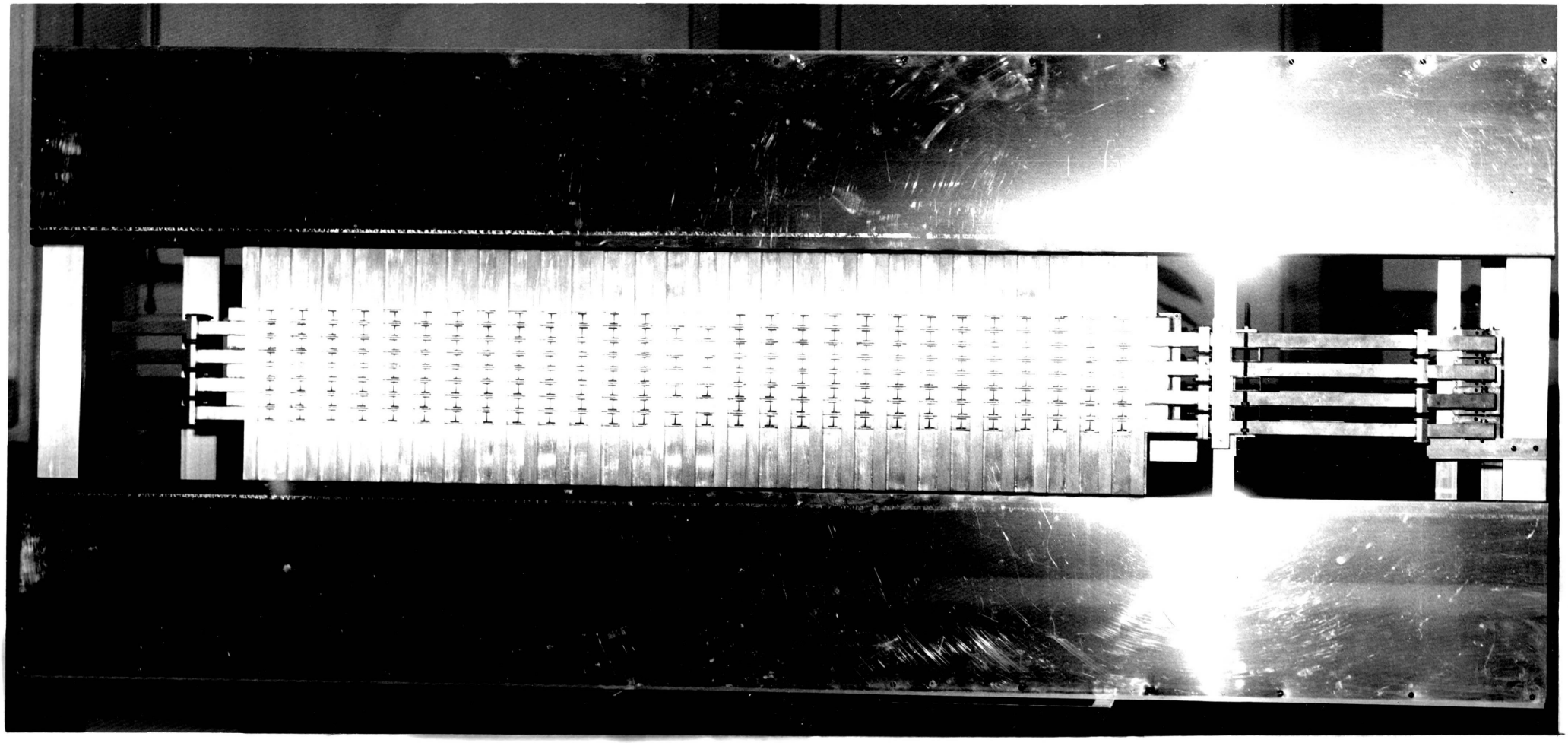

Plate 3 THE FRONT FACE OF THE ASSEMBLED ARRAY

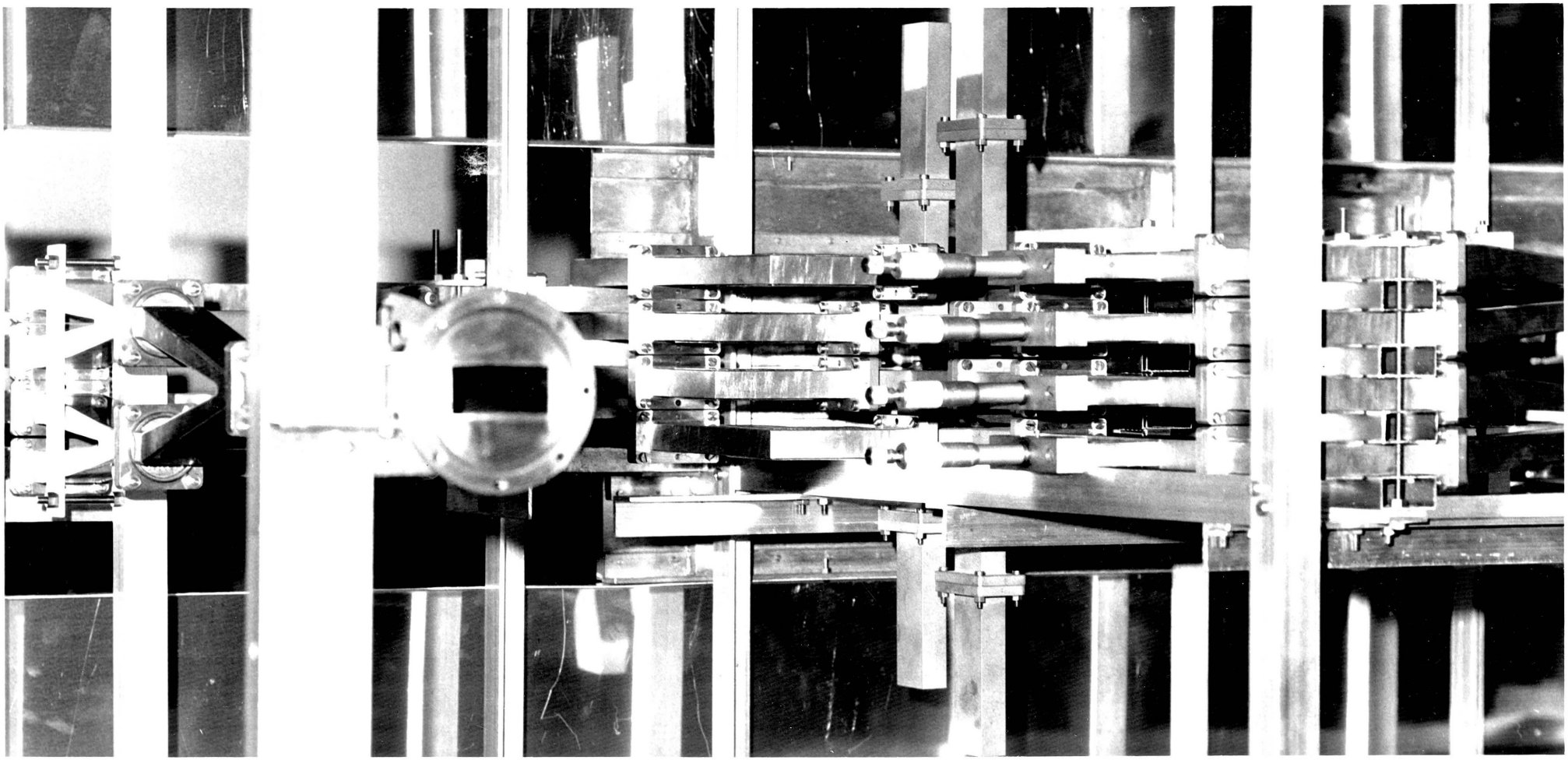

Plate [illegible] THE FEED NETWORK

Plate T FEED NETWORK